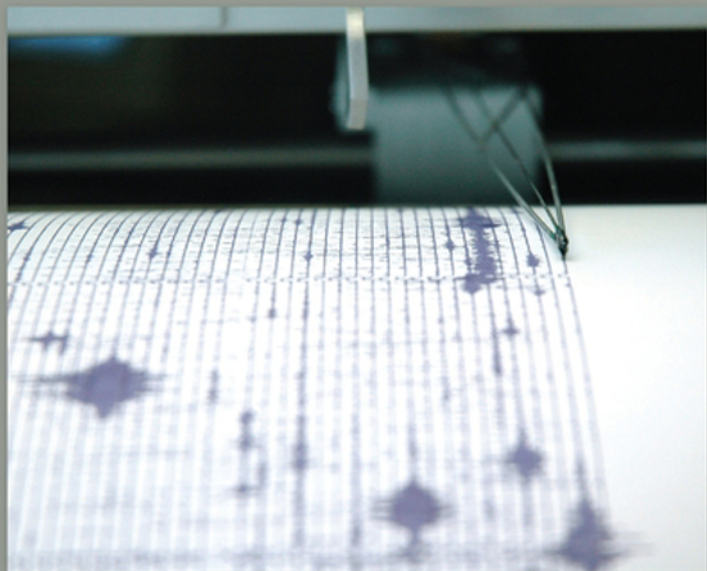


PREMIER REFERENCE SOURCE

Structural Seismic Design Optimization and Earthquake Engineering

Formulations and Applications



Vagelis Plevris, Chara Ch. Mitropoulou & Nikos D. Lagaros

Structural Seismic Design Optimization and Earthquake Engineering: Formulations and Applications

Vagelis Plevris

*School of Pedagogical and Technological Education,
Greece National Technical University of Athens, Greece*

Chara Ch. Mitropoulou

*Institute of Structural Analysis and Seismic Research,
National Technical University of Athens, Greece*

Nikos D. Lagaros

*Institute of Structural Analysis and Seismic Research,
National Technical University of Athens, Greece Hellenic Army, Greece*

Managing Director:	Lindsay Johnston
Senior Editorial Director:	Heather A. Probst
Book Production Manager:	Sean Woznicki
Development Manager:	Joel Gamon
Development Editor:	Myla Harty
Acquisitions Editor:	Erika Gallagher
Typesetter:	Nicole Sparano
Cover Design:	Nick Newcomer, Lisandro Gonzalez

Published in the United States of America by

Engineering Science Reference (an imprint of IGI Global)
701 E. Chocolate Avenue
Hershey PA 17033
Tel: 717-533-8845
Fax: 717-533-8661
E-mail: cust@igi-global.com
Web site: <http://www.igi-global.com>

Copyright © 2012 by IGI Global. All rights reserved. No part of this publication may be reproduced, stored or distributed in any form or by any means, electronic or mechanical, including photocopying, without written permission from the publisher. Product or company names used in this set are for identification purposes only. Inclusion of the names of the products or companies does not indicate a claim of ownership by IGI Global of the trademark or registered trademark.

Library of Congress Cataloging-in-Publication Data

Structural seismic design optimization and earthquake engineering: formulations and applications / Vagelis Plevris ... [et al.], editors.

p. cm.

Includes bibliographical references and index.

Summary: "This book focuses on the research around earthquake engineering, in particular, the field of implementation of optimization algorithms in earthquake engineering problems, including simulation issues for the accurate prediction of the seismic response of structures, design optimization procedures, soft computing applications, and other important advancements in seismic analysis and design"-- Provided by publisher.

ISBN 978-1-4666-1640-0 (hardcover) -- ISBN 978-1-4666-1641-7 (ebook) -- ISBN 978-1-4666-1642-4 (print & perpetual access) 1. Earthquake engineering. 2. Structural optimization. I. Plevris, Vagelis, 1976-

TA654.6.S8673 2012

624.1'762--dc23

2012003307

British Cataloguing in Publication Data

A Cataloguing in Publication record for this book is available from the British Library.

All work contributed to this book is new, previously-unpublished material. The views expressed in this book are those of the authors, but not necessarily of the publisher.

Editorial Advisory Board

Christoph Adam, *University of Innsbruck, Austria*

Christian Bucher, *Vienna University of Technology, Austria*

Tadeusz Burczynski, *Silesian University of Technology, Poland*

Luis Esteva Maraboto, *National University of Mexico, Mexico*

Dan M. Frangopol, *Lehigh University, USA*

Michalis Fragiadakis, *National Technical University of Athens, Greece*

Hector Jensen, *Universidad Técnica Federico Santa María, Chile*

Matthew G. Karlaftis, *National Technical University of Athens, Greece*

Manolis Papadrakakis, *National Technical University of Athens, Greece*

Shahram Pezeshk, *University of Memphis, USA*

Table of Contents

Foreword.....	xiii
Preface.....	xiv
Acknowledgment.....	xvi
Chapter 1	
Life Cycle Cost Considerations in Seismic Design Optimization of Structures	1
<i>Bora Gencturk, University of Illinois at Urbana-Champaign, USA</i>	
<i>Amr S. Elnashai, University of Illinois at Urbana-Champaign, USA</i>	
Chapter 2	
Performance-Based Seismic Design: A Search-Based Cost Optimization with Minimum Reliability Constraints	23
<i>Oscar Möller, University of Rosario, Argentina</i>	
<i>Marcelo Rubinstein, University of Rosario, Argentina</i>	
<i>Fabián Savino, University of Rosario, Argentina</i>	
<i>Ricardo O. Foschi, University of British Columbia, Canada</i>	
Chapter 3	
Discrete Variable Structural Optimization of Systems under Stochastic Earthquake Excitation	51
<i>Héctor Jensen, Universidad Tecnica Federico Santa Maria, Chile</i>	
<i>Marcos Valdebenito, Universidad Tecnica Federico Santa Maria, Chile</i>	
<i>Juan Sepúlveda, Universidad Tecnica Federico Santa Maria, Chile</i>	
<i>Luis Becerra, Universidad Tecnica Federico Santa Maria, Chile</i>	
Chapter 4	
A Multi-Hazard Framework for Optimum Life-Cycle Cost Design of Reinforced Concrete Bridges.....	76
<i>Azadeh Alipour, University of Massachusetts Amherst, USA</i>	
<i>Behrouz Shafei, University of Massachusetts Amherst, USA</i>	
<i>Masanobu Shinozuka, University of California, USA</i>	

Chapter 5	
Efficient Robust Optimization of Structures Subjected to Earthquake Load and Characterized by Uncertain Bounded System Parameters.....	105
<i>Subrata Chakraborty, Bengal Engineering and Science University, India</i>	
<i>Soumya Bhattacharjya, Bengal Engineering and Science University, India</i>	
Chapter 6	
Damage Assessment of Inelastic Structures under Simulated Critical Earthquakes	128
<i>Abbas Moustafa, Minia University, Egypt</i>	
Chapter 7	
Metaheuristic Optimization in Seismic Structural Design and Inspection Scheduling of Buildings.....	152
<i>Chara Ch. Mitropoulou, Institute of Structural Analysis and Seismic Research, National Technical University Athens, Greece</i>	
<i>Vagelis Plevris, School of Pedagogical and Technological Education (ASPETE), Greece</i>	
<i>Nikos D. Lagaros, Institute of Structural Analysis and Seismic Research, National Technical University Athens, Greece</i>	
Chapter 8	
Optimal Performance-Based Seismic Design.....	174
<i>Hamid Moharrami, Tarbiat Modares University, Iran</i>	
Chapter 9	
Optimal Seismic Performance-Based Design of Reinforced Concrete Buildings.....	208
<i>Xiao-Kang Zou, AECOM Asia Company Ltd., Hong Kong</i>	
Chapter 10	
Applications of Topology Optimization Techniques in Seismic Design of Structure	232
<i>Kazem Ghabraie, University of Southern Queensland, Australia</i>	
Chapter 11	
Overall Conceptual Seismic Design and Local Seismic Capacity Design for Components of Bridges.....	269
<i>Wan-Cheng Yuan, Tongji University, China</i>	
<i>Yu-Guo Zheng, Tongji University and Hunan University of Science and Technology, China</i>	
<i>Pak-Chiu Cheung, Tongji University, China</i>	
Chapter 12	
Optimum Design of Structures for Earthquake Loading by a Cellular Evolutionary Algorithm and Neural Networks	306
<i>Saeed Gholizadeh, Urmia University, Iran</i>	

Chapter 13	
Fuzzy Identification of Seismically Excited Smart Systems	323
<i>JinSeop Kim, Massachusetts Institute of Technology, USA</i>	
<i>Yeesock Kim, Worcester Polytechnic Institute, USA</i>	
<i>Tahar El-Korchi, Worcester Polytechnic Institute, USA</i>	
Chapter 14	
Health Assessment of Engineering Structures Using Graphical Models.....	342
<i>Abbas Moustafa, Minia University, Egypt</i>	
<i>Sankaran Mahadevan, Vanderbilt University, USA</i>	
Chapter 15	
Optimal Design of Nonlinear Viscous Dampers for Protection of Isolated Bridges	370
<i>Alexandros A. Taflanidis, University of Notre Dame, USA</i>	
<i>Ioannis G. Gidaris, University of Notre Dame, USA</i>	
Compilation of References	399
About the Contributors	430
Index.....	437

Detailed Table of Contents

Foreword	xiii
Preface	xiv
Acknowledgment	xvi

Chapter 1

Life Cycle Cost Considerations in Seismic Design Optimization of Structures	1
---	---

Bora Gencturk, University of Illinois at Urbana-Champaign, USA

Amr S. Elnashai, University of Illinois at Urbana-Champaign, USA

The life-cycle cost (LCC) of a structure in seismic regions, which includes the initial and the post-earthquake repair cost, is a critical parameter for structural engineers and other stakeholders. The LCC analysis has been gaining prominence in recent years since civil infrastructure sustainability has been identified as one of the grand challenges for engineering in the 21st century. The objective of this chapter is to first identify the components in LCC evaluation that directly affect the outcomes, and propose strategies to improve the reliability of the analysis. The shortcomings of existing studies on LCC optimization of structures are identified. These shortcomings include simplified analysis techniques to determine the structural capacity and earthquake demand, use of generalized definitions for structural limit states, and inadequacies in treating uncertainty. In the following, the problem formulation and a brief review of existing literature on LCC optimization of structures are provided. A LCC model is presented, and techniques are proposed to improve the above mentioned shortcomings. Finally, LCC analysis of an example reinforced concrete (RC) structure is employed to illustrate the methodology.

Chapter 2

Performance-Based Seismic Design: A Search-Based Cost Optimization with Minimum Reliability Constraints	23
---	----

Oscar Möller, University of Rosario, Argentina

Marcelo Rubinstein, University of Rosario, Argentina

Fabián Savino, University of Rosario, Argentina

Ricardo O. Foschi, University of British Columbia, Canada

An approach is presented to structural optimization for performance-based design in earthquake engineering. The objective is the minimization of the total cost, including repairing damage produced by future earthquakes, and satisfying minimum target reliabilities in three performance levels (operational, life safety, and collapse). The different aspects of the method are considered: a nonlinear dynamic structural

analysis to obtain responses for a set of earthquake records, representing these responses with neural networks, formulating limit-state functions in terms of deformations and damage, calculating achieved reliabilities to verify constraint violations, and the development of a gradient-free optimization algorithm. Two examples illustrate the methodology: 1) a reinforced concrete portal for which the design parameters are member dimensions and steel reinforcement ratios, and 2) optimization of the mass at the cap of a pile, to meet target reliabilities for two levels of cap displacement. The objective of this latter example is to illustrate model effects on optimization, using two different hysteresis approaches.

Chapter 3

Discrete Variable Structural Optimization of Systems under Stochastic Earthquake Excitation	51
---	----

Héctor Jensen, Universidad Tecnica Federico Santa Maria, Chile

Marcos Valdebenito, Universidad Tecnica Federico Santa Maria, Chile

Juan Sepúlveda, Universidad Tecnica Federico Santa Maria, Chile

Luis Becerra, Universidad Tecnica Federico Santa Maria, Chile

The reliability-based design optimization of structural systems under stochastic excitation involving discrete sizing type of design variables is considered. The design problem is formulated as the minimization of an objective function subject to multiple reliability constraints. The excitation is modeled as a non-stationary stochastic process with uncertain model parameters. The problem is solved by a sequential approximate optimization strategy cast into the framework of conservative convex and separable approximations. To this end, the objective function and the reliability constraints are approximated by using a hybrid form of linear, reciprocal, and quadratic approximations. The approximations are combined with an effective stochastic sensitivity analysis in order to generate explicit expressions of the reliability constraints in terms of the design variables. The explicit approximate sub-optimization problems are solved by an appropriate discrete optimization technique. Two example problems that consider structures with passive energy dissipation systems under earthquake excitation are presented to illustrate the effectiveness of the approach reported herein.

Chapter 4

A Multi-Hazard Framework for Optimum Life-Cycle Cost Design of Reinforced Concrete Bridges.....	76
---	----

Azadeh Alipour, University of Massachusetts Amherst, USA

Behrouz Shafei, University of Massachusetts Amherst, USA

Masanobu Shinozuka, University of California, USA

This chapter provides a comprehensive procedure for the time-dependant structural performance evaluation and life-cycle cost analysis of reinforced concrete highway bridges located in extreme chloride-laden environments. The penetration of chloride ions into the concrete is simulated through a finite difference approach, which takes into account all the parameters that can affect the corrosion process. From simulation results, the corrosion initiation time is predicted and the extent of structural degradation is calculated over the entire life of bridge. A group of detailed bridge models with various structural attributes are developed to evaluate the changes in the structural capacity and seismic response of corroded bridges. For the purpose of the probabilistic seismic risk assessment of bridges, the seismic fragility curves are generated and updated at regular time intervals. The time-dependent fragility parameters are employed to investigate the life-cycle cost of bridges by introducing a performance index which combines the effects of probable seismic events and chloride-induced corrosion. The proposed approach provides a multi-hazard framework, which leads to more realistic performance and cost estimates. It also indicates the inspection and maintenance intervals in a way that the inspection and maintenance costs are optimized, while the safety of bridge is ensured.

Chapter 5

Efficient Robust Optimization of Structures Subjected to Earthquake Load and Characterized by Uncertain Bounded System Parameters 105

Subrata Chakraborty, Bengal Engineering and Science University, India

Soumya Bhattacharjya, Bengal Engineering and Science University, India

An efficient robust design optimization (RDO) procedure is proposed in the framework of an adaptive response surface method (RSM) for structures subjected to earthquake load and characterized by uncertain but bounded system parameters. The basic idea of the proposed RDO approach is to improve the robustness of a design by using a new dispersion index which utilizes the relative importance of the gradients of the performance function. The same concept is also applied to the constraints. The repeated computations of stochastic responses and their sensitivities for evaluating the stochastic constraint of the associated optimization problem are efficiently obtained in the framework of an adaptive RSM. The proposed RDO approach is elucidated through the optimization of a three-storied concrete frame structure. The numerical study depicts that the proposed RDO results are in conformity with the conventional RDO results. However, definite improvements are achieved in terms of robustness and computational time requirements indicating its efficiency over the conventional RDO approach.

Chapter 6

Damage Assessment of Inelastic Structures under Simulated Critical Earthquakes 128

Abbas Moustafa, Minia University, Egypt

Damage of structures can be significantly reduced through robust prediction of possible future earthquakes that can occur during the life-time of the structure and through accurate modeling of the non-linear behavior of the structure under seismic loads. Modern seismic codes specify natural records and artificially generated ground accelerations as input to the nonlinear time-history analysis of the structure. The advantage of using natural records is the inclusion of all important characteristics of the ground motion (fault properties, path effects and local soil condition) in the design input. This option requires selecting and scaling a set of proper accelerograms from the available records. However, the site under consideration may have limited or scarce earthquake data. In such case, numerically simulated ground motions can be employed as input to the dynamic analysis of the structure. This chapter deals with the damage assessment of inelastic structures under numerically simulated critical earthquakes using non-linear optimization, inelastic time-history analysis, and damage indices.

Chapter 7

Metaheuristic Optimization in Seismic Structural Design and Inspection Scheduling of Buildings 152

Chara Ch. Mitropoulou, Institute of Structural Analysis and Seismic Research, National Technical University Athens, Greece

Vagelis Plevris, School of Pedagogical and Technological Education (ASPETE), Greece

Nikos D. Lagaros, Institute of Structural Analysis and Seismic Research, National Technical University Athens, Greece

Optimization is a field where extensive research has been conducted over the last decades. Many types of problems have been addressed, and many types of algorithms have been developed, while their range of applications is continuously growing. The chapter is divided into two parts; in the first part, the life-cycle cost analysis is used as an assessment tool for designs obtained by means of prescriptive and performance-based optimum design methodologies. The prescriptive designs are obtained through a single-objective formulation, where the initial construction cost is the objective to be minimized, while

the performance-based designs are obtained through a two-objective formulation where the life-cycle cost is considered as an additional objective also to be minimized. In the second part of the chapter, the problem of inspection of structures and routing of the inspection crews following an earthquake in densely populated metropolitan areas is studied. A model is proposed and a decision support system is developed to aid local authorities in optimally assigning inspectors to critical infrastructures. A combined particle swarm – ant colony optimization based framework is implemented, which proves to be an instance of a successful application of the philosophy of bounded rationality and decentralized decision-making for solving global optimization problems.

Chapter 8

Optimal Performance-Based Seismic Design 174

Hamid Moharrami, Tarbiat Modares University, Iran

In this chapter, the reader gets acquainted with the philosophy of performance-based design, its principles, and an overview of the procedures for performance evaluation of structures. The essential prerequisites of optimal performance-based design, including nonlinear analysis, optimization algorithms, and nonlinear sensitivity analysis, are introduced. The methods of nonlinear analysis and optimization are briefly presented, and the formulation of optimal performance-based design with emphasis on deterministic type, rather than probabilistic- (or reliability)-based formulation is discussed in detail. It is revealed how real performance-based design is tied to optimization, and the reason is given for why, without optimization algorithms, multilevel performance-based design is almost impossible.

Chapter 9

Optimal Seismic Performance-Based Design of Reinforced Concrete Buildings 208

Xiao-Kang Zou, AECOM Asia Company Ltd., Hong Kong

In order to meet the emerging trend of the performance-based design approach and to improve the design efficiency, this chapter presents a numerical optimization technique for both minimum material cost and life-cycle cost design of building structures subject to multiple levels of linear elastic and nonlinear elastic seismic drift performance design constraints. This chapter firstly introduces an elastic seismic drift design of reinforced concrete (RC) building structures based on elastic response spectrum analysis method; and then presents the inelastic design optimization based on the nonlinear pushover analysis method. Finally, the optimal seismic performance-based design of RC buildings is posed as a multi-objective optimization problem in which the life-cycle cost of a building is to be minimised subject to multiple levels of seismic performance design criteria. The computer based optimization methodology developed provides a powerful numerical design tool for performance-based design of RC building structures.

Chapter 10

Applications of Topology Optimization Techniques in Seismic Design of Structure 232

Kazem Ghabraie, University of Southern Queensland, Australia

During the last two decades, topology optimization techniques have been successfully applied to a wide range of problems including seismic design of structures. This chapter aims to provide an introduction to the topology optimization methods and a review of the applications of these methods in earthquake engineering. Two well-established topology optimization techniques are introduced. Several problems including eigenfrequency control of structures, compliance minimization under periodic loading, and maximizing energy absorption of passive dampers will be addressed. Numerical instabilities and approaches to overcome them will be discussed. The application of the presented approaches and methods will be illustrated using numerical examples. It will be shown that in seismic design of structures, topology optimization methods can be useful in providing conceptual design for structural systems as well as detailed design of structural members.

Chapter 11	
Overall Conceptual Seismic Design and Local Seismic Capacity Design for Components of Bridges.....	269

Wan-Cheng Yuan, Tongji University, China

Yu-Guo Zheng, Tongji University and Hunan University of Science and Technology, China

Pak-Chiu Cheung, Tongji University, China

From the perspective of “overall conceptual seismic design,” four design strategies are presented to decrease and balance the seismic force and displacement demands for some bridges working in a linear and elastic state: the adjustment of the layout and detail of piers and expansion joints for a typical long span continuous girder bridge, the adoption of a new-type spatial bridge tower for a long span cable-stayed bridge, the study on the isolation mechanism of an elastic cable seismic isolation device for another cable-stayed bridge, and the study on the seismic potential and performance for long span SCC (steel-concrete composite) bridges. From the perspective of “local seismic capacity design,” three earthquake resistant strategies are presented to achieve economical, applicable, and valid seismic design of local components of bridges working in a nonlinear state: the adoption and the study on a new cable sliding friction aseismic bearing, the study on the seismic capacities of single-column bridge piers wholly and locally reinforced with steel fiber reinforced concrete (SFRC), the study on the seismic capacities, and the hysteretic performance and energy dissipation capabilities of bridge pile group foundations strengthened with the steel protective pipes (SPPs). Research results show that these seismic design strategies are effective to improve the seismic performance of bridges.

Chapter 12	
Optimum Design of Structures for Earthquake Loading by a Cellular Evolutionary Algorithm and Neural Networks	306
<i>Saeed Gholizadeh, Urmia University, Iran</i>	

The present chapter deals with optimum design of structures for earthquake induced loads by taking into account nonlinear time history structural response. As the structural seismic optimization is a time consuming and computationally intensive task, in this chapter, a methodology is proposed to reduce the computational burden. The proposed methodology consists of an efficient optimization algorithm and a hybrid neural network system to effectively predict the nonlinear time history responses of structures. The employed optimization algorithm is a modified cellular genetic algorithm which reduces the required generation numbers compared with the standard genetic algorithm. Also, the hybrid neural network system is a combination of probabilistic and generalized regression neural networks. Numerical results demonstrate the computational merits of the proposed methodology for seismic design optimization of structures.

Chapter 13	
Fuzzy Identification of Seismically Excited Smart Systems	323
<i>JinSeop Kim, Massachusetts Institute of Technology, USA</i>	
<i>Yeesock Kim, Worcester Polytechnic Institute, USA</i>	
<i>Tahar El-Korchi, Worcester Polytechnic Institute, USA</i>	

In this chapter, a nonlinear modeling framework to identify nonlinear behavior of smart structural systems under seismic excitations is proposed. To this end, multi-input-multi-output (MIMO) autoregressive exogenous (ARX) input models and Takagi-Sugeno (TS) fuzzy models are coalesced as the MIMO ARX-TS fuzzy model. The premised part of the proposed MIMO ARX-TS fuzzy model is optimized using the hierarchical clustering (HRC) algorithm, while its consequent parameters are optimized via the

weighted linear least squares estimation. The performance of the proposed model is investigated using the dynamic response of a three-story shear planer frame structure equipped with a magnetorheological (MR) damper subject to earthquake disturbances. Furthermore, the impact of the HRC algorithm on the performance of the MIMO ARX-TS fuzzy model is compared with that of the subtractive and the fuzzy C-means clustering algorithms. The equivalence of the original and identified data is numerically shown to prove that the HRC MIMO ARX-TS fuzzy model introduced here is effective in estimating nonlinear behavior of a seismically excited building-MR damper system.

Chapter 14

Health Assessment of Engineering Structures Using Graphical Models 342

Abbas Moustafa, Minia University, Egypt

Sankaran Mahadevan, Vanderbilt University, USA

A hybrid qualitative-quantitative health assessment of structures using the bond graph theory is presented in this chapter. Bond graph (BG) is an energy-based graphical-modeling tool for physical dynamic systems, actuators, and sensors. BG provides domain-independent framework for modeling dynamic systems with interacting components from multiple domains. Discrete structures are modeled using one-to-one bond graph elements, while continuous structures are modeled using finite-mode bond graphs. BG facilitates the construction of temporal causal graph (TCG) that links the system response to the damaged component or faulty sensor. TCG provides qualitative damage isolation, which is not possible using most existing system identification techniques. This leads to rapid isolation of damage and significant reduction in computations. Quantitative identification of damage size is performed by analyzing the substructure containing the damaged component, using the nonlinear least-squares optimization technique, thus reducing the computations. The health assessment algorithm developed in this chapter combines the Generic Modeling Environment (GME), the Fault Adaptive Control Technology (FACT) software, and Matlab Simulink®. Numerical illustrations on BG modeling of a hydraulic actuator and system identification of a fifteen-story shear building and a high-rise structure under earthquake loads are provided.

Chapter 15

Optimal Design of Nonlinear Viscous Dampers for Protection of Isolated Bridges 370

Alexandros A. Taflanidis, University of Notre Dame, USA

Ioannis G. Gidaris, University of Notre Dame, USA

A probabilistic framework based on stochastic simulation is presented in this chapter for optimal design of supplemental dampers for multi - span bridge systems supported on abutments and intermediate piers through isolation bearings. The bridge model explicitly addresses nonlinear characteristics of the isolators and the dampers, the dynamic behavior of the abutments, and the effect of pounding between the neighboring spans to each other as well as to the abutments. A probabilistic framework is used to address the various sources of structural and excitation uncertainties and characterize the seismic risk for the bridge. Stochastic simulation is utilized for evaluating this seismic risk and performing the associated optimization when selecting the most favorable damper characteristics. An illustrative example is presented that considers the design of nonlinear viscous dampers for protection of a two-span bridge.

Compilation of References 399

About the Contributors 430

Index 437

Foreword

Earthquake engineering and aseismic structural design for many years was based on conventional methods of analysis, statistical description of earthquakes and very much engineering experience. Design engineers smugly say that the medium quality of ordinary structures, the low or uncontrollable quality of materials and the lack of guaranteed, maintenance in most parts of the world, did not justify the use of more sophisticated methods. On the other hand modern methods for the optimal design of structures, reliability analysis, and the most advanced methods of computational mechanics found their way into, mainly, mechanical engineering applications. Integration of electronics and control, resulting in the so-called smart structures, is another area with fruitful results. The existence of sensors allows us to think on structural health monitoring and much more. All these techniques stayed away from the seismic design of structures, although the safety of structures in which most of the population in earthquake-affected countries lives and works is of obvious importance.

I am happy to see that this gap is gradually closing. Technology and knowledge becomes available to broader parts of the population and is being applied to more ‘classical’ fields. The present edited volume contributes towards this direction. By studying selected topics of structural optimization, reliability-based, performance-based, robust design and life cycle cost structural analysis the authors of the book clearly demonstrate that sophisticated structural analysis and design tools slowly find their way in the design of ordinary structures. Both users of buildings and infrastructure and professional engineers will benefit from this development.

*Georgios E. Stavroulakis
Technical University of Crete, Greece*

Preface

Since the early seventies, optimization has been the subject of intensive research and several different approaches have been advocated for the optimal design of structures in terms of optimization methods or problem formulations. Most of the attention of the engineering community has been directed towards the optimum design of structures with the assumption of linear elastic structural behavior under static loading conditions. However, for a large number of real-life structural design problems, the assumption of linear response may lead to vulnerable structural configurations, while seismic loading has also to be taken into account in order to design earthquake resistant real-world structures. Parts of the book are devoted to the formulation of design optimization frameworks in the field of earthquake engineering.

In recent years, probabilistic-based formulations of the optimization problem have been developed in order to account for the uncertainty and randomness. The development of stochastic analysis methods over the last two decades has stimulated the interest for the probabilistic optimum design of structures. There are two distinguished design formulations that account for the probabilistic system response: Robust Design Optimization (RDO) and Reliability-Based Design Optimization (RBDO). RDO methods primarily seek to minimize the influence of stochastic variations on the nominal dimensions and values of the material properties of the design. On the other hand, the main goal of RBDO methods is to design for minimum weight, while satisfying the limit on the allowable probability of failure. Parts of the book are devoted to the formulation of optimization problems considering uncertainties under earthquake loading conditions.

The research fields described above define “hot” topics of Earthquake Engineering involving the use of advanced optimization tools. The basic idea of this book is to include all the aforementioned research topics into a volume taking advantage of the connecting link between them, which is optimization. In this direction, the book consists of 15 chapters in total. In the first chapter, the components in life-cycle cost (LCC) evaluation are identified that directly affect the outcomes and propose strategies to improve the reliability of the analysis, while the shortcomings of existing studies on LCC optimization of structures are identified.

In the second chapter an approach is presented to structural optimization for performance-based design in earthquake engineering where the objective is the minimization of the total cost, including repairing damage produced by future earthquakes, and satisfying minimum target reliabilities in three performance levels. In the next chapter the reliability-based design optimization of structural systems under stochastic excitation involving discrete sizing type of design variables is considered; while it is formulated as the minimization of an objective function subject to multiple reliability constraints.

In the fourth chapter, a comprehensive procedure for the time-dependent structural performance evaluation and life-cycle cost analysis of reinforced concrete highway bridges located in extreme

chloride-laden environments is provided. The chapter also indicates the inspection and maintenance intervals in a way that the inspection and maintenance costs are optimized while the safety of bridge is ensured. In the next chapter, an efficient RDO procedure is proposed in the framework of an adaptive response surface method for structures subjected to earthquake load and characterized by uncertain but bounded system parameters.

The sixth chapter deals with the problem of damage assessment of inelastic structures under numerically simulated critical earthquakes, implementing nonlinear optimization, inelastic time-history analysis, and damage indices. In the next chapter the life-cycle cost analysis is used as an assessment tool for designs obtained by means of prescriptive and performance-based optimum design methodologies; furthermore, the problem of inspection of structures and routing of the inspection crews following an earthquake in densely populated metropolitan areas is studied.

In the eighth chapter, the reader gets acquainted with the philosophy of performance-based design, its principles, and an overview of the procedures for performance evaluation of structures, while the essential prerequisites of optimal performance-based design, including nonlinear analysis, optimization algorithms, and nonlinear sensitivity analysis, are also introduced.

The ninth chapter presents a numerical optimization technique for both minimum material cost and life-cycle cost design of building structures subject to multiple levels of linear elastic and nonlinear elastic seismic drift performance design constraints. The next chapter aims at providing an introduction to the topology optimization methods and a review of the applications of these methods in earthquake engineering.

In the eleventh chapter, the overall conceptual seismic design and the local seismic capacity design methods are proposed to give clear and correct directions for seismic design optimization of bridges in order to obtain uniform and rational seismic demands and improved seismic capacities of structural components. The next chapter deals with the optimum design of structures for earthquake induced loads by taking into account the nonlinear time history structural response.

In the thirteenth chapter, a nonlinear modeling framework to identify nonlinear behavior of smart structural systems under seismic excitations is presented; to this end, multi-input-multi-output autoregressive exogenous input models and Takagi-Sugeno fuzzy models are coalesced.

In the fourteenth chapter of the book, a hybrid qualitative-quantitative health assessment of structures using the bond graph theory is presented. In the last chapter, a probabilistic framework based on stochastic simulation is presented for optimal design of supplemental dampers for multi-span bridge systems supported on abutments and intermediate piers through isolation bearings.

Vagelis Plevris

*School of Pedagogical and Technological Education,
Greece National Technical University of Athens, Greece*

Chara Ch. Mitropoulou

*Institute of Structural Analysis and Seismic Research,
National Technical University of Athens, Greece*

Nikos D. Lagaros

*Institute of Structural Analysis and Seismic Research,
National Technical University of Athens, Greece Hellenic Army, Greece*

Acknowledgment

The editors of the book would like to express their deep gratitude to all the contributors for their most valuable support during the preparation of this volume, for their time and effort devoted to the completion of their contributions, and for their great expert help in the review process. In addition, we are most appreciative to the members of the Editorial Advisory Board (EAB) of the book for their constructive comments and suggestions offered during the preparation process and for their contribution in reviewing some of the book chapters. We are also grateful to all the colleagues who, although they did not contribute chapters to the book, were kind enough to offer their expert help during the review process. Finally, we would also like to thank all the personnel of IGI Global Publishers, especially Myla R. Merkel, Lindsay Johnston, Emily E. Golesh, Erika L. Carter, and Kristin M. Klinger, for their most valuable continuous support for the publication of this book.

Vagelis Plevris
School of Pedagogical and Technological Education,
Greece National Technical University of Athens, Greece

Chara Ch. Mitropoulou
Institute of Structural Analysis and Seismic Research,
National Technical University of Athens, Greece

Nikos D. Lagaros
Institute of Structural Analysis and Seismic Research,
National Technical University of Athens, Greece Hellenic Army, Greece

Chapter 1

Life Cycle Cost Considerations in Seismic Design Optimization of Structures

Bora Gencturk

University of Illinois at Urbana-Champaign, USA

Amr S. Elnashai

University of Illinois at Urbana-Champaign, USA

ABSTRACT

The life-cycle cost (LCC) of a structure in seismic regions, which includes the initial and the post-earthquake repair cost, is a critical parameter for structural engineers and other stakeholders. The LCC analysis has been gaining prominence in recent years since civil infrastructure sustainability has been identified as one of the grand challenges for engineering in the 21st century. The objective of this chapter is to first identify the components in LCC evaluation that directly affect the outcomes, and propose strategies to improve the reliability of the analysis. The shortcomings of existing studies on LCC optimization of structures are identified. These shortcomings include simplified analysis techniques to determine the structural capacity and earthquake demand, use of generalized definitions for structural limit states, and inadequacies in treating uncertainty. In the following, the problem formulation and a brief review of existing literature on LCC optimization of structures are provided. A LCC model is presented, and techniques are proposed to improve the above mentioned shortcomings. Finally, LCC analysis of an example reinforced concrete (RC) structure is employed to illustrate the methodology.

INTRODUCTION

Structural optimization problems may be divided into three classes: sizing, shape and topology optimization. In sizing optimization, the locations and number of the structural elements are fixed and known. Usually, the problem is reduced to optimi-

zation of the properties of individual elements to find the optimal solution. In shape optimization, the contour of the boundary of a structural domain is optimized while keeping the connectivity of the structure the same, in other words, no new boundaries are formed. Topology optimization is the most general in the sense that both the size

DOI: 10.4018/978-1-4666-1640-0.ch001

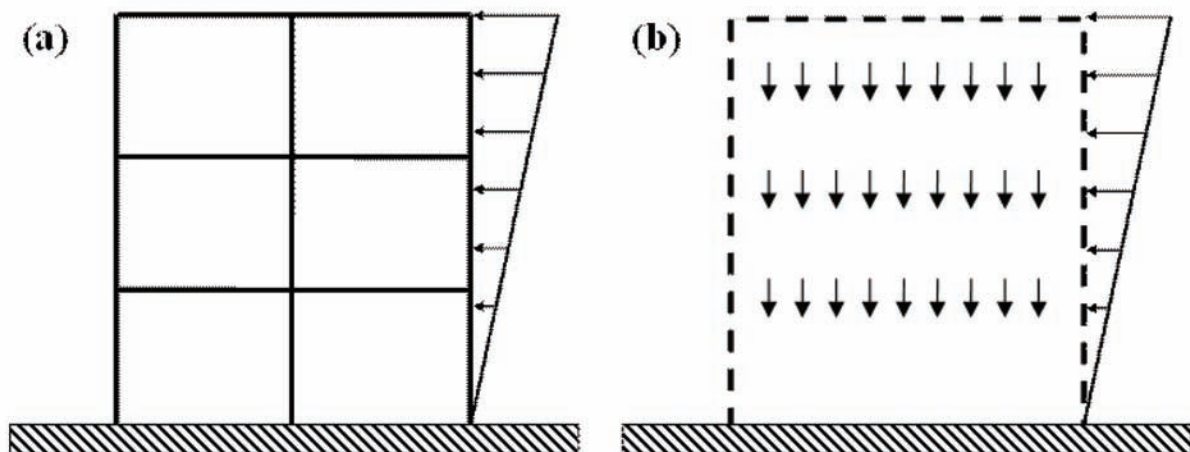
and location of structural members are determined and formation of new boundaries are allowed. The number of joints in the structure, the joint support locations, and number of members connected to each joint are unknown. In other words, topology and shape of the structure are optimized in addition to the shape of individual elements. Figure 1 illustrates the sizing and topology optimization problems for a structural frame. The structure being optimized may vary significantly from a component of a mechanical device to a member of a full-scale structure depending on the problem. Most problems in structural earthquake engineering fall into the category of sizing optimization and deal with full-scale structures.

The problems in structural optimization may also be classified based on the number of objectives, i.e. single- and multi-objective. For single-objective seismic design optimization problems, the objective is usually selected as the initial cost for reinforced concrete (RC) and total weight for steel structures; and the performance is determined based on the conformance to the requirements of a seismic design code. The code provisions are usually introduced to the problem as constraints. Some example studies include Moharrami and Grierson (1993), Adamu et al. (1994), Memari and Madhkhan (1999), Zou and Chan (2005) and

Sahab et al. (2005). As a consequence of the formulation of the problem, the majority of the single-objective optimization methods provide a single optimal solution (which minimizes the objective and satisfies the constraints). However, the decision maker does not have a broad view of to what extend the constraints are satisfied. Thus, she has to either accept or reject the optimal solution. On the other hand, since more than one objective is considered in multi-objective optimization problems, commonly a set of equivalently optimal solutions are obtained which provides the decision maker the flexibility to tradeoff between the solutions and she may base her selection on rather transparent results. Some example multi-objective studies include Li et al. (1999) and Liu et al. (2006).

It is natural to include multiple objectives (e.g. structural performance, initial and life-cycle costs) in the LCC optimization of structures; however, the number of objectives is not usually the only difference between LCC and initial cost optimization problems. The former necessitates the use of probabilistic formulations to evaluate the failure probability at different limit states in addition to the derivation of the probabilistic seismic hazard at different intensities. Whereas, in the latter the evaluation of the structural performance at

Figure 1. Example illustration of (a) sizing, and (b) topology optimization problems



predefined hazard level(s) is sufficient. A brief review of existing literature on LCC optimization of structures is provided in the following section. The objective of this chapter is to emphasize the importance of the following in LCC optimization:

1. Use of advanced analysis, which provides the most rigorous assessment of structural capacity and earthquake demand,
2. Evaluation of the structural capacity (that has direct impact on the LCC) by taking into account not only the global behavior of the structure but also the local response, such as reinforcement yielding and concrete crushing,
3. Use of system-specific limit states (rather than fixed value or generic limit states) to define the structural capacity,
4. Consideration of all major sources of uncertainty, from seismogenic source characteristics to material properties and structural modeling in calculating the limit state exceedance probabilities.

The majority of existing work on structural optimization uses either elastic dynamic or nonlinear static analysis for seismic performance assessment of structures. In cases where inelasticity is modeled, lumped plasticity models are adopted. The first item in the list above is significant because the oversimplification of the structural assessment, even though the optimization framework is robust and sound, might yield unrealistic results. This chapter highlights the importance of utilizing distributed inelasticity approach using which structural capacity and earthquake demand are evaluated through nonlinear pushover analysis and inelastic dynamic time history analysis, respectively. Widespread use of optimization tools for seismic design of structures can only be achieved by having practical and reliable approaches that can predict the structural performance with reasonable accuracy.

The second item is critical to the evaluation of LCC in that the repair cost (after an earthquake event) is more directly related to the local behavior, rather than the global. There is existing literature on relating the global structural response to local parameters (an example is predicting the damage state of a vertical member based on the interstory drift); however, it is not accurate to generalize these relationships to structural configurations other than that they are derived for. Therefore, in order to accurately evaluate the LCC proper response metrics need to be chosen.

As for the third item, the capacity of a structure depends on various factors, most importantly on the force resisting system employed in design. The limit state values for a bearing wall system will be significantly different from those for a frame system. It is simpler to use generic limit states, which also reduces computational demand; however, accurate evaluation of the structural capacity is key to seismic design and it warrants full consideration. In other words, structural capacity has to be evaluated specifically for the considered structural configuration.

Finally, for the fourth item, the sources of uncertainty have to be defined clearly. The uncertainty in exceedance probabilities of the structural damage states is mainly governed by the variability in ground motion processes; nevertheless, it is required to take into account the variability in material properties, and other capacity related parameters.

In the following, first the background information on structural optimization that will allow the reader to follow the rest of the chapter is provided. Then a framework for LCC optimization of structures that includes the definition of seismic hazard, evaluation of structural capacity and earthquake demand, LCC model and optimization algorithm, is proposed. Finally, the framework is applied to an example RC structural frame.

BACKGROUND ON STRUCTURAL OPTIMIZATION

In this section, first the terminology that is used in the chapter is described. Then an overview of the most commonly used optimization algorithms, with a focus on the advantages and shortcomings, is provided. Finally, existing work on LCC optimization of structures is briefly reviewed.

Terminology

- **Objective (merit) Function:** A function that measures the performance of design. For every possible design, the objective function takes a different value. Examples include the maximum interstory drift and initial cost.
- **Design (decision) Variables:** A vector that specifies design. Each element in the vector describes a different structural property that is relevant to the optimization problem. The design variables take different values throughout the optimization process. Examples include section dimensions and reinforcement ratios.
- **Performance Levels:** Predefined levels that describe the performance of the structure after an earthquake. Usually the following terminology is used to define the damage state (performance) of the structure: immediate occupancy, life safety and collapse prevention. Occurrence of each damage state is determined based on the exceedance of a threshold value in terms of structural capacity.
- **Hazard Levels:** Predefined levels used to describe the earthquake intensity that the structure is subjected to. Hazard levels are usually described by earthquake return periods (or annual frequencies of exceedance) and represented by acceleration response spectrum. It is required to consider multiple levels of hazard to calculate LCC

of a structure. Each hazard level is usually directly mapped to a single or multiple performance levels.

- **Space of Design (decision) Variables or Search Space:** The boundaries of the search space are defined by the ranges of the design variables. The dimension of the search space is equal to the number of design variables in the problem. The search space can be continuous for continuous design variables and discrete for discrete design variables or certain dimensions can be continuous and the rest can be discrete.
- **Solution (objective function) Space:** Usually the solution space is unbounded or semi-bounded. The dimension of the solution space is equal to the number of objective functions in the optimization problem. The optimal solution(s) is defined in the solution space. The set of optimal solutions in the solution space is referred to as Pareto-front or Pareto-optimal set, as described below.
- **Pareto-Optimality:** To define Pareto-optimality, consider the function $f : \Re^k \rightarrow \Re^l$ which assigns each point, \mathbf{x} in the space of decision variables to a point, $\mathbf{y} = f(\mathbf{x})$ in the solution space. Here f represents the objective functions, k is the number of decision variables and l is the number of objective functions to assess the performance of each, \mathbf{x} (or equal to the dimension of f). The Pareto-optimal set of solutions is constructed by comparing the points in the solution space based on the following definition: a point \mathbf{y} in the solution space strictly dominates another point $\bar{\mathbf{y}}$ if each element of \mathbf{y} is less than equal to the corresponding parameter of $\bar{\mathbf{y}}$ (that is $\mathbf{y}_i \leq \bar{\mathbf{y}}_i$) and at least one element, i^* , is strictly less (that is $\mathbf{y}_{i^*} < \bar{\mathbf{y}}_{i^*}$), assuming that this is a minimization problem. Thus, the Pareto-front is the subset of points in

the set of $\mathbf{Y} = f(\mathbf{X})$, that are not strictly dominated by another point in \mathbf{Y} . The Pareto-optimality is illustrated in Figure 2, the plot is in the solution space, and the figure axes are two objective functions, f_1 and f_2 . Assuming that the objective is minimization of both f_1 and f_2 , the Pareto-front lies at the boundary that minimizes both objectives as shown in the figure.

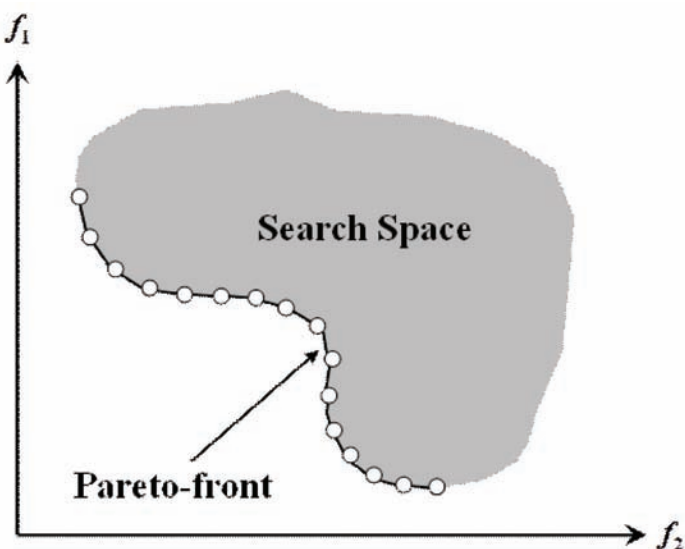
Review of Most Commonly Used Optimization Algorithms

The algorithms used in structural optimization may be divided into two categories: gradient-based and heuristic approaches. The earlier studies on structural optimization utilized conventional gradient-based algorithms to obtain the optimal solution (e.g. Bertero & Zagajeski, 1979; Cheng & Truman, 1985; Pezeshk, 1998). The most commonly used algorithms include optimality criteria, linear and nonlinear programming, feasible directions, and state-space steepest descent. Although the gradient-based approaches are

computationally efficient, the problems that could be solved are limited due to fact that the objective functions, constraints and their sensitivities should be expressed explicitly in terms of the design variables. The latter condition imposes a restraint on the analysis procedure that could be selected for structural assessment. Furthermore, the design variables should be continuous over the search domain. In other words, discrete design variables such as the reinforcement ratio in RC structures cannot directly be accounted for in gradient-based optimization algorithms. As a consequence, researchers used methods such as the principle of virtual work in order to express the objective function as well as the constraints analytically (e.g. Chan & Zou, 2004).

With the immense increase in available computational power in the recent years, researchers started to incorporate more accurate analysis tools in structural optimization such as the static push-over and dynamic time history analysis through finite element modeling. However, due to the fact that these analysis techniques required algorithms that do not entail the continuity of functions as well as the existence of derivatives, researchers

Figure 2. Illustration of Pareto-optimality



had to abandon the conventional gradient-based approaches. Heuristic optimization algorithms progressively became popular in structural optimization (Foley & Schinler, 2003; M. Fragiadakis, Lagaros, & Papadrakakis, 2006b; N. D. Lagaros & Papadrakakis, 2007; Min Liu, et al., 2006). The most commonly used approaches include genetic algorithms (GA), simulated annealing (SA), taboo search (TS), and shuffled complex evolution. A further advantage of the heuristic algorithms is that they are very effective in terms of finding the global minimum of highly nonlinear and/or discontinuous problems where the gradient-based algorithms are usually trapped at a local minimum.

Review of Studies on LCC Optimization of Structures

LCC analysis of structures has gained importance in the recent years due to concerns related to the civil infrastructure sustainability; therefore, studies on LCC optimization of structures are relatively new compared to the rest of the literature on structural optimization. Below, a brief review of existing studies on LCC optimization is provided. The section is not intended to be comprehensive; the goal is to highlight some of the critical components of seismic LCC analysis that are addressed in more detail in this chapter.

Wen and Kang (2001a) developed an analytical formulation to evaluate the LCC of structures under multiple hazards. The methodology is then applied to a 9-story steel building to find the minimum LCC under earthquake, wind and both hazards (Wen & Kang, 2001b). In this study, the simplified method based on an equivalent single-degree-of-freedom (SDOF) system developed by Collins et al. (1996) was used for structural assessment. Liu et al. (2003) investigated the optimal performance-based seismic design (PBSD) of steel moment frame structures. Merit functions were selected as the initial material and lifetime seismic damage costs. Reducing design complexity was also incorporated in the algorithm. Code

provisions were followed to determine the validity of design alternatives. Static pushover analysis was used to derive an equivalent SDOF system which was utilized in computing the maximum interstory drift ratios. Liu et al. (2004) studied the PBSD of steel moment-resisting frames using GA. Three merit functions were defined: the initial material and lifetime seismic damage costs, and the number of different steel section types. Maximum interstory drift was used for the performance assessment of the frames through static pushover analysis. Code provisions were taken into account in design. Different sources of uncertainty in estimating seismic demand and capacity were incorporated into analysis using the SAC/FEMA guidelines (Cornell, Jalayer, Hamburger, & Fouch, 2002). The results were presented as Pareto-fronts for competing merit functions. Final designs obtained from the optimization algorithm were assessed using inelastic dynamic time history analysis. Liu (2005) formulated an optimal design framework for steel structures based on the PBSD. The considered objectives were the material usage, initial construction expenses, degree of design complexity, seismic structural performance and lifetime seismic damage cost. Design variables were section types for members of the frames. The validity of designs was performed based on the existing code provisions. A lumped plasticity model was used for structural modeling. Both static pushover and inelastic dynamic (only when structural response parameters were directly taken as objective functions) analysis were used. Fragiadakis et al. (2006b) used evolutionary strategies for optimal design of steel structures. Initial construction and life cycle costs were considered as the two merit functions. The constraints were based on the provisions of the European design codes. A fiber-based finite element model was used to conduct static pushover analysis to determine the inelastic response of structures. Deterministic structural damage states based on the maximum interstory drift was employed; however, probabilistic formulations were adopted for calculating

the life cycle costs. Zou et al. (2007) used the method of virtual work to achieve an explicit formulation for multi-objective optimization of RC frames. Then, optimality criteria method was used to minimize the initial material cost and the expected damage loss in a Pareto optimal sense. The method was formulated in two stages: first elastic response spectrum analysis was performed where the cross-sectional dimensions were considered as the only design variables, second section sizes were kept constant and the reinforcement ratio was taken as the design variable for the static pushover analysis through which inelastic drift responses were calculated.

Although, LCC was not considered in the following studies, these studies are mentioned here because they are related to methods or derivations in this chapter by considering uncertainty, multiple hazard levels or advanced structural analysis to obtain the seismic demand on structures. In Liu et al. (2005) conflicting objectives were defined as the initial material cost (including the cost due to design complexity as a function of the number of different structural shapes) and the seismic performance. Two hazard levels were used and the performance criterion was selected as the maximum interstory drift. Structural assessment was conducted using static pushover analysis determined from seismic code provisions. GA were employed to solve the optimization problem. Fragiadakis et al. (2006a) used evolutionary strategies for optimal PBSD of steel structures. Minimization of cost subjected to constraints on interstory drift was targeted. Both inelastic static and inelastic dynamic analysis were employed. Discrete beam and column sections were selected as design variables. 10 earthquake records were used to represent each hazard level and mean structural response was taken as the performance measure. Uncertainty associated with structural modeling was also taken into account. Lagaros et al. (2006) evaluated modal, elastic and inelastic dynamic time history analysis in an optimization framework taking the European seismic design

code as a basis. Steel structures were considered and evolutionary strategies were used to solve the optimization problem. A fiber-based finite element modeling approach was adopted. Either 10 natural or 5 artificial records were used to represent the hazard. Material weight was selected as the design objective. It was observed that lighter structures could be obtained when inelastic dynamic time history analysis (instead of elastic dynamic time history or modal analysis) and natural records (instead of artificial records that were compatible with a certain design spectrum) were used. Fragiadakis and Papadrakakis (2008) studied the optimal design of RC structures. Both deterministic and reliability-based approaches were evaluated and the latter was found to provide more economical solutions as well as more flexibility to designer. The total cost of the structure was taken as the objective function and compliance with European design codes was applied as a condition. Evolutionary strategies were used to solve the optimization problem. Three hazard levels were considered. To reduce the computational time, fiber-based beam-column elements were used only at the member ends and inelastic dynamic analysis was performed only if non-seismic checks performed through a linear elastic analysis were met.

LCC oriented seismic design optimization of structures is a relatively new subject, a review of existing literature, as provided above, indicates that there is still need for further research due to following: (1) only a limited number of studies utilized advanced computational tools, structural performance assessment was usually performed using code-based formulations or elastic analysis, simplified modeling techniques were adopted whenever inelastic analysis was conducted; (2) existing studies overwhelmingly focused on the optimization of steel structures due to well defined design variables (i.e. section types) and availability of structural modeling tools; (3) most of the research effort was devoted to the development of optimization methods; the real engineering problem to be solved remained faint.

In the following section a LCC formulation is developed for optimal seismic design of RC structures. Fiber-based finite element modeling is used to construct the structural models. Inelastic dynamic time history analysis and static pushover analysis are used to accurately obtain the earthquake demand and structural capacity, respectively. In addition, randomness due to ground motion variability (aleatory uncertainty) and errors in structural modeling and inherent variability in material properties (epistemic uncertainty) are taken into account.

LIFE-CYCLE COST FORMULATION

Definition of the Seismic Hazard

In order to evaluate the LCC of a structure due to repair in future earthquakes, one has to evaluate the probability of demand exceeding capacity for the whole-life time of the structure. There is more than one way of defining the seismic hazard that a structure could experience throughout its life time. The most commonly used methods to evaluate the earthquake hazard for a given location with known historical seismicity are the deterministic and probabilistic seismic hazard analysis (DSHA and PSHA). The main difference between the two approaches is that PSHA incorporates the element of time in hazard assessment. It is beyond the scope of this chapter to assess and validate the two approaches for seismic hazard analysis; however, PSHA has well made its way into the seismic design codes. As examples, UBC (ICBO, 1997) and FEMA 450 (FEMA, 2003) represented design response spectrum based on probabilistic zonation maps. Therefore, here PSHA is used to characterize the seismic hazard for a selected site, while DSHA is also a valid option.

In PSHA mean annual frequency of exceedance (or probability of exceedance) is calculated for a range of a selected intensity measure that represents the earthquake hazard. The most commonly

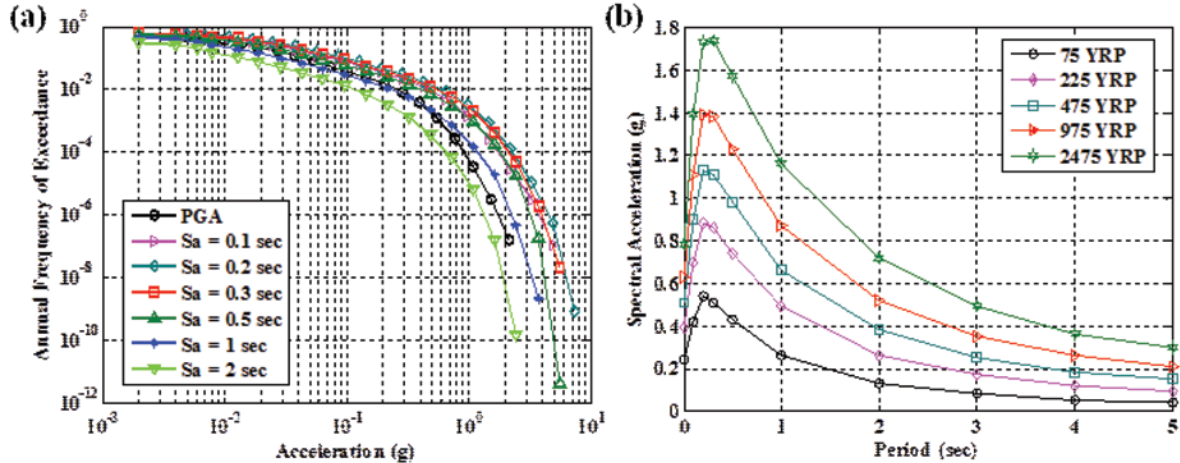
used intensity measures in seismic design are the peak ground acceleration (PGA) and spectral acceleration (S_a) at the fundamental period of the structure. Example hazard curves for PGA and S_a are shown in Figure 3(a). These curves are site specific and they can be obtained from PSHA for seismic design purposes.

For certain types of structural analysis such as modal response spectrum and time history analysis, it is required to obtain the design spectrum. The design spectrum could be obtained from the hazard curves depicted in Figure 3(a) at different return periods. The return period of an earthquake, T_R is simply the inverse of the mean annual frequency of exceedance, v , i.e. $T_R = 1/v$. As examples, design spectra at different return periods obtained from the hazard curves shown in Figure 3(a) are given in Figure 3(b). These are also referred to as uniform hazard spectra (UHS) because each spectral ordinate has the same probability of exceedance. As an alternative, the design spectra could be obtained from seismic design codes. Although, most codes provide the necessary information to draw design spectra for the maximum considered earthquake only (e.g. ICC, 2006) and it is not possible obtain the hazard at different return periods which is required for LCC analysis, more detailed seismic zonation maps have been developed in the recent years and design spectra for earthquake hazards with different probabilities of occurrence are now available (USGS, 2008).

Evaluation of the Structural Capacity and Earthquake Demand

As described in the previous section, the continuous probabilistic hazard at a selected site, Figure 3(a), is discretized at certain probabilities, represented with return period in Figure 3(b). The objective behind this manipulation is to have a means of evaluating the probability of failure; that is the probability of earthquake demand exceeding the structural capacity. By having the design spectra at different return periods, the hazard levels are

Figure 3. (a) Example hazard curves for different intensity measures obtained from PSHA, (b) design spectra at different return periods obtained from PSHA (YRP: years return period)



very well defined. The more challenging part is the definition of structural limit states and their correspondence to hazard levels. Studies on PBSD try to answer a similar question.

As opposed to traditional seismic codes that aim to provide structures with adequate strength and ductility for life safety, and stiffness for serviceability limits states, PBSD is a broader approach where the objective is to achieve stated performance objectives (levels) when the structures are subjected to stated seismic hazard levels. Using the multilevel (in terms of hazard) and multi-criteria (in terms of performance) approach offered by the PBSD it is aimed that the structural design will be under direct and explicit control and the expectations of stakeholders for more explicit codes for defining design objectives will be fulfilled. This is the very same reason for PBSD lending itself for use in LCC optimization of structures.

Vision 2000 (SEAOC, 1995) has been one of the key documents in the development of PBSD concepts. In Vision 2000, the hazard levels were expressed in terms of return periods as shown in Table 1. A performance level was defined as the maximum allowable damage to a building for a given earthquake design level. The performance

levels were determined by the condition of both the structural and nonstructural components. Four performance levels were defined: fully operational, operational, life-safety, and near collapse. Damage states of structural components were mapped to performance levels. Finally, a design performance objective was described as the desired performance level for the building for each earthquake design level. Design performance objectives were dependent on the building's occupancy, the importance of functions occurring within the building, economic considerations related to repair due to building damage and business interruption, and importance of the building as a historical or cultural asset. Recommended design performance objectives for buildings were mapped onto earthquake design levels as shown in Figure 4.

In FEMA 273 (FEMA, 1997) a similar framework to that of Vision 2000 (SEAOC, 1995) was presented. However, different design performance objectives and earthquake design levels were adopted (Figure 5). Threshold values for structural and nonstructural components at various performance levels were tabulated for various building types including steel, RC, masonry and

Table 1. Earthquake design levels in Vision 2000 (SEAOC, 1995)

Earthquake Design Level	Return Period	Probability of Exceedance
Frequent	43 years	50% in 30 years
Occasional	72 years	50% in 50 years
Rare	475 years	10% in 50 years
Very Rare	970 years	10% in 100 years

wood. System performance levels were described in terms of local (individual element) performance levels.

It is concluded from the review of documents Vision 2000 and FEMA 273 that conceptually PBSD framework is very similar. In other words, it is agreed that seismic design should be based on multiple performance objectives for stated earthquake hazard levels, however, the definition for earthquake design and performance levels show considerable variation. Furthermore, there is consensus neither on metrics to be selected as the indicators of performance levels, nor their relation to different damage states. However, interstory drift is mostly preferred since it is closely related to the development of P-Δ instabil-

ity (a system level indicator) and to the amount of local deformation imposed on the vertical elements and beam-column connections (component level indicators).

In this study the structural performance is defined in three levels: immediate occupancy (IO), life safety (LS) and collapse prevention (CP); and these performance levels are mapped onto the three hazard levels with return periods 75, 475 and 2475 years, respectively. The attainment of each performance level is described by reaching or exceeding a threshold value that defines the respective performance level (or structural limit state). It is noteworthy that the mapping between the performance and hazard levels does not indicate that the respective hazard level is considered only in evaluating the probability of attaining a given performance level. As described in the next section on the LCC model, first the fragility curve is derived and then it is integrated over the entire range of the earthquake intensity measure to obtain the probability of reaching or exceeding each structural limit (or damage) state.

The structural capacity and earthquake demand are coupled. In other words, the capacity of a structure is not independent from the earthquake

Figure 4. Recommended performance objectives for buildings in Vision 2000 (Adapted from SEAOC, 1995)

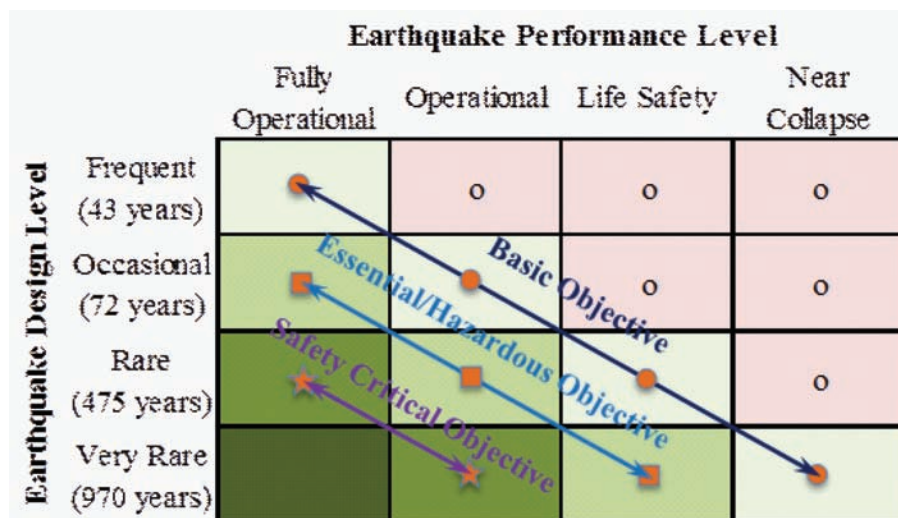


Figure 5. Recommended rehabilitation objectives for buildings in FEMA 273 (Adapted from FEMA, 1997)

		Building Performance Levels			
		Operational	Immediate Occupancy	Life Safety	Collapse Prevention
Earthquake Design Level	72 years	a	b	c	d
	225 years	e	f	g	h
	474 years	i	j	k	l
	2475 years	m	n	o	p

k + p = Basic Safety Objective
 k + p + any of a, e, i, m; or b, f, j, or n = Enhanced Objectives
 o = Enhanced Objective
 k alone or p alone = Limited Objectives
 c, g, d, h = Limited Objectives

demand imposed on the structure. The capacity varies during the strong ground shaking which also influences the seismic forces acting on the structure. The most elegant way of evaluating the failure probabilities is through the joint probability density function of capacity and demand which can be derived by Monte Carlo simulation (MCS). However, there are various sources of uncertainty in evaluation of the failure probabilities including the inherent variability of ground motions and randomness in material properties. Accounting for all the variability through MCS requires a large number of structural analyses. At the same time, accurate prediction of structural capacity and earthquake demand is critical for seismic design, and it is required to use analysis methods that yield reliable estimates. Performing MCS becomes infeasible when computationally demanding methods such as inelastic dynamic time history analysis is used. Therefore, here it is assumed that structural capacity is independent from earthquake demand and pushover analysis is used to evaluate the former while the latter is obtained by inelastic dynamic time history analysis.

Finite element model (based on distributed inelasticity) of the structure under consideration is built and pushover analysis is conducted. In order to establish the limit state threshold values that define the structural capacity, the response metrics obtained from the analysis such as stresses, strains, and interstory drifts are correlated to previously mentioned performance levels. Here only structural damage is considered; however, nonstructural damage could also be incorporated into the performance level definitions as suggested by Vision 2000 (SEAOC, 1995). Local (e.g. stresses and strains) and global (e.g. interstory drift) response measures could be combined to define different performance levels. Here, only the strains in longitudinal reinforcement and the core concrete are used as the criterion and the threshold values are represented in terms of interstory drift by mapping the strains onto the pushover curves. A typical pushover curve is shown in Figure 6(a) alongside the limit state points based on strains in the longitudinal reinforcement and the core concrete.

The LCC Model

Once the hazard and performance levels are defined, the next step is the calculation of the damage state probabilities, i.e. the probability of the structure attaining the pre-defined damage states throughout its lifetime. Once the damage state probabilities are calculated the cost of repair for each damage state is evaluated and the LCC of the structure is easily found. In the following the full derivation of a LCC model is provided.

The expected LCC of a structure is calculated as

$$E[C_{LC}(t)] = C_0 + t \cdot \sum_{i=1}^N C_i P_i \quad (1)$$

where C_0 is the initial construction cost, t is the service life of the structure, N is the total number of limit-states considered, P_i is the total probability that the structure will be in the i^{th} damage state throughout its lifetime, and C_i is the corresponding cost as a fraction of the initial cost of the structure. P_i is given by

$$P_i = P(\Delta_D > \Delta_{C,i}) - P(\Delta_D > \Delta_{C,i+1}) \quad (2)$$

where Δ_D is the earthquake demand and $\Delta_{C,i}$ is the structural capacity, usually in terms of drift ratio, defining the i^{th} damage state, as described in the previous section. The probability of demand being greater than capacity is evaluated as

$$P(\Delta_D > \Delta_{C,i}) = \int_0^\infty P(\Delta_D > \Delta_{C,i} | IM = im) \left| \frac{dv(IM)}{dIM} \right| dIM \quad (3)$$

where the first term inside the integral is the conditional probability of demand being greater than the capacity given the ground motion intensity, IM . This term is also known as the fragility function. The second term is the slope of the mean annual rate of exceedance of the ground motion intensity.

$v(IM)$ in Eqn. (3) defines the hazard curve, where IM is PGA for this study. The conditional probability of demand being greater than the capacity (or fragility) is

$$P(\Delta_D > \Delta_{C,i} | IM = im) = \int_0^\infty P(\Delta_D > \delta | IM = im) f_{C,i}(\delta) d\delta \quad (4)$$

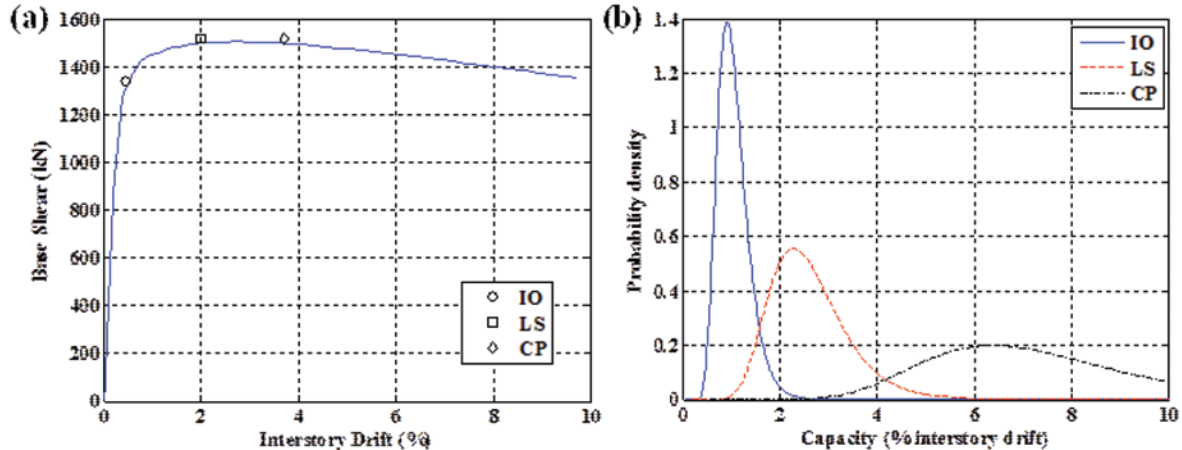
where δ is the variable of integration and $f_{C,i}$ is the probability density function for structural capacity for the i^{th} damage state. This formulation assumes that the demand and the capacity are independent of each other (as discussed in the previous section). Structural capacity is assumed to be lognormally distributed with $\Delta_{C,i}$ and β_C that are, respectively, the mean and the standard deviation of the corresponding normal distribution. As an example, the lognormal probability density functions for structural limit states are shown in Figure 6(b). In Figure 6(b), three limit states IO, LS, and CP with threshold values of 1%, 2.5% and 7% interstory drift, respectively, are assumed and β_C is taken as 0.3. The uncertainty in capacity (here represented with β_C) accounts for factors such as modelling error and variation in material properties. A more detailed investigation of capacity uncertainty is available in Wen et al. (2004) and Kwon and Elnashai (2006).

The structural demand is also assumed to follow a lognormal distribution and the probability of demand exceeding a certain value, δ , is given by

$$P(\Delta_D > \delta | IM = im) = 1 - \Phi \left[\frac{\ln(\delta) - \lambda_{D|IM=im}}{\beta_D} \right] \quad (5)$$

where $\Phi[\cdot]$ is the standard normal cumulative distribution, λ_D is the natural logarithm of the mean of the earthquake demand as a function of the ground motion intensity, and β_D is the standard deviation of the corresponding normal distribution of the earthquake demand. Although, β_C and β_D are dependent on ground motion intensity, in

Figure 6. (a) A typical pushover curve and the limit state points that delineate the performance levels, (b) illustration of lognormal probability distributions for the three structural limit states (IO: immediate occupancy, LS: life safety, CP: collapse prevention)



most studies they are taken as constants due to lack of information.

The dispersion in earthquake demand (here represented with β_D) due to variability in ground motions is established here using a simple structural system (2-story 1-bay RC frame) and three sets of earthquake ground motions each representing a different hazard level at return periods of 75, 475 and 2475 years. Each set includes seven ground motions which are selected from the PEER database (PEER, 2005) to represent the hazard at a selected site in San Francisco, CA (more details are given in the example application below). The correspondence between the hazard levels and the ground motions is achieved using three different methods. In the first method, the natural records are used without any modification. In the second method, the records are scaled based on PGA to match the PGA of the respective hazard level (in this case 75, 475 and 2475 years return period earthquakes are represented with a PGA of 0.24 g, 0.51 g and 0.78 g, respectively). And in the third method, spectrum matching is used to make the acceleration response spectrum of each record compatible with the UHS corresponding to each return period shown in Figure 3(b). The results

are shown in Figure 7. It is seen that although the mean of demand from three different methods are similar, a higher dispersion is obtained when natural and scaled ground motions are used. The dispersion also increases with increasing ground motion intensity (i.e. earthquake return period). The focus of this chapter is optimal seismic design of structures considering the LCC (not assessment); therefore, the use of spectrum compatible records is suggested. For assessment purposes, the use of unmodified (natural) records is recommended.

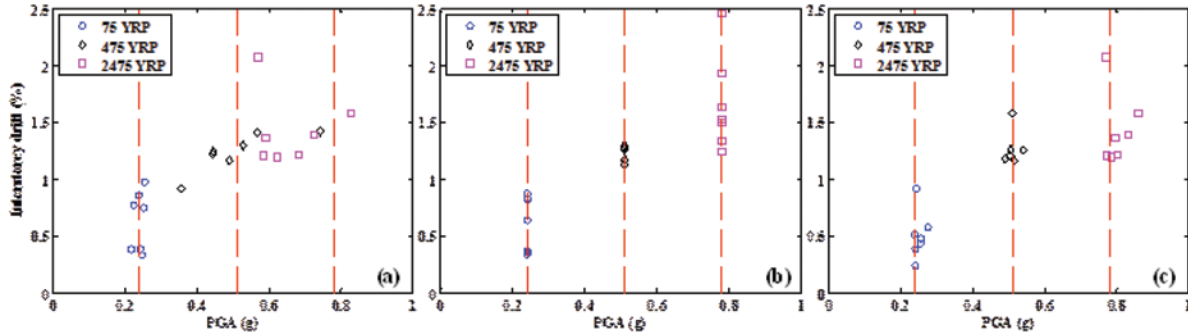
The mean, μ_D , and standard deviation, σ_D , of earthquake demand, as continuous functions of the ground motion intensity could be described using (Aslani & Miranda, 2005)

$$\mu_D (IM) = c_1 \cdot IM^{c_2} \text{ or } c_1 c_2^{IM} \cdot IM^{c_3} \quad (6)$$

$$\sigma_D (IM) = c_4 + c_5 \cdot IM + c_6 \cdot IM^2 \quad (7)$$

where the constants c_1 through c_3 and c_4 through c_6 are determined by curve fitting to the data points that match the PGA of the ground motions records with the mean and standard deviation,

Figure 7. Dispersion in earthquake demand for different representations of the earthquake hazard using: (a) natural, (b) scaled, and (c) spectrum compatible records



respectively, of earthquake demand evaluated using inelastic dynamic analysis. The mean and standard deviation are the parameters of the corresponding normal distribution that describes the earthquake demand. The curve fitting to the earthquake demand obtained from the spectrum compatible records that are mentioned above for the mean and standard deviation using the first option in Eqn. (6) and Eqn. (7), respectively, is shown in Figure 8.

The hazard curve can also be described in mathematical form

$$v(IM) = c_7 \cdot e^{c_8 \cdot IM} + c_9 \cdot e^{c_{10} \cdot IM} \quad (8)$$

where c_7 through c_{10} are constant to be determined from curve fitting to the hazard curve.

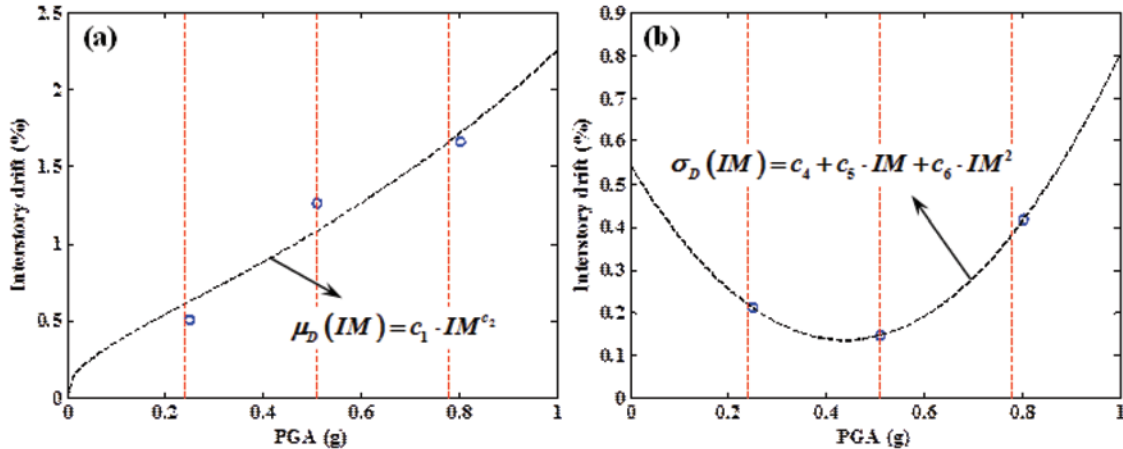
With the above described formulation each term in Eqn. (3) is represented as an analytical function of the ground motion intensity, IM . Thus, using numerical integration the desired probabilities of Eqn. (2) can easily be calculated. The cost of repair for the IO, LS, and CP limit states, C_i , are usually taken as a fraction of the initial cost of the structure. Finally, the LCC is evaluated through Eqn. (1).

The Optimization Algorithm

A brief review of most commonly used optimization algorithms is provided above. The objectives of the optimization problem considered here are highly nonlinear (due to the inelastic dynamic analysis that is used to predict earthquake demand) and the derivatives with respect to the design variables are discontinuous. Furthermore, the design variables (i.e. section sizes and reinforcement ratios) are discrete. Therefore, the use of gradient-based optimization algorithms is not well suited. The evolutionary algorithms have shown to be very efficient in solving combinatorial optimization problems as reviewed above. Here, the taboo search (TS) algorithm is selected and discussed in more detail. The same algorithm is also used to obtain the optimal solutions for the example application provided in the next section.

TS algorithm, first developed by Glover (1989, 1990), then it is adapted to multi-objective optimization problems by Baykasoglu et al. (1999a, 1999b). An advantage of TS algorithm is that a set of optimal solutions (Pareto-front or Pareto-set) could be obtained rather than a single optimal point in the objective function space. The methodology presented in Baykasoglu et al. (1999a, 1999b) is used here with further modifications as described below.

Figure 8. Curve fitting to obtain the (a) mean and (b) standard deviation of earthquake demand in continuous form



TS algorithm has also been applied to structural optimization problems. Bland (1998) applied TS algorithm to weight minimization of a space truss structure with various local minima and showed that TS algorithm was very effective in finding the global minimum when both reliability and displacement constraints were applied. Manoharan and Shanmuganathan (1999) investigated the efficiency of TS, SA, GA and branch-and-bound in solving the cost minimization steel truss structures. It was concluded that TS produced solutions better than or as good as both SA and GA and it arrives at the optimal solution quicker than both methods. In a more recent study, Ohsaki et al. (2007) explored the applicability of SA and TS algorithms for optimal seismic design of steel frames with standard sections. It was concluded that TS was more advantageous over SA in terms of the diversity of the Pareto solutions and the ability of the algorithm to search the solutions near the Pareto front.

To describe the modified TS algorithm used here, first, it is required to make the following definitions. The taboo list includes points in the design space for which the objective functions are evaluated for. Since inelastic dynamic time history analysis is computationally costly, this list is used

to avoid multiple runs with the same combination of design variables. That is, a point in the taboo list is not evaluated again. The Pareto list includes the points that are not dominated by other points within the set for which the evaluation of objective functions is performed (i.e. the taboo list). The seed list includes the points around which optimal solutions are looked for. The latter are called as the neighboring points and they are basically the adjacent elements of the multidimensional array, that defines the decision (or design) variables, around the given seed point. The modified TS algorithm works as follows:

- A. Start with the minimum cost combination (or initial design), evaluate the objective function and add this point into taboo, seed and Pareto lists. Use this point as the initial seed point.
- B. Find the neighboring points around the current seed. Here the number of neighboring points is chosen equal to the number of design variables and selected randomly amongst all the adjacent elements of the multidimensional array that defines the design variables.

- C. Evaluate the objective function for all the neighboring points and add these into taboo list.
- D. Find the Pareto-front using the set of points for which the objective function is evaluated and update the Pareto list as the current Pareto-front.
- E. Amongst the neighboring points for the current iteration choose the one that is on the Pareto-front and minimizes the cost function as the next seed point and add this point into the seed list. If there is no point which satisfies these conditions choose randomly one of the points from the Pareto list amongst the ones that are not already in the seed list.
- F. Check if the predetermined maximum number of objective function evaluations is exceeded; if yes stop, if not go to Step b.

The steps required to perform LCC oriented seismic design optimization according to the methodology presented in the preceding sections is outlined in Figure 9.

EXAMPLE APPLICATION

In this section, the formulations presented in the preceding sections are applied to a building as an illustration of the framework on LCC oriented seismic design optimization. The 2-story 2-bay RC frame structure show in Figure 10 is selected

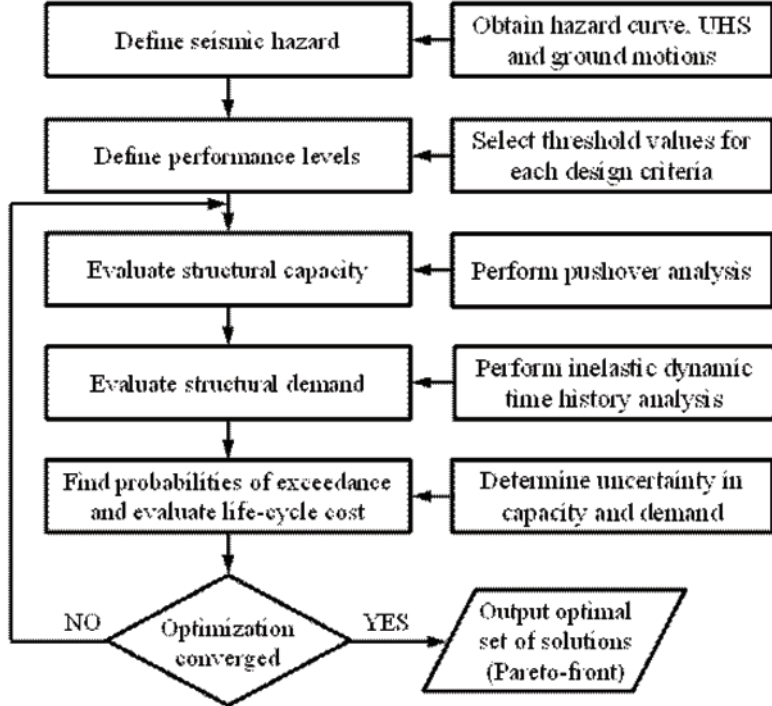
for the application. Seven design variables are defined for the optimization problem as given in Table 2, alongside the minimum and maximum values and increments. The combination of these design variables results in 30000 cases which constitute the search space. The objectives of the optimization problem are selected as initial and life-cycle cost, and structural performance in terms of maximum interstory drift. No constraints are defined because of the fact that code-based seismic design is not performed. The initial cost of the frames considers only the material costs. The unit prices for concrete and steel are assumed to \$0.13/liters and \$0.66/kg, respectively.

A site at the intersection of 2nd and Market Streets in San Francisco, CA (with coordinates 37° 47' 21.58'' N, 122° 24' 04.77'' W) is selected and the site-specific seismic hazard is consistently derived. The soil conditions might significantly alter the characteristics of the ground motions at a site, therefore, the soil conditions are also taken into account in the development of the hazard curves. The soil at the selected site is determined as D on the NEHRP (FEMA, 2003) scale with a shear wave velocity in the range from 180 m/sec to 360 m/sec. Site specific hazard curve for PGA is shown in Figure 11(a). UHS for three different return periods (i.e. 75, 475, and 2475 years) are obtained, see Figure 11(b), for record selection and scaling purposes. These return periods are mapped onto three structural limit states IO, LS and CP, respectively. One earthquake

Table 2. Design variables and ranges for the considered structural frame

	Minimum	Maximum	Increment
Column Reinforcement Ratio	1.0%	2.5%	0.50%
Beam Reinforcement Ratio	0.5%	2.0%	0.50%
Width of Exterior Columns (mm)	660.4	863.9	50.8
Width of Interior Columns (mm)	711.2	914.4	50.8
Depth of Columns (mm)	457.2	660.4	50.8
Width of Beams (mm)	508	711.2	50.8
Depth of Beams (mm)	406.4	508	50.8

Figure 9. Steps for performing LCC oriented seismic design optimization

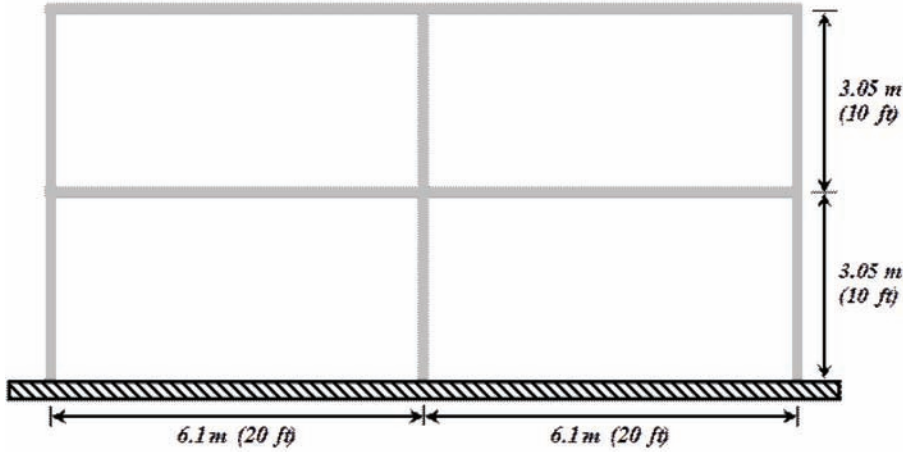


ground motion is selected for each return period (see the section “The LCC Model” for more information) and spectrum matching (Abrahamson, 1993) is used to achieve direct correspondence between the records and the hazard levels. The acceleration response spectra of the records after spectrum matching are shown in Figure 11(b).

The life-time of the structure, t , is considered as 50 years. The cost of repair for the IO, LS, and CP limit states, C_i , are taken as 30, 70 and 100 percent of the initial cost of the structure based on the correspondence of the limit states defined previously and the information provided by Fragiadakis et al. (2006b). The hazard curve as a function of PGA is shown in Figure 11(a). The functional form in Eqn. (8) is fitted to the hazard curve to allow for the numerical integration of Eqn. (3). The demand side of fragility relationship given in Eqn. (4), i.e. the first term, as a function of PGA, is obtained by finding the maximum interstory drift under the three hazard levels through inelastic dynamic analysis and it is rep-

resented analytically by curve fitting to mathematical form in Eqn. (6). The dispersion in earthquake demand, β_D , is quantified as 0.25, 0.35 and 0.45 for the three hazard levels with 75, 475 and 2475 years return period, respectively, by running additional analysis. The details of this derivation are omitted here for the sake of brevity. As mentioned earlier, the structural limit states are also established by carefully investigating different design alternatives in the search space by conducting pushover analysis and considering local response measures, i.e. strains in the longitudinal reinforcement and concrete core. The structural capacity is evaluated for a range of design variables and the mean values for the three limit states IO, LS and CP are obtained as 0.4%, 2% and 3.5% interstory drift. The uncertainty in capacity is assumed to be equal to 0.35 taking previous research as a reference (Wen, et al., 2004). First the conditional probability (fragility) in Eqn. (4), then the total probability in Eqn. (3) is calculated. The damage state probabilities are

Figure 10. RC frame structure used for the example application



found from Eqn. (2) and the expected LCC of the structure is obtained from Eqn. (1).

During the optimization process, TS algorithm is allowed to search 10% of the search space. In other words, the maximum number of objective function evaluations is set 3000 for each hazard level. Figure 12(a) shows the combinations of the design variables (in the solution space) that are searched by the TS algorithm to obtain the Pareto-front which is also shown in the same figure with a solid line with circle marks. It is seen that the algorithm is very effective in terms of narrowing down the search space to the points that are close

to the Pareto-front. The initial and the total costs of the building vs. the maximum interstory drift under the 2475 years return period earthquake is shown in Figure 12(b)[only for optimal solutions]. It is seen that there is a compromise between the initial cost, LCC and structural performance (represented with maximum interstory drift). As the initial cost increases it approaches the LCC and the maximum interstory drift is reduced (better structural performance) while the LCC and the maximum interstory drift are significantly higher for lower initial cost solutions. This type of a representation is very important for the use

Figure 11. (a) Site specific hazard curve, (b) UHS and spectrum compatible earthquake records

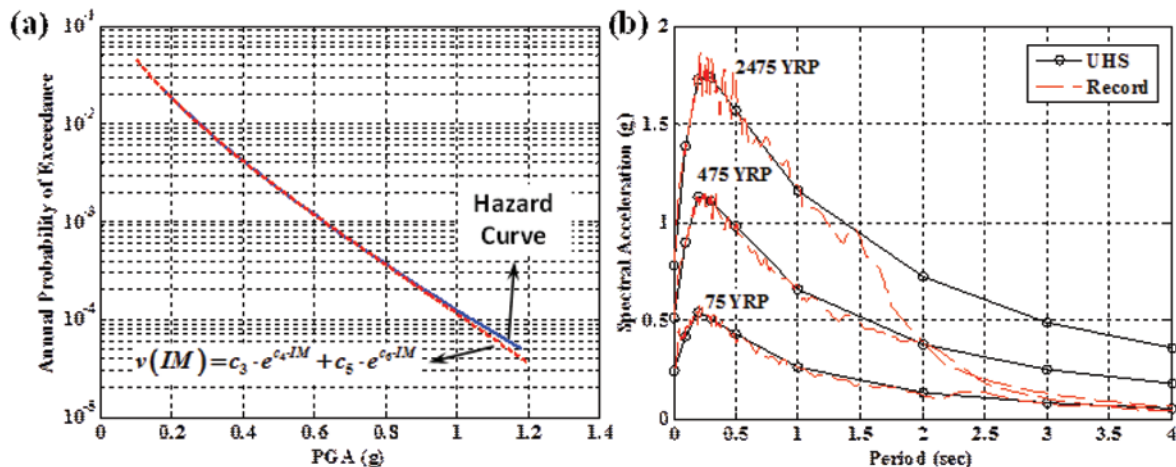
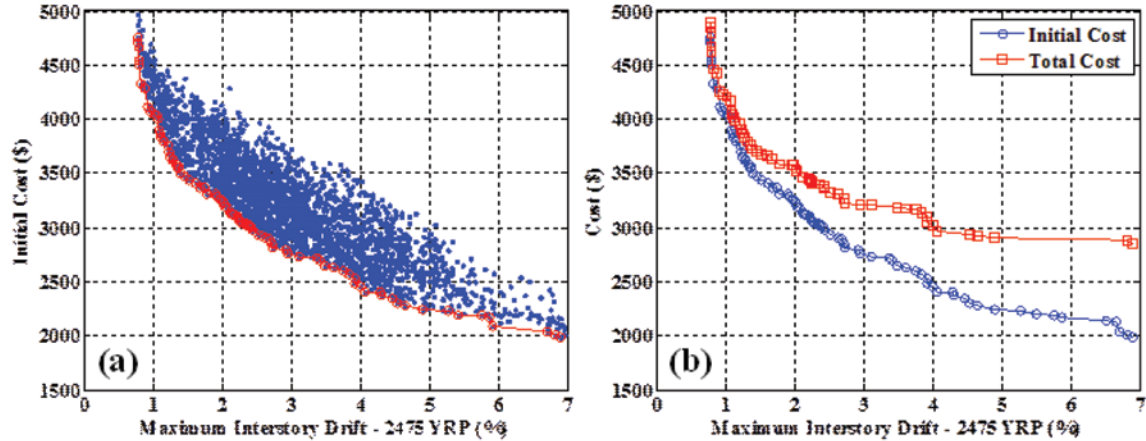


Figure 12. (a) Example Pareto-front obtained using TS algorithm, (b) initial and LCC of the building



of LCC oriented seismic design optimization by the decision makers such as owners and engineers as well as for its implementation in future seismic design codes, as the presentation of results in the Pareto-optimal form gives flexibility in the decision making process and can accommodate changes to the performance requirements throughout the course of design.

FUTURE RESEARCH DIRECTIONS

There are two major issues in LCC oriented seismic design of structures that requires further research. The first one is the application of the concept developed here to structural models with significant number design variables. The size of the search space increases exponentially with increasing number of design variables and without a compromise from the accuracy of structural assessment it becomes very difficult to cope with the computational demand. Although simplified structural models and analysis techniques are always an option, these undermine the main objective of the seismic design optimization by introducing additional uncertainty into the procedure.

The second issue is sensitivity of the LCC results to the assumptions made in the derivations.

Most importantly, for the formulation provided in this paper, the constants C_i in Eqn. (1) which define the cost of repair for the i^{th} damage state as a fraction of the initial cost have strong influence on the LCC. As discussed earlier, it is not straightforward to determine damage states for structures and the associated cost of repair. The effect of other parameters such as the dispersion in capacity and demand on the LCC should also be investigated. Eqn. (4) assumes that the structural capacity is independent of earthquake demand which is another simplification that is usually adopted. The evaluation of workmanship cost is difficult as it is dependent on various parameters (especially the local cost of labor). Finally, the cost of non-structural damage after an earthquake might exceed several times the cost of structural damage and this also needs to be investigated.

CONCLUSION

Optimization in structural design is a growing subject due to increased awareness of the community regarding the sustainability of civil infrastructure and the use Earth's nonrenewable resources. And the recent incidents have shown us once again that the initial cost of a structure is not a satisfactory

criterion for the economy objective of seismic design, as the repair and indirect costs due to damage in future earthquakes might be significantly higher than the initial cost, therefore the life-cycle cost (LCC) should also be considered. In this chapter the LCC considerations in seismic design optimization of structures is discussed emphasizing the importance of the following: (1) use of advanced analysis, which provides the most rigorous assessment of structural capacity and earthquake demand, (2) evaluation of the structural capacity by taking into account not only the global behavior of the structure but also the local response, (3) use of system-specific limit states to define the structural capacity, and (4) consideration of all major sources of uncertainty, from seismogenic source characteristics to material properties and structural modeling in calculating the limit state exceedance probabilities. A LCC formulation is provided where each component from seismic hazard, to structural assessment, LCC model and optimization algorithm are rigorously addressed. An example application is included to allow for easy implementation of the framework presented here.

REFERENCES

- Abrahamson, N. A. (1993). *Non-stationary spectral matching program RSPMatch: user's manual*.
- Adamu, A., Karihaloo, B. L., & Rozvany, G. I. N. (1994). Minimum cost design of reinforced concrete beams using continuum-type optimality criteria. *Structural and Multidisciplinary Optimization*, 7(1), 91–102.
- Aslani, H., & Miranda, E. (2005). Probability-based seismic response analysis. *Engineering Structures*, 27(8), 1151–1163. doi:10.1016/j.engstruct.2005.02.015
- Baykasoglu, A., Owen, S., & Gindy, N. (1999a). Solution of goal programming models using a basic taboo search algorithm. *The Journal of the Operational Research Society*, 50(9), 960–973.
- Baykasoglu, A., Owen, S., & Gindy, N. (1999b). A taboo search based approach to find the Pareto optimal set in multiple objective optimization. *Engineering Optimization*, 31(6), 731–748. doi:10.1080/03052159908941394
- Bertero, V. V., & Zagajeski, S. W. (1979). *Optimal inelastic design of seismic-resistant reinforced concrete framed structures*. Paper presented at the Nonlinear Design of Concrete Structures, CSCE-ASCE-ACI-CEB International Symposium, Ontario, Canada.
- Bland, J. (1998). Structural design optimization with reliability constraints using tabu search. *Engineering Optimization*, 30(1), 55–74. doi:10.1080/03052159808941238
- Chan, C. M., & Zou, X. K. (2004). Elastic and inelastic drift performance optimization for reinforced concrete buildings under earthquake loads. *Earthquake Engineering & Structural Dynamics*, 33(8), 929–950. doi:10.1002/eqe.385
- Cheng, F. Y., & Truman, K. Z. (1985). *Optimal design of 3-D reinforced concrete and steel buildings subjected to static and seismic loads including code provisions* (No. Final Report Series 85-20). Washington, DC, USA: prepared by University of Missouri-Rolla, National Science Foundation, US Department of Commerce.
- Collins, K. R., Wen, Y. K., & Foutch, D. A. (1996). Dual-level seismic design: A reliability-based methodology. *Earthquake Engineering & Structural Dynamics*, 25(12), 1433–1467. doi:10.1002/(SICI)1096-9845(199612)25:12<1433::AID-EQE629>3.0.CO;2-M

- Cornell, C. A., Jalayer, F., Hamburger, R. O., & Foutch, D. A. (2002). Probabilistic basis for 2000 SAC federal emergency management agency steel moment frame guidelines. *Journal of Structural Engineering*, 128(4), 526–533. doi:10.1061/(ASCE)0733-9445(2002)128:4(526)
- FEMA. (1997). *NEHRP guidelines for the seismic rehabilitation of buildings, FEMA 273*. Washington, DC: Federal Emergency Management Agency.
- FEMA. (2003). *NEHRP recommended provisions for seismic regulations for new buildings and other structures, FEMA 450, Part 1: Provisions*. Washington, DC: Federal Emergency Management Agency.
- Foley, C. M., & Schinler, D. (2003). Automated design of steel frames using advanced analysis and object-oriented evolutionary computation. *Journal of Structural Engineering*, 129(5), 648–660. doi:10.1061/(ASCE)0733-9445(2003)129:5(648)
- Fragiadakis, M., Lagaros, N. D., & Papadrakakis, M. (2006a). Performance-based earthquake engineering using structural optimisation tools. *International Journal of Reliability and Safety*, 1(1/2), 59–76. doi:10.1504/IJRS.2006.010690
- Fragiadakis, M., Lagaros, N. D., & Papadrakakis, M. (2006b). Performance-based multiobjective optimum design of steel structures considering life-cycle cost. *Structural and Multidisciplinary Optimization*, 32(1), 1–11. doi:10.1007/s00158-006-0009-y
- Fragiadakis, M., & Papadrakakis, M. (2008). Performance-based optimum seismic design of reinforced concrete structures. *Earthquake Engineering & Structural Dynamics*, 37(6), 825–844. doi:10.1002/eqe.786
- Glover, F. (1989). Tabu search - Part I. *ORSA Journal on Computing*, 1(3), 190-206.
- Glover, F. (1990). Tabu search - Part II. *ORSA Journal on computing*, 2(1), 4-32.
- International Building Code*. (2006).
- Kwon, O.-S., & Elnashai, A. (2006). The effect of material and ground motion uncertainty on the seismic vulnerability curves of RC structure. *Engineering Structures*, 28(2), 289–303. doi:10.1016/j.engstruct.2005.07.010
- Lagaros, N. D., Fragiadakis, M., Papadrakakis, M., & Tsompanakis, Y. (2006). Structural optimization: A tool for evaluating seismic design procedures. *Engineering Structures*, 28(12), 1623–1633. doi:10.1016/j.engstruct.2006.02.014
- Lagaros, N. D., & Papadrakakis, M. (2007). Seismic design of RC structures: A critical assessment in the framework of multi-objective optimization. *Earthquake Engineering & Structural Dynamics*, 36(12), 1623–1639. doi:10.1002/eqe.707
- Li, G., Zhou, R.-G., Duan, L., & Chen, W.-F. (1999). Multiobjective and multilevel optimization for steel frames. *Engineering Structures*, 21(6), 519–529. doi:10.1016/S0141-0296(97)00226-5
- Liu, M. (2005). Seismic design of steel moment-resisting frame structures using multiobjective optimization. *Earthquake Spectra*, 21(2), 389–414. doi:10.1193/1.1902952
- Liu, M., Burns, S. A., & Wen, Y. K. (2003). Optimal seismic design of steel frame buildings based on life cycle cost considerations. *Earthquake Engineering & Structural Dynamics*, 32(9), 1313–1332. doi:10.1002/eqe.273
- Liu, M., Burns, S. A., & Wen, Y. K. (2005). Multiobjective optimization for performance-based seismic design of steel moment frame structures. *Earthquake Engineering & Structural Dynamics*, 34(3), 289–306. doi:10.1002/eqe.426

- Liu, M., Burns, S. A., & Wen, Y. K. (2006). Genetic algorithm based construction-conscious minimum weight design of seismic steel moment-resisting frames. *Journal of Structural Engineering*, 132(1), 50–58. doi:10.1061/(ASCE)0733-9445(2006)132:1(50)
- Liu, M., Wen, Y. K., & Burns, S. A. (2004). Life cycle cost oriented seismic design optimization of steel moment frame structures with risk-taking preference. *Engineering Structures*, 26(10), 1407–1421. doi:10.1016/j.engstruct.2004.05.015
- Manoharan, S., & Shanmuganathan, S. (1999). A comparison of search mechanisms for structural optimization. *Computers & Structures*, 73(1-5), 363-372.
- Memari, A. M., & Madhkhan, M. (1999). Optimal design of steel frames subject to gravity and seismic codes' prescribed lateral forces. *Structural and Multidisciplinary Optimization*, 18(1), 56–66.
- Moharrami, H., & Grierson, D. E. (1993). Computer-automated design of reinforced concrete frameworks. *Journal of Structural Engineering*, 119(7), 2036–2058. doi:10.1061/(ASCE)0733-9445(1993)119:7(2036)
- Ohsaki, M., Kinoshita, T., & Pan, P. (2007). Multiobjective heuristic approaches to seismic design of steel frames with standard sections. *Earthquake Engineering & Structural Dynamics*, 36(11), 1481–1495. doi:10.1002/eqe.690
- PEER. (2005). *Pacific Earthquake Engineering Research (PEER) center: NGA database*. Retrieved January 1, 2009, from <http://peer.berkeley.edu/nga/>
- Pezeshk, S. (1998). Design of framed structures: An integrated non-linear analysis and optimal minimum weight design. *International Journal for Numerical Methods in Engineering*, 41(3), 459–471. doi:10.1002/(SICI)1097-0207(19980215)41:3<459::AID-NME293>3.0.CO;2-D
- Sahab, M. G., Ashour, A. F., & Toropov, V. V. (2005). Cost optimisation of reinforced concrete flat slab buildings. *Engineering Structures*, 27(3), 313–322. doi:10.1016/j.engstruct.2004.10.002
- SEAOC. (1995). *Vision 2000, performance based seismic engineering of buildings (Vol. I and II)*. Sacramento, CA: Structural Engineers Association of California.
- Uniform Building Code* (1997).
- USGS. (2008). *Documentation for the 2008 update of the United States national seismic hazard maps* (No. Open-File Report 2008-1128). Reston, VA: United States Geological Survey.
- Wen, Y. K., Ellingwood, B. R., & Bracci, J. M. (2004). *Vulnerability function framework for consequence-based engineering* (No. Project DS-4 Report). Urbana, IL: Mid-America Earthquake (MAE) Center.
- Wen, Y. K., & Kang, Y. J. (2001a). Minimum building life-cycle cost design criteria, I: Methodology. *Journal of Structural Engineering*, 127(3), 330–337. doi:10.1061/(ASCE)0733-9445(2001)127:3(330)
- Wen, Y. K., & Kang, Y. J. (2001b). Minimum building life-cycle cost design criteria, II: Applications. *Journal of Structural Engineering*, 127(3), 338–346. doi:10.1061/(ASCE)0733-9445(2001)127:3(338)
- Zou, X. K., & Chan, C. M. (2005). An optimal resizing technique for seismic drift design of concrete buildings subjected to response spectrum and time history loadings. *Computers & Structures*, 83(19-20), 1689–1704. doi:10.1016/j.compstruc.2004.10.002
- Zou, X. K., Chan, C. M., Li, G., & Wang, Q. (2007). Multiobjective optimization for performance-based design of reinforced concrete frames. *Journal of Structural Engineering*, 133(10), 1462–1474. doi:10.1061/(ASCE)0733-9445(2007)133:10(1462)

Chapter 2

Performance-Based Seismic Design: A Search-Based Cost Optimization with Minimum Reliability Constraints

Oscar Möller

University of Rosario, Argentina

Marcelo Rubinstein

University of Rosario, Argentina

Fabián Savino

University of Rosario, Argentina

Ricardo O. Foschi

University of British Columbia, Canada

ABSTRACT

An approach is presented to structural optimization for performance-based design in earthquake engineering. The objective is the minimization of the total cost, including repairing damage produced by future earthquakes, and satisfying minimum target reliabilities in three performance levels (operational, life safety, and collapse). The different aspects of the method are considered: a nonlinear dynamic structural analysis to obtain responses for a set of earthquake records, representing these responses with neural networks, formulating limit-state functions in terms of deformations and damage, calculating achieved reliabilities to verify constraint violations, and the development of a gradient-free optimization algorithm. Two examples illustrate the methodology: 1) a reinforced concrete portal for which the design parameters are member dimensions and steel reinforcement ratios, and 2) optimization of the mass at the cap of a pile, to meet target reliabilities for two levels of cap displacement. The objective of this latter example is to illustrate model effects on optimization, using two different hysteresis approaches.

INTRODUCTION

Structural optimization for performance-based design in earthquake engineering aims at finding optimum design parameters (e.g., dimensions of structural members, steel reinforcement ratios for concrete structures, characteristics of energy dissipation devices) corresponding to a minimum

objective (e.g., the total cost), with constraints specifying minimum reliability levels for each performance requirement. Three performance levels are normally considered in earthquake engineering: serviceability, life safety and collapse.

The objective of the present Chapter is to present a procedure for performance-based optimization of a preliminary design, taking into account the

DOI: 10.4018/978-1-4666-1640-0.ch002

uncertainties in the ground motion and structural properties, and at the same time minimizing the total cost. This includes, in addition to the initial cost of construction, that associated with repairs following each of a series of earthquakes within a given time interval. The preliminary design may be the result of applying capacity design approaches, according to existing Codes, in order to satisfy the performance levels.

The subsequent sections of this Chapter discuss the different aspects of the proposed design optimization process, including: 1) the quantification of the seismic hazard or possible ground motions at the site; 2) the use of a structural dynamics analysis model that represents, as best as possible, the nonlinear response and the hysteretic energy dissipation mechanisms; 3) the calculation of a response database for the estimated ranges of the different intervening input random variables and design parameters; 4) a functional representation for the discrete databases, using neural networks response surfaces; 5) implementation of the response surfaces in the calculation of the reliability levels achieved, at each performance level, for specific values of the design parameters; 6) representation of these reliability levels by neural networks in terms of the design parameters, in order to achieve an efficient calculation of reliability constraint violations and, finally, 7) an optimization algorithm that would search for a minimum total cost objective under minimum reliability constraints for each performance level.

Earthquakes show large ground motion uncertainties which must be coupled with those in the structural capacities, and the demands will likely trigger a nonlinear structural response. For each performance level, the formulation of the limit-state functions requires the estimation of maximum responses (e.g., maximum inter-story drift) during the duration of the earthquake. Since only discrete values can be obtained by numerical analyses for specific combinations of the variables and parameters, the responses need to be given a continuous functional representation

for optimization and reliability estimation. Each of the responses of interest can be approximately represented by using response surfaces which, when properly adjusted, can be used as substitutes for the dynamic analysis (Hurtado, 2004). Different forms for approximating surfaces have been studied (Möller et al., 2009b), and neural networks have been shown to offer advantages of flexibility and adaptability. Regardless of the type of response surface used, a major advantage of the substitute is the computational efficiency achieved with Monte Carlo-type simulations when estimating probabilities of non-performance.

The approach chosen in the optimization problem must consider the presence of constraints, the dimensionality and the form and number of objective functions. Optimization methods can use different approaches (Pérez López, 2005; Swisher et al., 2000), some requiring the calculation of gradients (steepest descent, conjugate gradients, Newton or quasi-Newton schemes) and others, not using gradients, implementing genetic or search algorithms. This Chapter proposes an efficient search-based algorithm which also accounts for constraints given by specified minimum reliability levels at each performance level. The optimization approach presented in this Chapter is based on previous work by the authors (Möller et al., 2007, 2008, 2009a,c), and introduces additional contributions as follows:

- The optimization process is started from a preliminary, deterministic seismic design;
- The previous search-based algorithm by the authors has been modified to minimize the possibility of encountering local minima;
- The damage repair costs introduced into the objective function take into account the occurrence of multiple seismic events during the life of the structure.

The optimization approach presented here is illustrated with two performance-based design

examples. The first is for a simple, reinforced concrete portal frame, for which the design parameters are the column and beam dimensions, as well as the steel reinforcement ratios. The optimality of the preliminary design is discussed, as well as the efficiency of the proposed optimization process. This example also considers the sensitivity of the optimal solution to the assumed relationship between calculated damage and repair costs, as well as to the reliability levels prescribed as minimum constraints for each of the performance levels.

Reliability estimates and optimization results are conditional on the analysis models used. The second example is the optimization for the permissible pile-cap mass carried by a pile foundation. This main objective in this example is to discuss the importance of the analysis model formulation in the final optimization results. Two different models are used, based on two different formulations for hysteretic energy dissipation.

1. THE OPTIMIZATION FORMULATION

1.1 General Objective

The aim of the optimization considered here is to find values for the design parameters, grouped in a vector \mathbf{x}_d , to minimize the objective function $C(\mathbf{x}_d)$. This function is the total cost, and it is given by the sum of the initial construction cost $C_0(\mathbf{x}_d)$ and the damage repair cost $C_d(\mathbf{x}_d)$, required after the occurrence of earthquakes during the service life of the structure. That is,

$$C(\mathbf{x}_d) = C_0(\mathbf{x}_d) + C_d(\mathbf{x}_d) \quad (1)$$

The minimum total cost must correspond to a structure that also satisfies minimum reliability requirements for different performance levels:

$$\beta_j(\mathbf{x}_d) \geq \beta_{jT} \quad , \quad j = 1, 2, 3 \quad (2)$$

in which $\beta_j(\mathbf{x}_d)$ are the reliability indices achieved with the design parameters \mathbf{x}_d for each of the three performance levels j : “operational”, “life safety or controlled damage” and “collapse”, with β_{jT} being the corresponding prescribed minimum targets over the design life T_D .

The design parameters \mathbf{x}_d could be, for example, either dimensions, steel reinforcement ratios, or statistical parameters for some of the random variables in the problem (e.g., the mean value of the required steel yield strength).

Given a procedure to verify reliability constraint compliance, as described in Section 2.2, an optimization technique is then applied to minimize the total cost while satisfying the minimum reliability indices for each performance level. The optimization algorithm proposed here is a gradient-free, search-based approach, as described in Section 5.

1.2 The Methodology for Reliability Evaluation

The optimization process requires the calculation of reliability levels achieved with the design parameters \mathbf{x}_d . This is implemented through the following steps, all prior to the optimization proper. These steps, to be addressed in the following sections, include:

- A. Definition of the random variables \mathbf{X} in the problem, and their corresponding upper and lower bounds;
- B. Selection of combinations for the variables \mathbf{X} within their corresponding bounds, using design of experiments;
- C. Construction of a structural response database: for each variable combination in b), and for each record in a set of earthquakes considered likely to occur at the site, determination of the maximum structural responses $R_i(\mathbf{X})$ that enter in the formulation of the performance functions, using a nonlinear dynamic time-step analysis;

- D. For each variable combination, determination of the mean maximum structural response and corresponding standard deviation over the set of earthquake records, followed by an approximation of these means and standard deviations by explicit, continuous neural network response surface functions $F_i(\mathbf{X})$.
- E. Using the mean and standard deviation for each maximum response to represent its corresponding cumulative probability distribution by a lognormal. In turn, with these distributions, implementing the neural networks from d), to calculate the probabilities of non-performance or the associated reliability indices β_j , for any given set of design parameters.
- F. For a set of parameters \mathbf{x}_d , chosen within their bounds, approximation of the discrete results from e) by means of neural network response surface functions for the reliabilities $\beta_j(\mathbf{x}_d)$. Using these approximations directly, during the optimization, to calculate the reliability achieved at each performance level for a particular vector \mathbf{x}_d , in order to efficiently evaluate constraint violations.

2. NONLINEAR DYNAMIC ANALYSIS MODEL

The optimization requires the development of a response database in terms of the random variables \mathbf{X} , for each earthquake record considered. This calculation implies the application of a nonlinear dynamic analysis and a step by step integration of the equations of motion over the duration of the earthquake. The focus of this Chapter is not on the details of the particular structural nonlinear dynamic analysis used. Many modeling techniques have been proposed, aiming at achieving an adequate balance between accuracy and simplicity. It is important to emphasize, however, that each approach has an associated modeling error, and

that the development of a response database is the task involving the greatest computational effort. A nonlinear model for reinforced concrete, based on bar elements, has been discussed elsewhere (Möller, 2001; Möller and Foschi, 2003) and has been used in the first application example presented here in Section 7.

The reliability and, ultimately, the optimization results, are conditional on the adequacy of the analysis model, and a proper “model error” variable must be included in the random set \mathbf{X} . Some of the issues to be addressed in the formulation of the dynamic analysis relate, for example, to how the hysteretic energy dissipation is represented. This issue is considered in the second application example in Section 8, a soil/structure interaction problem which highlights the dependence of the optimization results on the assumptions made in the analysis model.

3. RESPONSE REPRESENTATION BY NEURAL NETWORKS

3.1 Neural Networks

Neural networks are algorithms for the transmission of information between input and output. This technique has been used here to represent the structural response databases. Because the neural networks literature is quite extensive, only a brief description of the type of network used here is included for completeness.

Several input parameters are assumed to occupy individual “neurons” in an “input layer” and, similarly, several outputs can form the “output layer” containing the “output neurons”. The information between input and output is assumed to flow through intermediate or hidden neurons, the strength of the information between two neurons j and i being given by weight parameters W_{ji} . The architecture of the network is shown in Figure 1, for N inputs and K outputs. The information received by a hidden or output neuron is modi-

fied by a transfer function $h(t)$ before being sent forward along the network. The mathematical expression for this algorithm is

$$R(\mathbf{X}) \cong F(\mathbf{X}) = h \left(\sum_{j=1}^J W_{kj} h \left(\sum_{i=1}^N W_{ji} X_i + W_{j0} \right) + W_{k0} \right) \quad (3)$$

in which, in our case, $R(\mathbf{X})$ is the “true” value for the structural response obtained with the dynamic analysis for the input vector \mathbf{X} , with components X_i , $F(\mathbf{X})$ is the neural network approximation, W_{kj} and W_{ji} are the weight parameters, and $h(t)$ is the transfer function applied at the hidden and output neurons. This function could take different forms, and in this Chapter we use a sigmoid:

$$h(t) = \frac{1.0}{(1 + \exp(-t))} \quad (4)$$

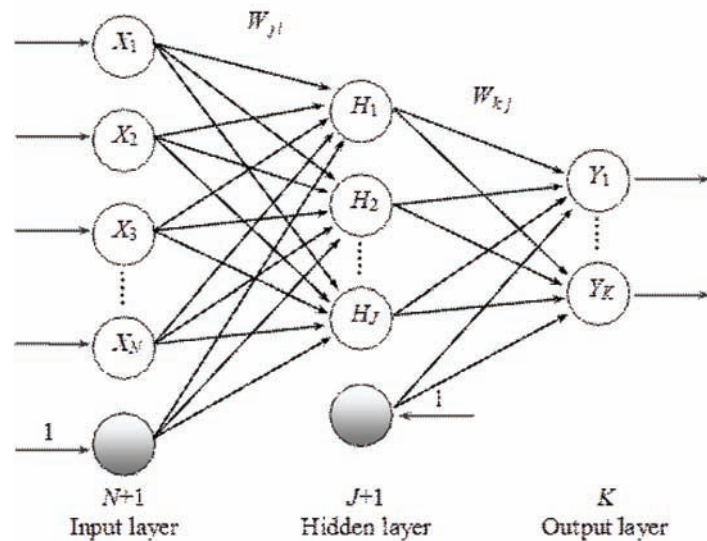
The weights W must be obtained in such a way that the differences between $R(\mathbf{X})$ and $F(\mathbf{X})$ be minimized. This optimization is defined as the “training” of the network, and different minimization algorithms can be implemented,

either gradient- or search-based. For example, the back-propagation or other Newtonian algorithms implement steepest descent with either a controlled or a calculated step. Although back-propagation is the commonly used training method, this Chapter presents in Section 4.2 a gradient-free search algorithm as a straight-forward approach to the training optimization.

3.2 Search-Based Optimization as a Training Algorithm

The following describes a gradient-free, search-based optimization algorithm for the neural network weights W . The optimization strategy is called OPT. Let N be the number of input variables and NP the number of input data combinations. The input values are then $X_0(i,k)$, with $i = 1, N$ and $k = 1, NP$. Before proceeding, the data are scaled to values $X(i,k)$, between the limits 0.01 and 0.99, in order to eliminate potential problems with different units and magnitudes. Similarly, the output results from the response analysis, $T_0(k)$, are also scaled to values $T(k)$ between 0.01 and 0.99, tak-

Figure 1. Neural network architecture



ing into account that the sigmoid transfer function $h(t)$ de Eq.(4) produces values between 0 and 1.

To start the optimization for the weights W , initial values are chosen randomly from an uniform distribution between -5 and 5. These limits are arbitrarily chosen, but are considered to be sufficiently wide to lead to a wide range in the predicted outputs $Y(k)$. For each weight selection (e.g., 5000 combinations in this Chapter) the corresponding prediction error E is calculated from Eq.(5),

$$E = \sum_{k=1}^{NP} (Y(k) - T(k))^2 \quad (5)$$

keeping the combination of weights W_0 which correspond to the minimum among the calculated errors E .

The absolute value of the NP errors ($|Y(k) - T(k)|$), corresponding to the weights W_0 , are ranked from smallest to largest. The set corresponding to 80% of the data with the largest errors is used for the network training, with the remaining 20% available for validation.

With W_0 representing an “anchor” point with corresponding error E_0 over the training set, new values for the weights W are randomly chosen within a neighborhood of W_0 , and the corresponding errors E are calculated with Eq.(5). Whenever a set W is found for which $E < E_0$, this set becomes the new W_0 and the search process is repeated around this new anchor. The maximum number of repetitions is limited to a prescribed number (500 in the work presented here).

The number of samples of weights W around a given anchor W_0 is limited, e.g., to 1000. If this limit is reached and all errors satisfy $E > E_0$, then convergence has been achieved and the minimum solution is estimated to be in correspondence with the anchor W_0 .

If either convergence has been achieved, or the number of repetitions has exceeded the stipulated maximum, then the NP individual errors are calculated and ranked, re-initiating the search

for the new 80% of the data corresponding to the greatest errors in absolute value. This process is repeated $NREP$ times (100 in the work presented here), looking for the possibility of local minima. The final solution corresponds to that W_0 with the minimum overall error E_0 .

3.3 Subsequent Optimization Using Gradients

The search-based algorithm described in 4.2 can be complemented with a gradient-based optimization starting from the final weights W_0 . The following alternatives may be pursued:

- A. Search for weights W trying to zero out the error E

If the error E is approximated as a linear function around E_0 ,

$$E = E_0 + \mathbf{G}_0^T (\mathbf{W} - \mathbf{W}_0) \quad (6)$$

in which \mathbf{G}_0 is the gradient vector at W_0 ,

$$\mathbf{G}_{0_i} = \left(\frac{\partial E}{\partial W_i} \right)_{W_0} \quad (7)$$

the objective is to find W to make $E = 0$. Thus, the vector $\mathbf{W} - \mathbf{W}_0$ is taken along the gradient direction (but in the negative direction):

$$(\mathbf{W} - \mathbf{W}_0) = -\lambda \mathbf{G}_0 \quad (8)$$

The step magnitude λ is then calculated from

$$E = E_0 + \mathbf{G}_0^T (-\lambda \mathbf{G}_0) = 0 \quad \rightarrow \quad \lambda = \frac{E_0}{\mathbf{G}_0^T \mathbf{G}_0} \quad (9)$$

giving a new W as

$$\mathbf{W} = \mathbf{W}_0 - \frac{E_0}{\mathbf{G}_0^T \mathbf{G}_0} \mathbf{G}_0 \quad (10)$$

Eq.(10) can be used to implement an iterative process which, however, may not converge. The process can be stopped when the new calculated error is greater than the previous one. To improve convergence, it is sometimes useful to advance only a fraction of λ .

B. Search for weights W trying to zero out the gradient G

A zero gradient is associated with a minimum value of the error E . Since, in general, the network predictions will not all agree exactly with the input data, searching for a minimum error is better than searching for $E = 0$. In this case, the gradient G is expressed as a linear function around the gradient G_0 evaluated for the weights W_0 ,

$$\mathbf{G} = \mathbf{G}_0 + \mathbf{H}_0 (\mathbf{W} - \mathbf{W}_0) \quad (11)$$

in which \mathbf{H}_0 is now the Hessian matrix

$$H_{0_{ij}} = \left(\frac{\partial^2 E}{\partial W_i \partial W_j} \right)_{W_0} \quad (12)$$

The search is now for a new vector $W - W_0$, also in the gradient direction, with the objective of achieving $G = 0$. Thus,

$$(\mathbf{W} - \mathbf{W}_0) = -\lambda \mathbf{G}_0 \quad (13)$$

The step magnitude λ is now obtained from

$$\lambda = \frac{\mathbf{G}_0^T \mathbf{G}_0}{\mathbf{G}_0^T \mathbf{H}_0 \mathbf{G}_0} \quad (14)$$

giving a new W as

$$\mathbf{W} = \mathbf{W}_0 - \frac{\mathbf{G}_0^T \mathbf{G}_0}{\mathbf{G}_0^T \mathbf{H}_0 \mathbf{G}_0} \mathbf{G}_0 \quad (15)$$

Eq.(15) can also be used to implement an iterative process, and convergence is improved if only a fraction of the step λ is applied. As a simplification, the full Hessian matrix can be replaced by using only its diagonal terms.

C. Combination of optimization approaches

The gradient-free search OPT described in 4.2 can be utilized to obtain a first solution for the optimum weights W . This approach can be subsequently combined with either the strategy described in a) or b), in an attempt to improve the optimization results. This can be done after each of the $NREP$ repetitions of OPT.

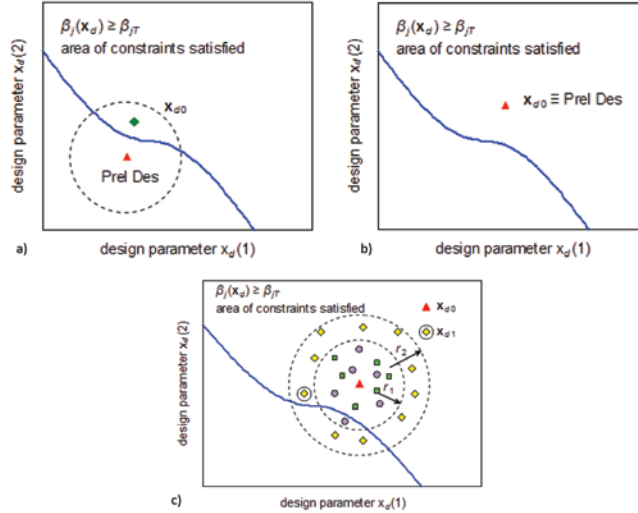
The components of the gradient or of the Hessian matrix are calculated numerically.

4. SEARCH-BASED OPTIMIZATION FOR THE DESIGN PARAMETERS

The optimization process OPT described in 4.2 for the training of neural networks can also be adapted to the problem of determining optimum design parameters, minimizing the total cost and satisfying the required minimum reliability constraints. Thus, the numerical procedure follows the steps represented in Figure 2.

The starting point or anchor, \mathbf{x}_{d0} , is the result of a preliminary design for the structure. This first step normally utilizes deterministic, simpler methods and may follow capacity design guidelines specified in the Codes. For this preliminary choice of the design parameters, the neural networks for the reliability indices are used to estimate the achieved levels $\beta_j(\mathbf{x}_{d0})$ and, using Eq.(1), the total cost $C(\mathbf{x}_{d0})$, Figure 2(a). This Figure shows, as a schematic illustration, the case of just two design parameters, $x_d(1)$ and $x_d(2)$, which could

Figure 2. Schematic for the design parameters' optimization process



either satisfy the reliability constraints or not. Should the preliminary design parameters \mathbf{x}_{d0} not satisfy the reliability constraints, a search is made according to the following steps, Figure 2(b), until one combination \mathbf{x}_d is found satisfying the constraints. This combination is then taken as the initial anchor.

Next, n combinations of \mathbf{x}_d are chosen randomly in the neighborhood of \mathbf{x}_{d0} , Figure 2(c), choosing each of the design parameters, x_{di} , within the interval $x_{d0i} \pm r_1 x_{d0i}$ (initially $r_1 = 0.1$). The reliability constraints are verified for each combination, choosing a new combination if the constraints are not satisfied. The total cost is calculated for the n combinations, keeping the one corresponding to the lowest cost. If this cost is lower than the one corresponding to the anchor, then the corresponding combination becomes the new anchor and the process is re-initiated. The work for this Chapter used $n = 100$.

If none of the n combinations leads to a cost lower than the one corresponding to the anchor, the search is densified by choosing more combinations within the interval, until one is found leading to a lower cost. The work for this chapter restricted the number of combinations to a maximum of $n = 500$.

If still no combinations are found leading to a cost lower than that for the anchor, the search factor radius r_1 is amplified to $r_2 = r_1 + \Delta r$, with $\Delta r = 0.3$ used in this work. A number m of combinations \mathbf{x}_d is chosen within the amplified search volume, satisfying the reliability constraints, and maintaining the same density as in the previous search domain corresponding to the radio r_1 . Of the m combinations (maximum of 2000), the first that is associated with a cost lower than that for the anchor is retained and used as the new anchor. This sequence is repeated three times in order to reduce the possibility of encountering a local minimum.

The search process is stopped when no combination is found, satisfying the constraints, with a cost lower than for the anchor.

5. OBJECTIVE FUNCTION: THE TOTAL COST

Costs associated with the occurrence of earthquakes and associated damage have been discussed by Lagaros et al. (2010). Here, the total cost $C(\mathbf{x}_d)$ in Eq.(1) includes the initial construction cost

$C_0(\mathbf{x}_d)$ and the damage repair cost $C_d(\mathbf{x}_d)$, assuming that the structure will be completely repaired after each earthquake that could occur during the service life.

5.1 Initial Cost

For a reinforced concrete structure, the initial cost is determined as a function of the concrete volumes V and steel weights W in beams and columns, and the unit costs of these items. Thus, if CUC is the unit cost for concrete, and CUS is the corresponding cost for steel,

$$C_0(\mathbf{x}_d) = [V_{c,beam}(\mathbf{x}_d) + V_{c,col}(\mathbf{x}_d)] CUC + [W_{s,beam}(\mathbf{x}_d) + W_{s,col}(\mathbf{x}_d)] CUS \quad (16)$$

The concrete volume and steel weight are functions of the design parameters \mathbf{x}_d . The unit costs should include not only those for materials but also for forming and labor. For the first application example in this Chapter, unit costs of 1500 \$/ m^3 and 500 \$/ KN have been used respectively, for concrete and steel.

5.2 Repair Costs

The repair costs, converted to present values, depend on the level of damage inflicted during the earthquakes, the uncertainty as to when these will occur and the number of earthquakes occurring during the life time T_D , and the interest rate to be applied to repair funds accumulated from the time of construction.

The nonlinear dynamic analysis should include a parallel calculation of the damage accumulated during the shaking. The analysis software used for the first application in this Chapter (Möller, 2001; Möller and Foschi, 2003) quantifies the global structural damage by means of an index $DIES$. If $C_f(DIES)$ is the function used to estimate the cost of repairing a damage $DIES$, and assuming that

this damage occurs at a time t , the present value $C_{f0}(DIES)$ is given by

$$C_{f0}(DIES) = C_f(DIES) \exp(-r t) \quad (17)$$

in which r is the interest rate. The expected value of $C_{f0}(DIES)$ can be calculated once the probability density function (PDF) for the time t is known. For this, a Poisson arrival process is assumed, with mean arrival rate v . Thus, the PDF for the time t to the first earthquake event, t_1 , is

$$f_{t_1}(t) = v \exp(-v t) \quad (18)$$

which allows the calculation of the mean for the time t_1 as

$$\bar{t}_1 = \int_0^\infty t f_{t_1}(t) dt = \frac{1}{v} \quad (19)$$

The probability $P(t_2 > t)$ that the time to the second event, t_2 , be greater than a time t must consider two possibilities: either that there are no events before t or that there is only one. Thus,

$$P(t_2 > t) = \exp(-v t) + v t \exp(-v t) \quad (20)$$

from which the cumulative distribution $F_{t_2}(t)$ for t_2 , and its PDF $f_{t_2}(t)$ become

$$P(t_2 \leq t) = 1 - (1 + v t) \exp(-v t) = F_{t_2}(t) \rightarrow f_{t_2}(t) = v^2 t \exp(-v t) \quad (21)$$

The expected time to the second event is

$$\bar{t}_2 = \int_0^\infty t f_{t_2}(t) dt = \frac{2}{v} \quad (22)$$

A similar reasoning allows the determination of the PDF for the arrival time t_n of the n^{th} event, and its mean value:

$$f_{t_n}(t) = \frac{\nu^n t^{n-1}}{(n-1)!} \exp(-\nu t) \rightarrow \bar{t}_n = \int_0^\infty t f_{t_n}(t) dt = \frac{n}{\nu} \quad (23)$$

Under the assumption that the structure is fully repaired after each event, the total expected cost (at present values and conditional on the damage index $DIES$) becomes:

$$C_d|_{DIES} = C_1|_{DIES} + C_2|_{DIES} + \dots + C_n|_{DIES} \quad (24)$$

in which

$$\begin{aligned} C_1|_{DIES} &= \int_0^{T_D} C_{f0}(DIES) f_{t_1}(t) dt \\ C_2|_{DIES} &= \int_0^{T_D} C_{f0}(DIES) f_{t_2}(t) dt \\ &\vdots \\ C_n|_{DIES} &= \int_0^{T_D} C_{f0}(DIES) f_{t_n}(t) dt \end{aligned} \quad (25)$$

Introducing Eq.(17) and (23) into Eq.(24) the final expected cost $C_d|_{DIES}$, conditional on a damage level $DIES$, becomes

$$C_d|_{DIES} = C_f(DIES) \nu \sum_{i=0}^{n-1} \left[\frac{\nu^i}{i!} \int_0^{T_D} t^i \exp(-(r+\nu)t) dt \right] \quad (26)$$

Eq.(26) is still conditional on the number n of earthquakes during the service life T_D . This number is itself a random quantity and, assuming that it obeys a Poisson distribution, the probability of n events in T_D is

$$P(X_{T_D} = n) = \frac{(\nu T_D)^n}{n!} \exp(-\nu T_D) \quad (27)$$

Finally,

$$C_d|_{DIES} = \sum_{n=1}^{\infty} C_n(DIES) \nu \sum_{i=0}^{n-1} \left[\frac{\nu^i}{i!} \int_0^{T_D} t^i \exp(-(r+\nu)t) dt \right] \frac{(\nu T_D)^n}{n!} \exp(-\nu T_D) \quad (28)$$

In general, the costs C_n increase with n , but this is compensated by the diminishing probability of occurrence of an increasing number of n events in T_D . Thus, the outcome from Eq.(28) converges to a finite number as n is increased. In the application results in this Chapter, the summation in Eq.(28) was truncated when the relative contribution of the last term was less than 0.001.

The function relating the cost C_f to the damage index $DIES$ (which ranges between 0 and 1) was assumed to be of the form

$$\begin{aligned} C_f(DIES) &= \alpha C_0 \left(\frac{DIES}{0.60} \right)^b && \text{for } DIES \leq 0.60 \\ C_f(DIES) &= \alpha C_0 && \text{when } DIES > 0.60 \end{aligned} \quad (29)$$

in which C_0 is the total replacement cost and the coefficient $\alpha = 1.20$ is assumed to contemplate extra costs for demolition and cleanup. Eq.(29) further assumes that complete replacement would be required should the damage index exceed a value $DIES_{\text{LIM}} = 0.60$. The exponent b needs to be set by calibration to practical experience, and in the applications in this Chapter has been assumed to be $b = 1$.

Finally, the total expected repair cost must consider the PDF for the damage index $DIES$,

$$C_d(\mathbf{x}_d) = \int_0^{\infty} C_d|_{DIES} \cdot f_{DIES}(DIES) \cdot d(DIES) \quad (30)$$

The PDF $f_{DIES}(DIES)$ in Eq.(30) is calculated by obtaining first, and then differentiating, the cumulative distribution of $DIES$, using simulation and the neural networks for the response $DIES$. This is represented by a Beta distribution, given that the damage index is bounded by 0 and 1.

In general, an earthquake does result in additional costs beyond those limited to the structure: losses associated with contents or non-structural components, cost for interruption of service, insurance and losses for injury or casualties. These additional costs can be taken into account within the format proposed here, but have not been considered in the applications shown next in this Chapter.

6. APPLICATION EXAMPLE1: OPTIMIZATION OF A SIMPLE PORTAL FRAME

6. 1 Random Variables, Response Databases, and Neural Network Representations

The structure chosen for this application example is a simple reinforced concrete portal frame, shown in Figure 3.

The main input variables for the determination of the response databases are shown in Table 1 with their corresponding bounds.

Within the bounds, 450 variable combinations were generated by experimental design (Zhang, 2003). For each combination, 10 sub-combinations were generated for the following secondary variables: (a) a set of random phase angles to generate an artificial earthquake record (Möller, 2001; Shinozuka, 1967), with the resulting record then scaled to the peak acceleration a_G included in the particular combination; and (b) the concrete and steel strength as they affect the variability in the parameters for the hysteretic relationship moment-curvature for beam and columns cross-sections (Möller et al., 2006).

The nonlinear dynamic analysis was then carried out for each of the combinations and for each sub-combination, obtaining a database for the following response parameters:

- **UMAX:** The maximum displacement at the top of the portal
- **DIST:** The maximum inter-story drift
- **DILO:** A maximum local damage index
- **DIES:** A maximum global damage index

Thus, to each of the response results R_i ($i = 1, 450$) obtained for the 450 combinations, corresponded $NS = 10$ results R_{ki} ($k = 1, 10$) for the set of sub-combinations. These results can be used to obtain the mean and the standard deviation of each R_i over the set of secondary variables (different earthquake records and hysteretic properties):

$$\bar{R}_i = \frac{1}{NS} \sum_{k=1}^{NS} R_{ki} \quad \sigma_{R_i} = \sqrt{\frac{1}{NS-1} \sum_{k=1}^{NS} (R_{ki} - \bar{R}_i)^2} \quad (31)$$

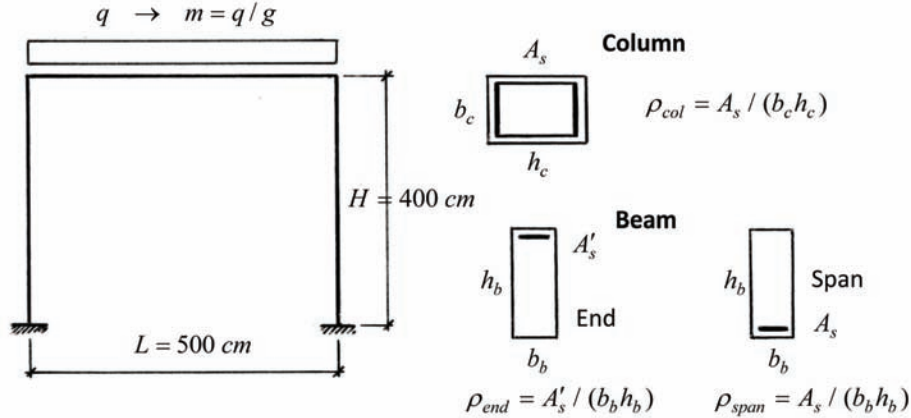
The data for these statistics form two databases, each with $NP = 450$ entries. Both databases are represented by neural networks with the main variables as input.

The training of the networks used the OPT algorithm, with a subsequent attempt to improve the solution by using a gradient-based approach as described in Section 4.3. This additional step only produced a small improvement in the results. The agreement between the data T and the neural network outputs Y , are shown in Figure 4 for the response $DIST$ as a typical case. To quantify the goodness of the regression, the linear correlation coefficient ρ_{YT} is calculated,

$$\rho_{YT} = \frac{\sigma_{YT}}{\sigma_Y \sigma_T} \quad \text{where} \quad \sigma_{YT} = \frac{1}{NP-1} \sum_{k=1}^{NP} (Y_k - \bar{Y})(T_k - \bar{T}) \quad (32)$$

The results in Figure 4 show a very good agreement and a correlation coefficient very close

Figure 3. Portal frame



to unity. Nevertheless, the lack of fit between the approximation $F(\mathbf{X})$ and the actual data $R(\mathbf{X})$ can be quantified by calculating the standard deviation of the relative error,

$$\sigma_{\varepsilon_r} = \sqrt{\frac{1}{NP-1} \sum_{k=1}^{NP} \left(\frac{Y_k - T_k}{Y_k} \right)^2} \quad (33)$$

in which Y_k is the value calculated by the network, T_k is the target data from the nonlinear dynamic analysis and $NP = 450$, the size of the database.

The neural network predictions can then be corrected to account for the lack of fit, as follows:

$$\bar{F}_i = \bar{Y}_i (1 + \sigma_{\varepsilon_m} X_{N_1}) \quad \sigma_{F_i} = \sigma_{Y_i} (1 + \sigma_{\varepsilon\sigma} X_{N_2}) \quad (34)$$

in which \bar{Y}_i , σ_{Y_i} are, respectively, the mean value and the standard deviation calculated with the corresponding neural network, and $\sigma_{\varepsilon m}$, $\sigma_{\varepsilon\sigma}$ are the corresponding standard deviations of the relative errors. X_{N_1} , X_{N_2} are two additional random variables associated with the fit error and assumed to be Standard Normals.

6.2 Performance Functions and Neural Networks for Reliability Estimates

The performance function G_i for the i^{th} -limit state can be written, in general, as

$$G_i(\mathbf{X}) = RLIM_i - R_i(\mathbf{X}) \cong RLIM_i - F_i(\mathbf{X}) \quad (35)$$

Eqs.(36) through (43) show the performance functions for the maximum relevant response parameter and for three performance levels: operational, life safety and collapse. Each of the capacity terms in these functions show, in parentheses, the mean and the coefficient of variation ($RLIM$, $CovRL$). In G_{11} , \bar{u}_y indicates the mean yield displacement for the frame, below which the structure remains elastic.

Operational:

- Elastic displacement limit
 $G_{11}(\mathbf{X}) = (\bar{u}_y, 0.10) - UMAX(\mathbf{X}) \quad (36)$

Table 1. Application 1, main random variables, and definitions

Variable	Lower bound	Upper bound	Definition
$X(1) = m \text{ (KN s}^2 / \text{cm}^2)$	2.15×10^{-4}	7.14×10^{-4}	Applied mass per unit length
$X(2) = b_b \text{ (cm)}$	15	30	Width of the beam cross-section
$X(3) = h_b \text{ (cm)}$	40	70	Height of the beam cross-section
$X(4) = b_c \text{ (cm)}$	20	40	Width of the column cross-section
$X(5) = h_c \text{ (cm)}$	40	100	Depth of the column cross-section
$X(6) = \rho_{span}$	0.00298	0.01389	Steel reinforcement ratio, beam span
$X(7) = \rho_{end}$	0.00298	0.01389	Steel reinforcement ratio, over beam support
$X(8) = \rho_{col}$	0.008	0.04286	Steel reinforcement ratio, columns
$X(9) = f_r / f'_{c0}$	0	0.15	Normalized concrete confinement pressure
$X(10) = a_g \text{ (cm / s}^2)$	25	1200	Ground peak acceleration
$X(11) = f_g \text{ (Hz)}$	2	3	Soil central frequency

- Interstory drift $G_{12}(\mathbf{X}) = (0.005, 0.10) - DIST(\mathbf{X})$ (37)

Life safety:

- Interstory drift $G_{21}(\mathbf{X}) = (0.015, 0.10) - DIST(\mathbf{X})$ (38)
- Maximum local damage index $G_{22}(\mathbf{X}) = (0.60, 0.10) - DILO(\mathbf{X})$ (39)
- Maximum global damage index $G_{23}(\mathbf{X}) = (0.40, 0.10) - DIES(\mathbf{X})$ (40)

Collapse:

- Interstory drift $G_{31}(\mathbf{X}) = (0.025, 0.10) - DIST(\mathbf{X})$ (41)
- Maximum local damage index $G_{32}(\mathbf{X}) = (1.00, 0.10) - DILO(\mathbf{X})$ (42)
- Maximum global damage index $G_{33}(\mathbf{X}) = (0.80, 0.10) - DIES(\mathbf{X})$ (43)

In these performance functions, each response demand $F(\mathbf{X})$ is a function of the main random variables \mathbf{X} , and is represented with a lognormal

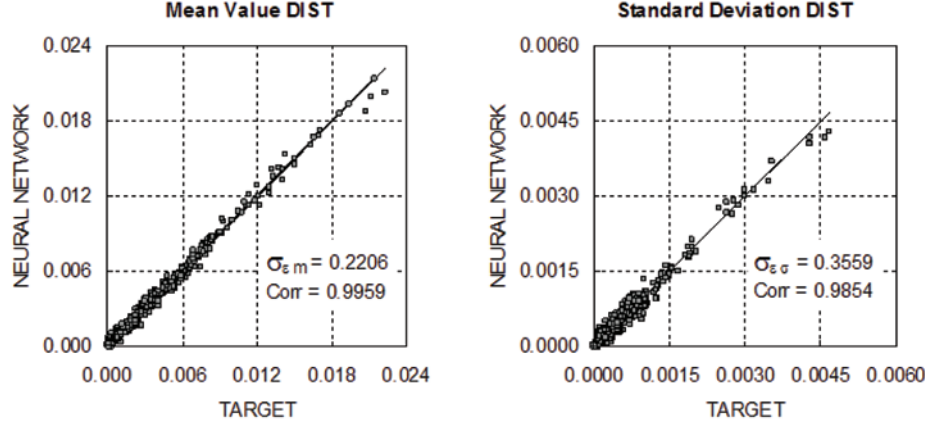
distribution over the sub-combinations. Thus, in general,

$$F(\mathbf{X}) = \frac{\bar{F}(\mathbf{X})}{\sqrt{1 + (\frac{\sigma_F(\mathbf{X})}{\bar{F}(\mathbf{X})})^2}} \exp \left[R_{N_1} \sqrt{\ln(1 + (\frac{\sigma_F(\mathbf{X})}{\bar{F}(\mathbf{X})})^2)} \right] \quad (44)$$

in which R_{N_1} is a Standard Normal variable that introduces the variability over the sub-combinations. $\bar{F}(\mathbf{X})$ and $\sigma_F(\mathbf{X})$ are, respectively, the mean and the standard deviation of the response calculated from the corresponding neural networks, using Eq.(34) to account for the regression error. Eq. (44) is applied to each response, for example, whether $F(\mathbf{X})$ is the maximum displacement $UMAX(\mathbf{X})$ or the maximum interstory drift $DIST(\mathbf{X})$.

Since the damage indices $DILO(\mathbf{X})$ and $DIES(\mathbf{X})$ are limited between 0 and 1, the $F(\mathbf{X})$ in these cases are represented by Beta distributions with the same limits, with the mean $\bar{F}(\mathbf{X})$ and standard deviation $\sigma_F(\mathbf{X})$. These, in turn, are

Figure 4. Neural networks agreement for the response DIST



obtained from the corresponding neural networks. The Beta distribution for each of the damage indices requires the introduction of an additional random variable, U_1 , uniformly distributed between 0 and 1.

The uncertainty in each of the capacities $RLIM$ is modeled with a normal distribution, introducing an additional Standard Normal variable $X_{N,3}$:

$$RLIM = \overline{RLIM} (1. + COVRL X_{N,3}) \quad (45)$$

A summary of the random variables, with their distribution types and parameters, is shown in Table 2. The statistics for the peak ground accelerations a_G correspond to the seismicity for the city of Mendoza, Argentina, as provided by INPRES (1995).

Table 2. Random variables

Variable	\bar{X}	σ_X	Type	Variable	\bar{X}	σ_X	Type
$X(1) = m$	5.1×10^{-4}	5.1×10^{-5}	Normal	$X(10) = \bar{a}_G$	94 cm/s^2	130 cm/s^2	Lognormal
$X(2) = b_b$	20 cm	1 cm	Normal	$X(11) = f_g$	2.50 Hz	0.375 Hz	Normal
$X(3) = h_b$? cm	$0.05 \bar{X}$	Normal	$X(12) = \sigma_{\bar{a}_G}$	0	0.25	Normal
$X(4) = b_c$	30 cm	1.5 cm	Normal	$X(13) = a_G$	$X(13) = X(10) [1.0 + X(12)]$		
$X(5) = h_c$? cm	$0.05 \bar{X}$	Normal	$X(14) = R_{N,1}$	0	1	Normal
$X(6) = \rho_{span}$?	$0.10 \bar{X}$	Lognormal	$X(15) = U_1$	0	1	Uniform
$X(7) = \rho_{end}$?	$0.10 \bar{X}$	Lognormal	$X(16) = X_{N,1}$	0	1	Normal
$X(8) = \rho_{col}$?	$0.10 \bar{X}$	Lognormal	$X(17) = X_{N,2}$	0	1	Normal
$X(9) = f_r / f'_{c0}$	0.10	0.01	Normal	$X(18) = X_{N,3}$	0	1	Normal

Each of the question marks (?) in this Table indicates an optimization design parameter (the mean values for the depth of the beams and columns, and for the longitudinal steel reinforcement ratios).

The reliability assigned to each performance level corresponds to a series system reliability for all the performance functions G included in that performance. Thus, the reliability for collapse corresponds to that of a series system consisting of the three limit states given by Eqs.(41) through (43).

Databases for achieved reliabilities are developed, as described, as a function of the design parameters, utilizing the performance functions and the response neural networks. These databases are themselves represented by neural networks, permitting the efficient estimation of reliabilities achieved for any choice of input design parameters (within their bounds). The databases included data from 180 design parameter combinations. Neural network agreement with the input data is shown in Figure 5 for the reliability indices β_1 , β_2 , β_3 corresponding to the three performance levels.

The dispersion or lack of agreement error is represented by a normal distribution following the same approach as described for Eq.(34). Figure 5 shows the very good approximation of the reliability data by means of the trained neural networks.

6.3 Preliminary Design: Initial Values for the Design Parameters

The preliminary design for the portal frame was achieved according to the procedure described by Rubinstein et al. (2006), followed by application of the capacity design guidelines specified in the Argentine norms INPRES-CIRSOC 103, Parte II (2005). The results of this preliminary calculation are shown in Table 3, and provide the first anchor combination \mathbf{x}_{d0} for the optimization.

The design parameters satisfy additional constraints to provide adequate resistance to the gravitational loads on the top beam. Thus, following Argentina's norm requirements,

$$\rho_{span} + \rho_{end} \geq \frac{1.4 q l_b^2}{6.48 b_b h_b^2 f_y} \quad (46)$$

Furthermore, to ensure a minimum ductility in the beam cross-sections, the steel reinforcement ratios satisfy

$$0.5 \rho_{end} \leq \rho_{span} \leq 2 \rho_{end} \quad (47)$$

Figure 5. Neural network agreement with data for the reliability indices β_1 , β_2 , β_3

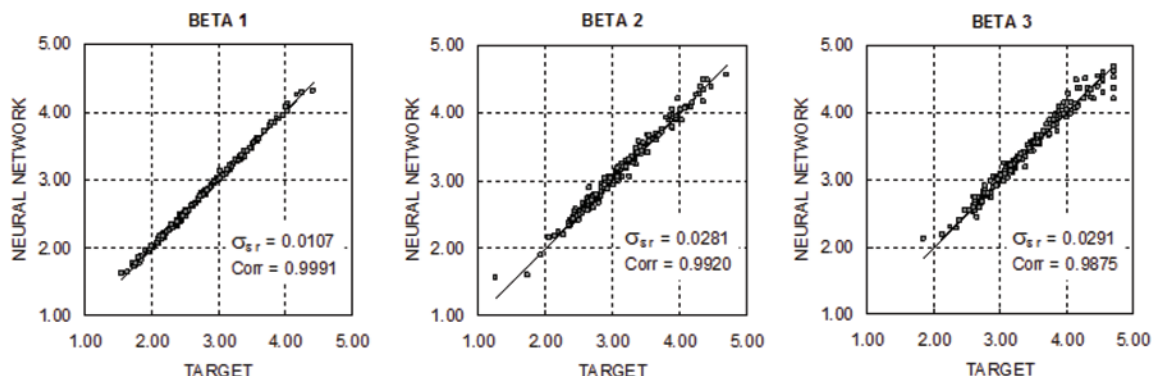


Table 3. Initial values for the design parameters

Design parameter	Initial value
$x_d(1) = \bar{X}(3) = h_b$ [cm]	50
$x_d(2) = \bar{X}(5) = h_c$ [cm]	45
$x_d(3) = \bar{X}(6) = \rho_{span}$	0.00804
$x_d(4) = \bar{X}(7) = \rho_{end}$	0.01143
$x_d(5) = \bar{X}(8) = \rho_{col}$	0.03148

6.4 Optimization Constraints: Minimum Reliability Levels

Minimum target reliabilities for each performance level are specified in terms of tolerable annual probabilities of non-performance, Pf_{annual} . Using a Poisson arrival process, with a mean arrival rate ν , the exceedence probability Pf_{annual} can be converted to a probability of non-performance P_f for the earthquake event, and finally expressed as a target event reliability index β :

$$Pf_{annual} = 1 - \exp[-\nu P_f] \rightarrow P_f \rightarrow \beta \cong -\Phi^{-1}(P_f) \quad (48)$$

A mean arrival rate $\nu = 0.20$, for earthquakes with magnitudes $M \geq 5$, was used for the city of Mendoza, Argentina. Table 4 shows annual and event target probabilities as recommended by Paulay and Priestley (1992). In this application, more stringent targets were also considered, as shown in Table 5, to evaluate the sensitivity of the optimization outcome to the levels used for the targets.

6.5 Optimization Results

The total cost and the reliability levels corresponding to the initial preliminary design are shown in

Table 6. It is seen that the reliability levels for this design already satisfy the minimum values shown in Tables 4 and 5. Starting from these preliminary parameters, the optimization process was applied, as described, using the target minimum reliabilities from Table 4 (Paulay y Priestley, 1992). The optimization took into account the bounds for the design parameters (minimum and maximum cross-sectional dimensions and steel reinforcement ratios) specified in Table 1 and used in the development of the response databases.

The final design parameters obtained are shown in Table 7, with the final total cost and the reliability levels achieved for each of the performance levels.

It is interesting to compare the optimum solutions obtained when the optimization is started from conditions other than the preliminary design. With this purpose, Table 8 shows five different initial combinations of design parameters, two of them “over-dimensioned in comparison to the preliminary design” and two “under-dimensioned”.

The evolution of the total cost during the optimization, in terms of the number of steps, is shown in Figure 6. Each step corresponds to one evaluation of total cost with all reliability constraints being satisfied. This figure shows that the optimization converges to approximately the same final total cost, regardless of the choice for the initial design parameters. Those corresponding to the preliminary design provide a cost solution which is already quite close to the optimum, showing the adequacy of the methodology employed for the preliminary estimation.

When the optimization starts from an under-designed combination, the first cost that is calculated is controlled by the requirement to satisfy the reliability constraints. It can be observed in Figure 6 that the number of steps needed to achieve the optimal solution varies, implying a varying number of anchor combinations and process repetitions. In each case, no lower total cost was found when the optimization search radius r_i was

Table 4. Target minimum reliability levels (Paulay and Priestley, 1992)

Performance level	Pf_{annual}	β_{annual}	Pf	β
Operational	2×10^{-2}	2.054	0.10101×10^0	1.276
Life safety	2×10^{-3}	2.878	0.10010×10^{-1}	2.326
Collapse	2×10^{-4}	3.540	0.10001×10^{-2}	3.090

Table 5. Target minimum reliability levels proposed

Performance level	Pf_{annual}	β_{annual}	Pf	β
Operational	1×10^{-2}	2.326	0.50252×10^{-1}	1.642
Life safety	1×10^{-3}	3.090	0.50025×10^{-2}	2.576
Collapse	1×10^{-4}	3.719	0.50003×10^{-3}	3.291

expanded, indicating that at least a local minimum had been found.

The different initial conditions lead eventually to essentially the same optimum total cost, but the solutions contain different optimal combinations of the individual parameters. This implies that the cost function may have different local minima, but that in this case these minima are approximately of the same magnitude, with the largest difference in total cost being only of the order of 2.1%. However, the difference in the column steel reinforcement ratio, for example, between using initially either the preliminary design or the Under-design 1, is closer to 81%. The final optimum results are shown in Table 9. It should be emphasized that all these different solutions satisfy the minimum reliability constraints, and that Table 9 implies a trade-off between the optimal depth of the beam, for example, and the optimal amount of steel used. If the constraints had been formulated in terms of specified narrow reliability intervals, rather than just only minima, the number of optimum design possibilities would have been correspondingly narrowed.

6.6 Optimization Sensitivity to Specified Minimum Target Reliabilities

In this section we discuss the influence that the definition of the minimum reliability constraints may have in the optimum solution. Figure 7 shows the evolution of the total cost either for the target reliabilities (β) in Table 4 (Paulay and Priestley, 1992) or for those proposed in Table 5. In both cases the starting configuration is the preliminary design. Figure 8 shows higher total costs as a result of imposing higher target reliability constraints, as expected.

At the optimum solution, the constraints for the different performance levels are met but not to the same degree. For example, for the minimum targets in Table 4, $\beta_1 = 1.276$, $\beta_2 = 2.326$ and $\beta_3 = 3.090$, the final (optimum) reliability levels in Table 7 show $\beta_1 = 1.697$, $\beta_2 = 2.422$ and $\beta_3 = 3.102$. Thus, the constraint is just met for the collapse performance level, and satisfied with a greater margin for performance levels 1 and 2.

Similar results are obtained using the proposed target reliabilities from Table 5 ($\beta_1 = 1.642$, $\beta_2 = 2.576$ and $\beta_3 = 3.291$). In this case, the reliability levels achieved at the optimum solution are $\beta_1 = 1.691$, $\beta_2 = 2.749$ and $\beta_3 = 3.296$.

Table 6. Initial costs and reliabilities, preliminary design

	Costs [\$]	Performance level	β
Initial $C_0(\mathbf{x}_d)$	2839	Operational	1.837
Repair $C_d(\mathbf{x}_d)$	1113	Life safety	2.846
Total	3952	Collapse	3.489

We analyze now the effect of changing the more significant constraints, 2 and 3, using as a base the minimum targets specified in Table 4. Thus, β_2 and β_3 are each individually changed by $\pm 10\%$, with the corresponding results shown in Figure 8.

When β_2 is decreased by 10%, the results are identical to those shown in Figure 7, since constraint 2 is more easily met and constraint 3 remains the determinant one. On the other hand, if β_2 is increased by 10%, constraints 2 and 3 now become jointly important, leading to different combinations of the design parameters but still with similar minimum total cost.

If the target β_3 is increased by 10%, the total cost for the optimum solution also increases as constraint 3 was already the most important. On the other hand, if β_3 is decreased by 10%, constraints 2 and 3 now have a similar influence, resulting again in a similar minimum total cost but with a different combination of design parameters.

6.6 Optimization Sensitivity to the Assumed Damage-Cost Relationship

Finally we consider the effect on the optimization of the form used for the cost-damage relationship (Eq.(29)). While maintaining $b=1$, the relationship is modified by changing the level of damage index $DIES_{LIMIT}$ at which the structure is considered to be destroyed and needs to be replaced. Thus, from the value assumed for the base results, $DIES_{LIMIT}=0.6$, two different possibilities were considered: 0.4 or 0.8. In the first, the cost increases more rapidly as a function of damage, while the reverse occurs in the second case. The results are shown in Figure 9, with corresponding differences of 15% and -7% with respect to the minimum total cost for the base relationship. However, the optimum values for the design parameters remain unaffected.

Table 7. Optimum results starting from the preliminary design

Design parameter	Optimal value		Costs [\$]	Performance level	β
$x_d(1) = \bar{X}(3) = h_b [cm]$	57.0	Initial $C_0(\mathbf{x}_d)$	2601	Operational	1.697
$x_d(2) = \bar{X}(5) = h_c [cm]$	40.3	Repair $C_d(\mathbf{x}_d)$	1020	Life safety	2.422
$x_d(3) = \bar{X}(6) = \rho_{span}$	0.00617	Total	3621	Collapse	3.102
$x_d(4) = \bar{X}(7) = \rho_{end}$	0.01028				
$x_d(5) = \bar{X}(8) = \rho_{col}$	0.02130				

Table 8. Different combinations of initial design parameters

Design parameter	Preliminary design	Over design 1	Over design 2	Under design 1	Under design 2
$x_d(1) = \bar{X}(3) = h_b [cm]$	50	60	65	45	45
$x_d(2) = \bar{X}(5) = h_c [cm]$	45	80	60	45	45
$x_d(3) = \bar{X}(6) = \rho_{spam}$	0.00804	0.01100	0.01300	0.00600	0.00390
$x_d(4) = \bar{X}(7) = \rho_{end}$	0.01143	0.01222	0.01011	0.00600	0.00390
$x_d(5) = \bar{X}(8) = \rho_{col}$	0.03148	0.03950	0.03950	0.00950	0.00890

7. APPLICATION EXAMPLE 2: OPTIMIZATION OF THE PILE-CAP MASS FOR A PILE FOUNDATION, AND SENSITIVITY TO THE ANALYSIS MODEL USED

The second application example illustrates the influence that the modeling approach may have in the optimization results. With this objective, Figure 10 shows a pile steel tube, of diameter D , wall thickness t and length L , supporting a pile-cap mass M . The pile is embedded into a sandy soil layer with relative density D_R . Under earthquake excitation, the mass will displace a maximum

amount Δ . The problem is the assessment of the probability that the displacement Δ (the response of interest) will exceed given levels, expressed as fractions of the pile diameter D . Furthermore, the mass M is to be optimized so that the probability of the displacement Δ exceeding a target be as specified.

The performance function G is defined as

$$G(X, d) = \lambda D - \Delta(a_G, \omega_s, T, M, D_R, r) \quad (49)$$

in which

Figure 6. Evolution of the total cost for different initial design parameters

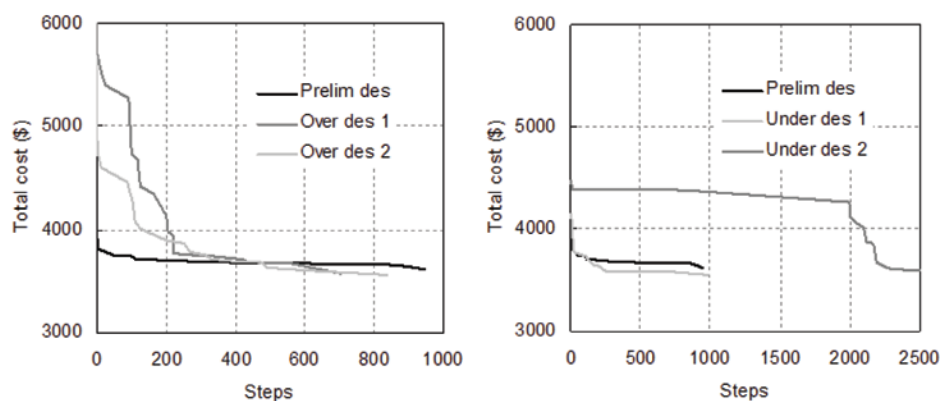


Table 9. Optimum results starting from different initial design parameters as per Table 8

Design parameter	Preliminary design	Over design 1	Over design 2	Under design 1	Under design 2
$x_d(1) = \bar{X}(3) = h_b [cm]$	57.0	58.4	56.5	53.6	58.0
$x_d(2) = \bar{X}(5) = h_c [cm]$	40.3	41.1	40.3	45.6	40.4
$x_d(3) = \bar{X}(6) = \rho_{span}$	0.00617	0.00586	0.00813	0.00711	0.00644
$x_d(4) = \bar{X}(7) = \rho_{end}$	0.01028	0.01122	0.01300	0.01303	0.01051
$x_d(5) = \bar{X}(8) = \rho_{col}$	0.02130	0.01672	0.01553	0.01152	0.01814
Initial cost $C_0(\mathbf{x}_d)$ [\$]	2601	2569	2559	2546	2568
Repair cost $C_d(\mathbf{x}_d)$ [\$]	1020	1008	1004	999	1007
Total cost [\$]	3621	3577	3563	3545	3575

λ = capacity factor, fraction of D defining the limit displacement;

a_g = peak ground acceleration;

ω_s = soil frequency in the Kanai-Tajimi Power Spectral Density function;

T = duration of the strong motion part of the accelerogram record;

M = applied mass;

D_R = soil relative density;

r = nominal variable representing the different ground motion records.

The pile is considered as an elasto-plastic beam on a nonlinear foundation. The pressure on the soil, $p(w)$, is a function of the displacement w which varies along the length L .

The structural analysis for the pile-cap displacement Δ can be done by considering the dynamic equilibrium of the mass M as a single degree of freedom system. Using a beam finite element model of the pile, the restoring hysteretic force $F(\Delta)$ can be calculated by integration of the reactions $p(w)$, after the deflected shape w is determined. The nonlinear, compression-only, soil reactions $p(w)$ take into account the development of gaps between the pile and the surrounding soil.

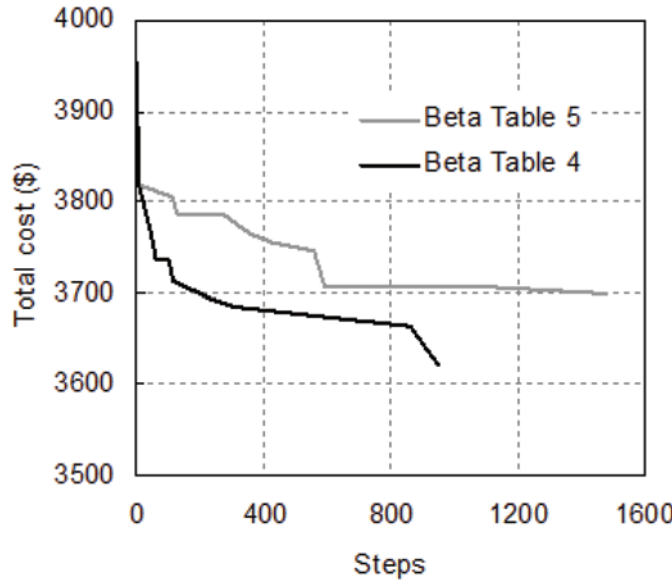
The resulting model, developed for the similar problem of a metal fastener in wood (Foschi, 2000) depends solely on mechanical properties of the pile and the soil, and produces the hysteretic loop for any input excitation, automatically developing the pinching and degradation characteristics. The $p(w)$ relationship used here was taken from Yan and Byrne (1992),

$$p(w) = \begin{cases} E_{\max} w & \text{if } w \leq \alpha^2 D \\ E_{\max} \alpha D \left(\frac{w}{d}\right)^{0.5} & \text{if } w > \alpha^2 D \end{cases} \quad (50)$$

in which $\alpha = 0.5 (D_R)^{0.8}$ and D_R is the soil relative density. The modulus E_{\max} depends on the specific weight of the soil and the depth of the soil layer and it is detailed by Yan and Byrne (1992). In this work only the relative density was considered to be a random variable.

The calculation of Δ can be integrated directly into the reliability calculation using the performance function in Eq.(49) or into the optimization for the mass M which can be sustained to match a prescribed reliability level. As a modeling alter-

Figure 7. Evolution of the total cost for different minimum target betas



native, a different formulation could be used in describing the hysteresis behavior. Thus, it could be matched to the response of the pile to a given cyclic displacement history for the pile-cap. This history, obtained by either experiments or by calculation, can then be fitted with a set of rules that permit the reproduction of the hysteresis observed for the specific cyclic displacements.

Many such set of rules are contained in dynamic analysis software packages. However, although a

good fit can be obtained for the cyclic response used for the matching, there is no guarantee that a similar good representation would be achieved when using the same fitted rules for any other cyclic history or earthquake record. Perhaps the most sophisticated of these calibrated approaches to hysteresis representation is to use cyclic data to determine parameters of a first-order differential equation, the solution of which, for a given history, can represent loops with pinching and degradation

Figure 8. Influence of β_2 and β_3 in the total cost

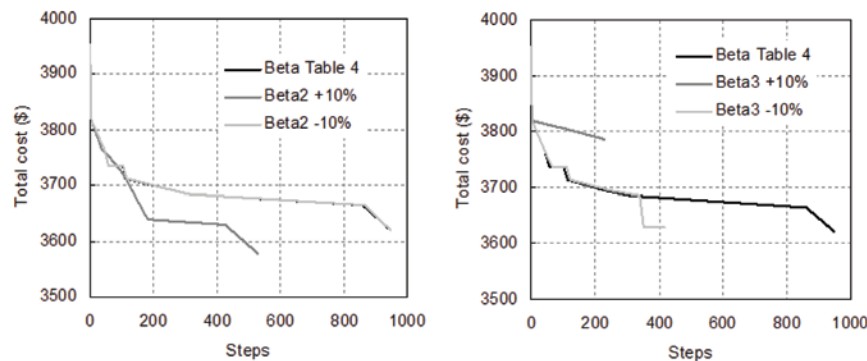
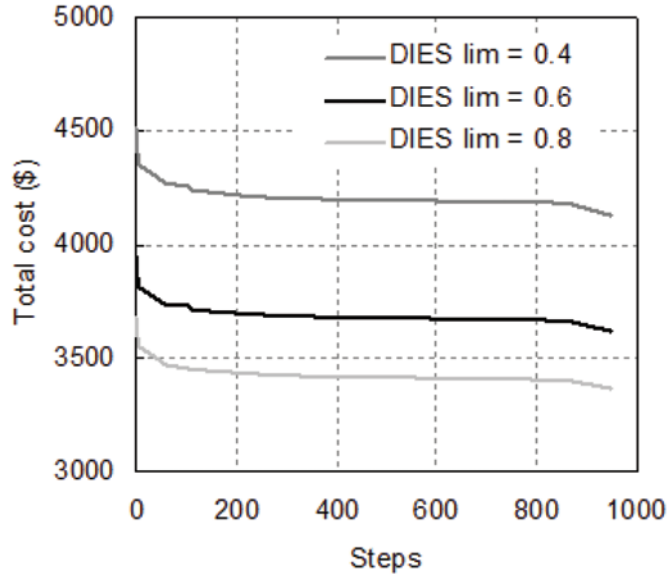


Figure 9. Influence of the cost-damage relationship used



characteristics. This model is commonly known as BWBN (Bouc, 1967; Baber et al., 1981, 1985).

The objective in this second application is a comparison of the influence that the two different hysteretic modeling techniques have in either reliability assessment or structural optimization.

The pile has a diameter $D = 0.356m$, with wall thickness $t = 0.10m$, and a length $L = 30m$. Yield strength and elastic modulus of the steel were assumed deterministic and to have nominal values (respectively, 250 Mpa and 200000 Mpa). Twenty earthquake records were simulated as stationary processes using a spectral representation based on the Clough-Penzien power spectrum density function (Clough and Penzien, 1975), an envelope modulation function (Amin and Ang, 1968), and twenty different sequences of random phase angles.

For different combinations of the intervening variables, databases were constructed for the mean response Δ and its standard deviation over the twenty records. These databases were then used to train corresponding neural networks, as

previously discussed. Finally, the response Δ in Eq.(49) was represented by using the lognormal format and the error representation as shown in Eqs.(44) and (34).

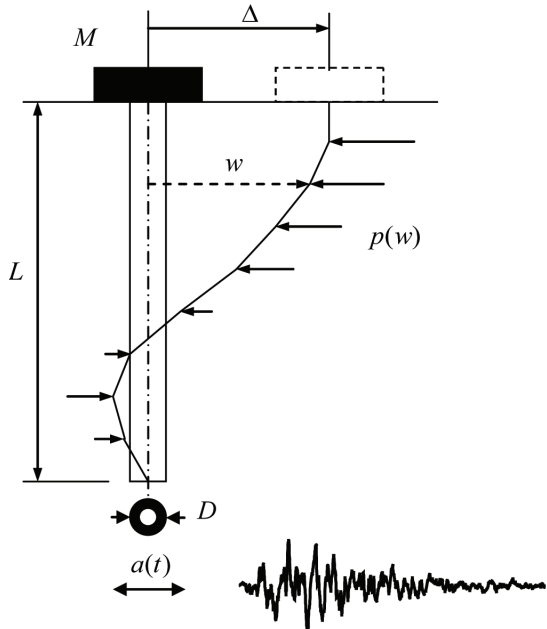
The pile was subjected to the displacement history $\Delta(t)$ in Figure 11. The finite element approach was used to calculate the hysteresis loop in Figure 12. This response was used to calibrate the parameters of a BWBN model, with the resulting loop shown in Figure 13.

Dynamic analyses for the different earthquake records were carried out with either the BWBN representation of the hysteretic restoring force or, alternatively, calculating each time the hysteresis via the finite-element model. In both cases, the neural network methodology previously described was applied.

Table 10 shows the statistical data assumed for the intervening variables, and Table 11 the reliability results obtained for different values of the capacity factor λ .

The parameters ω_s and T define, respectively, the Clough-Penzien power spectrum density func-

Figure 10. Pile foundation under earthquake excitation $a(t)$



tion and the duration T of the strong motion in the modulation function. The statistics for the peak ground acceleration a_G correspond to the event occurrence, and are consistent with a design acceleration (475 years return period) of $0.31g$, assuming that earthquakes have a Poisson arrival rate of 0.2 (one every five years).

Although the agreement between Figures 12 and 13 may be considered to be satisfactory, Table 11 shows that the calculated reliabilities, if not drastically different, clearly depend on the model used for the analysis.

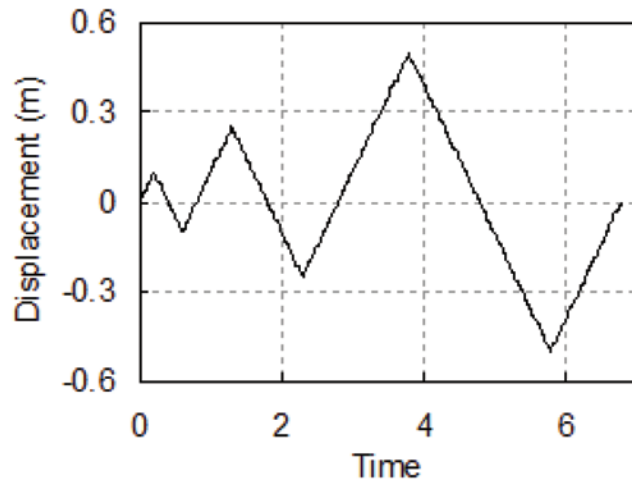
A similar conclusion may be reached if an optimization is carried out to determine the mass M that, optimally, will satisfy two performance criteria: a displacement associated with moderate damage level, with $\lambda = 0.40$, and another associated with more substantial damage, $\lambda = 1.0$. Target reliability levels are prescribed: $\beta = 2.5$ for the first criterion, and $\beta = 4.5$ for the second. The design

parameter is the mean value of the mass M , allowing for a coefficient of variation of 0.10. The results are shown in Table 12, comparing again results corresponding to the two approaches for analysis. It is seen that the model used has now a rather substantial effect on the optimal solution.

8. CONCLUSION

- This Chapter has considered different issues involved in performance-based design and optimization in earthquake engineering, using performance criteria specified in terms of displacements and damage. The study has led to a proposal for a systematic method of analysis, integrating the ground motion, a nonlinear dynamic analysis of the problem, neural network representation for the calculated responses and for the achieved reliabilities and, finally, a simple, search-based, optimization algorithm to minimize the total cost under minimum reliability constraints.
- Earthquake engineering design normally follows procedures and prescriptions given in Code guidelines. A design earthquake is used, which has been chosen with a relatively low probability of being exceeded (e.g., 0.02 in 50 years). The calculated structural responses for this earthquake are then modified by a set of coefficients which should be calibrated to lead to a desired performance reliability. For reinforced concrete structures, this preliminary design includes the determination of cross-sectional dimensions and steel reinforcements using a capacity design approach. The work presented in this Chapter considered the assessment of the reliability achieved for different performance criteria, and the possibility of optimizing the design in terms of the total cost, including construction and the repair of damage

Figure 11. Cyclic displacement history



caused by an uncertain number of earthquakes during the service life.

- The performance criteria must involve maximum structural displacement responses and the associated damage, the calculation of which requires a nonlinear dynamic analysis. This produces discrete values for the responses for different combinations of the intervening random variables. For reliability assessment and optimization, these discrete results must be represented

by continuous, smooth functions, and this Chapter has discussed the use of neural networks as an efficient approach to response representation.

- The random variables have been divided into two groups: a first set of main variables and a second set of secondary ones including those associated with the ground motion. An approach has been presented by means of which the analysis data are the mean and the standard deviation of

Figure 12. Loop for cyclic displacement history, finite element approach

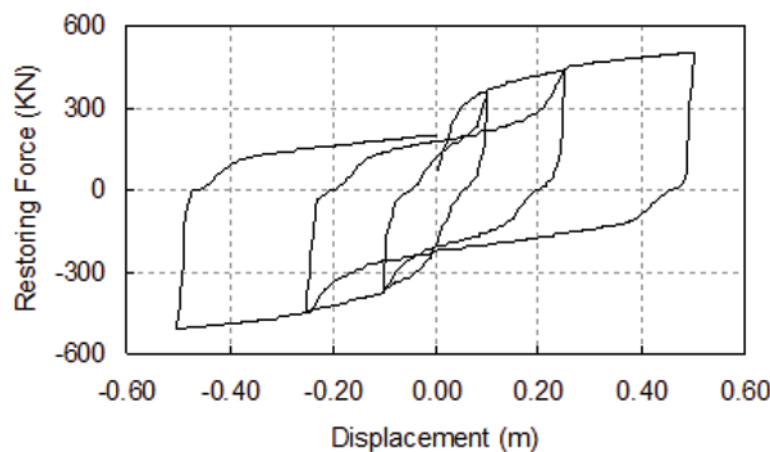
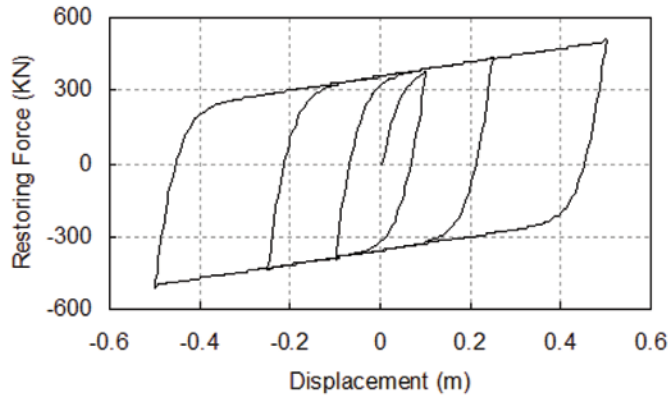


Figure 13. BWBN model regression for cyclic displacement history



the responses over the set of secondary variables. These means and standard deviations are then represented by neural networks with the main variables as the input. This approach facilitates the use of simulation in the estimation of the non-performance probabilities, at a great computational saving.

- The reliability indices β associated with the performance criteria are thus calculated in terms of the design parameters, and neural networks for the reliabilities are trained with those parameters as input.
- The design optimization is carried out for minimum total cost with minimum reliability constraints for each of the perfor-

mance criteria. The Chapter has described a search-based algorithm for the optimization, not requiring the calculation of gradients. The optimization requires initial values for the design parameters, and the work has considered initial values to be those from a preliminary design. Further, the Chapter considered the sensitivity of the optimal solution to the initial conditions, with the conclusion that the final result for total cost was essentially insensitive, but that the corresponding individual design parameters could be quite different.

Table 11. Reliability results and comparison between hysteretic representation approaches

Table 10. Statistical data for the intervening variables

Variable	Distribution	Mean	Standard Deviation
a_g (m/sec ²)	Lognormal	1.0	0.6
ω_s (rad/sec)	Normal	4π	π
T (sec)	Normal	12	2
M (kN·sec ² /m)	Normal	150	15
D_R	Normal	0.5	0.1

Limit displacement, capacity factor λ	Reliability index β	
	Hysteresis: Finite Element	Hysteresis: BWBN
0.1	-0.143	0.716
0.2	1.097	1.724
0.4	2.509	2.379
0.6	3.197	2.675
0.8	3.730	2.892
1.0	4.243	3.082

Table 12. Performance-based design

Hysteresis: Finite element			
Optimal Mean Mass (kN.sec ² /m)	Performing criterion λ	Target reliability β	Achieved reliability β
139.83	0.4	2.5	2.59
	1.0	4.5	4.51
Hysteresis: BWBN			
Optimal Mean Mass (kN.sec ² /m)	Performing criterion λ	Target reliability β	Achieved reliability β
102.19	0.4	2.5	2.76
	1.0	4.5	4.42

The optimization is then a problem which could admit multiple solutions. In practical terms, the design engineer has then the possibility of choosing from different alternatives, taking into account other practical requirements. It is also possible to add to the optimization additional constraints among the design parameters, orienting the optimum solution towards, for example, desired mechanisms for energy dissipation.

- Data are required on the relationship between a calculated damage and the corresponding repair cost. There is substantial uncertainty in this relationship, and the Chapter has also explored the sensitivity of the optimal solution to the form of the damage-cost function. For the first application example, it has been shown that there is a significant influence in the optimum minimum total cost, while the optimum design parameters are not affected. Further research is therefore needed to quantify the relationship, a task that must be guided by experiments and expert assessments.
- The Chapter has also explored the sensitivity of the optimal solution to the minimum target reliability levels prescribed for each performance criteria. In general, it can be concluded that the results show higher total costs as the minimum targets are increased. This is expected. However, since the de-

gree with which each minimum reliability constraint is met may vary, the relationship between the optimal solution and the prescribed targets is not simple. Increasing or decreasing a single target may affect the importance of another constraint, and the total cost for the optimal solution may or may not be affected.

- The assessment of reliability, and the optimization itself, are conditional on the quality of the response analysis model, particularly the quantification of the hysteretic energy dissipation during the shaking. In order to illustrate this influence, a second application example has been discussed involving the earthquake response of a steel pile foundation in a sandy soil. Two hysteretic representations are used: one implementing a calculation of the soil-structure interaction and the hysteretic force by means of a nonlinear finite element model; the other using a hysteresis model fitted to results from a cyclic displacement of the pile-cap. While the first model can self-adapt to different excitation histories or different earthquakes, the second approach can only be said to provide a good representation for the history to which it was fitted. The example considered the question of how significant is the influence of these different analyses on the reliability and optimization results. It was

concluded that indeed there is an influence, pointing to the use of an analysis as accurate as possible, or a careful evaluation of a model error to be used in conjunction with the approximate approach. This is contrary to the common assumption that structural or hysteretic modeling is not so important because any uncertainty associated with it is overwhelmed by the uncertainty in the ground motion.

- Sometimes it is proposed that reliability assessment in earthquake engineering should split the capacity from the hazard demand. Thus, in this alternate approach, the total probability of non-performance would be obtained by integrating the vulnerability, or probability of non-performance conditional on a hazard level, with the probability density for the hazard. This approach has not been considered in this Chapter because different vulnerabilities would have to be calculated each time that the design parameters are changed during the optimization process, with no savings in computational effort when compared to the approach proposed in this chapter.

ACKNOWLEDGMENT

This work was supported by grants from the Research Project “Diseño y optimización de estructuras bajo acciones dinámicas aleatorias”, IING 300, Universidad Nacional de Rosario, Argentina, and “Neural networks for reliability and performance-based design in earthquake engineering”, Natural Sciences and Engineering Research Council of Canada: RGPIN 5882-04, University of British Columbia, Vancouver, Canada.

REFERENCES

- Amin, M., & Ang, A. H.-S. (1968). Non-stationary stochastic models of earthquake motions. *Proceedings ASCE, Journal of Engineering Mechanics Division*, 94.
- Baber, T., & Noori, M. N. (1985). Random vibration of degrading, pinching systems. *Journal of Engineering Mechanics*, 111(8), 1010–1026. doi:10.1061/(ASCE)0733-9399(1985)111:8(1010)
- Baber, T., & Wen, Y. K. (1981). Random vibration of hysteretic degrading systems. *Journal of Engineering Mechanics*, 107(6), 1069–1089.
- Bouc, R. (1967). Forced vibration of mechanical systems with hysteresis. *Proceedings of the 4th Conference on Nonlinear Oscillations*, Prague, Czechoslovakia, Sept. 5-9.
- Clough, R. W., & Penzien, J. (1975). *Dynamics of structures*. McGraw-Hill.
- Foschi, R. O. (2000). Modeling the Hysteretic response of mechanical connectors for wood structures. *Proceedings, World Timber Engineering Conference*, Whistler, B.C.
- Hurtado, J. (2004). *Structural reliability – Statistical learning perspectives. Lecture Notes in Applied and Computational Mechanics*, 17. Springer Verlag.
- INPRES. (1995). *Microzonificación Sísmica del Gran Mendoza*. Instituto Nacional de Prevención Sísmica, Publicación Técnica N° 19.
- INPRES-CIRSOC 103. (1995). *Reglamento Argentino para construcciones sismorresistentes, Parte II: Construcciones de Hormigón Armado*, INTI.

- Lagaros, N. D., Naziris, I. A., & Papadrakakis, M. (2010). The influence of masonry infill walla in the Framework of the performance-based design. *Journal of Earthquake Engineering*, 14, 57–79. doi:10.1080/13632460902988976
- Möller, O. (2001). *Metodología para evaluación de la probabilidad de falla de estructuras sismorresistentes y calibración de códigos*. Tesis de Doctorado en Ingeniería, Universidad Nacional de Rosario.
- Möller, O., & Foschi, R. (2003). Reliability evaluation in seismic design: A response surface methodology. *Earthquake Spectra*, 19(3), 579–603. doi:10.1193/1.1598200
- Möller, O., Foschi, R., Quiroz, L., & Rubinstein, M. (2008). Optimización de pórticos con acciones sísmicas: diferentes estrategias numéricas utilizando redes neuronales. [AMCA.]. *Mecánica Computacional*, 28, 2583–2603.
- Möller, O., Foschi, R., Quiroz, L., & Rubinstein, M. (2009a). Performance-based seismic optimization implementing neural networks. In Frangopol, D. M. (Ed.), *Computational structural dynamics and earthquake engineering, structures and infrastructures series* (Vol. II, pp. 547–564). Taylor & Francis Group.
- Möller, O., Foschi, R., Quiroz, L., & Rubinstein, M. (2009c). Structural optimization for performance-based design in earthquake engineering: Applications of neural networks. *Structural Safety*, 31(6), 490–499. doi:10.1016/j.strusafe.2009.06.007
- Möller, O., Foschi, R., Rubinstein, M., & Quiroz, L. (2006). Momento-curvatura de secciones de hormigón armado sismorresistentes utilizando redes neuronales. [AMCA.]. *Mecánica Computacional*, 25, 2145–2162.
- Möller, O., Foschi, R., Rubinstein, M., & Quiroz, L. (2007). Optimización de pórticos sismorresistentes utilizando redes neuronales y algoritmo sin cálculo de gradientes. [AMCA.]. *Mecánica Computacional*, 26, 1824–1839.
- Möller, O., Foschi, R., Rubinstein, M., & Quiroz, L. (2009b). Seismic structural reliability using different nonlinear dynamic response surface approximations. *Structural Safety*, 31(5), 432–442. doi:10.1016/j.strusafe.2008.12.001
- Paulay, T., & Priestley, M. J. N. (1992). *Seismic design of reinforced concrete and masonry buildings*. John Wiley & Sons, Inc. doi:10.1002/9780470172841
- Pérez López, J. R. (2005). *Contribución a los métodos de optimización basados en procesos naturales y su aplicación a la medida de antenas en campo próximo*. Retrieved from <http://www.tesisenred.net/TDR-0305107-180847>
- Rubinstein, M., Giuliano, A., & Möller, O. (2006). Diseño preliminar de estructuras sismorresistentes: un tratamiento unificado de los efectos traslacionales y rotacionales. *Memorias XIX Jornadas Argentinas de Ingeniería Estructural*, 49.
- Shinozuka, M., & Sato, Y. (1967). Simulation of nonstationary random processes. *Journal of Engineering Mechanics*, 93(1), 11–40.
- Swisher, J. R., Hyden, P. D., Jacobson, S. H., & Schruben, L. W. (2000). A survey of simulation optimization techniques and procedures. In J. A. Jones, R. R. Barton, K. Kang, & P. A. Fishwick (Eds.), *2000 Winter Simulation Conference*.
- Yan, L., & Byrne, P. M. (1992). Lateral pile response to monotonic loads. *Canadian Geotechnical Journal*, 29, 955–970. doi:10.1139/t92-106
- Zhang, J. (2003). *Performance-based seismic design using designed experiments and neural networks*. PhD Thesis, Department of Civil Engineering, University of British Columbia, Canada.

Chapter 3

Discrete Variable Structural Optimization of Systems under Stochastic Earthquake Excitation

Héctor Jensen

Universidad Tecnica Federico Santa Maria, Chile

Marcos Valdebenito

Universidad Tecnica Federico Santa Maria, Chile

Juan Sepúlveda

Universidad Tecnica Federico Santa Maria, Chile

Luis Becerra

Universidad Tecnica Federico Santa Maria, Chile

ABSTRACT

The reliability-based design optimization of structural systems under stochastic excitation involving discrete sizing type of design variables is considered. The design problem is formulated as the minimization of an objective function subject to multiple reliability constraints. The excitation is modeled as a non-stationary stochastic process with uncertain model parameters. The problem is solved by a sequential approximate optimization strategy cast into the framework of conservative convex and separable approximations. To this end, the objective function and the reliability constraints are approximated by using a hybrid form of linear, reciprocal, and quadratic approximations. The approximations are combined with an effective stochastic sensitivity analysis in order to generate explicit expressions of the reliability constraints in terms of the design variables. The explicit approximate sub-optimization problems are solved by an appropriate discrete optimization technique. Two example problems that consider structures with passive energy dissipation systems under earthquake excitation are presented to illustrate the effectiveness of the approach reported herein.

DOI: 10.4018/978-1-4666-1640-0.ch003

INTRODUCTION

In a large number of practical design situations the design variables must be selected from a list of discrete values. Standard methods address discrete variable design optimization problems by employing discrete or integer variable algorithms to treat the problem directly in the primal variable space (branch and bound techniques, combinatorial methods, evolution-based optimization techniques, etc.) (Kovács, 1980; Goldberg, 1989; Scharage, 1989). These methods are quite general but are associated with a large number of function calls (evaluation of objective and constraint functions). On the other hand, in many practical applications the applied loads and system parameters may be subjected to uncertainty or variability. Under uncertain conditions the field of reliability-based optimization (RBO) provides a realistic and rational framework for structural design and optimization (Enevoldsen and Sørensen, 1994). Schemes for discrete structural optimization considering uncertainties have not been addressed as frequently as their deterministic counterpart. In most studies, ad hoc optimization algorithms have been integrated directly with a reliability method. For example, in (Hassan and Crossley, 2008), the problem of optimization under uncertainty has been approached by means of genetic algorithms and direct Monte Carlo simulation. As both the optimization and the reliability algorithms require a large number of function calls, numerical costs can be very high. In order to reduce the computational efforts related to reliability analysis, the application of optimization methods in combination with the first-order reliability methods was investigated in, for example, (Tolson et al, 2004, Gunawan and Papalambros, 2007). Another approach for reducing computational efforts is the application of meta-models, such as artificial neural networks (see, e.g. (Papadrakakis and Lagaros, 2002; Lagaros et al., 2008)). These approaches have been applied to solve RBO problems of a series

of physical systems characterized by uncertainty models of small and medium sizes (less than 30 random variables).

In this work attention is directed to discrete reliability-based optimization of structural systems under stochastic excitation. In particular, excitation models defined in terms of hundreds or thousands random variables (high dimensional models) are considered here. One of the difficulties in this type of problems is the high computational cost involved in the reliability analyses required during the optimization process. This is due to the fact that the reliability estimation of stochastic dynamical systems involves the estimation of failure probabilities in high-dimensional uncertain parameter spaces (Jensen et al., 2009; Valdebenito and Schuëller, 2011). The objective of this work is to present a general framework for solving this class of reliability-based optimization problems. The approach is based on the use of approximation concepts, the application of an effective stochastic sensitivity analysis, and the implementation of a globally convergent optimization scheme. Special attention is focused on the analysis and design of structures protected by means of passive energy dissipation systems. The basic function of these devices when incorporated into the structure is to absorb a portion of the input energy, thereby reducing energy dissipation demand on structural members and minimizing possible structural damage. In this regard, the consideration of discrete optimal design processes for protected structural systems is one of the novel aspects of this work. This type of problem is relevant from a practical point of view since the potential advantages of modern structural protective systems have lead to the design and construction of an increasing number of protected structures for the purpose of mitigating seismic impact.

The reliability-based optimization problem is formulated as the minimization of an objective function subject to multiple reliability constraints. All uncertainties involved in the problem (system parameters and loading) are considered explicitly

during the design process. The basic mathematical programming statement of the structural optimization problem is converted into a sequence of explicit approximate primal problems. For this purpose, the objective function and the reliability constraints are approximated by using a hybrid form of linear, reciprocal and quadratic approximations. An approximation strategy based on an incomplete quadratic conservative approximation is considered in the present formulation (Groenwold et al., 2007; Prasad, 1983). An adaptive Markov Chain Monte Carlo procedure, called subset simulation (Au and Beck, 2001), is used for the purpose of estimating the failure probabilities. The information generated by subset simulation is also used to estimate the sensitivity of the reliability constraints with respect to the design variables. The above information is combined with an approximation strategy to generate explicit expressions of the objective and reliability constraints in terms of the design variables. The explicit approximate primal problems are solved either by standard methods that treat the problem directly in the primal variable space (Goldberg, 1989; Kovács, 1980; Scharage, 1989; Tomlin, 1970) or by dual methods (Fleury and Braibant, 1986; Haftka and Gürdal, 1992; Jensen and Beer, 2010). The proposed optimization scheme exhibits monotonic convergence that is, starting from an initial feasible design, the scheme generates a sequence of steadily improved feasible designs. This ensures that the optimal solution of each approximate sub-optimization problem is a feasible solution of the original problem, with a lower objective value than the previous cycle.

The structure of the chapter is as follows. First, the design problem considering discrete sizing type of design variables is presented. Next, the structural and excitation models are discussed in detail. The solution strategy of the problem in the framework of conservative convex and separable approximations is then discussed. This is followed by the consideration of some implementation issues such as reliability and sensitivity estimation.

Finally, two numerical examples that consider structures with passive energy dissipation systems as structural protective systems are presented.

FORMULATION

Consider a structural optimization problem defined as the identification of a vector $\{y\}$ of design variables that minimizes an objective function, that is

$$\text{Minimize } f(\{y\}) \quad (1)$$

subject to design constraints

$$h_j(\{y\}) \leq 0 , \quad j = 1, \dots, n_c \quad (2)$$

where h_j represents a constraint function defined in terms of reliability measures, and n_c is the number of constraints. As previously pointed out a pure discrete variable treatment of the design problem is considered here. Thus, the side constraints for the discrete design variables are written as

$$y_i \in Y_i = \{\bar{y}_i^l, l = 1, \dots, n_i\}, \quad i = 1, \dots, n_d \quad (3)$$

where the set Y_i represents the available discrete values for the design variable y_i , listed in ascending order, and n_d is the number of design variables. It is assumed that the available values are distinct and they correspond to quantities such as cross sectional areas, moments of inertia, etc. The particular quantity to be used depends on the problem at hand. It is noted that alternative formulations to the one proposed here should be considered for cases where the possible values of the discrete design variables are linked to a number of properties simultaneously, for example, section groups in steel structures.

The objective function is defined in terms of initial, construction, repair, or downtime costs. In the context of reliability-based optimization of structural systems under stochastic excitation a reliability constraint can be written as

$$h_j(\{y\}) = P_{F_j}(\{y\}) - P_{F_j}^* \leq 0 \quad (4)$$

where $P_{F_j}(\{y\})$ is the probability of occurrence of the failure event F_j evaluated at the design $\{y\}$, and $P_{F_j}^*$ is the corresponding target failure probability. The failure probability function $P_{F_j}(\{y\})$ evaluated at the design $\{y\}$ can be expressed in terms of the multidimensional probability integral

$$P_{F_j}(\{y\}) = \int_{\Omega_{F_j}(\{y\})} q(\{\theta\}) p(\{\xi\}) d\{\xi\} d\{\theta\} \quad (5)$$

where $\Omega_{F_j}(\{y\})$ is the failure domain corresponding to the failure event F_j evaluated at the design $\{y\}$. The vectors $\{\theta\}, \theta_i, i = 1, \dots, n_u$, and $\{\xi\}, \xi_i, i = 1, \dots, n_T$ represent the vector of uncertain structural parameters and random variables that specify the stochastic excitation, respectively. The uncertain structural parameters $\{\theta\}$ are modeled using a prescribed probability density function $q(\{\theta\})$ while the random variables $\{\xi\}$ are characterized by a probability density function $p(\{\xi\})$. The failure probability function $P_{F_j}(\{y\})$ accounts for the uncertainty in the system parameters as well as the uncertainties in the excitation. It is noted that for structural systems under stochastic excitation the multidimensional integral (5) involves in general a large number of uncertain parameters (in the order of thousands). Therefore the reliability estimation for a given design constitutes a high dimensional problem which is extremely demanding from a numerical point of view. Finally, it is noted that constraint functions defined in terms of deterministic per-

formance functions can also be considered in the above formulation.

STRUCTURAL MODEL

A quite general class of dynamical systems under ground acceleration can be cast into the following form

$$\begin{aligned} [M]\{\ddot{x}(t)\} + [C]\{\dot{x}(t)\} + [K]\{x(t)\} = \\ -[M]\{g\}\ddot{x}_g(t) - \{f(\{x(t)\}, \{z(t)\})\} \end{aligned} \quad (6)$$

where $\{x(t)\}$ denotes the displacement vector of dimension n , $\{\dot{x}(t)\}$ the velocity vector, $\{\ddot{x}(t)\}$ the acceleration vector, $\{f(\{x(t)\}, \{z(t)\})\}$ the vector of non-linear restoring forces, $\{z(t)\}$ the vector of a set of variables which describes the state of the nonlinear components, and $\ddot{x}_g(t)$ the ground acceleration. The matrices $[M]$, $[C]$, and $[K]$ describe the mass, damping, stiffness, respectively. The vector $\{g\}$ couples the base excitation to the degrees of freedom of the structure. All these matrices are assumed to be constant with respect to time. This characterization of the nonlinear model is particularly well suited for cases where most of the components of the structural system remain linear, and only a small part behaves in a nonlinear manner. For a more general case, the formulation can still be applied at the expenses of more computational efforts due to possibly necessary updating of the damping and stiffness matrices of the system with respect to time. In general, the matrices involved in the equation of motion depend on the vector of design variables and uncertain system parameters and therefore the solution is also a function of these quantities. The evolution of the set of variables $\{z(t)\}$ is described by a first-order non-linear differential equation

$$\{\dot{z}(t)\} = \{h(\{x(t)\}, \{\dot{x}(t)\}, \{z(t)\})\} \quad (7)$$

Box 1.

$$\{z^{(j+1)}(t + \Delta t)\} = \{z(t)\} + \frac{1}{6}[\{k_1^{(j+1)}\} + 2\{k_2^{(j+1)}\} + 2\{k_3^{(j+1)}\} + \{k_4^{(j+1)}\}] \quad (10)$$

where $\{h\}$ is a non-linear vector function that characterizes the behavior of the non-linear components. From the last equation it is seen that the set of variables $\{z(t)\}$ is a function of the displacements $\{x(t)\}$ and velocities $\{\dot{x}(t)\}$, that is, $\{z(\{x(t)\}, \{\dot{x}(t)\})\}$.

Numerical Integration

Since the differential equation that satisfy the variables $\{z(t)\}$ is non-linear in terms of the response $\{x(t)\}$, Equations. (6) and (7) must be solved in an iterative manner. Equation (6) is solved first by any suitable step-by step integration scheme, leading from the solution at time t at the one at time $t + \Delta t$, that is

$$[M]\{\ddot{x}(t + \Delta t)\} + [C]\{\dot{x}(t + \Delta t)\} + [K]\{x(t + \Delta t)\} = -[M]\{g\}\ddot{x}_g(t + \Delta t) - \{f(\{x(t + \Delta t)\}, \{z(t + \Delta t)\})\} \quad (8)$$

It is seen that in order to compute the solution at time $t + \Delta t$, provided that the solution at time t is known, the value of $\{z(\cdot)\}$ is required at time $t + \Delta t$. To this end, at the beginning of the iteration within the time interval $[t, t + \Delta t]$, it is assumed that ($j = 0$)

$$\{z^{(j)}(\{x(t + \Delta t)\}, \{\dot{x}(t + \Delta t)\})\} = \{z(\{x(t)\}, \{\dot{x}(t)\})\} \quad (9)$$

The solution of Equation. (8), gives the responses $\{x^{(j+1)}(t + \Delta t)\}$ and $\{\dot{x}^{(j+1)}(t + \Delta t)\}$. Then, the nonlinear differential Equation (7) can be integrated to obtain new estimates for $\{z(\{x(t + \Delta t)\}, \{\dot{x}(t + \Delta t)\})\}$, and the right hand side $\{f(\{x(t + \Delta t)\}, \{z(t + \Delta t)\})\}$ in

Equation (8). The iteration starting with solving Equation. (8) needs to be repeated until the norm of the vector $\{z(t + \Delta t)\}$ is in two consecutive iterations sufficiently close. Numerical experience shows that in general only few iterations are required within each time interval $[t + \Delta t]$. The solution of the equation for the evolution of the set of variables $\{z\}$ is obtained by a modified Runge-Kutta method of fourth order. The solution at time $t + \Delta t$ is written in Box 1, 2, and 3.

For actual implementation, the characterization of the vector of non-linear restoring forces is modeled in local component specific coordinates (local displacements and velocities) with a minimal number of variables. Therefore, the relationships given by Equations (11) and (12) are evaluated in local displacements and velocities increasing in this manner the efficiency of the above numerical integration scheme.

EARTHQUAKE EXCITATION MODEL

The ground acceleration is modeled as a non-stationary stochastic process. In particular, a point-source model characterized by the moment magnitude M and epicentral distance r is considered here (Atkinson and Silva, 2000; Boore, 2003). The model is a simple, yet powerful, means for simulating ground motions and it has been successfully applied in the context of earthquake engineering. The time-history of the ground acceleration for a given magnitude M and epicentral distance r is obtained by modulating a white noise sequence by an envelope function and subsequently by a ground motion spectrum through the following steps:

Box 2.

$$\begin{aligned}
 \{k_1^{(j+1)}\} &= \Delta t \{h(\{x(t)\}, \{\dot{x}(t)\}, \{z(t)\})\} \\
 \{k_2^{(j+1)}\} &= \Delta t \{h(\{x^{(j+1)}(t + \Delta t / 2)\}, \{\dot{x}^{(j+1)}(t + \Delta t / 2)\}, \{z(t)\} + \frac{1}{2} \{k_1^{(j+1)}\})\} \\
 \{k_3^{(j+1)}\} &= \Delta t \{h(\{x^{(j+1)}(t + \Delta t / 2)\}, \{\dot{x}^{(j+1)}(t + \Delta t / 2)\}, \{z(t)\} + \frac{1}{2} \{k_2^{(j+1)}\})\} \\
 \{k_4^{(j+1)}\} &= \Delta t \{h(\{x^{(j+1)}(t + \Delta t)\}, \{\dot{x}^{(j+1)}(t + \Delta t)\}, \{z(t)\} + \{k_3^{(j+1)}\})\}
 \end{aligned} \tag{11}$$

Box 3.

$$\{x^{(j+1)}(t + \Delta t / 2)\} = \frac{\{x(t)\} + \{x^{(j+1)}(t + \Delta t)\}}{2}, \quad \{\dot{x}^{(j+1)}(t + \Delta t / 2)\} = \frac{\{\dot{x}(t)\} + \{\dot{x}^{(j+1)}(t + \Delta t)\}}{2} \tag{12}$$

1. Generate a discrete-time Gaussian white noise sequence
 $\omega(t_j) = \sqrt{I / \Delta t} \xi_j, j = 1, \dots, n_T$, where
 $\xi_j, j = 1, \dots, n_T$, are independent, identically distributed standard Gaussian random variables, I is the white noise intensity, Δt is the sampling interval, and n_T is the number of time instants equal to the duration of the excitation T divided by the sampling interval
2. The white noise sequence is modulated by an envelope function $e(t, M, r)$ at the discrete time instants
3. The modulated white noise sequence is transformed to the frequency domain
4. The resulting spectrum is normalized by the square root of the average square amplitude spectrum
5. The normalized spectrum is multiplied by a ground motion spectrum (or radiation spectrum) $S(f, M, r)$ at discrete frequencies $f_l = l / T, l = 1, \dots, n_T / 2$
6. The modified spectrum is transformed back to the time domain to yield the desired ground acceleration time history. Details of the characterization of the envelope function

$e(t, M, r)$ and the ground acceleration spectrum $S(f, M, r)$ are provided in the subsequent sections.

The probabilistic model for the seismic hazard at the emplacement is complemented by considering that the moment magnitude M and epicentral distance r are also uncertain. The uncertainty in moment magnitude is modeled by the Gutenberg-Richter relationship truncated on the interval $[M_{\min}, M_{\max}]$, which leads to the probability density function (Kramer, 2003)

$$p(M) = \frac{b e^{-bM}}{e^{-6.0b} - e^{-8.0b}}, \quad M_{\min} \leq M \leq M_{\max} \tag{13}$$

where b is a regional seismicity factor. For the uncertainty in the epicentral distance r , a lognormal distribution with mean value \bar{r} (km) and standard deviation σ_r (km) is used. The point source stochastic model previously described is well suited for generating the high-frequency components of the ground motion (greater than 0.1Hz). Low-frequency components can also be introduced in the analysis by combining the above

methodology with near-fault ground motion models (Mavroeidis and Papageorgiou, 2003).

Envelope Function

The envelope function for the ground acceleration is represented by (Saragoni and Hart, 1974; Boore, 2003)

$$e(t, M, r) = a_1 \left(\frac{t}{t_n} \right)^{a_2} e^{-a_3 \left(\frac{t}{t_n} \right)} \quad (14)$$

where

$$a_2 = \frac{-0.2 \ln(0.05)}{1 + 0.2(\ln(0.2) - 1)}, \quad a_3 = \frac{a_2}{0.2}, \quad a_1 = \left(\frac{e}{0.2} \right)^{a_2} \quad (15)$$

The envelope function has a peak equal to unity when $t = 0.2 t_n$, and $e(t, M, r) = 0.05$ when $t = t_n$, with $t_n = 2.0 T_{gm}$, where T_{gm} is the duration of ground motion, expressed as a sum of a path dependent and source dependent component $T_{gm} = 0.05\sqrt{r^2 + h^2} + 0.5 / f_a$, where r is the epicentral distance, and the parameters h and f_a (corner frequency) are moment dependent given by $\log(h) = 0.15M - 0.05$ and $\log(f_a) = 2.181 - 0.496M$ (Atkinson and Silva, 2000).

Ground Motion Spectrum

The total spectrum of the motion at a site $S(f, M, r)$ is expressed as the product of the contribution from the earthquake source $E(f, M)$, path $P(f, r)$, site $G(f)$ and type of motion $I(f)$, i.e.

$$S(f, M, r) = E(f, M) P(f, r) G(f) I(f) \quad (16)$$

The source component is given by

$$E(f, M) = C M_0(M) S_a(f, M) \quad (17)$$

where C is a constant, $M_0(M) = 10^{1.5M+10.7}$ is the seismic moment, and the factor S_a is the displacement source spectrum given by (Atkinson and Silva, 2000)

$$S_a(f, M) = \frac{1 - \varepsilon}{1 + \left(\frac{f}{f_a} \right)^2} + \frac{\varepsilon}{1 + \left(\frac{f}{f_b} \right)^2} \quad (18)$$

where the corner frequencies f_a and f_b , and the weighting parameter ε are defined, respectively, as

$$\begin{aligned} \log(f_a) &= 2.181 - 0.496M, \\ \log(f_b) &= 2.41 - 0.408M, \text{ and} \\ \log(\varepsilon) &= 0.605 - 0.255M. \end{aligned}$$

The constant C is given by $C = UR_\Phi VF / 4\pi\rho_s\beta_s^3 R_0$, where U is a unit dependent factor, R_Φ is the radiation pattern, V represents the partition of total shear-wave energy into horizontal components, F is the effect of the free surface amplification, ρ_s and β_s are the density and shear-wave velocity in the vicinity of the source, and R_0 is a reference distance. Next, the path effect $P(f, r)$ which is another component of the process that affects the spectrum of motion at a particular site is represented by functions that account for geometrical spreading and attenuation

$$P(f, r) = Z(R(r)) e^{-\pi f R(r)/Q(f)\beta_s} \quad (19)$$

where $R(r)$ is the radial distance from the hypocenter to the site given by $R(r) = \sqrt{r^2 + h^2}$. The attenuation quantity $Q(f)$ is taken as $Q(f) = 180f^{0.45}$ and the geometrical spreading function is selected as $Z(R(r)) = 1 / R(r)$ if $R(r) < 70.0$ km and $Z(R(r)) = 1 / 70.0$ other-

Table 1. Parameters for the stochastic ground acceleration model

Parameter	Numerical Value	Parameter	Numerical Value
\bar{r} (km)	20.0	σ_r (km)	9.0
b	1.8	U	10^{-20}
ρ_s (gm/cc)	2.8	β_s (km/s)	3.5
v	$1/\sqrt{2}$	R_Φ	0.55
F	2.0	R_0 (km)	1.0
T (s)	20.0	Δt (s)	0.01
M_{min}	6.0	M_{max}	8.0

wise (Atkinson and Silva, 2000). The modification of seismic waves by local conditions, site effect $G(f)$, is expressed by the multiplication of a diminution function $D(f)$ and an amplification function $A(f)$. The diminution function accounts for the path-independent loss of high frequency in the ground motions and can be accounted for a simple filter of the form $D(f) = e^{-0.03\pi f}$ (Anderson and Hough, 1984). The amplification function $A(f)$ is based on empirical curves given in (Boore et al., 1997) for generic rock sites. An average constant value equal to 2.0 is considered. Finally, the filter that controls the type of ground motion $I(f)$ is chosen as $I(f) = (2\pi f)^2$ for ground acceleration. The particular values of the different parameters of the stochastic ground acceleration model considered in this contribution are given in Table 1. For illustration purposes Figure 1 shows the envelope function, the ground motion spectrum and a corresponding sample of ground motion for a nominal distance $r = 20$ km, and moment magnitude $M=7.0$. For a detailed discussion of this point-source model the reader is referred to (Atkinson and Silva, 2000; Boore, 2003).

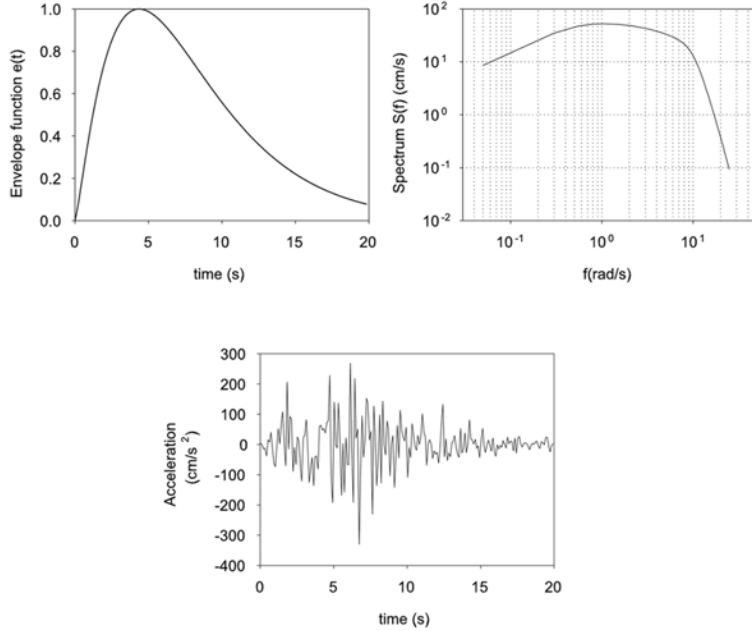
SEQUENTIAL OPTIMIZATION

The solution of the reliability-based optimization problem given by Equations (1, 2 and 3) is obtained by transforming it into a sequence of sub-optimization problems having a simple explicit algebraic structure. Thus, the strategy is to construct successive approximate analytical sub-problems. To this end, the objective and the constraint functions are represented by using approximate functions dependent on the design variables. In particular, a hybrid form of linear, reciprocal and quadratic approximations is considered in the present formulation (Haftka and Gürdal, 1992). For the purpose of constructing the approximations all design variables are assumed to be continuous.

First and Second-Order Approximations

Let $p(\{y\})$ be a generic function involved in the optimization problem, i.e. the objective or constraint functions, and $\{y^0\}$ a point in the feasible design space. The function $p(\{y\})$ is first approximated about the point $\{y^0\}$ by using a hybrid

Figure 1. Envelope function, ground acceleration spectrum and sample ground motion for epicentral distance $r=20$ km and moment magnitude $M=7$



form of linear and reciprocal approximations. In particular, the following approximation is considered

$$p(\{y\}) \approx p_{cl}(\{y\}) = p(\{y^0\}) + \sum_i \frac{\partial p(\{y^0\})}{\partial y_i} \delta_{pl}(y_i, y_i^0)(y_i - y_i^0) \quad (20)$$

where

$$\begin{aligned} \delta_{pl}(x_i, y_i^0) &= 1 \quad \text{if } \frac{\partial p(\{y^0\})}{\partial y_i} \geq 0, \quad \text{and} \\ \delta_{pl}(x_i, y_i^0) &= \frac{y_i^0}{y_i} \quad \text{if } \frac{\partial p(\{y^0\})}{\partial y_i} < 0 \end{aligned} \quad (21)$$

An attractive property of this approximation, called convex linearization, is that it yields the most conservative approximation among all possible combinations of direct/reciprocal variables (Fleury and Braibant, 1986). In principle, convex

linearization is not guaranteed to be conservative in an absolute sense. That is, it is not known that the approximations are more conservative than the original functions. One way to affect the conservatism of the approximation is by considering second-order terms. For example, introducing diagonal quadratic terms in the convex approximation (20) yields

$$p_{cq}(\{y\}) = p_{cl}(\{y\}) + \sum_i \delta_{pq}(y_i, y_i^0)(y_i - y_i^0)^2 \quad (22)$$

where $\delta_{pq}(y_i, y_i^0)$ are the coefficients of the second-order diagonal terms. These coefficients are defined in terms of the second-order derivatives of the convex approximation $p_{cl}(\{y\})$ at the point $\{y^0\}$ as

$$\delta_{pq}(y_i, y_i^0) = \chi_i \frac{\partial^2 p_{cl}(\{y^0\})}{\partial y_i^2} \quad (23)$$

Box 4.

$$\begin{aligned}
 f_{cq}(\{y\}) = & \sum_{(i^+)} \left(\frac{\partial f(\{y^0\})}{\partial y_i} y_i \right) - \sum_{(i^-)} \left(\frac{\partial f(\{y^0\})}{\partial y_i} \frac{(y_i^0)^2}{y_i} \right) - 2\chi_i^f \sum_{(i^-)} \left(\frac{\partial f(\{y^0\})}{\partial y_i} y_i \left(\frac{y_i}{y_i^0} - 2 \right) \right) + \\
 & f(\{y^0\}) - \sum_{(i^+)} \left(\frac{\partial f(\{y^0\})}{\partial y_i} y_i^0 \right) - \sum_{(i^-)} \left(\frac{\partial f(\{y^0\})}{\partial y_i} y_i^0 (2\chi_i^f - 1) \right)
 \end{aligned} \tag{25}$$

where

$$\begin{aligned}
 \frac{\partial^2 p_{cl}(\{y^0\})}{\partial y_i^2} = 0 & \text{ if } \frac{\partial p(\{y^0\})}{\partial y_i} \geq 0, \text{ and} \\
 \frac{\partial^2 p_{cl}(\{y^0\})}{\partial y_i^2} = & -2 \frac{\partial p(\{y^0\})}{\partial y_i} \text{ if } \frac{\partial p(\{y^0\})}{\partial y_i} < 0
 \end{aligned} \tag{24}$$

and χ_i is a user-defined positive scalar. The purpose of this parameter is to enforce the conservatism of the approximation. For continuously differentiable functions the manipulation of the higher-order curvatures will ensure the conservatism of the approximations at least locally (Groenwold et al., 2009). The enforcement of the conservatism will be carried out during inner loops throughout the optimization process (see Solution Scheme section). The conservatism of the approximations is important since affect the global convergence of the optimization process (Svanberg, 2002). It ensures that the optimal solution of the sub-optimization problem is a feasible solution of the original problem, with a lower objective value than the previous iteration. In this manner, the process generates a sequence of steadily improved feasible designs if the process starts from an initial feasible design. This property is significant from a practical view point since the optimization process can be stopped at any stage still leading to better designs than the initial feasible estimate.

Approximate Objective Function

Applying the above approximation approach to the objective function yields the following approximate function to be minimized as in Box 4. where the group (i^+) contains the variables for which the partial derivative of the objective function is positive and group (i^-) includes the remaining variables.

Approximate Constraint Functions

The construction of approximate constraint functions is based on the approximation of transformed failure probability functions. Specifically, the following transformation is considered (Jensen and Beer, 2010)

$$h_j^t(\{y\}) = \ln[P_{F_j}(\{y\})], \quad j = 1, \dots, n_c \tag{26}$$

The transformed failure probability functions are approximated by using the approximation approach previously defined. That is,

$$\begin{aligned}
 h_{cij}^t(\{y\}) = & \sum_{(i_j^+)} \left(\frac{\partial h_j^t(\{y^0\})}{\partial y_i} y_i \right) - \sum_{(i_j^-)} \left(\frac{\partial h_j^t(\{y^0\})}{\partial y_i} \frac{(y_i^0)^2}{y_i} \right) - \\
 & 2\chi_i^{h_j^t} \sum_{(i_j^-)} \left(\frac{\partial h_j^t(\{y^0\})}{\partial y_i} y_i \left(\frac{y_i}{y_i^0} - 2 \right) \right) + \bar{h}_j^t(\{y^0\}), \quad j = 1, \dots, n_c
 \end{aligned} \tag{27}$$

with

Box 5.

$$\sum_{(i^+)} \left(\frac{\partial f(\{y^0\})}{\partial y_i} y_i \right) - \sum_{(i^-)} \left(\frac{\partial f(\{y^0\})}{\partial y_i} \frac{(y_i^0)^2}{y_i} \right) - 2\chi_i^f \sum_{(i^-)} \left(\frac{\partial f(\{y^0\})}{\partial y_i} y_i \left(\frac{y_i}{y_i^0} - 2 \right) \right) \quad (30)$$

Box 6.

$$\sum_{(i_j^+)} \left(\frac{\partial h_j^t(\{y^0\})}{\partial y_i} y_i \right) - \sum_{(i_j^-)} \left(\frac{\partial h_j^t(\{y^0\})}{\partial y_i} \frac{(y_i^0)^2}{y_i} \right) - 2\chi_i^{h_j^t} \sum_{(i_j^-)} \left(\frac{\partial h_j^t(\{y^0\})}{\partial y_i} y_i \left(\frac{x_i}{y_i^0} - 2 \right) \right) \leq -\bar{h}_j^t(\{y^0\}) + \ln[P_{F_j}^*], \quad j = 1, \dots, n_c \quad (31)$$

$$\begin{aligned} \bar{h}_j^t(\{y^0\}) &= h_j^t(\{y^0\}) - \sum_{(i_j^+)} \left(\frac{\partial h_j^t(\{y^0\})}{\partial y_i} y_i^0 \right) \\ &\quad - \sum_{(i_j^-)} \left(\frac{\partial h_j^t(\{y^0\})}{\partial y_i} y_i^0 (2\chi_i^{h_j^t} - 1) \right) \end{aligned} \quad (28)$$

where $\sum_{(i_j^+)}$ and $\sum_{(i_j^-)}$ mean summation over the variables belonging to group (i_j^+) and (i_j^-) , respectively. Then, the approximate reliability constraints can be written as

$$h_{c_{qj}}(\{y\}) = h_{c_{qj}}^t(\{y\}) - \ln[P_{F_j}^*] \leq 0, \quad j = 1, \dots, n_c \quad (29)$$

Approximate Optimization Problem

Using the above approximations for the objective and constraint functions, the approximate sub-optimization problem defined at the point $\{y^0\}$, $P_{\{y^0\}}$, takes the form in Box 5 and 6.

$P_{\{y^0\}}$: Minimize (see Box 5) subject to (see Box 6) $j = 1, \dots, n_c$, where all terms have been previously defined.

Solution Scheme

The solution scheme of the optimization process proceeds as follows:

1. Start from a feasible design. At the beginning of the k^{th} design cycle ($k = 0, 1, 2, \dots$) the objective function $f(\{y\})$ and constraint functions $h_j(\{y\})$, $j = 1, \dots, n_c$ are approximated by using the approach introduced previously. The approximations require function evaluations ($f(\{y^k\})$, $h_j(\{y^k\})$, $j = 1, \dots, n_c$) and sensitivity analyses ($\nabla f(\{y^k\})$, $\nabla h_j(\{y^k\})$, $j = 1, \dots, n_c$). In this step, all design variables are assumed to be continuous.
2. Using this information an explicit sub-optimization problem is constructed. The explicit sub-optimization problem can be solved either by standard methods that treat the problem directly in the primal design variable space (branch and bound techniques, combinatorial methods, evolution-based optimization techniques, etc.) or by dual methods (Fleury and Braibant, 1986). In the present implementation, a genetic algorithm is applied to solve the sub-optimization problem.

3. The new point $\{y^{*k}\}$ is tested if it is acceptable in terms of a conservative criterion, i.e. if $f_{cq}(\{y^{*k}\}) \geq f(\{y^{*k}\})$ and if $h_{eq}(\{y^{*k}\}) \geq h_j(\{y^{*k}\}), j = 1, \dots, n_c$. If these conditions are satisfied (conservative step) the point $\{y^{*k}\}$ is used as the current design for the next cycle, that is, $\{y^{k+1}\} = \{y^{*k}\}$. If the design $\{y^{*k}\}$ does not represent a conservative step an inner loop is initiated to effect conservatism. For functions which are not conservative at $\{y^{*k}\}$ the corresponding coefficients of the second-order diagonal terms are increased by multiplying the scalars χ_i by a constant greater than one. The modified approximations are used to construct a new sub-optimization problem to obtain a new point.
4. The overall design process is continued until some convergence criterion is satisfied.

It is noted that the requirement of a conservative step in the algorithm can be relaxed and demand that a feasible descent step is made instead, i.e., if $f(\{y^{*k}\}) < f(\{y^{*(k-1)}\})$ and if $h_j(\{y^{*k}\}) \leq 0, j = 1, \dots, n_c$. In this case, the conservatism is only enforced when a feasible descent step could not be made. This approach which is called, relaxed conservatism, inherits the global convergence properties of the algorithm that enforces conservatism at each design cycle. In general the above optimization scheme is very effective when the curvatures of the functions involved in the optimization problem are not too large and relatively uniform throughout the design space. For other cases, methods based on local response surfaces, trust regions and line search methodologies may be more appropriate (Alexandrov et al., 1998; Bucher and Bourgund, 1990; Jensen et al., 2009).

STOCHASTIC ANALYSIS

The characterization of the sub-optimization problems $P_{\{y^k\}}, k = 0, 1, 2, \dots$ requires the estimation of failure probabilities and their sensitivities. For that purpose an advanced simulation technique is adopted and implemented in the present formulation.

Reliability Estimation

Subset simulation is adopted in this formulation for the purpose of estimating the corresponding failure probabilities during the design process (Au and Beck, 2001). In the approach, the failure probabilities are expressed as a product of conditional probabilities of some chosen intermediate failure events, the evaluation of which only requires simulation of more frequent events. Therefore, a rare event simulation problem is converted into a sequence of more frequent event simulation problems. For example, the failure probability $P_{F_j}(\{y\})$ can be expressed as the product

$$P_{F_j}(\{y\}) = P(F_{j,1}(\{y\})) \prod_{k=1}^{m_{F_j}-1} P(F_{j,k+1}(\{y\}) / F_{j,k}(\{y\})) \quad (32)$$

where $F_{j,m_{F_j}}(\{y\}) = F_j(\{y\})$ is the target failure event and:

$$F_{j,m_{F_j}}(\{y\}) \subset F_{j,m_{F_j}-1}(\{y\}) \dots \subset F_{j,1}(\{y\})$$

is a nested sequence of failure events. Equation (32) expresses the failure probability $P_{F_j}(\{y\})$ as a product of $P(F_{j,1}(\{y\}))$ and the conditional probabilities:

$$P(F_{j,k+1}(\{y\}) / F_{j,k}(\{y\})), k = 1, \dots, m_{F_j} - 1.$$

It is seen that, even if $P_{F_j}(\{y\})$ is small, by choosing m_{F_j} and $F_{j,k}(\{y\})$, $k = 1, \dots, m_{F_j} - 1$ appropriately, the conditional probabilities can still be made sufficiently large, and therefore they can be evaluated efficiently by simulation because the failure events are more frequent. The intermediate failure events are chosen adaptively using information from simulated samples so that they correspond to some specified values of conditional failure probabilities (Au and Beck, 2001).

Sensitivity Estimation

As previously pointed out the approximation of the reliability constraints requires the estimation of the gradient of the transformed failure probability functions h_j^t . For the purpose of estimating the gradients, it is assumed that the optimization variables can have non-discrete values during the solution process. Therefore, all design variables are treated as continuous during the first step of the optimization process (see Solution Scheme section). The sensitivity of the transformed failure probability functions with respect to the design variables is estimated by an approach recently introduced in (Valdebenito and Schuëller, 2011). The approach is based on the approximate representation of two different quantities. The first approximation involves the performance function κ_j while the second includes the failure probability function. Recall that the failure domain Ω_{F_j} for a given design $\{y\}$ is defined as

$$\Omega_{F_j}(\{y\}) = \{\{\theta\}, \{\xi\} \mid \kappa_j(\{y\}, \{\theta\}, \{\xi\}) \leq 0\}. \quad (33)$$

If $\{y^k\}$ is the current design, the performance function is approximated in the vicinity of the current design as

$$\bar{\kappa}_j(\{y\}, \{\theta\}, \{\xi\}) = \kappa_j(\{y^k\}, \{\theta\}, \{\xi\}) + \{\delta\kappa_j\}^T \{\Delta y\} \quad (34)$$

where $\{y\} = \{y^k\} + \{\Delta y\}$ and $\{\delta\kappa_j\}$ is a vector of constant, real valued coefficients. For samples $(\{\theta_i\}, \{\xi_i\})$, $i = 1, \dots, m_s$ near the limit state surface, that is, $\kappa_j(\{y\}, \{\theta_i\}, \{\xi_i\}) \approx 0$ the performance function is evaluated at $n_s = q_s \times m_s$ points in the neighborhood of $\{y^k\}$. That is, for each sample $(\{\theta_i\}, \{\xi_i\})$, q_s designs are defined. These points are generated as

$$\{y^{lk}\} - \{y^k\} = \{\Delta y\} = \frac{\{\eta_l\}}{\|\{\eta_l\}\|} R, \quad l = 1, \dots, n_s \quad (35)$$

where the components of the vector $\{\eta_l\}$ are independent, identically distributed standard Gaussian random variables, and R is a user-defined small positive number. This number defines the radius of the hypersphere $(\{\eta_l\} / \|\{\eta_l\}\|)R$ centered at the current design $\{y^k\}$. The coefficients $\{\delta\kappa_j\}$ are computed by least squares. To this end the following set of equations is generated

$$\begin{aligned} \kappa_j(\{y^{lk}\}, \{\theta_i\}, \{\xi_i\}) &= \kappa_j(\{y^k\}, \{\theta_i\}, \{\xi_i\}) \\ &+ \{\delta\kappa_i\}^T \frac{\{\eta_l\}}{\|\{\eta_l\}\|} R \\ l &= i + (q - 1) \times m_s, \quad q = 1, \dots, q_s, \quad i = 1, \dots, m_s \end{aligned} \quad (36)$$

where the index l indicates a double loop in terms of the indices i and q . Since the samples $(\{\theta_i\}, \{\xi_i\})$, $i = 1, \dots, m_s$ are chosen near the limit state surface the approximate performance function $\bar{\kappa}_j$ is expected to be representative, on the average, of the behavior of the failure domain Ω_{F_j} in the vicinity of the current design $\{y^k\}$ (Jensen et al., 2009). Next, the failure domain Ω_{F_j} for a given design $\{y\}$ can also be defined in terms of the normalized demand function as

$$\Omega_{F_j}(\{y\}) = \{\{\theta\}, \{\xi\} \mid D_j(\{y\}, \{\theta\}, \{\xi\}) \geq 1\}. \quad (37)$$

where $D_j(\{y\}, \{\theta\}, \{\xi\}) = 1 - \kappa_j(\{y\}, \{\theta\}, \{\xi\})$. The failure probability function, evaluated at the current design $\{y^k\}$, is approximated locally as an explicit function of the normalized demand around $D_j^* = 1$ as

$$P[D_j(\{y^k\}, \{\theta\}, \{\xi\}) \geq D_j^*] \approx e^{\psi_0 + \psi_1(D_j^* - 1)}, \quad (38)$$

$$D_j^* \in [1 - \varepsilon, 1 + \varepsilon]$$

where D_j^* is a threshold of the normalized demand (in the neighborhood of one) and ε represents a small tolerance. The coefficients ψ_0 and ψ_1 can be calculated by least squares with samples of the performance function κ_j (or normalized demand function D_j) generated at the last stage of subset simulation (Valdebenito and Schuëller, 2011). The gradient of the j -th transformed failure probability function at $\{y^k\}$ (see Equation (26)) is given by

$$\frac{\partial h_j^t(\{y\})}{\partial y_l} \Bigg|_{\{y\}=\{y^k\}} = \frac{1}{P_{F_j}(\{y^k\})} \times \frac{\partial P_{F_j}(\{y\})}{\partial y_l} \Bigg|_{\{y\}=\{y^k\}}$$

$$l = 1, \dots, n_d \quad (39)$$

where n_d is the total number of design variables. On the other hand, the gradient of the j -th failure probability function can be estimated by means of the limit:

$$\frac{\partial P_{F_j}(\{y\})}{\partial y_l} \Bigg|_{\{y\}=\{y^k\}} = \lim_{\Delta y_l \rightarrow 0} \frac{P_{F_j}(\{y^k\} + \{\delta(l)\}\Delta y_l) - P_{F_j}(\{y^k\})}{\Delta y_l},$$

$$l = 1, \dots, n_d \quad (40)$$

where $\{\delta(l)\}$ is a vector of length n_d with all entries equal to zero, except for the l -th entry,

which is equal to one. Considering the definition of failure probability in terms of the performance function, the linear expansion of the performance function in (34), and the approximation of the failure probability function given in (38), the partial derivatives of the j -th transformed failure probability function can be expressed as (Jensen et al., 2009)

$$\left. \frac{\partial h_j^t(\{y\})}{\partial y_l} \right|_{\{y\}=\{y^k\}} \approx \frac{1}{P_{F_j}(\{y^k\})} \times \lim_{\Delta y_l \rightarrow 0} \frac{e^{\psi_0 + \psi_1 \delta \kappa_{jl}} - e^{\psi_0}}{\Delta y_l}$$

$$= \psi_1 \delta \kappa_{jl}, \quad l = 1, \dots, n_d \quad (41)$$

where $\delta \kappa_{jl}$ is the l -th element of the vector $\{\delta \kappa_j\}$, and all other terms have been previously defined. It is noted that the previous approach for estimating the gradients of the failure probability functions requires a single reliability analysis plus the evaluation of the performance functions in the vicinity of the current design. Validation calculations have shown that this approach is quite efficient for estimating the sensitivity of failure probability functions with respect to design variables (Jensen et al., 2009; Valdebenito and Schuëller, 2011).

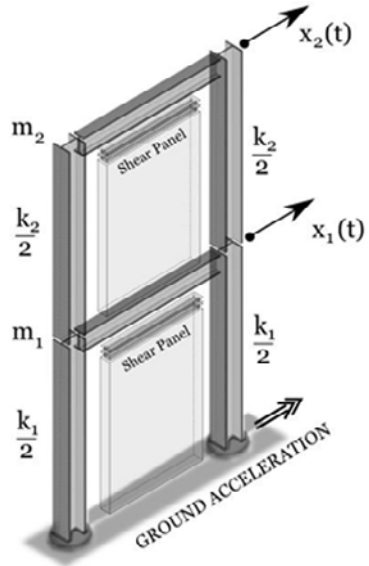
NUMERICAL EXAMPLES

Example No.1

Description

Consider the reliability-based optimization of the two-story frame structure under earthquake loading shown in Figure 2. The floor masses are $m_i = 10^7 \text{ kg}$, $i = 1, 2$, and the initial linear inter-story stiffnesses are $K_1 = 9.0 \times 10^9 \text{ N/m}$ and $K_2 = 7.0 \times 10^9 \text{ N/m}$. A 3% of critical damping is assumed in the model. The damping ratio is treated as uncertain and modeled as a log-normal

Figure 2. Structural system with a passive energy dissipation system under ground acceleration



random variable with a coefficient of variation of 40 %. This high coefficient of variation accounts for the considerable uncertainty in estimating damping ratios in real structural systems.

For an improved earthquake resistance, the model is reinforced with a passive energy dissipation system (shear panel) at each floor. The shear panels follow the inter-story restoring force law

$$r(t) = k_d(\delta(t) - q^1(t) + q^2(t)) \quad (42)$$

where k_d denotes the initial stiffness of the device, $\delta(t)$ is the relative displacement between floors, and $q^1(t)$ and $q^2(t)$ denote the plastic elongations of the device. Using the auxiliary variable $u(t) = \delta(t) - q^1(t) + q^2(t)$, the plastic elongations are specified by the differential equations

$$\dot{q}^i(t) = \lambda_i \dot{\delta}(t) g_i(\dot{\delta}(t), u(t)), i = 1, 2 \quad (43)$$

where the nonlinear functions g_i are specified by (Pradlwarter and Schuëller, 1993)

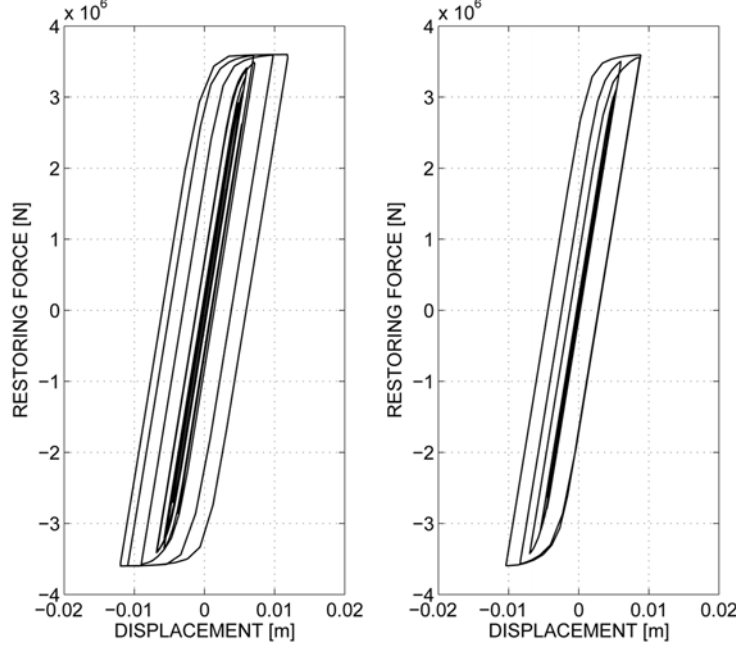
$$\begin{aligned} g_i(\dot{\delta}(t), u(t)) &= H(\lambda_i \dot{\delta}(t)) \times \\ &\left[H(\lambda_i u(t) - u_y) \frac{\lambda_i u(t) - u_y}{u_p - u_y} \right. \\ &\left. H(u_p - \lambda_i u(t)) + H(\lambda_i u(t) - u_p) \right] \end{aligned} \quad (44)$$

where $\lambda_i = -1^{(i-1)}$, $i = 1, 2$, $H(\cdot)$ denotes the Heaviside step function, u_y is a parameter specifying the onset of yielding, and $k_d u_p$ is the maximum restoring force of the device. The values $u_p = 6.0 \times 10^{-3}$ m, $u_y = 0.7 u_p$, and $k_d = 6.0 \times 10^8$ N/m are used for each nonlinear element. Because of the yielding, energy dissipation due to hysteresis is introduced in the structural response. For illustration purposes the behavior of the friction devices at the initial design ($K_1 = 9.0 \times 10^9$ N/m, and $K_2 = 7.0 \times 10^9$ N/m) is shown in Figure 3. In this figure typical displacement-restoring force curves of the friction devices at the first and second floor are presented. The non-linear incursion of the devices is clear from the figure. In general the overall effect of the dissipation system is to decrease the response of the structural system. The system is subjected to a ground acceleration that is modeled as described in a previous Section. Note that the duration of the excitation is 20 s and the sampling interval is equal to 0.01 s (see Table (1)). Therefore the number of random variables involved in the characterization of the excitation is equal to 2000. This in turn implies that the estimation of the failure probability for a given design represents a high dimensional reliability problem.

Discrete Optimization Problem

The objective function is defined in terms of an initial cost which is assumed to be proportional to the linear interstory stiffnesses. The reliability constraints are given in terms of the interstory drift ratios. Failure is assumed to occur when the

Figure 3. Typical displacement-restoring force curves of the shear panels at the initial design. The first and the second floor



interstory drift ratio reaches some critical level for the first time. A threshold level value equal to 0.02 m is considered in this case, and the failure events are defined as

$$F_i = \max_{t \in [0, T]} |\delta_i(t)| > 0.02, \quad i = 1, 2 \quad (45)$$

where $\delta_1(t)$ and $\delta_2(t)$ are the relative displacements of the first and second floor, respectively. The target failure probability is taken equal to 10^{-3} . The optimization variables are the linear inter-story stiffnesses K_1 and K_2 , with initial design $K_{01} = 9.0 \times 10^9$ N/m and $K_{02} = 7.0 \times 10^9$ N/m. The optimization problem is written as

$$\text{Min } f(K_1, K_2) = K_1 + K_2 \quad (46)$$

subject to

$$P_{F_j}(K_1, K_2) \leq P_{F_j}^*, \quad j = 1, 2 \quad (47)$$

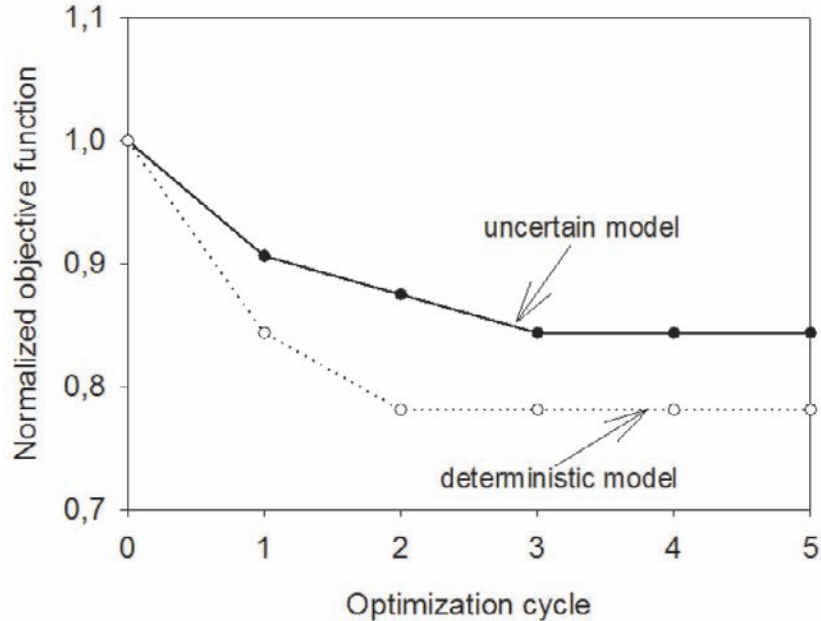
with side constraints

$$\begin{aligned} \frac{K_1}{10^9} &\in \{3.0, 3.5, 4.0, 4.5, 5.0, 5.5, 6.0, 6.5, 7.0, 7.5\} \\ \cup \quad &\{8.0, 8.5, 9.0, 9.5, 10.0, 10.5, 11.0, 11.5, 12.0\} \text{N/m} \end{aligned} \quad (48)$$

$$\begin{aligned} \frac{K_2}{10^9} &\in \{3.0, 3.5, 4.0, 4.5, 5.0, 5.5, 6.0, 6.5, 7.0, 7.5\} \\ \cup \quad &\{8.0, 8.5, 9.0, 9.5, 10.0, 10.5, 11.0, 11.5, 12.0\} \text{N/m} \end{aligned} \quad (49)$$

The problem is solved by using the sequential approximate optimization approach previously described. Subset simulation is used to estimate the failure probabilities and their sensitivities. To smooth the variability of the estimates, the average of failure probability estimates over five independent simulation runs is considered at each design. The value of the parameter that controls the curvature of the second-order terms in the approximations is taken as $\chi = 0.5$. It is noted

Figure 4. Iteration history in terms of the objective function. Deterministic and uncertain models(Example 1)



that the optimal choice of this parameter from the algorithm performance point of view depends on the particular type of problem. The reader is referred to (Svanberg, 2002) for a general discussion of the values of this parameter in the context of conservative, convex and separable approximations.

Results

The iteration history of the optimization process in terms of the objective function and the reliability constraints is shown in Figure 4 and figure 5, respectively. For comparison, the results obtained with the deterministic model are also shown in the figures. In this context, the deterministic model considers the damping ratio equal to its most probable value. The objective function is normalized by the cost of the initial design. It is seen that, starting from a feasible initial design, the process converges in less than four iterations. Therefore, the entire optimization process takes few excursion probability and sensitivity estima-

tions. It is observed that the value of the objective function at the final design of the uncertain model is greater than the corresponding value of the deterministic model. This in turn implies that the structural components (columns) of the uncertain model are bigger than the corresponding components of the deterministic model. This result can be seen from Figure 6, where the final designs of the deterministic and uncertain models are shown in the design space corresponding to the uncertain model. Note that the final design obtained from the deterministic model is not feasible. Finally, it is seen from Figures 4 and 5 that the method generates a series of steadily improved feasible designs that move toward the optimum.

Example No.2

Structural Model

A four-story reinforced concrete building under earthquake motion is considered for analysis. A 3D view of the system is shown in Figure 7. Each

Figure 5. Iteration history in terms of the reliability constraints. Deterministic and uncertain models (Example 1)

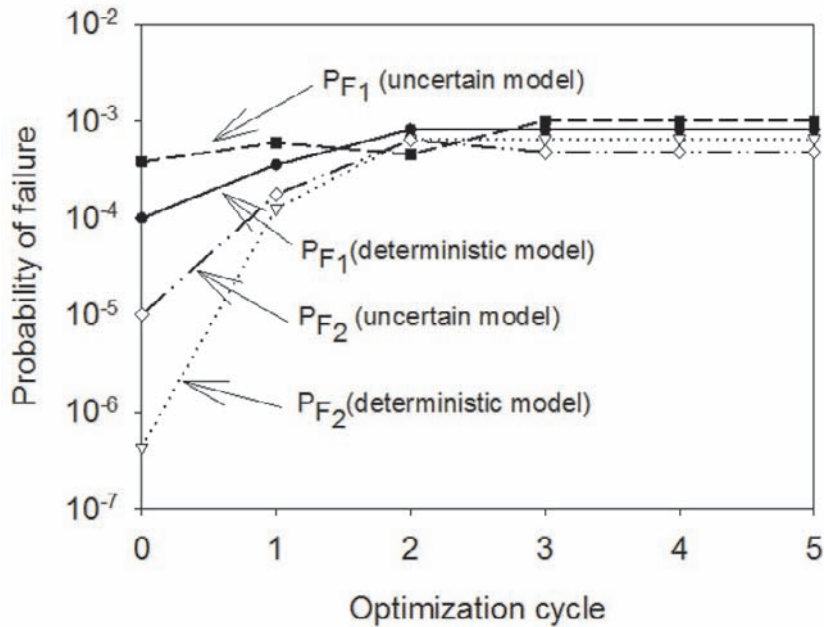


Figure 6. Final designs of the deterministic and uncertain models in the design space

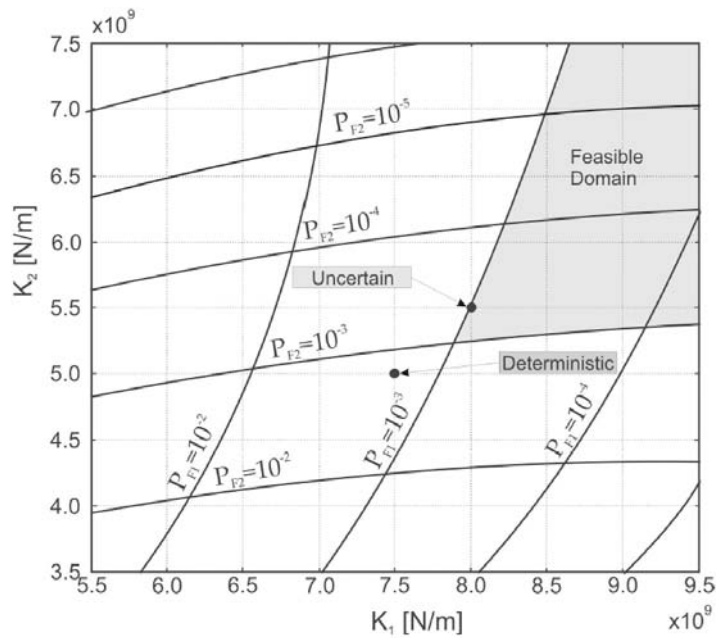
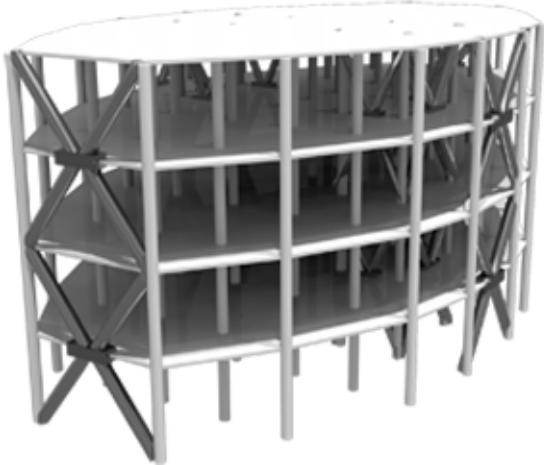


Figure 7. Four-story building model under earthquake excitation



of the four floors is supported by 43 columns of circular cross section. All floors have a constant height equal to 3.0 m, leading to a total height of 12.0 m. It is assumed that each floor may be represented sufficiently accurately as rigid within the $x - y$ plane when compared with the flexibility of the columns. Hence, each floor can be represented by three degrees of freedom, i.e. two translatory displacements in the direction of the x axis and y axis, and a rotational displacement. The associated active masses in the x and y direction are taken constant for all floors and equal to 658 ton, while the mass moment of inertia is equal to 1.8×10^5 ton-m² for all floors. The Young's modulus E and the modal damping ratios ρ_i of the structural model are treated as uncertain system parameters. The Young's modulus is modeled as a Gaussian random variable with most probable value $\bar{E} = 2.5 \times 10^{10}$ N/m², and coefficient of variation of 20%, while the damping ratios are modeled by independent Log-normal random variables with mean values $\bar{\rho}_i = 0.05$ and coefficients of variation of 40%. The structural model is excited horizontally by a ground acceleration applied at 45° with respect to the plan of the system. The induced ground

acceleration is modeled as described in a previous Section.

Dissipation Model

For an improved earthquake performance the structural system is enforced with vibration control devices.

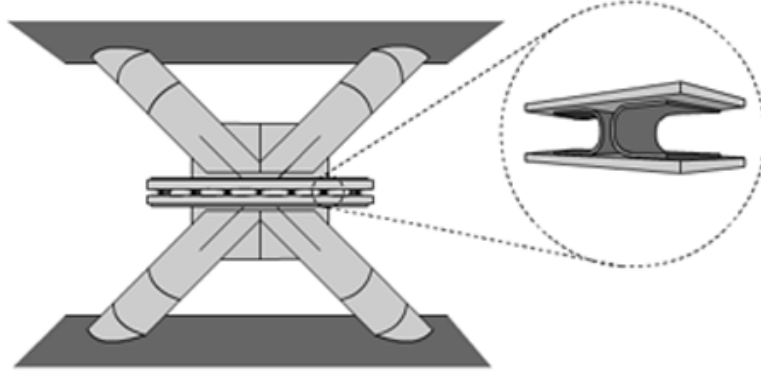
Ten devices connected to the structure every two floors as indicated in Figure (7) are placed in the structural system. A typical configuration of the devices is shown in Figure (8). They consist of brace and plate elements as indicated in the figure. Between the plates there are a series of dissipators in the form of metallic U-shaped flexural plates (UFP).

The devices exhibit a one-dimensional hysteretic type of non-linearity modeled by the restoring force law

$$r(t) = n_{ufp} r_{ufp}(t) \quad (50)$$

where n_{ufp} is the number of U-shaped flexural plates in the device and $r_{ufp}(t)$ is the dissipator force given by

Figure 8. Vibration control device and metallic U-shape flexural plates



$$r_{ufp}(t) = \alpha k_e \delta(t) + (1 - \alpha) k_e U^y z(t) \quad (51)$$

where k_e is the pre-yield stiffness, U^y is the yield displacement, α is the factor which defines the extent to which the restoring force is linear, $z(t)$ is a dimensionless hysteretic variable, and $\delta(t)$ is the relative displacement between the floors where the device is connected. The nonlinear restoring force of the device acts between the floors where it is placed with the same orientation as the relative displacement $\delta(t)$. The hysteretic behavior of each U-shaped flexural plate is defined in terms of the auxiliary variable $z(t)$ which satisfies the first-order non-linear differential equation

$$U^y \dot{z}(t) = \dot{\delta}(t) [\beta_1 - z(t)(\beta_2 \text{sgn}(\dot{\delta}(t)) + \beta_3 \text{sgn}(z(t)))] \quad (52)$$

where β_1 , β_2 and β_3 are dimensionless quantities that characterize the properties of the hysteretic behavior, $\text{sgn}(\cdot)$ is the sign function, and all other terms have been previously defined. The quantities β_1 , β_2 and β_3 correspond to scale, loop fatness and loop pinching parameters, respectively. The above characterization of the hysteretic behavior corresponds to the Bouc-Wen type model (Baber and Wen, 1981). The values

$k_e = 4 \times 10^8 \text{ N/m}$, $U^y = 5 \times 10^{-3} \text{ m}$, $\alpha = 0.01$, $\beta_1 = 1.0$, $\beta_2 = 2.0$, $\beta_3 = -0.5$ are used in this case. These model parameters generate hysteretic behaviors similar to the one observed from experimental data (De La Llera et al., 2004)

Design Problem

The design variables denoted by $d_i, i = 1, \dots, n_d$, are the diameters of the reinforced concrete column elements. Each floor is associated to one design variable and therefore $n_d = 4$ in this example. The objective function f is proportional to the total volume of the resistant elements (columns), while the failure events are defined in terms of the interstory drift ratios, and given by

$$F_i(\{d\}, \{\theta\}, \{\xi\}) = \max_{t_k, k=1, \dots, 2001} |\delta_i(t_k, \{d\}, \{\theta\}, \{\xi\})| > \delta^* \quad (53)$$

where $\delta_i(t_k, \{d\}, \{\theta\}, \{\xi\})$ is the relative displacement between the $(i-1, i)$ -th floor evaluated at the design $\{d\}$, t_k are the discrete time instants, δ^* is the critical threshold level and equal to 0.006 m (0.2% of the floor height), $\{\theta\}$ is the vector that represents the uncertain structural parameters (Young's modulus and damping ratios), and $\{\xi\}$

is the vector that specifies the stochastic excitation. The corresponding multidimensional probability integrals involved in the estimation of the probabilities of failure include more than two thousand random variables in this case. Thus, as in the previous example the estimation of the failure probability for a given design represents a high-dimensional reliability problem. The reliability-based optimization problem is written as

$$\text{Min } f(\{d\}) \quad (54)$$

subject to

$$P_{F_i}(\{d\}) \leq P_F^* = 10^{-3} \quad i = 1, 2, 3, 4 \quad (55)$$

with side constraints

$$d_i \in D_i, i = 1, \dots, 4 \quad (56)$$

where the set D_i represents the available discrete values for the design variable d_i . The set D_i is defined as $D_i = \{0.40, 0.41, \dots, 0.75\}$ m. It is seen that each of the design variables can be chosen from a discrete set of 36 diameters. Therefore, the discrete set of design variables involves more than 10^6 possible combinations. The optimization problem is solved by the sequential approximate optimization strategy discussed in previous sections.

Final Designs

The initial and the final designs of the structural system are presented in Table 2. The corresponding iteration history of the optimization process in terms of the objective function is shown in Figure 9. Note that the initial design is an interior point in the design space, as it is required by the algorithm (see first step of the Solution Scheme section). For comparison the final design of the system without vibration control devices is also

indicated. The objective function is normalized by its value at the initial design. From Table 2 and figure 9 it is observed that the dimensions of the column elements at the final design of the system without the vibration control devices are greater than the corresponding elements of the model with the devices, as expected. The total weight of the unprotected model increases almost 40 % with respect to the weight of the enforced model. This result highlights the beneficial effects of the vibration control devices in protecting the structural system. For illustration purposes Figure 10 shows a typical displacement-restoring force curve of one of the U-shaped flexural plates at the final design. The nonlinear incursion of the dissipator is clear from the figure.

It is found that the process converges in less than four iterations in this case and therefore the design process takes few excursion probability and sensitivity estimations. This computational cost is substantially different for the case of direct optimization. In that case the number of excursion probability and sensitivity estimations increases dramatically with respect to the proposed approach. In direct optimization the excursion probabilities and their sensitivities need to be estimated for every change of the design variables during the optimization process. As in the previous example the method generates a series of steadily improved feasible designs that moves toward the final design. That is, the design process has monotonic convergence properties.

CONCLUSION

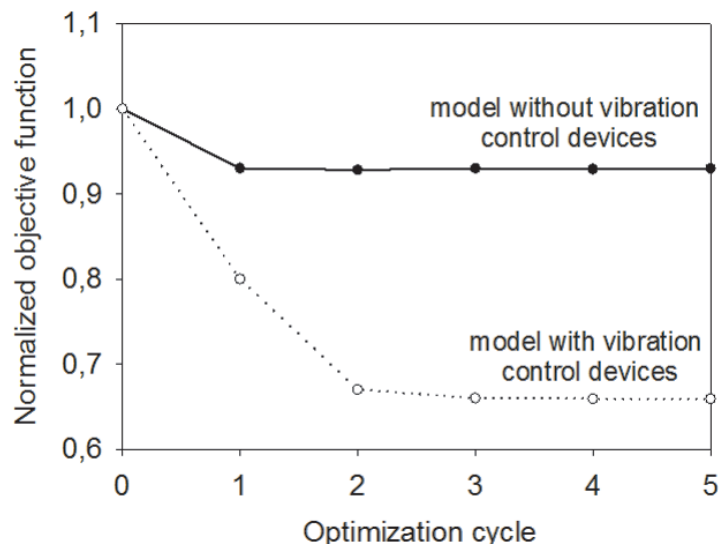
A general framework for reliability-based design optimization of a class of stochastic systems involving discrete sizing type of design variables has been presented. The reliability-based design problem is formulated as an optimization problem with a single objective function subject to multiple reliability constraints. The high computational cost associated with the solution of the

Table 2. Final designs

Design variable	Initial design	Final design	
		ND	D
d_1 (m)	0.75	0.71	0.62
d_2 (m)	0.70	0.68	0.59
d_3 (m)	0.65	0.64	0.54
d_4 (m)	0.60	0.56	0.44
Normalized objective function	1.00	0.92	0.66

ND= without devices, D= with devices

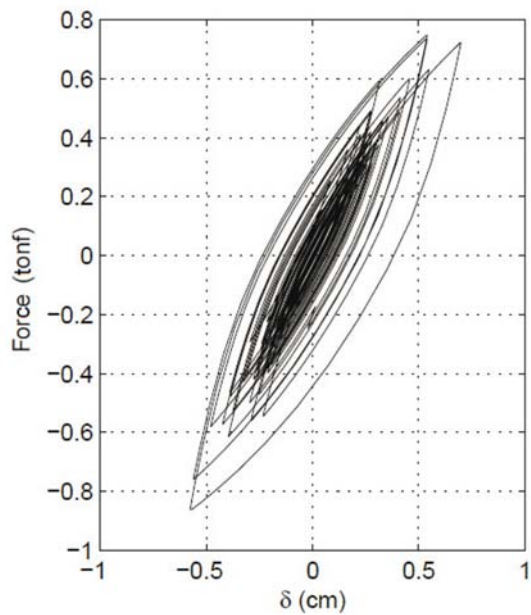
Figure 9. Iteration history in terms of the objective function (Example 2)



optimization problem is addressed by the use of approximate reliability analyses during portions of the optimization process. This is achieved by implementing a sequential optimization approach based on global conservative, convex and separable approximations. The combined use of approximation concepts, advanced simulation techniques, efficient sensitivity analyses and discrete optimization techniques provides an effective reliability-based design optimization strategy for sizing problems which involve discrete design variables. The proposed approach

takes into account the uncertainty in structural and excitation model parameters explicitly during the optimization process. The design scheme exhibits monotonic convergence that is, starting from an initial feasible design the scheme generates a sequence of steadily improved feasible designs. This property is important from a practical view point since the optimization process can be stopped at any stage still leading to better designs than the initial feasible estimate. Recall that each design cycle involves a considerable computational effort for complex structural systems. Numerical results

Figure 10. Typical displacement-restoring force curves of one of the U-shaped flexural plates at the final design



obtained from the example problems and from additional validation calculations have shown that the number of reliability estimations required during the optimization process is in general very small. The results have also indicated that the presence of passive vibration control devices has a positive impact on the reliability and global performance of systems under stochastic loading. In fact, the results of this study highlight the beneficial effect of these devices in protecting structural systems under environmental loads such as earthquake excitations. Based on the previous observations it is concluded that the proposed methodology can be very advantageous from a numerical point of view for solving discrete variable structural optimization problems of an important class of stochastic dynamical systems.

ACKNOWLEDGMENT

This research was partially supported by CONICYT (National Commission for Scientific and Technological Research) under grant number 1110061. This support is gratefully acknowledged by the authors.

REFERENCES

- Alexandrov, N., Dennis, J. Jr, Lewis, R., & Torczon, V. (1998). A trust-region framework for managing the use of approximation models in optimization. *Structural Optimization*, 15(1), 16–23. doi:10.1007/BF01197433
- Anderson, J., & Hough, S. (1984). A model for the shape of the Fourier amplitude spectrum of acceleration at high frequencies. *Bulletin of the Seismological Society of America*, 74(5), 1969–1993.
- Atkinson, G., & Silva, W. (2000). Stochastic modeling of California ground motions. *Bulletin of the Seismological Society of America*, 90(2), 255–274. doi:10.1785/0119990064
- Au, S., & Beck, J. (2001). Estimation of small failure probabilities in high dimensions by subset simulation. *Probabilistic Engineering Mechanics*, 16(4), 263–277. doi:10.1016/S0266-8920(01)00019-4
- Baber, T., & Wen, Y. (1981). Random vibration hysteretic, degrading systems. *Journal of the Engineering Mechanics Division*, 107(6), 1069–1087.
- Boore, D. (2003). Simulation of ground motion using the stochastic method. *Pure and Applied Geophysics*, 160(3), 635–676. doi:10.1007/PL00012553

- Boore, D., Joyner, W., & Fumal, T. (1997). Equations for estimating horizontal response spectra and peak acceleration from western North American earthquakes: A summary of recent work. *Seismological Research Letters*, 68(1), 128–153. doi:10.1785/gssrl.68.1.128
- Bucher, C., & Bourgund, U. (1990). A fast and efficient response surface approach for structural reliability problems. *Structural Safety*, 7(1), 57–66. doi:10.1016/0167-4730(90)90012-E
- De la Llera, J., Esguerra, C., & Almazán, J. (2004). Earthquake behavior of structures with copper energy dissipators. *Earthquake Engineering & Structural Dynamics*, 33(3), 329–358. doi:10.1002/eqe.354
- Enevoldsen, I., & Sørensen, J. (1994). Reliability-based optimization in structural engineering. *Structural Safety*, 15(3), 169–196. doi:10.1016/0167-4730(94)90039-6
- Fleury, C., & Braibant, V. (1986). Structural optimization: A new dual method using mixed variables. *International Journal for Numerical Methods in Engineering*, 23(3), 409–428. doi:10.1002/nme.1620230307
- Goldberg, D. (1989). *Genetic algorithms in search, optimization, and machine learning*. Reading, MA: Addison Wesley.
- Groenwold, A., Etman, L., Snyman, J., & Rooda, J. (2007). Incomplete series expansion for function approximation. *Structural and Multidisciplinary Optimization*, 34(1), 21–40. doi:10.1007/s00158-006-0070-6
- Groenwold, A., Wood, D. W., Etman, L. F. P., & Tosserams, S. (2009). Globally convergent optimization algorithm using conservative convex separable diagonal quadratic approximations. *AIAA Journal*, 47(11), 2649–2657. doi:10.2514/1.41975
- Gunawan, S., & Papalambros, P. Y. (2007). Reliability optimization with mixed continuous-discrete random variables and parameters. *Journal of Mechanical Design*, 129(2), 158–165. doi:10.1115/1.2406085
- Haftka, R., & Gürdal, Z. (1992). *Elements of structural optimization* (3rd ed.). Kluwer.
- Hassan, R., & Crossley, W. (2008). Reliability-based optimization under uncertainty including discrete variables. *Journal of Spacecraft and Rockets*, 45(2), 394–405. doi:10.2514/1.28827
- Jensen, H., & Beer, M. (2010). Discrete-continuous variable structural optimization of systems under stochastic loading. *Structural Safety*, 32(5), 293–304. doi:10.1016/j.strusafe.2010.03.007
- Jensen, H., Valdebenito, M., Schuëller, G., & Kusanovic, D. (2009). Reliability-based optimization of stochastic systems using line search. *Computer Methods in Applied Mechanics and Engineering*, 198(49–52), 3915–3924. doi:10.1016/j.cma.2009.08.016
- Kovács, L. (1980). Combinatorial methods of discrete programming. *Mathematical Methods of Operation Research*, 2.
- Kramer, S. (2003). *Geotechnical earthquake engineering*. Prentice Hall.
- Lagaros, N., Garavela, A. T., & Papadrakakis, M. (2008). Innovative seismic design optimization with reliability constraints. *Computer Methods in Applied Mechanics and Engineering*, 198, 28–41. doi:10.1016/j.cma.2007.12.025
- Mavroeidis, G., & Papageorgiou, A. (2003). A mathematical representation of near-fault ground motions. *Bulletin of the Seismological Society of America*, 93(3), 1099–1131. doi:10.1785/0120020100

- Papadrakakis, M., & Lagaros, N. (2002). Reliability-based structural optimization using neural networks and Monte Carlo simulation. *Computer Methods in Applied Mechanics and Engineering*, 191, 3491–3507. doi:10.1016/S0045-7825(02)00287-6
- Pradlwarter, H. J., & Schuëller, G. I. (1993). Equivalent linearization - A suitable tool for analyzing MDOF-systems. *Probabilistic Engineering Mechanics*, 8(2), 115–126. doi:10.1016/0266-8920(93)90005-G
- Prasad, B. (1983). Approximation, adaptation and automation concepts for large scale structural optimization. *Engineering Optimization*, 6(3), 129–140. doi:10.1080/03052158308902462
- Saragoni, G., & Hart, G. (1974). Simulation of artificial earthquakes. *Earthquake Engineering & Structural Dynamics*, 2(3), 249–267. doi:10.1002/eqe.4290020305
- Scharage, L. (1989). *Optimization modeling with LINGO*. Technical report, LINDO Systems inc., Chicago.
- Svanberg, K. (2002). A class of globally convergent optimization methods based on conservative convex separable approximations. *SIAM Journal on Optimization*, 12(2), 555–573. doi:10.1137/S1052623499362822
- Tolson, B. A., Maier, H. R., Simpson, A. R., & Lence, B. J. (2004). Genetic algorithms for reliability-based optimization of water distribution systems. *Journal of Water Resources Planning and Management*, 130(1), 63–72. doi:10.1061/(ASCE)0733-9496(2004)130:1(63)
- Tomlin, J. (1970). Integer and non-linear programming. In *Branch and bound methods for integer and non-convex programming* (pp. 437–450). Amsterdam, The Netherlands: North Holland.
- Valdebenito, M., & Schuëller, G. (2011). Efficient strategies for reliability-based optimization involving non linear, dynamical structures. *Computers & Structures*, 89(19-29), 1797-1811.

Chapter 4

A Multi-Hazard Framework for Optimum Life-Cycle Cost Design of Reinforced Concrete Bridges

Azadeh Alipour

University of Massachusetts Amherst, USA

Behrouz Shafei

University of Massachusetts Amherst, USA

Masanobu Shinohzuka

University of California Irvine, USA

ABSTRACT

This chapter provides a comprehensive procedure for the time-dependant structural performance evaluation and life-cycle cost analysis of reinforced concrete highway bridges located in extreme chloride-laden environments. The penetration of chloride ions into the concrete is simulated through a finite difference approach, which takes into account all the parameters that can affect the corrosion process. From simulation results, the corrosion initiation time is predicted and the extent of structural degradation is calculated over the entire life of bridge. A group of detailed bridge models with various structural attributes are developed to evaluate the changes in the structural capacity and seismic response of corroded bridges. For the purpose of the probabilistic seismic risk assessment of bridges, the seismic fragility curves are generated and updated at regular time intervals. The time-dependent fragility parameters are employed to investigate the life-cycle cost of bridges by introducing a performance index which combines the effects of probable seismic events and chloride-induced corrosion. The proposed approach provides a multi-hazard framework, which leads to more realistic performance and cost estimates. It also indicates the inspection and maintenance intervals in a way that the inspection and maintenance costs are optimized, while the safety of bridge is ensured.

DOI: 10.4018/978-1-4666-1640-0.ch004

1. INTRODUCTION

From a long-term point of view, the durability of reinforced concrete (RC) highway bridges is significantly impacted by the deterioration of their structural members. When investigating the damaged bridges, the deterioration caused by the corrosion of reinforced concrete members is usually found to be one of the main sources of structural degradation which may eventually result in the serviceability failure of bridges under service or extreme loading conditions. An accurate estimation of the extent of degradation during the structure's life-cycle provides both engineers and decision-makers with valuable information which helps to ensure the safety of bridges while reducing the associated costs. Towards this goal, the current chapter focuses on the corrosion process caused by the chloride ions attack and evaluates its effects on the life-cycle performance and cost of RC bridges.

Chloride-induced corrosion is one of the deterioration mechanisms caused by the rapid intrusion of chloride ions into the concrete. This mode of corrosion is expected when the bridge is exposed to aggressive environments (e.g., coastal environments or the application of deicing salts). The penetration profile of chloride ions in a reinforced concrete member demonstrates the highest chloride content near the surface with a decreasing trend towards the depth of the member. The chloride transport mechanism in concrete is a complex phenomenon that may occur in several forms, such as ionic diffusion, capillary suction, and permeation. When the concentration of chloride ions in the pore solution within the vicinity of reinforcing bars becomes high enough to depassivate the protection film of the reinforcement, the layers of rust start to form on the reinforcing bar surface and the corrosion of steel begins.

In this chapter, an integrated computational methodology is developed to simulate the penetration of chloride ions into the reinforced concrete members. Through a comprehensive study, the effects of various influential parameters, such as

water-to-cement ratio, ambient temperature, relative humidity, concrete age, free chloride content, and binding capacity, are considered to obtain a precise prediction of the chloride content in different depths of RC members with the progression of time. By comparing the chloride content values with certain critical thresholds suggested in the literature, the corrosion initiation time is estimated. After corrosion initiation, the time-dependent characteristics of corroded bridges are identified through the extent of the cracking and spalling of the concrete cover, reduction of the steel bar cross-section area, and decrease in the yield strength of reinforcing bars. Based on that, the probabilistic life time fragility parameters of a group of RC bridges with different structural attributes are evaluated over the time using fragility analysis procedure.

Furthermore, the life-cycle cost of RC bridges under corrosion attack is studied in this chapter. The total life-cycle cost of the bridge is calculated from the present value of the construction cost, inspection and maintenance costs, serviceability and earthquake-induced failure costs, and finally user costs associated with them. These costs are reviewed in detail and the relevant assumptions are discussed to provide a more realistic estimation of the total cost. Among the mentioned costs, a special attention is paid to the serviceability and earthquake-induced failure cost. The serviceability failure cost is incurred from necessary repair and replacement actions due to the concrete cover spalling and steel rebar corrosion while the earthquake-induced failure cost is due to the repair and rehabilitation actions after a specific seismic event and is dependent on the occurrence probability of different damage states. This cost is estimated here from the results of probabilistic life-time fragility analysis by introducing a performance index which represents the expected performance of a corroded bridge under a particular seismic hazard risk. This index is updated regularly over the time and takes into account the combined effects of seismic hazard and chloride-induced corrosion in the calculation of life-cycle cost of RC bridges.

2. CORROSION INITIATION AND PROPAGATION

Chloride-induced corrosion is identified as one of the major causes for the structural deterioration of reinforced concrete bridges. This type of corrosion is initiated by the ingress of chloride ions into structural concrete members during the concentration and diffusion cycles. The sources of chloride ions are mainly air-borne sea-salts in coastal areas and deicing salts used in winter times. This chapter focuses on the corrosion resulting from sea-salt particles floating in the air and assumes that the diffusion process is the dominant mode of chloride intrusion. In order to study the diffusion process, it is essential to find the changes in the chloride content at different depths of the concrete member. The total chloride content refers to the total acid-soluble chloride in concrete, which is the summation of free chlorides and bound chlorides. The relationship among the total, C_t , free, C_f , and bound, C_b , chloride content in unsaturated concrete is as follows:

$$C_t = C_b + w_e C_f \quad (1)$$

where w_e is the evaporable water content (m^3 of evaporable water per m^3 of concrete). According to the Fick's second law which is based on the mass conservation principle, the diffusion process is expressed as the change in the free chloride content over the time, t (Equation 2).

$$\frac{\partial C_f}{\partial t} = -\text{div} \left[\frac{D_{Cl}}{1 + (1/w_e)(\partial C_b / \partial C_f)} \nabla (C_f) \right] \quad (2)$$

where D_{Cl} is the chloride diffusion coefficient and $(\partial C_b / \partial C_f)$ is the binding capacity. The chloride binding capacity characterizes the relationship between the free and bound chloride ions in concrete at a constant temperature and it is also referred to as the binding isotherm. Martin-Perez et al.

(2000) suggest an idealized isotherm which simulates the exposure conditions of marine structures. This isotherm is called Freundlich isotherm and its relationship can be expressed as:

$$C_b = \alpha_F C_f^{\beta_F} \rightarrow \frac{\partial C_b}{\partial C_f} = \alpha_F \beta_F C_f^{\beta_F - 1} \quad (3)$$

where α_F and β_F are the Freundlich binding constants equal to 1.05 and 0.36, respectively. The chloride diffusion coefficient in Equation 2, D_{Cl} , is calculated by taking into account the effects of major influential parameters, such as water to cement ratio, ambient temperature, relative humidity, age of the concrete, free chloride content, and chloride binding capacity. The chloride diffusion coefficient can be determined from a diffusion coefficient estimated for a reference temperature and humidity, $D_{Cl,ref}$ multiplied by the modification factors as below:

$$D_{Cl} = D_{Cl,ref} F_1(T) F_2(h) F_3(t_e) F_4(C_f) \quad (4)$$

where $F_1(T)$ accounts for the dependence of chloride diffusion coefficient on the ambient temperature, $F_2(h)$ represents the influence of relative humidity, $F_3(t_e)$ denotes the influence of concrete age, and $F_4(C_f)$ considers the effects of free chloride content. Table 1 summarizes the mathematical expressions for the modification factors used in Equation 4 (Bažant and Najjar, 1972, Saetta et al., 1993, Bamforth and Price, 1996, Xi and Bažant, 1999, Martin-Perez et al., 2001, and Kong et al., 2002).

In Table 1, $F_1(T)$ is calculated using the temperature data, T , gathered for a specific region where the structure is located. In the current study, the temperature data of the Los Angeles area during last 15 years (from 1995 to 2009) has been collected from the National Oceanic and Atmospheric Administration (NOAA). It is evident from this database that the temperature has a periodic trend over the year and a sinusoidal func-

Table 1. Summary of modification factors used for the estimation of chloride diffusion coefficient

Formulation	Parameters	Assigned values
$\log D_{Cl,ref} = a + b \log(w / c)$	a, b : empirical coefficients	$a = -10.6, b = 1.9$
$F_2(T) = \exp\left[\frac{E}{R}\left(\frac{1}{T_{ref}} - \frac{1}{T}\right)\right]$	E : activation energy for diffusion process R : gas constant T_{ref} : reference temperature	$E = 44.6 \pm 4.3 \text{ (kJ/mol)}$ $R = 8.314 \text{ (kJ/mol. }^\circ\text{K)}$ $T_{ref} = 296 \text{ (}^\circ\text{K)}$
$F_3(h) = 1 / \left[1 + \left(\frac{1-h}{1-h_c}\right)^4\right]$	h_c : critical humidity level	$h_c = 0.75$
$F_4(t_e) = \left(\frac{t_{ref}}{t}\right)^m$	t_{ref} : reference time m : empirical age factor	$t_{ref} = 28 \text{ (day)}$ $m = 0.04$
$F_5(C_f) = 1 - \kappa(C_f)^n$	k, n : empirical parameters	$k = 8.366, n = 0.5$

tion can be fit very well to that. The temperature at the j -th day of the year can be found from Equation 5:

$$T(\text{ }^\circ\text{K}) = 291 - 15 \sin(2\pi j / 365) \quad (5)$$

Similar to the ambient temperature, the local humidity information is needed for $F_2(h)$. The average monthly relative humidity data for the Los Angeles area has been obtained from NOAA to find the annual trend of humidity. The relative humidity is periodic in nature and is repeated throughout the years. Hence, it can be simulated for the j -th day by a half-sinusoidal function as below:

$$h(\%) = 0.65 + 0.13 \sin(\pi j / 365) \quad (6)$$

A review of Table 1 shows that the chloride diffusion coefficient is a nonlinear parameter which varies over the time. Hence, the governing partial differential equation given by Equation 2 cannot be solved without using appropriate numerical

methods. In the current study, a finite difference algorithm is developed to evaluate the chloride diffusion process at different time steps by constant updating of the diffusion coefficient. This algorithm considers the effects of all influential parameters and provides a more accurate estimation of chloride content in the concrete.

For the numerical solution, it is assumed that the free chloride content in the concrete is zero at the initial condition. This value will gradually increase by the intrusion of chloride ions over the time. On the other hand, the free chloride content is always constant at the concrete surface. The surface chloride content, C_s , depends on various parameters, such as the composition of the concrete, location of the structure, orientation of its surface, chloride concentration in the environment, and general conditions of exposure with regard to rain and wind (Bertolini, 2008). A range of 2.95 kg.m^{-3} (McGee, 1999) to 7.00 kg.m^{-3} (Val, 2004) has been suggested for the surface chloride content at bridges located near coastlines. In this study the average value of 5.00 kg.m^{-3} is assigned to C_s .

Using the developed finite difference algorithm, a set of simultaneous equations are solved in one-day time steps to determine the chloride content in the concrete. Assuming that the water to cement ratio is equal to 0.5, the calculated free chloride content at the depth of 50 mm has been shown in Figure 1. After obtaining the free chloride content at each time step, the bound and total chloride contents can be calculated using Equations 1 and 3. The changes in bound and total chloride contents during a 30-year period can also be found in Figure 1.

The calculated free chloride content at different time steps can be used to estimate the corrosion initiation time, t_i . The corrosion initiation time is determined as the time when the chloride concentration near the reinforcing bars reaches the threshold chloride concentration. This means:

$$C_f(t_i, d_c) = C_{critical} \quad (7)$$

where d_c is the depth at which the reinforcing bars are placed (usually equal to the concrete cover depth). In Equation 7, the $C_{critical}$ is the threshold

chloride concentration causing depassivation of the concrete protection film and initiation of the corrosion process. There have been many research efforts during the past three decades to determine an appropriate threshold for the critical chloride content. It had been first suggested that the critical value should be determined by investigating the free chloride concentration, but the study of Glass and Buenfeld (2000) on the chemical aspects of chloride binding capacity showed that the bound chloride should also be taken into account. As a result, the threshold value is expected to represent the total chloride content. Figure 2 demonstrates a summary of data available in the literature regarding the measured or suggested values for the critical chloride concentration. For this study, the critical chloride concentration is considered to be 1% of the cement weight which is assumed to equal 350 kg.m^{-3} .

The total chloride content profile given in Figure 1 can be used to evaluate the corrosion initiation time. Assuming the threshold value as 3.5 kg.m^{-3} (1% of cement weight), the initiation time can be estimated accordingly as 12.66 year for. It is evident that different chloride binding

Figure 1. Change in the free, bound, and total chloride contents during a 30-year period

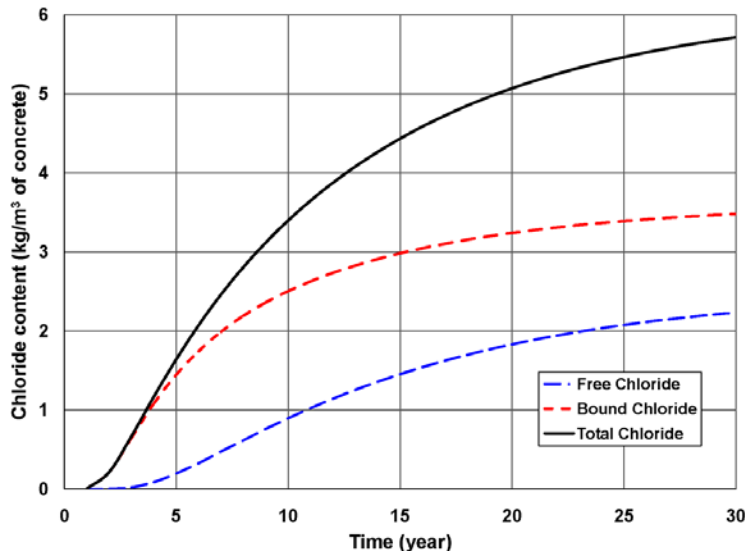
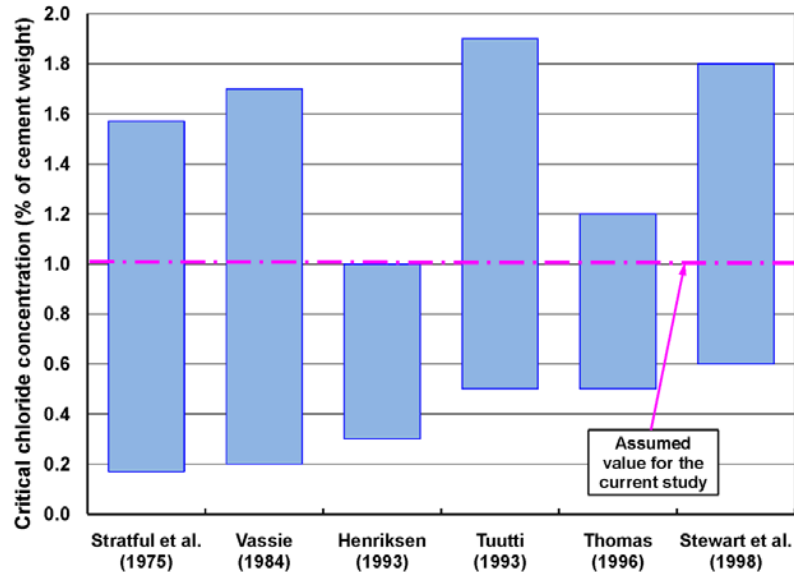


Figure 2. Summary of data available in literature for the critical chloride concentration required to initiate the corrosion process



isotherms result in some change in the estimation of the corrosion initiation time, which indicates the importance of a reasonable choice for the chloride binding model. The initiation time for different cover depths of 40, 50, and 60 mm would respectively be 7.23, 10.40, and 14.20 years (Figure 3). It can be seen that the values of corrosion initiation time obtained from the developed algorithm lie well within the range of 7 to 20 years, observed by Kong et al. (2002).

3. STRUCTURAL DEGRADATION DUE TO CORROSION

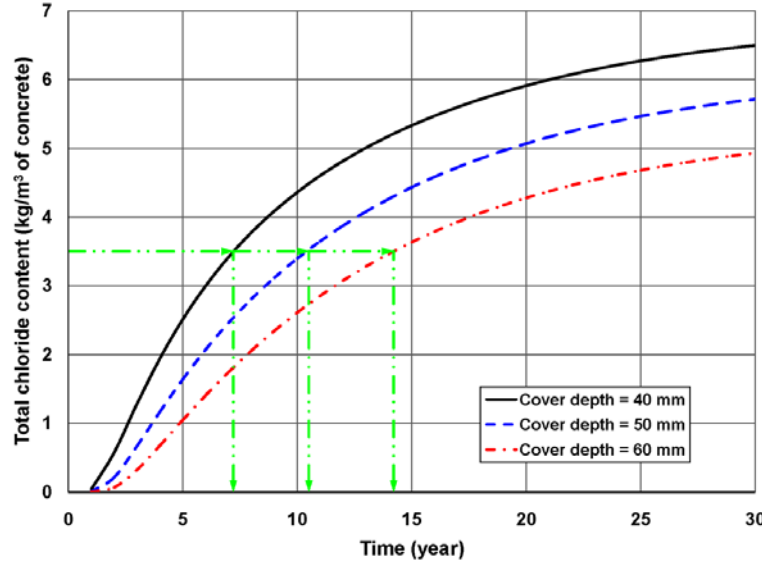
After the corrosion initiation time, the protection film of the reinforcing bar is depassivated and the transport of iron ions starts. This results in the formation of rust layers around the rebar during the corrosion process. This process continues until the volume of rust reaches a level that causes the concrete to crack due to the excessive expansion of rust layers. In this study the crack initiation time is calculated using the Faraday's law which

relates the mass of steel consumed over the time to the amount of current that flows through the electrochemical corrosion cell. The rate of mass loss per unit length of bar subjected to the corrosion, ΔM_{loss} (gr.cm^{-1}), for a time step of Δt (sec) can be described as:

$$\Delta M_{\text{loss}}(t) = k\pi D(t)i_{\text{corr}}\Delta t \quad (8)$$

where $D(t)$ is the reduced diameter of reinforcing bar during the corrosion process, k , the mass transport coefficient equal to 2.893×10^{-9} , and i_{corr} , the current per unit area of the reinforcing bar. For the i_{corr} in Equation 8, a range of 10 to 25 $\mu\text{A.cm}^{-2}$ has been suggested by Rodriguez et al. (1994). This range corresponds to the high reinforcement corrosion risk because it is larger than 1 $\mu\text{A.cm}^{-2}$ (Andrade et al., 1993). In the current study, i_{corr} is assumed to equal 10 $\mu\text{A.cm}^{-2}$. By taking the steel mass density, ρ_s , equal to 7.8 (gr.cm^{-3}), the change in the volume of corroded steel, ΔV_{loss} ($\text{cm}^3.\text{cm}^{-1}$), can be simply calculated from ΔM_{loss} . The reduced rebar diameter after each time step of corrosion is calculated as:

Figure 3. Estimation of corrosion initiation time for the cover depths of 40, 50, and 60 mm



$$D(t) = \sqrt{D_0^2 - 4\Delta V_{loss}(t) / \pi} \quad (9)$$

where D_0 is the initial diameter of the rebar.

The residual strength of corroded reinforcing bars was investigated experimentally by Du et al. (2005a and b). They conducted both accelerated and simulated corrosion tests on the bars embedded in the concrete and concluded that the strength of steel bars decreases significantly with chloride penetration. Their test results are in reasonable agreement with other studies, such as Andrade et al. (1991), Lee et al. (1996), and Morinaga (1996). Therefore, the below empirical equation proposed by Du et al. (2005a and b) is used to estimate the time-dependent loss of yield strength in corroded reinforcing bars:

$$f_y(t) = (1 - 0.005m(t)) f_{y0} \quad (10)$$

where $f_y(t)$ is the yield strength of corroded reinforcement at each time step, f_{y0} the yield strength of non-corroded reinforcement, t , the time elapsed since corrosion initiation (year), and $m(t)$, the percentage of steel mass loss over the time. The

$m(t)$ is equal to the consumed mass of steel per unit length divided by the original steel mass. The reduced diameter and the remaining yield strength of rebars are calculated at different time steps during the life-cycle of the bridge (Table 2). These values are used to update the characteristics of bridge models during the structural capacity estimation and seismic performance evaluation of corroded bridges.

Through a step-by-step analysis, the time in which the concrete starts cracking is determined as the time when the percentage of steel mass loss, $m(t)$, becomes equal to a critical level, $m_{critical}$. The $m_{critical}$ which can be defined as a function of rebar dimensions and concrete properties (El Maaddawy and Soudki, 2007) is calculated in the present study equal to 20%. Based on this critical level, the crack initiation time is found to be 51 days (0.14 year) for the structures under consideration. To calculate the crack width after crack initiation, w_{crack} (mm), the analytical equation proposed by Vidal et al. (2004) can be used:

$$w_{crack}(t) = K_{crack} (\Delta A_s(t) - \Delta A_0) \quad (11)$$

Table 2. Reduction in the mass, diameter, and yield strength of reinforcing bars at 5-year time intervals

Time* (year)	0	5	10	15	20	25	30	35	40	45	50
(M _{loss} /M ₀)x100	0.00	6.38	12.24	18.10	23.96	29.82	35.68	41.54	47.40	53.26	59.12
D (mm)	35.80	34.75	33.61	32.46	31.32	30.17	29.03	27.88	26.74	25.59	24.45
f _y /f _{y0}	1.00	0.97	0.94	0.91	0.88	0.85	0.82	0.79	0.76	0.73	0.70

*after corrosion initiation

where $\Delta A_s(t)$ is the steel loss of the rebar cross section during the corrosion process (mm^2), ΔA_0 , the steel loss of the cross section needed for crack initiation (mm^2), and K_{crack} , an empirical coefficient equal to 0.0577. Assuming the crack width of 0.3 mm as one of the first serviceability limits, the time in which this limit is exceeded has been calculated to equal 117 days (0.32 year). Comparing the time to crack initiation (0.14 year) and the time to exceed the crack width of 0.3 mm (0.32 years) with the time to corrosion initiation (10.40 years), it can be clearly seen that the two former times are negligible within the whole life-cycle of the bridge. Hence, considering the fact that the crack initiation occurs shortly after the corrosion initiation time, it is assumed that the time corresponding to the serviceability threshold is equal to the corrosion initiation time. Furthermore, it is widely accepted that a crack width of more than 1 mm indicates the performance failure of the concrete cover. The time required for reaching this crack width limit has also been calculated to equal 542 days (1.48 year) after corrosion initiation. Since the capacity of structures under study will be evaluated every 5 years after the corrosion initiation time, it is assumed that the concrete cover is destroyed from the first analysis interval.

4. BRIDGE MODELING

To develop the probabilistic life time fragility parameters of RC bridges located in chloride-laden environments, a group of 9 box girder bridge models are developed and analyzed in this study.

This group consists of two-span bridges with three variations in the span lengths, representing the short-, medium-, and long-span bridges. All the bridges have two columns at each bent and their height varies from 7.5 to 12.5 m. This provides a range of span length-to-column height ratios from 1.2 to 6.0. For the purpose of this study, the effect of skewness is not considered and as a result, the skew angle is assumed to equal zero degrees. A schematic view of the bridges under study is illustrated in Figure 4 and their dimensions are summarized in Table 3.

OpenSees (2009) is used in this study to carry out a series of static and dynamic analyses which can provide a comprehensive performance assessment of the bridges subjected to the time-dependent corrosion process. At different bridge ages, the remained structural capacity and expected seismic response are calculated by analyzing the bridge mathematical models which consist of a variety of elements defined for the superstructure, pier, abutment, and foundation. The developed models are representative of the bridge geometric characteristics, boundary conditions, material properties, mass distribution, and nonlinear behavior of selected components. The detailed assumptions made for each of the bridge components are discussed below.

1. **Material Properties:** The compressive strength of concrete, f'_c , is assumed to equal 35 MPa for the bridge columns and superstructure. The Poisson's ratio is 0.2 and the concrete modulus of elasticity, E_c , is calculated for the normal weight concrete using:

$E_c = 4700\sqrt{f'_c}$ (ACI-318, 2008). To capture the effects of confinement in columns, the properties of confined and unconfined concrete are both taken into account following the equations given by Mander et al. (1988). For the reinforcing bars, the yield strength is assumed to equal 470 MPa before corrosion begins. As discussed in the previous section, the steel yield strength decreases over the time due to the corrosion progress (Equation 10).

2. **Superstructure Model:** The bridge superstructure has been designed for four traffic lanes, two in each direction (as it can be seen in Figure 4). The roadway width is equal to 23.0 m and the concrete cross-sectional area is 12 m². The bridge deck is modeled by linear-elastic beam-column elements placed at the centroid of the deck cross section. These elements are subjected to linear-distributed loads which represent the bridge mass per unit length. Since the columns and abutments are designed to experience the nonlinear behavior, no nonlinear properties are assigned to the superstructure elements and they always remain in the elastic range. Furthermore, because the concrete superstructure always experiences some cracks due to loading conditions, the flexural stiffness of deck section is modified by a factor of 0.75 according to the recommendation of Caltrans seismic design criteria (SDC, 2006).
3. **Pier Columns:** A nonlinear three dimensional beam-column element is used to model the bridge columns. This element is based on the iterative force formulation and considers the spread of plasticity along the column (OpenSees, 2009). The concrete cross section is discretized into a number of fibers (total of 18 wedges and 20 rings) defined by the fiber module available in OpenSees (2009) and the steel reinforcement

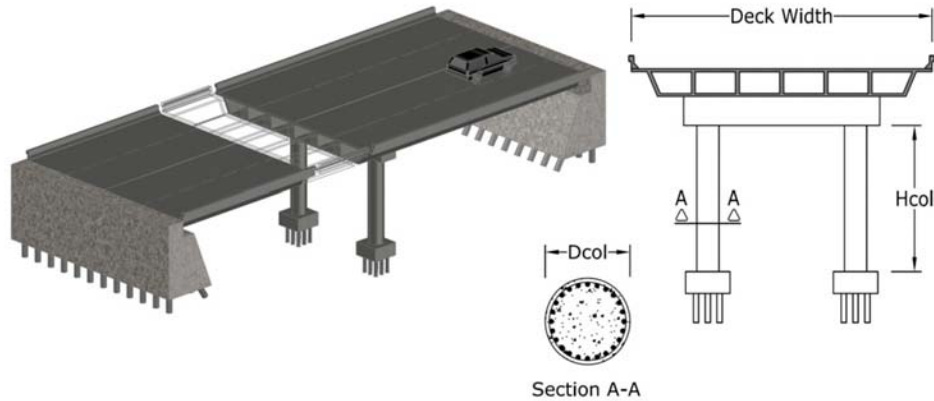
is considered by two additional circular layers of rebars.

4. **Abutments:** The bridge abutment is modeled using a rigid element with a length equal to the superstructure width, connected to the superstructure centerline through a rigid joint. This element is supported at each end by three springs in longitudinal, transverse, and vertical directions. While an elastic spring is used for the vertical direction, the longitudinal and transverse springs are expected to present a nonlinear behavior. For this purpose, nonlinear zero-length elements are placed in the perpendicular horizontal directions with the properties determined from the Caltrans seismic design criteria (SDC, 2006). The abutment stiffness and maximum resistance are dependent upon the material properties of abutment backfill and account for an expansion gap, here assumed to equal 5 cm.

As discussed earlier, the corrosion process may cause a significant structural capacity loss which directly affects the bridge performance under any service and extreme loading conditions. From a multi-hazard point of view, the combined effects of a natural event, here an earthquake, and an environmental stressor, here chloride-induced corrosion, are studied over the time and the vulnerability of bridge as one of the key infrastructure components is evaluated. Towards this goal, the nonlinear time-history analysis is employed to estimate the seismic response of various bridges at different ages. Obtained results will be used later for the probabilistic life-time fragility analysis.

In order to perform nonlinear time-history analysis, a suite of 60 earthquake ground motions is selected. These ground motions were originally generated through the FEMA/SAC project (1997) for the Los Angeles area and include records from historic earthquakes as well as artificially-generated time histories. The selected suite consists of

Figure 4. A schematic view of the two -span bridges under study



three sets of records corresponding to earthquakes with 4.04×10^{-4} , 2.10×10^{-3} , and 1.39×10^{-2} annual frequency of exceedance, which are equivalent to 2%, 10%, and 50% probability of occurrence in 50 years. Figure 5 shows the spectral acceleration values over a range of natural periods for the three categories mentioned. For each category of records, the median spectral acceleration has also been indicated which represents the expected level of seismic demand.

Using the selected suite of ground motions, the dynamic response of the bridge cases are evaluated. A series of 60 nonlinear time-history analysis is performed for each bridge case and

response time-histories are recorded as forces and displacements at various bridge components. For the sake of brevity, the current study demonstrates the seismic response only in terms of deck drift ratio which is one of reliable response measures among diverse response parameters. The deck drift ratio (DDR) is defined as the relative displacement of deck centroid divided by the column height. This ratio is calculated in both longitudinal and transverse directions, but since the ground motions are applied in the longitudinal direction, the transverse DDR can be neglected compared to the longitudinal one. The distribution of longitudinal DDR at different time steps is shown in

Table 3. Main dimensions of the reinforced concrete bridges under study

Bridge Case No.	Number of Spans	Span Length (m)	Column Height (m)	Column Diameter (m)
1	2	15-15	7.5	1.3
2	2	15-15	10	1.3
3	2	15-15	12.5	1.3
4	2	30-30	7.5	1.6
5	2	30-30	10	1.6
6	2	30-30	12.5	1.6
7	2	45-45	7.5	1.9
8	2	45-45	10	1.9
9	2	45-45	12.5	1.9

Figure 6 for the bridge with medium span length and column height of 10.0 m. The review of the drift data at each time step indicates that a log-normal distribution can be fit very well to the DDR response. It can be seen that both the median and standard deviation of the obtained distributions increase as the corrosion progresses and the scatter plot tends to the higher DDRs.

5. PROBABILISTIC LIFE-TIME FRAGILITY ANALYSIS

Fragility analysis is considered as a powerful tool for the probabilistic seismic risk assessment of highway bridges. Through this analysis, a set of fragility curves is developed to estimate the conditional probability statements of the bridge vulnerability as a function of ground motion intensity measure. The damageability of the bridge can be assessed by expert opinions (ATC, 1985), empirical data from past earthquakes (Basoz and Kiremidjian, 1999 and Shinotzuka et al., 2000a), and analytical methods (Mander and Basoz, 1999 and Shinotzuka et al., 2000b). The current study uses the later approach and defines four limit states of damage. The definitions of damage states are derived from HAZUS-MH (2007) and can be summarized as: (at least) slight, E_1 , (at least) moderate, E_2 , (at least) extensive, E_3 , and complete damage, E_4 . Based on these damage states, the analytical fragility curves of the bridge cases are generated at different ages after the corrosion initiation time.

To perform fragility analysis, the column curvature ductility is taken here as the primary damage measure. The curvature ductility is defined as the ratio of maximum column curvature recorded from a nonlinear time-history analysis to the column yield curvature obtained from moment-curvature analysis. Following the procedure given by Priestley et al. (1996), the curvature ductility values of all the bridge cases are calculated under the set of 60 ground motions and then compared with damage limit states. In

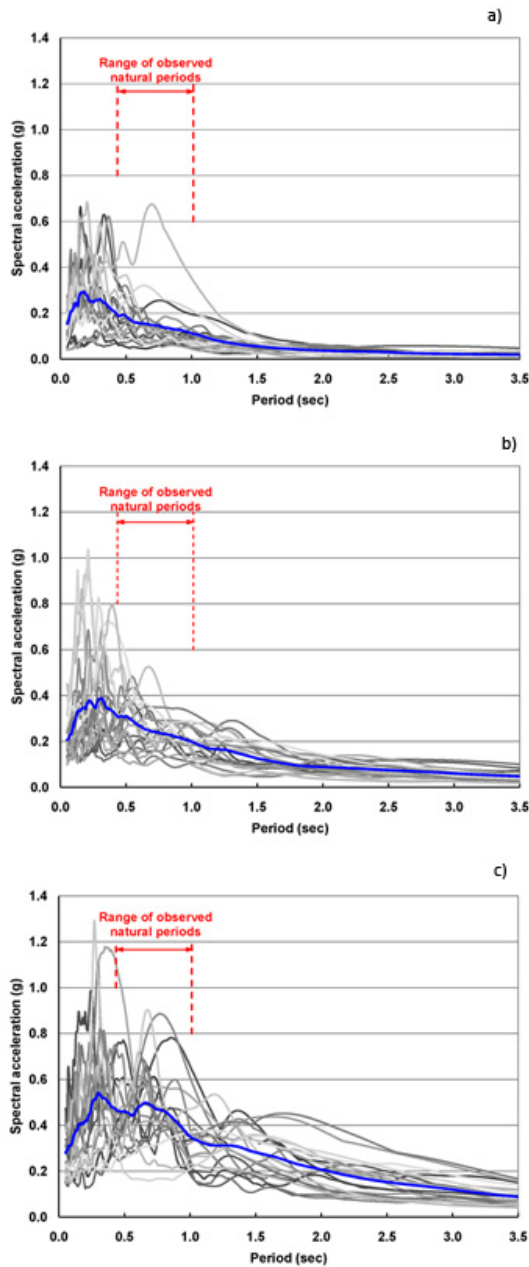
this study, the damage limit states are assumed to equal the ductility of 1.0, 2.0, 4.0, and 7.0 for the slight, moderate, extensive, and complete damage states, respectively. The estimation of these limit states are beyond the scope of this chapter, but the suggested values are in accordance with the limit states available in the literature for similar bridges (Hwang et al., 2000, Choi et al., 2004, and Yang et al., 2009).

Under a ground motion excitation with the peak ground acceleration of PGA_i (here $i = 1, \dots, 60$), a bridge sustains failure in a specific damage state if its ductility is larger than the ductility corresponding to that damage state. Depending on whether or not the bridge sustains the state of damage under different ground motions, the parameters of each fragility curve (i.e., median, c_k and log-standard deviation, ζ_k) are estimated using the maximum likelihood procedure given in Shinotzuka et al. (2000b). For the k -th damage state ($k = 1, 2, 3$, and 4), the fragility curve is developed following the formula below:

$$F_k(PGA_i | \zeta_k, c_k) = \Phi \left[\frac{\ln(PGA_i / c_k)}{\zeta_k} \right] \quad (12)$$

where F_k is the probability of exceeding the damage state of k and $\Phi[\cdot]$ is the standard normal distribution function. The fragility curves of the intact two-span bridges with the column height of 10.0 m, having a range of short, medium, and long span lengths, are illustrated in Figure 7. Additionally, the estimated median values (c_k) of the fragility curves developed for all the bridges under study are summarized in Table 4 for the four damage states considering the intact bridge conditions before the corrosion initiation time. For the log-standard deviation (ζ_k), it is seen that different deviation values may result in intersecting the fragility curves of different damage states. To avoid any intersection, Shinotzuka et al. (2000b) suggest considering one common deviation value for all the damage states. In this study, since the

Figure 5. Spectral acceleration plots developed for three sets of 20 ground motions with different seismic hazard levels: (a) 50% probability of occurrence in 50 years; (b) 10% probability of occurrence in 50 years; (c) 2% probability of occurrence in 50 years



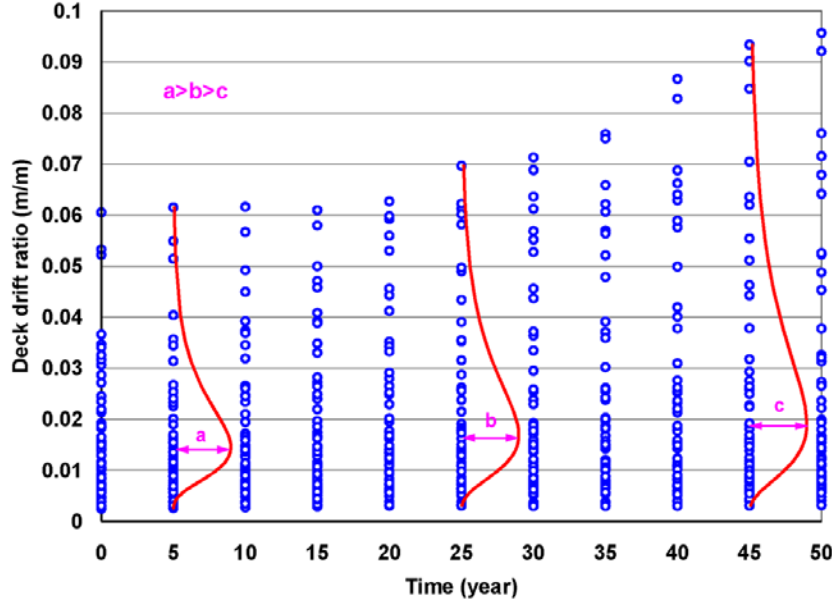
estimated log-standard deviations are very close to each other (ranging from 0.50 to 0.70), the median value of log-standard deviations (equal to 0.60) is selected as the identical log-standard deviation.

To evaluate the effects of chloride-induced corrosion on the seismic damageability of RC bridges, the fragility curves are generated for the case-study bridges at different time steps during their life-cycle. Considering the extent of structural degradation (as discussed in Section 3), the median and log-standard deviation of fragility curves are estimated for the corroded bridges following the procedure described for the intact bridges. The change in the median values of fragility curves is shown in Figure 8 for all the bridges with the column height of 10.0 m. This figure indicates that after 50 years, the overall average of median values obtained for the four damage states drops by 38%. For further illustration, the time-dependent fragility curves of the bridges with medium span length and column height of 10.0 m are depicted in Figure 9. It can be understood from this figure that for a specific PGA value, the probability of exceeding any damage state increases over the time due to the corrosion process. This increases the seismic damageability of bridge and makes it more vulnerable to natural hazards. The time-dependent fragility curves developed in this section will also be used to predict the life-cycle cost of bridges in a multi-hazard framework.

6. LIFE-CYCLE COST ANALYSIS OF DEGRADED BRIDGES

The life-cycle cost (LCC) of a structure is defined as the total cost of the structure from the beginning of planning for construction to the end of its service life time. The LCC analysis provides a framework that helps to allocate appropriate

Figure 6. The distribution of DDR response over the time for the two-span bridge with the medium span length and column height of 10 m



resources for design, construction, and operation of the structure. The focus of the current study is on the LCC analysis of RC bridges located in extreme chloride-laden environments. From the resources point of view, it is important to optimize the inspection and maintenance schedules in a way so that the total cost of structure is minimized while the structure satisfies the performance requirements.

The LCC of a bridge consists of a one-time initial cost associated with design and construction of the bridge and regular inspection and maintenance costs necessary at certain time intervals. The general formula for LCC analysis can be expressed as follows:

$$LCC = C_c + [C_{IN} + C_M + C_M^u] + [C_{sf} + C_{sf}^u] \quad (13)$$

where C_c is the initial construction cost, C_{IN} , the inspection cost, C_M , the maintenance cost, C_M^u , the user cost associated with the maintenance procedure, C_{sf} , the bridge service failure cost, and

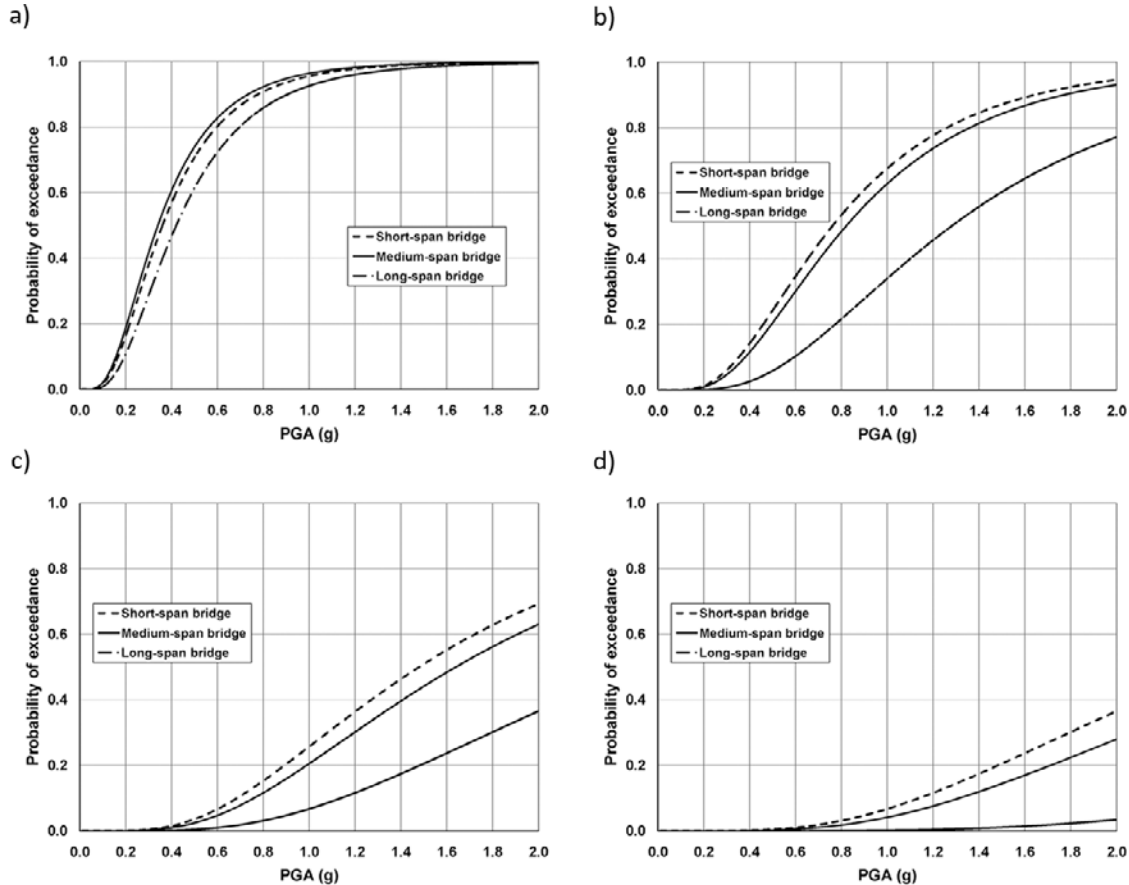
C_{sf}^u , the user cost associated with the probable service failure. The inflation is also taken into account by dominating future maintenance expenditures in base year prices. These recurrent maintenance costs are combined by weighing them according to a discount factor that takes into account the time value of the money. The discount factor, $z(t)$, is defined as:

$$z(t) = (1 + r)^{-t} \quad (14)$$

where r is the discount rate indicating the expected market rate of return on an investment. The choice of discount rate is often disputable in LCC analysis. In practice, the discount rate ranges from 2% to 8%. Generally, choosing a high discount rate favors short service life time while a low discount rate encourages a longer service life time.

The initial cost of construction is assumed to be the summation of the costs of the bridge components. The cost of the deck is computed as the

Figure 7. Fragility curves developed for different damage states of the intact two-span bridges with the medium span length and column height of 10 m: (a) at least slight damage state; (b) at least moderate damage state; (c) at least extensive damage state; (d) complete damage state



total area of the deck multiplied by a cost per unit deck area. Caltrans contract cost data (2008) suggests \$380 per m^2 for deck construction cost. For

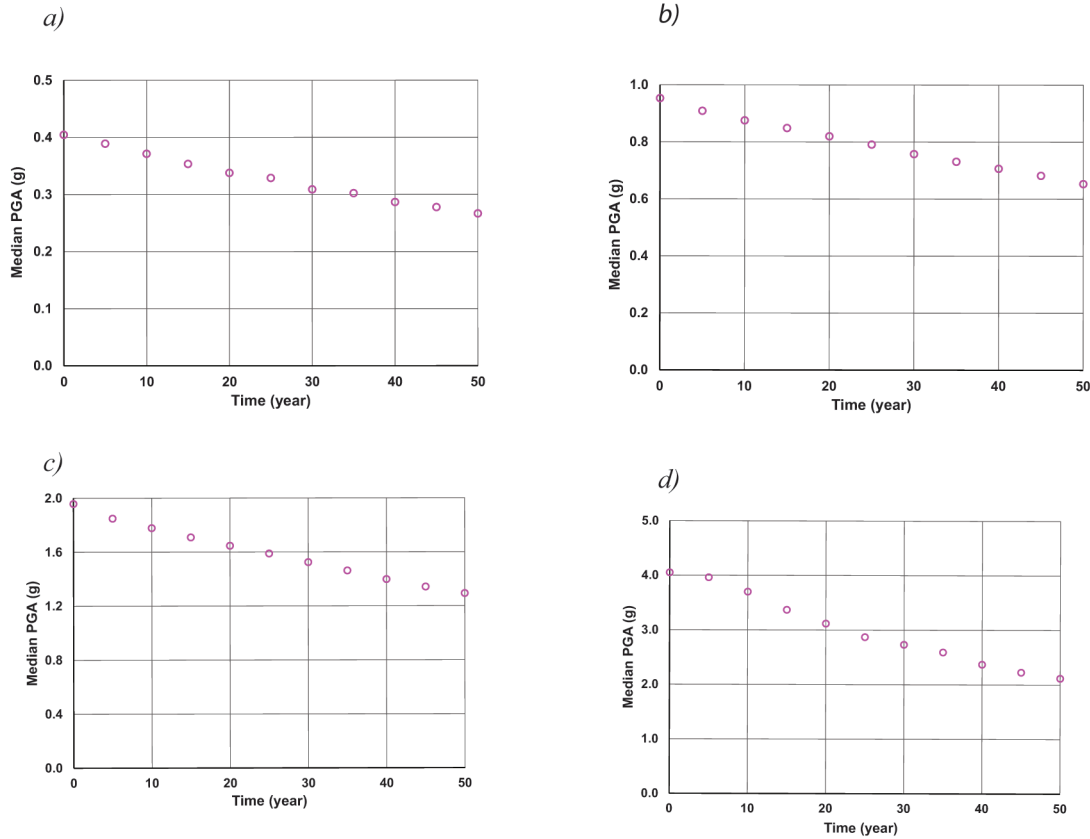
bridge piers, the construction cost includes the cost of steel work and concrete work. After calculating the total volumes of the steel and concrete, the

Table 4. Median values of the fragility curves estimated for all the bridge cases under different damage states

Two-Span	short-span				medium-span				long-span			
Damage State	E ₁	E ₂	E ₃	E ₄	E ₁	E ₂	E ₃	E ₄	E ₁	E ₂	E ₃	E ₄
H _{col} = 7.5 m	0.38	0.90	2.46	6.0*	0.32	0.68	1.36	1.90	0.42	0.78	1.36	1.90
H _{col} = 10.0 m	0.42	1.28	2.46	6.0*	0.34	0.82	1.64	2.84	0.36	0.76	1.48	2.46
H _{col} = 12.5 m	0.66	1.66	2.84	6.0*	0.38	0.82	2.46	6.0*	0.36	0.88	1.56	3.36

* indicates that no case of complete damage, E₄, was observed.

Figure 8. Time-dependant median values of fragility curves obtained for the two -span bridges with the column height of 10 m: (a) at least slight damage state; (b) at least moderate damage state; (c) at least extensive damage state; (d) complete damage state



pier cost can be estimated by assuming \$4 per kg of steel and \$840 per m³ of concrete according to Caltrans contract cost data (2008). The average total construction cost of short-, medium-, and long-span bridges under study can be seen in Table 5. Their inspection and maintenance costs as well as their failure costs will be discussed in the upcoming sections.

6.1. Inspection and Maintenance Costs

The cost of inspection and maintenance is expected to be incurred at regular time intervals, Δt . The inspection cost is calculate as:

$$C_{IN} = \sum_{i=1}^n S z(i\Delta t) \quad (15)$$

where S is the cost of each inspection, n , the number of maintenance intervals, and z , the discount factor from Equation 14. It can be seen that by increasing the number of inspections, n , during the life-cycle of the bridge, the inspection cost rises accordingly. For the bridges under study, the inspection cost is assumed to equal 0.5% of the construction cost. The maintenance cost over a structure's life span can be expressed as:

Figure 9. Time-dependant fragility curves for the two-span bridge with the medium span length and column height of 10 m; (a) at least slight damage state; (b) at least moderate damage state; (c) at least extensive damage state; (d) complete damage state

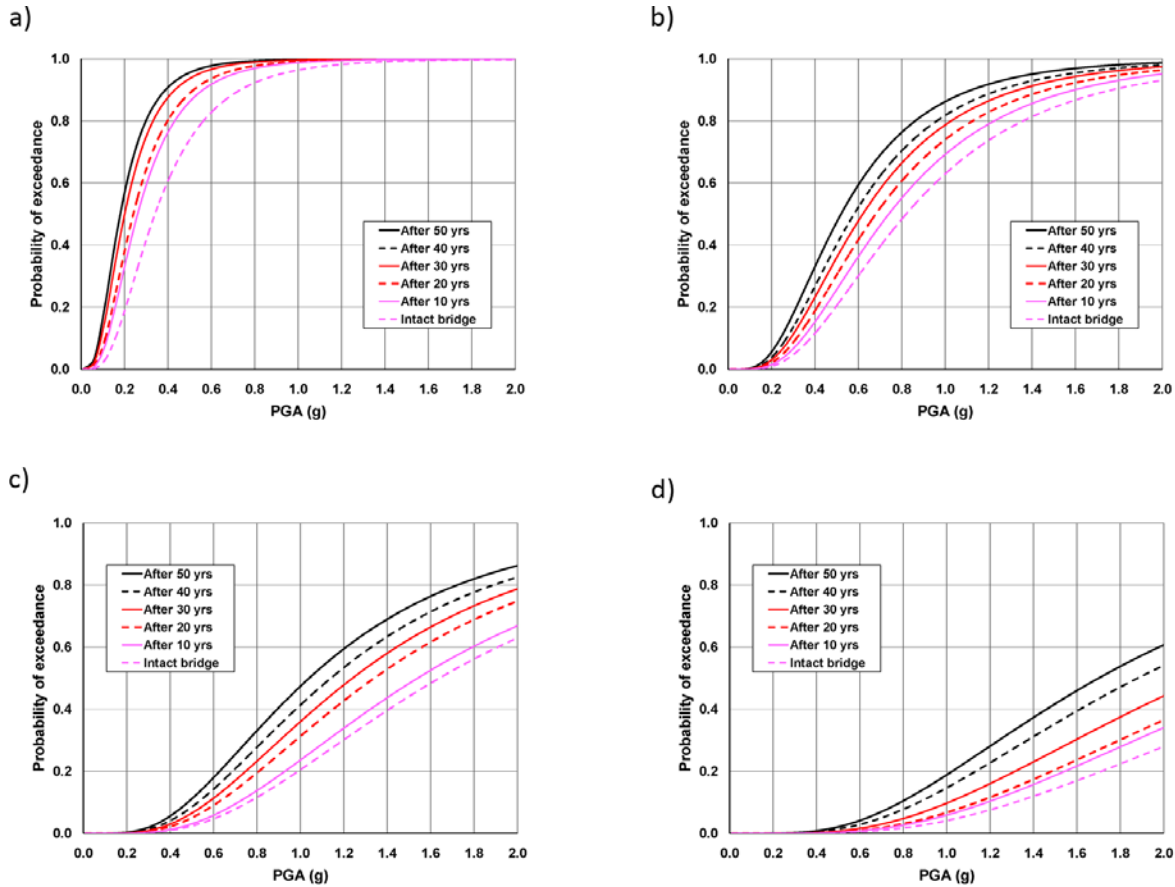


Table 5. Life-cycle cost of short-, medium-, and long-span bridges under study, including initial construction cost, inspection and maintenance costs, and service failure costs

Bridge Case	short-span	medium-span	long-span
C_c	\$361,151	\$500,117	\$639,083
C_{IN}	\$122,557	\$169,716	\$216,874
C_M	\$154,744	\$214,288	\$273,832
C_M^u	\$95,171	\$95,171	\$95,171
C_{sf}	\$90,085	\$124,749	\$159,412
C_{sf}^u	\$45,471	\$45,471	\$45,471
C_{total}	\$869,179	\$1,149,512	\$1,429,843

$$C_M = \sum_{i=1}^n Mz(i\Delta t) \quad (16)$$

where M is the cost of maintenance activity in base year prices. The maintenance cost is usually assumed between 0.5% to 1.0% of the construction cost, but since it is expected that the maintenance cost increases as the bridge ages, it is assumed here that the maintenance cost has a linear increasing trend from 0.5% to 1.0% during the structure's service life time.

In addition to the direct maintenance costs, the user cost associated with the temporary closure of facilities should also be considered. The actual user cost during the regular maintenance work depends on the extent and duration of service disruption (Chang and Shinozuka, 1996). This can be expressed as:

$$C_M^u = \sum_{i=1}^n t_m b_m u z(i\Delta t) \quad (17)$$

where t_m is the duration of maintenance activities, and b_m , the index of usage disruption ($0 \leq b_m \leq 1$). For example, if maintenance entails closure of one of the two lanes of a bridge, b_m would be 0.5. In Equation 17, u is the unit user cost which depends on the volume and type of traffic crossing the bridge as well as the availability of convenient alternative routes. The user cost also typically includes the increased costs associated with travel delays and accidents. In the current study, it is assumed that for the maintenance program, only 1/4 of bridge is closed at each period of time for one week. Hence, the average hourly user cost is calculated to be \$8.75 per vehicle. The annual traf-

fic is assumed to be 100,000 hour.vehicle.year⁻¹, which makes the user cost of the maintenance program equal to \$875,000. It is also assumed here that the inspection procedure is so short that it leads to negligible disruptions on bridge traffic, and as a result, it causes no user cost.

6.2. Service Failure Costs

The expected value for the service failure cost of a bridge can be calculated using Equation 18:

$$C_{sf} = \sum_{i=1}^n C_f z(i\Delta t) \Delta p_f(i) \quad (18)$$

where C_f is the repair cost due to the service failure, assumed to be equal to 20% of the construction cost. In order to obtain the expected service failure cost, the repair cost should be multiplied by the relevant probability of failure during each time interval of the bridge life-cycle. Since the current chapter studies the effects of the corrosion process on LCC of bridges, the probability of failure due to the corrosion process between $(i-1)$ -th and i -th time intervals, $\Delta p_f(i)$, has been calculated using a recursive formula suggested by Val and Stewart (2003) in Box 1: where p is the cumulative distribution function for the time of service failure. Since the crack initiation and propagation time (calculated in Section 4.2) is small comparing to the corrosion initiation time, the service failure is assumed to occur after the corrosion initiation time. The values of $\Delta p_f(i)$ have been calculated for different inspection intervals and are shown in Figure 10 for the entire life-cycle of the bridge, which is

Box 1.

$$\Delta p_f(i) = p(i\Delta t) - p[(i-1)\Delta t] + \sum_{j=1}^{i-1} \Delta p_f(j) \{ p[(i-j)\Delta t] - p[(i-j-1)\Delta t] \} \quad (19)$$

assumed to be 50 years after the corrosion initiation time. It is evident that as the number of inspections decreases, the probability of failure due to the corrosion process increases. According to Chang and Shinozuka (1996), the expected user cost associated with the probable service failure can be calculated as below:

$$C_{sf}^u = \sum_{i=1}^n t_{sf} b_{sf} u z(i\Delta t) \Delta p_f(i) \quad (20)$$

where t_{sf} is the duration of repair activities after failure, and b_{sf} the usage disruption parameter due to the service failure. In this study, it is assumed that it takes one month for the bridge to be repaired and during this time half of the bridge will be closed to traffic.

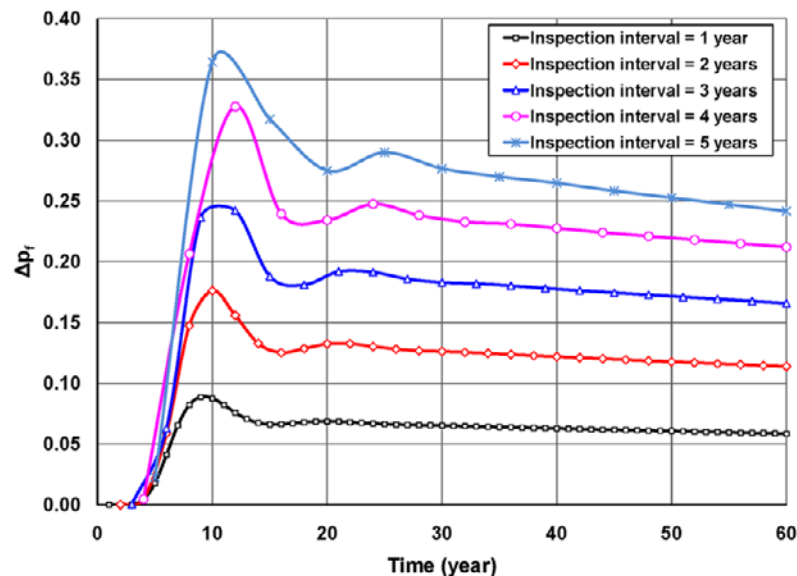
6.3. Optimized Inspection and Maintenance Intervals

Based on the total construction cost of the short-, medium-, and long-span bridge cases, the inspec-

tion and maintenance costs as well as the service failure costs of all the bridges are calculated and the average costs are summarized in Table 5. The values of Table 5 are obtained with the assumption of 4% annual inflation rate and scheduling annual inspection and maintenance program. This table shows that the user associated costs, C_M^u and C_{sf}^u , do not change for different bridge types, which indicates that they are independent of the construction cost.

In order to evaluate the effects of inspection and maintenance intervals on the LCC of bridges, different inspection and maintenance strategies have been examined. In this study, it is assumed that the inspection and maintenance intervals are the same and can be scheduled every 1, 2, 3, 4, or 5 years. Table 6 indicates the average inspection, maintenance, and service failure costs for the medium-span bridge inspected and maintained according to the proposed time schedules. The ratio of different cost types to the initial construction cost are depicted in Figure 11. Referring to Table 6 and Figure 11, when the inspection intervals

Figure 10. Probability of service failure due to the corrosion process for various inspection intervals



increase, the costs associated with the inspection and maintenance decrease but this causes a significant increase in the service failure cost. The total LCC of the bridge has been shown in Figure 12, considering the decreasing trend of inspection and maintenance costs and increasing trend of the service failure costs. From this figure, it can be understood that the total LCC of the bridge can be minimized if the inspection and maintenance intervals are scheduled for every 2 or 3 years. This schedule optimizes the inspection and maintenance costs while ensuring the safety of the bridge.

6.4. Earthquake-Induced Failure Cost

This section focuses on the LCC analysis of RC bridges considering the combined effects of natural hazards and environmental stressors on the estimation of the LCC. The extent of structural degradation and capacity loss due to the corrosion process were discussed in the previous sections and it is evident that an optimized plan for the inspection and maintenance of bridges is necessary to avoid any structural failure under the service or seismic loads. To satisfy overall performance requirements while minimizing the total resource costs, the LCC of bridges is evaluated in this study by taking into account the structural performance criteria in addition to the key cost parameters.

As mentioned earlier the total LCC of the bridge includes a one-time initial cost required for the design and construction of the bridge, some regular inspection and maintenance costs necessary at certain time intervals, and the costs associated with the serviceability failure of the corroded bridge due to earthquake events. Based on the mentioned costs, Equation 13 is updated as follows to account for the earthquake-induced failure cost for the degraded bridges.

$$LCC = C_c + [C_{IN} + C_M + C_M^u] + [C_{ef} + C_{ef}^u] \quad (21)$$

where C_{ef} is the bridge failure cost due to earthquake event, and C_{ef}^u , the user cost associated with the probable bridge failure.

The failure cost is assumed to equal the cost associated with the repair and replacement of the damaged parts of a bridge during probable natural hazards. Since the current chapter evaluates the seismic performance of corroded bridges, the state of damage after an earthquake event can be considered as an assessment measure for the estimation of failure cost. Through a probabilistic approach, the expected service failure cost is calculated for each of the damage states and the results are then combined with appropriate weighting factors. This procedure is repeated over the entire life-cycle of the bridge (n time intervals) to calculate the total failure cost by taking into account the failure probabilities which are updated at each time interval based on the corrosion process. The general formula for the estimation of failure cost is as below:

$$C_{ef} = \sum_{i=1}^n \sum_{k=1}^4 PI(d_k, i\Delta t) r_k z(i\Delta t) C_c \quad (22)$$

where r_k is the damage ratio (will be discussed later) and PI is the performance index for the damage state of d_k ($k = 1, 2, 3$, and 4) at i -th time interval. The performance index represents the overall performance of a particular corroded state of the bridge under a specified seismic hazard risk and it can be determined in terms of the annual probability of exceeding a given damage state considering the effects of deteriorating mechanisms. This index is calculated from Equation 23, as follows:

$$PI(d_k, i\Delta t) = \int_0^\infty P_{k,i}(DS > d_k | x) \left| \frac{dH(x)}{dx} \right| dx \quad (23)$$

Table 6. Effects of inspection/maintenance intervals on the life cycle cost of the medium-span bridge

Interval	annual	2-year	3-year	4-year	5-year
C_c	\$500,117	\$500,117	\$500,117	\$500,117	\$500,117
C_{IN}	\$169,716	\$86,887	\$54,368	\$39,966	\$32,798
C_M	\$214,288	\$112,618	\$69,391	\$51,288	\$43,249
C_M^u	\$95,171	\$48,723	\$30,488	\$22,412	\$18,392
C_{sf}	\$124,749	\$237,982	\$340,877	\$431,840	\$500,949
C_{sf}^u	\$45,471	\$86,744	\$124,249	\$157,405	\$182,595
C_{total}	\$1,149,512	\$1,073,071	\$1,119,490	\$1,203,028	\$1,278,100

where $P_{k,i}$ is the probability of suffering the damage state of d_k (i.e., $DS > d_k$) under the ground motion intensity (here PGA) of x . This probability can be obtained at each time interval from the updated fragility curve developed for that damage state. On the other hand, the probability of exceeding the ground motion intensity of x during the service life-time of the bridge can be calculated from a seismic hazard curve, $H(x)$, generated for the specific

location of the bridge. For further clarification, the current chapter demonstrates an application of the explained approach in the calculation of the failure cost of the case study bridges. It is assumed that these bridges are located at three different parts of the Los Angeles area which are similar in terms of exposure to chloride ions but are different in terms of the seismic hazard risk. The seismic hazard curves corresponding to these

Figure 11. Ratio of different cost items to the initial construction cost

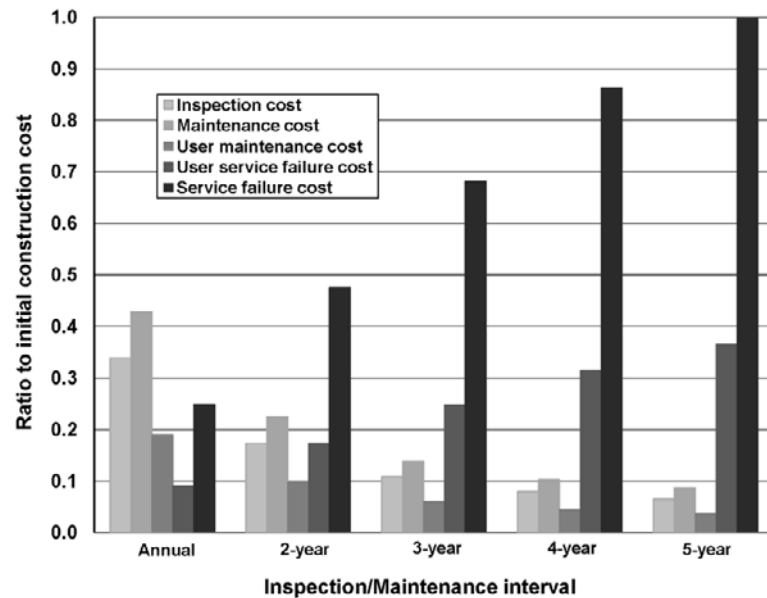
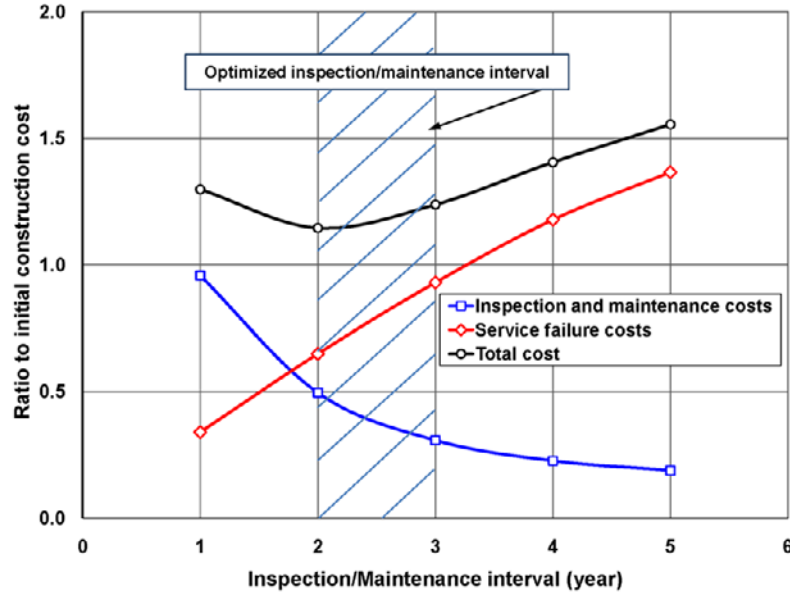


Figure 12. Total LCC of the medium-span bridge obtained for different inspection and maintenance intervals



locations have been extracted from the USGS database and shown in Figure 13. For the purpose of this study, these hazard curves represent high, medium, and low hazard risks and indicate a PGA of 0.48, 0.32, and 0.20g for 10% probability of exceedance in 50 years, respectively.

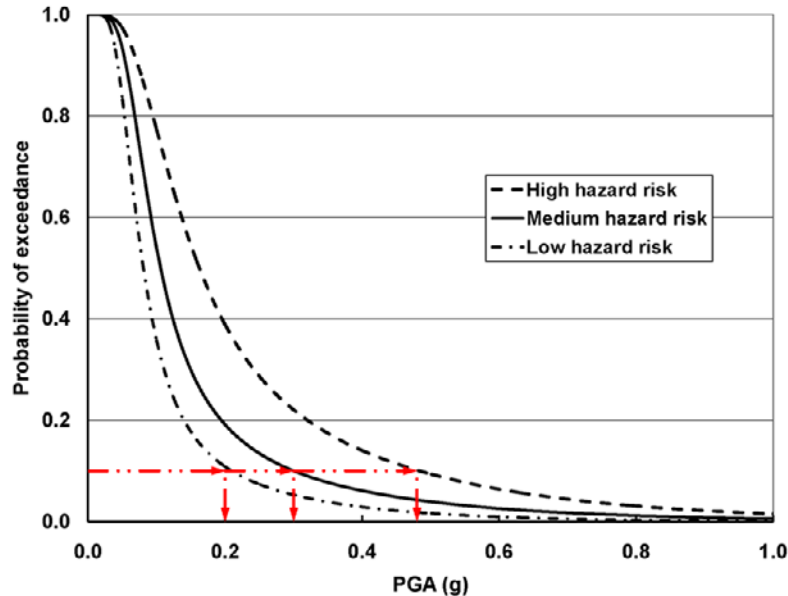
Using Equation 23, the performance indices for the three levels of seismic hazard risk are calculated in different states of damage at a range of PGA values. The obtained results are multiplied by damage ratios, r_k , which are employed as weighting factors to adjust the economic loss due to the different damage states. HAZUS-MH (2007) provides some ranges for damage ratios and also suggests the best estimates within each range for the slight, moderate, extensive, and complete damage states (Table 7). By repeating the explained procedure for all time steps, the earthquake induced failure cost is estimated from Equation 22.

The required steps for this procedure have also been schematically illustrated in Figure 14.

In addition to the failure cost which is directly related to the repair and replacement costs of a bridge, there are user costs associated with the closure of part or whole of a bridge to traffic after an earthquake. Similar to the user cost of the maintenance procedure, the total user cost of the bridge failure is calculated based on a unit user cost, u , which is assumed to be identical in both cases. By taking into account the time- and damage-dependent performance indices obtained from Equation 16, the total user cost of the bridge failure, C_{ef}^u , can be expressed as:

$$C_{ef}^u = \sum_{i=1}^n \sum_{k=1}^4 PI(d_k, i\Delta t) [t_f(d_k) b_f(d_k) u] z(i\Delta t) \quad (24)$$

Figure 13. Seismic hazard curves for three different locations in the Los Angeles area (USGS)



where t_f is the duration of repair activity and b_f is the usage disruption parameter due to the seismic damage ($0 \leq b_f \leq 1$). These two parameters depend on the state of damage, d_k , and the values assigned to them are summarized in Table 8.

The summation of failure cost and its associated user cost is calculated for each of the bridge cases and then the total failure cost is normalized to the relevant initial construction cost for comparison purposes. There are also three assumptions

for the regular inspection and maintenance activities, which include 1-, 2-, and 5-year time intervals. Considering three levels of seismic hazard risk, the ratio of total failure cost to initial construction cost is shown in Figure 15 for all the bridge cases. As it can be seen from this figure, the obtained ratios have an increasing trend when the inspection and maintenance activities are less frequent and as a result, the bridges have become more vulnerable to seismic events. As a case in

Table 7. Damage ratios for RC highway bridges (HAZUS-MH,2007)

Damage State	Range of Damage Ratios	Best Estimate Damage Ratio
slight	0.01-0.03	0.03
moderate	0.02-0.15	0.08
extensive	0.10-0.40	0.25
complete	0.03-1.00	1.00*

*If the number of spans is greater than two, then the best estimate damage ratio for complete damage is [2/(number of spans)]

Figure 14. Summary of required steps for the calculation of the failure cost of corroded bridges due to probable earthquake events

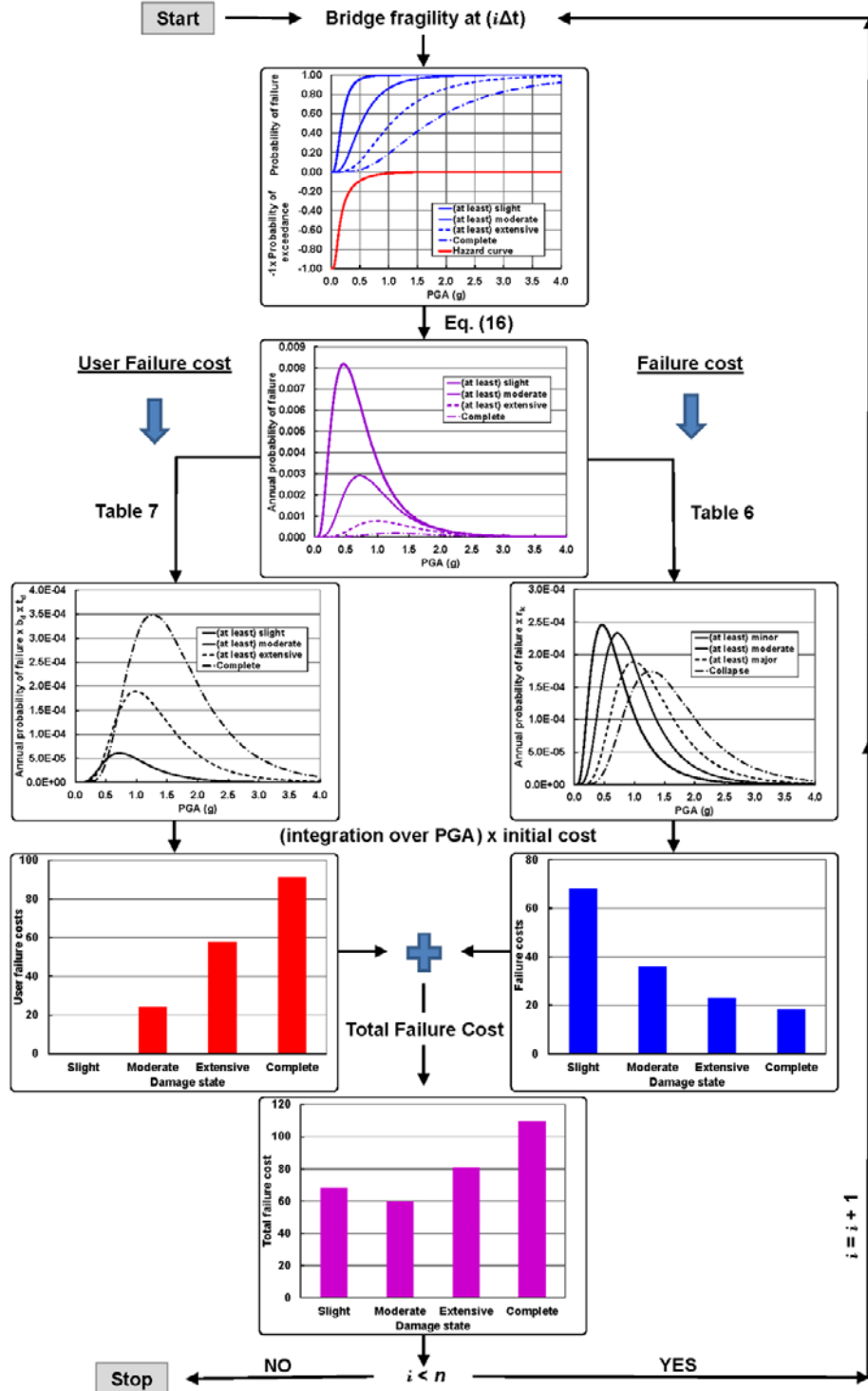


Figure 15. Ratio of total failure cost to initial construction cost for three levels of seismic hazard risk (Note: The geometric characteristics of each bridge case number can be found in Table 3): (a) low seismic hazard risk; (b) medium seismic hazard risk; (c) high seismic hazard risk

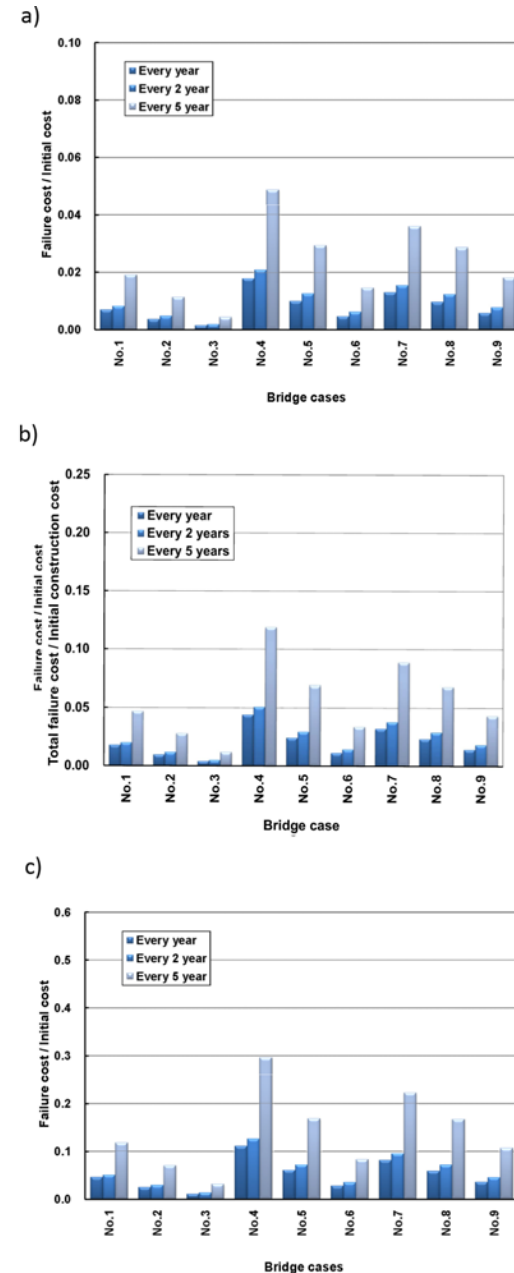


Table 8. Values assumed for b_f and t_f at different damage states

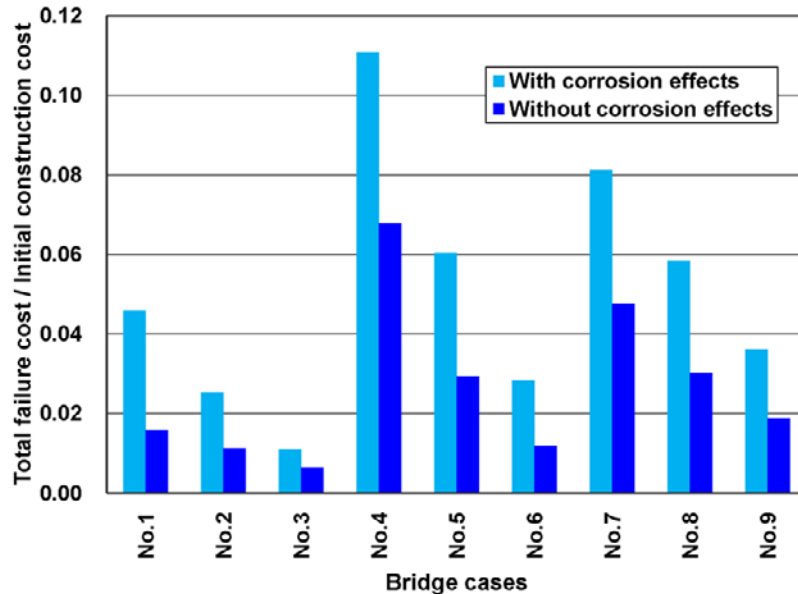
Damage State	b_f	t_f
slight	0	0
moderate	0.25	1 month
extensive	0.50	6 months
complete	1.00	24 months

point, the ratio of total failure cost increases between 5% to 19% for various bridge cases as the inspection and maintenance interval changes from every 1 year to every 5 years. On the other hand, planning for more frequent inspection and maintenance intervals may cause an increase in the total life-cycle cost of a bridge. Selecting the two-span bridge with the medium span length and column height of 10.0 m as the case-study, it is found that the ratio of total life-cycle cost (LCC) to initial construction cost is equal to 2.7, 2.4, and 3.3 for the inspection and maintenance intervals of 1, 2, and 3 years, respectively. This indicates that a 2-year interval would be probably an optimized interval which saves more money while limiting the probability of bridge failure.

As discussed earlier, the current chapter provides a multi-hazard framework for the estimation of the total life-cycle cost of bridges. But one may question the importance of the proposed framework considering the efforts required to take into account the deterioration process in addition to the seismic hazard risk. To respond to this concern, a comparison has been made between the ratios of total failure cost to initial construction cost calculated with and without the effects of the corrosion process (Figure 16). It can be found that this ratio is underestimated by a factor of 47% on average in case that the corrosion process is ignored. This indicates that the accuracy of life-cycle cost estimations can be improved significantly through the developed framework.

In order to simplify the evaluation of the corrosion process and easily incorporate it into the

Figure 16. Comparison between the ratios of total failure cost to initial construction cost calculated with and without the effects of corrosion (Note: The geometric characteristics of each bridge case number can be found in Table 3)



life-cycle cost analysis, adoption of some relationships which predict the extent of change in the performance of a bridge over the time is proposed. For this purpose, the performance index is chosen here as an appropriate measure since it considers the combined effects of corrosion and earthquake scenarios and can be directly used in the calculation of the life-cycle cost. For the bridges considered in the current study, with the given structural degradation rate and seismic hazard risk, a series of linear regression analysis is conducted to provide the users with an equation which updates the value of the performance index over the life-cycle of the bridge. This Equation can be expressed as follows:

$$PI(d_k, t) = PI_0(d_k) + A(d_k)t \quad (25)$$

where $PI_0(d_k)$ is the performance index calculated for a bridge in the intact condition (no deterioration) and $A(d_k)$ is the slope of the line which shows

the rate of change in the performance index value over the time given a specific state of damage (d_k). The expected values of $A(d_k)$ obtained from the detailed analysis of the bridge cases for different seismic hazard risks and damage states are summarized in Table 9. The performance indices extracted from Equation 18 can be used to predict the failure costs in bridge cases with similar deterioration scenarios and seismic hazard conditions.

7. CONCLUSION

Reinforced concrete highway bridges are continuously exposed to different environmental stressors during their service life time. Chloride-induced corrosion is one of deterioration mechanisms that causes serious structural degradation and may result in the service failure of the entire bridge. This chapter develops a comprehensive framework to study the chloride intrusion mechanisms and

Table 9. Suggested values for $A(d_k)$ in Equation 25

Damage State	Seismic Hazard Risk		
	Low	Medium	High
slight	3.26×10^{-5}	5.44×10^{-5}	9.93×10^{-5}
moderate	5.53×10^{-6}	1.05×10^{-5}	2.38×10^{-5}
extensive	1.66×10^{-6}	3.74×10^{-6}	9.12×10^{-6}
complete	5.46×10^{-7}	1.43×10^{-6}	3.66×10^{-6}

predict the progress of corrosion in reinforced concrete members. Through this study, the effects of various influential parameters, such as water to cement ratio, ambient temperature, relative humidity, concrete age, free chloride content, and binding capacity, are carefully considered for an accurate estimation of the chloride penetration profile in deteriorating structural members over the time.

The corrosion initiation time is estimated by comparing the chloride content values in the vicinity of reinforcing bars with critical thresholds. After the determination of the corrosion initiation time, the rate of reduction in geometry and material properties due to the corrosion process is calculated at different time steps. This chapter specifically considers the reduction rate of diameter and yield strength of reinforcing bars in corroded members. The crack initiation and propagation in concrete cover is also investigated in order to modify the confinement assumptions required for capacity evaluation. Based on the updated structural characteristics of corroded members, the capacity loss of a group of RC bridges with short, medium, and long spans is evaluated. In addition to the structural degradation, the effects of the corrosion process on the life-cycle cost of bridges are also studied. From the detailed calculation of construction, inspection, maintenance, and service failure costs of the bridges, this chapter examines various inspection and maintenance strategies and suggests the optimized inspection and maintenance intervals. The proposed procedure minimizes the

total life-cycle cost of the bridge while maintains its expected structural performance.

This chapter also provides a multi-hazard framework that evaluates the life-cycle performance and cost of reinforced concrete highway bridges. The bridges under consideration are located in seismic areas and they are continuously exposed to the attack of chloride ions. As a result, it is necessary to study the combined effects of a natural hazard and an environmental stressor over the time. The time-dependent seismic fragility curves of the bridges are then generated using a set of damage states for the purpose of seismic risk assessment. In addition to the probabilistic structural evaluation, the results of fragility analysis are employed to estimate the total life-cycle cost of the bridges. To consider both earthquake and corrosion scenarios, a performance index is introduced which represents the vulnerability of a corroded bridge under a specified seismic hazard risk. Comparing the life-cycle costs calculated with and without the effects of corrosion, it is found that the suggested performance index plays a key role in obtaining more realistic estimates of the total costs and it provides valuable information to optimize the inspection and maintenance intervals. The time-dependent variation of this index is also formulated to be directly used in the life-cycle cost analysis of similar cases without going through the detailed corrosion models.

REFERENCES

- American Concrete Institute. (2008). *ACI-318: Building code requirements for structural concrete and commentary*. ACI.
- Andrade, C., Alonso, C., Garcia, D., & Rodriguez, J. (1991). Remaining life time of reinforced concrete structures: effect of corrosion in mechanical properties of the steel, life prediction of corrodible structures. *Proceedings of the International Symposium of the National Association of Corrosion Engineers*, 12/1-12/11, Cambridge, U. K.
- Andrade, C., Alonso, C., & Molina, F. J. (1993). Cover cracking as a function of rebar corrosion: Part I: Experimental test. *Materials and Structures*, 26(3), 345–353.
- Applied Technology Council. (1985). *ATC-13: Earthquake damage evaluation data for California*. Redwood City, CA: ATC.
- Bamforth, P. B., & Price, W. F. (1996). *An international review of chloride ingress into structural concrete*. Rep. No. 1303/96/9092. Middlesex, UK: Taywood Engineering Ltd., Technology Division.
- Basoz, N., & Kiremidjian, A. (1999). Development of empirical fragility curves for bridges. *Proceedings of 5th US Conference on Lifeline Earthquake Engineering*, ASCE, New York, USA.
- Bazant, Z. P., & Najjar, L. J. (1972). Nonlinear water diffusion in unsaturated concrete. [Paris, France]. *Materials and Structures*, 5(25), 3–20.
- Bertolini, L. (2008). Steel corrosion and service life of reinforced concrete structures. *Structure and Infrastructure Engineering*, 4(2), 123–137. doi:10.1080/15732470601155490
- California Department of Transportation. (2006). *Caltrans seismic design criteria*. Sacramento, CA: Author.
- California Department of Transportation. (2008). *Caltrans contract cost data*. Sacramento, CA: Author.
- Chang, S., & Shinozuka, M. (1996). Life cycle cost analysis with natural hazard risk. *Journal of Infrastructure Systems*, 2(3), 118–126. doi:10.1061/(ASCE)1076-0342(1996)2:3(118)
- Choi, E., DesRoches, R., & Nielson, B. (2004). Seismic fragility of typical bridges in moderate seismic zones. *Journal of Engineering Structures*, 26(2), 187–199. doi:10.1016/j.engstruct.2003.09.006
- Du, Y. G., Clark, L. A., & Chan, A. H. C. (2005a). Residual capacity of corroded reinforcing bars. *Magazine of Concrete Research*, 57(3), 135–147. doi:10.1680/macr.2005.57.3.135
- Du, Y. G., Clark, L. A., & Chan, A. H. C. (2005b). Effect of corrosion on ductility of reinforcing bars. *Magazine of Concrete Research*, 57(7), 407–419. doi:10.1680/macr.2005.57.7.407
- El Maaddawy, T., & Soudki, K. (2007). A model for prediction of time from corrosion initiation to corrosion cracking. *Journal of Cement and Concrete Composites*, 29(3), 168–175. doi:10.1016/j.cemconcomp.2006.11.004
- Glass, G. K., & Buenfeld, N. R. (2000). The influence of chloride binding on the chloride induced corrosion risk in reinforced concrete. *Corrosion Science*, 42(2), 329–344. doi:10.1016/S0010-938X(99)00083-9
- HAZUS-MH/MR3. (2007). FEMA's software program for estimating potential losses from disasters.
- Hwang, H., Liu, J. B., & Chiu, Y.-H. (2001). *Seismic fragility analysis of highway bridges*. Tennessee, USA: Center of Earthquake Research and Information, The University of Memphis.

- Kong, J. S., Ababneh, A. N., Frangopol, D. M., & Xi, Y. (2002). Reliability analysis of chloride penetration in saturated concrete. *Journal of Probabilistic Engineering Mechanics*, 17(3), 302–315. doi:10.1016/S0266-8920(02)00014-0
- Lee, H. S., Tomosawa, F., & Noguchi, T. (1996). Effect of rebar corrosion on the structural performance of single reinforced beams. In Lacasse, M. A., & Vanier, D. J. (Eds.), *Durability of building material and components* (pp. 571–580). London, UK: E & FN Spon.
- Mander, J. B., & Basoz, N. (1999). Seismic fragility curve theory for highway bridges. *Proceedings of the 5th US Conference on Earthquake Engineering TCLEE No.16*, (pp. 31-40).
- Mander, J. B., Priestly, M. J. N., & Park, R. (1988). Theoretical stress-strain model for confined concrete. *Journal of the Structural Division*, 114(8), 1804–1826. doi:10.1061/(ASCE)0733-9445(1988)114:8(1804)
- Martin-Perez, B., Pantzopoulou, S. J., & Thomas, M. D. A. (2001). Numerical solution of mass transport equations in concrete structures. *Journal of Computers and Structures*, 79(13), 1251–1264. doi:10.1016/S0045-7949(01)00018-9
- McGee, R. (1999). Modeling of durability performance of Tasmanian bridges. *Proceedings of the ICASP8 Conference*, (pp. 297-306). Sydney, Australia.
- Morinaga, S. (1996). *Remaining life of reinforced concrete structures after corrosion cracking. Durability of Building Material and Components* (pp. 127–136). London, UK: E & FN Spon.
- OpenSees Development Team. (2009). *OpenSees: Open system for earthquake engineering simulation*. Berkeley, CA, USA.
- Priestly, M. J. N., Seible, F., & Calvi, G. M. (1996). *Seismic design and retrofit of bridges*. USA: John Wiley and Sons Inc. doi:10.1002/9780470172858
- Rodriguez, J., & Ortega, L. M. (1994). *Assessment of structural elements with corroded reinforcement. Corrosion and Corrosion Protection in Concrete*. Sheffield, UK: Sheffield Academic press.
- Saetta, A. V., Schrefler, B. A., & Vitaliani, R. V. (1993). The carbonation of the concrete and the mechanism of moisture, heat and carbon dioxide flow through porous material. *Journal of Cement and Concrete Research*, 23(4), 761–772. doi:10.1016/0008-8846(93)90030-D
- Shinozuka, M., Feng, M. Q., Kim, H.-K., & Kim, S.-H. (2000b). Nonlinear static procedure for fragility curve development. *Journal of Engineering Mechanics*, 126(12), 1287–1296. doi:10.1061/(ASCE)0733-9399(2000)126:12(1287)
- Shinozuka, M., Feng, M. Q., Lee, J., & Naanuma, T. (2000a). Statistical analysis of fragility curves. *Journal of Engineering Mechanics*, 126(12), 1224–1231. doi:10.1061/(ASCE)0733-9399(2000)126:12(1224)
- Somerville, P., Smith, N., Punyamurthula, S., & Sun, J. (1997). *Development of ground motion time histories for Phase 2 of the FEMA/SAC steel project*. SAC joint venture, California, USA. U.S. Geological Survey. (USGS). Retrieved from www.usgs.gov
- Val, D., & Stewart, M. G. (2003). Life-cycle cost analysis of reinforced concrete structures in marine environments. *Journal of Structural Safety*, 25(4), 343–362. doi:10.1016/S0167-4730(03)00014-6
- Val, D. V. (2004). *Aspects of corrosion in reinforced concrete structures and its influence on structural safety*. Report No. 2002950, National Building Research Institute.

- Vidal, T., Catel, A., & Francois, R. (2004). Analyzing crack width to predict corrosion in reinforced concrete. *Cement and Concrete Research*, 34(1), 165–174. doi:10.1016/S0008-8846(03)00246-1
- Xi, Y., & Bazant, Z. P. (1999). Modeling chloride penetration in saturated concrete. *Journal of Materials in Civil Engineering*, 11(1), 58–65. doi:10.1061/(ASCE)0899-1561(1999)11:1(58)
- Yang, C. S., DesRoches, R., & Padgett, J. E. (2009). Fragility curves for a typical California box girder bridge. *Proceedings of the 2009 ASCE Technical Council on Lifeline Earthquake Engineering Conference*, San Francisco, California, USA.

Chapter 5

Efficient Robust Optimization of Structures Subjected to Earthquake Load and Characterized by Uncertain Bounded System Parameters

Subrata Chakraborty

Bengal Engineering and Science University, Shibpur, India

Soumya Bhattacharjya

Bengal Engineering and Science University, Shibpur, India

ABSTRACT

An efficient robust design optimization (RDO) procedure is proposed in the framework of an adaptive response surface method (RSM) for structures subjected to earthquake load and characterized by uncertain but bounded system parameters. The basic idea of the proposed RDO approach is to improve the robustness of a design by using a new dispersion index which utilizes the relative importance of the gradients of the performance function. The same concept is also applied to the constraints. The repeated computations of stochastic responses and their sensitivities for evaluating the stochastic constraint of the associated optimization problem are efficiently obtained in the framework of an adaptive RSM. The proposed RDO approach is elucidated through the optimization of a three-storied concrete frame structure. The numerical study depicts that the proposed RDO results are in conformity with the conventional RDO results. However, definite improvements are achieved in terms of robustness and computational time requirements indicating its efficiency over the conventional RDO approach.

DOI: 10.4018/978-1-4666-1640-0.ch005

INTRODUCTION

The response of a structural system under environmental loads such as wind, water wave, earthquake, etc. is highly uncertain and can be best modelled as a stochastic process. The optimization of structure under such loads is normally dealt in the literature in the form of standard nonlinear optimization problem. The dynamic responses to define the stochastic constraints of the related optimization problem are obtained by random vibration theory. Subsequently, a standard nonlinear optimization problem is formulated where the weight of the structure or a desired stochastic response quantity is minimized. The procedure is termed as stochastic structural optimization (*SSO*). The details of the relevant developments can be found in (Nigam, 1972), Kang et al. (2006). It may be underlined here that in a typical *SSO* procedure the dynamic load is considered to be the only source of randomness in many cases and all other system parameters are assumed to be deterministic. But, uncertainty in the system parameters is inevitable to model a realistic structural system and incorporation of such uncertainty creates an interaction between the stochastic descriptions of the loads and the uncertain parameters (Jensen, 2002). Furthermore, the effect of system parameter uncertainty is important as the safety of structure may be endangered due to this (Chaudhuri, & Chakraborty, 2006) and can affect the final optimal design significantly (Schuëller, & Jensen, 2008). Thus, there is a growing interest to consider the effect of uncertainty in the optimization process for economic design of structure ensuring necessary safety requirements.

The developments in the optimum design of structure under uncertainty can be divided into three broad categories: (i) performance based design optimization (*PBDO*), (ii) reliability based design optimization (*RBDO*), and (iii) robust design optimization (*RDO*). The limitation of the *PBDO* is quite obvious as it optimizes the mean

or nominal value of a performance function disregarding its variation due to uncertainty. The *RBDO* ensures a target reliability of a design for a specific limit state. An efficient *RBDO* was presented for linear (Jensen, 2005) and nonlinear (Jensen, 2006) deterministic dynamic systems under earthquake load. Jensen et al. (2008) have further extended the approach to include the randomness in the system parameters. Lagaros et al. (2008) proposed an *RBDO* procedure for computationally intensive system under earthquake load and random system parameters. Mohsine et al. (2005) presented an *RBDO* method where solution has been achieved in a hybrid design space (HDS) considering probabilistic variations of parameters under deterministic dynamic load. The HDS considers reliability level in the same design space of the objective functions and constraints. An optimum seismic design criterion was proposed by Marano et al. (2006) for elastic structures considering deterministic system parameters. The optimum design of structure considering system parameter uncertainty as discussed above is mainly accomplished in the framework of *RBDO* to ensure a target reliability of structure with respect to desired performance modes. It may be noted here that the studies on the optimization of dynamic system considering system parameter uncertainty primarily apply the total probability theory concept to obtain the unconditional response or the failure probability of the system which is subsequently used as the performance measure. However, the optimization has been performed without any consideration to the possible variation of the performance of the structure due to system parameter uncertainty. It may be realized that such a design approach not necessarily corresponds to an optimum design in terms of minimum dispersion of the performance objective of the design. Rather, the system may be sensitive to the variations of the system parameters due to uncertainty. In order to obtain a more viable optimum design, the *RDO* approach is more desirable which optimizes a performance

index expressed in terms of the mean value of the performance function (obtained by the so called *RBDO* approach) as well as its dispersion due to uncertainty. Thereby, a design configuration of the structure can be achieved so that the performance objective is less sensitive to the variations due to system parameter uncertainty. Furthermore, the *RBDO* of structure, based on a probabilistic description of uncertain parameters attains its limitation when sufficient reliable data are not available for describing the system parameter uncertainty of a real life system. In fact, often a probabilistic description of uncertainty arising from insufficient information is warned in order to incorporate our partial knowledge about the system. A preferable approach is to model the system parameters as uncertain but bounded (*UBB*) type. In such a case, the *RDO* approach becomes an attractive alternative to the *RBDO* approach. The *RDO* approach is fundamentally concerned with minimizing the effect of uncertainty in the Design Variables (*DVs*) (the specific system parameters designer needs to optimize to achieve a desired performance) and the Design Parameters (*DPs*) (which cannot be controlled by the designer or are difficult and expensive to control). The subject of the present chapter is the *RDO* of structures under stochastic load (earthquake to be specific) considering *UBB* type system parameters.

BACKGROUND

To present the proposed *RDO* approach, it will be informative to discuss the background of *RDO* of structures with emphasis on optimization of stochastic dynamic system. In doing so, the related developments in the field of *RDO* are presented first to justify the relevance of the present study. Subsequently, the concept of conventional *RDO* approach, the *SSO* under earthquake load assuming deterministic system parameters and the metamodelling based approximation of stochastic dynamic responses are briefly presented.

The RDO Method: Developments

The concepts of *RDO* have been developed independently in different scientific disciplines and the developments in the recent past are noteworthy as evident from the works of Park et al. (2006); Beyer, & Sendhoff (2007). The limited information on uncertainty is usually integrated with a nondeterministic optimization framework to obtain an *RDO* (Park, Lee, & Hwang, 2006). This approach is often referred as sensitivity based approach. There are various such *RDO* approaches adopted by different researchers e.g. robust counterpart approach (Lewis, 2002), semi-definite programming (Ben-Tal, & Nemirovski, 2002; Bertsimas, & Sim, 2004), worst case sensitivity region concept (Gunawan, & Azarm, 2005), minimization of sensitivity matrix (Al-Widyan, & Angeles, 2005) etc. A new semi-analytical method to calculate the sensitivity of stability boundary for a system of delay differential equations was presented by Kurdi et al. (2008). Guo et al. (2009) proposed a bi-level programming technique using a semi-definite programming to solve *RDO* problem under non-probabilistic and non-convex stiffness and load uncertainties. The study on *RDO* procedure in the field of stochastic dynamic systems is comparatively a less attempted area compared to the deterministic design optimization (*DDO*) and the *RBDO* procedures. Hwang et al. (2001) minimized the mean and the variance of displacement at the first resonance frequency of an automobile mirror considering system parameter uncertainty. Zang et al. (2005) reviewed the applications of optimization of dynamic system and presented an *RDO* procedure for a vibration absorber considering mass and stiffness uncertainties under deterministic sinusoidal load. Son and Savage (2007) proposed a probabilistic design of vibration absorber parameters to reduce the mean as well the variance of dynamic performance measure. Marano et al. (2008) investigated *RDO* solution for a tuned mass damper (TMD) system in seismic vibration mitigation. Taflanidis and

Beck (2008) proposed an *RDO* procedure for a base-isolation system under earthquake load considering system parameter uncertainty. The unconditional performance function was evaluated through stochastic simulation. Guedri et al. (2009) proposed a stochastic metamodel based approach integrated with an *RDO* procedure to reduce the cost of uncertainty analysis. In a recent study, Marano et al. (2010) presented an *RDO* criterion for a TMD system in seismic vibration control of structures. Taflanidis (2010) presented an *RDO* procedure of a linear dynamic system under stochastic stationary excitation using simulation based approach.

The review of currently available literature reveals that the developments in the field of *RDO* procedures have been taken place in three distinct areas: (i) mathematical formulation of *RDO* procedure as a *SSO* problem or deterministic programming (Du, & Chen, 2000; Lee, & Park, 2001; Gunawan, & Azarm, 2005), (ii) solution strategies (Du, Sudjianto, & Chen, 2004; Beyer, & Sendhoff, 2007), and (iii) assessment of robustness (Huang, & Du, 2007). The literature on *RDO* procedures largely indicates that the applications of *RDO* procedures in dynamics is lesser compared to its applications in static. Moreover, in many such applications, the dynamic load is considered to be deterministic in nature. It is generally observed that the existing *RDO* formulations put equal importance to each individual gradient of the performance function and constraints. But, it is well-known to the structural reliability community that all the gradients of a performance function are not of equal importance (Gupta, & Manohar, 2004; Haldar, & Mahadevan, 2000). In fact, when a large numbers of *DVs* and *DPs* are involved in a structural reliability analysis problem, the dominant parameters having relatively stronger influence on the reliability are identified by using the relative importance of the gradients. The concept has been successfully used in the reduction of number of random variables in large scale reliability analysis problems. Thus,

it is intuitively expected that the importance of the individual gradient should also provide useful information to measure the robustness of the performance of a design and the concept can be applied in the *RDO* procedure. In this regard, it is of worth mentioning that most of the engineering design problems are strongly based on computationally expensive complex computer code and numerical analysis. For a large-scale system design, a preferable strategy is to utilize the metamodeling technique to approximate the implicit performance functions and constraints (Jurecka, Ganser, & Bletzinger, 2007). However, the accuracy of the metamodel based optimization approach relies on how accurate the response surface method (*RSM*) is in capturing the performance variations during the iteration cycles of a typical numerical optimization procedure (Jin, Chen, & Simpson, 2001). Generally, the *RSM* is based on the least-squares method (*LSM*) which is primarily a global approximation of scatter position data (Myers, & Montogmery, 1995). It is well-known that the *LSM* is one of the major sources of error in the response approximation by the *RSM*. The moving least-squares method (*MLSM*), basically a local approximation approach is found to be more efficient in this regard (Kim, Wang, & Choi, 2005). However, the studies addressing the *RDO* of structure using the *MLSM* based metamodeling technique is observed to be scarce than the applications of the *MLSM* addressing the *RBDO* or the *DDO* procedures.

The focus of the present chapter is on an improved *RDO* strategy for structures subjected to stochastic earthquake load and characterized by *UBB* type *DVs* and *DPs*. The formulation is proposed in the framework of *MLSM* based adaptive *RSM*. The basic idea of the proposed *RDO* approach is to improve the robustness of the performance function using a new dispersion index, which utilizes the weight factors proportional to the importance of each gradient of the performance function. The same concept is also applied to the constraints. The repeated computations of the

stochastic dynamic responses and their sensitivities for evaluating the stochastic constraint of the related optimization problem have been avoided by applying the *MLSM* based adaptive *RSM*. The proposed *RDO* approach is elucidated through the optimization of a three-storied concrete frame. The numerical results obtained by the conventional and the proposed *RDO* approaches are presented to demonstrate the effectiveness of the proposed *RDO* approach.

The Conventional RDO Approach

Most of the developments in the field of *RDO* as discussed in the previous section primarily use the weighted sum method (*WSM*) for examples as adopted by Du & Chen (2000), Lee & Perk (2001). This approach is termed in the present study as ‘the conventional *RDO* approach’ in which the robustness of a design performance is expressed in terms of the dispersion of performance function from its nominal value.

Let, $\mathbf{u} = (\mathbf{x}, \mathbf{z})$ is a vector composed of n -dimensional DVs, $\mathbf{x} = [x_1, x_2, \dots, x_n]$ and l -dimensional DPs, $\mathbf{z} = [z_1, z_2, \dots, z_l]$. The lower and upper bounds of the i th UBB type DV or DP, u_i^I are denoted by u_i^l and u_i^u , respectively. In interval mathematics u_i^I is expressed in Box 1 (Moore, 1979).

In the above, \bar{u}_i is the nominal value of u_i , and Δu_i denotes the maximum variation of u_i from its’ nominal value, termed as dispersion. If a practical estimate of the nominal value is available, it can be directly assigned to \bar{u}_i . In absence of that, \bar{u}_i is usually taken as, $(u_i^l + u_i^u) / 2$. Then,

for a performance function, $f(\mathbf{u})$, its nominal value is obtained as: $\bar{f} = f(\bar{\mathbf{u}})$, where $\bar{\mathbf{u}}$ is a vector comprising of nominal values of \mathbf{u} . Generally, the *RDO* is performed by improving the robustness of the performance function by minimizing a gradient index obtained through first-order Taylor series expansion (Lee, & Perk, 2001) as defined below:

$$\Delta f = \sum_{i=1}^N \left| \frac{\partial f}{\partial u_i} \right| \Delta u_i \quad (2)$$

where, N is the total number of DVs and DPs and Δu_i quantifies their uncertainty amplitudes. The objective of an *RDO* is to achieve optimum performance of the design as well as its less sensitivity with respect to the variations of DVs and DPs due to uncertainty. This leads to a dual criteria performance function. This dual criteria performance function is transformed to an equivalent single objective function as following:

$$\text{minimize: } (1 - \alpha) \frac{\bar{f}}{f^*} + \alpha \frac{\Delta f}{\Delta f^*}, \quad 0 \leq \alpha \leq 1 \quad (3)$$

where, α is a weighting factor in the above bi-objective optimization problem, \bar{f}^* and Δf^* are the optimal solutions at two ideal situations obtained for $\alpha = 1.0$ and 0.0 , respectively. The maximum robustness will be achieved for $\alpha = 0.0$, and $\alpha = 1.0$ indicates optimization without any consideration for robustness.

Box 1.

$$u_i^I = [u_i^l, u_i^u] = [\bar{u}_i - \Delta u_i, \bar{u}_i + \Delta u_i] = [\bar{u}_i, \bar{u}_i] + [-\Delta u_i, \Delta u_i] \quad (1)$$

The constraint functions are exactly satisfied in a DDO. However, these are expected to vary due to the presence of uncertainty in the DVs and DPs. As a consequence, the final design obtained by the DDO approach may become infeasible in presence of uncertainty and the constraint functions are required to be revised to include the effect of their variations due to uncertainty. The robustness of a constraint is the feasibility of the constraint that needs to be guaranteed for the considered uncertainty ranges of the DVs and DPs. Further details of this can be found in the works of Lee, & Park (2001); Wang, Peng, Hu, & Cao (2009). When the DVs and DPs are characterized by random variables with known probability density function (pdf), the probabilistic feasibility of the constraint can be approximated ensuring a target reliability level for the considered constraint (Zang, Friswell, & Mottershead, 2005). A general probabilistic feasibility formulation for j th constraint can be expressed as: $P[g_j(\mathbf{u}) \leq 0] \geq P_{oj}$, $j = 1, \dots, m$, where, P_{oj} is the probability one desires to satisfy for the j th constraint feasibility. Assuming $g_j(\mathbf{u})$ to be normally distributed, this probabilistic feasibility of the constraint can be approximated as $g_j(\bar{\mathbf{u}}) + k_j \sigma_{g_j} \leq 0$, where, $g_j(\bar{\mathbf{u}})$ and σ_{g_j} are the mean and standard deviation of $g_j(\mathbf{u})$. The penalty factor, k_j is used to enhance the feasibility of $g_j(\mathbf{u})$ and can be obtained from, $k_j = \Phi^{-1}(P_{oj})$, where $\Phi^{-1}(\cdot)$ is the inverse of the cumulative density function of a standard normal distribution. For example, to ensure a reliability level of $P_{oj} = 99.87\%$, one should take $k_j = 3.0$.

However, when the DVs and DPs are of UBB type, above probabilistic feasibility formulation for the constraints cannot be adopted. In order to enhance the feasibility of the j th constraint, an additional quantity (Δg_j) is introduced to consider the effect of uncertainty in the DVs and DPs. The maximum variation (Δg_j) of the j th constraint with respect to its nominal value, $\bar{g}_j = g_j(\bar{\mathbf{u}})$ due

to uncertainty in the DVs and DPs can be estimated through first-order Taylor series expansion of the constraint function (Du, & Chen, 2000) as:

$$\Delta g_j = \sum_{i=1}^N \left| \frac{\partial g_j}{\partial u_i} \right| \Delta u_i \quad (4)$$

To further enhance the quality of robustness of the constraint, it is multiplied by a penalty factor, k_j and the constraint function can be expressed as (Lee, & Park, 2001):

$$g_j(\mathbf{u}) = \bar{g}_j + k_j \Delta g_j \leq 0 \quad (5)$$

It may be noted that a direct relationship to ensure a target reliability level can not be achieved in case of UBB type DVs and DPs and the value of k_j is introduced in equivalence to the probabilistic feasibility formulation, thereby indirectly ensuring safety requirement of a design. The selection of k_j is somewhat ad hoc. Obviously, the larger value of k_j means one is more conservative to enhance the feasibility of the associated constraint.

Finally, the conventional RDO formulation is expressed by combining Eqs. (3) and (5) as:

$$\begin{aligned} \text{minimize: } & (1 - \alpha) \frac{\bar{f}}{\bar{f}^*} + \alpha \frac{\Delta f}{\Delta f^*}, & 0 \leq \alpha \leq 1 \\ \text{such that: } & \bar{g}_j + k_j \Delta g_j \leq 0, & j = 1, 2, \dots, m. \end{aligned} \quad (6)$$

The conventional RDO approach as presented above and also by the proposed RDO formulation to be presented in the later part of the chapter are based on linear perturbation based approximation of response functions about the mean values of the UBB parameters. The accuracy and efficiency of such linear perturbation based approach are well documented in stochastic finite element literatures (Vanmarcke et al., 1986; Ghanem, & Spanos, 1990; Kleiber, & Hien, 1992). The study of accuracy

of perturbation based approach for evaluation of nominal response and its dispersion in this regard may be found in Chen, Song, & Chen, (2007). It has been numerically shown that the error in estimation by linear perturbation approximation goes up as the amplitude of uncertainty of the interval variables increases. Thus, the approach will be applicable for systems having small degree of uncertainty so that the linear perturbation based analysis will be satisfactory. An extension to the linear perturbation analysis is to use higher order perturbation method. Stochastic simulation approach may be also applied for larger amplitude of uncertainty (Datta, 2010). However, the stochastic simulation will require assumptions of pdf functions. One may choose conservative uniform distribution for this purpose. This aspect needs further study and it is beyond the scope of the present chapter.

Stochastic Structural Optimization (SSO)

As already discussed, the SSO procedure under random earthquake load involves solution of a nonlinear optimization problem involving stochastic performance measure. The constraint in a generic form can be stated as, the probability of not to exceed a given threshold of a stochastic response measure in a given time period, must be greater than some prescribed minimum value. The related formulation of stochastic dynamic analysis to obtain the constraint of the related optimization problem is briefly presented here.

The dynamic equilibrium equation of a linear multi degree of freedom (MDOF) system under seismic excitation can be written as,

$$[\mathbf{M}]\{\ddot{\mathbf{Y}}(t)\} + [\mathbf{C}]\{\dot{\mathbf{Y}}(t)\} + [\mathbf{K}]\{\mathbf{Y}(t)\} = -[\mathbf{M}]\{\mathbf{L}\}\ddot{u}_g(t) \quad (7)$$

Where, $[\mathbf{M}]$, $[\mathbf{C}]$ and $[\mathbf{K}]$ are the global mass, damping and stiffness matrix, respectively. $\mathbf{Y}(t)$

is the vector comprising of displacements of the MDOF system due to ground motion $\ddot{u}_g(t)$ at base of the system. $\{\mathbf{L}\}$ is the influence coefficient matrix. The displacement of the system subjected to ground motion, $\ddot{u}_g(t) = \ddot{u}_g(\omega)e^{i\omega t}$ can be assumed as $\{\mathbf{Y}(t)\} = \{\mathbf{H}_Y(\omega)e^{i\omega t}\}$, where $\{\mathbf{H}_Y(\omega)\}$ is the complex frequency response function (FRF) vector. Using this, the equation of motion can be expressed in the frequency domain as following:

$$([\mathbf{K}] - \omega^2 [\mathbf{M}] + i\omega [\mathbf{C}])\{\mathbf{H}_Y(\omega)\} = -[\mathbf{M}]\{\mathbf{L}\}\ddot{u}_g(\omega) \text{ i.e. } [\mathbf{D}(\omega)]\{\mathbf{H}_Y(\omega)\} = \{\mathbf{F}(\omega)\}. \quad (8)$$

In the above, $[\mathbf{D}(\omega)]$ is the dynamic stiffness matrix, $\{\mathbf{F}(\omega)\}$ is the forcing vector and $\ddot{u}_g(\omega)$ is the Fourier amplitude of ground motion. In Eq. (8), $\{\mathbf{H}_Y(\omega)\}$ is a function of \mathbf{u} and can be explicitly re-written as,

$$[\mathbf{D}(\omega, \mathbf{u})]\{\mathbf{H}_Y(\omega, \mathbf{u})\} = \{\mathbf{F}(\omega, \mathbf{u})\} \text{ or } \{\mathbf{H}_Y(\omega, \mathbf{u})\} = [\mathbf{D}(\omega, \mathbf{u})]^{-1}\{\mathbf{F}(\omega, \mathbf{u})\} \quad (9)$$

For a linear dynamic system, the power spectral density (PSD) function $[\mathbf{S}_{YY}(\omega, \mathbf{u})]$ of any response variable $Y(t)$ can be readily obtained as (Lutes, & Sarkani, 1997; Datta, 2010),

$$[\mathbf{S}_{YY}(\omega, \mathbf{u})] = \{\mathbf{H}_Y(\omega, \mathbf{u})\} S_{\ddot{u}_g \ddot{u}_g}(\omega) \{\mathbf{H}_Y^*(\omega, \mathbf{u})\}^T \quad (10)$$

Where, $\{\mathbf{H}_Y^*(\omega, \mathbf{u})\}$ is the complex conjugate of $\{\mathbf{H}_Y(\omega, \mathbf{u})\}$ and $S_{\ddot{u}_g \ddot{u}_g}(\omega)$ is the known PSD function of stochastic ground motion.

The records of the ground motion at site are necessary for realistic seismic reliability analysis. However, in scarcity of sufficient data for statistical descriptions, various statistical models are developed to describe the stochastic ground motion process. The simplest such stochastic

model is the well-known stationary white noise process, whose correlation function is Delta Dirac and associated PSD function is constant at each frequency. However, it cannot sufficiently describe the spectral behaviour of many real stochastic dynamic loads. To improve the spectral characterization of ground motion, a second order filter is introduced to colour the white noise, known as the Kanai-Tajimi model (Tajimi, 1960). This model has been widely applied in the random vibration analysis of structures as it provides a simple way to describe the ground motion characterized by a single dominant frequency. However, actual earthquake recorded data show a non-stationary nature both in the amplitude and frequency contents and a more generalized non-stationary model obtained by enveloping the stationary input stochastic process should be used for more refined analysis. The Kanai-Tajimi PSD function used in the present study is represented by,

$$S_{\ddot{u}_g \ddot{u}_g}(\omega) = S_0 \frac{(4\xi_g^2 \omega_g^2 \omega^2 + \omega_g^4)}{(\omega^2 - \omega_g^2)^2 + 4\xi_g^2 \omega_g^2 \omega^2} \quad (11)$$

where, ω_g and ξ_g denote the natural frequency and damping ratio of the soil layer, respectively. The PSD of the white noise process at bed rock, S_0 can be related to the peak acceleration, ($\ddot{x}_{g,max}$) by,

$$S_0 = \frac{0.0707 \xi_g \ddot{x}_{g,max}^2}{\omega_g (1 + 4\xi_g^2)} \quad (12)$$

The spectral moments (λ_j) and the associated root mean square (RMS) values (σ_Y and $\sigma_{\dot{Y}}$) of the responses useful for reliability evaluation can be evaluated as,

$$\begin{aligned} \lambda_j(\mathbf{u}) &= \int_{-\infty}^{\infty} |\omega|^j \mathbf{S}_{YY}(\omega, \mathbf{u}) d\omega, \\ \sigma_Y(\mathbf{u}) &= \sqrt{\lambda_o(\mathbf{u})} \quad \text{and} \quad \sigma_{\dot{Y}}(\mathbf{u}) = \sqrt{\lambda_2(\mathbf{u})} \end{aligned} \quad (13)$$

The reliability of the structure based on the first passage failure criterion for double barrier problem can be obtained as,

$$r(T) = r_0 \exp \left(- \int_0^T h(t) dt \right) \quad (14)$$

where, r_0 is the survival probability at time, $t=0$ and $h(t)$ is the hazard function and T is the duration of the ground motion. Following the Poisson's assumption of rare and independent threshold crossings events, $h(t)$ can be replaced with unconditional threshold crossing rate, ν_Y^+ which can be expressed as:

$$\nu_Y^+(\beta) = \frac{1}{2\pi} \frac{\sigma_{\dot{Y}}}{\sigma_Y} \left\{ -\frac{1}{2} \left(\frac{\beta}{\sigma_Y} \right)^2 \right\} \quad (15)$$

In the above, β is the first time bi-lateral displacement crossing barrier. If the failure is due to double symmetric threshold crossing (as considered herein), the threshold crossing rate can be given by,

$$\nu(\beta) = 2\nu_Y^+(\beta) \quad (16)$$

The applicability of the above is limited to the assumptions that the structure can recover immediately after suffering failure (threshold crossing) and such failures arrive independently, that is, they constitute a Poisson process. More

Box 2.

$$g(\mathbf{u}) = \nu(\beta, \mathbf{u}) - \frac{\log(1/R_{min})}{T} = \frac{1}{\pi} \frac{\sigma_Y}{\sigma_Y} \exp\left\{-\frac{1}{2}(\beta/\sigma_Y)^2\right\} - \frac{\log(1/R_{min})}{T} \leq 0 \quad (19)$$

details may be found in Lutes, & Sarkani, (1997); Datta, (2010).

The limit state corresponds to the first excursion of a structural response $\mathbf{Y}(\mathbf{u}, t)$ can be expressed as, $G[\mathbf{Y}(\mathbf{u}, t)] > 0$, where G is a function. For a stationary stochastic process, the reliability of structure can be written as,

$$R(t, \mathbf{u}) = P\{G[\mathbf{Y}(\mathbf{u}, t)] \geq 0 |_{t < T}\}. \quad (17)$$

The optimum DVs must satisfy one or more probabilistic constraint(s) consisting of limiting the failure probability for a given value of reliability, R_{min} . For a specified threshold barrier (β), the stochastic constraint becomes,

$$R(\beta, T, \mathbf{u}) = P\{G[\mathbf{Y}(\mathbf{u}, t)] \geq 0 |_{t < T}\} = \exp(-\nu(\beta, \mathbf{u})T) \geq R_{min} \quad (18)$$

Using Eqs. (15) and (16), the constraint can be finally expressed in Box 2.

Finally, the SSO problem under stationary earthquake model can be expressed in Box 3.

In the above, $f(\mathbf{u})$ is the objective function of the optimization problem. Usually the weight of the structure or some important stochastic response measure is considered as the objective function. The SSO presented here is based on the

stochastic dynamic response of structure under earthquake load modelled as stationary stochastic process. However, application of the proposed RDO presented in this chapter is not restricted to such stochastic random process only and extension to non-stationary earthquake model will be straight forward. However, this will involve time dependent response statistics evaluations and subsequently to deal with time dependent performance function in the optimization procedure.

Stochastic Dynamic Response Approximation

It can be noted that in a typical SSO procedure, the safety measures are required to be evaluated several times to obtain an optimal design. The evaluations of safety measures for every change of the DVs require several evaluations of the dynamic responses of a structural system. The dynamic responses as described by Eq. (9) are implicit function of \mathbf{u} and normally obtained by numerical methods like the finite element procedure. Furthermore, the formulations described in the previous section assume that all the DVs and DPs are deterministic. If the effects of uncertainty are considered in the analysis, $\mathbf{D}(\omega, \mathbf{u})$ and thereby the FRF vector will also involve uncertainty. Therefore, the analysis will require

Box 3.

$$\begin{aligned} &\text{find } \{\mathbf{x}\} \text{ to minimize: } f(\mathbf{u}) \\ &\text{such that : } g(\mathbf{u}) = \nu(\beta, \mathbf{u}) - \frac{\log(1/R_{min})}{T} = \frac{1}{\pi} \frac{\sigma_Y}{\sigma_Y} \exp\left\{-\frac{1}{2}(\beta/\sigma_Y)^2\right\} - \frac{\log(1/R_{min})}{T} \leq 0. \end{aligned} \quad (20)$$

complex sensitivity analysis of the stochastic dynamic system (Chaudhuri, & Chakraborty, 2004) as the RDO problem requires the gradients of the objective function and associated constraints. For systems of practical interest, repeated evaluations of dynamic responses and their sensitivities will be extremely time-consuming. Thus, the use of direct optimization procedure is not suitable to perform RDO under stochastic excitation. In the present study, an alternative to the direct optimization methods is proposed. An RSM based approximation is adopted judiciously to approximate the dynamic response required to obtain the stochastic constraint of the related SSO problem. The MLSM, a local approximation approach is observed to be elegant in this regard (Kim, Wang, & Choi, 2005) is adopted in the present study. The essential concept of the MLSM is briefly described here in order to outline the procedure. The further details about this may be found elsewhere (Kim, Wang, & Choi, 2005; Bhattacharjya, & Chakraborty, 2009; Kang, Koh, & Choo, 2010).

The MLSM based RSM is a weighted LSM that has varying weight functions with respect to the position of approximation. The weight associated with a particular sampling point x_i decays as the prediction point x moves away from x_i . The weight function is defined around the prediction point x and its magnitude changes with x . If y_i is the i th response ($i=1,2,\dots,q$) with respect to

the variable x_{ij} , which denotes the i th observation of the j th variable x_j obtained by a suitable design of experiments (DOE), following matrix form can express the relationship between the responses (\mathbf{y}) and the variables (\mathbf{x}),

$$\mathbf{y} = \mathbf{x}\mathbf{a} + \boldsymbol{\mu}_y \quad (21)$$

In the above, \mathbf{x} , \mathbf{y} , \mathbf{a} and $\boldsymbol{\mu}_y$ are the design matrices containing the input data obtained by the DOE, the response vector, the unknown coefficient vector and the error vector, respectively. The least-squares function $L_y(x)$ can be defined as the sum of the weighted errors,

$$L_y(x) = \sum_{i=1}^q w_i \varepsilon_i^2 = \boldsymbol{\mu}^T \mathbf{W}(x) \boldsymbol{\mu} = (\mathbf{y} - \mathbf{x}\mathbf{a})^T \mathbf{W}(x) (\mathbf{y} - \mathbf{x}\mathbf{a}) \quad (22)$$

where, $\mathbf{W}(x)$ is the diagonal matrix of the weight function. It can be obtained by utilizing the weighting function such as constant, linear, quadratic, higher order polynomials, exponential functions, etc. (Kim, Wang, & Choi, 2005), as described in Box 3.

R_I is the approximate radius of the sphere of influence, chosen as twice the distance between the centre point and extreme most experimental point. The value of R_I is chosen to secure sufficient number of neighbouring experimental points to

Box 3.

$$w(x-x_i) = w(d)$$

$$= \begin{cases} & \text{(if } d / R_I \leq 1.0\text{)}, \\ & \left\{ \begin{array}{ll} \text{Constant:} & 1.0 \\ \text{Linear:} & 1 - d / R_I \\ \text{Quadratic:} & 1 - (d / R_I)^2 \\ \text{4}^{\text{th}} \text{ order polynomial:} & 1 - 6(d / R_I)^2 + 8(d / R_I)^3 - 3(d / R_I)^4 \\ \text{Exponential:} & \exp(-d / R_I) \end{array} \right. \\ & \text{(if } d / R_I \geq 1.0\text{)}, \end{cases}$$

$$(23)$$

avoid singularity. An exponential form of weight function has been adopted in the present numerical study. Eventually, a weight matrix $\mathbf{W}(x)$ can be constructed by using the weighting function in the diagonal terms as:

$$\mathbf{W}(x) = \begin{bmatrix} w(x-x_1) & 0 & 0 & 0 \\ 0 & w(x-x_2) & .. & 0 \\ .. & .. & .. & .. \\ .. & .. & .. & .. \\ 0 & 0 & .. & w(x-x_n) \end{bmatrix} \quad (24)$$

By minimizing the least-squares estimators $L_y(x)$, the coefficients $\mathbf{a}(x)$ can be obtained by the matrix operation as below,

$$\mathbf{a}(x) = [\mathbf{x}^T \mathbf{W}(x) \mathbf{x}]^{-1} \mathbf{x}^T \mathbf{W}(x) \mathbf{y} \quad (25)$$

It is important to note here that the coefficients $\mathbf{a}(x)$ are the function of the location x , where the approximation is sought. Thus, the procedure to calculate $\mathbf{a}(x)$ is a local approximation and “moving” processes performs a global approximation throughout the whole design domain.

The Proposed RDO APPROACH

As mentioned earlier, the present chapter deals with an efficient RDO procedure for structures subjected to stochastic earthquake load and characterized by UBB type DVs and DPs. A heuristic algorithm is proposed here which allows the use of importance factor obtained using the respective sensitivity information of the performance function and constraints. In the following subsections, the related theoretical developments, implementation of the algorithm and numerical study are presented.

Theoretical Formulation

It is well-known that the sensitivity information are useful to a designer as it provides a measure of performance deviations in a design associated with an increase or decrease of the respective variables. To reduce the number of significant random variables before in reliability evaluation process the use of importance measure as given below is quite common (Bjerager, & Krenk, 1989; Haldar, & Mahadevan, 2000; Gupta, & Manohar, 2004):

$$I_i = \left(\frac{\partial G}{\partial u_i} \right)^2 \Bigg/ \left[\sum_{k=1}^N \left(\frac{\partial G}{\partial u_k} \right)^2 \right] \quad (26)$$

where, G is the failure surface defining the safe and unsafe regions and N is the total number of random variables in a generic structural reliability analysis problem. The applicability of the above form of importance measure was studied by Gupta, & Manohar (2004) through Monte Carlo Simulation (MCS) study. Based on the entries of I_i 's, the uncertain variables can be grouped into ‘important’ and ‘unimportant’ variables. The uncertain variables for which the failure surface is more sensitive are identified as dominant variables. This is hinged on the fact that all the gradients are not equally important in the expression of the failure surface in a typical reliability analysis problem. This intuitively indicates that all the gradients do not have equal importance in the expression of the dispersion of the performance function as defined by Eq. (2). Hence, it is apparent that the importance measure should also play a role to indicate the measure of robustness of the performance.

It can be readily realized from Eq. (2) that the dispersion Δf depends on two factors: (i) the amplitude of uncertainty in the DVs and DPs represented by the corresponding dispersion, Δu_i 's and (ii) the gradients of the performance

function, $\partial f / \partial u_i$'s. If the amplitudes of uncertainty, i.e. the dispersions of DVs and DPs do not change, the dispersion of the performance function Δf will solely depend on the gradients $\partial f / \partial u_i$'s. It is obvious that a change in the dispersion Δf_i (due to the variation of the i th DV or DP) will be more than Δf_j (due to the variation of the j th DV or DP) if the associated importance measure $I_i > I_j$ or vice versa. Hence, it seems to be more logical to use the importance measure of the associated gradients as well in defining the measure of robustness. A new measure of robustness is thus proposed in the present RDO study by redefining the performance dispersion as following:

$$\Delta f_w = \sum_{i=1}^N \left| \frac{\partial f}{\partial u_i} \right| I_{fi} \Delta u_i, \text{ where, } I_{fi} = N \left(\frac{\partial f}{\partial u_i} \right)^2 / \left[\sum_{k=1}^N \left(\frac{\partial f}{\partial u_k} \right)^2 \right] \quad (27)$$

In the above, Δf_w is the new dispersion index and I_{fi} is the importance factor for the i th DV or DP. It is to be noted here that the importance factor as defined above is multiplied by the total number (N) of the DVs and DPs. However, the summation of all such factors will be always equal to N , whatever is the individual value of the importance factor. This will keep the consistency of the definition of this index to measure the robustness with the usual dispersion index used in the conventional RDO approach.

The basic idea to improve the robustness of the performance function using the new index utilizing the importance factors proportional to the importance of the gradients of the performance function can be readily extended to the constraints as well. A new dispersion index to achieve the robustness of j th constraint feasibility is defined as:

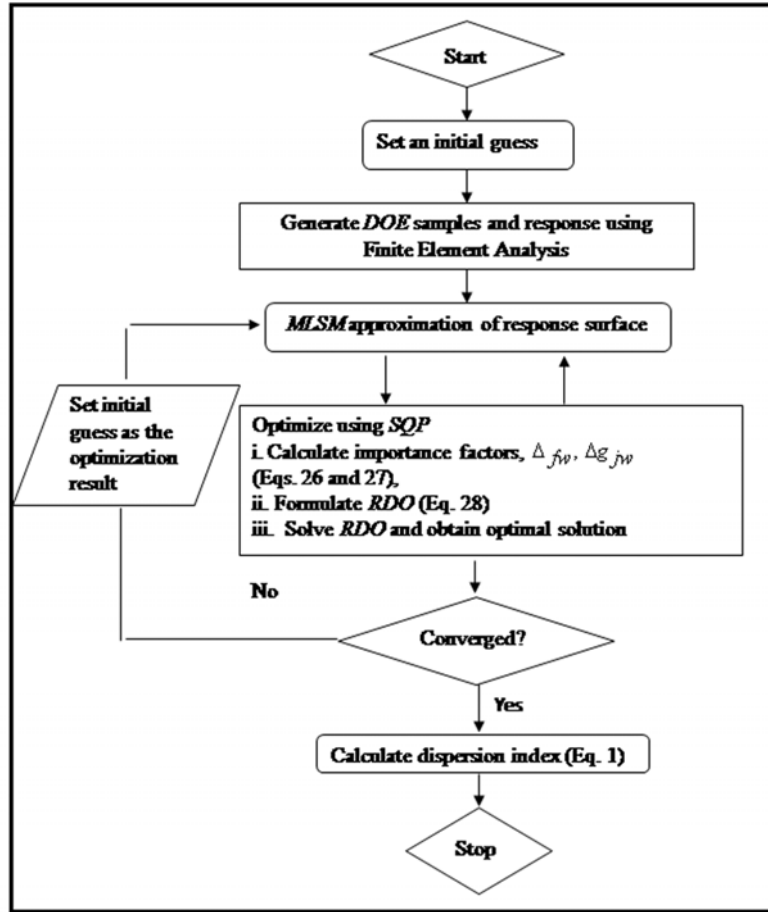
$$\Delta g_{jw} = \sum_{i=1}^N \left| \frac{\partial g_j}{\partial u_i} \right| I_{gj} \Delta u_i, \text{ where, } I_{gj} = N \left(\frac{\partial g_j}{\partial u_i} \right)^2 / \left[\sum_{k=1}^N \left(\frac{\partial g_j}{\partial u_k} \right)^2 \right] \quad (28)$$

Integrating the information presented so far, the proposed RDO scheme can be finally represented as an equivalent DDO problem as following:

$$\begin{aligned} \text{minimize: } & (1 - \alpha) \frac{\bar{f}}{f^*} + \alpha \frac{\Delta f_w}{\Delta f_w^*} \\ \text{such that: } & \bar{g}_j + k_j \Delta g_{jw} \leq 0, \quad j = 1, 2, \dots, m, \end{aligned} \quad (29)$$

In the above, k_j is as defined in Eq. (5). The above nonlinear optimization problem can be solved by available optimization techniques. Once the optimum design point is obtained by the proposed importance factor based RDO approach, the dispersion of the performance function can be evaluated at the optimum design point using Eq. (2). It may be noted that the importance factors are directly incorporated in the optimization formulation and such factors are evaluated at updated design point during each iteration cycle of the optimization process. Doing so, more sensitive DVs and DPs are automatically got re-amplified yielding a better robust solution in lesser computational time. Basically, the incorporation of the importance factors changes the feasible domain of the original optimization problem and captures the more flat zone of the performance function. In this regard, it is worth mentioning that many researchers adopt a separate sub-problem to find a search direction for a quick convergence towards the robust optima (Lee, & Park, 2001; Wang et al., 2009). The search direction should emphasize on the more sensitive variables for an efficient and quick convergence to the robust optima. As the importance factor based dispersion index includes this aspect of assigning more importance to more sensitive DVs and DPs, the proposed RDO procedure converges to robust optima efficiently without requiring any such separate sub-problem for direction finding.

Figure 1. Implementation of the proposed RDO



Implementation of the RDO Approach

The implementation procedure of the proposed RDO for linear dynamic system is demonstrated through a flow chart in Figure 1. The procedure is basically a three-stage interlinked procedure, viz.: i) stochastic dynamic analysis of the finite element model for selected set of input variables as per the DOE to obtain the required stochastic responses and subsequently the constraint of the optimization problem, ii) evaluation of the constraint function at the iteration point following the MLSM based RSM during each iteration of the optimization process utilizing the computed

responses as per the DOE in step (i), and iii) finally checking the convergence to obtain the robust optimum solution. It can be noted from the flow chart that during each update of the DVs in the optimization process the MLSM based response approximation is re-called and a new approximation function is formed. However, this is not the case for the LSM based RSM, where a single approximation function gets operated throughout the optimization process. It is worth mentioning here that the choice of initial solution is an important issue in metamodel based optimization procedure. For the conventional LSM based RSM approach, a poor initial guess not only increases the number of iterations, but also warns the convergence of

the optimization problem. As the MLSM based approximation technique can capture the actual response even beyond the sampling zone, the convergence is faster than the conventional LSM based techniques (Kim, Wang, & Choi, 2005).

Numerical Study

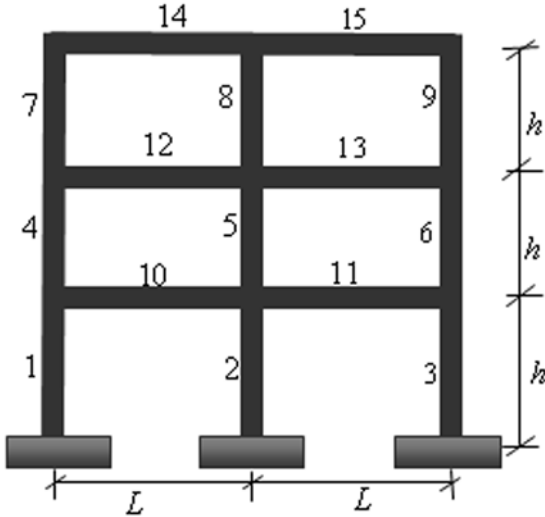
A three storied concrete building frame (as shown in Figure 2) subjected to earthquake motion is taken up to elucidate the effectiveness of the proposed RDO approach. The frame structure is idealized by fifteen two-noded plane frame elements having three degrees of freedom at each node. Both the DVs and DPs are considered to be of UBB type and are described by their respective dispersions, Δu_i , representing the maximum possible ranges of variations expressed in terms of the percentage of the corresponding nominal values. The necessary information with associated notations are summarized in Table 1. The deterministic dimension L and h are taken as 6.0 m and 4.0 m, respectively. The natural frequency (ω_g) and the damping ratio (ξ_g) of the soil layer are considered to be 18.85 rad/sec and 0.65, respectively. The peak ground acceleration ($\ddot{x}_{g,\max}$) is taken as 0.2g, where g is the acceleration due to gravity.

The objective function f(u) considered in the present study is the weight of the frame. Apart from the stochastic constraint, as discussed earlier, a size constraint (g2) limiting the ratio between the depth and width of the beam members is also considered in the SSO formulation. The SSO formulation under earthquake load with deterministic DVs and DPs can be defined as:

$$\begin{aligned} \text{find } \mathbf{x} = \{ b_c \quad d_b \quad b_b \} \text{ to minimize: } f &= (9hb_c^2 + 6Lb_b d_b)\rho_c \\ \text{such that: } g_1(\mathbf{x}, \mathbf{z}) : \frac{1}{\pi} \frac{\sigma_Y}{\sigma_y} \exp \left[-\frac{1}{2} \left(\frac{\beta}{\sigma_y} \right)^2 \right] - \frac{\log(1/R_{\min})}{T} &\leq 0 \\ g_2(\mathbf{x}, \mathbf{z}) : d_b - 3b_b &\leq 0 \quad 0.1 \leq b_c, b_b, d_b \leq 1.2 \end{aligned} \quad (30)$$

Unless mentioned specifically R_{\min} , T and β are taken as 0.99, 10 sec and $3\sigma_Y$ (σ_Y is the maximum RMS displacement), respectively. The MLSM based adaptive RSM technique as discussed previously is used to approximate the constraint function. In the present numerical study, the second-order polynomial without cross terms is considered. The DOE is constructed considering the centre and axial points following the Saturated Design (SD) method (Bucher, & Macke, 2005). However, the points chosen are at the nominal value (\bar{x}_i) of the input variable (xi) and at axial points $x_i = \bar{x}_i \pm h_i \Delta x_i$, where h_i is a positive integer. For each input variable six axial points ($h_i=1, 2, \dots, 6$) are considered on each axis taking Δx_i as 5% of \bar{x}_i to cover the different amplitude levels of uncertainty. Thus, for the present study, the number of required training points with respect to dimension of the input vector (N) is: $(6 \times 2N + 1)$ i.e. the total number of sampling points is sixty one with five input variables. As more axial points are considered than that required by the SD method, the design becomes a redundant design (Bucher, & Macke, 2005). To study the effectiveness of the MLSM based adaptive RSM, the computed responses are compared with that obtained by the conventional LSM based RSM. The maximum RMS displacement of the frame is shown for a wide range of column size in Figure 3. The results obtained by the direct random vibration analysis are also shown in the same figure for ease in comparison. It can be readily observed from the figure that the predicted responses by the MLSM based RSM better matches with the direct random vibration analysis results. The error using the conventional LSM based RSM drastically increases beyond the range of data points which are used in the DOE to construct the metamodel. During the iteration stage of any gradient-based optimization algorithm, the DVs may take values outside the sampling range

Figure 2. The building frame



depending on the specific nature of the optimization problem. This is a potential problem in iterative optimization process and warns the applicability of the LSM based RSM approach for RDO of complex dynamic system under stochastic load. Furthermore, to study the suitability of the proposed adaptive RSM, the statistical metrics as described below have been also computed (Bouazizi, Ghanmi, & Bouhaddi, 2009):

The Root Mean Square Error (RMSE) is defined as:

$$RMSE = \sqrt{\sum_{i=1}^p \frac{(\hat{y}_i - y_i)^2}{p}} \quad (31)$$

In the above, \hat{y}_i is the predicted response obtained by the considered LSM or MLSM based metamodel and y_i is the actual response obtained by the direct MCS for i th sample. The sample size, p is taken as 1000 for the present numerical investigation.

The coefficient of determination (R^2) is defined as:

$$R^2 = \left(\sum_{i=1}^p (\hat{y}_i - \bar{y}_i)^2 \right) / \left(\sum_{i=1}^p (y_i - \bar{y}_i)^2 \right) \quad (32)$$

where, \bar{y}_i is the mean value of the actual response. The value of this coefficient close to one represents a good metamodel for response approximation.

The average prediction error (ε_m) is defined as,

$$\varepsilon_m = 100 \frac{|\hat{y}_i - y_i|}{y_i} \quad (33)$$

Table 2 shows the results of the statistical test for both the LSM and MLSM based metamodels. It can be observed that the lesser RMSE and ε_m values and the higher R^2 value are attained by the MLSM based RSM compared to the LSM based RSM. This clearly indicates the accuracy of the MLSM based RSM over the LSM based RSM. The CPU time required for complete generation of all y_i by the direct MCS is about 2.5 hrs, whereas the CPU time needed for computation of \hat{y}_i is only 11 minutes by the LSM based RSM and 12 minutes by the MLSM based RSM. The MLSM based RSM needs more computational time compare to the LSM based RSM due to the fact that the MLSM based approach needs repeated evaluation of the response surface as it is required to be generated afresh for each updated DV set. Whereas, the LSM based approach may need more rigorous DOE compare to the MLSM based RSM to obtain a comparable accuracy level. It may be noted here that one needs to evaluate the structural responses analysis at all these training points involving the solution of a system having number of unknowns in the order of few thousands to million. This obviously in-

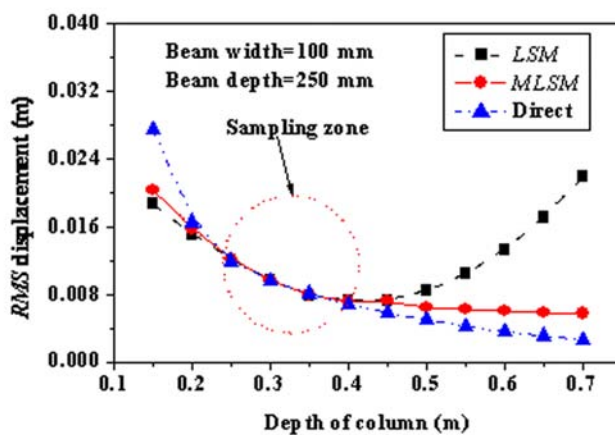
Table 1. The details of the uncertainty in the DVs and DPs

DPs	Nominal values	Dispersion
Density of concrete, ρ_c	2400 kg/m ³	10%
Modulus of Elasticity of concrete, E_c	20 GPa	10%
DVs		
Size of square column, b_c	To be optimized	10%
Depth of beam, d_b	To be optimized	10%
Width of beam, b_b	To be optimized	10%

Table 2. Performance of the LSM and MLSM based RSM

	RMSE	R^2	ε_m
LSM based RSM	7.91%	0.97	2.5%
MLSM based RSM	4.72%	0.99	0.07%

Figure 3. The comparison of RMS displacement by the LSM and MLSM based RSM



creases the time requirement by the LSM based approach. Thus the computational involvement with regard to generation of training data point will be substantially high whereas, there is a higher computational demand with regard to repeated evaluation of response surface. Of course, it needs further study to comprehend which one will be more efficient.

Now, the optimization task is performed by the sequential quadratic programming (SQP) using built-in MATLAB routine. The weight of the frame is optimized by the proposed importance factor based RDO approach as described by Eq. (29) and the conventional RDO approach as described by Eq. (6) considering uncertainty in both the DVs and DPs. The results are studied through Figures 4, 5, 6, 7 and 8. The optimal weight of the frame versus the dispersion of the DVs and DPs are plotted in Figure 4. For comparison, the results obtained by the conventional RDO approach are also shown in the same figure. The variations of the optimal weight of the frame (indicates the measure of robustness) versus the dispersion of the input DVs and DPs, as obtained by the proposed and conventional RDO approaches are depicted in Figure 5. The value of

the penalty factor, k_j and the bi-objective weight factor, α are considered to be 1.0 and 0.5, respectively. It can be noted that the optimization results obtained by the proposed approach indicate an improved robustness compared to the conventional RDO method.

The optimal weight and its dispersion are plotted in the Figures 6 and 7, respectively, with respect to the upcrossing level, β for different values of k_j . The dispersion of the inputs and α are set as 10% and 0.5, respectively. It can be noted from these figures that the same nature of variations and improvement are observed for all the values of k_j considered in the study. In general, it has been observed that the effect on the robustness is more prominent for smaller values of β . This is obvious as the smaller value of β represents more stringent failure criterion and makes the constraints more critical. Thus, the effect of the importance of the sensitivity derivatives introduced by the proposed RDO approach becomes more.

One of the important tasks in an RDO procedure like any other multi-objective optimization problem is to obtain the Pareto front (Deb, 2001). It is generally observed that there is a trade-off between the objective value of a design and its

Figure 4. The optimal weight of the frame with increasing range of uncertainty

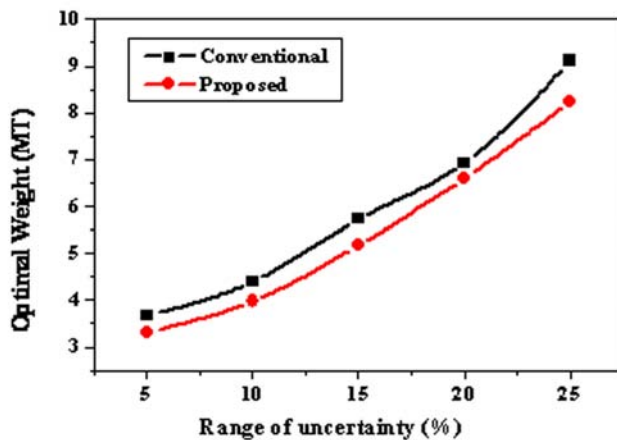


Figure 5. The variation of optimal weight of the beam with increasing range of uncertainty

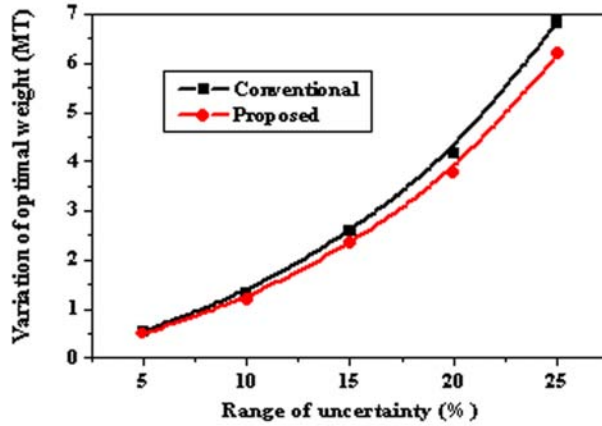
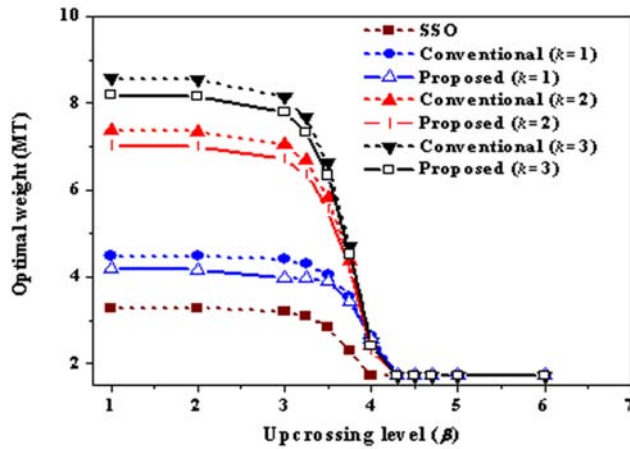


Figure 6. The optimal weight of the frame with varying upcrossing level



robustness. If one desires more robustness, the design will be further away from its ideal optimal value. The situation can be studied further in terms of Pareto-front. The Pareto-front is one where any improvement in one objective can only achieve through worsening of at least one other objective. If one chooses a design that is not Pareto-optimal, one essentially forfeits improvements that would otherwise entail no compromise. The Pareto fronts obtained by the proposed and the conventional

RDO approaches are plotted in Figure 8. The uncertainty ranges of the DVs and DPs are taken as per Table 1 and k_j is considered to be 1.0 to develop this figure. The Pareto front is determined by evaluating the optimal solutions (the objective function and its associated dispersion) for different settings of α . Maximum robust solution is obtained when α is 1.0. The designer puts maximum emphasis on optimal objective, not on its robustness, if α is zero. Thus, the designer can

Figure 7. The dispersion of optimal weight of the frame with varying upcrossing level

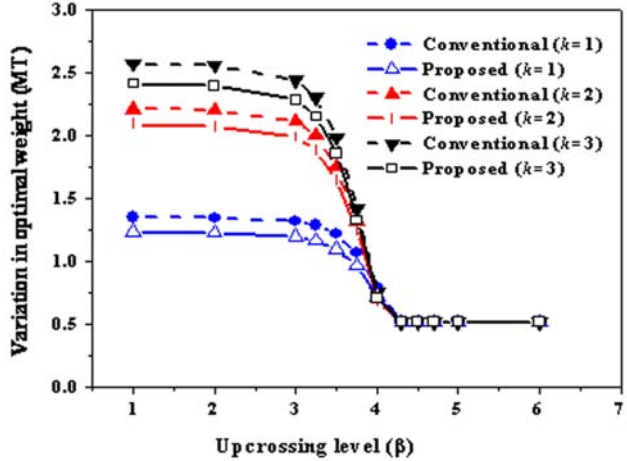
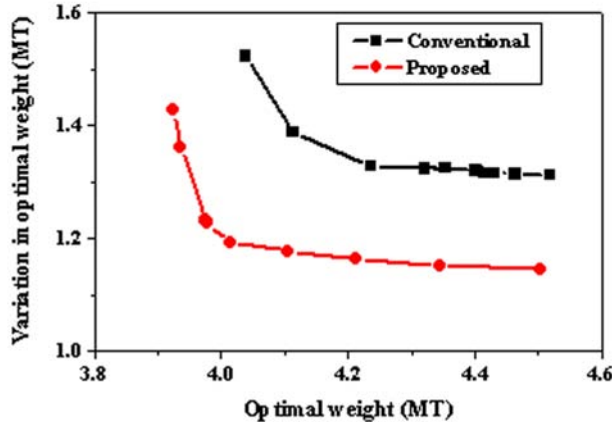


Figure 8. Comparison of Pareto front as obtained by the proposed and the conventional RDO approaches



tune the robustness of a solution through suitable choice of this parameter. It can be clearly observed from the figure that for a specific level of dispersion Δf , if the desired objective is to minimize the weight of the frame, the proposed RDO approach always yields lesser weight compared to the conventional RDO approach. Furthermore, for a prescribed weight of the frame, the dispersion of the optimal weight Δf obtained by the proposed

RDO approach is also observed to be lesser than that obtained by the conventional RDO approach. To quantify the computational involvement of the proposed RDO approach, the CPU time required to generate the complete Pareto front by both the approaches are computed. It is observed that the proposed RDO approach needs 25 minutes whereas the conventional RDO approach needs 40 minutes for this purpose. This clearly indicates

the efficiency of the proposed RDO approach. In this regard, it is worth mentioning here that one may fail to identify the complete Pareto front by the present WSM approach for non-convex Pareto front. This is a potential drawback of WSM and to overcome this limitation Evolutionary algorithms like Non-domination Sorting Genetic Algorithm-II (Deb, 2001) can be applied.

SUMMARY AND CONCLUSION

An efficient *RDO* procedure for structural system subjected to stochastic earthquake load and characterized by *UBB* type *DVs* and *DPs* is presented. The associated stochastic constraint is derived by imposing a limit on the failure probability. To exclude the complexity of repeated evaluations of random dynamic responses and their sensitivities (required for *RDO* solution), the implicit constraint function is approximated through a potentially superior *MLSM* based adaptive *RSM* method. The proposed *RDO* approach improves the robustness of the performance function using a new dispersion index which utilizes the weight factors proportional to the importance of the gradients of the performance function with respect to uncertain *DVs* and *DPs*. The improvement is achieved in terms of more robustness in the optimization by allowing more importance to the uncertain variables which influence the variations of the performance function and the constraint violations. Numerical results indicate that the trends and variations of the optimization results are in conformity with the well-known two criteria *RDO* results. It can be noted that the economy is not affected in achieving better robustness, as the proposed *RDO* approach yields more reduction of weight for a specified dispersion of the weight. This implies that the importance factor based *RDO* approach captures the optimal design point on a comparatively flat region than the optimal point captured by the conventional *RDO* approach. However, how much improvement in robustness

is possible to achieve compare to the conventional *RDO* approach is problem dependent. It will specifically depend on the nature of the performance function and the entire solution domain, i.e., the nature of the variation of the objective function and constraints. This of course needs further study. The results shown in the numerical example are for some specific values of the bi-objective weight factor and penalty factor. However, the general trend is observed to be similar for other values. The proposed *RDO* approach is generic in nature and can be applied to optimum *RDO* of structures under other stochastic dynamic load, like wind, wave, etc.

REFERENCES

- Al-Widyan, K., & Angeles, J. (2005). Model-based formulation of robust design. *Journal of Applied Mechanics Transaction*, 127(3), 388–396. doi:10.1115/1.1829728
- Ben-Tal, A., & Nemirovski, A. (2002). Robust optimization-methodology and applications. *Mathematical Programming*, 92(3), 453–480. doi:10.1007/s101070100286
- Bertsimas, D., & Sim, M. (2006). Tractable approximations to robust conic optimization problems. *Mathematical Programming*, 107(1-2), 5–36. doi:10.1007/s10107-005-0677-1
- Beyer, H., & Sendhoff, B. (2007). Robust optimization -A comprehensive survey. *Computer Methods in Applied Mechanics and Engineering*, 196(33-34), 3190–3218. doi:10.1016/j.cma.2007.03.003
- Bhattacharjya, S., & Chakraborty, S. (2009). Robust optimization of linear dynamic system with random parameters under stochastic earthquake excitation. *International Journal of Reliability Quality and Safety Engineering*, 16(3), 261–279. doi:10.1142/S0218539309003393

- Bjerager, P., & Krenk, S. (1989). Parametric sensitivity in first order reliability theory. *Journal of Engineering Mechanics*, 115(7), 1577–1582. doi:10.1061/(ASCE)0733-9399(1989)115:7(1577)
- Bouazizi, M.-L., Ghanmi, S., & Bouhaddi, N. (2009). Multi-objective optimization in dynamics of the structures with nonlinear behavior: Contributions of the metamodels. *Finite Elements in Analysis and Design*, 45(10), 612–623. doi:10.1016/j.finel.2009.03.007
- Bucher, C., & Macke, M. (2005). Response surfaces for reliability assessment. In Nikolaidis, E., Ghiocel, D. M., & Singhal, S. (Eds.), *Engineering design reliability handbook*. Boca Raton, FL: CRC Press.
- Chaudhuri, A., & Chakraborty, S. (2004). Sensitivity evaluation in seismic reliability analysis of structures. *Computer Methods in Applied Mechanics and Engineering*, 193(1-2), 59–68. doi:10.1016/j.cma.2003.09.007
- Chaudhuri, A., & Chakraborty, S. (2006). Reliability of linear structures with parameter uncertainty under nonstationary earthquake. *Structural Safety*, 28(3), 231–246. doi:10.1016/j.strusafe.2005.07.001
- Chen, S. H., Song, M., & Chen, Y. D. (2007). Robustness analysis of vibration control structures with uncertain parameters using interval algorithm. *Structural Safety*, 29(2), 94–111. doi:10.1016/j.strusafe.2006.03.001
- Datta, T. K. (2010). *Seismic analysis of structures*. Singapore: John Wiley & Sons. doi:10.1002/9780470824634
- Deb, K. (2001). *Multi-objective optimization using evolutionary algorithms*. New York, NY: John Wiley & sons.
- Du, X., & Chen, W. (2000). Towards a better understanding of modelling feasibility robustness in engineering design. *ASME Journal of Mechanical Design*, 122(4), 385–394. doi:10.1115/1.1290247
- Du, X., Sudjianto, A., & Chen, W. (2004). An interval framework for optimization under uncertainty using inverse reliability strategy. *ASME Journal of Mechanical Design*, 126(4), 562–570. doi:10.1115/1.1759358
- Ghanem, R., & Spanos, P. D. (1990). *Stochastic finite element analysis: A spectral approach*. Berlin, Germany: Springer.
- Guedri, M., Ghanmi, S., Majed, R., & Bouhaddi, N. (2009). Robust tools for prediction of variability and optimization in structural dynamics. *Mechanical Systems and Signal Processing*, 23(4), 1123–1133. doi:10.1016/j.ymssp.2008.08.013
- Gunawan, S., & Azarm, S. (2005). Multi-objective robust optimization using a sensitivity region concept. *Structural and Multidisciplinary Optimization*, 29(1), 50–60. doi:10.1007/s00158-004-0450-8
- Guo, X., Bai, W., Zhang, W., & Gao, X. (2009). Confidence structural robust design and optimization under stiffness and load uncertainties. *Computer Methods in Applied Mechanics and Engineering*, 198(41-44), 3378–3399. doi:10.1016/j.cma.2009.06.018
- Gupta, S., & Manohar, C. S. (2004). An improved response surface method for the determination of failure probability and importance measures. *Structural Safety*, 26(2), 123–139. doi:10.1016/S0167-4730(03)00021-3
- Haldar, A., & Mahadevan, S. (2000). *Reliability assessment using stochastic finite element analysis*. USA: John Wiley and Sons.
- Huang, B., & Du, X. (2007). Analytical robustness assessment for robust design. *Structural and Multidisciplinary Optimization*, 34(2), 123–127. doi:10.1007/s00158-006-0068-0

- Hwang, K.-H., Lee, K.-W., & Park, G.-J. (2001). Robust optimization of an automobile rearview mirror for vibration reduction. *Structural and Multidisciplinary Optimization*, 21(4), 300–308. doi:10.1007/s001580100107
- Jensen, H. (2002). Reliability-based optimization of uncertain systems in structural dynamic. *AIAA Journal*, 40(4), 731–738. doi:10.2514/2.1705
- Jensen, H. (2005). Structural optimization of linear dynamical systems under stochastic excitation: A moving reliability database approach. *Computer Methods in Applied Mechanics and Engineering*, 194(12-16), 1757-1778.
- Jensen, H. (2006). Structural optimization of non-linear systems under stochastic excitation. *Probabilistic Engineering Mechanics*, 21(4), 397–409. doi:10.1016/j.probengmech.2006.02.002
- Jensen, H. A., Valdebenito, M. A., & Schuëller, G. I. (2008). An efficient reliability-based optimization scheme for uncertain linear systems subject to general Gaussian excitation. *Computer Methods in Applied Mechanics and Engineering*, 198(12-16), 72-87.
- Jin, R., Chen, W., & Simpson, T. (2001). Comparative studies of metamodeling techniques under multiple modeling criteria. *Structural and Multidisciplinary Optimization*, 23(1), 1–13. doi:10.1007/s00158-001-0160-4
- Jurecka, F., Ganser, M., & Bletzinger, K. U. (2007). Update scheme for sequential spatial correlation approximations in robust design optimization. *Computers & Structures*, 85(10), 606–614. doi:10.1016/j.compstruc.2006.08.075
- Kang, B., Park, G. J., & Arora, J. S. (2006). A review of optimization of structures subjected to transient loads. *Structural and Multidisciplinary Optimization*, 31(2), 81–95. doi:10.1007/s00158-005-0575-4
- Kang, S.-C., Koh, H.-M., & Choo, J. F. (2010). An efficient response surface method using moving least squares approximation for structural reliability analysis. *Probabilistic Engineering Mechanics*, 25(4), 365–371. doi:10.1016/j.probengmech.2010.04.002
- Kim, C., Wang, S., & Choi, K. K. (2005). Efficient response surface modelling by using moving least-squares method and sensitivity. *AIAA Journal*, 43(1), 2404–2411. doi:10.2514/1.12366
- Kleiber, M., & Hien, T. D. (1992). *The stochastic finite element method*. Chichester, UK: John Wiley and Sons.
- Kurdi, M. H., Haftka, R. T., Schmitz, T. L., & Mann, B. P. (2008). A robust semi-analytical method for calculating the response sensitivity of a time delay system. *Journal of Vibration and Acoustics*, 130(6), 1–6. doi:10.1115/1.2981093
- Lagaros, N. D., Garavelas, A. T., & Papadrakakis, M. (2008). Innovative seismic design optimization with reliability constraints. *Computer Methods in Applied Mechanics and Engineering*, 198(1), 28–41. doi:10.1016/j.cma.2007.12.025
- Lee, K., & Park, G. (2001). Robust optimization considering tolerances of design variable. *Computers & Structures*, 79(1), 77–86. doi:10.1016/S0045-7949(00)00117-6
- Lewis, A. S. (2002). *Robust regularization. Technical Report*. Columbia: Simon Fraser University.
- Lutes, L. D., & Sarkani, S. (1997). *Stochastic analysis of structural and mechanical vibrations*. Upper Saddle River, NJ: Prentice Hall.
- Marano, G. C., Greco, R., & Sgobba, S. (2010). A comparison between different robust optimal design approaches: Application to tuned mass dampers. *Probabilistic Engineering Mechanics*, 25(1), 108–118. doi:10.1016/j.probengmech.2009.08.004

- Marano, G. C., Sgobba, S., Greco, R., & Mezzina, M. (2008). Robust optimum design of tuned mass dampers devices in random vibrations mitigation. *Journal of Sound and Vibration*, 313(3-5), 472–492. doi:10.1016/j.jsv.2007.12.020
- Marano, G. C., Trentadue, F., & Greco, R. (2006). Optimal design criteria for elastic structures subject to random dynamic loads. *Engineering Optimization*, 38(7), 853–871. doi:10.1080/03052150600913028
- Moore, R. E. (1979). *Methods and applications of interval analysis*. Philadelphia, PA: SIAM Bookmart, PA.
- Mohsine, A., Kharmanda, G., & El-Hami, A. (2005). Reliability-based design optimization study using normal and lognormal distributions with applications to dynamic structures. In G. Augusti, G. I. Schuëller, & M. Ciampoli (Eds.), *Proceedings of the 9th International Conference on Structural Safety and Reliability*, 19-23 June 2005 Rome, Italy (pp. 3773-3779). Rotterdam, The Netherlands: Millpress.
- Myers, R. H., & Montogmery, D. C. (1995). *Response surface methodology: Process and product optimization using designed experiments*. USA: John Wiley and Sons.
- Nigam, N. C. (1972). Structural optimization in random vibration environment. *AIAA Journal*, 10(4), 551–553. doi:10.2514/3.50151
- Park, G. J., Lee, T. H., Lee, K., & Hwang, K. H. (2006). Robust design: An overview. *AIAA Journal*, 44(1), 181–191. doi:10.2514/1.13639
- Schuëller, G., & Jensen, H. (2008). Computational methods in optimization considering uncertainties- An overview. *Computer Methods in Applied Mechanics and Engineering*, 198(1), 2–13. doi:10.1016/j.cma.2008.05.004
- Son, Y. K., & Savage, G. J. (2007). Optimal probabilistic design of the dynamic performance of a vibration absorber. *Journal of Sound and Vibration*, 307(1-2), 20–37. doi:10.1016/j.jsv.2007.06.032
- Taflanidis, A. A. (2010). Reliability-based optimal design of linear dynamical systems under stochastic stationary excitation and model. *Engineering Structures*, 32(5), 1446–1458. doi:10.1016/j.engstruct.2010.01.023
- Taflanidis, A. A., & Beck, B. L. (2008). An efficient framework for optimal robust stochastic system design using stochastic simulation. *Computer Methods in Applied Mechanics and Engineering*, 198(1), 88–101. doi:10.1016/j.cma.2008.03.029
- Tajimi, H. (1960). A statistical method of determining the maximum response of a building during earthquake. In G. W. Housner (Ed.), *Proceedings of the Second World Conference on Earthquake Engineering*, 11-18 July 1960 Tokyo and Kyoto, Japan, (pp. 781-797). Tehran, Iran: University press.
- Vanmarcke, E. H., Shinozuka, M., Nakagiri, S., Schuëller, G. I., & Grigoriu, M. (1986). Random fields and stochastic finite elements. *Structural Safety*, 3(3), 143–166. doi:10.1016/0167-4730(86)90002-0
- Wang, W. M., Peng, Y. H., Hu, J., & Cao, Z. M. (2009). Collaborative robust optimization under uncertainty based on generalized dynamic constraints network. *Structural and Multidisciplinary Optimization*, 38(2), 159–170. doi:10.1007/s00158-008-0271-2

Chapter 6

Damage Assessment of Inelastic Structures under Simulated Critical Earthquakes

Abbas Moustafa
Minia University, Egypt

ABSTRACT

Damage of structures can be significantly reduced through robust prediction of possible future earthquakes that can occur during the life-time of the structure and through accurate modeling of the nonlinear behavior of the structure under seismic loads. Modern seismic codes specify natural records and artificially generated ground accelerations as input to the nonlinear time-history analysis of the structure. The advantage of using natural records is the inclusion of all important characteristics of the ground motion (fault properties, path effects and local soil condition) in the design input. This option requires selecting and scaling a set of proper accelerograms from the available records. However, the site under consideration may have limited or scarce earthquake data. In such case, numerically simulated ground motions can be employed as input to the dynamic analysis of the structure. This chapter deals with the damage assessment of inelastic structures under numerically simulated critical earthquakes using nonlinear optimization, inelastic time-history analysis, and damage indices.

1. INTRODUCTION

Damage indices describe the state of the structural damage and correlate well with actual damage displayed during earthquakes. The critical ground motion for a give structure is estimated by solving an inverse nonlinear dynamic problem in time domain using constrained nonlinear optimiza-

tion techniques. The critical excitation method relies on the high uncertainty associated with the occurrence of the earthquake phenomenon and on the safety requirements of important and lifeline structures. The earthquake input is taken to maximize the damage index of the structure while satisfying predefined constraints that are quantified from the earthquake data available at the site. Numerical illustrations for damage assessment of

DOI: 10.4018/978-1-4666-1640-0.ch006

one-storey and two-storey plane frame structures under possible future earthquakes are presented.

Earthquakes continue to claim thousands of lives and to damage structures every year (Comartin et al, 2004). Each earthquake brings out new surprises and lessons with it. In fact, the unexpected loss of lives and the severe damage of infrastructures and buildings during past strong earthquakes (e.g., 1994 Northridge, 1995 Kobe, 2010 Haiti and the most recent 2011 Tohoku earthquakes) have raised significant concern and questions on life safety and performance of engineering structures under possible future earthquakes. The occurrence of strong earthquakes in densely populated regions, especially in developing countries with vulnerable building stock and fragile infrastructure, could lead to catastrophic consequences. A notable example is the 2010 Haiti earthquake that killed 250,000 people and left a long-term suffering for the residents of this developing country (USGS/EERI 2010). On the other hand, the severe damage caused by the 2011 Tohoku earthquake and associated tsunami in Japan has raised significant challenges to one of the most developed countries as well (Takewaki et al, 2011). Hence, the assessment of seismic performance of structures under strong ground motions is an important problem in earthquake engineering. Structures need to resist unknown future earthquakes which adds more complexity to the problem (Moustafa 2011, 2009, Moustafa & Takewaki 2010a, Abbas & Manohar 2007, Takewaki 2002a, 2007). The consideration of the earthquake inherent uncertainty, the variability in the structure parameters and modeling the nonlinear behavior of the structure is essential for the accurate prediction of the actual response of the structure. Earthquake uncertainties include time, location, magnitude, duration, frequency content and amplitude, referred to as aleatory uncertainties.

The earthquake-resistant design of structures has been an active area of research for many decades (e.g., Penelis & Kappos 1997). The structural engineer aims to ensure safe performance of

the structure under possible future earthquakes while maintaining optimal use of the construction material. The design objectives in current seismic building codes are to ensure life safety and to prevent damage of the structure in minor and moderate frequent earthquakes, and to control local and global damage (prevent total collapse) and reduce life loss in a rare major earthquake. This can be achieved through: (1) robust prediction of expected future strong ground motions at the site, (2) accurate modeling of the material behavior under seismic loads, and (3) optimal distribution of the construction material.

Early works on seismic design have dealt with the specification of earthquake loads using the response spectrum method, the time history of the ground acceleration or using the theory of random vibrations. The nonlinear time-history analysis method is recognized as the most accurate tool for dynamic analysis of structures (Pinho, 2007). Many researchers have also established deterministic and probabilistic hazard spectra for the site (Reiter, 1990, McGuire, 1995). The development of mathematical models to describe the hysteretic nonlinear behavior of the structure during earthquakes has also been pursued in several studies (e.g., Takeda et al, 1970, Otani, 1981, Akiyama, 1985). New design concepts and methods, such as energy-, performance- and displacement-based design, base-isolation and structural control have been recently developed (Priestely et al, 2007, Takewaki, 2009, Fardis, 2010). Similarly, the optimal design of the structures under earthquake loads has been investigated in several studies (Fardis, 2010, Elishakoff & Ohsaki, 2010, Plevris, 2009, Haldar, 2006, Liang, 2005). The evaluation of the current procedures and new practical procedures for ground motion selection and modification are provided in the recent special issue on earthquake ground motion selection and modification for nonlinear dynamic analysis of structures (Kalkan & Luco, 2011). The two edited books by Papadrakakis et al (2009) and Tsompanakis et al. (2008) and the doctoral

thesis by Plevris (2009) present the state-of-the-art on advances and applications of optimal seismic design of structures considering uncertainties.

The definition of the worst (also known as critical) ground motion represents a major challenge in earthquake-resistance design of structures. This is because of the high uncertainty involved in the occurrence of the earthquake phenomenon compared to the relatively low variability in the structure's properties. Strasser & Bommer (2009) pose an important question on whether we have seen the worst ground motion yet, and the answer is not. They identify the worst ground motions as those having large amplitude. It may be emphasized that the worst ground motion for a structure may not be the worst input for a different structure. For example, the 2002 earthquake of magnitude 7.9 occurred along Alaska's Denali fault killed no one and did a little serious damage (Worth 2005), while the 1995 Kobe earthquake of 6.9 magnitude killed 5,100 people and caused billion of dollars in structural damage. Early studies on defining severity of strong ground motion and earthquake capability to create large damage have focused on the earthquake intensity, peak values of ground acceleration, velocity and displacement (PGA, PGV, PGD), effective PGV, etc. (Housner, 1970, Housner & Jennings, 1976). Near-field ground motion with pulse-like characteristic is a phenomenon representing one scenario of severity in the near-field region. Other scenarios of earthquake severity include repeated occurrence of ground motion in sequences (Elnashai et al, 1998, Moustafa & Takewaki 2009). Deep soft soils can also amplify earthquake amplitudes and modify frequency content. Secondary causes include also the travel path effects. In reality, some of these causes could exist together.

To carry out nonlinear time-history analysis, a set of suitable accelerograms need to be selected from available records (see, e.g., PEER, 2011). In this context, the criteria based on which records are selected and scaled represents an interesting subject. A notable effort in this direction

and other related subjects has been extensively investigated by several researchers, especially at Stanford University (e.g., Baker & Cornell, 2006, Moustafa et al, 2010, Baker, 2011, Baker et al, 2011, Haselton et al, 2011, Buratti et al 2011, Bommer & Acevedo 2004). If the number of the available records is small, records from other sites with similar soil condition or artificially simulated ground motions could be employed. The critical excitation method provides another alternative in case of scarce, inhomogeneous or limited earthquake data at the site. This method has been used to assess the structure's response under mathematically simulated earthquake inputs representing possible worst future earthquakes (e.g., Moustafa, 2011, 2009, Takewaki, 2002a, 2007). The method relies on the high uncertainty associated with the occurrence of the earthquake phenomenon, associated characteristics and also on the safety requirements of important and lifeline structures (nuclear plants, storage tanks, industrial installations, etc.). The critical earthquake input for a given structure is computed by minimizing the structure's performance while satisfying pre-defined constraints observed in real earthquake records. The structural performance may be described in terms of the structure's response or in terms of reliability measures or damage indices (Abbas & Manohar, 2007, Moustafa, 2009). The optimum design of the structure under varying critical earthquake loads has also been studied (e.g., Fujita et al, 2010, Saikat & Manohar, 2005, Takewaki, 2002b). Several practical applications have evolved from the concept of critical excitations. This includes design of structures to critical excitations, deriving critical response spectra for the site, estimating critical cross power spectral density functions of multi-point and spatially-varying ground motions, and reliability analysis of structures to partially specified earthquake loads. The method of critical excitations has also been employed in identifying resonant accelerations and in selecting critical recorded accelerograms based on the notion of the entropy principle (Moustafa,

2009, 2010). Comprehensive reviews on these aspects can be found in Moustafa (2011).

This chapter deals with the damage assessment for inelastic structures under worst future earthquakes using the critical excitations method. The novelty of this research is in combining damage indices, for the first time, with nonlinear optimization and nonlinear time-history analysis for assessing the structural performance under possible future ground motions. The use of damage indices provides a quantitative measure for damage and necessary repair for the structure. Bilinear and elastic-plastic force-displacement relationships are taken to model the material nonlinearity, and thus the present work is limited to non-deteriorating structures. Numerical examples for one-storey and two-storey plane frames without irregularities are provided. Future practical applications of the proposed methodology in seismic analysis and design of structures are also discussed.

2. DAMAGE ASSESSMENT OF INELASTIC STRUCTURES UNDER EARTHQUAKE LOADS

Damage assessment for structures is generally based on the nonlinear response quantities under earthquake loads (see Table 1). The bilinear and the elastic-plastic models are shown in Figure 1. The evaluation of the structural damage is usually carried out using damage indices which are quantified in terms of the structure response and the associated absorbed energy. Therefore, the quantification of damage indices is carried out after performing nonlinear time-history analysis for the structure. The nonlinear time-history analysis for the structure is performed by solving the equations of motions using numerical integration schemes (Moustafa, 2009, Hart & Wong 2000).

2.1 Energy Dissipated by Inelastic Structures

The energy dissipated by an N multi-degree-of-freedom (MDOF) structure under the ground acceleration $\ddot{x}(t)$ can be computed by integrating the equations of motion as follows (Zahrah & Hall, 1984, Akiyama, 1985, Uang & Bertero, 1990, Takewaki, 2004, Kalkan & Kunnath, 2008):

$$E_K(t) = \int_0^t \dot{\mathbf{X}}^T(\tau) \mathbf{M} \ddot{\mathbf{X}}(\tau) d\tau = \frac{1}{2} \sum_{i=1}^N m_i \dot{x}_i^2(t) \quad (1a)$$

$$E_D(t) = \int_0^t \dot{\mathbf{X}}^T(\tau) \mathbf{C} \dot{\mathbf{X}}(\tau) d\tau = \sum_{i=1}^N \int_0^t \dot{x}_i(\tau) f_{Di}(\tau) d\tau \quad (1b)$$

$$E_H(t) = \sum_{i=1}^N \int_0^t \dot{x}_i(\tau) f_{si}(\tau) d\tau - E_s(t) \quad (1c)$$

where, \mathbf{M} , \mathbf{C} , are the mass and damping matrices of the structure, respectively, $f_{si}(t)$ is the i th hysteretic restoring force, $\mathbf{X}(t)$ is the structure displacement vector and dot indicates differentiation with respect to time. The quantities $E_K(t)$, $E_D(t)$, $E_s(t)$ and $E_H(t)$ represent the kinetic, damping, strain and hysteretic energies, respectively (Moustafa, 2009). For viscous damping models, the damping energy reduces to

$$\sum_{i=1}^N \sum_{j=1}^N \int_0^t c_{ij} \dot{x}_i(\tau) \dot{x}_j(\tau) d\tau .$$

Note that equations (1) provide the relative energy terms. Note also that, by the end of the earthquake duration the kinetic and elastic strain energies diminish. Thus, the earthquake input energy to the structure is dissipated by hysteretic and damping energies. The next section demonstrates the use of the structure's response and the hysteretic energy in developing damage indices.

Table 1. Response descriptors for inelastic buildings under earthquake ground motion

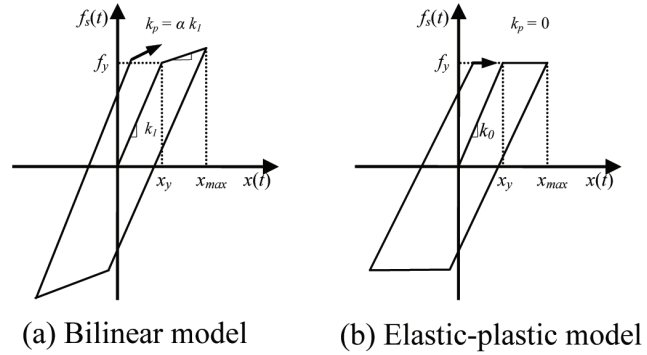
Response parameter	Definition
Maximum ductility	$\mu_{\max} = \max_{0 \leq t \leq t_f} \left \frac{x(t)}{x_y} \right $
Number of yield reversals	Number of times velocity changes sign
Maximum normalized plastic deformation range	$\Delta \bar{x}_{p,i} = \max_{0 \leq t \leq t_f} \left \frac{\Delta x_{p,i}}{x_y} \right $
Normalized cumulative ductility	$\mu_{ac.} = \sum_{i=1}^N \frac{ \Delta x_{p,i} }{x_y} + 1$
Residual (permanent) ductility	$\mu_{res} = \left \frac{x(t_f)}{x_y} \right $
Normalized earthquake input energy	$\bar{E}_I = \frac{1}{f_y x_y} \int_0^{t_f} E_I(t) dt$
Normalized total hysteretic energy dissipated	$\bar{E}_H = \frac{1}{f_y x_y} \int_0^{t_f} E_H(t) dt$
Ratio of total hysteretic energy to input energy	$r_E = \frac{\bar{E}_H}{\bar{E}_I}$
Maximum rate of normalized input energy	$P_{I,\max} = \frac{1}{f_y x_y} \max_{0 \leq t \leq t_f} \left[\frac{dE_I(t)}{dt} \right]$
Maximum rate of normalized damping energy	$P_{D,\max} = \frac{1}{f_y x_y} \max_{0 \leq t \leq t_f} \left[\frac{dE_D(t)}{dt} \right]$
Maximum rate of normalized hysteretic energy	$P_{H,\max} = \frac{1}{f_y x_y} \max_{0 \leq t \leq t_f} \left[\frac{dE_H(t)}{dt} \right]$

2.2 Damage Measures for Inelastic Structures

The literature on damage measures for structures under earthquake loads is vast (e.g., Cosenza et al, 1993, Ghobarah et al, 1999). Damage indices are quantified in terms of a single or a combination of structural response parameters. Table 1 summarizes several damage measures that are based on a single response parameter (Powell & Allahabadi 1988, Cosenza et al, 1993). The first measure represents the ultimate ductility produced

during the ground shaking. This measure does not incorporate information on how the earthquake input energy is imparted on the structure nor how this energy is dissipated. Earthquake damage occurs due to the maximum deformation or ductility and the hysteretic energy dissipated by the structure. Therefore, the definition of structural damage in terms of the ductility is inadequate. The last three measures indicate the rate of the earthquake input energy to the structure (i.e., how fast the input energy E_I is imparted by the earth-

Figure 1. (a) Force-displacement relation for nonlinear materials



quake and how fast it gets dissipated). Damage indices can be estimated by comparing the response parameters demanded by the earthquake with the structural capacities. Powell & Allahabadi (1988) proposed a damage index in terms of the ultimate ductility (capacity) μ_u and the maximum ductility attained during ground shaking μ_{\max} :

$$DI_\mu = \frac{x_{\max} - x_y}{x_u - x_y} = \frac{\mu_{\max} - 1}{\mu_u - 1} \quad (2)$$

However DI_μ does not include effects from hysteretic energy dissipation. Additionally, this damage index may not be zero for undamaged structures. A damage index that overcomes this problem has been proposed by Khashaee (2004):

$$DI_K = \frac{1 - \mu_{\max}^{-1}}{1 - \mu_u^{-1}} \quad (3)$$

Fajfar (1992) and Cosenza et al., (1993) quantified damage based on the structure hysteretic energy E_H :

$$DI_H = \frac{E_H / (f_y x_y)}{\mu_u - 1} \quad (4)$$

A robust damage measure should include not only the maximum response but also the effect of repeated cyclic loading. Park and co-workers developed a simple damage index, given as (Park et al, 1985, Park & Ang 1985, Park et al, 1987):

$$DI_{PA} = \frac{x_{\max}}{x_u} + \beta \frac{E_H}{f_y x_u} = \frac{\mu_{\max}}{\mu_u} + \beta \frac{E_H}{f_y x_y \mu_u} \quad (5)$$

Here, x_{\max} , E_H are the maximum absolute displacement and the dissipated hysteretic energy excluding elastic energy. x_u is the ultimate deformation capacity under monotonic loading and β is a positive constant that weights the effect of cyclic loading on structural damage. Note that if $\beta = 0$, the contribution to DI_{PA} from cyclic loading is omitted.

The state of the structure damage is defined as: (a) repairable damage, when $DI_{PA} < 0.40$, (b) damaged beyond repair, when $0.40 \leq DI_{PA} < 1.0$, and (c) total or complete

collapse, when $DI_{PA} \geq 1.0$. These criteria are based on calibration of DIPA against experimental results and field observations in earthquakes (Park et al., 1987). Note that Eq (5) reveals that both maximum ductility and hysteretic energy dissipation contribute to the structural damage during earthquakes. Eq. (5) expresses damage as a linear combination of the damage caused by excessive deformation and that contributed by repeated cyclic loading effect. Note also that the quantities x_{\max} , E_H depend on the loading history while the quantities β , x_u , f_y are independent of the loading history and are determined from experimental tests. It should also be emphasized that Eqs (2-5) can be used to estimate damage for a member in a structure which defines the local damage. To estimate the global damage of the structure, a weighted sum of the local damage indices need to be estimated (Park et al, 1987). In this chapter, Eq (5) is adopted in quantifying the structural damage. The next section develops the mathematical modeling of critical future earthquake loads.

3. DERIVATION OF WORST FUTURE EARTHQUAKE LOADS

The worst future ground acceleration is represented as a product of a Fourier series and an envelope function in Box 1.

Here, A_0 is a scaling constant and the parameters α_1, α_2 impart the transient trend to $\ddot{x}_g(t)$. R_i and φ_i are $2N_f$ unknown amplitudes and phase angles, respectively and ω_i , $i = 1, 2, \dots, N_f$ are the frequencies presented in the ground accelera-

Box 1.

$$\ddot{x}_g(t) = e(t) \sum_{i=1}^{N_f} R_i \cos(\omega_i t - \varphi_i) = A_0 [\exp(-\alpha_1 t) - \exp(-\alpha_2 t)] \sum_{i=1}^{N_f} R_i \cos(\omega_i t - \varphi_i) \quad (6)$$

tion which are selected to span satisfactory the frequency range of $\ddot{x}_g(t)$. In constructing critical seismic inputs, the envelope function is taken to be known. The information on energy E , peak ground acceleration (PGA) M_1 , peak ground velocity (PGV) M_2 , peak ground displacement (PGD) M_3 , upper bound Fourier amplitude spectra (UBFAS) $M_4(\omega)$, and lower bound Fourier amplitude spectra (LBFAS) $M_5(\omega)$ are also taken to be available which enables defining the following nonlinear constraints (Abbas & Manohar, 2002, Abbas, 2006):

$$\begin{aligned} \left[\int_0^{\infty} \ddot{x}_g^2(t) dt \right]^{\frac{1}{2}} &\leq E \\ \max_{0 < t < \infty} |\ddot{x}_g(t)| &\leq M_1 \\ \max_{0 < t < \infty} |\dot{x}_g(t)| &\leq M_2 \\ \max_{0 < t < \infty} |x_g(t)| &\leq M_3 \\ M_5(\omega) &\leq X_g(\omega) \leq M_4(\omega) \end{aligned} \quad (7)$$

Here, $X_g(\omega)$ is the Fourier transform of $\ddot{x}_g(t)$. Note that the constraint on the earthquake energy is related to the Arias intensity (Arias 1970). The spectra constraints aim to replicate the frequency content and amplitude observed in past recorded accelerograms on the future earthquake. The ground velocity and displacement are obtained from Eq. (6) and seen in Box 2:

Making use of the conditions $x_g(0) = 0$ and $\lim_{t \rightarrow \infty} \dot{x}_g(t) \rightarrow 0$ (Shinozuka & Henry, 1965), the constants in the above equation can be shown to be given as (Abbas & Manohar, 2002, Abbas, 2006):

Box 2.

$$\dot{x}_g(t) = \sum_{i=1}^{N_f} \int_0^t R_i e(\tau) \cos(\omega_i \tau - \varphi_i) d\tau + C_1; x_g(t) = \sum_{i=1}^{N_f} \int_0^t R_i e(\tau) (t - \tau) \cos(\omega_i \tau - \varphi_i) d\tau + C_1 t + C_2 \quad (8)$$

$$C_2 = 0; C_1 = -\sum_{i=1}^{N_f} \int_0^\infty R_i e(\tau) \cos(\omega_i \tau - \varphi_i) d\tau \quad (9)$$

The constraints of Eq (7) can be expressed in terms of the variables $R_i, \varphi_i, i = 1, 2, \dots, N_f$ (see Box 3)

Here $i = \sqrt{-1}$. To quantify the constraints quantities E, M1, M2, M3, $M_4(\omega)$, and $M_5(\omega)$ it is assumed that a set of Nr earthquake records denoted by $\ddot{v}_{gi}(t), i = 1, 2, \dots, N_r$ are available for the site under consideration or from other sites with similar geological soil conditions. The values of energy, PGA, PGV and PGD are obtained for each of these records. The highest of these values across all records define E, M1, M2 and M3. The available records are further normalized such that the Arias intensity of each record is set to unity (i.e., $[\int_0^\infty \ddot{v}_{gi}^2(t) dt]^{1/2} = 1$, Arias, 1970), and are denoted by $\{\ddot{v}_{gi}\}_{i=1}^{N_r}$. The bounds $M_4(\omega)$ and $M_5(\omega)$ are obtained as:

$$M_4(\omega) = E \max_{1 \leq i \leq N_r} |\bar{V}_{gi}(\omega)|; M_5(\omega) = E \min_{1 \leq i \leq N_r} |\bar{V}_{gi}(\omega)| \quad (11)$$

Here $\bar{V}_{gi}(\omega), i = 1, 2, \dots, N_r$ denotes the Fourier transform of the ith normalized accelerogram $\ddot{v}_{gi}(t)$. The bound $M_4(\omega)$ has been considered earlier (Shinozuka, 1970, Takewaki, 2001, 2002). The lower bound was considered by Moustafa (2002) and Abbas & Manohar (2002).

Finally, the problem of deriving critical future earthquake loads on inelastic structures can be posed as determining the optimization variables $y = \{R_1, R_2, \dots, R_{N_f}, \varphi_1, \varphi_2, \dots, \varphi_{N_f}\}^t$ such that the damage index DIPA is maximized subjected to the constraints of Eq (10). The solution to this nonlinear constrained optimization problem is tackled by using the sequential quadratic programming method (Arora, 2004). The following convergence criteria are adopted:

$$|f_j - f_{j-1}| \leq \varepsilon_1; |y_{i,j} - y_{i,j-1}| \leq \varepsilon_2 \quad (12)$$

Herein, f_j is the objective function at the j th iteration, $y_{i,j}$ is the i th optimization variable at the j th iteration and $\varepsilon_1, \varepsilon_2$ are small quantities to be specified. The structure inelastic deformation is estimated using the Newmark β -method which is built as a subroutine inside the optimization program. The details of the optimization procedures involved in the computation of the critical earthquake and the associated damage index are shown in Figure 2. Further details can also be found in Abbas (2006).

It may be emphasized that the quantities $\mu(t)$ and $E_H(t)$ do not reach their respective maxima at the same time. Therefore, the optimization is performed at discrete points of time and the optimal solution

$$y^* = [R_1^*, R_2^*, \dots, R_{N_f}^*, \varphi_1^*, \varphi_2^*, \dots, \varphi_{N_f}^*]^t$$

is the one that produces the maximum DIPA across all time points. The critical earthquake loads are characterized in terms of the critical accelerations

Box 3.

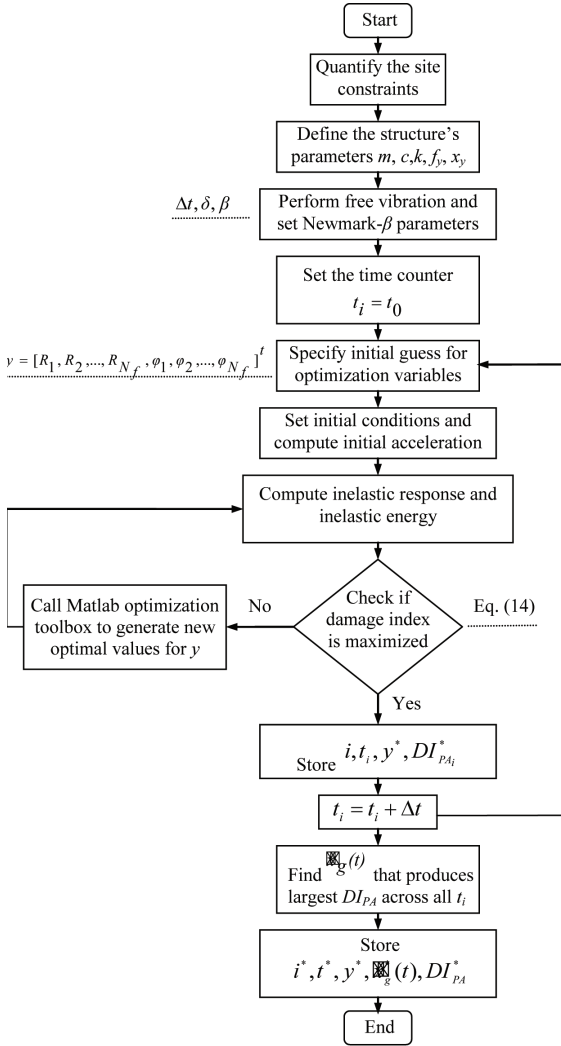
$$\begin{aligned}
 & \left[A_0^2 \sum_{m=1}^{N_f} \sum_{n=1}^{N_f} R_m R_n \int_0^\infty [\exp(-\alpha_1 t) - \exp(-\alpha_2 t)]^2 \cos(\omega_m t - \varphi_m) \cos(\omega_n t - \varphi_n) dt \right]^{\frac{1}{2}} \leq E \\
 & \max_{0 < t < \infty} |A_0[\exp(-\alpha_1 t) - \exp(-\alpha_2 t)] \sum_{n=1}^{N_f} R_n \cos(\omega_n t - \varphi_n)| \leq M_1 \\
 & \max_{0 < t < \infty} |A_0 \sum_{n=1}^{N_f} \int_0^t R_n [\exp(-\alpha_1 \tau) - \exp(-\alpha_2 \tau)] \cos(\omega_n \tau - \varphi_n) d\tau - \\
 & A_0 \sum_{n=1}^{N_f} \int_0^\infty R_n [\exp(-\alpha_1 \tau) - \exp(-\alpha_2 \tau)] \cos(\omega_n \tau - \varphi_n) d\tau| \leq M_2 \\
 & \max_{0 < t < \infty} |A_0 \sum_{n=1}^{N_f} \int_0^t R_n [\exp(-\alpha_1 \tau) - \exp(-\alpha_2 \tau)] (t - \tau) \cos(\omega_n \tau - \varphi_n) d\tau - \\
 & A_0 t \sum_{n=1}^{N_f} \int_0^\infty R_n [\exp(-\alpha_1 \tau) - \exp(-\alpha_2 \tau)] \cos(\omega_n \tau - \varphi_n) d\tau| \leq M_3 \\
 & M_5(\omega) \leq |A_0 \sum_{n=1}^{N_f} \int_0^\infty R_n \{\exp[-\alpha_1 \tau] - \exp[-\alpha_2 \tau]\} \cos(\omega_n \tau - \varphi_n) \exp[-i\omega\tau] d\tau| \leq M_4(\omega)
 \end{aligned} \tag{10}$$

and associated damage indices, inelastic deformations and energy dissipated by the structure. The next section provides numerical illustrations for the formulation developed in this section.

In the numerical analysis, the constraints quantities E , M_1 , M_2 , M_3 , $M_4(\omega)$, and $M_5(\omega)$ are estimated using past recorded earthquake data. This approach is considered to be consistent with the aspirations of the ground motion models that are commonly used by engineers, which, aim to replicate the gross features of recorded motions, such as, amplitude, frequency content, nonstationarity trend, local soil amplification effects, and duration. It is of interest to note in this context that, predictive or physical models for ground motions, which take into account several details, such as, fault dimension, fault orientation, rupture velocity, magnitude of earthquake, attenuation, stress drop, density of the intervening medium, local soil condition and epicentral distance, have

also been developed in the existing literature, mainly by seismologists (see, e.g., Brune, 1970, Hanks & McGuire, 1981, Boore, 1983, Queck et al, 1990). In using these models, one needs to input values for a host of parameters and the success of the model depends on how realistically this is done. It is possible to formulate the critical earthquake models based on the latter class of models in which one can aim to optimize the parameters of the model so as to realize the least favorable conditions. Note that the class of admissible functions, in the determination of critical excitations, in this case, becomes further constrained by the choice that one makes for the physical model. The approach adopted in this study, in this sense, is nonparametric in nature. A comparison of results based on this approach with those from ‘model-based’ approaches is of interest; however, these questions are not considered in the present study.

Figure 2. Flowchart for deriving critical earthquake loads



4. NUMERICAL EXAMPLES

4.1 Bilinear Inelastic Frame Structure

A SDOF frame structure with mass 9×103 kg, initial stiffness $k_1 = 1.49 \times 105$ N/m and viscous damping of 0.03 damping ratio is considered (initial natural frequency = 4.07 rad/s). The strain hardening ratio is taken equal to 0.05. These

parameters are changed later to study their influence on the estimated worst earthquake loads and the associated damage. The yield displacement is taken as 0.10 m and the structure is taken to start from rest. The objective function is adopted as the Park and Ang damage index DIPA given by Eq(5). The parameters of the Newmark β -method are taken as $\delta = 1/2$; $\alpha = 1/6$ and $\Delta t = 0.005$ s.

4.1.2 Quantification of Constraints

A set of 20 earthquake records is used to quantify the constraint bounds E , M_1 , M_2 , M_3 , $M_4(\omega)$ and $M_5(\omega)$ (COSMOS, 2005). Table 2 provides information on these records. Based on numerical analysis of these records, the constraints were computed as $E = 4.17$ m/s^{1.5}, $M_1 = 4.63$ m/s² (0.47 g), $M_2 = 0.60$ m/s and $M_3 = 0.15$ m and the average dominant frequency was about 1.65 Hz. The envelope parameters were taken as $A_0 = 2.17$, $\alpha_1 = 0.13$, and $\alpha_2 = 0.50$. The convergence limits $\varepsilon_1, \varepsilon_2$ were taken as 10-6 and the convergence criterion on the secant stiffness is taken as 10-3 N/m. The frequency content for $\ddot{x}_g(t)$ is taken as (0.1-25) Hz. Additionally, in distributing the frequencies $\omega_i, i = 1, 2, \dots, N_f$ in the interval (0.1, 25), it was found advantageous to select some of these ω_i to coincide with the natural frequency of the elastic structure and also to place relatively more points within the modal half-power bandwidth.

The constraint scenarios considered in deriving the worst earthquake inputs are listed in Table 3. The constrained nonlinear optimization problem is solved using the sequential quadratic optimization algorithm ‘fmincon’ of the Matlab optimization toolbox (Caleman et al, 1999). In the numerical calculations, alternative initial starting solutions, within the feasible region, were examined and were found to yield the same optimal solution. To select the number of frequency terms N_f a parametric study was carried out and $N_f =$

51 was found to give satisfactory results. Figure 3 depicts the influence of N_f on the convergence of the objective function for constraints scenarios 1 and 4 (see Table 3).

4.1.3 Numerical Results and Discussions

The numerical results obtained are presented in Figures 4, 5, 6, 7, 8 and 9 and Table 4. Figure 4 shows results for constraint scenario 1 and similar results for case 4 are shown in Figure 5. Each of these figures shows the Fourier amplitude spectrum of the worst ground acceleration, the inelastic deformation, the hysteretic force and the energy dissipated by the structure. Figure 6 shows the time history of the ground acceleration. Based on extensive analysis of the numerical results, the major observations are summarized below.

The frequency content and Fourier amplitude of the worst earthquake are strongly dependent on the constraints imposed (see Table 3). If available information on earthquake data is limited to

the total energy and PGA, the worst input is narrow band (highly resonant) and the structure deformation is conservative (see Figure 4 and Table 4). Furthermore, most of the power of the Fourier amplitude is concentrated at a frequency close to the natural frequency of the elastic structure. This amplitude gets shifted towards a higher frequency when the strain hardening ratio increases. The Fourier amplitudes at other frequencies are low and uniformly distributed. This result is substantially different from that for the elastic structure where all power of the acceleration amplitude is concentrated around ω_0 with no amplitude at other frequencies (Abbas & Manohar, 2002). Additional constraints on the Fourier amplitude spectra (see Table 3) force the Fourier amplitude of the worst acceleration to get distributed across other frequencies. The critical acceleration possesses a dominant frequency that is close to the average dominant frequency observed in past records (see Figure 5). The realism of the earthquake input is also evident from the maximum damage index it produces. For instance, the dam-

Table 2. Information on past recorded ground motion records for a firm soil site

Earthquake date	Magnitude	Epic. Dist. (km)	Comp- onent	PGA (m/s ²)	PGV (m/s)	PGD (m)	Energy* (m/s ^{1.5})	Site
Mammoth lakes 05.25.1980	6.2	1.5	W	4.02	0.21	0.05	3.73	Convict Greek
Loma prieta 10.18.1989	7.0	9.7	S	3.92	0.23	0.05	4.01	Capitola
Morgan hill 04.24.1984	6.1	4.5	W	3.91	0.31	0.07	3.82	Halls valley
San Fernando 02.09.1971	6.6	27.6	S	4.63	0.36	0.11	2.61	Castaic old ridge
Parkfield 12.20.1994	5.0	9.1	S60E	3.06	0.40	0.07	2.33	Parkfield fault
Caolinga 05.02.1983	6.5	30.1	S30W	1.53	0.30	0.02	1.64	Cantuac creek
Northridge 01.17.1994	6.7	5.9	N	2.66	0.28	0.10	2.47	Canoga park
Cape Mendocino 04.25.1992	7.0	5.4	S74E	3.81	0.60	0.12	4.17	Petrolia general
Westmorland 04.26.1981	5.0	6.6	S16W	3.43	0.34	0.09	3.50	Westmorland fire
Imperial valley 10.15.1979	6.4	17.4	E	3.25	0.45	0.15	2.44	Calexico fire
			S	2.89	0.24	0.08	2.31	
			S45W	4.35	0.33	0.11	3.26	
			N45W	3.54	0.44	0.15	3.25	
				2.68	0.22	0.10	2.30	
				1.98	0.19	0.15	2.14	

$$* E = \left[\int_0^\infty \ddot{v}_g^2(t) dt \right]^{1/2} \text{ (Arias, 1970).}$$

Table 3. Nomenclature of constraint scenarios considered

Case	Constraints imposed
1	Energy and PGA
2	Energy, PGA, PGV and PGD
3	Energy, PGA and UBFAS
4	Energy, PGA, UBFAS and LBFAS

age index for case 4 is 0.37 which is substantially smaller than 1.15 for case 1 (Table 4). The constraints on PGV and PGD were not found to be significant in producing realistic critical inputs compared to the constraints on UBFAS and LB-FAS. Also, the realism of the critical acceleration for case 4 can be examined by comparing the Fourier amplitude spectra and frequency content of the worst acceleration (Figures 4, 5) with the Fourier amplitude spectra of past recorded earthquakes (Figure 7). Note that, while the constraint scenario 1 leads to pulse-like ground motion, such scenario is observable in past recorded earthquakes (e.g., 1971 San Fernando, 1985 Mexico, and 1995 Kobe earthquakes). Resonant or pulse-like earthquakes are also observable in near-field ground motion with directivity focusing, known as forward- and backward-directivity ground motion (Housner & Hudson, 1958, Kalkan & Kunnath, 2006, He & Agrawal, 2008, Moustafa 2008). The realism of worst earthquake loads can be also

examined by comparing maximum response from these accelerations with those from past recorded ground motions. Thus, the maximum ductility factor of the structure from the worst earthquake is about 3.9 (case 1) and 2.6 (case 4) times that from the Kobe earthquake and is 2.7 (case 1) and 1.5 (case 4) times that from the San Fernando earthquake.

To examine the effect of the strain hardening ratio on the design earthquake acceleration computed, limited studies were carried out. The value of α was changed and the critical input was determined by solving a new optimization problem. Namely, α was taken as 0.20, 0.10, 0.05, and 0.01. The strain hardening ratio was not seen to significantly influence the frequency content of the critical earthquake input. It was observed, however, that the inelastic structure with lower values of α yields more frequently compared to the same system with higher α values. Accordingly, the cumulative hysteretic energy dissipated was observed to decrease for higher values of α (Figure 8(a)). This feature is particularly remarkable at the end of the earthquake duration. It was also observed that the results on critical earthquake accelerations for bilinear inelastic structure with $\alpha = 0.01$ are close to those for the elastic-plastic structure (Abbas, 2006).

Figure 3. Convergence of objective function in terms of frequency terms N_f (a) Case 1 (b) Case 4

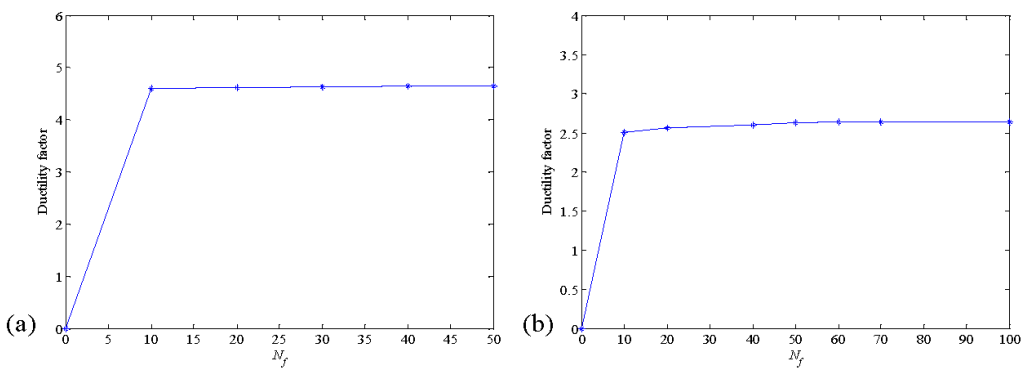
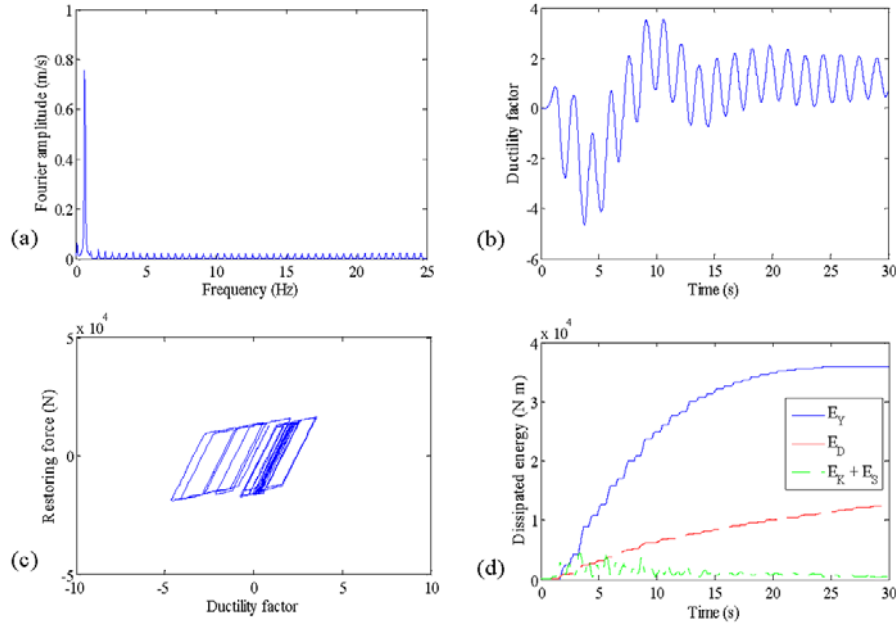


Figure 4. Optimal earthquake input and associated structural responses for case 1 (a) Fourier amplitude of the ground acceleration (b) Normalized inelastic deformation (c) Hysteretic restoring force (d) Dissipated energy

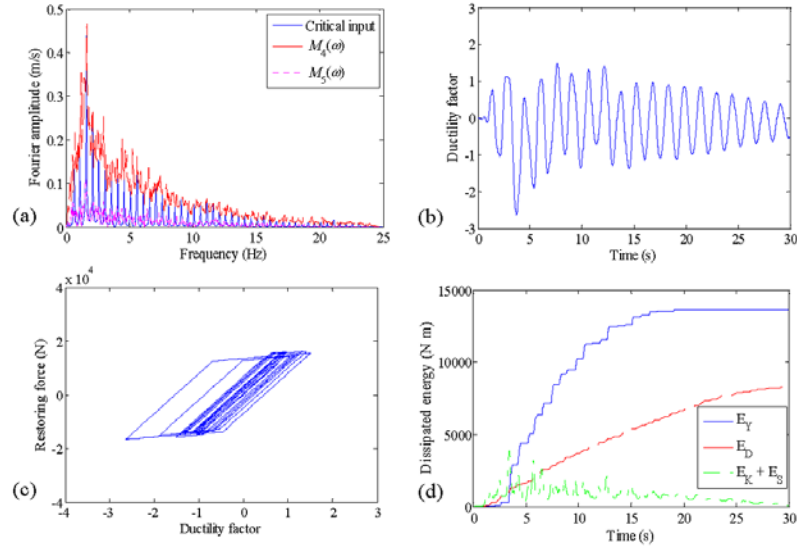


To investigate the influence of the damping ratio on the computed worst earthquake load, limited studies were carried out. The damping ratio was changed, namely, 0.01, 0.03 and 0.05, while all other parameters were kept unchanged. The critical earthquake is computed by solving a new optimization problem for each case. The effect of the change in η_0 was seen to be similar to that due to α . In other words, the value of the damping ratio was not seen to significantly influence the frequency content of the earthquake acceleration. It was observed, however, that the ductility ratio and the maximum inelastic deformation of the structure decrease for higher damping ratios. Thus, the ductility ratio decreases to 2.43 when the damping ratio is taken as 0.05 while the ductility ratio increases to 2.89 when the damping ratio reduces to 0.01. It was also observed that the inelastic structure with higher damping ratio dissipates more energy through damping

compared with the same structure with lower damping ratio (see Figure 8(b)). The damage index also reduces when the damping ratio increases.

To assess the structure safety, Eq. (5) was used to estimate the damage index of the structure subjected to the critical earthquake load. The effect of the parameter β on the damage index is examined first. Based on experimental tests, it was reported that β ranges between 0.05 and 0.20 with an average value of 0.15 as suggested by Park et al., (1987). Figure 9(a) shows the influence of β on the damage index. To study the effect of the initial natural frequency of the structure on the damage index, the structure stiffness was varied while keeping all other parameters unchanged and the critical earthquake was computed for each case. Subsequently, the value of DIPA was calculated for each case. In the numerical calculations β was taken as 0.15 and

Figure 5. Optimal earthquake input and associated structural responses for case 4 (a) Fourier amplitude of the ground acceleration (b) Normalized inelastic deformation (c) Hysteretic restoring force (d) Dissipated energy



x_{\max}, μ_{\max} are taken as 0.10 m and 2.64, respectively.

The value of μ_u was taken as 6 in Figures. 9(a) and 8 in Figure 9(b). It was found that the damage index for the structure with initial natural frequency smaller than 1.65 is higher than 0.40 and thus either total collapse or damage beyond repair

of the structure is expected. The value of DIPA for the structure with ω_0 greater than about 1.70 Hz is less than 0.40 and thus the structure does not experience total damage but repairable damage. This observation is consistent since the site dominant frequency is around 1.65 Hz and since the Fourier amplitude of the ground acceleration

Figure 6. Optimal earthquake acceleration and velocity (a) Case 1 (b) Case 4

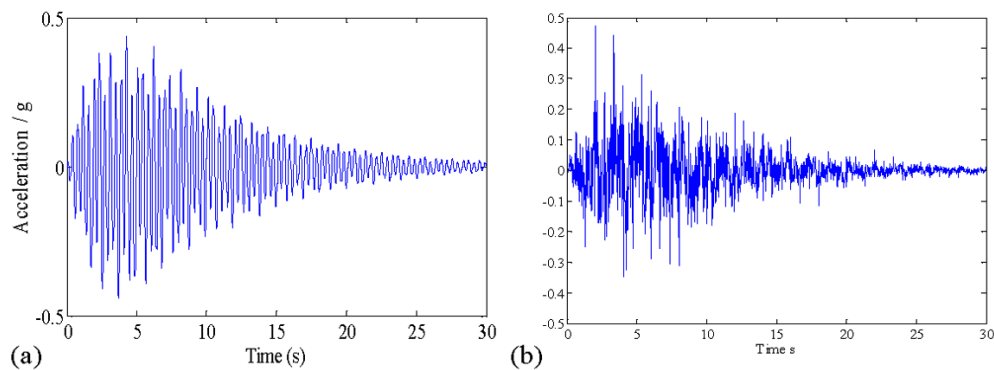


Figure 7. Fourier amplitude of recorded earthquakes (a) San Fernando 1971 (b) Hyogoken-Nanbu 1995

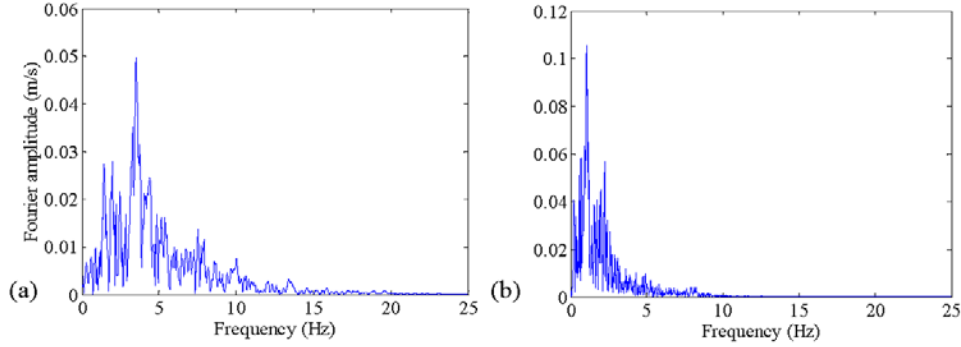


Figure 8. (a) Effect of strain hardening ratio on dissipated yield energy (b) Effect of damping on dissipated damping energy

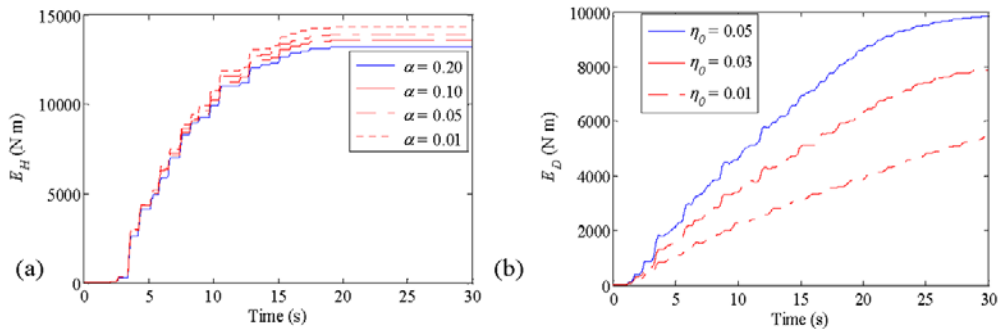


Figure 9. (a) Effect of the value of β on the damage index (b) damage spectra for inelastic SDOF buildings

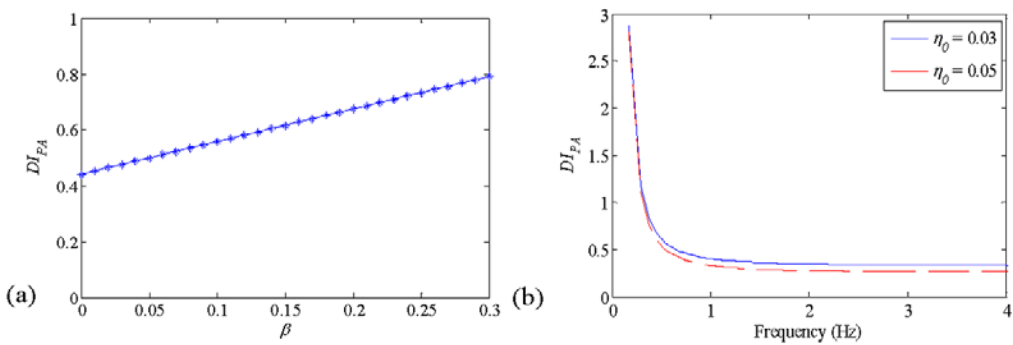


Table 4. Response parameters for alternative constraint scenarios ($\alpha = 0.05$, $\zeta = 0.03$)

Case	x_{\max} (m)	μ_{\max}	x_p (m)	N_{rv}^*	DI_{PA}	Damage status
1	0.47	4.65	0.07	60	1.15	Total collapse
2	0.45	4.53	0.06	54	0.97	Damaged beyond repair
3	0.41	4.14	0.07	49	0.72	Damaged beyond repair
4	0.26	2.64	0.05	44	0.37	Repairable damage

* N_{rv} = number of yield reversals (see Table 1)

is seen to be located in the stiff side of the initial frequency of the inelastic structure.

4.2 Inelastic Two-Story Frame Structure

A two-story braced building frame is considered to demonstrate the formulation developed in this chapter for MDOF inelastic structures (Moustafa 2009). The material behavior of the braces is taken as bilinear ($k_2 = \gamma k_1$) as shown in Figure 1(a). The floor masses are taken as $m_1 = m_2 = 1.75 \times 10^5$ Ns²/m, the cross-sectional areas of the braces are $A_1 = A_2 = 6.45 \times 10^{-4}$ m², the Young's modulus = 2.59×10^{11} N/m², and the strain hardening ratio = 0.10 (i.e., ratio of the post-yield stiffness to the pre-yield stiffness). When both braces are behaving elastically, the stiffness matrix $\mathbf{K}_s = \mathbf{K}_{el}$, if brace 1 yields $\mathbf{K}_s = \mathbf{K}_1$, if brace 2 yields $\mathbf{K}_s = \mathbf{K}_2$ and if both braces yield $\mathbf{K}_s = \mathbf{K}_{12}$. These matrices are given in Moustafa (2009). The structure is assumed to start from rest. The first two natural frequencies of the elastic structure were computed as $\omega_1 = 6.18$ rad/s and $\omega_2 = 16.18$ rad/s. A Rayleigh proportional damping $\mathbf{C} = a\mathbf{M} + b\mathbf{K}_s$ with $a = 0.2683$, $b = 0.0027$ is adopted. These values are selected such that the damping ratio in the first two modes is 0.03. This implies that the damping forces in braces are nonlinear hysteretic functions of the deformed shape of the structure. Let the yield strain of the braces $\varepsilon_y = 0.002$ for both tension and compression. The braces will yield at a relative displacement

$$x_y = L\varepsilon_y / \cos \theta = 0.0381 \text{ m.}$$

Thus, brace 1 yields when $|x_1| = 0.0381$ m and brace 2 yields when $|x_2 - x_1| = 0.0381$ m. The objective function is taken as the weighted damage indices in braces 1 and 2. In the numerical analysis, the parameters of the Newmark β -method were taken as $\delta = 1/2$; $\alpha = 1/6$ and the time step $\Delta t = 0.005$ s.

The results of this example are shown in Figures 10 and 11. In general, the feature observed for the future earthquakes in the previous example was also observed in this example. However, the inelastic deformation and the associated damage were seen to depend on the two vibration modes. Thus, the maximum ductility ratio μ for case 1 is 4.34 while that produced from constraint case 4 is 2.27. Similarly, the maximum response reduces from 0.15 m to 0.08 m when the constraints on UBFAS and LBFAS are brought in. The earthquake input energy to the inelastic system is mainly dissipated by yielding and nonlinear damping of the structure. The hysteretic and damping energies are significantly higher than the recoverable strain and kinetic energy. The kinetic and recoverable strain energies are small and diminish near the end of the ground shaking. The energy dissipated by yielding is significantly higher than that dissipated by damping. The weighted damage index for case 1 was about 0.96 implying total collapse while for case 4 the damage index was about 0.35 implying repairable damage.

It may be noted that the numerical illustrations of the formulation developed in this paper were demonstrated for simple structures with bilinear

Figure 10. Critical acceleration $\ddot{x}_g(t)$ for inelastic structure for case 1 (a) Time history (b) Fourier amplitude spectrum

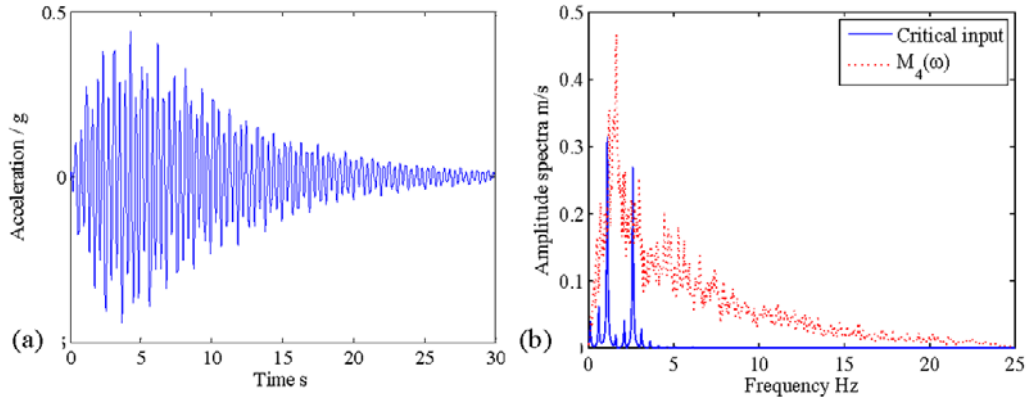
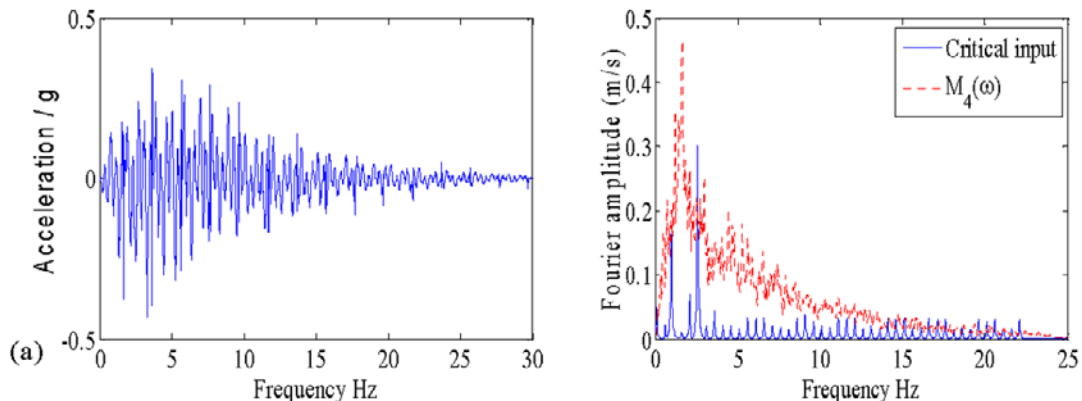


Figure 11. Critical acceleration $\ddot{x}_g(t)$ for inelastic structure for case 2 (a) Time history (b) Fourier amplitude spectrum



and elastic-plastic force-deformation laws. The application of the proposed method to more complex structures and the use of more detailed degradation models (e.g., trilinear degradation, Takeda and Clough models) need to be investigated. Additionally, in this paper Park and Ang damage index has been used to assess the structure performance. It may be emphasized that this damage index has some limitations (Mehanny & Deierlein, 2000, Bozorgnia & Bertero 2003).

This includes: (1) the weak cumulative component for practical cases given the typical dominance of the peak displacement term over the accumulated energy term, (2) the use of a linear combination of deformation and energy in spite of the obvious nonlinearity of the problem and the interdependence of the two quantities, and (3) the lack of considering the loading sequence effect in the cumulative energy term. Furthermore, when $E_H = 0$ (elastic behavior), the value of DI_{PA} should

be zero. However, the value of DI_{PA} computed from Eq (5) will be greater than zero. Similarly, when the system reaches its maximum monotonic deformation, while DI_{PA} should be 1.0, however, Eq (5) leads to DI_{PA} greater than 1.0. Chai et al (1995) proposed modification to DI_{PA} to correct for the second drawback only. The study, also, examined experimentally the implication of the energy-based linear damage model of DI_{PA} . Despite the drawbacks of DI_{PA} , it has been extensively used by many researchers, mainly due to its simplicity and the extensive calibration against experimentally observed seismic structural damage during earthquakes (mainly for reinforced concrete structures). Bozorgnia & Bertero (2003) proposed two improved damage indices that overcome some of the drawbacks associated with DI_{PA} .

In this chapter, worst earthquakes that maximize the structure's damage were obtained using deterministic methods. Critical earthquakes can be formulated using stochastic processes, random vibration theory and reliability analysis which provides a powerful alternative to the methodology developed here (see, e.g., Abbas & Manohar, 2005, 2007).

5. CONCLUDING REMARKS

A methodology for assessing damage in structures under critical future earthquake loads is developed in this chapter. The novelty of this research lies in combining damage indices, nonlinear optimization and nonlinear time-history analysis in assessing the structural performance under future earthquakes. Damage descriptors are introduced in deriving the worst earthquake ground motion. The structural damage is quantified in terms of Park and Ang damage indices. As is well known, damage indices describe the damage state of the structure and correlate well with the actual damage displayed during earthquakes. The quantification of the structure's damage using damage indices

is of substantial importance in deriving critical earthquake loads for inelastic structures. This is because damage indices imply that the structure is damaged by a combination of repeated stress reversals and high stress excursions. This also facilitates assessing the safety of the structure by providing a quantitative measure on the necessary repair.

In this chapter, the worst earthquake load is derived based on available information using inverse nonlinear dynamic analysis, optimization techniques and damage indices. It was seen that if available information is limited to the energy and PGA, the resulting earthquake is highly resonant and produces conservative damage. When extra information on the Fourier amplitude spectra is available, more realistic earthquake loads (in terms of frequency content, amplitude, inelastic deformations and damage indices produce) are obtained. The influences of the strain hardening and damping ratios on the estimated design loads were studied. Critical damage spectra for the site were also established. These spectra provide upper bounds on the structural damage and necessary repair under possible future earthquakes. The formulation developed in this chapter was demonstrated for inelastic frame structures modeled with bilinear and elastic-plastic force-deformation laws. In other words, non-deteriorating structures are only considered. Future extension of the present research requires the use of nonlinear degradation models that facilitate the development of plastic hinges in the structure. In this case the computations will increase considerably due to the complexity in estimating the structural response. Finally, it may be emphasized that in the present work, the structural properties have been kept unchangeable. It is possible to apply the proposed methodology for optimal design of the structure under future earthquakes. Herein, an initial guess for the dimensions of the structure's members needs to be assumed and an iterative procedure has to be carried out leading to the optimal design of the structure, the system-dependent worst

earthquake and the associated damage (Takewaki, 2002b, 2007, Saikat & Manohar, 2005, Fujita et al, 2010).

ACKNOWLEDGMENT

This research work is partly supported by research funds from the Japanese Society for the Promotion of Science (JSPS) under Grant No. JSPS-P-08073. The support is gratefully acknowledged.

REFERENCES

- Abbas, A. M. (2006). Critical seismic load inputs for simple inelastic structures. *Journal of Sound and Vibration*, 296, 949–967. doi:10.1016/j.jsv.2006.03.021
- Abbas, A. M., & Manohar, C. S. (2002). Investigations into critical earthquake load models within deterministic and probabilistic frameworks. *Earthquake Engineering & Structural Dynamics*, 31, 813–832. doi:10.1002/eqe.124
- Abbas, A. M., & Manohar, C. S. (2005). Reliability-based critical earthquake load models. Part 2: Nonlinear structures. *Journal of Sound and Vibration*, 287, 883–900. doi:10.1016/j.jsv.2004.12.003
- Abbas, A. M., & Manohar, C. S. (2007). Reliability-based vector nonstationary random critical earthquake excitations for parametrically excited systems. *Structural Safety*, 29, 32–48. doi:10.1016/j.strusafe.2005.11.003
- Akiyama, H. (1985). *Earthquake-resistant limit-state design for buildings*. Tokyo, Japan: University of Tokyo Press.
- Arias, A. (1970). *A measure of earthquake intensity: Seismic design of nuclear power plants* (pp. 438–468). Cambridge, MA: MIT Press.
- Arora, J. S. (2004). *Introduction to optimum design*. San Diego, CA: Elsevier Academic Press.
- Baker, J. W. (2011). Conditional mean spectrum: Tool for ground motion selection. *Journal of Structural Engineering*, 137(3), 322–331. doi:10.1061/(ASCE)ST.1943-541X.0000215
- Baker, J. W., & Cornell, C. A. (2006). Spectral shape, epsilon and record selection. *Earthquake Engineering & Structural Dynamics*, 35, 1077–1095. doi:10.1002/eqe.571
- Baker, J. W., Lin, T., Shahi, S. K., & Jayaram, N. (2011). *New ground motion selection procedures and selected motions for the PEER transportation research program*. PEER Technical Report 2011/03. 106p.
- Bommer, J. J., & Acevedo, A. B. (2004). The use of real earthquake accelerograms as input to dynamic analysis. *Journal of Earthquake Engineering*, 1, 43–91. doi:10.1080/13632460409350521
- Boore, D. M. (1983). Stochastic simulation of high-frequency ground motions based on seismological models of the radiated spectra. *Bulletin of the Seismological Society of America*, 73, 1865–1894.
- Bozorgnia, Y., & Bertero, V. V. (2003). Damage spectra: Characteristics and applications to seismic risk reduction. *Journal of Structural Engineering*, 129(4), 1330–1340. doi:10.1061/(ASCE)0733-9445(2003)129:10(1330)
- Bozorgnia, Y., & Bertero, V. V. (Eds.). (2004). *Earthquake engineering*. New York, NY: CRC Press. doi:10.1201/9780203486245
- Brune, J. N. (1970). Tectonic stress and the spectra of seismic shear waves from earthquakes. *Journal of Geophysical Research*, 75, 4997–5009. doi:10.1029/JB075i026p04997
- Buratti, N., Stafford, P. J., & Bommer, J. J. (2011). Earthquake accelerogram selection and scaling procedures for estimating the distribution of drift response. *Journal of Structural Engineering*, 137(3), 345–357. doi:10.1061/(ASCE)ST.1943-541X.0000217

- Caleman, T., Branch, M. A., & Grace, A. (1999). *Optimization toolbox for the use with Matlab. User's guide.* USA: The MATH WORKS Inc.
- Chai, Y. H., Romstad, K. M., & Bird, S. M. (1995). Energy-based linear damage model for high-intensity seismic loading. *Journal of Structural Engineering*, 121(5), 857–864. doi:10.1061/(ASCE)0733-9445(1995)121:5(857)
- Choi, H., & Kim, J. (2006). Energy-based design of buckling-restrained braced frames using hysteretic energy spectrum. *Engineering Structures*, 28, 304–311. doi:10.1016/j.engstruct.2005.08.008
- Comartin, C., Brvez, S., Naeim, F., Greene, M., Blondet, M., & Cherry, S. (2004). A challenge to the earthquake engineering professionals. *Earthquake Spectra*, 20(4), 1049–1056. doi:10.1193/1.1809130
- Conte, J. P., & Peng, B. F. (1997). Fully nonstationary analytical earthquake ground motion model. *Journal of Engineering Mechanics*, 123, 15–24. doi:10.1061/(ASCE)0733-9399(1997)123:1(15)
- Cosenza, C., Manfredi, G., & Ramasco, R. (1993). The use of damage functionals in earthquake engineering: A comparison between different methods. *Earthquake Engineering & Structural Dynamics*, 22, 855–868. doi:10.1002/eqe.4290221003
- COSMOS. (2005). *Consortium organizations for strong-motion observation systems*. Retrieved from <http://db.cosmos-eq.org/scripts/default.plx>
- Decanini, L. D., & Mollaioli, F. (2001). An energy-based methodology for the assessment of seismic demand. *Soil Dynamics and Earthquake Engineering*, 21, 113–137. doi:10.1016/S0267-7261(00)00102-0
- Drenick, R. F. (1977). The critical excitation of nonlinear systems. *Journal of Applied Mechanics*, 18, 333–336. doi:10.1115/1.3424047
- Elishakoff, I., & Ohsaki, M. (2010). *Optimization and anti-optimization of structures under uncertainty*. Singapore: Imperial College Press. doi:10.1142/9781848164789
- Fajfar, P. (1992). Equivalent ductility factors, taking into account low-cyclic fatigue. *Earthquake Engineering & Structural Dynamics*, 21, 837–848. doi:10.1002/eqe.4290211001
- Fajfar, P., & Krawinklere, H. (1997). *Seismic design methodologies for the next generation of codes*. Rotterdam, The Netherlands: Balkema.
- Fardis, M. N. (Ed.). (2010). *Advances in performance-based earthquake engineering*. New York, NY: Springer.
- Fujita, K., Moustafa, A., & Takewaki, I. (2010). Optimal placement of viscoelastic dampers and supporting members under variable critical excitations. *Earthquakes and Structures*, 1(1), 43–67.
- Ghobara, A., Abou-Elfath, H., & Biddah, A. (1999). Response-based damage assessment of structures. *Earthquake Engineering & Structural Dynamics*, 28, 79–104. doi:10.1002/(SICI)1096-9845(199901)28:1<79::AID-EQE805>3.0.CO;2-J
- Goel, R. K. (1997). Seismic response of asymmetric systems: Energy-based approach. *Journal of Structural Engineering*, 123(11), 1444–1453. doi:10.1061/(ASCE)0733-9445(1997)123:11(1444)
- Haldar, A. (Ed.). (2006). *Recent developments in reliability-based civil engineering*. Singapore: World Scientific Publishing Co. Pte. Ltd. doi:10.1142/9789812707222
- Hanks, T. G., & McGuire, R. K. (1981). The character of high frequency ground motions based on seismic shear waves. *Bulletin of the Seismological Society of America*, 71, 2071–2095.

- Hart, G. C., & Wong, K. (2000). *Structural dynamics for structural engineers*. New York, NY: John Wiley & Sons.
- Haselton, C., Baker, J. W., Liel, A. B., & Deierlein, G. G. (2011). Accounting for ground motion spectral shape characteristics in structural collapse assessment through an adjustment for epsilon. *Journal of Structural Engineering*, 137(3), 332–344. doi:10.1061/(ASCE)ST.1943-541X.0000103
- He, W. L., & Agrawal, A. K. (2008). Analytical model of ground motion pulses for the design and assessment of seismic protective systems. *Journal of Structural Engineering*, 134(7), 1177–1188. doi:10.1061/(ASCE)0733-9445(2008)134:7(1177)
- Housner, G. W., & Hudson, D. E. (1958). The Port Hueneme earthquake of March 18, 1957. *Bulletin of the Seismological Society of America*, 48, 163–168.
- Iyengar, R. N. (1972). Worst inputs and a bound on the highest peak statistics of a class of nonlinear systems. *Journal of Sound and Vibration*, 25, 29–37. doi:10.1016/0022-460X(72)90593-7
- Kalkan, E., & Kunath, S. K. (2006). Effects of fling step and forward directivity on seismic response of buildings. *Earthquake Spectra*, 22(2), 367–390. doi:10.1193/1.2192560
- Kalkan, E., & Kunath, S. K. (2008). Relevance of absolute and relative energy content in seismic evaluation of structures. *Advances in Structural Engineering*, 11(1), 1–18. doi:10.1260/136943308784069469
- Kalkan, E., & Luco, N. (Eds.). (2011). Earthquake ground motion selection and modification for nonlinear dynamic analysis of structures. *Journal of Structural Engineering*, 137(3), 277–467. doi:10.1061/(ASCE)ST.1943-541X.0000355
- Khashaee, P. (2004). Damage-based seismic design of structures. *Earthquake Spectra*, 21(2), 371–387. doi:10.1193/1.1896366
- Kiureghian, A. D., & Crempien, J. (1989). An evolutionary model for earthquake ground motion. *Structural Safety*, 6, 235–246. doi:10.1016/0167-4730(89)90024-6
- Liang, Q. Q. (2005). *Performance-based optimization of structures*. New York, NY: Spon Press. doi:10.4324/9780203334713
- Mahin, S. A., & Bertero, V. V. (1981). An evaluation of inelastic seismic design spectra. *Journal of the Structural Division*, 107(ST9), 1777–1795.
- McGuire, R. K. (1995). Probabilistic seismic hazard analysis and design earthquake: Closing the loop. *Bulletin of the Seismological Society of America*, 85, 1275–1284.
- Mehanny, S. S., & Deierlein, G. G. (2000). *Modeling of assessment of seismic performance of composite frames with reinforced concrete columns and steel beams*. Report No. 135, The John Blume Earthquake Research Center, Stanford University.
- Moustafa, A. (2002). *Deterministic/reliability-based critical earthquake load models for linear/nonlinear engineering structures*. Doctoral dissertation, Department of Civil Engineering, Indian Institute of Science, Bangalore, India.
- Moustafa, A. (2009). Critical earthquake load inputs for multi-degree-of-freedom inelastic structures. *Journal of Sound and Vibration*, 325, 532–544. doi:10.1016/j.jsv.2009.03.022
- Moustafa, A. (2009). Discussion of the effect of energy concentration of earthquake ground motions on the nonlinear response of RC structures. *Soil Dynamics and Earthquake Engineering*, 29, 1181–1183. doi:10.1016/j.soildyn.2009.02.004

- Moustafa, A. (2009). Discussion of a new approach of selecting real input ground motions for seismic design: The most unfavourable real seismic design ground motions. *Earthquake Engineering & Structural Dynamics*, 38, 1143–1149. doi:10.1002/eqe.885
- Moustafa, A. (2010). Identification of resonant earthquake ground motion. *Indian Academy of Sciences*, 35(3), 355–371.
- Moustafa, A. (2010). Discussion of analytical model of ground motion pulses for the design and assessment of seismic protective systems. *Journal of Structural Engineering*, 137(1), 229–230. doi:10.1061/(ASCE)ST.1943-541X.134
- Moustafa, A. (2010). Closure to discussion of critical earthquake load inputs for multi-degree-of-freedom inelastic structures. *Journal of Sound and Vibration*, 330, 356–360. doi:10.1016/j.jsv.2010.09.002
- Moustafa, A. (2011). Damage-based design earthquake loads for SDOF inelastic structures. *Journal of Structural Engineering*, 137(3), 456–467. doi:10.1061/(ASCE)ST.1943-541X.0000074
- Moustafa, A., & Mahadevan, S. (2010). Probabilistic critical earthquake excitations using earthquake response spectra. [Building and Housing]. *Asian Journal of Civil Engineering*, 11(3), 295–319.
- Moustafa, A., & Takewaki, I. (2010). Modeling critical strong ground motion sequences on inelastic structures. *Advances in Structural Engineering*, 13(4), 665–679. doi:10.1260/1369-4332.13.4.665
- Moustafa, A., & Takewaki, I. (2010). Deterministic and probabilistic representation of near-field pulse-like ground motion. *Soil Dynamics and Earthquake Engineering*, 30, 412–422. doi:10.1016/j.soildyn.2009.12.013
- Moustafa, A., & Takewaki, I. (2010). Characterization and modeling of near-fault pulse-like strong ground motion via damage-based critical excitation method. *Structural Engineering & Mechanics*, 34(6), 755–778.
- Moustafa, A., & Takewaki, I. (2011). Response of nonlinear SDOF structures to random acceleration sequences. *Engineering Structures*, 33(4), 1251–1258. doi:10.1016/j.engstruct.2011.01.002
- Moustafa, A., Takewaki, I., & Wijeyewickrema, A. K. (2010). *Selection of earthquake records for time-history analysis of structures*. Joint 7th International Conference on Urban Earthquake Engineering and 5th International Conference on Earthquake Engineering, 3–5 March, Tokyo, Japan.
- Moustafa, A., Ueno, K., & Takewaki, I. (2010). Critical earthquake loads for SDOF inelastic structures considering evolution of seismic waves. *Earthquakes and Structures*, 1(2), 147–162.
- Nakashima, M., Saburi, K., & Tsuji, B. (1996). Energy input and dissipation behavior of structures with hysteretic dampers. *Earthquake Engineering & Structural Dynamics*, 25, 483–496. doi:10.1002/(SICI)1096-9845(199605)25:5<483::AID-EQE564>3.0.CO;2-K
- Newmark, N. M., & Hall, W. J. (1982). *Earthquake spectra and design. Monograph*. Earthquake Engineering Research Institute. EERI.
- Otani, S. (1981). Hysteretic models of reinforced concrete for earthquake response analysis. *Journal of the Faculty of Engineering. University of Tokyo*, 36(2), 407–441.
- Pacific Earthquake Research (PEER) Center. (2011). Retrieved from http://peer.berkeley.edu/peer_ground_motion_database

- Papadrakakis, M., Charmpis, D. C., Lagaros, N. D., & Tsompanakis, Y. (Eds.). (2009). *Computational structural dynamics and earthquake engineering*. London, UK: Taylor & Francis.
- Park, Y. J., & Ang, A. H.-S. (1985). Mechanistic seismic damage model for reinforced concrete. *Journal of Structural Engineering*, 111(4), 722–739. doi:10.1061/(ASCE)0733-9445(1985)111:4(722)
- Park, Y. J., Ang, A. H.-S., & Wen, Y. K. (1985). Seismic damage analysis of reinforced concrete buildings. *Journal of Structural Engineering*, 111(4), 740–757. doi:10.1061/(ASCE)0733-9445(1985)111:4(740)
- Park, Y. J., Ang, A. H.-S., & Wen, Y. K. (1987). Damage-limiting aseismic design of buildings. *Earthquake Spectra*, 3(1), 1–26. doi:10.1193/1.1585416
- Pecker, A. (Ed.). (2007). *Advanced earthquake engineering analysis*. Udine, Italy: Springer. doi:10.1007/978-3-211-74214-3
- Penelis, G. G., & Kappos, A. J. (1997). *Earthquake-resistant concrete structures*. London, UK: E & FN SPON.
- Philippacopoulos, A. J., & Wang, P. C. (1984). Seismic inputs for nonlinear structures. *Journal of Engineering Mechanics*, 110, 828–836. doi:10.1061/(ASCE)0733-9399(1984)110:5(828)
- Pinho, R. (2007). Non linear dynamic analysis of structures subjected to seismic action. In Pecker, A. (Ed.), *Advanced earthquake engineering analysis*. New York, NY: Springer Wien. doi:10.1007/978-3-211-74214-3_5
- Plevris, V. (2009). *Innovative computational techniques for the optimum structural design considering uncertainties*. Ph. D. dissertation, Institute of Structural Analysis and Seismic Research, National Technical University of Athens, June 2009.
- Priestely, M. J. N., Calvi, G. M., & Kowalsky, M. J. (2007). *Displacement-based seismic design of structures*. Pavia, Italy: IUSS Press.
- Quek, S. T., Teo, Y. P., & Balendra, T. (1990). Non-stationary structural response with evolutionary spectra using seismological input model. *Earthquake Engineering & Structural Dynamics*, 19, 275–288. doi:10.1002/eqe.4290190210
- Reiter, L. (1990). *Earthquake hazard analysis*. New York, NY: Columbia University Press.
- Riddell, F. (1995). Inelastic design spectra accounting for soil conditions. *Earthquake Engineering & Structural Dynamics*, 24, 1491–1510. doi:10.1002/eqe.4290241106
- Saikat, S., & Manohar, C. S. (2005). Inverse reliability based structural design for system dependent critical earthquake loads. *Probabilistic Engineering Mechanics*, 20, 19–31. doi:10.1016/j.probengmech.2004.03.006
- Sarkar, A. (2003). Linear stochastic dynamical system under uncertain load: Inverse reliability analysis. *Journal of Engineering Mechanics*, 129(6), 665–671. doi:10.1061/(ASCE)0733-9399(2003)129:6(665)
- SEAOC. Vision Committee. (2002). *Performance based seismic design engineering*. Sacramento, CA: Structural Engineers Association of California (SEAOC) Report.
- Shinozuka, M. (1970). Maximum structural response to seismic excitations. *Journal of Engineering Mechanics*, 96, 729–738.
- Shinozuka, M., & Henry, L. (1965). Random vibration of a beam column. *Journal of Engineering Mechanics*, 91, 123–143.
- Strasser, F. O., & Bommer, J. J. (2009). Review: Strong ground motions – Have we seen the worst? *Bulletin of the Seismological Society of America*, 99(5), 2613–2637. doi:10.1785/0120080300

- Takeda, T., Sozen, M. A., & Nielsen, N. (1970). Reinforced concrete response to simulated earthquakes. *Journal of the Structural Division*, 96(ST12), 2557–2573.
- Takewaki, I. (2001). Probabilistic critical excitation for MDOF elastic-plastic structures on compliant ground. *Earthquake Engineering & Structural Dynamics*, 30, 1345–1360. doi:10.1002/eqe.66
- Takewaki, I. (2002a). Seismic critical excitation method for robust design: A review. *Journal of Structural Engineering*, 128, 665–672. doi:10.1061/(ASCE)0733-9445(2002)128:5(665)
- Takewaki, I. (2002b). Robust building stiffness design for variable critical excitations. *Journal of Structural Engineering*, 128(12), 1565–1574. doi:10.1061/(ASCE)0733-9445(2002)128:12(1565)
- Takewaki, I. (2004). Bound of earthquake input energy. *Journal of Structural Engineering*, 130, 1289–1297. doi:10.1061/(ASCE)0733-9445(2004)130:9(1289)
- Takewaki, I. (2007). *Critical excitation methods in earthquake engineering*. Elsevier Science.
- Takewaki, I. (2009). *Building control with passive dampers*. Singapore: John Wiley & Sons. doi:10.1002/9780470824931
- Takewaki, I., Murakami, S., Fujita, K., Yoshihomi, S., & Tsuji, M. (2011). The 2011 off the Pacific coast of Tohoku earthquake and response of high-rise buildings under long-period ground motions. *Soil Dynamics and Earthquake Engineering*, 31(11), 1511–1528. doi:10.1016/j.soildyn.2011.06.001
- Tsompanakis, Y., Lagaros, N. D., & Papadrakakis, M. (Eds.). (2008). *Structural design optimization considering uncertainties*. London, UK: Taylor & Francis.
- Uang, C.-M., & Bertero, V. V. (1990). Evaluation of seismic energy in structures. *Earthquake Engineering & Structural Dynamics*, 19, 77–90. doi:10.1002/eqe.4290190108
- USGS/EERI Advance Reconnaissance Team. (2010). *The Mw 7.0 Haiti earthquake of January 12, 2010*.
- Westermo, B. D. (1985). The critical excitation and response of simple dynamic systems. *Journal of Sound and Vibration*, 100, 233–242. doi:10.1016/0022-460X(85)90417-1
- Wong, K. K. F., & Yong, R. (2002). Earthquake response and energy evaluation of inelastic structures. *Journal of Engineering Mechanics*, 128(3), 308–317. doi:10.1061/(ASCE)0733-9399(2002)128:3(308)
- Yamaguchi, H., & El-Abd, A. (2003). Effect of energy input characteristics on hysteretic damper efficiency. *Earthquake Engineering & Structural Dynamics*, 32, 827–843. doi:10.1002/eqe.250
- Zahrah, T. F., & Hall, W. J. (1984). Earthquake energy absorption in sdof structures. *Journal of Structural Engineering*, 110, 1757–1772. doi:10.1061/(ASCE)0733-9445(1984)110:8(1757)

Chapter 7

Metaheuristic Optimization in Seismic Structural Design and Inspection Scheduling of Buildings

Chara Ch. Mitropoulou

Institute of Structural Analysis and Seismic Research, National Technical University Athens, Greece

Vagelis Plevris

School of Pedagogical and Technological Education (ASPETE), Greece

Nikos D. Lagaros

Institute of Structural Analysis and Seismic Research, National Technical University Athens, Greece

ABSTRACT

Optimization is a field where extensive research has been conducted over the last decades. Many types of problems have been addressed, and many types of algorithms have been developed, while their range of applications is continuously growing. The chapter is divided into two parts; in the first part, the life-cycle cost analysis is used as an assessment tool for designs obtained by means of prescriptive and performance-based optimum design methodologies. The prescriptive designs are obtained through a single-objective formulation, where the initial construction cost is the objective to be minimized, while the performance-based designs are obtained through a two-objective formulation where the life-cycle cost is considered as an additional objective also to be minimized. In the second part of the chapter, the problem of inspection of structures and routing of the inspection crews following an earthquake in densely populated metropolitan areas is studied. A model is proposed and a decision support system is developed to aid local authorities in optimally assigning inspectors to critical infrastructures. A combined particle swarm – ant colony optimization based framework is implemented, which proves to be an instance of a successful application of the philosophy of bounded rationality and decentralized decision-making for solving global optimization problems.

DOI: 10.4018/978-1-4666-1640-0.ch007

INTRODUCTION

Earthquake loading transfers large amounts of energy in short periods of time, which might produce severe damages on the structural systems. During the last century, significant advances have been made towards the improvement of the seismic design codes. The philosophy underlying modern codes is that the building structures should remain elastic for frequent earthquake events. Under rare earthquakes, however, damages are allowed given that life safety is guaranteed. Hence, the main task of the design procedures is to achieve more predictable and reliable levels of safety and operability against natural hazards. Through extensive research studies it was found that the Performance-Based Design (PBD) concept can be integrated into a structural design procedure in order to obtain designs that fulfill the provisions of a safety structure in a more predictable way (ATC-40, 1996, FEMA-350, 2000, ASCE/SEI Standard 41-06, 2006, FEMA-445, 2006, ATC-58, 2009). According to the PBD framework the structural behavior is assessed in multiple hazard levels of increased intensity. Consequently, it is very important to use robust and computationally efficient methods for predicting the seismic response of the structure in order to assess its capacity under different seismic hazard levels.

In the first part of the chapter, 3D reinforced concrete (RC) buildings with regular and irregular plan views were considered in order to examine the sensitivity of life-cycle cost value with reference to the analysis procedure (static or dynamic), the number of seismic records imposed, the performance criterion used and the structural type (regular or irregular). In particular, nonlinear static analysis and multiple stripe analysis, which is a variation of IDA, were applied for the calculation of the maximum inter-story drift and the maximum floor acceleration. The life-cycle cost was calculated for both regular and irregular in plan test examples taking into consideration the damage repair cost, the cost of loss of contents due to structural damage, quantified by the

maximum inter-story drift and floor acceleration, the loss of rental cost, the income loss cost, the cost of injuries and the cost of human fatalities. Furthermore, the influence of uncertainties on the seismic response of structural systems and their impact on Life Cycle Cost Analysis (LCCA) is examined. In order to take into account the uncertainty on the material properties, the cross-section dimensions and the record-incident angle, the Latin hypercube sampling method is integrated into the incremental dynamic analysis procedure. In addition, the LCCA methodology is used as an assessment tool for the designs obtained by means of prescriptive and performance-based optimum design methodologies. The prescriptive design procedure is formulated as a single-objective optimization problem where the initial construction cost is the objective to be minimized; while the performance-based design procedure is defined as a two-objective optimization problem where the life-cycle cost is considered as an additional objective also to be minimized.

Infrastructure networks are vital for the well-being of modern societies; national and local economies depend on efficient and reliable networks that provide added value and competitive advantage to an area's social and economic growth. The significance of infrastructure networks increases when natural disasters occur since restoration of community functions is highly dependent on the affected regions receiving adequate relief resources. Infrastructure networks are frequently characterized as the most important lifelines in cases of natural disasters; recent experience from around the World (hurricanes Katrina and Wilma, Southeastern Asia Tsunami, Loma Prieta and Northridge earthquakes and others) suggests that, following a natural disaster, infrastructure networks are expected to support relief operations, population evacuation, supply chains and the restoration of community activities.

Infrastructure elements such as bridges, pavements, tunnels, water and sewage systems, and highway slopes are highly prone to damages caused by natural hazards, a result of possible

poor construction or maintenance, of design inconsistencies or of the shear magnitude of the natural phenomena themselves. Rapid network degradation following these disasters can severely impact both short and long run operations resulting in increased fatalities, difficulties in population evacuation and the supply of clean water and food to the affected areas. Much of the state of the art in this research area indicates that attention must be given to three important actions: (i) Fail-safe design and construction of infrastructure facilities; (ii) Effective maintenance and management of the available facilities; and, (iii) Planning and preparing actions to deal with rapid reparation of infrastructure following the disasters (Altay et al. 2006, Dong et al., 1987, Peizhuangm et al. 1986, Tamura et al., 2000, Mendonca et al., 2001, Mendonca et al., 2006, Karlaftis et al. 2007, Lagaros et al., 2011).

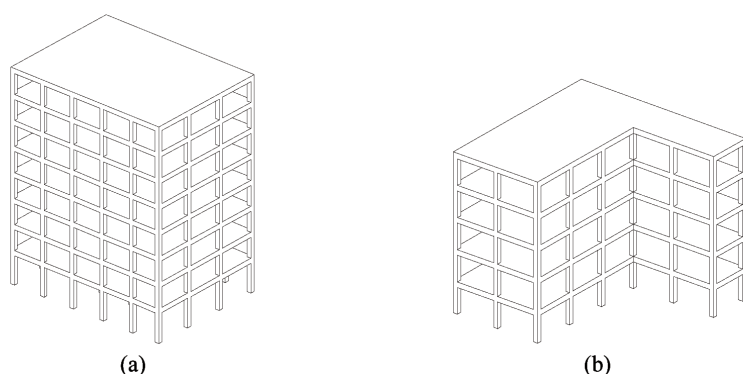
The second part of the chapter focuses on issues that are related to inspecting and repairing infrastructure elements damaged by earthquakes, a highly unpredictable natural disaster of considerable importance to many areas around the world. An explicit effort is made to initiate the development of a process for handling post-earthquake emergency response in terms of optimal infrastructure condition assessment, based on a combined Particle Swarm Optimization (PSO)–Ant Colony Optimization (ACO) framework. Some of the

expected benefits of this work include improvements in infrastructure network restoration times and minimization of adverse impacts from natural hazards on infrastructure networks.

LIFE-CYCLE COST ASSESSMENT OF OPTIMALLY DESIGNED REINFORCED CONCRETE BUILDINGS UNDER SEISMIC ACTIONS

In the framework of the present study, two multi-story 3D RC buildings, shown in Figure 1 (a) and (b), have been optimally designed to meet the Eurocode (EC2 (2004) and EC8 (2004)) or the PBD requirements. Furthermore, the two buildings (optimally designed according to EC2 and EC8) have been considered in order to study the influence of various factors on LCCA procedure and to perform critical assessment of seismic design procedures. Therefore, the investigation presented in this study is composed by three parts. In the first part the single and multi-objective optimization problems are solved, in the second part the influence of various parameters on the LCCA procedure is quantified while in the last part a critical assessment of the two design procedures with reference to the life-cycle cost is presented.

Figure 1. Test cases: (a) Eight-story 3D view, (b) Five-story 3D view



Single and Multi-Objective Optimization Problems

In the following paragraphs, the single and the two-criteria design optimization problems and the optimum designs obtained are presented.

Problem Formulations

The mathematical formulation of the optimization problem for the single-objective formulation, as it was presented in (Lagaros et al., 2004), is defined as follows:

$$\begin{aligned}
 \min_{\mathbf{s} \in F} \quad & C_{IN}(\mathbf{s}) \\
 \text{where} \quad & C_{IN}(\mathbf{s}) = C_b(\mathbf{s}) + C_{sl}(\mathbf{s}) + C_{cl}(\mathbf{s}) + C_{ns}(\mathbf{s}) \\
 \text{subject to} \quad & g_j^{SERV}(\mathbf{s}) \leq 0 \quad j=1, \dots, m \\
 & g_j^{ULT}(\mathbf{s}) \leq 0 \quad j=1, \dots, k
 \end{aligned} \tag{1}$$

where \mathbf{s} represents the design vector, F is the feasible region where all the serviceability and ultimate constraint functions (g^{SERV} and g^{ULT}) are satisfied. In this formulation the boundaries of the feasible region are defined according to the recommendations of the EC8. The single objective function considered is the initial construction cost C_{IN} , while $C_b(\mathbf{s})$, $C_{sl}(\mathbf{s})$, $C_{cl}(\mathbf{s})$ and $C_{ns}(\mathbf{s})$ correspond to the total initial construction cost of beams, slabs, columns and non-structural elements, respectively. The term “initial cost” of a new structure corresponds to the cost just after construction. The initial cost is related to material, which includes concrete, steel reinforcement, and labor costs for the construction of the building. The solution of the resulting optimization problem is performed by means of Evolutionary Algorithms (EA) (Mitropoulou, 2010).

In practical applications of sizing optimization problems, the initial cost rarely gives a representative measure of the performance of the structure. In fact, several conflicting and usually incommensurable criteria usually exist

in real-life design problems that have to be dealt with simultaneously. This situation forces the designer to look for a good compromise among the conflicting requirements. Problems of this kind constitute multi-objective optimization problems. In general, a multi-objective optimization problem can be stated as follows:

$$\begin{aligned}
 \min_{\mathbf{s} \in F} \quad & [C_{IN}(\mathbf{s}), C_{LS}(\mathbf{s})]^T \\
 \text{where} \quad & C_{IN}(\mathbf{s}) = C_b(\mathbf{s}) + C_{sl}(\mathbf{s}) + C_{cl}(\mathbf{s}) + C_{ns}(\mathbf{s}) \\
 \text{subject to} \quad & g_j^{Capacity}(\mathbf{s}) \leq 0 \quad j=1, \dots, k \\
 & g_j^{PBD}(\mathbf{s}) \leq 0 \quad j=1, \dots, k
 \end{aligned} \tag{2}$$

where \mathbf{s} represents the design vector, F is the feasible region where all the constraint functions $g^{Capacity}$ and g^{PBD} are satisfied for the PBD formulation. The objective functions considered are the initial construction cost C_{IN} and the life-cycle cost C_{LS} . Several methods have been proposed for treating structural multi-objective optimization problems (Coello, 2000, Marler & Arora, 2004). In this work, the Nondominated Sorting Evolution Strategies II (NSES-II) algorithm, proposed by Lagaros and Papadrakakis (2007), is used in order to handle the two-objective optimization problem at hand. This algorithm is denoted as NSES-II($\mu+\lambda$) or NSES-II(μ,λ), depending on the selection operator.

Various sources of uncertainty are considered: on the ground motion excitation which influences the level of seismic demand and on the modeling and the material properties which affects the structural capacity. The structural stiffness is directly connected to the modulus of elasticity E_s and E_c of the longitudinal steel reinforcement and concrete respectively, while the strength is influenced by the yield stress f_y of the steel and the cylindrical strength for the concrete f_c and the hardening b of the steel. In addition to the material properties, the cross-sectional dimensions are considered as random variables. Thus, both for beams and columns four random variables are

considered; the modulus of elasticity (E_s and E_c), the yield and cylindrical strength stresses (f_y and f_c), the hardening parameter b of the stress-strain curve and the cross-sectional dimensions (B and H). One random variable is considered for both confined and unconfined concrete. Furthermore, one random variable is considered for the ground motion excitation and one for the incident angle. In order to account for the randomness of the incident angle, the ground motions are applied with a random angle with respect to the structural axes uniformly distributed in the range of 0 to 180 degrees. The characteristics of the random variables are given in Table 1, i.e. probability density function (PDF), mean value, coefficient of variation (CoV) and type. Therefore, the total number of random variables considered is: 54 (4+2 groups of structural elements times 9 random variables) for the eight-story RC building (since 4 groups of columns and 2 groups of beams are considered) and 45 (3+2 groups of structural elements times 9 random variables) for the five-story RC building (since 3 groups of columns and 2 groups of beams are considered) plus one random variable for the seismic record and one for the incident angle.

Optimum Design Results

For both formulations the designs variables of the optimization problems are defined through the dimensions of the columns' and beams' cross-section. The columns are chosen to be rectangular and they are grouped into four categories (C1, C2, C3 and C4) for the eight-story test example while they are grouped into three categories (C1, C2 and C3) for the five-story test example, while the beams for both test examples are grouped into two categories (more details can be found in a study of Lagaros et al. (2004)). The two dimensions of the columns/beams along with the longitudinal, transverse reinforcement and its spacing are the five design variables that are assigned to each group of the columns/beams. Therefore, the structural elements (beams and columns) are separated into 14 groups, 12 groups for the columns and 2 for the beams, resulting into 70 design variables for the eight-story test example; while for the five-story test example the structural elements (beams and columns) are separated into 10 groups, 8 for the columns and 2 for the beams, resulting in 50 design variables in total.

Table 1. Random variables (Ellingwood et al., 1980, Dolsek, 2009)

Random variable	Distribution (PDF)	Mean	CoV	Type
Earthquake	Uniform	-	-	aleatory
Incident angle*	Uniform	-	-	aleatory
Material	mean f_c	Lognormal	20 MPa	4%
	f_c	Lognormal	mean f_c	15%
	E_c	Lognormal	2.9×10^7 kN/m ²	15%
	mean f_y (steel)	Lognormal	500 MPa	4%
	f_y (steel)	Lognormal	mean f_y	5%
	E_s (steel)	Lognormal	2.1×10^8 kN/m ²	5%
	b (steel)	Lognormal	1%	5%
Design variables	b	Normal	design value	5%
	h	Normal	design value	5%

* In the Range of 0 to 180 degrees.

Based on the prescriptive seismic design formulation, both buildings have been designed for minimum initial cost following an optimization strategy proposed by Mitropoulou *et al.* (2010). In particular, for the solution of the single objective optimization problem formulated as shown in Eq. (4) the EA($\mu + \lambda$) optimization scheme is employed (Lagaros *et al.* 2004) with ten parent and offspring ($\mu=\lambda=10$) design vectors for both test examples. On the other hand, the second optimization problem is formulated as a two-criteria design optimization problem, as presented in Eq. (5) where the initial construction cost C_{IN} and the life-cycle cost C_{LS} are the two objectives both to be minimized, while for solving the problem the NSES-II(100+100) optimization scheme was employed.

Solving the optimization problem of Eq. (4) results to a single design denoted as D_{descr} corresponding to the prescriptive design procedure. On the other hand, solving the optimization problem of Eq. (5) results to a group of designs that define the Pareto curve. In order to compare the behavior of the different designs of the Pareto front curve two characteristic designs were selected, corresponding to the PBD optimum designs, which they are denoted as D_{PBD1} obtained from the region where

the initial cost is the dominant criterion and D_{PBD2} obtained from the region where the life-cycle cost is the dominant criterion. The steel and concrete quantities for the columns and the beams along with the RC frame cost and total initial cost, for the three optimum designs, are presented in Tables 2 and 3 corresponding to the designs of the eight-story and five-story test example, respectively.

For the eight-story symmetric test example, as shown in Table 2, it can be said that compared to D_{descr} the D_{PBD1} requires 9% more concrete both for beams and columns while it requires 22% and 31% more longitudinal steel reinforcement for the beams and the columns, respectively. On the other hand, D_{PBD2} requires 37% and 30% more concrete for beams and columns, respectively; while it requires 70% and 56% more longitudinal steel reinforcement for the beams and the columns, respectively. Furthermore, with reference to the RC frame initial cost, where the cost of the plates is also included, it can be said that D_{PBD1} is by 10% more expensive compared to D_{descr} ; while D_{PBD2} is by 26% more expensive. On the other hand though, with reference to the initial cost, the three designs vary by 2% and 4% only.

The five-story non-symmetric test example has a similar trend. Based on the concrete and steel

Table 2. Eight-story test example: comparison of steel and concrete quantities in the three designs

Design procedure	Columns		Beams		$C_{IN, RC Frame} (10^3 MU)$	$C_{IN} (10^3 MU)$
	Concrete (m ³)	Steel (kg.)	Concrete (m ³)	Steel (kg.)		
D_{descr}	1.68E+02	1.84E+04	2.27E+02	1.06E+04	2.40E+02	1.44E+03
D_{PBD1}	1.84E+02	2.41E+04	2.48E+02	1.29E+04	2.64E+02	1.46E+03
D_{PBD2}	2.19E+02	2.87E+04	3.11E+02	1.80E+04	3.03E+02	1.50E+03

Table 3. Five-story test example: comparison of steel and concrete quantities in the three designs

Design procedure	Columns		Beams		$C_{IN, RC Frame} (10^3 MU)$	$C_{IN} (10^3 MU)$
	Concrete (m ³)	Steel (kg.)	Concrete (m ³)	Steel (kg.)		
D_{descr}	8.86E+01	5.20E+03	6.57E+01	1.45E+03	1.11E+02	7.36E+02
D_{PBD1}	1.04E+02	6.87E+03	7.40E+01	1.75E+03	1.20E+02	7.45E+02
D_{PBD2}	1.27E+02	8.24E+03	9.16E+01	2.50E+03	1.33E+02	7.58E+02

reinforcement quantities and initial costs given in Table 3, it can be said that compared to D_{descr} the D_{PBD1} requires 13% and 18% more concrete for beams and columns, respectively; while it requires 21% and 32% more longitudinal steel reinforcement for the beams and the columns, respectively. On the other hand, D_{PBD2} requires 39% and 43% more concrete for beams and columns, respectively; while it requires 72% and 59% more longitudinal steel reinforcement for the beams and the columns, respectively. Furthermore, with reference to the RC frame initial cost, where the cost of the plates is also included, it can be said that D_{PBD1} is by 8% more expensive compared to D_{descr} ; while D_{PBD2} is by 19% more expensive. On the other hand though, with reference to the initial cost, the three designs vary by 1% and 3% only.

Prescriptive vs Performance-Based Design

The difference between EC8 and PBD formulations is demonstrated in terms of the life-cycle cost analysis of selected designs. The EC8 formulation implements a linear analysis procedure where the behavioral factor q is used to take into account the inelastic behavior of the structure. Most of the contemporary seismic design codes rely on the ability of the structure to absorb energy through inelastic deformation using the reduction or behavior factor q . The capacity of a structure to resist seismic actions in the nonlinear range generally permits the design seismic loads to be smaller than the loads corresponding to a linear

elastic response. Thus, the seismic design loads are reduced by the behavior factor q . According to EC8, the nonlinear deformation of the structure caused by the seismic load is equal to q times the corresponding deformation of the linear analysis.

In accordance to the previous section, the three designs are also considered for the comparative study with reference to the life-cycle cost and the impact of the various sources of randomness of the LCCA procedure. The median values of the life-cycle cost of the three designs are shown in Tables 4 to 7 corresponding to the deterministic and probabilistic formulations, while the histograms of Figures 2 and 3 show the probabilistic distribution of the life-cycle cost values for the deterministic and probabilistic formulations implemented into the Multi-Stripe Dynamic Analysis (MSDA) for the three different designs along with the 90% confidence bounds.

For the eight-story symmetric test example, comparing the histograms of Figures 2(a) and 2(b) it can be noticed that the width of the 90% confidence bounds of the life-cycle cost values of design D_{PBD2} , is much narrower compared to the other two confidence bounds both for the deterministic and probabilistic formulations. Furthermore, it can be said that with reference to the mean value of the life-cycle cost (as shown in Table 4) D_{PBD1} is by 18% less expensive compared to D_{descr} ; while D_{PBD2} is by 52% less expensive when the deterministic formulation is implemented for 60 records. On the other hand, as shown in Table 5, it can be said that design D_{PBD1} is by 5% less expensive compared to D_{descr} ; while

Table 4. Eight-story test example: median value of the life-cycle cost (10^3 MU) for the four cases and the three designs for the deterministic formulation

Design	Number of records			
	10	20	40	60
D_{descr}	3.13E+03	2.73E+03	2.61E+03	2.72E+03
D_{PBD1}	2.87E+03	2.02E+03	1.83E+03	2.30E+03
D_{PBD2}	1.91E+03	1.82E+03	1.79E+03	1.79E+03

D_{PBD2} is by 57% less expensive when the probabilistic formulation is also implemented for 60 records. For the five-story symmetric test example, comparing the histograms of Figure 3(a) it can be noticed that the width of the 90% confidence bounds of the life-cycle cost values, of design D_{descr} , is much narrower compared to the other two confidence bounds both for the deterministic formulation while for the probabilistic one it is D_{PBD2} design that shows the narrower confidence bounds. Furthermore, it can be said that with reference to the mean value of the life-cycle cost (as shown in Table 6) D_{PBD1} is by 38% less expensive compared to D_{descr} ; while D_{PBD2} is

by 52% less expensive when the deterministic formulation is implemented for 60 records. On the other hand, as shown in Table 7, it can be said that design D_{PBD1} is by 40% less expensive compared to D_{descr} ; while D_{PBD2} is by 53% less expensive when the probabilistic formulation is also implemented for 60 records. Comparing the deterministic with the probabilistic formulation with reference to the median values, they appear to be increased by 12% to 30% for the eight-story test example and by 11% to 13% for the five-story building.

Figure 2. Eight-story test case – Prescriptive vs PBD (a) frequency of occurrence deterministic approach and (b) frequency of occurrence probabilistic approach, all for the case of 60 records

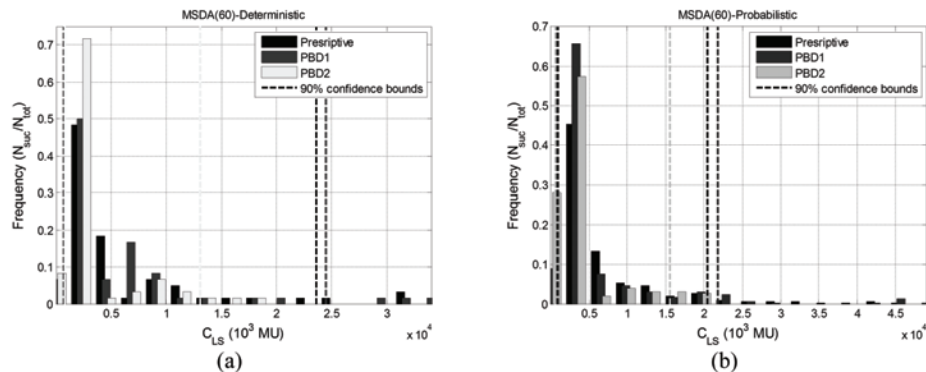


Figure 3. Five-story test case – Prescriptive vs PBD (a) frequency of occurrence deterministic approach and (b) frequency of occurrence probabilistic approach, all for the case of 60 records

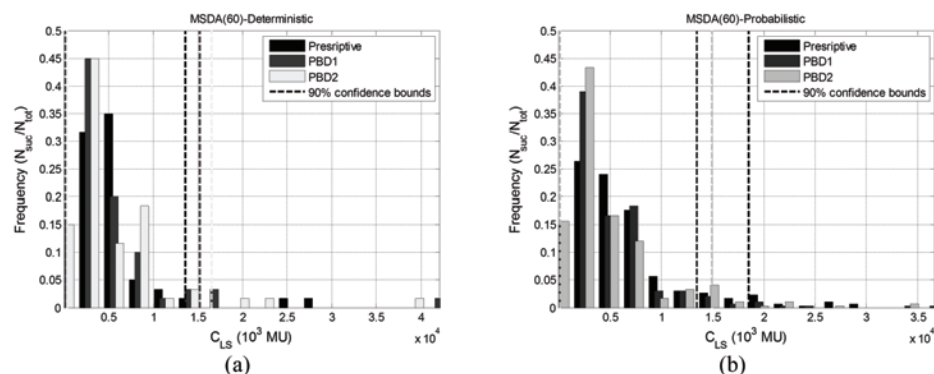


Table 5. Eight-story test example: median value of the life-cycle cost (10^3 MU) for the four cases and the three designs for the probabilistic formulation

Design	Number of records			
	10	20	40	60
D_{descr}	3.16E+03	3.04E+03	3.08E+03	3.14E+03
D_{PBD1}	3.25E+03	2.97E+03	2.95E+03	2.98E+03
D_{PBD2}	2.05E+03	2.00E+03	1.99E+03	2.00E+03

Table 6. Five-story test example: median value of the life-cycle cost (10^3 MU) for the four cases and the three designs for the deterministic formulation

Design	Number of records			
	10	20	40	60
D_{descr}	5.10E+03	3.54E+03	3.28E+03	4.18E+03
D_{PBD1}	4.70E+03	3.17E+03	2.84E+03	3.04E+03
D_{PBD2}	4.37E+03	2.58E+03	2.27E+03	2.75E+03

Table 7. Five-story test example: median value of the life-cycle cost (10^3 MU) for the four cases and the three designs for the probabilistic formulation

Design	Number of records			
	10	20	40	60
D_{descr}	4.79E+03	4.71E+03	4.47E+03	4.72E+03
D_{PBD1}	3.90E+03	3.26E+03	3.17E+03	3.36E+03
D_{PBD2}	3.66E+03	3.00E+03	2.90E+03	3.08E+03

METAHEURISTIC OPTIMIZATION FOR THE INSPECTION SCHEDULING OF BUILDINGS

Natural hazards such as earthquakes, floods and tornadoes can cause extensive failure of critical infrastructures including bridges, water and sewer systems, gas and electricity supply systems, and hospital and communication systems. Following a natural hazard, the condition of structures and critical infrastructures must be assessed and damages have to be identified; inspections are therefore necessary since failure to rapidly inspect

and subsequently repair infrastructure elements will delay search and rescue operations and relief efforts. The objective of this work is scheduling structure and infrastructure inspection crews following an earthquake in densely populated metropolitan areas. A model is proposed and a decision support system is designed to aid local authorities in optimally assigning inspectors to critical infrastructures. A combined Particle Swarm – Ant Colony Optimization based framework is developed which proves an instance of a successful application of the philosophy of bounded rationality and decentralized decision-

making for solving global optimization problems (Plevris et al., 2010).

Problem Formulation

A general formulation of a nonlinear optimization problem can be stated as follows

$$\begin{aligned} \min_{x \in R^n} f(x) \quad x = [x_1, \dots, x_n]^T \\ \text{Subject to} \\ g_k(x) \leq 0 \quad k = 1, \dots, m \\ x^L \leq x \leq x^U \end{aligned} \quad (3)$$

where x is the design variables vector of length n , $f(x): R^n \rightarrow R$ is the objective function to be minimized, the vector of m inequality constraint functions $g(x): R^n \rightarrow R^m$ and x^L, x^U are two vectors of length n defining the lower and upper bounds of the design variables, respectively.

The main objective of this work is to formulate the problem of inspecting the structural systems of a city/area as an optimization problem. This objective is achieved in two steps: in the first step, the structural blocks to be inspected are optimally assigned into a number of inspection crews (assignment problem), while in the second step the problem of hierarchy is solved for each group of blocks (inspection prioritization problem). In the formulation of the optimization problems considered in this work, the city/area under investigation is decomposed into N_{SB} structural blocks while N_{IG} inspection crews are considered for inspecting the structural condition of all structural and infrastructure systems of the city/area.

STEP 1: OPTIMUM ASSIGNMENT PROBLEM

The assignment problem is defined as a nonlinear programming optimization problem as follows

$$\begin{aligned} \min & \sum_{i=1}^{N_{IG}} \sum_{k=1}^{n_{SB}^{(i)}} [d(SB_k, C_i) \cdot D(k)] \\ x_{C_i} &= \frac{1}{n_{SB}^{(i)}} \sum_{k=1}^{n_{SB}^{(i)}} x_k \\ y_{C_i} &= \frac{1}{n_{SB}^{(i)}} \sum_{k=1}^{n_{SB}^{(i)}} y_k \\ D(k) &= A(k) \cdot BP(k) \end{aligned} \quad (4)$$

where $n_{SB}^{(i)}$ is the number of structural blocks allocated to the i^{th} inspection crews, $d(SB_k, C_i)$ is the distance between the SB_k building block from the centre of the i^{th} group of structural blocks (with coordinates x_{C_i} and y_{C_i}), while $D(k)$ is the demand for the k^{th} building block defined as the product of the building block total area times the built-up percentage (i.e. percentage of the area with a structure). This is defined as a discrete optimization problem since the design variables x are integer numbers denoting the inspection crews to which each built-up block has been assigned and thus the total number of the design variables is equal to the number of structural blocks and the range of the design variables is $[1, N_{IG}]$.

STEP 2: INSPECTION PRIORITIZATION PROBLEM

The definition of this problem is a typical *Traveling Salesman Problem* (TSP) (Colomi et al., 1992) which is a problem in combinatorial optimization studied in operations research and theoretical computer science. In TSP a salesman spends his time visiting N cities (or nodes) cyclically. Given a list of cities and their - pair-wise - distances, the task is to find a Hamiltonian tour of minimal length, i.e. to find a closed tour of minimal length that visits each city once and only once. For an N city asymmetric TSP if all links are present then there are $(N-1)!$ different tours. TSP problems are also defined as integer optimization problems,

similar to all problems that have been proven to be NP-hard (Lawler, 1985).

Consider a TSP with N cities (vertices or nodes). The TSP can be represented by a complete weighted graph $G=(N,A)$, with N the set of nodes and A the set of arcs (edges or connections) that fully connects the components of N . A cost function is assigned to every connection between two nodes i and j , that is the distance between the two nodes $d_{i,j}$ ($i \neq j$). In the symmetric TSP, it is $d_{i,j} = d_{j,i}$. A solution to the TSP is a permutation $\mathbf{p} = \{p(1), \dots, p(N)\}$ of the node indices $\{1, \dots, N\}$, as every node must appear only once in a solution. The optimum solution is the one that minimizes the total length $L(\mathbf{p})$ given by

$$L(\mathbf{p}) = \sum_{i=1}^{N-1} (d_{p(i), p(i+1)}) + d_{p(N), p(1)} \quad (5)$$

Thus, the corresponding prioritization problem is defined as follows

$$\min \left[\sum_{k=1}^{n_{SB}^{(i)}-1} d(SB_k, SB_{k+1}) + d(SB_{n_{SB}^{(i)}}, SB_1) \right], i = 1, \dots, N_{IG} \quad (6)$$

where $d(SB_k, SB_{k+1})$ is the distance between the building block SB_k and $k+1^{\text{th}}$. The main objective is to define the shortest possible route between the structural blocks that have been assigned in *Step 1* to each inspection group.

PARTICLE SWARM OPTIMIZATION ALGORITHM

In a PSO formulation, multiple candidate solutions coexist and collaborate simultaneously. Each solution is called a “particle” that has a position and a velocity in the multidimensional design space. A particle “flies” in the problem search space looking for the optimal position. As “time” passes through its quest, a particle adjusts its velocity

and position according to its own “experience” as well as the experience of other (neighbouring) particles. Particle’s experience is built by tracking and memorizing the best position encountered. As every particle remembers the best position it has visited during its “flight”, the PSO possesses a memory. A PSO system combines local search method (through self-experience) with global search method (through neighbouring experience), attempting to balance exploration and exploitation.

Mathematical Formulation of PSO

Each particle maintains two basic characteristics, velocity and position, in the multi-dimensional search space that are updated as follows

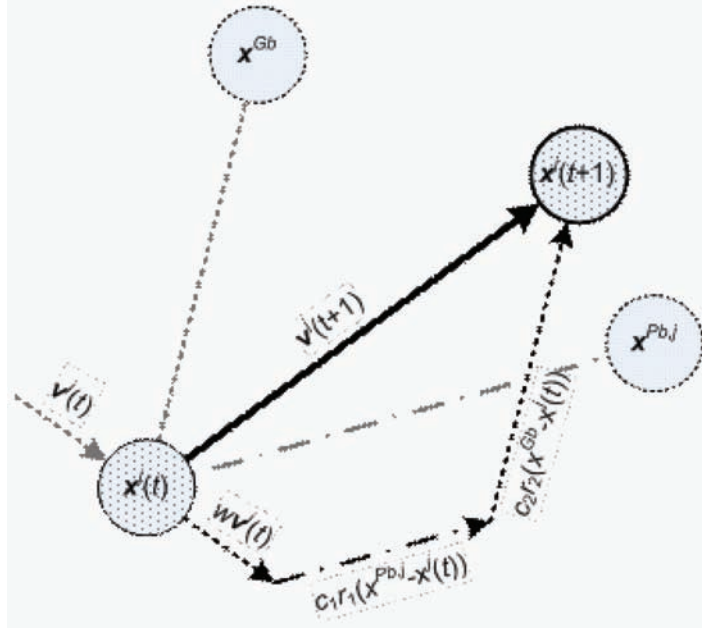
$$\mathbf{v}^j(t+1) = w\mathbf{v}^j(t) + c_1 \mathbf{r}_1 \circ (\mathbf{x}^{\text{Pb},j} - \mathbf{x}^j(t)) + c_2 \mathbf{r}_2 \circ (\mathbf{x}^{\text{Gb}} - \mathbf{x}^j(t)) \quad (7)$$

$$\mathbf{x}^j(t+1) = \mathbf{x}^j(t) + \mathbf{v}^j(t+1) \quad (8)$$

where $\mathbf{v}^j(t)$ denotes the velocity vector of particle j at time t , $\mathbf{x}^j(t)$ represents the position vector of particle j at time t , vector $\mathbf{x}^{\text{Pb},j}$ is the personal ‘best ever’ position of the j^{th} particle, and vector \mathbf{x}^{Gb} is the global best location found by the entire swarm. The acceleration coefficients c_1 and c_2 indicate the degree of confidence in the best solution found by the individual particle (c_1 - cognitive parameter) and by the whole swarm (c_2 - social parameter), respectively, while \mathbf{r}_1 and \mathbf{r}_2 are two random vectors uniformly distributed in the interval $[0, 1]$. The symbol “ \circ ” of Eq. (7) denotes the Hadamard product, i.e. the element-wise vector or matrix multiplication.

Figure 4 depicts a particle’s movement, in a two-dimensional design space, according to Eqs. (7) and (8). The particle’s current position $\mathbf{x}^j(t)$ at time t is represented by the dotted circle at the lower left of the drawing, while the new position $\mathbf{x}^j(t+1)$ at time $t+1$ is represented by the dotted bold circle at the upper right hand of the

Figure 4. Visualization of the particle's movement in a two-dimensional design space



drawing. It can be seen how the particle's movement is affected by: (i) it's velocity $v(t)$; (ii) the personal best ever position of the particle, x^{Pbj} , at the right of the figure; and (iii) the global best location found by the entire swarm, x^{Gb} , at the upper left of the figure.

In the above formulation, the global best location found by the entire swarm up to the current iteration (x^{Gb}) is used. This is called a fully connected topology (fully informed PSO), as all particles share information with each other about the best performer of the swarm. Other topologies have also been used in the past where instead of the global best location found by the entire swarm, a local best location of each particle's neighbourhood is used. Thus, information is shared only among members of the same neighbourhood.

The term w of Eq. (7) is the inertia weight, essentially a scaling factor employed to control the exploration abilities of the swarm, which scales the current velocity value affecting the updated velocity vector. The inertia weight was not part of the original PSO algorithm (Kennedy

& Eberhart, 1995), as it was introduced later by Shi and Eberhart (1998) in a successful attempt to improve convergence. Large inertia weights will force larger velocity updates allowing the algorithm to explore the design space globally. Similarly, small inertia values will force the velocity updates to concentrate in the nearby regions of the design space.

The inertia weight can also be updated during iterations. A commonly used inertia update rule is the linearly-decreasing, calculated by the formula:

$$w_{t+1} = w_{\max} - \frac{w_{\max} - w_{\min}}{t_{\max}} \cdot t \quad (9)$$

where t is the iteration number, w_{\max} and w_{\min} are the maximum and minimum values, respectively, of the inertia weight. In general, the linearly decreasing inertia weight has shown better performance than the fixed one.

Particles' velocities in each dimension i ($i = 1, \dots, n$) are restricted to a maximum velocity v_{\max}^i . The vector v^{\max} of dimension n holds the maximum

absolute velocities for each dimension. It is more appropriate to use a vector rather than a scalar, as in the general case different velocity restrictions can be applied for different dimensions of the particle. If for a given particle j the sum of accelerations of Eq. (7) causes the absolute velocity for dimension i to exceed $v_{max,i}^{max}$, then the velocity on that dimension is limited to $\pm v_{max,i}^{max}$. The vector parameter v^{max} is employed to protect the cohesion of the system, in the process of amplification of the positive feedback. The basic PSO has only few parameters to adjust. In Table 8 there is a list of the main parameters, their typical values as well as other information (Perez & Behdinan, 2007).

Convergence Criteria

Due to the repeated process of the PSO search, convergence criteria have to be applied for the termination of the optimization procedure. Two widely adopted convergence criteria are the maximum number of iterations of the PSO algorithm and the minimum error requirement on the calculation of the optimum value of the objective function. The selection of the maximum number of iterations depends, generally, on the complexity of the optimization problem at hand. The second

criterion presumes prior knowledge of the global optimal value, which is feasible for testing or fine-tuning the algorithm in mathematical problems when the optimum is known a priori, but this is certainly not the case in practical structural optimization problems where the optimum is not known a priori.

In our study, together with the maximum number of iterations, we have implemented the convergence criterion connected to the rate of improvement of the value of the objective function for a given number of iterations. If the relative improvement of the objective function over the last k_f iterations (including the current iteration) is less or equal to a threshold value f_m , convergence is supposed to have been achieved. In mathematical terms, denoting as $Gbest_t$ the best value for the objective function found by the PSO at iteration t , the relative improvement of the objective function can be written for the current iteration t as follows

$$\frac{Gbest_{t-k_f+1} - Gbest_t}{Gbest_{t-k_f+1}} \leq f_m \quad (10)$$

In Table 9 there is a list of the convergence parameters of the PSO used in this study with description and details.

Table 8. Main PSO parameters

Symbol	Description	Details
NP	Number of particles	A typical range is 10 – 40. For most problems 10 particles is sufficient enough to get acceptable results. For some difficult or special problems the number can be increased to 50-100.
n	Dimension of particles	It is determined by the problem to be optimized.
w	Inertia weight	Usually is set to a value less than 1, i.e. 0.95. It can also be updated during iterations.
x^L, x^U	Vectors containing the lower and upper bounds of the n design variables, respectively	They are determined by the problem to be optimized. Different ranges for different dimensions of particles can be applied in general.
v^{max}	Vector containing the maximum allowable velocity for each dimension during one iteration	Usually is set half the length of the allowable interval for the given dimension: $v_{max,i}^{max} = (x_{i,U}^U - x_{i,L})/2$. Different values for different dimensions of particles can be applied in general.
c_1, c_2	Cognitive and social parameters	Usually $c_1=c_2=2$. Other values can also be used, provided that $0 < c_1+c_2 < 4$ (Perez & Behdinan, 2007)

Table 9. PSO convergence parameters

Symbol	Description	Details
t_{\max}	Maximum number of iterations for the termination criterion.	Determined by the complexity of the problem to be optimized, in conjunction with other PSO parameters (n, NP).
k_f	Number of iterations for which the relative improvement of the objective function satisfies the convergence check.	If the relative improvement of the objective function over the last k_f iterations (including the current iteration) is less or equal to f_m , convergence has been achieved.
f_m	Minimum relative improvement of the value of the objective function.	

PSO for Integer Optimization

Since both problems defined in previous section are integer optimization problems, discrete optimization algorithms are required. For the Step 1 optimization problem described in previous section, a discrete version of the PSO algorithm is employed. In the continuous version of the PSO method, both particle positions and velocity are initialized randomly. In this work, the particle positions are generated randomly over the design space using discrete Latin Hypercube Sampling, thus guaranteeing that the initial particle positions will be integers in the acceptable range. Furthermore, in the case of discrete optimization and in particular in integer programming, at every step of the optimization procedure, integer particle positions should also be generated. In order to satisfy this, Eq. (7) is modified as follows

$$\mathbf{v}^j(t+1) = \text{round} \left[u\mathbf{v}^j(t) + c_1 \mathbf{r}_1 \circ (\mathbf{x}^{\text{Ph},j} - \mathbf{x}^j(t)) + c_2 \mathbf{r}_2 \circ (\mathbf{x}^{\text{Gb}} - \mathbf{x}^j(t)) \right] \quad (11)$$

where the vector function $\text{round}(\mathbf{x})$ rounds each element of the vector \mathbf{x} into the nearest integer.

ANT COLONY OPTIMIZATION

The *Ant Colony Optimization* (ACO) algorithm is a population-based probabilistic technique for solving optimization problems, mainly for finding optimum paths through graphs (Dorigo, 1992).

The algorithm was inspired by the behaviour of real ants in nature. In many ant species, individuals initially wander randomly and upon finding a food source return to their colony, depositing a substance called *pheromone* on the ground. Other ants smell this substance, and its presence influences the choice of their path, i.e. they tend to follow strong pheromone concentrations rather than travelling completely randomly, returning and reinforcing it if they eventually find food. The pheromone deposited on the ground forms a *pheromone trail*, which allows the ants to find good sources of food that have been previously identified by other ants.

As time passes, the pheromone trails start to evaporate, reducing their strength. The more time it takes for an ant to travel down a path and back again, the more time the pheromone trail has to evaporate. A short path gets marched over faster than a long one, and thus the pheromone density remains high as it is laid on the path faster than it can evaporate. If there was no evaporation, the paths chosen by the first ants would tend to be excessively attractive to the following ants and as a result the exploration of the solution space would be constrained. In that sense, pheromone evaporation helps also to avoid convergence to a locally optimal solution. Positive feedback eventually leads to most of the ants following a single “optimum” path.

The idea of the ant colony algorithm is to mimic this behaviour with simulated ants walking around the graph representing the problem to solve. The

first algorithm was aiming to search for an optimal path in a graph. The original idea has since diversified to solve a wider class of numerical problems and, as a result, several problems have emerged, drawing on various aspects of the behaviour of ants. The initial applications of ACO were in the domain of NP-hard combinatorial optimization problems, while it was soon also applied to routing in telecommunication networks.

In ACO, a set of software agents called *artificial ants* search for good solutions to the optimization problem of finding the best path on a weighted graph. The ants incrementally build solutions by moving on the graph. The solution construction process is stochastic and it is biased on a *pheromone model*, that is, a set of parameters associated with graph components (either nodes or edges) whose values are modified at runtime by the ants.

To apply ACO to the TSP, the *construction graph* is considered, defined by associating the set of cities with the set of vertices on the graph. The construction graph is fully connected and the number of vertices is equal to the number of cities, since in the TSP it is possible to move from any given city to any other city. The length of the edges (connections) between the vertices are set to be equal to the corresponding distances between the nodes (cities) and the pheromone values and heuristic values are set for the edges of the graph. Pheromone values are modified during iterations at runtime and represent the cumulated experience of the ant colony, while heuristic values are problem dependent values that, in the case of the TSP, are set to be the inverse of the lengths of the edges.

During an ACO iteration, each ant starts from a randomly chosen vertex of the construction graph. Then, it moves along the edges of the graph keeping a memory of its path. In order to move from one node to another it probabilistically chooses the edge to follow among those that lead to yet unvisited nodes. Once an ant has visited all the nodes of the graph, a solution has been constructed. The probabilistic rule is biased by pheromone values and heuristic information:

the higher the pheromone and the heuristic value associated to an edge, the higher the probability the ant will choose that particular edge. Once all the ants have completed their tour, the iteration is complete and pheromone values on the connections are updated: each of the pheromone values is initially decreased by a certain percentage and then it receives an amount of additional pheromone proportional to the quality of the solutions to which it belongs.

Ant Colony Optimization Algorithm

Consider a population of m ants where at each iteration of the algorithm every ant constructs a “route” by visiting every node sequentially. Initially, ants are put on randomly chosen nodes. At each construction step during an iteration, ant k applies a probabilistic action choice rule, called random proportional rule, to decide which node to visit next. While constructing the route, an ant k currently at node i , maintains a memory M^k which contains the nodes already visited, in the order they were visited. This memory is used in order to define the feasible neighbourhood N_i^k that is the set of nodes that have not yet been visited by ant k . In particular, the probability with which ant k , currently at node i , chooses to go to node j is

$$p_{i,j}^k = \frac{(\tau_{i,j})^\alpha \cdot (\eta_{i,j})^\beta}{\sum_{\ell \in N_i^k} ((\tau_{i,\ell})^\alpha \cdot (\eta_{i,\ell})^\beta)}, \quad \text{if } j \in N_i^k \quad (12)$$

where $\tau_{i,j}$ is the amount of pheromone on connection between i and j nodes, α is a parameter to control the influence of $\tau_{i,j}$, β is a parameter to control the influence of $\eta_{i,j}$ and $\eta_{i,j}$ is a heuristic information that is available a priori, denoting the desirability of connection i,j , given by

$$\eta_{i,j} = \frac{1}{d_{i,j}} \quad (13)$$

According to Eq. (13), the heuristic desirability of going from node i to node j is inversely proportional to the distance between i and j . By definition, the probability of choosing a city outside N_i^k is zero. By this probabilistic rule, the probability of choosing a particular connection i,j increases with the value of the associated pheromone trail $\tau_{i,j}$ and of the heuristic information value $\eta_{i,j}$.

The selection of the superscript parameters α and β is very important: if $\alpha=0$, the closest cities are more likely to be selected which corresponds to a classic stochastic greedy algorithm (with multiple starting points since ants are initially randomly distributed over the nodes). If $\beta=0$, only pheromone amplification is at work, that is, only pheromone is used without any heuristic bias (this generally leads to rather poor results (Dorigo & Stützle, 2004).

Pheromone Update Rule

After all the m ants have constructed their routes, the amount of pheromone for each connection between i and j nodes, is updated for the next iteration $t+1$ as follows

$$\tau_{i,j}(t+1) = (1 - \rho) \cdot \tau_{i,j}(t) + \sum_{k=1}^m \Delta\tau_{i,j}^k(t), \quad \forall(i, j) \in A \quad (14)$$

where ρ is the rate of pheromone evaporation, a constant parameter of the method, A is the set of arcs (edges or connections) that fully connects the set of nodes and $\Delta\tau_{i,j}^k(t)$ is the amount of pheromone ant k deposits on the connections it has visited through its tour T^k , typically given by

$$\Delta\tau_{i,j}^k = \begin{cases} \frac{1}{L(T^k)} & \text{if connection } (i,j) \text{ belongs to } T^k \\ 0 & \text{otherwise} \end{cases} \quad (15)$$

The coefficient ρ must be set to a value <1 to avoid unlimited accumulation of trail (Colorni et

al., 1992). In general, connections that are used by many ants and which are parts of short tours, receive more pheromone and are therefore more likely to be chosen by ants in future iterations of the algorithm.

CASE STUDY

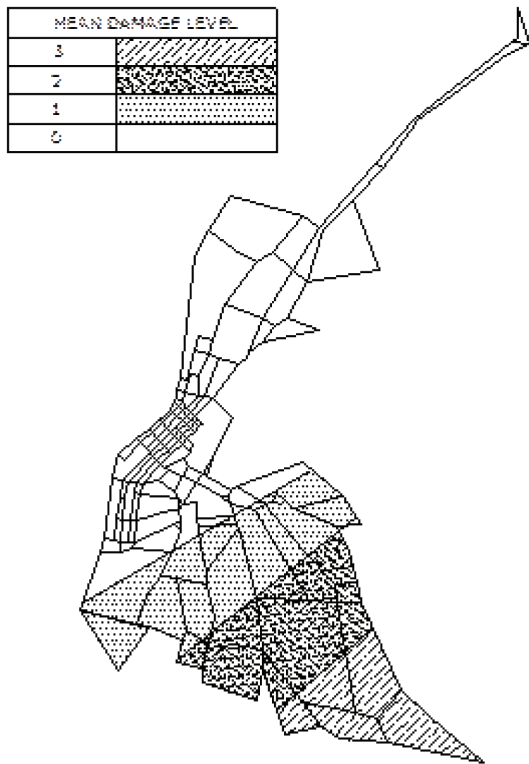
The real world case study considered is the city of Patras in Greece, which is used in order to define both the problem of the inspection assignment and the inspection prioritization. The city of Patras is decomposed into 112 structural blocks having different areas and built-up percentages, while two different sets of inspection groups (crews of inspectors) are considered. A non-uniform distribution of damages is examined with respect to the damage level encountered on the structures due to a strong earthquake. Four areas with different structural damage levels are considered: (i) Level 0 – no damages, (ii) Level 1 – slight damages, (iii) Level 2 – moderate damages and (iv) Level 3 – extensive damages. The subdivision of the city of Patras into 112 structural blocks and the mean damage level for each region are shown in Figure 5. Damages are assumed to follow the Gaussian distribution with mean value 0, 1, 2 and 3 for the four zones of Figure 5. The final distribution of damages over the structural blocks can be seen in Figure 6, where a big circle denotes severe damage.

In order to account for the influence of the distribution of the damages in the city's regions, the formulation of the optimal assignment problem given in Eq. (4) is modified as follows

$$\min \sum_{i=1}^{N_{IG}} \sum_{k=1}^{n_{SB}^{(i)}} [d(SB_k, C_i) \cdot D(k) \cdot DF(k)] \quad (16)$$

where $DF(k)$ is the damage factor corresponding to each damage level, as shown in Table 10. Figures 7(a) and 7(b) depict the solutions obtained for the

Figure 5. City of Patras – Subdivision into structural blocks and the mean damage level distributed over the structural blocks



optimum allocation problem for the two different numbers of inspection crews.

In the second step, the inspection prioritization problem defined in Eq. (6) is solved by means of the Ant Colony Optimization algorithm. Figures 8(a) and 8(b) depict the optimum routes achieved, corresponding to the least time consuming route required for each inspection group imitating from their base. The base is the same for every inspection crew. The distances for the first and second group are 17121 and 31540 respectively for the two inspection groups while for the four are 9633.7, 10939, 11383 and 15740.

Figure 9 depicts the convergence histories of the ACO algorithm. The vertical axis is the minimum distance path among the ants for every iteration.

Table 10. Damage Factor (DF) corresponding to each damage level

Damage level	Damage Factor (DF)
0	1.0
1	1.2
2	1.5
3	2.0

CONCLUSION

In this study the application of metaheuristic optimization and in particular Evolution Strategies, Particle Swarm Optimization and Ant Colony Optimization is examined in two problems of great significance, the structural seismic design optimization problem and the inspection scheduling problem after a seismic hazard attack.

In the first problem examined in this study it was found that with reference to the factors influencing the life-cycle cost estimation it can be concluded that 10 to 20 records are not enough to obtain reliable life-cycle cost analysis prediction results. The structural type of the building affects its structural performance. It has been verified that a symmetrical structure sustains less damage and therefore less repair cost during its life compared to a non-symmetric structure. In both test examples the effect of the other sources of uncertainty like material properties, damping and mass properties is very significant varying considerably the mean, the standard deviation and the fractiles of the seismic response. Neglecting the influence of modeling uncertainties (i.e. material properties and design variables) in the prediction of the seismic response can significantly underestimate the values of the seismic damage indices considered. As a result the estimated value of the life cycle cost varies considerably (up to 30%) compared to the case where the cumulative impact of all sources of randomness is considered. Furthermore, it has been shown that designs obtained in accordance to the European seismic design code are more

Figure 6. City of Patras – Distribution of the damage levels

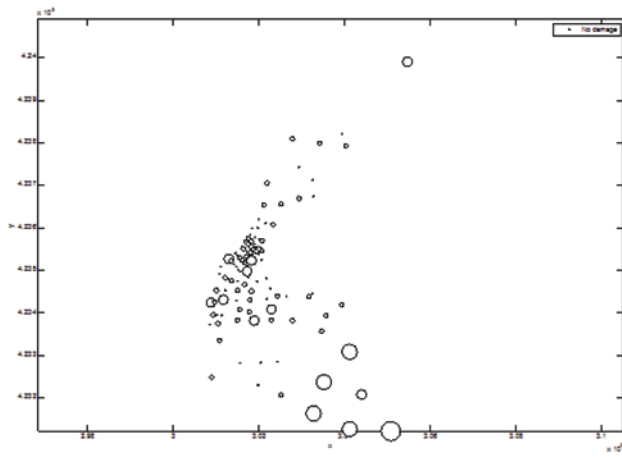


Figure 7. City of Patras - Subdivision into structural blocks (a) two and (b) four inspection crews

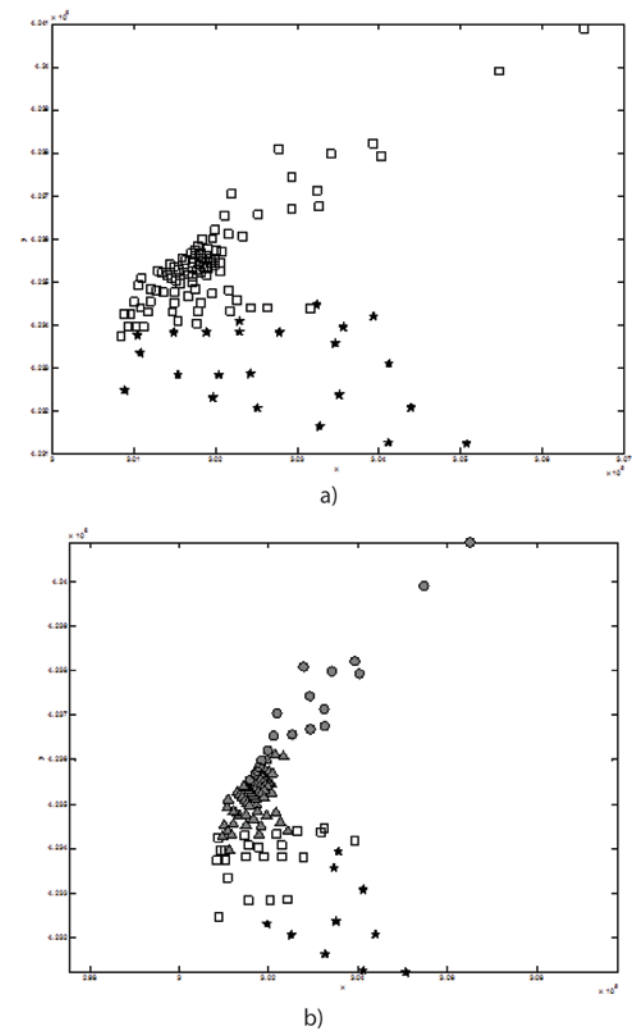


Figure 8. City of Patras – Best route (a) two and (b) four inspection crews

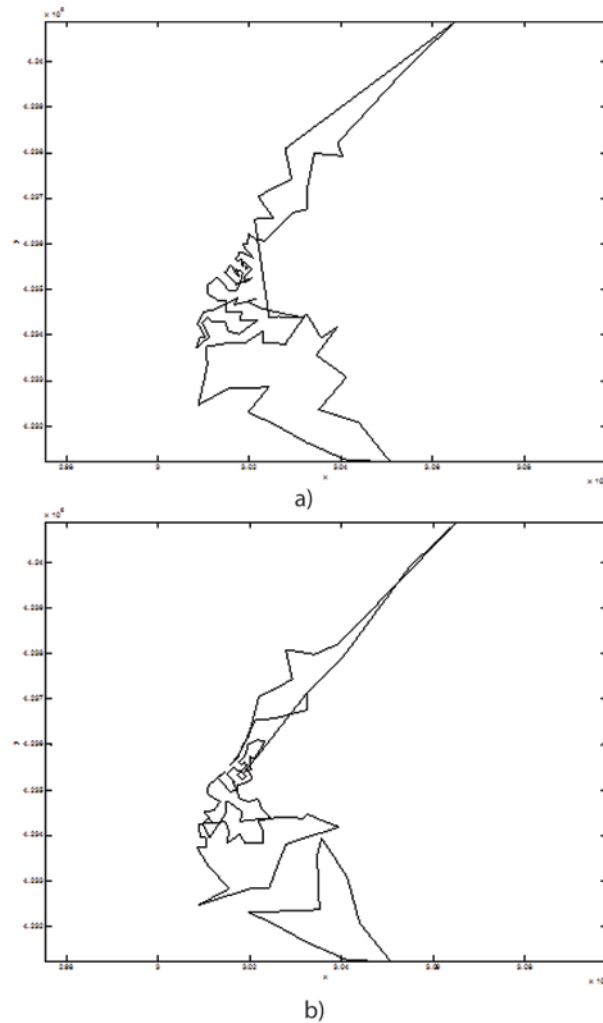
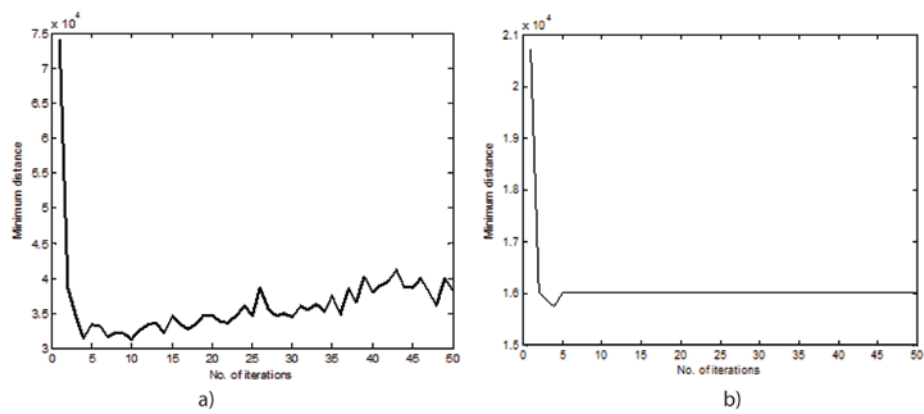


Figure 9. City of Patras – Optimization history of the last group (a) for the case of two and (b) the case of four inspection crews



vulnerable to future earthquakes compared to similar designs, in terms of initial construction cost, obtained with the performance-based design procedure. This vulnerability increases for designs selected from the part of the Pareto front curves where the initial construction cost is the dominant criterion. Even though these conclusions cannot be generalized, they provide an indication of the quality of the designs obtained according to a prescriptive design code and to a performance-based design procedure.

On the other hand following a natural hazard, the condition of the critical infrastructures must be assessed and damages have to be identified. Inspections are therefore necessary, immediately after the catastrophic event, since failure to quickly inspect, repair and/or rehabilitate the infrastructure system, particularly in densely populated metropolitan regions, might delay search and rescue operations and relief efforts, which increases the suffering of the survivors. Specialized crews must be dispatched and inspect critical infrastructures. The objective of the present work was to schedule critical infrastructures inspection crews following an earthquake in densely populated metropolitan regions. In this work two formulations have been successfully implemented: in the first, the structural blocks are assigned to different inspection groups with an effort to equally distribute the workload between the groups, while in the second the optimal route for each group was determined with an effort to minimize the distance that each inspection group has to cover. A Particle Swarm Optimization and an Ant Colony Optimization-based framework were implemented for dealing with the problem at hand and they both resulted in tractable and rapid response models.

REFERENCES

- Altay, N., & Greene, W. G. (2006). OR/MS research in disaster operations management. *European Journal of Operational Research*, 175, 475–493. doi:10.1016/j.ejor.2005.05.016
- ASCE/SEI Standard 41-06. (2006). *Seismic rehabilitation of existing buildings*, prepublication edition. Structural Engineering Institute, American Society of Civil Engineers, 2006. ATC-40. (1996). *Seismic evaluation and retrofit of concrete buildings*. Redwood City, CA: Applied Technology Council.
- ATC-58. (2009). Guidelines for seismic performance assessment of buildings. Redwood City, CA: Applied Technology Council.
- Coello, C. A. (2000). An updated survey of GA-based multi-objective optimization techniques. *ACM Computing Surveys*, 32(2), 109–143. doi:10.1145/358923.358929
- Colorni, A., Dorigo, M., & Maniezzo, V. (1992). An investigation of some properties of an ant algorithm. In R. Manner, & B. Manderick (Eds.), *Proceedings of the Parallel Problem Solving from Nature Conference (PPSN 92)*, (pp. 509–520). Brussels, Belgium: Elsevier Publishing.
- Colorni, A., Dorigo, M., & Maniezzo, V. (1992). Distributed optimization by ant colonies. In F. Varela & P. Bourgine (Eds.), *Proceedings of the First European Conference on Artificial Life*, (pp. 134–142). Paris, France: Elsevier Publishing.
- Dolsek, M. (2009). Incremental dynamic analysis with consideration of modelling uncertainties. *Earthquake Engineering & Structural Dynamics*, 38(6), 805–825. doi:10.1002/eqe.869
- Dong, W. M., Chiang, W. L., & Shah, H. C. (1987). Fuzzy information processing in seismic hazard analysis and decision making. *Soil Dynamics and Earthquake Engineering*, 6(4), 202–226. doi:10.1016/0267-7261(87)90003-0

- Dorigo, M. (1992). *Optimization, learning and natural algorithms*. Milano, Italy: Politecnico di Milano.
- Dorigo, M., & Stützle, T. (2004). *Ant colony optimization*. The MIT Press.
- EC2. (2004). *Eurocode 2. Design of concrete structures—Part 1: General rules and rules for buildings. (The European Standard EN 1992-1-1)*. Brussels, Belgium: European Committee for Standardisation.
- EC8. (2004). *Eurocode 8: Design of structures for earthquake resistance. (The European Standard EN 1998-1)*. Brussels, Belgium: European Committee for Standardisation.
- Ellingwood, B. R., Galambos, T. V., MacGregor, J. G., & Cornell, C. A. (1980). *Development of a probability-based load criterion for American national standard A58*. Washington, DC: National Bureau of Standards. FEMA-350. (2000). *Recommended seismic design criteria for new steel moment-frame buildings*. Washington, DC: Federal Emergency Management Agency. FEMA-445. (2006). *Next-generation performance-based seismic design guidelines, program plan for new and existing buildings*. Washington, DC: Federal Emergency Management Agency.
- Karlaftis, M. G., Kepaptsoglou, K. L., & Lampropoulos, S. (2007). Fund allocation for transportation network recovery following natural disasters. *Journal of Urban Planning and Development*, 133(1), 82–89. doi:10.1061/(ASCE)0733-9488(2007)133:1(82)
- Kennedy, J., & Eberhart, R. (1995). Particle swarm optimization. *IEEE International Conference on Neural Networks*, Piscataway, NJ, (pp. 1942–1948).
- Lagaros, N. D., Fragiadakis, M., & Papadrakakis, M. (2004). Optimum design of shell structures with stiffening beams. *AIAA Journal*, 42(1), 175–184. doi:10.2514/1.9041
- Lagaros, N. D., & Karlaftis, M. G. (2011). A critical assessment of metaheuristics for scheduling emergency infrastructure inspections. *Swarm and Evolutionary Computation*, 1(3), 147–163. doi:10.1016/j.swevo.2011.06.002
- Lagaros, N. D., & Papadrakakis, M. (2007). Seismic design of RC structures: A critical assessment in the framework of multi-objective optimization. *Earthquake Engineering & Structural Dynamics*, 36(12), 1623–1639. doi:10.1002/eqe.707
- Lagaros, N. D., & Papadrakakis, M. (2007). Robust seismic design optimization of steel structures. *Structural and Multidisciplinary Optimization*, 33(6), 457–469. doi:10.1007/s00158-006-0047-5
- Lawler, E. L., Lenstra, J. K., Rinnooy Kan, A. H. G., & Shmoys, D. B. (1985). *The traveling salesman problem: A guided tour of combinatorial optimization*. New York, NY: Wiley.
- Marler, R. T., & Arora, J. S. (2004). Survey of multi-objective optimization methods for engineering. *Structural and Multidisciplinary Optimization*, 26(6), 369–395. doi:10.1007/s00158-003-0368-6
- Mendonca, D., Beroggi, G. E. G., van Gent, D., & Wallace, W. A. (2006). Designing gaming simulations for the assessment of Group decision support Systems in emergency response. *Safety Science*, 44, 523–535. doi:10.1016/j.ssci.2005.12.006
- Mendonca, D., Beroggi, G. E. G., & Wallace, W. A. (2001). Decision support for improvisation during emergency response operations. *International Journal of Emergency Management*, 1(1), 30–38. doi:10.1504/IJEM.2001.000507

- Mitropoulou, C., Lagaros, N. D., & Papadrakakis, M. (2010). Building design based on energy dissipation: A critical assessment. *Bulletin of Earthquake Engineering*, 8(6), 1375–1396. doi:10.1007/s10518-010-9182-x
- Peizhuangm, W., Xihui, L., & Sanchez, E. (1986). Set-valued statistics and its application to earthquake engineering. *Fuzzy Sets and Systems*, 18(3), 347–356. doi:10.1016/0165-0114(86)90011-4
- Perez, R. E., & Behdinan, K. (2007). Particle swarm approach for structural design optimization. *Computers & Structures*, 85, 1579–1588. doi:10.1016/j.compstruc.2006.10.013
- Plevris, V., Karlaftis, M. G., & Lagaros, N. D. (2010). A swarm intelligence approach for emergency infrastructure inspection scheduling. In Gopalakrishnan, K., & Peeta, S. (Eds.), *Sustainable and resilient critical infrastructure systems: Simulation, modeling, and intelligent engineering*. Springer. doi:10.1007/978-3-642-11405-2_8
- Shi, Y., & Eberhart, R. (1998). A modified particle swarm optimizer. *IEEE World Congress on Computational Intelligence*, Anchorage, AK, USA, (pp. 69-73).
- Tamura, H., Yamamoto, K., Tomiyama, S., & Hatono, I. (2000). Modelling and analysis of decision making problem for mitigating natural disaster risks. *European Journal of Operational Research*, 122(2), 461–468. doi:10.1016/S0377-2217(99)00247-7

Chapter 8

Optimal Performance–Based Seismic Design

Hamid Moharrami
Tarbiat Modares University, Iran

ABSTRACT

In this chapter, the reader gets acquainted with the philosophy of performance-based design, its principles, and an overview of the procedures for performance evaluation of structures. The essential prerequisites of optimal performance-based design, including nonlinear analysis, optimization algorithms, and nonlinear sensitivity analysis, are introduced. The methods of nonlinear analysis and optimization are briefly presented, and the formulation of optimal performance-based design with emphasis on deterministic type, rather than probabilistic- (or reliability)-based formulation is discussed in detail. It is revealed how real performance-based design is tied to optimization, and the reason is given for why, without optimization algorithms, multilevel performance-based design is almost impossible.

INTRODUCTION

According to the archaeologists' discoveries the ancient Egyptians believed that to keep a ceiling safely supported by columns, the columns have to have one third of area of the ceiling. Since ever, the effort of engineers has been devoted to minimizing the size of columns to retrieve more space. This indicates that *ENGINEERING* has an intui-

tive meaning of *OPTIMIZATION*; i.e., the degree of professionalism of any engineering design can be measured based on its degree of optimality. This aspiration has been followed in two directions: 1) A better understanding from the behaviour of structure for enhancing design knowledge and 2) Achieving the best (optimum) design in the framework of structural design knowledge.

Improving Design Practice

In the traditional design of structures, attention was mostly paid to strength of structure and the deformation control was often a secondary check. The designer aimed to design a structure in such a way that it withstands the applied loads with sufficient reserved resistance capacity. The structure was in fact designed for amplified loads and checked for deflection or side-sway. It is not too far that the philosophy of design changed to load and resistance factored design (LRFD) in which reduced ultimate strengths of structural elements are compared to the corresponding amplified internal forces. In this method, different loads are amplified differently based on the reliability of their evaluation; and the resistance is decreased differently for bending moment, shear, etc. for similar reasoning. After California earthquakes, including the 1989 Loma Prieta and 1994 Northridge events, the need for a better control on performance of structure became more serious. Seismic-related optimization was supposed to address this problem. Alternatively, Performance-Based Design (PBD) of structures that aims to design a structure for required ductility and targeted displacement in expected risk levels was proposed to satisfy this need. This latter new design philosophy is so attractive that has the potential of being the next generation of design philosophy.

In this new design philosophy, the structure is expected to be such designed that it behaves nonlinearly under severe loadings while it behaves linearly under service loads, small wind and minor earthquake effects. The design has to have enough ductility to tolerate specified drift for severe wind and earthquakes. Depending on behaviour of material used in the structure, being ductile or brittle, the importance of the structure, the risk level and the severity of loading, different design criteria may apply. In other words, different performances may be expected from a structure with different material and different load intensities including

wind, earthquake, etc. In this chapter, we will learn how to find the performance level of a structure. To that end, since some methods of performance-based designs require nonlinear analysis, a brief introduction to nonlinear analysis procedures is also provided to complete the discussion.

Optimizing the Design for Seismic Effects

The desire of optimum design has a long history and goes back to the time of Galileo and even before. However, the new era of structural optimization starts with the time of emergence of electronic computers. Considerable research works can be found in the literature that have focused on the structural optimization under static loading. Many of them have suggested efficient algorithms with relatively good degrees of success.

As the design practice evolved and the demand for structural design under earthquake effects increased, the research on optimizing the structural design for seismic effects increased. The primary works in this field were devoted to structural optimization under dynamic loads. Most of research works in the field considered the elastic behaviour of structures. The degree of success was not fully satisfactory because of the complexity of the problem, objectives to be optimized, mathematical formulation, and the solution schemes for nonlinear optimization problems. Among these research works some attempted to suggest a mathematical model for a better solution of optimization problems and speed up of the solution process; some tried to change the dynamic behaviour of the structure. Among the others, some recent papers by Masson et al. (2002), Basset and Jezequel(2007), Chen, et al. (2002), and Mills-Curran (1985), may be consulted in this field. Park et al. (2003, 2005 & 2010) suggested an equivalent static loading procedure that generates the same response field in linear static analysis that nonlinear dynamic

analysis does. Moharrami and Alavinasab (2006) proposed a method for structural optimization under equivalent static and pseudo-dynamic earthquake loading. In their method, the effect of change of structural components on the amplitude of equivalent static loading (because of change in natural period of the structure) was accounted for. In this way, they could end up to a solution that had maximum ductility leading to minimum lateral earthquake loads and consequently lowest cost.

A different approach to seismic-related optimization was also followed in seismic design, by considering the uncertainties that encounter in demand and capacity assessment. This topic attracted considerable research works in different branches. Some researchers considered the uncertainties involved in the response and performance prediction of a structure during its life. This type of problem formulation that is called life-cycle design optimization is a more general aspect of optimal design, and may be considered as an overall performance-based design optimization. The optimization of the structural system on life-cycle performance has to consider the initial cost of construction of a building, vulnerability of damage to structural components, its expected costs of preventive maintenance, the expected costs of inspection, the estimated costs of repair or rehabilitation, and predicted costs of consequences of failure. This in turn, requires some deep study on risk-related engineering applications including studies about risk analysis on system survival and possibilities of partial or total collapse of a structure and corresponding damage assessment. It is also necessary to have a highly efficient and robust algorithm to estimate the deformation capacity of the structure and evaluate the damage to the structure for given deformation. To that end, some vulnerability and damage functions have to be defined in monetary terms that take into account not only the damage and rehabilitation-related costs, but also the cost of social consequences of structural collapse related to human life.

Since the goal of this chapter is to promote the readers in particular young researchers and practicing engineers to become acquainted with practical performance-based design optimization, and on the other hand, from the practical point of view the life-cycle design optimization requires development of quantitative definitions for qualitative subjects that are not yet well documented, this second type of performance-based design, despite its generality, is not covered in this chapter. However, for those readers who are interested in having more information in this field, among many others, the papers by Frangopol (2011), Fragiadakis and Lagaros (2011), Lagaros et al (2008), Jalayer and Cornell (2009), Cornell(2008), and Esteva et al. (2010) are suggested to start with.

With the promotion of deterministic performance-based design philosophy, some researchers in the field of structural optimization focused their attention to various aspects of this new subject with different approaches to the problem. Since optimal performance-based design is the main subject of this chapter, some selected research works in the field will be reviewed in more detail in the forthcoming sections.

When we seek the optimum performance-based seismic design (OPBSD), we need to know: how to formulate our optimization problem, what are the prerequisites of the problem formulation, how to choose the design variables and how to choose the optimization algorithm to solve it. In this chapter, all these items will be discussed. The prerequisites of the OPBSD will be briefly explained to enable the reader write his own computer program for his especial type of structure and material properties. Special attention will be paid to the sensitivity analysis that is a fundamental tool for classical optimization algorithms. Two types of formulations of sensitivity analysis for 2D steel and reinforced concrete structures will be discussed. The differences between the sensitivity analyses will be presented by some samples from the literature.

INTRODUCTION TO PERFORMANCE-BASED DESIGN

As was mentioned before, the performance-based design integrates the design for deformation with the design for strength. In this new design philosophy, the “ductility of structure” and the “resistance for the internal forces” have the same order of importance. It is expected from the design engineer, to design the structure in such a way that it exhibits different desired behaviours under different intensities of loads. Although this design strategy is general, it is mainly proposed and used for design of structure under earthquake excitation. Accordingly in this chapter our discussion is limited to this field of application.

Although Japanese are likely the first who proposed and used the performance-based design, the studies made in the United States of America are the best known and the most referred ones. Since this design philosophy is not yet mandatory for newly designed structures, but is essential in rehabilitation of buildings, most of research works, practical recommendations and applications are made in seismic rehabilitation of buildings. As an introduction to the research activities in this field, one may consult a paper by Ghobarah (2001) who has reviewed the serious challenges up to 2001.

ASCE41 (2007) that is the latest published recommendations for rehabilitation, considers four levels of performances for structures. These performance levels that are virtually adopted worldwide are:

- A. Operational (OP), which is the level of performance in which no damage is accepted for the structure, and it behaves elastically under service loads, minor wind, and earthquake effects.
- B. Immediate Occupancy (IO), that is the level of performance in which little damage may occur in the structure, and it is safe to be reoccupied immediately following the earthquake.

- C. Life Safety (LS), in which the structure tolerates sever damage, but it remains safe for the occupants to evacuate the building.
- D. Collapse Prevention (CP). This level of performance is the final stage of life of a structure in which the structure has reached its instability level, and an increase in load or deflection results in collapse of the structure.

Depending on the degree of importance of a structure, it may be desirable to have different levels of performances for different levels of earthquake intensities. For example, it may be desirable to design a hospital so that even for severe earthquake excitations, its performance does not go beyond life safety (LS) situation. This is because hospitals are to serve to the people after earthquake. For a residential building, it may be uneconomic to be designed similar to a hospital; therefore, it may be designed such that it experiences CP situation for severe earthquakes. Table 1 shows an example of this kind of strategies.

FEMA356 (2000) suggests a more general definition as in Table 2 for rehabilitation objectives. Here, we call it performance objectives.

According to FEMA356, the basic safety objective (BSO) for an ordinary building is to satisfy the K+P criteria. i.e., every building has to be safe enough to satisfy LS criteria under an earthquake with the probability of 10% per fifty years, and withstand the earthquake with the probability of 2% per fifty years with CP condition. Any design that satisfies either of M, N or O alone, or satisfies any of A, E, I, B, F, and J in addition to K+P, is considered to have enhanced performance objective. Reversely, if a design does not meet K or P criteria is designated as limited performance objective. A design that uses a lower seismic hazard or lower target Building Performance Level than the BSO may be called a reduced performance design.

To design a structure for specified performance level, the design engineer needs to know the target displacement; i.e., the extent of deformations that

Table 1. A sample of desired performances for different buildings

Earthquake hazard level	OP	IO	LS	CP
The most severe in 72 years				
The most severe in 225 years				
The most severe in 474 years				
The most severe in 2475 years				
	Unimportant building such as a sunshade			
	Ordinary buildings such as residential buildings			
	Important buildings such as hospitals			

Table 2. Performance objectives (FEMA356, 2000)

Earthquake hazard level	OP	IO	LS	CP
50% per 50 years	A	B	C	D
20% per 50 years	E	F	G	H
10% per 50 years	I	J	K	L
2% per 50 years	M	N	O	P

the structure has to tolerate for the specified performance level. Some publications in the literature claim that once the target displacement is known, it is possible to determine the design base shear and consequently to design the structure for the base shear. A book by Priestley et al. (2007), that instructs the direct displacement-based seismic design methodology, and research works by Fajfar (2000) that propose the N2 method, and research works by Aschheim (1999) that suggest YPS method may be consulted in this regard. Since these methods have not yet been adopted by design codes, the iterative performance-based design is often used. The iterative process consists of assuming a trial design, finding its performance level, modifying the design and repeating the process again and again until the required specifications that meet the performance criteria are obtained.

How to Find the Performance Level of a Structure

The spirit of almost all seismic evaluation methods is a comparison between the capacity of structure

and the demand that an earthquake imposes to it, in respect to its strength and ductility characteristics. This comparison is made in member level as well as structure level.

The capacity of a structure is a resultant of capacity of its components. If a force-deformation relation is defined for elements of a structure, the capacity of structure can be found from nonlinear analysis. Since computer programming for nonlinear analysis is difficult and is time consuming, engineers prefer to conduct a linear analysis. Four methods of analyses are accepted for seismic evaluation of a structure:

1. Linear static analysis
2. Linear dynamic analysis
3. Nonlinear static analysis
4. Nonlinear dynamic analysis

If a static type of analysis is performed, a modification factor has to be applied to the results to make them reflect the nonlinear behavior. This will be discussed later.

The Vertical Distribution of Lateral Load

To perform a linear or nonlinear static analysis, the distribution of base shear or pseudo-lateral force over the storys in the vertical direction of a building, has to be such applied that it simulates the earthquake effect accounting for dynamic characteristics. According to ASCE41, the base shear should be vertically distributed according to the following equations.

$$F_x = C_{vx} V \quad (1)$$

$$C_{vx} = \frac{w_x h_x^k}{\sum_{i=1}^n w_i h_i^k} V \quad (2)$$

where

C_{vx} = vertical distribution factor;

k = 2.0 for $T \geq 2.5$ sec; k = 1.0 for $T \leq 0.5$ sec and linear interpolation shall be used to calculate values of k for intermediate values of T .

V = Base shear or pseudo-lateral force;

w_i = portion of the effective seismic weight W located on or assigned to floor level i ;

w_x = portion of the effective seismic weight W located on or assigned to floor level x ;

h_i = height from the base to floor level i ; and h_x = height from the base to floor level x .

Linear Analyses

Among the above four methods, the first one is the most accessible method for engineers. However, there are some limitations on its use for irregular structures. The distribution of demands predicted by a linear dynamic analysis (the 2nd method), is

usually more accurate than those predicted by the linear static analysis; accordingly compared to the first method, there are fewer limitations on use of linear dynamic analysis. Whenever applicable, either of the response spectrum method or time history method may be used for linear dynamic analysis.

When the linear type of analysis is used for demand evaluation, the structure is loaded to the extent that reaches the target displacement. At this stage, every structural component experiences a deformation and corresponding internal force. All structural components have to be checked against acceptance criteria pertaining to the desired performance level. Discussion on "how the acceptance criteria are obtained" is out of the scope of this chapter, but it worth knowing that these criteria are specified using actual laboratory test results, supplemented by the engineering judgment of various development teams of FEMA¹. Acceptance criteria are different for deformation-controlled (ductile) and force-controlled (inductile) members. They also vary depending on the type of structural component, (i.e., beam, column etc.), its material, physical properties, and performance level. Acceptance criteria are given differently for the results of linear and nonlinear type of structural analyses. For forced controlled members, depending on the type of structural element and the performance level in question, if a linear type of analysis is used, the internal force of member due to lateral load is multiplied by a reduction factor, to rationalize it for the given performance level. Alternatively for deformation controlled components, the strength of structural component is multiplied by an m -factor and checked against design forces due to the gravity and earthquake loads. FEMA356 (2000) recommends the following formula for deformation-controlled components:

$$mkQ_{CE} \geq Q_{UD} \quad (3)$$

where, m is the component or element demand modifier (factor), to account for expected ductility associated with this action at the selected Structural Performance Level; i.e., the m -factors modify the results so as to be similar to the results of a nonlinear analysis. The m -factors are specified in Chapters 4 through 8 of FEMA356.

Q_{CE} is the expected strength of the component or element at the deformation level under consideration for deformation-controlled actions.

Q_{UD} is Deformation-controlled design action due to gravity loads and earthquake loads.

k is the Knowledge factor (0.75 or 1.0) depending on the accuracy of collected data and performance objectives.

For a force-controlled structural component, in the absence of either a nonlinear or limit state analysis the following formula applies to the design force, Q_{UF} .

$$Q_{UF} = Q_G \pm \frac{Q_E}{C_1 C_2 C_3 J} \quad (4)$$

Q_{UF} is the Force-controlled design force due to gravity plus earthquake loads. J is Force-delivery reduction factor defined by FEMA356 and is greater than 1. Coefficients $C1$, $C2$, and $C3$ are amplification factors and are defined in FEMA356. They are used to amplify the design base shear for achieving displacement target at the desired performance level. This pre-standard recommends the following formula for forced controlled members.

$$kQ_{CL} > Q_{UF} \quad (5)$$

k was previously defined. Q_{CL} is Lower-bound strength of a component or element at the deformation level under consideration for force-controlled actions.

If structural components have capacities more than the demand, it satisfies the performance level

in question. Otherwise, a lower performance level is examined.

Nonlinear Analyses

Parallel and simultaneous improvements in computational facilities in commercial software and the theories supporting nonlinear static seismic (pushover) analysis, is making the pushover method more accessible and reliable for engineers, and from a practical point of view, it is foreseen to be the most popular analysis procedure in the future for performance-based seismic design. The outcome of pushover analysis is the inelastic capacity curve of the structure. This curve defines the capacity of the building independent of any earthquake. To make it useful for evaluation of performance point for a given earthquake, this curve has to be converted to spectral ordinates. This will be discussed later.

On the other hand because of its complexity, the nonlinear dynamic analysis (the 4th method) is hardly used by engineers. However, since it is a reliable analysis method, it is more often used for research purposes. When this method is used the demand data can be directly used for evaluation of performance of the structure. Design optimization using nonlinear dynamic analysis is an extraordinarily difficult subject that is not yet used for practical design problems.

When nonlinear analysis is used for demand evaluation, similar to deformations, the internal forces obtained for components, are used without substantial modification. One should realize that unlike to nonlinear dynamic analysis, nonlinear static (pushover) analysis does not fully reflect the nonlinear behaviour of a structure. It does not account for cycle strength and stiffness degradation. Also, the ductility demand concentration of individual stories is not tracked in this method. Two accepted methods i.e., the method of coefficients and method of capacity spectrum have been proposed to convert the outcome of nonlinear

pushover analysis, the capacity curve, to usable data as of nonlinear dynamic analysis.

The Coefficient Method

In the coefficient method that is recommended by FEMA273, FEMA356 and ASCE41, the target displacement, δ_t at roof level, shall be calculated in accordance with an equation similar to Eq. (6). The internal forces and deformation of every component will be accordingly obtained. The coefficients C_i and S_a , have slightly different definitions in these references, but they are essentially the same. According to ASCE41, that is believed to provide better results compared to FEMA356, the target displacement is obtained from the following equation.

$$\delta_t = C_0 C_1 C_2 S_a \frac{T_e^2}{4\pi^2} g \quad (6)$$

where:

T_e is the effective fundamental period of building in the direction under consideration. (clause 3.3.3.2.6)

C_0 is the modification factor to relate spectral displacement of an equivalent SDOF system to the roof displacement of the MDOF building system.

C_1 is modification factor to relate expected maximum inelastic displacements to displacements calculated for linear elastic response. It is calculated from the following equation. According to ASCE41, some limitations apply.

$$C_1 = 1 + \frac{(R - 1)}{\alpha T_e^2} \quad (7)$$

α is site class factor given by ASCE41.

R is the ratio of elastic strength demand to calculated yield strength.

$$R = \frac{S_a}{V_y/W} C_m \quad (8)$$

V_y is yield strength calculated using nonlinear static pushover analysis.

W is effective seismic weight.

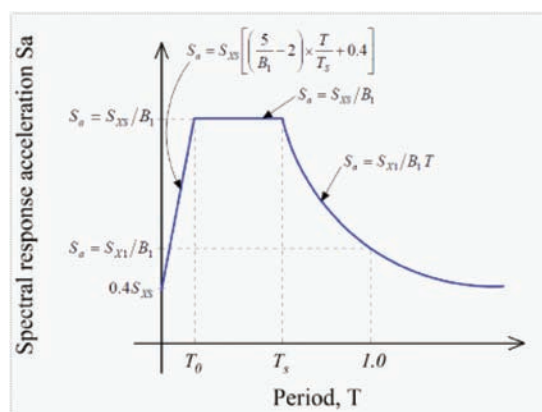
C_m is effective mass factor and is given in a table in ASCE41.

S_a is the response spectrum acceleration, at the effective fundamental period and damping ratio of the building in the direction under consideration. It is shown graphically in Figure 1 in which T_s is characteristic period of response spectrum and B_1 is obtained from $B_1 = 4/[5.6 - \ln(100\beta)]$ and β is effective viscose damping ratio.

C_2 is the adjustment factor to represent the effect of pinched hysteretic shape, cyclic stiffness degradation and strength deterioration on maximum displacement response. For $T_e > 0.7$ sec, $C_2 = 1$.

$$C_2 = 1 + \frac{1}{800} \left(\frac{R - 1}{T_e} \right)^2 \quad (9)$$

Figure 1. General horizontal response spectrum



With this target displacement, the internal forces and deformation of structural components are obtained and checked to the acceptance criteria. From this comparison, the performance level of structure is known. The checking process is similar to linear analysis, but with different criteria; i.e., it is similar in the sense that it depends on the properties of structural component whether it is deformation-controlled or force-controlled component.

The Capacity Spectrum Method

In the capacity spectrum method that is recommended by ATC40, the performance point that is alternatively called the target point is obtained by intersecting the capacity spectrum and demand spectrum. The capacity spectrum is indeed the capacity curve converted from force-displacement ordinates to spectral acceleration-spectral displacement ordinates. This is done by converting the base-shear to S_a and displacement to S_d . The following formulae apply.

$$S_a = \frac{V/W}{\alpha_1} \quad (10)$$

$$S_d = \frac{\Delta_{roof}}{PF_1(\varphi_{roof,1})} \quad (11)$$

$$\alpha_1 = \frac{1}{W} \frac{\left(\sum_{i=1}^n m_i \varphi_{i1} \right)^2}{\sum_{i=1}^n m_i (\varphi_{i1})^2} \quad (12)$$

$$PF_1 = \frac{\sum_{i=1}^n m_i \varphi_{i1}}{\sum_{i=1}^n m_i (\varphi_{i1})^2} \quad (13)$$

Having the capacity curve converted to capacity spectrum curve it remains to draw the demand response spectrum in the same coordinate. Noting that response spectrum as specified by a design code is a curve specified in S_a -T coordinates, and we need demand spectrum in S_a - S_d coordinates, the horizontal axis should be transformed to S_d simply noting that $S_d = T^2/4\pi^2 S_a g$. The outcome of this conversion is an acceleration-displacement response spectrum (ADRS) curve.

As building yields in response to seismic demand, it dissipates energy with hysteretic damping; that means its damping increases. With an increase in damping, the demand spectrum reduces. i.e., the ADRS curve is not unique, and it depends on the effective damping property of the structure. According to ATC 40, the effective equivalent viscose damping, is obtained from $\beta_{eq} = \beta_0 + 0.05$ in which 0.05 is the inherent viscose damping of the structure that is considered to be constant. β_0 is the hysteretic damping represented as viscose-equivalent hysteresis damping and is calculated from: $\beta_0 = E_D / (4\pi E_{so})$ in which E_D is the damping dissipated energy and E_{so} is the maximum strain energy. According to ATC 40 (section 8.2.2), E_D and E_{so} are calculated based on performance point that is the intersection of the ADRS curve and the reduced demand spectrum. This implies that the performance point is obtained through an iterative process.

There are several techniques for finding this intersection. Here, we explain one of them. Since the intersection of demand and capacity spectra, (the target/performance point) is not known a priori, an initial target point is assumed on the capacity spectrum curve. Then with the information of this point and the capacity spectrum curve, the corresponding viscose-equivalent hysteresis damping β_0 and β_{eq} are obtained and the corresponding reduced demand spectrum is constructed and intersected to capacity spectrum curve to produce a new performance/target point. If the obtained target point is close enough to the assumed one, the performance point is found;

otherwise a new target point has to be assumed on capacity spectrum, and the process should be repeated. Figure 2 illustrates the procedure.

Having the nonlinear demand obtained via any of aforementioned analyses and subsequent techniques, and comparing it to the specification of acceptance criteria at desired performance level(s) identifies the performance level of a structure.

A BRIEF LOOK INTO NONLINEAR ANALYSES

Any nonlinear analysis procedure requires the establishment of nonlinear set of equations of equilibrium as follows:

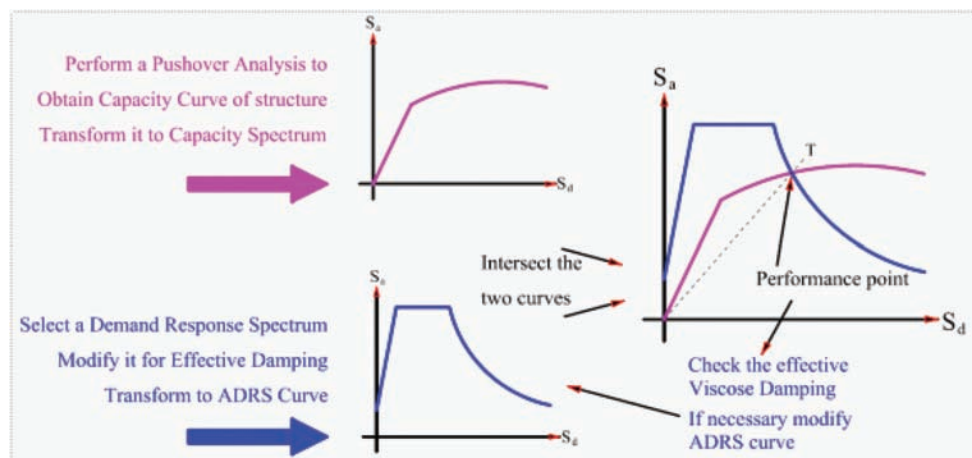
$$[K(x, \Delta)]\{\Delta\} = \{P\} \quad (14)$$

This in turn, necessitates the definition of a force-deformation relation in member level. If the force-deformation relation is known in its explicit mathematical form, the assembly of explicit nonlinear stiffness matrix is theoretically possible, otherwise, as it often happens, the stiffness matrix will be a numerically established matrix that is an implicit function of deformation.

If for a certain degree of freedom at a node, the internal forces of all members connected to that node are summed up and equated to the corresponding external load, an equation of equilibrium for that particular degree of freedom will be generated. If this is done for all degrees of freedoms, a set of nonlinear equations can be obtained. The nonlinear analysis procedure is the art of finding a displacement vector that satisfies the set of all nonlinear equations of equilibrium in Eq.(14), simultaneously. Once the displacement vector in Eq.(14) is obtained, it remains to calculate the internal forces in all members. At this stage, the pre-defined force-deformation relation is used to obtain internal forces.

Since the performance-based design in its general form requires nonlinear analysis, design engineers in this field are recommended to study in details some useful publications before employing any commercial software. This will help to understand the merits of different nonlinear schemes with respect to each other. Crisfield (2000) and Owen and Hinton (1980) have cited good summaries of classical nonlinear analysis techniques. A brief description of some of these methods that are suitable for monotonically increasing curves is provided hereunder and summarized graphically in Figure 3.

Figure 2. Capacity spectrum method

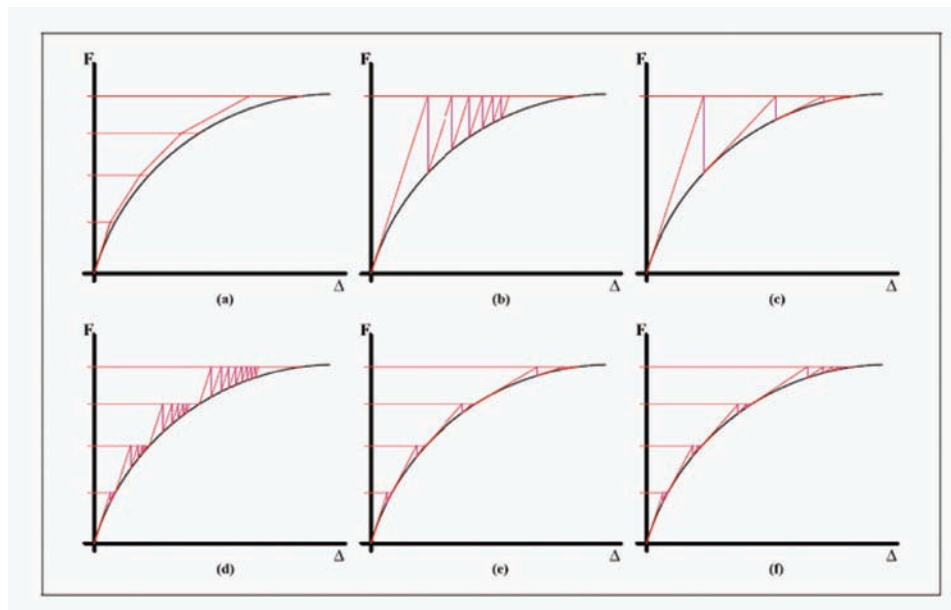


- **Incremental Scheme:** As shown in Figure 3a, in this method, displacement is found by gradual loading and modification of the stiffness matrix of the structure at the beginning of each load increment. To get a satisfactory result from this method, loading increments should be quite small; otherwise, it results in incorrect displacement values.
- **Initial Stiffness method:** In this method, which is shown in Figure 3b, the structure is analyzed with its initial stiffness. After each analysis, internal forces of members, which can be measured by the previously obtained displacement, are used to find the unbalanced forces in nodes. The unbalanced forces are then applied again to the structure with its initial stiffness. The process of analysis of structure under unbalanced forces is repeated until external and internal forces and moments reach equilibrium.
- **Newton-Raphson method:** As Figure 3c shows, this method is similar to the ini-

tial stiffness method in the sense that both methods start with the initial stiffness and continue analysis with unbalanced loads, however, Newton Raphson method uses tangential stiffness of the structure at the beginning of each analysis instead of initial stiffness. In this method too, the process continues until the unbalanced load becomes infinitesimally small.

- **Combined Methods:** To achieve a more efficient method, the above techniques can be combined. For example, Figure 3d demonstrates the combination of the initial stiffness method with the incremental solution. Figure 3e shows Newton Raphson method in conjunction with the incremental loading scheme. A combination of three methods can also be seen in Figure 3f. In this latter method, loading on structure is divided into several segments. At the beginning of every loading increment, stiffness matrix of structure is established/modified and displacement vector of struc-

Figure 3. A schematic presentation of nonlinear analysis



ture is obtained using iterative initial stiffness technique.

There are also some other techniques that have been established for inelastic analysis of structures based on theorems of Structural Variation. Structural variation theory studies the effect of change of properties, or even removal, of a member on the entire structure. It takes advantage of linear analysis and sensitivity of structure to some self equilibrating unit loads that are applied at the end nodes of changing members. This technique has been applied to analysis of several types of inelastic skeletal structures including space trusses, frames, and grids, etc. It has been also extended to nonlinear finite elements analysis. Although this method takes advantage of initial stiffness matrix and does not require a change in the stiffness matrix of structure during the analysis process, it is a hierarchical and step by step method of analysis in which every step uses information from the previous step and is not a proper nonlinear analysis that is to be joined to a performance-based design program. As an example in this field one may start with a paper by Saka (1997).

Nonlinear analysis of structures by the mathematical programming is another field of research in this ground. De Donato (1977) presented fundamentals of this method for both holonomic (path independent) and nonholonomic material behaviors. In this method, it is assumed that displacement of nodes of an elasto-plastic structure comprises two parts namely elastic and plastic parts. Then, the problem of finding total displacement vector of a structure is formulated in the form of a quadratic programming (QP) problem with some complementary yield constraints. These yield constraints state that individual members either are stressed within elastic limits and do not accept plastic deformations or, are stressed up to yield limit, and as a result, undergo some plastic deformations. The output of this sub-problem is linear and nonlinear deformation of the structure.

Despite its robustness, this method suffers from the considerable number of variables that enter in the QP sub-problem. Recently Tin Loi has improved this technique. Among others, a paper by Tangaramvong and Tin Loi (2011) may be consulted in this field.

DESIGN OPTIMIZATION

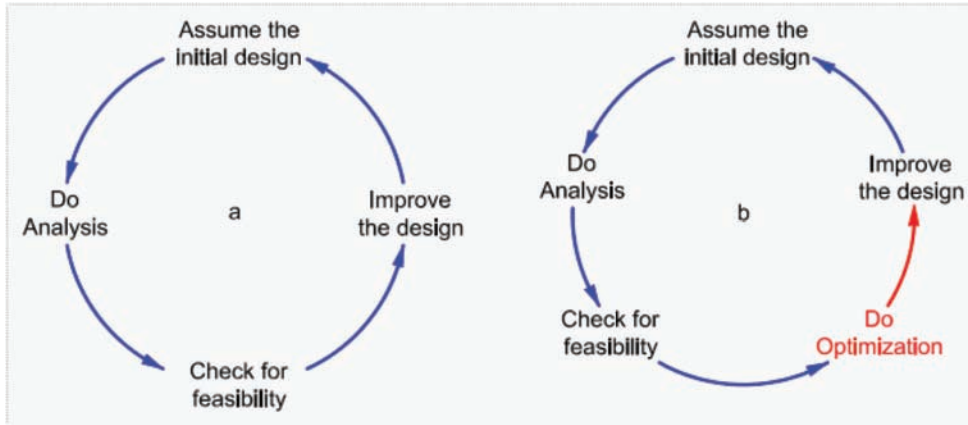
The traditional design as shown in Figure 4a consists of a cycle of four components. They are: *Design*, *Analysis*, *Feasibility-check* and *Design improvement*. If the initial design is not satisfactory or feasible, a revision on the initial design is made, and the design cycle is repeated. The process stops when the design is deemed satisfactory. A design that is obtained in this way may be satisfactory but not optimum. If, as shown in Figure 4b, in the design cycle an optimization component is added to enhance the design intelligently, the outcome of the design cycle may be both satisfactory and optimum.

Therefore, the design optimization may be defined as a mathematical means that is used to evolve a structure from its initial form to a final form with characteristics of being the optimum. This process may be employed for a member by member optimization or whole-structure. To optimize a design, it should be written in the form of the standard optimization problem as follows:

$$\begin{aligned} & \text{Minimize} \quad Z(\vec{x}) \\ & \text{Subject to : } g_j(\vec{x}) \leq 0 \quad ; j = 1, 2, \dots, m \\ & \quad h_k(\vec{x}) = 0. \quad ; k = 1, 2, \dots, p \end{aligned} \tag{15}$$

where \vec{x} is the generalized vector of design variables including x_1 to x_n . The design variables establish the design space. Z is the objective function. g and h are inequality and equality design constraints, respectively. Design constraints divide the design space into feasible and infeasible sec-

Figure 4. Design cycles: a) traditional, b)optimal



tions. The solution of constrained optimization problem places within feasible space. The feasible space for problems with equality constraints is the boundary constructed by the intersection of all equality constraints. In the engineering design problems, we rarely confront to problems with equality constraints. Considerable research effort has been paid to propose some solution algorithms that efficiently solve the problem. Depending on the order of derivatives that optimization algorithms use for solution, Haftka (1992) divides them into three main groups. They are: zero order, first order and second order algorithms.

Zero order algorithms do not use any derivative of objective functions or constraints. There are a few zero order classical algorithms, but there are many hierarchical and probabilistic algorithms such as Genetic Algorithms, Particle Swarm Optimization, Ant Colony, etc. Most of zero order algorithms are used for unconstrained optimization problems. Since almost all engineering design optimization problems are constrained problems, to use a zero order algorithm for their solution, the constrained optimization problems have to be converted to unconstrained optimization problems via one of Penalty Function methods. A book by Arora (2004) will assist in this regard. The first order algorithms use the first order derivatives of constraints. This group of algorithms comprise

a large part of body of classical optimization and are most commonly used. The second order optimization algorithms that use the second order derivatives of constraints are fairly efficient algorithms, but because of calculation of second order derivatives, they are not proper algorithms for problems with numerous design variables.

Many attempts have been made to formulate the optimization problem in such a way that it is easily solved. Optimization problems may be categorized into linear and nonlinear. If the constraints and objective function of a problem are linear, the problem is called a linear programming problem and may be solved by Simplex method. Most of structural design optimization problems are naturally nonlinear problems because of the nonlinear nature of indeterminate structures. For determinate structures, the fully stressed design (FSD) optimization or similar algorithms (such as simultaneous failure mode (SFM), etc.) which are a member to member optimization strategy may be used. In most of engineering problems, the design constraints cannot be defined in explicit form in terms of design variables. Accordingly, the Taylor series expansion is used to express the constraints in explicit form as follows:

$$F(\vec{x}) = F(\vec{x}^0) + \nabla F(\vec{x}^0)^T \Delta \vec{x} + \frac{1}{2} \Delta \vec{x}^T \nabla^2 F(\vec{x}^0) \Delta \vec{x} + \dots \quad (16)$$

where, \vec{x} is the vector of design variables; $\nabla F(\vec{x}^0)$ is the gradient of the function F at the current point and $\nabla^2 F(\vec{x}^0)$ is the matrix of second order derivatives, named Hessian matrix of the function. Although the design constraint may be implicit function of design variables, its derivatives can be numerically obtained by sensitivity analysis. The calculation of Hessian of a function, particularly if it is a function of numerous design variables is relatively difficult and computationally time consuming. Some algorithms such as DFP and BFGS use the first order derivatives to gradually construct the Hessian matrix or its inverse from its first order derivatives.

If a function is approximated with its first two terms of Taylor series, it is called linearized form of the function. Keeping the first three terms of Taylor series approximates the function with a quadratic form. Except for problems with a few design variables, the quadratic term is rarely used. Expressing the constraints and objective function in their linear form, makes it possible to define a Linear Programming (LP) sub-problem and solve it by Simplex algorithm. Objective function is usually given explicitly in terms of design variables. If the objective function is written in quadratic form and the constraints expressed in linear form, a Quadratic Programming (QP) problem is established. The solution of an optimization problem can be sought by converting it to LP or QP sub-problem and solving it. The QP and LP problems have a straight-forward solution scheme and most of mathematical programming software have these solution options. The outcome of LP or QP sub-problem will not necessarily insure the feasibility and optimality of the solution because the constraints of these problems are some approximation of actual design problem. Therefore, the process of establishing and solution of LP or

QP sub-problems should be repeated. These strategies are called Sequential Linear Programming (SLP) and Sequential Quadratic Programming (SQP), respectively. Although SLP and SQP can often capture the optimum solution, they are not so much efficient algorithms. Considerable effort has been paid to find efficient and robust optimization algorithms. Among successful optimization algorithms are Dual method and Conlin algorithm by Fleury (1983 and 1989) and DOT algorithm by Vanderplatts (1997). The degree of success for an optimization algorithm somehow depends on the nature of the optimization problem. An algorithm may work very well for a problem and not well for another. There is not a firm conclusion about the efficiency and robustness of any especial optimization algorithm. An optimization algorithm may solve one optimization problem efficiently, and not solve another. For example if an optimization problem is expressed in terms of reciprocals of design variables, it may be solved in an excellent way, but if it is defined in terms of direct design variables it may not be solved properly. This may happen vice versa.

As a conclusion, the choice of the optimization algorithm for a design optimization problem does not have a certain rule. However, some algorithms have shown that in many applications are often more efficient than the others. Optimality Criteria (OC) methods are believed to be more efficient than other classical optimization algorithms. These methods do not directly consider the objective function in the solution process. They seek the optimality of the solution in satisfaction of some predefined criteria. The FSD and SFM methods are among this group of optimization algorithms. Some research works focused their attempt to combine the principals of OC methods with those of classical optimization algorithms. The Kuhn-Tucker-based OC method is an example of this kind. In this type of OC algorithm, the necessary conditions for optimality of a design point that are called Kuhn-Tucker conditions, are chosen as a basis for the establishment of recursive for-

mulae for updating design variables. Moharrami (2006) improved the convergence of this type of OC algorithm by establishing and solving a QP sub-problem for finding the Lagrange Multipliers. This improvement completes the efficiency and robustness of the algorithm.

SENSITIVITY ANALYSIS

The change in a behaviour B_j of structure due to change in a design variable d_i that is expressed as

$$\frac{\partial B_j}{\partial d_i}$$

is called the sensitivity of B_j with respect to d_i . The sensitivity calculation is performed in several ways. Here, we point to some of them.

Finite Difference Method

As was mentioned before, the behaviour B is usually implicit function of design variable. Therefore, it is not possible to find the sensitivity via a direct differentiation of a function. As a remedy for this problem, the Finite Difference (FD) method has been widely used. In this method, the difference between the values of a function at two adjacent points are used to find the approximate slope of the curve (sensitivity) at the desired point as follows:

$$\frac{\partial B_j}{\partial d_i} \approx \frac{B_j(d^1) - B_j(d^2)}{(d_i^1 - d_i^2)} \quad (17)$$

The numerator of the right side of Eq.(17) is the difference between the values of B_j at two adjacent design points d^1 and d^2 where all components of vector of design variables remain unchanged except d_i that can assume any value of $d_i^1 \pm \delta d_i$ i.e., the current point and a point before, or current point and the point after, or the points before and after the current point. The accuracy

of FD method depends on the degree of nonlinearity of the function and the value of δd_i . Habibi and Moharrami (2010) showed that FD method not only does not give accurate sensitivity values but also sometimes results in false evaluation.

Analytical Sensitivity Analysis

Another way of evaluating the sensitivity of a structural behavior is to differentiate the basic equation from which that behavior is evaluated.

As an example, the sensitivity of the displacement vector when a structure behaves linearly can be derived as follows:

The basic equation that the displacement vector is calculated from is:

$$K\Delta = P \quad (18)$$

Differentiating this equation with respect to any generic design variable, d_i results in:

$$\frac{\partial K}{\partial d_i} \Delta + K \frac{\partial \Delta}{\partial d_i} = \frac{\partial P}{\partial d_i} \quad (19)$$

Rearranging the above equation for $\partial \Delta / \partial d_i$ results in the sensitivity equation as follows:

$$\frac{\partial \Delta}{\partial d_i} = K^{-1} \left(\frac{\partial P}{\partial d_i} - \frac{\partial K}{\partial d_i} \Delta \right) \quad (20)$$

Note that all terms in the right hand side of the above equation is known and although Δ is not known explicitly in terms of design variables, its derivatives can be calculated accurately. To calculate the sensitivity $\partial \Delta / \partial d_i$ from the above equation efficiently, the paper by Arora and Haug,(1979) is recommended for study.

As another example, consider the evaluation of sensitivity of a number of vibrating frequencies of a structure. The basic equation for calculating

the frequencies and modal shapes is the following equation:

$$[K - M\omega^2]\varphi = 0 \quad (21)$$

Differentiating the above equation with respect to the design variable, d_i , and rearranging the terms results in the following equation.

$$[K - M\omega^2] \frac{\partial \varphi}{\partial d_i} = \left[2M\omega \frac{\partial \omega}{\partial d_i} + \omega^2 \frac{\partial M}{\partial d_i} - \frac{\partial K}{\partial d_i} \right] \varphi \quad (22)$$

If the above equation is pre-multiplied by φ^T and noted that

$$\varphi^T [K - M\omega^2] = [K - M\omega^2] \varphi = 0 ,$$

then the following equation is obtained:

$$2\omega \frac{\partial \omega}{\partial d_i} \varphi^T M \varphi + \omega^2 \varphi^T \frac{\partial M}{\partial d_i} \varphi - \varphi^T \frac{\partial K}{\partial d_i} \varphi = 0 \quad (23)$$

If the vector f is normalized in such a way that $\varphi^T M \varphi = 1$, then the sensitivity of frequency can be obtained easily from the following expression:

$$\frac{\partial \omega}{\partial d_i} = \frac{1}{2\omega} \varphi^T \left[\frac{\partial K}{\partial d_i} - \omega^2 \frac{\partial M}{\partial d_i} \right] \varphi \quad (24)$$

Nonlinear Sensitivity Analysis

In the sensitivity calculations in Eqs.(18-20), since the structure is in its linear behaviour state, the stiffnesses of structural members do not depend on the deformation, Δ , and therefore, $\partial K/\partial d_i$ and consequently $\partial \Delta/\partial d_i$ are easily calculated. However, if the structure is in nonlinear behavior state, the equation of equilibrium becomes as in Eq.(14) that is repeated here.

$$[K(d, \Delta)]\{\Delta\} = \{P\} \quad (14)$$

That is the stiffness matrix itself becomes a function of displacement. Provided that the nonlinear relation of the stiffness matrix with the displacement vector is explicitly known, theoretically saying, the equation of equilibrium can be solved by mathematics and the specific displacement vector can be obtained in terms of design variables. However, if the relation is not known explicitly, the calculation of displacement vector Δ and its derivative $\partial \Delta/\partial d_i$ has to be followed in a different manner. Differentiating the above equation with respect to any design variable d_i , results in the following complicated equation:

$$\left[\frac{\partial K(d, \Delta)}{\partial d_i} + \sum_{r=1}^{ndf} \frac{\partial K(d, \Delta)}{\partial \Delta_r} \times \frac{\partial \Delta_r}{\partial d_i} \right] \{\Delta\} + [K(d, \Delta)] \left\{ \frac{\partial \Delta}{\partial d_i} \right\} = \left\{ \frac{\partial P}{\partial d_i} \right\} \quad (25)$$

Obviously the above equation cannot be easily solved for $\partial \Delta/\partial d_i$; therefore, a different strategy has to be followed for the sensitivity of structural nonlinear behavior. There are a number of papers that have paid attention to this problem. For the sake of illustrations, the sensitivity calculations in moment resisting steel frames by Gong (2003) is explained and compared to those of reinforced concrete frames by Habibi and Moharrami (2010).

A Sensitivity Analysis Procedure for Nonlinear Steel Frame

In his research for performance-based design, Gong used a special nonlinear static (pushover) analysis scheme proposed by Hasan et al.(2002). In this nonlinear analysis, the progressive degradation of stiffness of a frame structure is referenced to its plastification. As the bending moment, M , goes beyond the yielding moment M_y , a partial plasticity (Plastification) develops in the section. As the plastification increases, the rigidity of the

section decreases. Hasan et al. simulated the partial plasticity in a section with a semi-rigid connection in which the rigidity of connection is progressively decreased as the moment in the section is increased. In particular, a potential plastic-hinge section was simulated with a semi-rigid connection whose stiffness variation is measured by a plasticity-factor p that ranges from unity, for ideal elastic, to zero, for fully plastic. If this degradation is monitored, its influence on the nonlinear behavior of the member and the overall behavior of a structure under increasing lateral load can be traced. Hasan et al. assumed an elliptic moment-curvature relation for post elastic behavior of a section. Then he replaced the plasticity factor with rigidity factor and performed the nonlinear analysis in an incremental scheme. As the lateral load is gradually increased in infinitesimal steps, the stiffness matrix of the structure is deteriorated. This deterioration is considered by modifying the C_s and C_g coefficient matrices in the following formula based on plasticity factors.

$$K = S \cdot C_s + G \cdot C_g \quad (26)$$

where, S is the standard elastic stiffness matrix; C_s is a correlation matrix expressed in terms of plasticity factors; G is the standard geometric stiffness matrix and C_g is corresponding correction matrix, formulated in terms of plasticity factors. In this way, they could obtain the magnitude of overall deformation of the whole-structure as well as all members.

The sensitivity analysis that Gong proposed for his problem is defined in this framework of analysis. Since the sensitivity of displacement is the basis of evaluation of sensitivities of other structural behaviours, it is usually found first. To obtain sensitivity of displacement vector, Eq. (14) was written in the following form.

$$F(d, \Delta) = P(d) \quad (27)$$

This is to say that sum of internal forces at a node is equal to external loads. Differentiating Eq.(27) with respect to any design variable d_i results in the following relation.

$$\frac{\partial F}{\partial d_i} + \frac{\partial F}{\partial \Delta} \cdot \frac{\partial \Delta}{\partial d_i} = \frac{\partial P}{\partial d_i} \quad (28)$$

Noting that $\partial F/\partial \Delta$ is actually the global tangential stiffness matrix, Eq.(28) can be written as:

$$K_T \cdot \frac{\partial \Delta}{\partial d_i} = \frac{\partial P}{\partial d_i} - \frac{\partial F}{\partial d_i} \quad (29)$$

As per above explanations, the tangential stiffness matrix, K_T , for a given displacement vector is easily calculated. Therefore, the sensitivity of displacement can be obtained from the following equation that is similar to Eq.(20) except that the calculation of $\partial P/\partial d_i$ and $\partial F/\partial d_i$ requires further consideration.

$$\frac{\partial \Delta}{\partial d_i} = K_T^{-1} \cdot \left(\frac{\partial P}{\partial d_i} - \frac{\partial F}{\partial d_i} \right) \quad (30)$$

In the above equation, the first term in parenthesis is indeed the change in the external earthquake forces. Recalling Eq.(1), this may be interpreted in two ways. First, the change in the base shear V , that may occur due to change in the stiffness of the structure, as a result of change in design variables. The second, the change in the vertical distribution factor C_{vx} . However, since in the nonlinear pushover analysis, the load level is invariant of design variables, the sensitivity of lateral load depends on sensitivity of vertical distribution of lateral loads that is a function of parameter k in Eq.(2) and k is given in terms of natural period of the structure. See FEMA356 or ASCE41 in this regard. Therefore, utilizing chain

rule in differentiation, the sensitivity of lateral load distribution becomes as follows:

$$\frac{\partial C_{vx}}{\partial d_i} = \frac{\partial C_{vx}}{\partial k} \cdot \frac{\partial k}{\partial T} \cdot \frac{\partial T}{\partial d_i} \quad (31)$$

If Eq.(24) is used for finding the sensitivity of natural period of the structure, and the change of the mass of the structure due to change in the design variables is ignored, one can easily find:

$$\frac{\partial T}{\partial d_i} = -\frac{T^3}{8\pi^2} \varphi^T \frac{\partial K}{\partial d_i} \varphi \quad (32)$$

The second term in the parenthesis of Eq.(30), however, is the variation of internal forces due to a change in design variable when there is no change in external loads. This is in fact, the main challenge in nonlinear sensitivity analysis. To calculate this quantity, Gong pointed out that internal forces in members are the accumulation of their incremental forces, δF , induced in members during incremental analysis procedure i.e.:

$$\frac{\partial F^n}{\partial d_i} = \sum_{l=1}^n \frac{\partial \delta F}{\partial d_i} = \sum_{l=1}^n \frac{\partial K_T^l}{\partial d_i} \delta \Delta_l \quad (33)$$

Therefore, the sensitivity of internal force can be accumulatively obtained at every load step as follows:

$$\frac{\partial F^n}{\partial d_i} = \frac{\partial F^{n-1}}{\partial d_i} + \frac{\partial K_T^n}{\partial d_i} \delta \Delta_n \quad (34)$$

Noting that K_T^n is the tangential stiffness matrix at iteration n and is an explicit function of plasticity index that in turn is a function of internal forces in members, one can easily calculate the value of $\partial K_T^n / \partial d_i$. Having $\delta \Delta_n$ calculated from analysis at the iteration n, the second term in the right hand side of Eq.(34) is known, and

the value of $\partial F^n / \partial d_i$ can be computed in an accumulative process. It is now sufficient to substitute for $\partial F / \partial d_i$ and $\partial P / \partial d_i$ in Eq.(30) to obtain the sensitivity of displacement vector to change in a design variable.

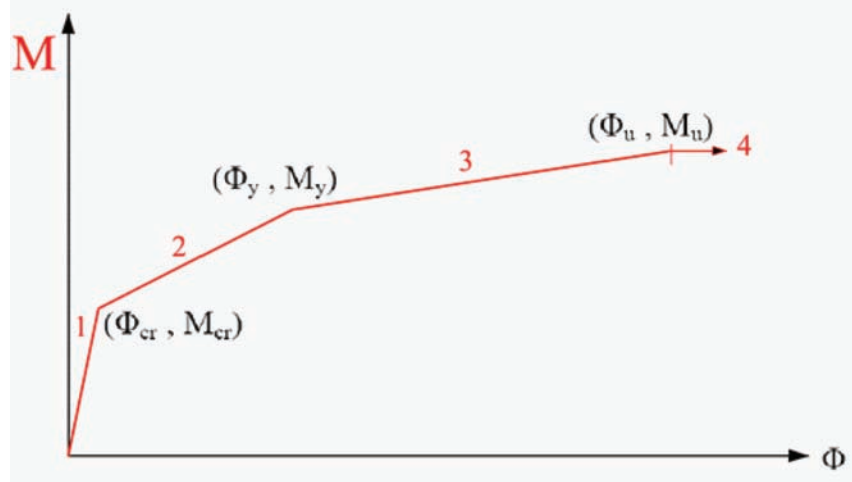
A Sensitivity Analysis procedure for nonlinear reinforced Concrete frame

In this section the sensitivity analysis proposed by Habibi and Moharrami (2010), will be described to show a different sensitivity analysis procedure and emphasize on the fact that formulation of any design sensitivity analysis has to be derived based on assumptions made on the corresponding nonlinear analysis.

As per any nonlinear analysis of structures that requires the stiffness-displacement relation for assembling Eq.(14), and requires force-displacement relation for solution of nonlinear Eq.(14) in the form of Eq.(27), it is necessary to define a nonlinear moment-curvature and a stiffness-curvature relation for concrete structural elements. Habibi adopted a tri-linear moment-curvature relation, proposed by Park and Ang (1985) as shown in Figure 5. This assumption helps to achieve the amount of curvature for a given moment and amount of the moment for a given curvature.

The first line represents the without-crack situation. The second line stands for post-crack to yielding state and the third line corresponds to yield to the ultimate state. With the help of these definitions, the distribution of curvature of a beam under applied loads can be obtained and plotted as per Figure 6a. The distribution of curvature makes it possible to create a nonlinear model at the element level. Park et al. (1987) proposed a nonlinear model for R/C members (used in IDARC software) in which the flexural stiffness in any section is related to its curvature. Since both flexural deformation and flexibility have reciprocal relation with stiffness of element, there will be an analogy between flexibility of the section

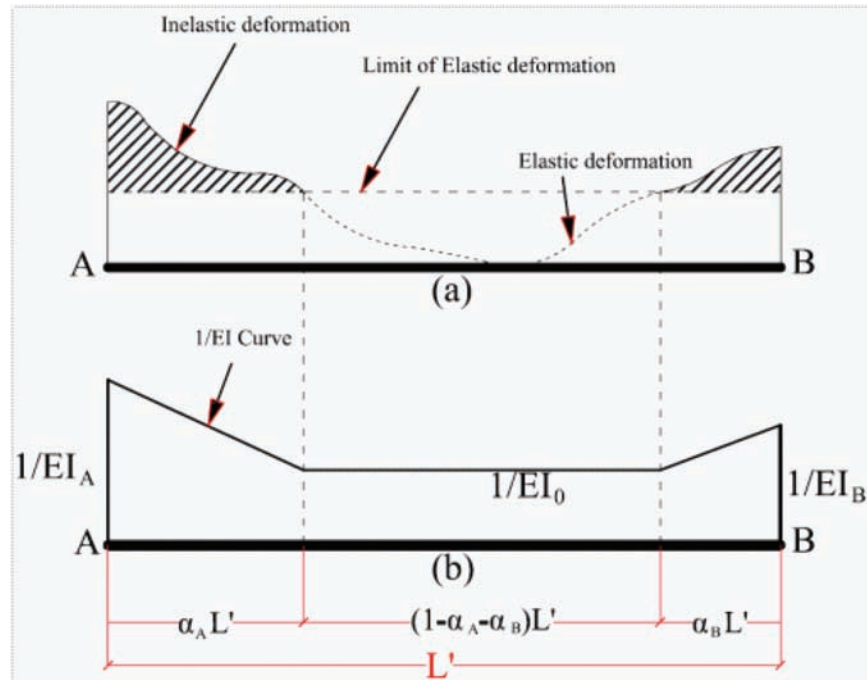
Figure 5. A trilinear moment curvature relation



and its flexural deformation. Accordingly Figure 6b can be considered for the flexibility distribution in the RC elements. In Figure 6b, EI_A and EI_B are the flexural stiffness of the section at end 'A' and end 'B', respectively, and EI_0 is the initial stiffness of the element; α_A and α_B are the yield

penetration coefficients, and L' is the free length of the element. Having α_A and α_B together with EI_A and EI_B , facilitates obtaining the flexibility curve of a member and its corresponding deformation, etc.

Figure 6. (a) Curvature distribution along a RC element, (b) flexibility assumption along a RC element



Habibi and Moharrami (2010) adopted the Park's nonlinear model and modified it to take the axial force into account and formulated the nonlinear stiffness matrix of the nonlinear concrete elements based on these assumptions. For a reinforced concrete frame under gravity and lateral loads, it was assumed that prior to execution of lateral loads, the structure behaves linearly. The nonlinear behavior starts when the lateral loads are applied and increased to a certain level. Similar to nonlinear analysis of steel frames, it is assumed that in the reinforced concrete frame, the unloading does not happen. Habibi (2008) used the Modified Newton Raphson method for nonlinear analysis. In this form of nonlinear analysis, the internal forces in members are obtained using tangential stiffness matrix. At the beginning of every load step, as shown in Figure 3f the tangential stiffness matrix, K^l , is updated, and the displacement vector is obtained assuming an elastic behavior for the structure. With the displacement found, the internal forces in all members are obtained from the following equation and the equilibrium is checked in all nodes.

$$\delta F_e^{l,j} = K_e^l \Delta_e^{j-1} \quad (35)$$

where, Δ_e^{j-1} is the displacement sub-vector for the element at $(j-1)^{th}$ iteration of load step l . Realizing that the internal forces in members at any analysis stage is the sum of increments, the following equation is used.

$$F_e^{l,j} = F_e^{l-1} + \delta F_e^{l,j} \quad (36)$$

If equilibrium is not satisfied in any node, the unbalanced force in the node is calculated and the structure is analyzed for unbalanced forces in all nodes. This gives the increment in the displacement vector. This process is repeated several times until the unbalance forces in all nodes become

negligible. The following equations are used to find the displacement vector in the nonlinear Modified Newton Raphson method.

$$K_T^l \delta \Delta^j = P^l - F^{j-1} \Rightarrow \delta \Delta^j = K_T^{l-1} (P^l - F^{j-1}) \quad (37)$$

$$\Delta^l = \sum_j \delta \Delta^j \quad ; \quad D = \sum_l \Delta^l \quad (38)$$

where, K_T^l is the tangential stiffness matrix at the beginning of load step l ; $\delta \Delta^j$ is the incremental displacement due to the unbalanced force $(P^l - F^{j-1})$ at the j^{th} iteration of the l^{th} load step; Δ^l is the subtotal displacement for the load step l and $D = \sum_l \Delta^l$ is the total displacement for all load steps, up to load level l .

The sensitivity analysis proposed by Habibi and Moharrami (2010) is based on the foregoing nonlinear analysis. Assuming linear behavior during every unbalanced force analysis, the Eq.(37) can be utilized to produce the sensitivity of incremental displacement $\delta \Delta^j$ with respect to any design variable d_i as follows:

$$\frac{\partial \delta \Delta^j}{\partial d_i} = K_T^{l-1} \left(\frac{\partial P^l}{\partial d_i} - \frac{\partial F^{j-1}}{\partial d_i} - \frac{\partial K_T^l}{\partial d_i} \delta \Delta^j \right) \quad (39)$$

Noting that during any load segment, the properties of tangential stiffness matrix and the load level presumably do not change, their derivatives remain unchanged within any load step. Therefore, Eq.(30) can be used during repeated analysis in any particular load segment, and the sensitivity of displacement vector at any level of loading can be obtained as follows:

$$\frac{\partial \Delta^j}{\partial d_i} = \sum_l \frac{\partial \delta \Delta^j}{\partial d_i} = K_T^{l-1} \left(n^l \times \frac{\partial P^l}{\partial d_i} - \sum_l \frac{\partial F^{j-1}}{\partial d_i} - \frac{\partial K_T^l}{\partial d_i} \Delta^j \right) \quad (40)$$

where, n^l is the number of iterations of N-R process at the relative load step l . The sensitivity

$\partial P^I / \partial x_i$ can be calculated based on how it is obtained. For example, if Eq.(1) is used for its calculation, this equation should be differentiated with respect to design variables and Eqs.(31 & 32) should be used. Since we know how to calculate P in terms of design variables, its derivatives may be easily obtained.

The second term in Eq.(40) is derivative of the resultant of internal forces in nodes. It can be calculated by summing up the derivatives of internal forces in elements. The derivatives of internal forces in elements, in turn, can be calculated using Eq.(33) and (34). Note that in Eq.(40), the second term is the derivative of internal forces in the previous iteration, and from Eqs.(35 & 36) it is understood that the internal forces themselves are determined based of deformations of previous loadings.

The third term in the right hand side of Eq.(40), is easily calculated by assembling the derivatives of the stiffness matrix of all elements with respect to any design variable. This is because for any specific amount of deformation, the tangential stiffness matrix can be expressed explicitly, and its derivatives can be obtained accordingly.

Summing up the derivatives of displacements in all load segments, results the derivative of total displacement in a nonlinear force-displacement environment.

Discussion on Sensitivity Analyses

In previous sub-sections, two distinctive sensitivity analyses were briefly described. Here in this section some similarities and dissimilarities of the two methods are discussed to suggest any future research activities in this field.

A common point in these two methods was the fact that the formulation of nonlinear sensitivity analysis in both methods was established based on the nonlinear procedures that were followed for nonlinear analyses. For example, Gong who used an enhanced incremental method similar

to Figure 3a, followed a similar procedure for sensitivity analysis of displacement. On the other hand, Habibi used the modified Newton-Raphson method as shown in Figure 3f. In this method, consideration of unbalanced forces is a must. Therefore, in the establishment of corresponding sensitivity analysis, this matter was taken care of. Another common point in the two sensitivity methods was the fact that sensitivity assessment was obtained through an accumulative calculation process. This is not to say that the sensitivity calculation is an iterative process, but is to say that during the analysis process, some derivatives have to be obtained and summed up for use in sensitivity computation in upcoming stages.

In Gong's method of analysis, a lumped inelasticity was considered, and a plasticity factor was defined to simulate the partial plasticity with rigidity degradation in a semi-rigid connection. This particular model with all its circumstances was exactly used for sensitivity analysis. Obviously the outcome of the sensitivity analysis is consistent with the basic assumptions made. However, in Habibi's nonlinear analysis, a spread plasticity model was adopted for consideration of nonlinear flexibility and nonlinear stiffness characteristics of a concrete beam column. There is no doubt that the corresponding sensitivity analysis procedure is fundamentally different from Gong's method. Another difference between the two methods returns to the method of natural period evaluation. Gong used a Rayleigh method for determination of natural period of the structure while Habibi used the analytical method for evaluation of natural period. Of course, the sensitivity calculations for $\partial T / \partial d_i$ are remarkably different.

As a conclusion, the nonlinear sensitivity analysis formulation has to be built based on adopted nonlinear analysis procedure; otherwise, the results may not be consistent and may result in difficulty in convergence of the optimization algorithm. The similarities and dissimilarities of

the sensitivity procedures may be interpreted in the context of nonlinear analysis procedure.

OPTIMIZATION IN PERFORMANCE-BASED DESIGN

To optimally design a structure, as was already mentioned, the design problem should be expressed mathematically in terms of design variables in the framework of a standard optimization problem, Eq.(15). To express design constraints in its explicit form, Eq.(16) is employed. The derivatives in this equation are obtained from sensitivity analysis. Some examples of sensitivity analysis were discussed. In this section, the general formulation of OPBSD is presented and some, not all, published research works in the field will be described.

General OPBSD Problem

For optimal Performance-based seismic design, the general standard optimization problem can be written in the form seen in Box 1.

In the above formulation, Z is the objective or cost function. C_1 to C_5 are groups of constraints. The superscript p relates to the performance level and np is the number of performance levels. If it is to design a structure for four performance levels, $np=4$. The superscript lp denotes the load

pattern. The load pattern can be different for various levels of risks. It also can be different in a single risk level for different directions. The lateral earthquake load pattern can be either uniform, triangular, exponential, or etc.; FEMA356 recommends the exponential form. To be in the safe side one may use more than one or two load patterns. n_δ , n_θ and n_s are number of stories, number of sections that the plastic rotation has to be controlled, and number of sections for strength check, respectively. δ and $\bar{\delta}$ are inter-story drift and its allowable upper limit. Similarly, θ and $\bar{\theta}$ are plastic rotation and its allowable upper bound. F and S are internal force and strength respectively. DI stands for damage index for any load pattern and performance level; damage index should be less than the pre-specified value \overline{DI}^p .

The constraint group $C1$ and $C2$ are the main constraints in PBS; they control the drift and plastic rotation. The constraint group $C3$ are strength constraints and for higher performance levels, may be considered as secondary performance constraints. The C_4 set of constraints are not used so much. They are optional and stand for limitations on damage index. One may adopt different upper bounds for different performance levels on a certain damage index. The C_5 group of constraints are lower bound and upper bounds for design variables. Obviously some other constraints can be added to the optimization problem. For

Box 1.

$\text{Minimize } Z = C(X)$ $\text{Subject to } \begin{aligned} C_1 : & \quad {}^{lp}\delta_s^p - \bar{\delta}^p \leq o & (s = 1, 2, \dots, n_\delta); (p = 1, \dots, np); (lp = 1, \dots, nlp) \\ C_2 : & \quad {}^{lp}\theta_r^p - \bar{\theta}_r^p \leq o & (r = 1, 2, n_\theta) \\ C_3 : & \quad {}^{lp}F_i^p - S_i^p \leq o & (i = 1, 2, \dots, n_s) \\ C_4 : & \quad {}^{lp}DI^p - \overline{DI}^p \leq o \\ C_5 : & \quad x_j^l - x_j \leq o, \quad x_j - x_j^u \leq o & (j = 1, 2, \dots, n_x) \end{aligned}$	(41)
---	--------

example if it is desired to provide some constraint on protection of equipments and contents in a floor, some constraints such as limits on velocity or acceleration of floors have to be added to the design optimization problem. Evidently the formulation of these particular constraints requires employing a nonlinear dynamic analysis. It is noted that the C_1 , C_2 , C_3 and C_4 group of constraints may be different for various levels of performances, and they all can enter into the optimization problem. The difference between research works on the OPBSD is a consequence of their assumption on the objective function, constraints and the solution procedure. Some examples of recent research works in this ground that utilize the classical optimization algorithms are discussed hereunder. Many other researches have been excluded not because of their scientific value, but because of their weak relation to the subject of this chapter. For example, Ganzerli et al. (2000), who were probably the first that incorporated pushover analysis and the performance-based design concept, used the idea of OPBSD for a one story one bay R/C frame with pushover analysis. They minimized the cost of R/C frame including costs of concrete and reinforcements under plastic rotation constraints at the ends of members. They considered performance constraints at immediate occupancy, and checked for the satisfaction of design conditions in other levels. However, in their publication, there was no sensitivity analysis and no explicit design constraints. Therefore, their work is not presented here in detail.

Example 1

The procedure of OPBSD of reinforced concrete frames suggested by Zou and Chan (2005) is a good example to be presented here. These authors decomposed the optimal design process into two single-criterion phases. The first phase involved an elastic design optimization in which the cost of concrete is minimized subject to elastic spectral displacement constraints due to a minor

earthquake. The second phase involved minimizing the cost of steel reinforcement subject to constraints on inelastic displacements. Pushover analysis was performed based on the assumption that the fundamental mode of vibration was the predominate response and did not change during nonlinear behavior.

The details of the first phase that produces the optimal dimensions of members for minor wind or earthquake loadings was previously addressed by Moharrami (1993) and is not the concern of this chapter. The detail of the second phase, as it is addressed by Zou and Chan, is presented hereunder. To establish a nonlinear analysis procedure, the following assumptions were made for the structural model of reinforced concrete frame.

1. All inelastic deformations occur at the plastic hinges, which are located at the ends of each frame member and, members are perfectly elastic between the plastic hinges.
2. Beam –column connections are rigid zone, and the plastic hinges are assumed to be frictionless and have zero length.

As a requirement for the solution of nonlinear equations of equilibrium, Eq.(14), the authors expressed the pushover displacement in two parts i.e. elastic and plastic (inelastic) displacements.

$$\Delta_j = \Delta_{j,e} + \Delta_{j,p} \quad (42)$$

In Eq.(42), j stands for the story number. Using the principle of virtual load method, $\Delta_{j,e}$ and $\Delta_{j,p}$ can be obtained from Eq.(43) and Eq.(44) respectively. It is to be noted that f_s and m_s are internal forces and moments due to application of a unit load in the direction in question, and F_s and M_s are internal forces due to applied loads.

$$\Delta_{j,e} = \sum_{i=1}^{N_i} \left[\int_0^{L_i} \left(\frac{F_X f_{X,i}}{EA_X} + \frac{F_Y f_{Y,i}}{GA_Y} + \frac{F_Z f_{Z,i}}{GA_Z} + \frac{M_X m_{X,i}}{GI_X} + \frac{M_Y m_{Y,i}}{EI_Y} + \frac{M_Z m_{Z,i}}{EI_X} \right) dx \right] \quad (43)$$

$$\Delta_{j,p} = \sum_{i=1}^{N_i} \left[\sum_{h=1}^2 m_{ph}^0 \theta_{ph} \right]_i \quad (44)$$

Zou and Chan (2005) also adopted the following assumptions for relating the plastic rotation to the moment and reinforcements in the beam and column.

They assumed a bilinear M-θ relation similar to the one shown in Figure (7); accordingly a linear relation, as in Eq.(45), can be found between θ_p , the plastic rotation, and the moment in excess of M_y .

$$\theta_p = \theta_p^U \left(\frac{M - M_y}{M_U - M_y} \right) \quad (45)$$

Zou and Chan assumed $M_U = 1.1M_y$ and could write θ_p as a function of M

Zou and Chan (2005) used an explicit relationship between M_y and reinforcement ratios ρ and ρ' for beams, Eq.(46), and beam-columns, Eq.(47), as follows:

$$M_y = 0.5f_c B J d \left(Jd/3 - d' \right) + f_y B d (d - d') \rho \quad ;$$

$$J = \sqrt{\left(\rho + \rho' \right)^2 n_{sc}^2 + 2 \left(\rho + \rho' \frac{d'}{d} \right) n_{sc}} - \left(\rho + \rho' \right) n_{sc} \quad (46)$$

$$M_y = \frac{f_y B D}{2n_{sc}} \cdot \left(\frac{D}{2} - \frac{Jd}{3} \right) \cdot \frac{J^2}{1-J} + \frac{f_y B d (d - d')^2}{2d} \cdot \frac{\rho}{1-J} \quad ;$$

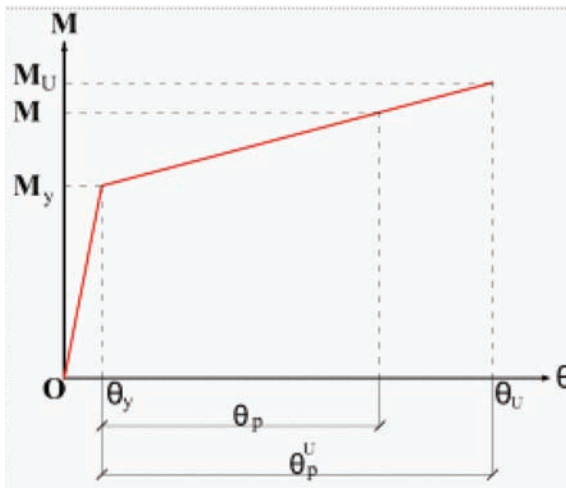
$$J = - \left(2\rho + \frac{F_x}{f_y B d} \right) n_{sc} + \sqrt{\left(2\rho + \frac{F_x}{f_y B d} \right)^2 n_{sc}^2 + 2n_{sc} \left(\rho \frac{D}{d} + \frac{F_x}{f_y B d} \right)} \quad (47)$$

in which n_{sc} is the ratio of modules of elasticity of steel, E_s and concrete E_c . ρ and ρ' are the ratios of reinforcements in tensile and compression zone of concrete beam. Zou and Chan (2005) assumed that ρ and ρ' are linearly dependent to each other. They were assumed equal in columns.

They expressed the relationship between plastic rotation and reinforcement ratios by second order Taylor series expansion as follows:

$$\theta_p(\rho) = \theta_p(\rho^0) + \frac{\partial \theta_p(\rho^0)}{\partial \rho} (\rho - \rho^0) + \frac{1}{2} \frac{\partial^2 \theta_p(\rho^0)}{\partial \rho^2} (\rho - \rho^0)^2 \quad (48)$$

Figure 7. A bilinear M-θ relation



To find the derivatives of θ_p with respect to design variables it is noted that Eqs.(46 and 47) provide explicit relation between M and ρ . Therefore, using Eq.(45) θ_p can be expressed in terms of ρ and the derivatives can be easily obtained. Substituting θ_p from Eq.(48) into Eq.(44) and utilizing chain rule in differentiating, produces an explicit relation between pushover displacement and reinforcement ratios.

$$\Delta_j(\rho_i) = \Delta_j(\rho_i^0) + \sum_{i=1}^{N_i} \frac{\partial \Delta_j(\rho_i^0)}{\partial \rho_i} (\rho_i - \rho_i^0) + \frac{1}{2} \sum_{i=1}^{N_i} \frac{\partial^2 \Delta_j(\rho_i^0)}{\partial \rho_i^2} (\rho_i - \rho_i^0)^2 \quad (49)$$

Upon establishing the explicit formulation of the inelastic displacement, Eq. (49), Zou and Chan could explicitly write the optimization problem of minimizing the steel construction cost of a multistory RC building with drift constraints in terms of the design variables, ρ_i .

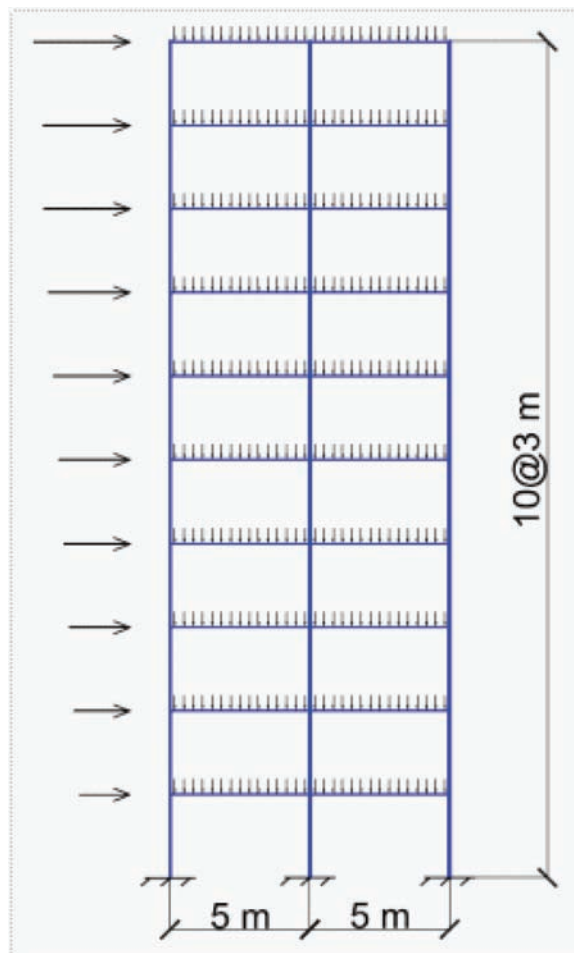
In Zou and Chan's study (2005), since the dimensions of frame elements were fixed, the objective function of the OPBSD problem W_s was the volume or weight of reinforcements. The drift constraints were written in terms of design variables, ρ , in the form of quadratic functions at the target displacement. The design optimization problem became in Box 2. Where d_j^U is the upper limit on story drift and ψ_{1i} and ψ_{2i} are first and second derivatives of differential displacement $\delta\Delta_j$ with respect to ρ . They are expressed in terms of two end moments and first and second derivatives of plastic hinge rotations, θ , with respect to ρ . (See Zou and Chan 2005).

The above optimization problem was solved utilizing Optimality Criteria method for a ten story 2D frame of Figure (8), in which, the concrete cylinder strength and steel reinforcement yield strength, f_y , for all members were assumed to be 20 and 335 MPa, respectively.

The problem was solved for two different gravity loads, to show the effect of axial force on the pushover performance and capacity of framework. The followings have been reported as the outcome of design optimization process.

In the load Case A, the gravity is 30 kN/m while that of Case B is 10 kN/m. The results show that, as expected, more reinforcements are required for the beams in Case A relative to Case B. This is because the gravity forces have more influence on bending moment of beams compared to columns. For columns, the situation is somehow different. Most of columns in Case B required more reinforcement in comparison to Case A and there were more plastic hinges in columns of Case B compared to A. This might be because the gravity forces have a reverse effect compared to lateral

Figure 8. The ten story reinforced concrete frame, Example 1



loads on tensile reinforcement of columns. After design optimization, there were 45 plastic hinges in Case A while there were 55 plastic hinges in Case B. The distribution of plastic hinges was albeit different in the two Cases. Overall, the reinforcement in Case B was more than Case A.

Example 2

As the second example consider the three story 2D frame in Figure (9) that was studied by Xu et al. (2006).

Box 2.

Minimize	$F(\rho_i) = \sum_{i=1}^{N_i} W_{si} \rho_i$
Subject to :	$g_j(\rho_i) = \frac{1}{h_j} \left[\delta \Delta_j(\rho^0) + \sum_{i=1}^{N_i} \Psi_{1i} \times (\rho_i - \rho_i^0) + \frac{1}{2} \sum_{i=1}^{N_i} \Psi_{2i} \times (\rho_i - \rho_i^0)^2 \right] \leq d_j^U \quad j = 1, 2, 3, \dots, N_j$ $\rho_i^L \leq \rho_i \leq \rho_i^U \quad i = 1, 2, 3, \dots, N_i$

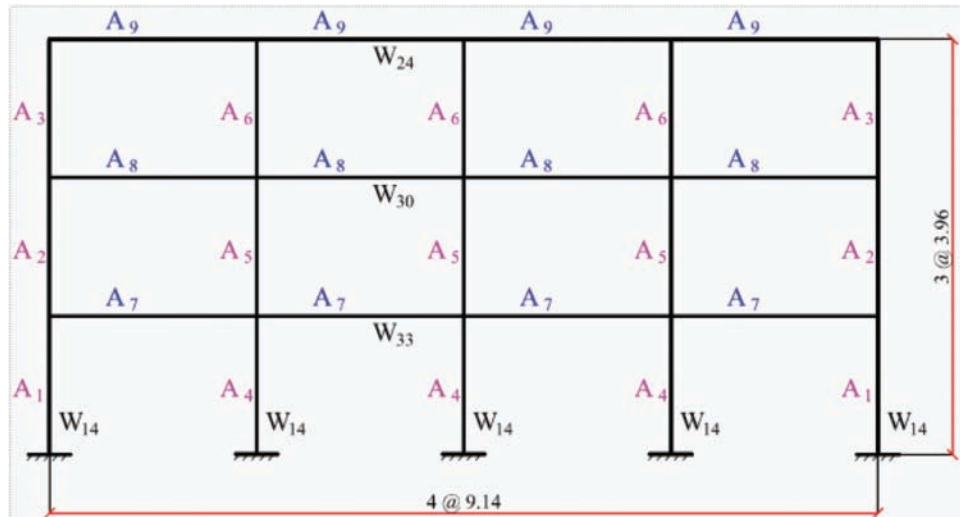
To optimize the design of this frame under applied earthquake load, Xu et al. (2006) considered a combination of two objective functions for this example. The first is F_1 , a measure of weight of the structure, and the second is F_2 , a measure of uniformity of distribution of relative drift (see Box 3).

In Eq.(51), Δ and H stand for lateral displacement and height, respectively; r and s represent the roof and story; A_i^U is the upper bound of area A_i of member i . ω_1 and ω_2 are named combination factors, and for this example they were taken $\omega_1=0.95$ and $\omega_2=0.05$. The first objective function, F_1 , is an explicit function of design variables, A , while the second objective function, F_2 , is an implicit function of design variables. Xu et al.

used one set of constraints, C_1 , in Eq.(41). The constraints of group C_3 as well as C_5 , were treated as side constraints; i.e. they were checked after analysis; if they were violated, the design was scaled via a proper way.

The pushover analysis of Hasan (2002) was used for determining the displacements under applied earthquake load at IO, LS and CP levels. To express the objective function explicitly in terms of design variables, as a requirement of Eq.(16), the derivative of F_2 had to be calculated using a proper sensitivity analysis technique. Xu et al. (2006) realized that a better approximation can be obtained using reciprocal variables. Accordingly, they reformulated the problem in terms of reciprocal variables and used the sensitivity analysis technique of Gong (2003), i.e. Eq.(30) for the

Figure 9. A three story four bay moment frame, (Xu et al. 2006)



Box 3.

$$F = \omega_1 F_1 + \omega_2 F_2 \quad ; \quad F_1(x) = \frac{\sum_{i=1}^n \rho L_i A_i}{\sum_{i=1}^n \rho L_i A_i^U} \quad ; \quad F_2(x) = \frac{1}{ns} \sum_{s=1}^{ns-1} \left(\frac{\Delta_s / H_s}{\Delta_r / H_r} - 1 \right)^2 \quad (51)$$

sensitivity calculations. Having the optimization problem fully defined, it was solved by the Dual method by Fleury (1983). Table 3 shows some of the history of the change in design variables during the optimization process.

Table 4 shows how the drift ratio for different performance levels varied during the optimization history.

The most critical constraint was satisfied with a response ratio of 1. The plastic states of the optimal design corresponding to the LS and CP

Table 3. Example 2: primary design variable results (Xu et al. 2006)

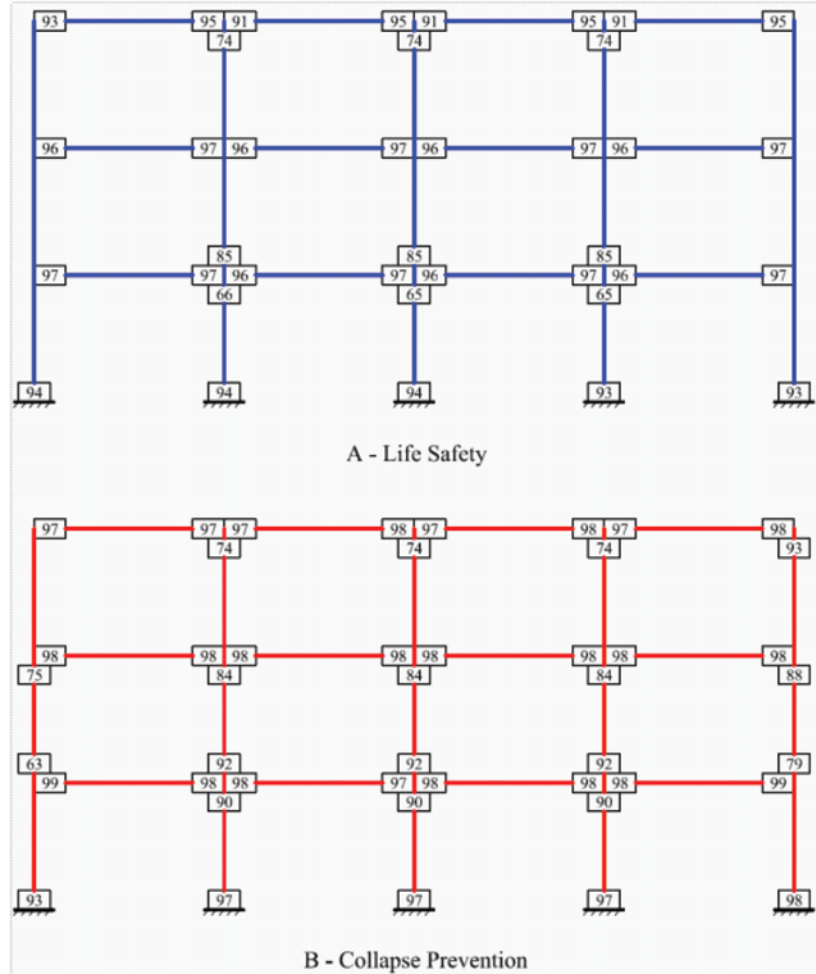
Cycle	A_1	A_2	A_3	A_4	A_5	A_6	A_7	A_8	A_9
index	(mm ²)								
1	152.900	152.900	152.900	152.900	152.900	152.900	67.100	90.320	92.900
4	67.440	49.605	42.595	74.970	71.835	59.624	35.095	37.093	26.600
7	55.460	38.210	32.100	64.115	63.030	49.960	30.985	30.465	19.880
10	50.010	34.460	29.860	57.820	61.250	49.850	29.825	27.680	17.870
Discrete	48.770	33.420	33.420	58.970	65.160	48.770	31.930	28.060	17.900
Design	W14×257	W14×176	W14×176	W14×311	W14×342	W14×257	W33×169	W30×148	W24×94

Table 4. Design history for critical drift, objective functions f_1 and F_2 (Xu et al. 2006)

Design Cycles		Δ/H Overall (roof) drift δ_s/h_s Critical story drift			Structural Weight/ W_{max}	Ductility Demand	
		IO	LS	CP	(f1)	(f2)	
1	{}	0.0020	0.0027	0.0042	1.000	0.067	
		0.0024 [2] [‡]	0.0033 [2]	0.0051 [2]			
4	{}	0.0058	0.0078	0.0162	0.402	0.045	
		0.0067 [2]	0.0089 [2]	0.0188 [2]			
7	{}	0.0067	0.0087	0.0305	0.333	0.037	
		0.0075 [2]	0.0098 [2]	0.0349 [2]			
10	{}	0.0070	0.0091	0.0476	0.311	0.026	
		0.0077 [3]	0.0101 [3]	0.0510 [2]			
Discrete design		0.0069	0.0090	0.0456	0.319	0.022	
		0.0078 [3]	0.0102 [3]	0.0481 [2]			

[‡] The numbers in brackets show the critical story.

Figure 10. Structural plastification: A) At LS level, B) At CP level, (Xu et al. 2006)



performance levels _i.e., 2.5% and 5% roof drift can be compared in Figure 10A and figure 10B, respectively.

Example 3

Habibi (2008) whose method of nonlinear analysis and nonlinear sensitivity analysis were discussed earlier, formulated the OPBSD of reinforced concrete frame of example 1, a ten story two bay RC frame, in the form of the standard design optimization problem of Eq.(41). He wrote his own optimization software named CONOPT. This

computer program utilizes the CONLIN optimization algorithm with some modifications made.

Habibi optimized the example 1, with CONOPT software, for several design assumptions. In his design optimization formulation, the dimensions of beams, columns as well as reinforcement ratios, were chosen as design variables; i.e. he nearly doubled the design variables and significantly increased the number of design constraints because of considering almost all groups of constraints in Eq.(41). He even entered the voluntary constraints of damage index into the design optimization problem. He used the stiffness degradation index (DI) = $1 - (k_j / k_{OP})$

suggested by Ghobarah (1999) as a damage index. He suggested and applied different damage indices for different performance levels. To investigate the effectiveness of design optimization algorithm, Habibi first assumed the same dimensions for frame elements that Zou and Chan had considered in their second phase optimization. The results were compared to the results of Zou-Chan and Asadi (2006) who optimized the same RC frame.

It worth to mention that Asadi sought the *uniform inter-story drift* for his measure of optimality of design, and similar to Zou and Chan assumed that distribution of rebars in R/C frames has a substantial effect on the drift control. Therefore, considering fixed values for dimensions of frame members and variable reinforcement, he indeed chose the same design variables as Zou and Chan's but followed different design objective.

As an alternative design optimization, Habibi considered variable dimensions and considered the cost of formwork in addition to the cost of concrete and reinforcement. As a general rule, when the number of design variables increases, a more optimal design can be achieved. On the other hand, when the number of constraints increase, the cost function increases. Obviously Habibi could reduce the cost of material used in trade of more computational effort. Table 5 shows the comparison of the results.

To see what happens to performance point, the demand and capacity spectra have to be drawn after completion of design optimization. Evi-

dently the target point displaces from the initial point. Corresponding curves to Zou and Chan is shown in Figure 11-a while that of Habibi is in Figure 11-b.

This figure shows that in both solutions, the spectral accelerations and consequently the base shears have increased and corresponding target point or spectral displacements have been decreased. In the automated performance design, it is possible to impose any constraint on behavior of the structure. Here in this example the drift has been limited to 1% in both solution strategies. In both studies while the initial designs pertained to more expensive cost, they included some violated constraint but the optimal designs not only reduced the cost, but also satisfied all drift constraint. In fact, this is the advantage of automated optimum design that reduces the cost while satisfies user-defined conditions/constraints.

FUTURE RESEARCH DIRECTIONS

As was stated earlier, the trend of design philosophy is towards performance-based design. The second and third examples, especially the comparison of the results from the first and the third example, clearly showed that to design a structure for several performance levels simultaneously, there is no way other than optimization. In fact, optimization puts the design problem in a mathematical framework and solves the design

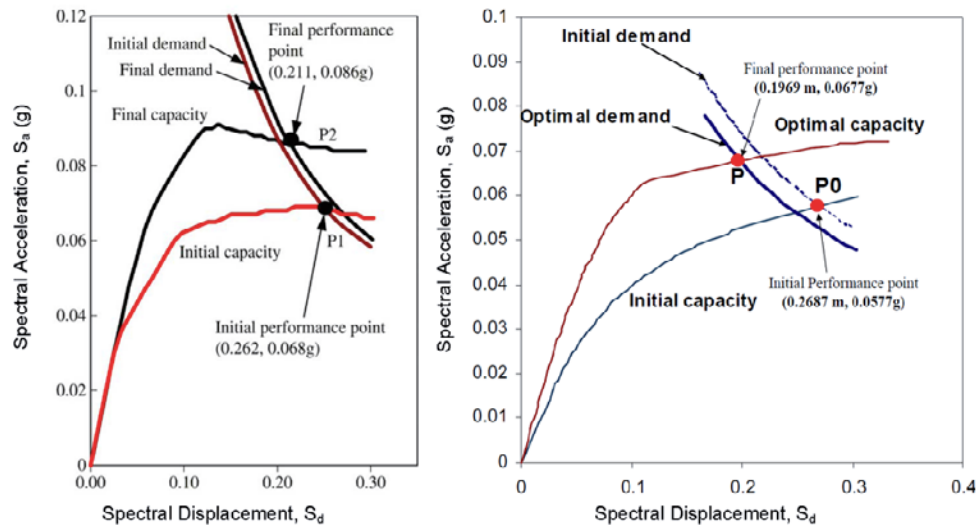
Table 5. Cost of initial and optimal design of ten story frame

Cost basis (US\$)	Initial Design	Optimal Design			
		OC [†]	UD [‡]	CONOPT (Fixed Dimensions)	CONOPT (Variable Dimensions)
Reinforcement	3386	3956	3204	2972	2333
Concrete +Formwork	3558	3558	3558	3558	3382
Total	6994	7515	6762	6530	5722

[†] Optimality Criteria algorithm used by Zou and Chan (2005)

[‡] Uniform Ductility distribution criterion by Asadi (2006)

Figure 11. The initial and final (optimal) target point. a)Zou and Chan(2005), used with permission, b)Habibi



problem mathematically. When we need simultaneous solution of a number of equalities and inequalities one way is to satisfy equalities and check for inequalities. This is the common practice in design offices. The design engineers satisfy equilibrium equalities and check for acceptance criteria inequalities for a structure. Another way to solve the set of equalities and inequalities is to get assisted by mathematics. The design optimization is this second way. Design optimization helps the designer to design a structure in such a way that not only satisfies the equilibrium and acceptance criteria but also reduces the cost. In this methodology, the designer is allowed to put all self-interested conditions among the constraints. Albeit, the constraint limits require experience to be determined realistically. It is the responsibility of all Engineering faculties to consider the design optimization as a highly vital subject and put it among the obligatory courses. This will help more understanding about this subject and provides the ground for more developments in the field.

The OPBSD has a bright future. This methodology can be used as a powerful robust tool for scientist engineers, to revise their suggestions on acceptance criteria based on correlations that may be discovered between several aspects of optimally designed structures. For example, a design engineer may have queries on the specification of a good design so as to have proper energy dissipation, limited plastic rotations in connections, controlled relative drift, comfort of occupants, etc. These questions may be answered by a massive research on different types of optimally designed structure including different objectives and constraints. This tool may be also used to discover the controversy of different outcomes for different design criteria.

Preparing the ground for application of OPBSD can be followed in several directions:

- A. Enhancing the knowledge on the material nonlinearity models for better predicting the response of a structure.

- B. Improving the nonlinear analysis and corresponding sensitivity analysis procedures.
- C. Developing more efficient optimization algorithms.
- D. Rationalizing acceptance criteria and correlating them to structure's overall behaviour with the help of OPBSD.
- E. Developing optimal performance-based seismic design criteria applicable in combination with nonlinear dynamic analysis
- F. Establishing relations between expected values of the response and performance indicators, estimated by means of refined models of the system with those estimated with the aid of structural analysis and design ordinarily applied in typical structural design practice.

CONCLUSION

In this chapter, performance-based design and its prerequisites were briefly introduced. Due to shortage of space, and wideness of the field, we could only point to titles of the related subjects. However, this chapter provides a ground for more deep studies in the subject for the interested reader. The performance-based design philosophy and corresponding practical procedures were explained on the whole, to provide an overview of what is going on in design offices. The goal of design optimization and its application to some design problems was briefly presented. The sensitivity calculation that is an essential task in practical design optimization was explained. It was shown how nonlinear sensitivity calculation has to be built on nonlinear analysis assumptions and procedure. Some examples of the research activities in the field of Optimum Performance-Based Seismic Design were presented, and various aspects of this progressing desire were discussed within the description of examples. The aim of the author was to help the interested reader to obtain an overall understanding of the subject,

such that he/she could begin to write his own computer program for OPBSD. The start points for different parts of an OPBSD program including the knowledge for starting performance-based design, nonlinear analysis, formulation of design optimization problem and sensitivity analysis were clearly introduced. The algorithms of optimization, although were particularly relevant to the subject of this chapter, were not explained much because of shortage of space; however, some useful references were introduced. If the interested reader establishes his own performance-based design optimization problem, its solution may be facilitated by one of available optimization software.

REFERENCES

- Arora, J. S. (2004). *Introduction to optimum design*. San Diego, CA: Elsevier Academic Press.
- Arora, J. S., & Haug, E. J. (1979). Methods of design sensitivity analysis in structural optimization. *AIAA Journal*, 17(9), 970–974. doi:10.2514/3.61260
- Asadi, P. (2006) *Optimization of distribution of reinforcement in the seismic design of R/C frames*. MSc. Thesis Civil Eng. Dept., Sharif University of Technology.
- ASCE. (2007). *Seismic rehabilitation of existing buildings* (pp. 41–06). Reston, VA: ASCE Publications.
- Aschheim, M. (1999). Yield point spectra: A simple alternative to the capacity spectrum method. *SEAOC 1999 Convention*, (pp. 373-379).
- Basset, S., & Jezequel, L. (2007). Optimization of structural dynamic behaviour based on effective modal parameters. *International Journal for Numerical Methods in Engineering*, 70(5), 523–542. doi:10.1002/nme.1890

- Chen, J., Che, J., Sun, H., Ma, H., & Cui, M. (2002). Structural dynamic optimization with probability constraints of frequency and mode. *Structural Engineering & Mechanics*, 13(5), 479–490.
- Cornell, A. C. (2008). Uncertainty propagation in probabilistic seismic loss estimation. *Structural Safety*, 30(3), 236–252. doi:10.1016/j.strusafe.2006.11.003
- Crisfield, M. A. (2000). *Non-linear finite element analysis of solids and structures, Vol. 1: Essentials; Vol. 2: Advanced topics*. New York, NY: John Wiley & Sons.
- De Donato, O. (1977). Fundamentals of elastic-plastic analysis. In Cohn, M. Z., & Maier, G. (Eds.), *Engineering plasticity by mathematical programming* (pp. 325–349). New York, NY: Pergamon Press.
- Esteva, L., López, O. D., & Hernández, E. I. (2010). Seismic vulnerability functions of multi-story buildings: estimation and applications. *Structure and Infrastructure Engineering Special Issue: Vulnerability Assessment of Structures and Infrastructures*, 6(1-2), 3–16.
- Fajfar, P. (2000). A nonlinear analysis method for performance-based seismic design. *Earthquake Spectra*, 16(3), 573–599. doi:10.1193/1.1586128
- FEMA. 356. (2000). *Prestandard and Commentary for the seismic rehabilitation of buildings*. Reston, VA: ASCE Publications.
- Fleury, C. (1983). Dual methods for optimizing finite element flexural systems. *Computer Methods in Applied Mechanics and Engineering*, 37(3), 249–275. doi:10.1016/0045-7825(83)90078-6
- Fleury, C. (1989). CONLIN: An efficient dual optimizer based on convex approximation concepts. *Structural Optimization*, 1(2), 81–89. doi:10.1007/BF01637664
- Fragiadakis, M., & Lagaros, N. D. (2011). An overview to structural seismic design optimisation frameworks. *Computers & Structures*, 89(11-12), 1155–1165. doi:10.1016/j.compstruc.2010.10.021
- Frangopol, D. M. (2011). Life-cycle performance, management, and optimisation of structural systems under uncertainty: Accomplishments and challenges. *Structure and Infrastructure Engineering*, 7(6), 389–413. doi:10.1080/15732471003594427
- Ganzerli, S., Pantelides, C. P., & Reaveley, L. D. (2000). Performance-based design using structural optimization. *Earthquake Engineering & Structural Dynamics*, 29(11), 1677–1690. doi:10.1002/1096-9845(200011)29:11<1677::AID-EQE986>3.0.CO;2-N
- Ghobarah, A. (2001). Performance-based design in earthquake engineering: State of development. *Journal of Engineering Structures*, 23(8), 878–884. doi:10.1016/S0141-0296(01)00036-0
- Ghobarah, A., Abou-Elfath, H., & Biddah, A. (1999). Response-based damage assessment of structures. *Earthquake Engineering & Structural Dynamics*, 28(1), 79–104. doi:10.1002/(SICI)1096-9845(199901)28:1<79::AID-EQE805>3.0.CO;2-J
- Gong, Y. (2003). *Performance-based design of steel building frameworks under seismic loading*. PhD Thesis, University of Waterloo, Ontario, Canada, 2003.
- Habibi, A. (2008). *Optimal seismic performance-based design of 2D reinforced concrete frames*. Doctoral dissertation, Tarbiat Modares University, Tehran, Iran.
- Habibi, A., & Moharrami, H. (2010). Nonlinear sensitivity analysis of reinforced concrete frames. *Finite Elements in Analysis and Design*, 46(7), 571–584. doi:10.1016/j.finel.2010.02.005

- Haftka, R. T., & Gurdal, Z. (1992). *Elements of structural optimization*. Norwell, MA: Kluwer Academic Publishers.
- Hasan, R., Xu, L., & Grierson, D. E. (2002). Push-over analysis for performance-based seismic design. *Computers & Structures*, 80(31), 2483–2493. doi:10.1016/S0045-7949(02)00212-2
- Jalayer, F., & Cornell, C. A. (2009). Alternative non-linear demand estimation methods for probability-based seismic assessments. *Earthquake Engineering & Structural Dynamics*, 38(8), 951–972. doi:10.1002/eqe.876
- Kim, Y.-I., & Park, G. J. (2010). Nonlinear dynamic response structural optimization using equivalent static loads. *Computer Methods in Applied Mechanics and Engineering*, 199(9-12), 660–676. doi:10.1016/j.cma.2009.10.014
- Lagaros, N. D., Garavelas, A. T., & Papadrakakis, M. (2008). Innovative seismic design optimization with reliability constraints. *Computer Methods in Applied Mechanics and Engineering*, 198(1), 28–41. doi:10.1016/j.cma.2007.12.025
- Masson, G., Cogan, S., Bouhaddi, N., Lombard, J. P., & Bonini, J. (2002). Parameterized reduced models for efficient optimization of structural dynamic behavior. *Collection of Technical Papers - AIAA/ASME/ASCE/AHS/ASC Structures, Structural Dynamics and Materials Conference*, (pp. 1434-1440).
- Mills-Curran, W. C., & Schmit, L. A. (1985). Structural optimization with dynamic behaviour constraints. *AIAA Journal*, 23(1), 132–138. doi:10.2514/3.8881
- Moharrami, H. (1993). *Design optimization of reinforced concrete frameworks*. Ph.D. Thesis, The University of Waterloo, Waterloo, Ontario, Canada
- Moharrami, H. (2006). *Optimality criteria: A robust nonlinear optimization algorithm*. The 7th International Congress on Civil Engineering, Tarbiat Modarres University, Tehran, Iran.
- Moharrami, H., & Alavinab, A. (2006). An optimization procedure for automated design of seismic resistant steel frames. *International Journal of Civil Engineering*, 4(2), 86–105.
- Owen, D. R. J., & Hinton, E. (1980). *Finite elements in plasticity- Theory and practice*. Swansea, UK: Pineridge Press.
- Park, G. J., & Kang, B. S. (2003). Validation of a structural optimization algorithm transforming dynamic loads into equivalent static loads. *Journal of Optimization Theory and Applications*, 118(1), 191–200. doi:10.1023/A:1024799727258
- Park, K. J., Lee, J. N., & Park, G. J. (2005). Structural shape optimization using equivalent static loads transformed from dynamic loads. *International Journal for Numerical Methods in Engineering*, 63(4), 589–602. doi:10.1002/nme.1295
- Park, Y. J., & Ang, A. H. S. (1985). Mechanistic seismic damage model for reinforced concrete. *Journal of Structural Engineering*, 111(4), 722–739. doi:10.1061/(ASCE)0733-9445(1985)111:4(722)
- Park, Y. J., Reinhorn, A. M., & Kunnath, S. K. (1987). *IDARC: Inelastic damage analysis of frame shear-wall structures*. Technical Report NCEER-87-0008, National Center for Earthquake Engineering Research, State University of New York at Buffalo.
- Priestley, M. J. N., Calvi, G. M., & Kowalsky, M. J. (2007). *Displacement-based seismic design of structures*. Pavia, Italy: IUSS Press.

- Saka, M. P. (1997). The theorems of structural variation for grillage systems. In Topping, B. H. V., & Leeming, M. B. (Eds.), *Innovation in computer methods for civil and structural engineering* (pp. 101–111). Edinburgh, UK: Civil Comp Press. doi:10.4203/ccp.50.8.2
- Tangaramvong, S., & Tin Loi, F. (2011). Mathematical programming approaches for the safety assessment of semirigid elastoplastic frames. *International Journal of Solids and Structures*, 48(6), 1011–1023. doi:10.1016/j.ijsolstr.2010.12.003
- Vanderplaats, G. M. (1997). *DOT user's manual*. Colorado Springs, CO: VMA.
- Xu, L., Gong, Y., & Grierson, D. E. (2006). Seismic design optimization of steel building frameworks. *Journal of Structural Engineering*, 132(2), 277–286. doi:10.1061/(ASCE)0733-9445(2006)132:2(277)
- Zou, X. K., & Chan, C. M. (2005). Optimal seismic performance-based design of reinforced concrete buildings using nonlinear pushover analysis. *Engineering Structures*, 27(8), 1289–1302. doi:10.1016/j.engstruct.2005.04.001

ENDNOTE

- ¹ Federal Emergency Management Agency (FEMA) of USA

Chapter 9

Optimal Seismic Performance-Based Design of Reinforced Concrete Buildings

Xiao-Kang Zou

AECOM Asia Company Ltd., Hong Kong

ABSTRACT

In order to meet the emerging trend of the performance-based design approach and to improve the design efficiency, this chapter presents a numerical optimization technique for both minimum material cost and life-cycle cost design of building structures subject to multiple levels of linear elastic and nonlinear elastic seismic drift performance design constraints. This chapter firstly introduces an elastic seismic drift design of reinforced concrete (RC) building structures based on elastic response spectrum analysis method; and then presents the inelastic design optimization based on the nonlinear pushover analysis method. Finally, the optimal seismic performance-based design of RC buildings is posed as a multi-objective optimization problem in which the life-cycle cost of a building is to be minimised subject to multiple levels of seismic performance design criteria. The computer based optimization methodology developed provides a powerful numerical design tool for performance-based design of RC building structures.

1. INTRODUCTION

The concept of performance-based design appears to be the future direction of seismic design codes (SEAOC 1995; ATC-40 1996; FEMA 356 2000; FEMA 440 2005; FEMA 445 2006; ASCE41 2007). According to the newly developed performance-based seismic design approach, an acceptability analysis needs to be conducted at various design load levels in order to ensure that the corresponding performance objectives are

satisfactory. The acceptability checking procedures may employ various linear or nonlinear analysis methods to assess the seismic responses of structures in relation to the acceptable design criteria. Response spectrum analysis, which is one of the most common linear elastic methods, provides designers with a simple but rational basis for determining the responses of structures under minor or moderate earthquake loading. In the advent of advanced computational techniques, nonlinear analysis procedures become

DOI: 10.4018/978-1-4666-1640-0.ch009

significantly necessary to identify the pattern and level of damage and to understand the modes of failure of structures during severe seismic events. In assessing the nonlinear seismic behaviour of framework structures, pushover analysis has provided an effective means for distinguishing between good and bad seismic performance of structures (Krawinkler 1994).

It has been recognized that the displacement or lateral drift performance of a multi-story building can be a good measure of structural and non-structural damage of the building under various levels of earthquake motions (Moehle and Mahin 1991). The performance-based seismic design provisions for multi-story buildings can be based upon controlling story drifts to prescribed limit states under different design levels of earthquakes. Lateral drift design requires the consideration of a proper distribution of the stiffness of all structural elements and, in a severe seismic event, also the occurrence and redistribution of plasticity in structure elements.

Numerous studies on structural optimization in the seismic design of structures have been published in the past two decades, including Cheng and Botkin (1976), Feng et al. (1977), Bhatti and Pister (1981), Balling et al. (1983), Cheng and Truman (1982), Arora (1999). However, most of these previous research efforts were concerned with optimization through prescriptive-based design concepts. Recently, Beck and his associates (1998) developed an optimization methodology for performance-based design of structural systems operating in an uncertain dynamic environment. Foley (2002) provided a comprehensive literature review of current state-of-the-art seismic performance-based design procedures and presented a vision for the development of performance-based design optimization. It has been recognized that there is a pressing need for developing optimized performance-based design procedures for seismic engineering of structures

(Charney 2000; Foley 2002). Zou (2002), Chan and Zou (2004), Zou and Chan (2001, 2005a, b), Zou et al (2007a, b), Zou (2008), Wang et al (2010) and Zou et al (2010) had been working at the performance-based seismic design optimization of RC building structure and developed an effective method for design optimization of buildings subject to seismic elastic and inelastic seismic drift performance criteria.

The traditional prescriptive design optimization based on linear elastic techniques has been researched for many years. One major drawback of these elastic techniques is that it does not directly address structural inelastic seismic responses and thus cannot effectively deal with damage loss due to structural and non-structural failure during earthquakes. As a result, the long-term risk and benefit implications cannot be assessed using the traditional linear elastic design method. In seismic performance-based design, the design objective function may consist of two main parts: initial construction cost and expected future failure loss caused by earthquakes (SEAOC 1995; Foley 2002). The final design should be established considering a good balance between the initial structural cost and its loss expectation in the design life period. Due to the fact that the life-cycle cost involves the consideration of construction cost and damage loss which are inherently conflicting, the minimum life-cycle cost design can be viewed as a multi-objective optimization problem. Given with the initial conditions of a building project, it is, in general, a relatively easy task to estimate the construction cost of the building. However, the estimation of the seismic damage to a building is such a complex problem that it involves not only engineering cost but also costs associated with social, economic, political, cultural and ethical aspects. A number of different damage loss models, established by numerous researchers (Park and Ang 1985; Gao and Bao 1985; Park et al. 1987; Ang et al. 1997; Wen and Kang 1997, 2001), in-

volve realistic modelling of loading and resistance uncertainty, initial construction cost, damage cost, failure consequence cost, maintenance cost and discount cost of distant future failure. Cheng and Chang (1988), Cheng and Li (1997), Li (1998) and Zou et al (2007b) studied the application of minimum expected life-cycle cost. Recently, Liu et al. (2003) presented a multi-objective genetic algorithm for optimal seismic design of steel frames based on life cycle cost considerations. All these research efforts indicate the importance of consideration of a life-cycle cost on making rational design decisions.

This chapter presents an effective single- or multi-objective optimization technique for the elastic and inelastic seismic drift performance design of reinforced concrete buildings under response spectrum loading and pushover loading. Using the principle of virtual work, the modal drift response can be explicitly formulated in terms of element sizing variables and the peak drift values can be estimated by modal combination methods. With careful tracking of the location and extent of plastic hinge occurrence, the inelastic pushover drift can also be explicitly expressed in terms of the sizing variables using the same principle of virtual work and the Taylor series approximation. The total life-cycle cost optimization is formulated as a multi-objective optimization problem subject to seismic inelastic inter-story drift responses under pushover loading. Once the multi-objective function (including both the initial material cost and the predicted damage loss) and the design performance constraints are explicitly formulated, the ϵ -constraint method is then applied to produce a Pareto optimal set, from which the decision of the best compromise solution for the multi-objective design problem can be achieved. The optimization methodology for each Pareto optimal solution is basically established based on a rigorously derived Optimality Criteria (OC) approach. Finally, one RC building frame example is presented to illustrate the effectiveness and applicability of the proposed automated optimization approaches.

2. SINGLE OBJECTIVE DESIGN OPTIMIZATION PROBLEM

In seismic design, it is commonly assumed that a building behaves linearly elastic under minor earthquakes and may work nonlinearly inelastic when subjected to moderate and severe earthquakes. Under such an assumption, the entire design optimization process can therefore be decomposed into two phases (Zou and Chan 2001; Zou 2002). The first phase is an elastic design optimization in which the structural concrete cost can be minimized subject to elastic spectral drift responses under minor earthquake loading; and concrete member sizes are taken as design variables since concrete material plays a more dominant role in improving elastic drift performance of a building. In this phase, all concrete sections are assumed to be uncracked and to behave linear- elastically. Once the optimal structural member sizes are determined at the end of the first phase of the optimization, the steel reinforcement quantities can then be considered as design variables in the second phase. In controlling the inelastic drift responses, steel reinforcement is the most effective element that provides the ductility of RC building structure beyond first yielding (Zou 2002). In this second design phase or the so-called inelastic design optimization, the member sizes are kept unchanged and the cost of steel reinforcement is minimized subject to inelastic inter-story drift performance constraints based on nonlinear pushover analysis.

2.1 First Phase: Elastic Design Optimization Problem

Consider a multi-story concrete framework having $i = 1, 2, \dots, N$ member (or member fabrication groups). Assuming that the concrete elements are uncracked and have rectangular cross sections such that the width (B_i) and depth (D_i) are taken as design variables, the design objective of

the first phase elastic optimization is to minimize the concrete material cost of the structure as expressed explicitly in terms of design variables as

$$\text{Minimize: concrete cost } f_{1c} = \sum_{i=1}^{N_i} w_{ci} B_i D_i \quad (1)$$

where w_{ci} is the unit cost coefficient of concrete for member i .

The intent of the elastic drift design is to ensure that a building remains operational or serviceable under the action of minor earthquakes. In checking the seismic drift response of a building, an elastic analysis procedure can be employed and the $j = 1, 2, \dots, N_j$ inter-story drift should comply with the following requirement:

$$\frac{\Delta u_j}{h_j} \leq \psi_j \quad (j = 1, 2, \dots, N_j) \quad (2)$$

where Δu_j is the elastic inter-story drift of the j th story; h_j is the j th story height and ψ_j is the specified inter-story drift ratio limit for the j th story.

Elastic linear response spectrum analysis method, widely used in modern building codes such as UBC (1997) and GB5011-2001 (2001), is adopted in this study. This method eliminates the time variable and provides a relatively simple method for determining the maximum structural responses in which individual modal responses are first calculated and the maximum responses are then obtained by combination rules.

Based on the modal response of a building, which is computed by commonly available engineering software, the n th modal elastic displacement at the j th floor level, $u_j^{(n)}$, can be expressed explicitly by the principle of the virtual work in Box 1. where L_i is the length of member i ; E and G are the axial and shear elastic material moduli; A_x , A_y , and A_z are the axial and shear areas for the cross-section; I_x , I_y , and I_z are the torsional and flexural moments of inertia for the cross-section; $F_X^{(n)}$, $F_Y^{(n)}$, $F_Z^{(n)}$, $M_X^{(n)}$, $M_Y^{(n)}$, and $M_Z^{(n)}$ are the n th modal element internal forces and moments; fXj , fYj , fZj , mXj , mYj , and mZj are the virtual element forces and moments due to a unit of virtual load applied to the building at the location corresponding to the story displacement, u_j .

Considering rectangular concrete elements with the width (B_i) and depth (D_i) taken as design variables and expressing the cross section properties in terms of B_i and D_i , the modal displacement Eq. (3) can be simplified as

$$u_j^{(n)}(B_i, D_i) = \sum_{i=1}^{N_i} \left[\begin{aligned} & \left(\frac{1}{B_i D_i} \int_0^{L_i} \left(\frac{F_X^{(n)} f_{Xj}}{E} + \frac{F_Y^{(n)} f_{Yj} + F_Z^{(n)} f_{Zj}}{5G/6} \right)_i dx + \right. \\ & \left. \frac{1}{B_i D_i^3} \int_0^{L_i} \left(\frac{M_Z^{(n)} m_{Zj}}{E/12} \right)_i dx + \right. \\ & \left. \left(\frac{1}{B_i^3 D_i} \int_0^{L_i} \left(\frac{M_X^{(n)} m_{Xj}}{G\beta} + \frac{M_Y^{(n)} m_{Yj}}{E/12} \right)_i dx \right) \right] \end{aligned} \right] \quad (4)$$

β denotes the torsional coefficient that depends on the ratio value of depth to width of the element i . For typical rectangular sections, it can be approximately set to 0.2.

Once the modal story displacement is formulated explicitly, the maximum value of the inter-

Box 1.

$$u_j^{(n)} = \sum_{i=1}^{N_i} \int_o^{L_i} \left(\frac{F_X^{(n)} f_{Xj}}{EA_X} + \frac{F_Y^{(n)} f_{Yj}}{GA_Y} + \frac{F_Z^{(n)} f_{Zj}}{GA_Z} + \frac{M_X^{(n)} m_{Xj}}{GI_X} + \frac{M_Y^{(n)} m_{Yj}}{EI_Y} + \frac{M_Z^{(n)} m_{Zj}}{EI_Z} \right)_i dx \quad (3)$$

story drifts can be expressed using the general and accurate complete quadratic combination (CQC) method as

$$[\Delta u_j(B_i, D_i)]_{CQC} = \sqrt{\sum_{n=1}^{N_n} \sum_{m=1}^{N_m} \rho_{nm} (u_j^{(n)} - u_{j-1}^{(n)}) (u_j^{(m)} - u_{j-1}^{(m)})} \quad (5)$$

where N_n denotes the total number of modes considered in the response spectrum analysis ; $u_{j-1}^{(n)}, u_{j-1}^{(m)}, u_j^{(m)}$ are the respective nth and mth modal elastic displacements at the (j-1)th and jth floor levels; ρ_{nm} is a modal correlation coefficient for the nth and mth modes, which can be obtained from the following equation with the constant damping ratio, ξ , as

$$\rho_{nm} = \frac{8\xi^2(1 + \beta_{nm})\beta_{nm}^{3/2}}{(1 - \beta_{nm}^2)^2 + 4\xi^2\beta_{nm}(1 + \beta_{nm})^2} \quad (6)$$

where

$$\beta_{nm} = \frac{\omega_n}{\omega_m} \leq 1 \quad (7)$$

Upon establishing the explicit formulation of the elastic inter-story drift Eqs. (4) and (5), based on the response spectrum analysis method, elastic spectral inter-story drift constraints using the CQC method can be written in terms of the design variables, B_i and D_i , as

Subject to:

$$g_j(B_i, D_i) = \frac{1}{\psi_j^e h_j} \Delta u_j(B_i, D_i) \leq 1 \quad (j = 1, 2, \dots, N_j) \quad (8)$$

Besides, the member sizing constraints can be defined as,

$$B_i^L \leq B_i \leq B_i^U; D_i^L \leq D_i \leq D_i^U \quad (i = 1, 2, \dots, N_i) \quad (9)$$

where B_i^L and B_i^U , D_i^L and D_i^U correspond to the lower and upper size bounds specified for the section width, B_i , and depth, D_i , respectively.

2.2 Second Phase – Inelastic Design Optimization Problem

2.2.1 Nonlinear Analysis Procedure

In the newly developed performance-based seismic design approach, nonlinear analysis procedures become important in identifying the patterns and levels of damage to assess a structure's inelastic behaviour and to understand the modes of failure of the structure during severe seismic events. Pushover analysis is a simplified, static, nonlinear procedure in which a predefined pattern of earthquake loads is applied incrementally to framework structures until a plastic collapse mechanism is reached. This analysis method generally adopts a lumped-plasticity approach that tracks the spread of inelasticity through the formation of nonlinear plastic hinges at the frame element's ends during the incremental loading process.

As graphically presented in Figure 1, the nonlinear static analysis procedure requires determination of three primary elements: capacity, demand and performance. The capacity spectrum can be obtained through the pushover analysis, which is generally produced based on the first mode response of the structure assuming that the fundamental mode of vibration is the predominant response of the structure. This pushover capacity curve approximates how a structure behaves beyond the elastic limit under seismic loadings. The demand spectrum curve is normally estimated by reducing the standard elastic 5% damped design spectrum by the spectral reduction method. The intersection of the pushover capacity and demand spectrum curves defines the "performance point" as shown in Figure 1. At the performance point, the resulting responses of the building should then be checked using certain acceptability criteria. The

responses can be checked against acceptability limits on both global system levels (such as the lateral load stability and the inter-story drift) and local element levels (such as the element strength and the sectional plastic rotation) (ATC-40 1996). When the responses of a structure do not meet the targeted performance level, the structure needs to be resized and the design process repeated until a solution for the desired performance level is reached. In general, the determination of the satisfactory performance response that fulfills both the system level response and element level response requires a highly iterative trial-and-error design procedure even with the aid of today's finite element analysis software.

2.2.2 Design Optimization Problem and Explicit Drift Formulation

While the concrete material plays an important role in controlling the elastic displacement response of a RC building, the steel reinforcement can have a significant effect on the inelastic displacement and ductility of the RC building beyond the linear elastic limit. Moreover, when an RC structure works in the inelastic stage, steel reinforcement is generally the more cost-effective

element to be used to control the inelastic performance of the structure. Based on these considerations, in the second phase, the tension steel reinforcement ratio, ρ_i , and the compression steel reinforcement ratio, ρ'_i , of rectangular cross sections are taken as design variables, for a flexural concrete building having $i=1, 2, \dots, N_i$ members and $2N_i$ plastic hinges (assuming one hinge at each end of a member). The width B_i and depth D_i of the cross section are fixed in this phase.

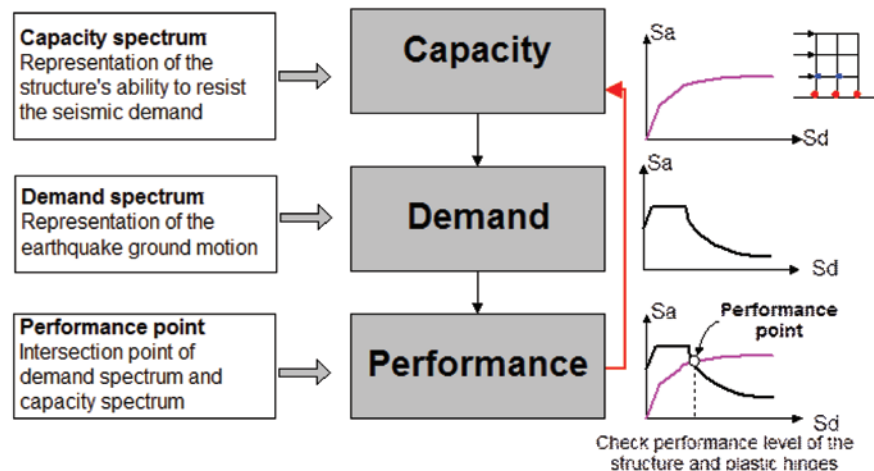
If the topology of a building structural system is predefined, the design objective of the reinforced concrete framework in the second inelastic design phase is to minimize the steel reinforcement cost f_{1s} , which can be expressed in terms of steel reinforcement design variables:

Minimize: steel cost

$$f_{1s} = \sum_{i=1}^{N_i} w_{si} (L_{si}\rho_i + L'_{si}\rho'_i) \quad (10)$$

where w_{si} is the cost coefficient for steel reinforcements; and L_{si} and L'_{si} are the lengths of the lower and upper steel reinforcements for member i . Herein, only the longitudinal reinforcement of member sections is considered as design variables and the transverse reinforcement is assumed to

Figure 1. Nonlinear analysis procedure



be invariant in the optimization under the presupposition that adequate shear strength is provided for all members.

The total construction cost, f_1 , of a reinforced concrete framework, which consists of the concrete cost f_{1c} given in Eq. (1) and the steel reinforcement cost f_{1s} shown in Eq. (10), can be expressed as

$$f_1(B_i, D_i, \rho_i, \rho'_i) = f_{1c} + f_{1s} = \sum_{i=1}^{N_i} w_{ci} B_i D_i L_i + \sum_{i=1}^{N_i} w_{si} (L_{si} \rho_i + L'_{si} \rho'_i) \quad (11)$$

It has been previously shown that, in the elastic design optimization, the concrete material cost of the structure with respect to the width, B_i , and depth, D_i , is minimized and is kept to the minimum value in the inelastic design optimization. Under the condition that the concrete element dimensions are fixed to their minimum values, the steel material cost is to be minimized in the inelastic design stage.

In seismic performance-based design, it is necessary to check the “capacity” of a structure against the “demand” of an earthquake. At the performance point, where capacity equals demand as shown in Figure 1, the resulting responses of the building should then be checked using certain acceptability criteria. In this chapter, the inelastic drift responses at the performance point of a building, generated by a severe earthquake demand, are to be checked against appropriate limits corresponding to a given performance objective. The inelastic interstory drift constraint at the performance point is defined as below.

$$\frac{\Delta u_j}{h_j} = \frac{u_j - u_{j-1}}{h_j} \leq \psi_j \quad (j = 1, 2, \dots, N_j) \quad (12)$$

where u_j and u_{j-1} are the respective displacement of two adjacent j and j-1 floor levels; ψ_j is the specified inelastic inter-story drift ratio limit for the j th story in the inelastic design phase.

In order to facilitate a numerical solution of the drift design problem, it is necessary that the implicit story drift constraint Eq. (12) be expressed explicitly in terms of the design variables, ρ_i and ρ'_i . Before the drift formulation can be discussed, three assumptions must be made. The first is that all the inelastic deformation is assumed to occur at the plastic hinges, which are located at the ends of each frame member and members are fully elastic between the plastic hinges. Secondly, the plastic hinges are assumed to be frictionless and have zero length. The third assumption is that beam-column joints are much stronger than any adjacent framing components so that the joint region may be modelled as a stiff or rigid zone.

Based on the internal element forces and moments of the structure obtained from the pushover analysis at the performance point, the principle of virtual work can be employed to express the pushover displacement. The pushover story displacement, u_j , at the performance point includes the virtual work, $u_{j,memb}$, produced by the structural members and the virtual work, $u_{j,hinge}$, generated by the plastic hinges. That is,

$$u_j = u_{j,memb} + u_{j,hinge} \quad (13)$$

in which

$$u_{j,memb} = \sum_{i=1}^{N_i} \left[\int_o^{L_i} \left(\frac{F_x f_{xj}}{EA_x} + \frac{F_y f_{yj}}{GA_y} + \frac{F_z f_{zj}}{GA_z} + \frac{M_x m_{xj}}{GI_x} + \frac{M_y m_{yj}}{EI_y} + \frac{M_z m_{zj}}{EI_z} \right) dx \right] \quad (14)$$

$$u_{j,hinge} = \sum_{i=1}^{N_i} \left[\sum_{h=1}^2 m_{pjh}^0 \theta_{ph} \right] \quad (15)$$

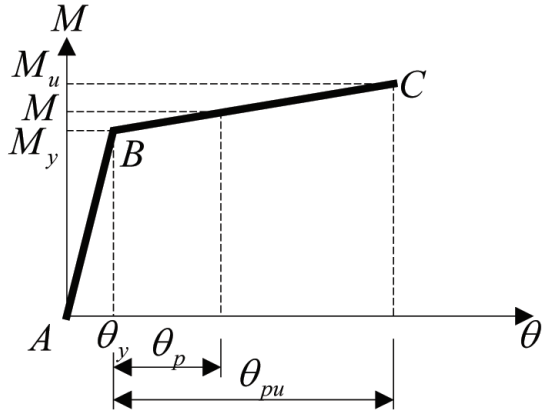
Considering rectangular concrete elements with width (B_i) and depth (D_i) and expressing the cross sectional properties in terms of B_i and D_i , the displacement, $u_{j,memb}$, in Eq. (14) can be simplified in terms of B_i and D_i , as shown in

Eq.(4). During the inelastic drift design optimization process, $u_{j,memb}$ is kept unchanged since B_i and D_i of each member section are fixed. The emphasis here is on the displacement, $u_{j,hinge}$, caused by the formation of the plastic hinges. In Eq. (15), m_{ph}^0 is the virtual end moment at the location of the hth hinge of a member; θ_{ph} is the actual plastic rotation experienced by the hth plastic hinge, which is equal to zero when no plastic hinge is found. As shown in Figure 2, the behaviour of a plastic hinge is modelled as a bilinear curve: the elastic segment, AB, and the hardening segment, BC. Based on the line segments A-B-C, the plastic rotation, θ_p , can be given as follows

$$\theta_p = \frac{M - M_y}{M_u - M_y} \theta_p^U \leq \theta_p^U \quad (16)$$

where θ_p^U is the ultimate plastic rotation which can be established based on experimental tests or can be obtained directly from design guidelines such as the ATC-40 (1996); M is the applied moment at the location of the plastic hinge; M_y is the bending moment at the first yielding of the tensile steel; and M_u is the ultimate moment of resistance. Given the quantity of the steel reinforcement used in a concrete section, the values of M_y and M_u can then be determined. For simplicity, M_u can be approximately related to M_y as $M_u = 1.1M_y$ (ATC-40 1996). For the explicit problem formulation, it is necessary that the plastic rotation, θ_p , be accurately expressed in terms of the design variables (i.e., ρ and ρ'). Furthermore, a good formulation should reflect accurately the change in the plastic rotation, θ_p , due to a change in the design variables during the optimization resizing process. In other words, any change in the design variables, ρ and ρ' , during

Figure 2. Moment-rotation curve



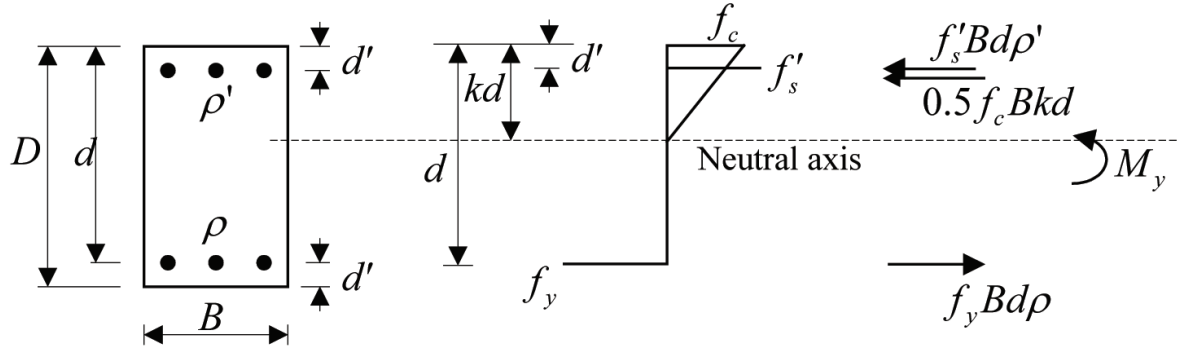
the inelastic optimization process requires a corresponding update on the values of M and M_y .

In pushover analysis, pure moment hinges as well as axial moment hinges are widely used and are generally assigned to the two ends of each beam or column. In fact, the inelastic displacement, $u_{j,hinge}$, in Eq.(13) includes the displacement generated by moment hinges (usually in the beams) and that generated by axial moment hinges (usually in the columns). By the force equilibrium shown in Figure 3, where f_c is the stress at the extreme compression concrete fibre, f'_s is the stress in the compression steel, f_y is the yield strength of the tension steel, and d is the effective depth, which is equal to the distance from the extreme compression fibre to the centroid of the tension steel, M_y for a moment hinge (where there is no co-existent axial force) can be expressed in terms of design variables, ρ and ρ' , as

$$M_y = 0.5f_cBkd\left(\frac{kd}{3} - d'\right) + f_yBd(d - d')\rho \quad (17)$$

where k is the neutral axis depth factor at the first yield and it is given as

Figure 3. Double reinforced member section at first yield



Section

Stress

Resultant force

$$k = \sqrt{(\rho + \rho')^2 n_{sc}^2 + 2(\rho + \rho' \frac{d'}{d}) n_{sc}} - (\rho + \rho') n_{sc} \quad (18)$$

in which $n_{sc} = E_s/E_c$ where E_c and E_s are the moduli of elasticity of the concrete and the steel, respectively.

Similarly, M_y for an axial-moment hinge (wherein there is co-existent axial force) can be expressed in terms of design variables, ρ and ρ' as

$$M_y = \frac{f_y Bd}{2n_{sc}} \cdot \left(\frac{D}{2} - \frac{k d}{3} \right) \cdot \frac{k^2}{1-k} + \frac{f_y Bd(d-d')^2}{2d} \cdot \frac{\rho}{1-k} \quad (19)$$

where k is given as

$$k = -\left(2\rho + \frac{F_x}{f_y Bd}\right) n_{sc} + \sqrt{\left(2\rho + \frac{F_x}{f_y Bd}\right)^2 n_{sc}^2 + 2n_{sc} \left(\rho \frac{D}{d} + \frac{F_x}{f_y Bd}\right)} \quad (20)$$

To take into account the change in θ_p due to a change in ρ and ρ' while maintaining an instantaneously fixed value of M , a second-order Tay-

lor series approximation for evaluating the value of θ_p is given as

$$\theta_p(\rho) = \theta_p \Big|_{\rho=\rho^0} + \frac{\partial \theta_p}{\partial \rho} \Big|_{\rho=\rho^0} (\rho - \rho^0) + \frac{1}{2} \frac{\partial^2 \theta_p}{\partial \rho^2} \Big|_{\rho=\rho^0} (\rho - \rho^0)^2 \quad (21)$$

where the tension steel ratio, ρ , is considered as the major design variable; for simplicity, the compression steel ratio, ρ' , is assumed to be linearly related to ρ for beams and to be the same as ρ for columns. Given the explicit expression of M_y as a function of ρ from Eqs. (17) and (19), the gradient, $\frac{\partial \theta_p}{\partial \rho}$, and the second-order term, $\frac{\partial^2 \theta_p}{\partial \rho^2}$, can be analytically calculated from Eq. (16).

By substituting the explicit plastic rotation, $\theta_p(\rho)$, given in Eq. (21) into Eq. (15), the pushover displacement, u_j , in Eq. (13) can also be explicitly expressed in terms of the design variable, ρ_i in Box 2.

Box 2.

$$u_j(\rho_i) = u_j \Big|_{\rho_i=\rho_i^0} + \sum_{i=1}^{N_i} \frac{\partial u_j}{\partial \rho_i} \Big|_{\rho_i=\rho_i^0} (\rho_i - \rho_i^0) + \frac{1}{2} \sum_{i=1}^{N_i} \frac{\partial^2 u_j}{\partial \rho_i^2} \Big|_{\rho_i=\rho_i^0} (\rho_i - \rho_i^0)^2 \quad (22)$$

2.2.3 Plastic Rotation Constraint and Sizing Constraint

Besides checking the inter-story drift responses discussed above, local response quantities (i.e., sectional plastic rotation and strength of all members) at the performance point also must not exceed appropriate response limits. Therefore, the plastic rotation, θ_{ph} , at the hth end of member i (where the subscript h represents one end of a member and $h=1,2$) should be constrained in the optimization by

$$\theta_{ph} \leq \theta_p^U \quad (23)$$

where θ_p^U is the rotation limit of member i for a specific performance level. Once the designer determines the performance levels of the structure (e.g., Immediate Occupancy, Life Safety, Collapse Prevention), the corresponding limiting value of θ_p^U is then determined. In addition, in order to reduce the practical building design problem to a manageable size, the strength design of each member is not considered explicitly as a design constraint; rather, the strength-based steel reinforcement ratios in accordance with code specifications are first calculated and these values are then taken as the lower size bound for each member in the inelastic seismic drift design optimization.

It is found from Figure 2 that, in order to maintain the relationship of $0 \leq \theta_p \leq \theta_p^U$, the internal moment, M , leading to the occurrence of a plastic hinge must satisfy the following condition:

$$M_y \leq M \leq M_u \quad (24)$$

On the one hand, by setting $M_y = M$ where M_y can be found from Eq. (17) for a moment hinge and Eq. (19) for an axial-moment hinge, the corresponding value of ρ_i can be solved and this value can then be taken as the instantaneous upper bound value of ρ_i such that $\rho_i^U = \rho_i$. On the other hand, by setting $M_u = M$ and assuming $M_u = 1.1M_y$, the instantaneous lower bound value of ρ_i can then be found such that $\rho_i^L = \rho_i$. As a result, based on Eq. (24), the lower and upper bounds of ρ_i for each plastic hinge can be instantaneously established during the OC iterative resizing process.

2.2.4 Design Optimization Problem Formulation

Upon establishing the explicit inelastic drift formulation, Eq. (22), the optimization problem of minimizing the steel construction cost Eq.(10) can be explicitly written in terms of the design variable, ρ_i , as

$$\text{Minimize: } f_{1s}(\rho_i) = \sum_{i=1}^{N_i} w'_{si} \rho_i \quad (25)$$

Subject to:

$$g_j(\rho_i) = \frac{1}{\psi_j^p h_j} \left[\Delta u_j \Big|_{\rho_i=\rho_i^0} + \sum_{i=1}^{N_i} \alpha_{1i} (\rho_i - \rho_i^0) + \frac{1}{2} \sum_{i=1}^{N_i} \alpha_{2i} (\rho_i - \rho_i^0)^2 \right] \leq 1 \quad (j = 1, 2, 3, \dots, N_j) \quad (26)$$

$$\rho_i^L \leq \rho_i \leq \rho_i^U \quad (i = 1, 2, 3, \dots, N_i) \quad (27)$$

where

$$\alpha_{1i} = \frac{\partial \Delta u_j}{\partial \rho_i} \Big|_{\rho_i=\rho_i^0} = \left[\sum_{h=1}^2 m_{jh}^0 \frac{\partial \Delta \theta_{ph}}{\partial \rho} \Big|_{\rho_i=\rho_i^0} \right]_i \quad (28)$$

$$\alpha_{2i} = \frac{\partial^2 \Delta u_j}{\partial \rho_i^2} \Big|_{\rho_i=\rho_i^0} = \left[\sum_{h=1}^2 m_{jh}^0 \frac{\partial^2 \Delta \theta_{ph}}{\partial \rho^2} \Big|_{\rho_i=\rho_i^0} \right]_i \quad (29)$$

In Eq. (25), w'_{si} is the cost coefficient for the steel reinforcement, ρ_i ; ψ_j^p is the allowable inelastic inter-story drift ratio. Eq. (26) defines the set of seismic inelastic inter-story drift performance constraints under specified earthquake ground motions. Eq. (27) defines the sizing constraints for the steel reinforcement, where ρ_i^L and ρ_i^U correspond to the lower and upper size bounds specified for the tensile steel reinforcement variable, ρ_i , and they should be updated after each nonlinear pushover analysis. For the sake of simplicity, the compressive steel reinforcement, ρ'_i , has been assumed to be simply related to ρ_i and therefore, it is not included in the explicit optimization problem Eqs. (25)-(29).

2.3 Design Procedure

The overall design optimization procedure for limiting lateral elastic and inelastic drifts of an RC building structure is listed as follows:

1. Assume the initial member sizes and determine the design spectra corresponding to minor and severe earthquakes.
2. In the first phase, i.e., the elastic design optimization, carry out the response spectrum analysis of the structure subject to a minor earthquake and conduct a static virtual load

analysis using commercially available software such as SAP2000 (2000).

3. Read all the necessary input and output results of the analysis and establish the explicit elastic design optimization formulation of Eqs. (1) and (9).
4. Apply the recursive OC optimization algorithm to resize the concrete element sizes.
5. Repeat Steps 2 and 4 for statically indeterminate structures until the concrete cost of the structure between two successive design cycles converges to be within certain acceptable criteria (say, 0.5%).
6. After the elastic design optimization, fix the optimal member sizes, B_i and D_i , in the inelastic design optimization. Based on the member size derived from the elastic optimization, determine the minimum and maximum size bounds of the steel reinforcement ratios, ρ_i and ρ'_i , in accordance with the strength-based code requirements.
7. Carry out the nonlinear pushover analysis to determine the inelastic responses of the structure at the performance point.
8. Read all the necessary input and output results of the pushover analysis, establish the lower and upper bounds of ρ_i for the members with plastic hinges using Eq. (24) and determine the values of the first-order and second-order derivatives of inelastic drift responses using Eqs (28) and (29).
9. Establish the explicit inelastic inter-story drift constraints using a second-order Taylor series approximation and formulate the explicit inelastic design problem, Eqs (25)-(29).
10. Apply the recursive OC optimization algorithm to resize all steel reinforcement design variables.
11. Repeat Steps 7 and 10 until the convergence of the values of the steel cost objective function and the inelastic drift design constraints is achieved.

3. MULTIOBJECTIVE DESIGN OPTIMIZATION PROBLEM

3.1 Objective Function

In seismic performance based design, the total life-cycle cost of structures should be considered and the final design should be established based on a good balance between the initial structural cost and its loss expectation in the design life period. Due to the fact that the life-cycle cost involves the consideration of construction cost and damage loss which are inherently conflicting, i.e., the decrease of one increases the other, it is necessary to formulate the design optimization as a multi-objective optimization problem. In this research study, the initial construction cost of an RC building frame is estimated simply in terms of the material costs of the concrete member sizes and steel reinforcements. In contrast, the establishment of an approximate but rational cost function to explicitly represent the expected damage loss of building structures in terms of sizing design variables remains one of the challenging difficulties.

If the topology of a building structural system is predefined, the design objective is to minimize the multi-objective life-cycle cost of the structure. Using F to denote the life-cycle cost function including the initial structure cost f_1 and expected future damage loss f_2 , the multi-objective function can be expressed as

$$\text{Minimize: } F = \{f_1, f_2\} \quad (30)$$

In order to facilitate the numerical solution of the optimization problem, the implicit objective function in Eq. (11) needs to be first expressed explicitly in terms of the design variables. As presented previously, the initial structure cost f_1 of an RC framework is simply assumed to be the summation of the concrete material cost f_{1c} and

the steel reinforcement cost f_{1s} , as given in Eq. (11).

3.2 Expected Future Structural Loss f_2

The structural failure losses due to an earthquake attack consist of direct loss and indirect loss. The direct loss is the cost of repair or replacement of structural members, contents, non-structural components and equipment, and so on. The indirect loss may include the losses associated with structural malfunction, injuries and fatalities, psychological and political influence, etc. The accurate estimation of both direct and indirect losses is generally a very complex task involving not only engineering analysis but also many other issues. The failure of each structural performance may lead to a different failure loss. Herein, Li's work (1998) is introduced as an example of derivation of the expected future structural loss f_2 for convenient discussion in the following. According to the work by Li (1998), the total loss expectation can be defined by the summation of the product of the occurrence probability of earthquake and the system failure loss. That is, for N_r performance levels, the loss expectation function f_2 can be stated as

$$f_2 = \sum_{r=1}^{N_r} P_r \times L_r \quad (31)$$

where r denotes the seismic design level and $r = 1, 2, \dots, N_r$; P_r is the occurrence probability of an earthquake for the r th seismic design level, which can be determined from specified code requirements; L_r is the structural failure loss including direct and indirect losses under the r th seismic design level. In Li's study (1998), the damage loss of a structure corresponding to different discrete levels of performance criteria is expressed in terms of the maximum inter-story drift index under minor, moderate and severe

earthquakes. Five classes of structural damage (namely negligible, slight, moderate, severe and complete damage) of a building are given based on the maximum inter-story drift value in accordance with the Chinese code for seismic design of buildings (GB50011-2001). Due to the fact that the classification of the five different degrees of damage is discrete in nature and the set of inter-story drift responses of a building is continuous, the fuzzy-decision theory is employed to best estimate the damage loss with specified probabilities of occurrence of different levels of earthquakes. For simplicity, τ is used to represent the inter-story drift index such that $\tau = \Delta u \times R/h$, where Δu is the inter-story drift; h is the story height; R is equal to 500 for concrete frames and 1000 for concrete shear-wall structures and frame-wall structures. Finally, the total structural damage loss f_2 presented in Eq. (31) can be explicitly expressed in terms of the variable $\tau(\Delta u)$ as

$$f_2 = f_1 \sum_{r=1}^{N_r} \left\{ P_r \times \left[\sum_{j=1}^{N_j} (a_1 \tau(\Delta u_j) + a_2) \right] \right\} \quad (32)$$

where a_1 and a_2 are the coefficients of an expected failure loss, which depend on not only damage levels but also building classes and details are presented in Li (1998). For example, assuming that the importance of a frame building belongs to Class B, the values of a_1 and a_2 can be derived as shown in Table 1. Details of derivation can be found in Zou (2002) and Zou et al (2007).

3.3 Explicit Multi-Objective Problem Formulation

Upon obtaining the explicit nonlinear objective function (i.e., the initial structure cost f_1 in Eq. (11) and the damage loss f_2 in Eq. (32)), and the explicit inelastic drift formulation in Eq. (22), the multi-objective design optimization problem can be written in terms of the design variables ρ_i as

Minimize:

$$F(\rho_i) = \{f_1, f_2\} \quad (33)$$

Subject to:

$$g_j(\rho_i) = \frac{1}{h_j \psi_j^p} \left[\Delta u_j \Big|_{\rho_i=\rho_i^0} + \sum_{i=1}^{N_i} \alpha_{1i} (\rho_i - \rho_i^0) + \frac{1}{2} \sum_{i=1}^{N_i} \alpha_{2i} (\rho_i - \rho_i^0)^2 \right] \leq 1 \quad (j = 1, 2, \dots, N_j) \quad (34)$$

$$\rho_i^L \leq \rho_i \leq \rho_i^U \quad (i = 1, 2, 3, \dots, N_i) \quad (35)$$

Eqs. (33) defines the life-cycle cost function F , which consists of the construction cost f_1 and the damage loss f_2 ; Eq. (34) defines the inelastic inter-story drift constraint at the structural performance point for a specified ground motion; Eq. (35) defines the lower and upper size bounds specified for the design variables, ρ_i ; α_1 and α_2 are given in Eqs.(28)-(29).

Table 1. The coefficients of expected failure loss for a Class B building

	$\tau < 0.5$	$0.5 \leq \tau < 1.5$	$1.5 \leq \tau < 3$	$3 \leq \tau < 7$	$7 \leq \tau < 10$	$\tau \geq 10$
a_1	0.000	0.080	0.800	1.350	4.770	0.000
a_2	0.02	-0.020	-1.100	-2.750	-26.667	21.000

3.4 Multi-Objective Optimization Algorithm

The multi-objective optimization problem given in Eqs. (33)-(35) can be solved by a *Pareto optimal set* – formed by a large number (infinite number) of Pareto optimal solutions. The Pareto optimal set can provide an overview of all the tradeoffs to the designer. To establish a Pareto optimum point, multi-objective optimization algorithms should be constructed, one of which transforms the multi-objective problem into a single-objective optimization. The key to the transformation is that the solution of the single-objective problem should be a point in the Pareto set with respect to a feasible region and a set of objective functions. Among transformation methods, the ε -constraint method is one of the commonly used approaches in practical problems (Kaisa 1999; Marler and Arora 2004). The ε -constraint method is a technique that transforms a multi-criteria objective function into a single criterion by retaining one selected objective function as the primary criterion to be optimized and treating the remaining criteria as constraints.

Herein, the construction cost, $f_1(\rho_i)$, is taken as a primary objective, while the damage loss, $f_2(\rho_i)$, is transformed into a design constraint. The reason for this consideration is that both the damage loss $f_2(\rho_i)$ in Eq. (32) and the inter-story drift constraints in Eq. (34) are expressed explicitly in terms of the inter-story drifts. The similarity may bring advantages in numerical calculations. Thus, the multi-objective optimization problem given in Eqs. (33)-(35) can be transformed as

$$\text{Minimize: } f_1(\rho_i) \quad (36)$$

$$\text{Subject to: } f_2(\rho_i) \leq \varepsilon_2 \quad (37)$$

$$g_j(\rho_i) \leq 1 \quad (j = 1, 2, \dots, N_j) \quad (38)$$

$$\rho_i^L \leq \rho_i \leq \rho_i^U \quad (i = 1, 2, \dots, N_i) \quad (39)$$

By varying the upper bound value, ε_2 , for the objective $f_2(\rho_i)$ and minimizing the objective $f_1(\rho_i)$, all Pareto optimal points are, in principle, attainable. Theoretically, there is no limitation on the range of ε_2 ($-\infty \leq \varepsilon_2 \leq +\infty$) regardless of the convexity conditions. However, this may result in extensive computational time to find a Pareto set. In fact, the main difficulty of the ε -constraint method lies in finding the range of reasonable values for the upper bound, ε_2 . Details can be found in Zou (2002) and Zou et al (2007).

3.5 Multi-Objective Design Optimization Procedure

The multi-objective inelastic optimal design procedure is outlined as follows:

1. The optimal member sizes B_i and D_i are first found based on the elastic design optimization, which are fixed in the inelastic design optimization. The initial reinforcement ratios for each member are taken as the minimum values of the design variable, ρ_i , obtained from the elastic optimization results.
2. Establish the explicit optimization problem given in Eqs. (33)-(35).
3. Transfer multi-objective design problem Eqs. (33)-(35) into a single objective optimization Eqs.(36)-(39).
4. Change ε_2 in Eq.(40) and generate one Pareto optimum solution by employing the OC method. The global convergence is checked based on the change in the objective function and the violation of the constraints.
5. Repeat Steps 4 and 5 until the upper bounds of the active design variables are achieved.

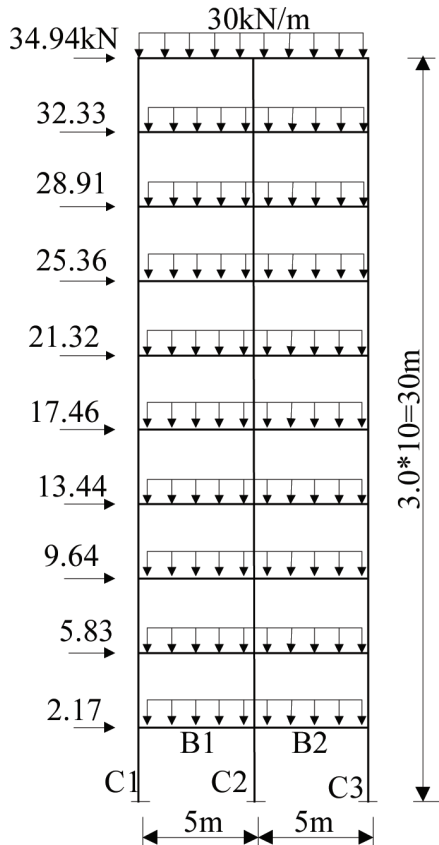
4. ILLUSTRATIVE EXAMPLE

A ten-story, two-bay planar frame is used to illustrate the proposed optimal design method. The geometry of the example is given in Figure 4(a). Concrete with the cylinder strength of 20MPa and steel reinforcement with the yield strength, f_y , of 335MPa are used for all members. To illustrate the effectiveness of the optimal design technique, three cases are conducted in this example. Cases A and B are elastic and inelastic design optimization for a single objective, respectively, while Case C considers life-cycle cost, i.e., multi-objective optimization where other conditions are the same as Case B.

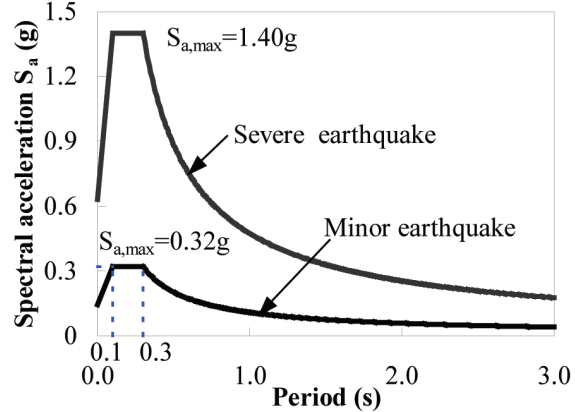
4.1 A Single Objective Optimization (i.e., Cases A and B)

Two levels of earthquake loads are considered in this example. One represents a minor earthquake load with a peak acceleration of 0.32g according to the acceleration response spectrum in GB5011-2001(2001), as shown in Figure 4(b). Another load level represents a severe earthquake with an initial peak acceleration of 1.4g. In the elastic phase of the optimization, the concrete cost of the

Figure 4. A ten-story, two-bay frame



a) Geometry



b) Design response spectra

structure is to be minimized subject to the elastic spectral drift constraints under the minor earthquake loading condition. The unit construction cost of concrete is assumed to be US\$90/m³, including the concrete material cost and labour cost. Elastic inter-story drift constraints are taken into account with an allowable inter-story drift ratio limit of 1/450. The initial sizes are arbitrarily chosen to be 350 × 350mm for the columns and 200 × 350mm for the beams. Size bounds are defined as 350~1000mm for the depths and the widths of the columns, 200~350mm for the widths of the beams and 350~450mm for the depths of the beams.

In the inelastic phase of the optimization, the design objective is to minimize the steel reinforcement cost subject to the performance-based inelastic drift constraints under the severe earthquake loading condition. The unit construction cost of steel reinforcement is assumed to be US\$960/tonne including the steel material cost and the labour cost. Inelastic inter-story drift constraints are considered with an allowable inter-story drift ratio limit of 1/100 and the P-Delta effect is considered in the example. Initial reinforcement ratios are calculated based on the strength requirements of members after the elastic phase design process. Such strength-based reinforcement ratios are taken as the lower bounds for the inelastic design process. Their upper bounds are assumed to be 6.0% for columns and 4.0% for beams. For simplicity, symmetrical arrangement of steel reinforcement is assumed such that $\rho_i = \rho'_i$. Flexural moment hinges and axial-moment hinges are assigned to the end locations of the beams and columns, respectively. The ultimate plastic hinge rotation, θ_p^U , is assumed to be 0.02 radian for the moment hinges on the beams and 0.015 radian for the axial-moment hinges on the columns.

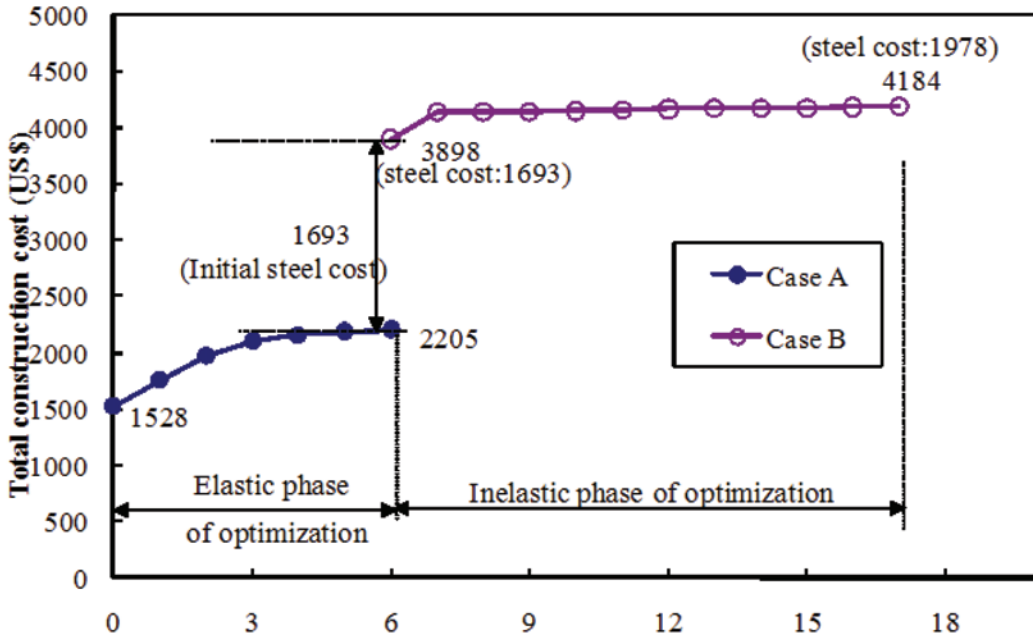
Initial applied lateral loads applied in push-over analysis are shown in Figure 4(a), which is proportional to the product of the story mass and the first mode shape of the elastic model of the

structure. During the pushover analysis, the lateral loads are applied incrementally in proportion to the initial loads but the gravity loads, shown in Figure 4(a), are assumed to be fixed. The design process is deemed to converge when the difference in the structure costs for two successive design cycles is within 0.5% and when the difference between the active inter-story drift value and its allowable limit at the performance point is within 0.5%.

Figure 5 presents the optimal design history for both the elastic and inelastic drift optimization processes. In the elastic optimal design, rapid and steady convergence of the concrete cost from the initial US\$1528 to the final US\$2205 after 6 design cycles has been found. The rapid convergence can be explained by the fact that the member force distribution for such structures is somewhat insensitive to changes in member size. In contrast, the inelastic optimal design process converges quite slowly but steadily in 11 design cycles. Relatively slow, but steady, convergence is inevitable due to the need of maintaining a small change in the steel reinforced ratios during the nonlinear design optimization process. However, the OC design method is able to achieve a smooth and steady convergence to the optimal design as evidently shown in Figure 5.

In the elastic design optimization subject to elastic inter-story drift constraints, the total material cost only includes the concrete cost, which is minimized from the arbitrary, initial US\$1528 to the final US\$2205. In the inelastic design optimization subject to inelastic inter-story drift constraints, the initial total cost US\$3898 consists of the steel reinforcement cost of US\$1693 calculated based on code-specified strength requirements and the concrete cost of US\$2205, which is to be fixed in this inelastic phase of the optimization. Since initial violations in inelastic inter-story drift constraints are found in the strength-based design, an increase in the steel reinforcement is necessary, resulting in a final total construction cost of US\$4184. In addition, it is found from Case B that there is a relatively large increase of

Figure 5. Design history of structural cost



16% in the steel cost from the initial US\$1693 to US\$1978.

Figure 6 presents the optimal steel reinforcement ratios for Cases A and B. In the elastic phase, the member sizes are increased after the elastic design optimization since the initial design is found to be infeasible. The starting strength-based design, in the second inelastic design phase, is also found to be infeasible in terms of the assumed allowable inter-story drift limit. After the inelastic design optimization, the steel reinforcement ratios of the beams greatly increase particularly in the lower levels of the structure, while those of columns are found with little changes for Case B. Reasons lie on that the columns of Case B are found to be mainly controlled by the minimum strength requirements with the final steel ratios being set to the initial strength based limits, whilst the beams are governed by the inelastic inter-story drift performance requirements with the final steel ratios being larger than the initial strength based limits.

The initial and final inter-story drift ratios are shown in Figure 7(a) for Case A and Figure 7(b) for Case B. The initial inter-story drift constraints at the second through the eighth floors are found to violate substantially the allowable inter-story drift ratio limit of 1/100 for both cases, resulting in the occurrence of the weak stories on the these floor levels of the building. However, these push-over inter-story drift constraints are found to be close to and within the allowable values after the optimization, indicating that a rather uniform inter-story drift distribution over the height of the building has been achieved and the occurrence of weak story has been prevented at the final performance point.

Figure 8(a) includes a table showing the number of plastic hinges at three different performance states, i.e., Immediate Occupancy (IO), Life Safety (LS) and Collapse Prevention (CP) for Case B. Figures 8(b)-(c) show the initial and final plastic hinge distributions under the pushover loading at the performance point of the structure.

Figure 6. Optimal member sizes and reinforcement ratios for three cases

Element type	Story level	Member group	Case A		Case B		Case C	
			Optimal sizes		Steel ratios		Steel ratios	
			Width (mm)	Depth (mm)	Initial (%)	Optimal (%)	At Point C0 (%)	At Point C* (%)
Column	9th~10th	C1,C3	350	350	0.990	1.096	1.096	1.100
		C2	350	350	1.386	1.386	1.278	1.386
	8th	C1,C3	350	350	0.849	0.860	0.860	1.034
		C2	350	475	0.958	0.958	0.958	0.958
	7th	C1,C3	350	350	1.163	1.163	1.186	1.354
		C2	350	475	1.092	1.092	1.092	1.092
	6th	C1,C3	350	400	0.854	0.864	0.854	0.854
		C2	350	575	0.831	0.831	0.831	0.831
	5th	C1,C3	350	400	0.969	1.004	1.004	1.012
		C2	350	575	1.002	1.002	1.002	1.002
Beam	4th	C1,C3	350	450	0.833	0.873	0.833	0.833
		C2	350	600	0.739	0.739	0.739	0.739
	3rd	C1,C3	350	450	0.825	0.876	0.876	0.928
		C2	350	600	0.857	0.857	0.857	0.857
	2nd	C1,C3	350	450	1.044	1.124	1.044	1.066
		C2	350	650	1.225	1.225	1.224	1.225
	1st	C1,C3	350	450	1.514	1.514	1.514	1.514
		C2	350	650	1.844	1.844	1.844	1.844
	9th~10th	B1,B2	200	400	0.800	0.800	0.800	0.800
	8th	B1,B2	200	450	0.838	0.941	0.941	1.098

Figure 7. Interstory drift responses of three cases

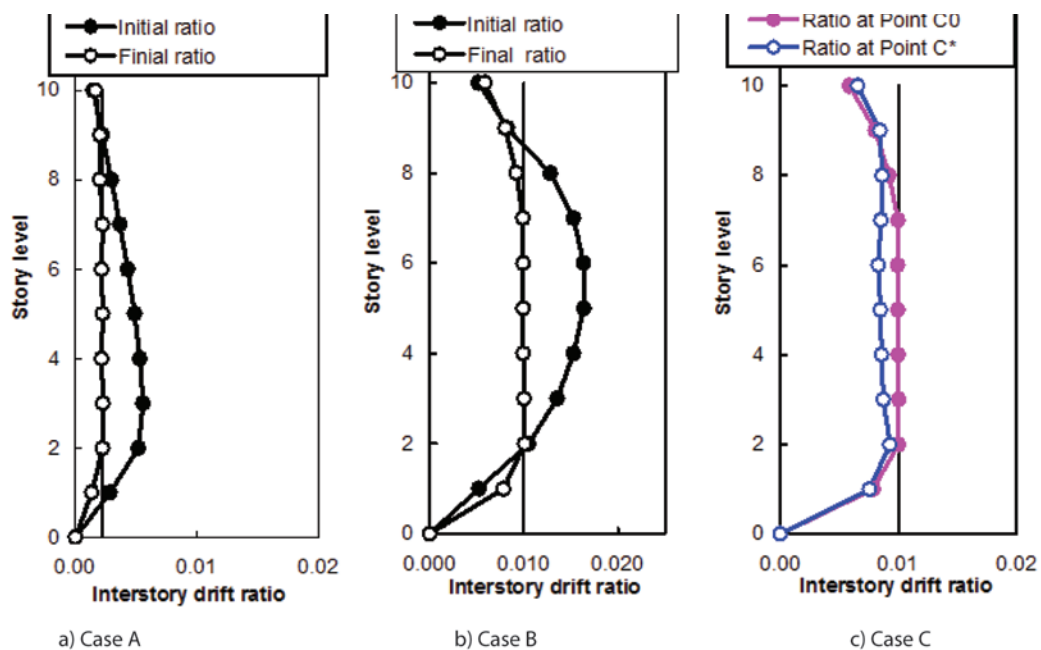
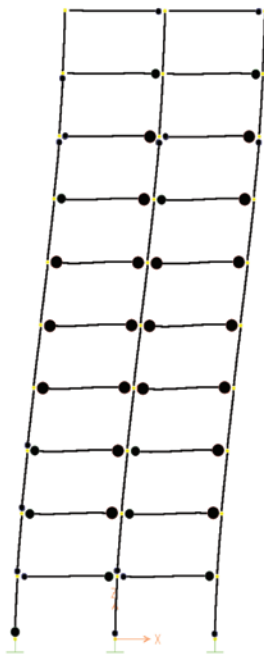


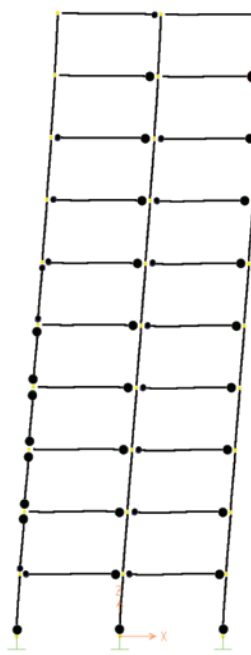
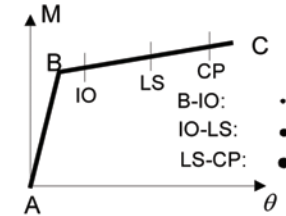
Figure 8. Initial and final plastic hinge distribution of Case B

Case B	Number of plastic hinges			Total number of plastic hinges
	B-IO	IO-LS	LS-CP	
Initial design	16	11	20	47
Final design	16	28	1	45

(a) Number of plastic hinges



(b) Case B: initial design



(c) Case B: final design

No plastic hinge rotation is found to exceed the specified threshold of plastic rotation, θ_p^U . As shown in Figure 8(b), the rotations of twenty plastic hinges of the initial design are found to be located between the LS-CP state. However, after the optimization, most of the plastic hinges are found to be in the B-IO and IO-LS states and only one hinge is in the LS-CP state, as can be observed from the optimized framework in Figure 8(c). Furthermore, the inter-story drifts along the height of the building are also found to be almost all fully constrained at the optimum, resulting in a

rather linear deflected profile of the inelastic design. Such a result further indicates that the optimization method developed can automatically resize the steel reinforcements of all members to attain a uniform ductility demand along the height of the multi-story building.

4.2 Multi-Objective Optimization (Case C)

The occurrence probability P_r for the severe earthquake is assumed to be 3.9% according to

the design return period of 50 years. This building frame is assumed to be a Class B building in this example and the coefficients of expected failure loss are shown in Table 1. Other conditions stay the same as Case B.

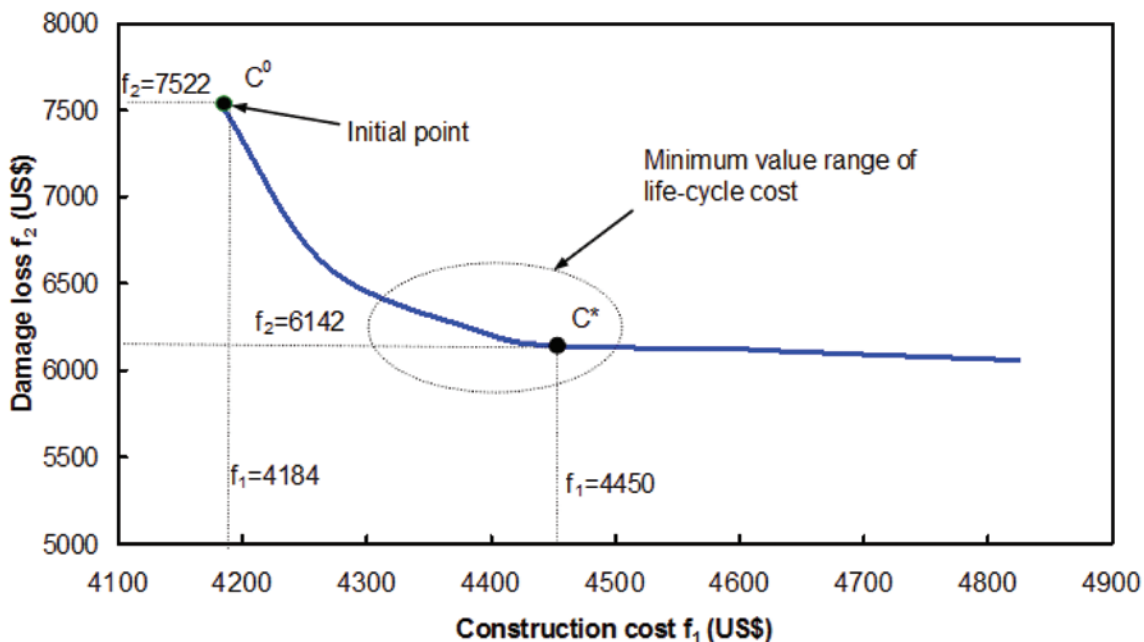
Figure 9 presents a Pareto optimal set, which provides the best compromise between the initial structure cost, f_1 , and the damage loss, f_2 . The minimum structure cost, f_1 , for the single objective optimal design problem given in Eqs. (36)-(39), i.e., corresponds to Point C0 in Figure 8 where $f_1 = \text{US\$}4184$ and the corresponding damage loss, f_2 , is found to be $\text{US\$}7522$. The optimal steel reinforcement ratios corresponding to Point C0 are taken as initial steel ratios of members in the subsequent multi-objective inelastic design optimization (see Eqs. (33)-(35)) and the optimal Pareto set curve can then be generated. Besides, $\text{US\$}4184$ at Point C0 is the minimum value of the initial structure cost, f_1 , satisfying design constraints at this Pareto curve; correspondingly,

$\text{US\$}7522$ at Point C0 is the maximum value of the damage loss, f_2 .

Firstly, it is observed from Figure 9 that an improvement in the damage loss leads to an increase in the initial material cost of the structure. From the Pareto optimal set, a designer can have an overview of the tradeoffs. Secondly, any point in the Pareto optimal set can be selected as an optimum design, which represents a designer's preference. A designer has many choices rather than only one and he/she may finally choose a particular solution, which he/she thinks, should be realized. Thirdly, the life-cycle cost can be further written as $F = \varphi_1 f_1 + \varphi_2 f_2$, where φ_1 and φ_2 are the weighting factors and their magnitudes are dependent on a designer's decision. A preferred balance of the initial and damage losses can therefore be obtained. It is worth noting that different values of φ_1 and φ_2 will lead to different minimum values of the life-cycle cost.

Figure 6 lists the optimal steel reinforcement ratios at Points C⁰ and C*, respectively. The steel

Figure 9. A Pareto optimal set of Case C



reinforcement ratios of beams are largely increased from the first to the eighth floors from Point C⁰ to Point C* (i.e., an increase of 17%~47%), while there is no change of steel reinforcement ratios in most columns due to no occurrence of plastic hinges. Such an increase indicates that steel reinforcement has a significant effect on improving inelastic drift performance and further reducing damage loss.

Figure 7(c) presents the results of the inter-story drift ratios at Points C⁰ and C*, respectively. It is found that all the inelastic inter-story drift constraints are satisfied corresponding to either Point C⁰ or Point C*. In the optimal solution (i.e., corresponding to Point C⁰) of the single objective design optimization, the inter-story inelastic drift constraints from the second to the seventh floors are close to the limiting ratio of 1%. However, in the multi-objective design optimization (i.e., Point C*), all final drift constraints are not necessarily found to be close to the limiting ratio 1%. This is due to the fact that steel ratios of the structure members are further enhanced in order to meet the best balance between the initial structure cost and damage loss. Such a result seems to indicate that for the multi-objective design optimization, the lateral load resisting system can be automatically improved by the OC procedure to seek the best balance so that lateral drift constraints are satisfied simultaneously with the least life-cycle cost.

5. CONCLUSION

Using the principle of virtual work, both the elastic spectral drift constraints and the nonlinear pushover inelastic drift constraints have been explicitly formulated in terms of the design variables. Rapid and steady convergence for elastic drift optimization has been found. In contrast, the inelastic optimal design process converges quite slowly but steadily. The restrictive move limit imposed on the steel reinforcement design variables is

found necessary to ensure a smooth and steady convergence of the inelastic drift design process.

It has been demonstrated that steel reinforcement plays a significant role in controlling the lateral drift beyond first yielding and in providing ductility to an RC building framework. It is also demonstrated that the OC design method is able to attain automatically and gradually the optimal performance-based inter-story drift design. At optimum, a uniform lateral drift or ductility demand over all stories of the building with the minimum cost is achieved, thus preventing the occurrence of soft story mechanisms in such structures.

The optimization technique developed for the nonlinear multi-objective design of inelastic drift performance of RC frameworks under pushover loadings provides a very effective way to simultaneously optimize the structural life-cycle cost while satisfying all drift performance design criteria. A multi-objective optimization algorithm, the ϵ -constraint method, has been effectively applied to handle the conflicts between the initial structure cost and damage loss by producing a Pareto optimal set, from which a decision maker can directly select the best compromise solution.

It is believed that the single- and multi-objective optimization methodology provides a powerful computer-based technique for seismic performance-based design of multi-story RC building structures. The proposed optimization methodology provides a good basis for more comprehensive performance-based optimization of structures as multiple levels of performance criteria and design objectives are to be considered.

ACKNOWLEDGMENT

The author would acknowledge the thoughtful suggestions and support from Prof. C.M. Chan of the Department of Civil Engineering, the Hong Kong University of Science and Technology.

REFERENCES

- Ang, A. H.-S., Lee, J.-C., & Pires, J. A. (1997). Cost-effectiveness evaluation of design criteria. *Proceedings of the International Workshop on Optimal Performance of Civil Infrastructure Systems* (pp.1-16). New York, NY: ASCE.
- Arora, J. S. (1999). Optimization of structures subjected to dynamic loads. In Leondes, C. T. (Ed.), *Structural dynamic systems computational techniques and optimization* (pp. 1–73). Gordon and Breach Science Publishers.
- ASCE. 41. (2007). Seismic rehabilitation of existing buildings ASCE/SEI 41/06. ASCE Standard No. ASCE/SEI 41-06. *ATC-40*. (1996). Seismic evaluation and retrofit of concrete buildings, Vol. 1. *ATC-40 Report*. Redwood City, CA: Applied Technology Council.
- Balling, R. J., Pister, K. S., & Ciampi, V. (1983). Optimal seismic-resistant design of a planar steel frame. *Earthquake Engineering & Structural Dynamics*, 11, 541–556. doi:10.1002/eqe.4290110407
- Beck, J. L., Papadimitriou, C., Chan, E., & Irfanoglu, A. (1998). *A performance-based optimal structural design methodology*. Report No. EERL 97-03, CA, USA.
- Bhatti, M. A., & Pister, K. S. (1981). A dual criteria approach for optimal design of earthquake-resistant structural systems. *Earthquake Engineering & Structural Dynamics*, 9, 557–572.
- Chan, C. M. (1997). How to optimize tall steel building frameworks. *Guide to structural optimization* (pp. 165-195). ASCE Manuals and Reports on Engineering Practice No.90.
- Chan, C. M., & Zou, X. K. (2004). Elastic and inelastic drift performance optimization for reinforced concrete building under earthquake loads. *Earthquake Engineering & Structural Dynamics*, 33(8), 929–950. doi:10.1002/eqe.385
- Charney, F. A. (2000). Needs in the development of a comprehensive performance based design optimization process. In M. Elgaaly (Ed.), *Advanced Technology in Structural Engineering - Structural Congress 2000*, ASCE, May 8-10, (CD-ROM).
- Cheng, F. Y., & Botkin, M. E. (1976). Nonlinear optimum design of dynamic damped frames. *Journal of the Structural Division*, 102, 609–628.
- Cheng, F. Y., & Chang, C. C. (1988). *Safety-based optimum design of nondeterministic structures subjected to various types of seismic loads*. NSF Report, U.S. Department of Commerce, VA, NTIS No. PB90-133489/AS.
- Cheng, F. Y., & Li, D. (1997). Multiobjective optimization design with Pareto genetic algorithm. *Journal of Structural Engineering*, 123(9), 1252–1261. doi:10.1061/(ASCE)0733-9445(1997)123:9(1252)
- Cheng, F. Y., & Truman, K. Z. (1982). Optimization algorithm of 3-D building systems for static and seismic loading. In Ames, W. F. (Ed.), *Modeling and simulation in engineering* (pp. 315–326). North-Holland Pub. Co.
- Computer and Structures, Inc. (CSI). (2000). *SAP2000/NL-PUSH software*, Version 7.40. Berkeley, CA: Computer and Structures, Inc.
- Federal Emergency Management Agency. (2000). Prestandard and commentary for the seismic rehabilitation of buildings. *FEMA-356*. Washington, DC.
- Federal Emergency Management Agency. (2005). Improvement of nonlinear static seismic analysis procedure. *FEMA-440*. Washington, DC.
- Federal Emergency Management Agency. (2006). Next-generation performance-based seismic design guidelines. *FEMA-445*. Washington, DC.

- Feng, T. T., Arora, J. S., & Huang, E. J. (1977). Optimal structural design under dynamic loads. *International Journal for Numerical Methods in Engineering*, 11(1), 39–52. doi:10.1002/nme.1620110106
- Foley, C. M. (2002). Optimized performance-based design for buildings. In Burns, S. A. (Ed.), *Recent advances in optimal structural design* (pp. 169–240). American Society of Civil Engineers.
- Gao, X. W., & Bao, A. B. (1985). Probabilistic model and its statistical parameters for seismic load. *Earthquake Engineering and Engineering Vibration*, 5(1), 13–22.
- International Conference of Building Officials. (1997). *Uniform building code* (UBC). Whittier, California, USA.
- Kaisa, M. (1999). *Nonlinear multiobjective optimization*. USA: Kluwer Academic Publishers.
- Krawinkler, H. (1994). Static pushover analysis. *Proceedings SEAONC 1994 Fall Seminar on the Developing Art of Seismic Engineering*. San Francisco, CA.
- Li, G. (1998). *Reliability and performance based optimal design for seismic high-rising structures*. Ph.D. Dissertation, Dalian University of Technology, China.
- Li, G., Zhou, R.-G., Duan, L., & Chen, W.-F. (1999). Multiobjective and multilevel optimization for steel frames. *Engineering Structures*, 21(6), 519–529. doi:10.1016/S0141-0296(97)00226-5
- Liu, M., Burns, S. A., & Wen, Y. K. (2003). Optimal seismic design of steel frame buildings based on life cycle cost considerations. *Earthquake Engineering & Structural Dynamics*, 32(9), 1313–1332. doi:10.1002/eqe.273
- Marler, R. T., & Arora, J. S. (2004). Survey of multi-objective optimization methods for engineering. *Structural and Multidisciplinary Optimization*, 26(6), 369–395. doi:10.1007/s00158-003-0368-6
- Moehle, J. P., & Mahin, S. A. (1991). Observations on the behavior of reinforced concrete buildings during earthquakes. American Concrete Institute SP-127. In Ghosh, S. K. (Ed.), *Earthquake-resistant concrete structures – Inelastic response and design*.
- National Standard of the People's Republic of China. (2001). *Chinese code for seismic design buildings (GB50011-2001)*. Beijing, China: New World Press.
- Park, Y. J., & Ang, A. H.-S. (1985). Mechanistic seismic damage model for reinforced concrete. *Journal of Structural Engineering*, 111(4), 722–739. doi:10.1061/(ASCE)0733-9445(1985)111:4(722)
- Park, Y. J., Ang, A. H.-S., & Wen, Y. K. (1987). Damage-limiting aseismic design of buildings. *Earthquake Spectra*, 3(1), 1–26. doi:10.1193/1.1585416
- Vision, S. E. A. O. C. (2000). *Committee. (1995). Performance based seismic engineering of buildings, part 2: Conceptual framework*. Sacramento, CA: Structural Engineers Association of California.
- Wang, Q., Fang, H., & Zou, X. K. (2010). Application of micro-GA for optimal cost base isolation design of bridges subject to transient earthquake loads. *Structural and Multidisciplinary Optimization*, 36(5), 493–507.
- Wen, Y. K., & Kang, Y. J. (1997). Optimal seismic design based on life-cycle cost. *Proceedings of the International Workshop on Optimal Performance of Civil Infrastructure Systems 1997*, (pp. 194–210). New York, NY: ASCE.

- Wen, Y. K., & Kang, Y. J. (2001). Minimum building life-cycle cost design criteria. I: Methodology. *Journal of Structural Engineering*, 127(3), 330–337. doi:10.1061/(ASCE)0733-9445(2001)127:3(330)
- Zou, X. K. (2002). *Optimal seismic performance-based design of reinforced concrete buildings*. Ph.D. Dissertation, Hong Kong University of Science and Technology.
- Zou, X. K. (2008). Integrated seismic design optimization of nonlinear base-isolated RC buildings. *Structural and Multidisciplinary Optimization*, 36(5), 493–507. doi:10.1007/s00158-007-0184-5
- Zou, X. K., & Chan, C. M. (2001). Optimal drift performance design for nonlinear pushover response of concrete structures. *WCSMO-4: Proceedings of the Fourth World Congress of Structural and Multidisciplinary Optimization*, June 4-8, Dalian, China.
- Zou, X. K., & Chan, C. M. (2005a). An optimal resizing technique for seismic drift design of concrete buildings subjected to response spectrum and time history loadings. *Computers & Structures*, 83, 1689–1704. doi:10.1016/j.compstruc.2004.10.002
- Zou, X. K., & Chan, C. M. (2005b). Optimal seismic performance-based design of reinforced concrete buildings using nonlinear pushover analysis. *Engineering Structures*, 27, 1289–1302. doi:10.1016/j.engstruct.2005.04.001
- Zou, X. K., Chan, C. M., Li, G., & Wang, Q. (2007b). Multiobjective optimization for performance-based design of concrete structures. *Journal of Structural Engineering*, 133(10), 1462–1474. doi:10.1061/(ASCE)0733-9445(2007)133:10(1462)
- Zou, X. K., Teng, J. G., Xia, S. H., & Wong, Y. L. (2007a). Optimal performance-based seismic retrofit design of FRP-confined concrete buildings. *Composite Part B: Engineering International Journal*, 38, 584–597. doi:10.1016/j.compositesb.2006.07.016
- Zou, X. K., Wang, Q., Li, G., & Chan, C. M. (2010). Integrated reliability-based seismic drift design optimization of base-isolated concrete buildings. *Journal of Structural Engineering*, 136(10), 1282–1295. doi:10.1061/(ASCE) ST.1943-541X.0000216

Chapter 10

Applications of Topology Optimization Techniques in Seismic Design of Structure

Kazem Ghabraie

University of Southern Queensland, Australia

ABSTRACT

During the last two decades, topology optimization techniques have been successfully applied to a wide range of problems including seismic design of structures. This chapter aims to provide an introduction to the topology optimization methods and a review of the applications of these methods in earthquake engineering. Two well-established topology optimization techniques are introduced. Several problems including eigenfrequency control of structures, compliance minimization under periodic loading, and maximizing energy absorption of passive dampers will be addressed. Numerical instabilities and approaches to overcome them will be discussed. The application of the presented approaches and methods will be illustrated using numerical examples. It will be shown that in seismic design of structures, topology optimization methods can be useful in providing conceptual design for structural systems as well as detailed design of structural members.

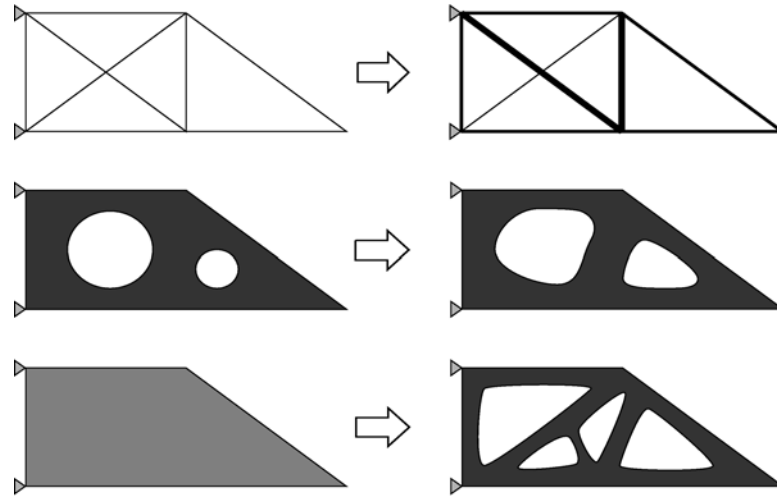
1. INTRODUCTION

Solving optimization problems is an inherent part of engineering design where one seeks the best design to minimize or maximize an objective

function subject to some constraints. In structural optimization, depending on the nature of the design variables, three different optimization categories can be recognized. *Sizing optimization* arises when the design variables are connected to the dimensions of the elements. It can be useful where the layout and the shapes of the members

DOI: 10.4018/978-1-4666-1640-0.ch010

Figure 1. The three levels of structural optimization: top) sizing optimization; middle) shape optimization; bottom) topology optimization



are known and it is desired to find the optimum dimensions. On another level, one can choose the design variables to control the shape of the boundaries of the members. Such selection will lead to *shape optimization*. If the overall layout of the members is known and it is already decided where to put each member, in order to find the best shapes of the members, one can use shape optimization. In order to optimize the topology, connectivity, or layout of a system, *topology optimization* techniques should be used. In topology optimization the design variables control the topology and connectivity of the design. Figure 1 schematically illustrates these three categories of structural optimization.

Starting from topology optimization and feeding the results to shape and sizing optimization routines will generally result in far greater savings than merely using shape and sizing optimization. Topology optimization techniques can thus be considered as important and powerful tools in hand of design engineers.

In this chapter we review the application of topology optimization techniques in seismic design of structures. We start with a brief review of the

history of topology optimization. Then we focus on two general optimization problems in seismic design of structures, the eigenvalue optimization problem and the problem of maximizing the energy absorption.

2. TOPOLOGY OPTIMIZATION

Initially addressed by Culmann (1866), the layout optimization problem is not quite new. The interesting work of Michell (1904) laid down the principles of topology optimization of structures more than a century ago. After that, the field remained untouched for nearly seven decades until Prager and Rozvany improved and generalized the Michell's theory (e.g. refer to Prager 1969, 1974 and Rozvany 1972a,b). Yet the field didn't attract much attention until Bendsøe and Kikuchi (1988) proposed a finite element-based numerical method for topology optimization of continuum structures. Usually referred to as the *homogenization method*, this approach soon became a basis upon which other topology optimization techniques have been developed.

In their approach, Bendsøe and Kikuchi considered special microstructures as the building cells of the structure and employed the homogenization method to find the macro-scale properties of the cells in terms of their micro-scale dimensions. By considering the dimensional properties of the microstructures as design variables, they reduced the topology optimization of the structure to sizing optimization of its microstructures.

Using the idea behind the homogenization method, Bendsøe (1989) introduced a simpler approach to optimize the topology of structures. In this new approach instead of using the microstructures and homogenization, Bendsøe proposed an artificial material interpolation scheme relating the material properties of the elements to their relative density. After Rozvany et al. (1992), this approach is referred to as ‘Solid Isotropic Microstructures with Penalization (SIMP)’. The SIMP approach is now one of the most established and popular methods in topology optimization.

A simple FE-based topology optimization technique was later proposed by Xie and Steven (1993). Named Evolutionary Structural Optimization (ESO), the technique was based on the idea of evolving the structure towards an optimum design by progressively removing its inefficient elements. The Bi-directional ESO (BESO) was the main successor of the ESO method. Initially introduced by Querin (1997), Querin et al. (1998) and Yang et al. (1999a), the BESO algorithm was capable of adding as well as removing elements. This method is now a well-known topology optimization technique which is widely used due to its clear topology results and ease of application.

The SIMP and BESO techniques will be detailed and used in later sections of this chapter. In the next section we investigate the equation of motion of a structural system to find out which parameters shape the responses of structures under dynamic loads.

3. STRUCTURAL RESPONSES UNDER DYNAMIC LOADS

Consider the equation of motion for a finite element discretized linear system

$$\mathbf{M}\ddot{\mathbf{u}} + \mathbf{C}\dot{\mathbf{u}} + \mathbf{K}\mathbf{u} = \mathbf{p} \quad (1.1)$$

where \mathbf{M} , \mathbf{C} and \mathbf{K} are mass, damping and stiffness matrices respectively and \mathbf{u} and \mathbf{p} are time-dependent vectors of nodal displacement and nodal force respectively, i.e., $\mathbf{u} \equiv \mathbf{u}(t)$ and $\mathbf{p} \equiv \mathbf{p}(t)$. We assume a classical damping (Chopra 1995), for example Reyliugh damping of the form

$$\mathbf{C} = a_M \mathbf{M} + a_K \mathbf{K} \quad (1.2)$$

where a_M and a_K are constants.

We now expand the displacements in terms of modal contributions

$$\mathbf{u}(t) = \sum_{r=1}^{N_d} q_r(t) \boldsymbol{\varphi}_r \quad (1.3)$$

where N_d is the number of degrees of freedom and

$$q_r(t) = C_r \cos \omega_r t + S_r \sin \omega_r t, \quad r = 1, \dots, N_d \quad (1.4)$$

are harmonic functions and C_r and S_r are constants of integration associated with the r th degree of freedom. The natural frequencies ω_r and natural modes $\boldsymbol{\varphi}_r$ are solutions of the following eigenvalue problem

$$\mathbf{K}\boldsymbol{\varphi}_r = \omega_r^2 \mathbf{M}\boldsymbol{\varphi}_r \quad (1.5)$$

which represents the free vibration of the undamped system. For simplicity, we further require that the modes are \mathbf{M} -orthonormal, i.e.,

$$\Phi_n^T \mathbf{M} \Phi_r = \delta_{nr}, \quad n, r = 1, \dots, N_d \quad (1.6)$$

where δ_{nr} is the Kronecker's delta which equals 1 for $n = r$ and 0 otherwise. Premultiplying Equation (1.5) by Φ_n^T and using Equation (1.6) we get

$$\Phi_n^T \mathbf{K} \Phi_r = \omega_r^2 \delta_{nr}, \quad n, r = 1, \dots, N_d \quad (1.7)$$

which means the modes are also \mathbf{K} -orthogonal. Using Equation (1.3) in Equation (1.1) and premultiplying by Φ_n^T we obtain

$$\sum_{r=1}^{N_d} \Phi_n^T \mathbf{M} \Phi_r \ddot{q}_r + \sum_{r=1}^{N_d} \Phi_n^T \mathbf{C} \Phi_r \dot{q}_r + \sum_{r=1}^{N_d} \Phi_n^T \mathbf{K} \Phi_r q_r = \Phi_n^T \mathbf{p} \quad (1.8)$$

We now make use of \mathbf{M} -orthonormality of the modes and the classical damping Equation (1.2) to simplify Equation (1.8) to

$$\ddot{q}_n + 2\zeta_n \omega_n \dot{q}_n + \omega_n^2 q_n = \Phi_n^T \mathbf{p} \quad (1.9)$$

where $\zeta_n = \frac{a_M}{2} \frac{1}{\omega_n} + \frac{a_K}{2} \omega_n$ is the damping ratio of the n -th mode (Chopra 1995).

According to Equation (1.9), the response of a structure under a dynamic load depends on its natural frequencies ω_n and damping ratios ζ_n .

4. MAXIMIZING EIGENFREQUENCIES IN FREE VIBRATION

As seen in the previous section, controlling the response of structures can involve eigenfrequency optimization. In this section we address the problem of maximizing the fundamental frequency of a structure in free vibration. This problem was initially addressed by Díaz and Kikuchi (1992) using the homogenization method. Here, we formulate the problem using the SIMP approach. This formulation can be simply extended to maximiz-

ing (or minimizing) any combination of natural frequencies. A practically useful example of such extensions will be briefly addressed in section 6. It is worth noting that maximizing fundamental frequency results in structures with a reasonable stiffness against static loads in general (Bendsøe and Sigmund 2003).

Damping effects are ignored and linear elastic material behavior is assumed in this section. Also all material parameters are taken as deterministic quantities. Random variability of material strength parameters can significantly affect the ductility and energy absorption capacities of structures subjected to seismic loading (Kuwamura and Kato 1989, Elnashai and Chryssanthopoulos 1991). Uncertainties of variables can be considered in structural optimization by integrating Reliability Analysis (see e.g. Kharmanda et al. 2004 and Papadrakakis et al. 2005) or through Robust Optimization (see e.g. Beyer and Sendhoff 2007).

Using the finite element discretization and the SIMP approach we introduce the following material interpolation scheme to express the Young's modulus E_e of element e in terms of its relative density x_e as

$$E_e(x_e) = x_e^p \bar{E} \quad (1.10)$$

where \bar{E} is the Young's modulus of the base isotropic material. The power $p > 1$ is known as the penalty factor and is introduced to push the solutions towards a solid-void topology. A typical value for the penalty factor is $p = 3$ (Bendsøe and Sigmund 1999). The relative densities are changing in the range $0 \leq x_e \leq 1$ in which $x_e = 1$ represents solids and $x_e = 0$ represents void areas. In order to avoid singularities in the stiffness matrix of the system, Equation (1.10) may be replaced by

$$E_e(x_e) = \underline{E} + x_e^p (\bar{E} - \underline{E}) \quad (1.11)$$

in which \underline{E} is a small elastic modulus assigned to voids. Based on Equation (1.10), the (local

level) stiffness matrix of the element e can be expressed as

$$\mathbf{K}_e(x_e) = \underline{\mathbf{K}}_e + x_e^p (\bar{\mathbf{K}}_e - \underline{\mathbf{K}}_e) \quad (1.12)$$

in which $\bar{\mathbf{K}}_e$ and $\underline{\mathbf{K}}_e$ are the stiffness matrices of the element e when it is made of the base material and void (in its solid and void states) respectively. Similarly for the density and the mass matrix of the element e we can write

$$\rho_e(x_e) = x_e \bar{\rho} \quad (1.13)$$

and

$$\mathbf{M}_e(x_e) = x_e \bar{\mathbf{M}}_e \quad (1.14)$$

Where $\bar{\rho}$ is the density of the base material and $\bar{\mathbf{M}}_e$ is the mass matrix of the element e in its solid state.

Using these material interpolation schemes one can change element e from solid to void and backwards by changing the value of x_e . Thus by choosing x_e -s as design variables, one can produce different topologies without altering the finite element mesh.

We can now formulate the optimization problem. The fundamental frequency optimization problem can be stated as finding the best topology of a structure to maximize its fundamental frequency given a fixed amount of material. The problem can thus be formulated as

$$\begin{aligned} \max_{x_1, x_2, \dots, x_N} \quad & \left\{ \lambda_1 = \min_{j=1,2,\dots,N_d} \lambda_j \right\} \\ \text{such that} \quad & \mathbf{K}\Phi_j = \lambda_j \mathbf{M}\Phi_j, \quad j = 1, 2, \dots, N_d \\ & \sum_{e=1}^N x_e v_e \leq \bar{v} \\ & 0 \leq x_e \leq 1, \quad e = 1, 2, \dots, N \end{aligned} \quad (1.15)$$

where $\lambda_j = \omega_j^2, j = 1, \dots, N_d$ and N is the number of elements. The second constraint restricts the volume of the design to an upper limit denoted by \bar{v} . In this statement v_e is the volume of the element e .

4.1. Sensitivity Analysis

Solving Problem (1.15) requires finding the sensitivities of λ_1 with respect to design variables x_e . Differentiating $\mathbf{K}\Phi_j = \lambda_j \mathbf{M}\Phi_j$ we can write

$$\frac{\partial \mathbf{K}}{\partial x_e} \Phi_j + \mathbf{K} \frac{\partial \Phi_j}{\partial x_e} = \frac{\partial \lambda_j}{\partial x_e} \mathbf{M}\Phi_j + \lambda_j \frac{\partial \mathbf{M}}{\partial x_e} \Phi_j + \lambda_j \mathbf{M} \frac{\partial \Phi_j}{\partial x_e} \quad (1.16)$$

Premultiplying by Φ_j^T and rearranging the terms we obtain

$$\Phi_j^T \left(\frac{\partial \mathbf{K}}{\partial x_e} - \lambda_j \frac{\partial \mathbf{M}}{\partial x_e} \right) \Phi_j = \frac{\partial \lambda_j}{\partial x_e} \Phi_j^T \mathbf{M}\Phi_j - \Phi_j^T (\mathbf{K} - \lambda_j \mathbf{M}) \frac{\partial \Phi_j}{\partial x_e} \quad (1.17)$$

Using the symmetry of \mathbf{K} and \mathbf{M} , we can readily conclude that

$$\Phi_j^T (\mathbf{K} - \lambda_j \mathbf{M}) = [(\mathbf{K} - \lambda_j \mathbf{M}) \Phi_j]^T = 0.$$

We also use Equation (1.16) in Equation (1.17) to finally express the sensitivities as

$$\frac{\partial \lambda_j}{\partial x_e} = \Phi_j^T \left(\frac{\partial \mathbf{K}}{\partial x_e} - \lambda_j \frac{\partial \mathbf{M}}{\partial x_e} \right) \Phi_j \quad (1.18)$$

The stiffness and mass derivatives in Equation (1.18) can be calculated using Eqs. (1.12) and (1.14).

4.2. Solution Method

Having the sensitivities in Equation (1.18), the optimization problem (1.15) can be solved using

suitable gradient-based techniques. Noting that the number of design variables (number of elements) can be very large, one should adopt a solution method capable of solving large-scale problems. The method of moving asymptotes (MMA) proposed by Svanberg (1987) is a well-known solution method used in topology optimization problems. Another common approach is using optimality criteria (OC) based algorithms. In the following, after deriving the optimality criteria for the optimization problem (1.15), we propose a heuristic iterative fixed-point algorithm to solve the optimization problem based on the optimality criteria.

The eigenvalue equation, $\mathbf{K}\boldsymbol{\varphi}_j = \lambda_j \mathbf{M}\boldsymbol{\varphi}_j$ can be satisfied separately using finite element analysis. Excluding this equation, the Lagrangian of Problem (1.15) takes the form

$$\mathcal{L} = \lambda_1 + \Gamma \left(\bar{v} - \sum_{e=1}^N x_e v_e \right) + \sum_{e=1}^N [\bar{\gamma}_e (1 - x_e) + \underline{\gamma}_e x_e] \quad (1.19)$$

where Γ , $\bar{\gamma}_e$ and $\underline{\gamma}_e$ are Lagrange multipliers. Using Karush-Kuhn-Tucker results (Karush 1939; Kuhn and Tucker 1951), the necessary optimality conditions for Problem (1.15) can be expressed as follows

$$\begin{aligned} \frac{\partial \mathcal{L}}{\partial x_e} &= \frac{\partial \lambda_1}{\partial x_e} - \Gamma v_e - \bar{\gamma}_e + \underline{\gamma}_e = 0 \\ \Gamma \left(\bar{v} - \sum_{e=1}^N x_e v_e \right) &= 0; \quad \bar{v} - \sum_{e=1}^N x_e v_e \geq 0; \quad \Gamma \geq 0 \\ \bar{\gamma}_e (1 - x_e) &= 0; \quad 1 - x_e \geq 0; \quad \bar{\gamma}_e \geq 0, \quad e = 1, \dots, N \\ \underline{\gamma}_e x_e &= 0; \quad x_e \geq 0; \quad \underline{\gamma}_e \geq 0, \quad e = 1, \dots, N \end{aligned} \quad (1.20)$$

If we define $\gamma_e = \bar{\gamma}_e - \underline{\gamma}_e$ and use it in Equation (1.20), we can rewrite the optimality criteria as

$$\begin{aligned} D_e &= \frac{\partial \lambda_1}{\partial x_e} - \Gamma v_e = \gamma_e \\ \Gamma \left(\bar{v} - \sum_{e=1}^N x_e v_e \right) &= 0; \quad \bar{v} - \sum_{e=1}^N x_e v_e \geq 0; \quad \Gamma \geq 0 \\ x_e = 0 &\Rightarrow \gamma_e \leq 0 \\ 0 < x_e < 1 &\Rightarrow \gamma_e = 0 \\ x_e = 1 &\Rightarrow \gamma_e \geq 0 \\ e &= 1, \dots, N \end{aligned} \quad (1.21)$$

To increase the fundamental frequency, we add a vector of increments $\Delta \mathbf{x} = (\Delta x_1, \Delta x_2, \dots, \Delta x_N)^T$ to the design variables $\mathbf{x} = (x_1, x_2, \dots, x_N)^T$. The subsequent change in the fundamental frequency and the design volume can then be evaluated as

$$\Delta \lambda_1 = (\nabla \lambda_1)^T \Delta \mathbf{x} \quad (1.22)$$

$$\Delta v = \mathbf{v}^T \Delta \mathbf{x} \quad (1.23)$$

where $\nabla \lambda_1 = \left(\frac{\partial \lambda_1}{\partial x_1}, \frac{\partial \lambda_1}{\partial x_2}, \dots, \frac{\partial \lambda_1}{\partial x_N} \right)^T$ is the gradient vector of λ_1 and $\mathbf{v} = (v_1, v_2, \dots, v_N)^T$.

Let us now define the increments of design variables as

$$\Delta \mathbf{x} = \mathbf{D} = \nabla \lambda_1 - \Gamma \mathbf{v} \quad (1.24)$$

If the volume constraint is inactive, we will have $\Gamma = 0$ and thus $\Delta \mathbf{x} = \nabla \lambda_1$ which results in $\Delta \lambda_1 = (\nabla \lambda_1)^T \nabla \lambda_1 \geq 0$ after substituting in Equation (1.22).

If the volume constraint is active, on the other hand, we will have

$$\Delta v = \mathbf{v}^T \Delta \mathbf{x} = 0 \quad (1.25)$$

Using Equation (1.24) in Equation (1.25) and solving for Γ we obtain

$$\Gamma = \frac{\mathbf{v}^T \nabla \lambda_1}{\mathbf{v}^T \mathbf{v}} \quad (1.26)$$

If the boxing conditions are all inactive, i.e. if $0 < x_e < 1$, we can use Equation (1.26) in Equation (1.24) and then Equation (1.24) in Equation (1.22) to write

$$\Delta \lambda_1 = (\nabla \lambda_1)^T \left(\nabla \lambda_1 - \frac{\mathbf{v}^T \nabla \lambda_1 \mathbf{v}}{\mathbf{v}^T \mathbf{v}} \right) \quad (1.27)$$

It can be easily verified that the right hand side of Equation (1.27) is a form of Cauchy–Bunyakovsky–Schwarz inequality and thus $\Delta \lambda_1 \geq 0$.

Based on this discussion, we propose the following update scheme to solve Problem (1.15)

$$\mathbf{x}_{(k+1)} = \max \left\{ \begin{array}{l} 0, (\mathbf{x}_{(k)} - \eta), \\ \min \left\{ 1, (\mathbf{x}_{(k)} + \eta), \left| \mathbf{x}_{(k)} + \eta \mathbf{D}_{(k)} \right|^{\frac{1-p}{p}} \right\} \end{array} \right\} \quad (1.28)$$

Here the subscripts denote the iteration number and η is a tuning parameter defining the move limit. The vector \mathbf{D} is defined in Equation (1.24). Note that p used here is the previously defined penalty power for stiffness. The value of the Lagrange multiplier Γ can be calculated using bisection method in an inner loop. In finding Γ , one should note that $\partial v / \partial \Gamma < 0$.

Note that the same algorithm can be used to maximize any of the natural frequencies. To maximize the k th eigenvalue, for example, one needs to replace λ_1 and ϕ_1 by λ_k and ϕ_k respectively.

4.3. Numerical Instabilities

Most of the material distribution techniques, including homogenization, SIMP and BESO methods, are known to be prone to three major numerical instabilities, namely checkerboard problem, mesh dependency, and local minima

(Sigmund and Petersson 1998). Checkerboard problem refers to the formation of alternating solid and void elements in a checkerboard-like pattern resulting in artificially high stiffness. Mesh dependency refers to obtaining different optimal topologies for the same problem using different mesh sizes. Local minima refers to the problem of obtaining different optimal topologies using the same mesh but different algorithmic parameters and/or initial design.

One of the simplest yet effective approaches to overcome checkerboard and mesh dependence problems is filtering sensitivities (Sigmund and Petersson 1998). In this approach the calculated sensitivities are replaced by filtered sensitivities which are calculated as a weighted average of the sensitivities of the neighboring elements. A simple linear filter takes the form

$$\widehat{\frac{\partial \lambda}{\partial x_i}} = \frac{\sum_{e=1}^N x_j \frac{\partial \lambda}{\partial x_j} w_{ij}}{x_i \sum_{j=1}^N w_{ij}} \quad (1.29)$$

in which $w_{ij} = \max \{0, R - d_{ij}\}$. R is known as the filtering radius and d_{ij} denotes the distance between the centers of the elements i and j . The filtering scheme (1.29) can be activated by choosing the filtering radius R bigger than the size of elements h . This can eliminate the checkerboard problem.

In this scheme, the filtering radius R imposes a local minimum length scale to the solutions. More precisely, using this sensitivity filter, the width of bars appearing in the resulting topologies could not be smaller than $2R$. This property is useful in achieving mesh independency. By defining R as a ratio of the actual length of the design domain, the mesh dependence problem can be rectified.

Unlike the first two types of numerical instabilities, the local minima problem is mostly due to the use of gradient-based optimization algorithm which can be trapped in local minima of usually non-convex objective functions. On the other

hand, the extremely large size of the problems in topology optimization is a great barrier in using non-gradient-based optimization techniques such as Genetic Algorithm (GA) and Neural Networks. The *continuation* method is a simple approach used and suggested by many researchers to overcome this problem in gradient-based optimization methods (Sigmund and Petersson 1998). In this approach, one would start solving the problem in a more relaxed form and gradually apply restrictions. For example, one can start the solution considering no penalty factor ($p = 1$) and gradually increase p upon convergence of the solution.

Apart from these three problems – which are common in all types of topology optimization problems – some numerical artifacts are unique to eigenvalue problems. The ‘artificial modes’ problem comes under this category. These are localized modes appearing in regions with relatively high mass to stiffness ratio. Pedersen (2000) points that due to the interpolation schemes for stiffness and mass (Eqs. (1.12) and (1.14) respectively), the mass to stiffness ratio rises steeply for small values of x which ultimately results in localized modes. To overcome this problem, a modification in the stiffness interpolation scheme is suggested by Pedersen (2000) to limit the mass to stiffness ratio in low density areas (typically $x < 0.1$). Following the same principle, Du and Olhoff (2007) proposed a different approach by modifying the mass interpolation scheme. The latter approach is adopted here. To this end, we replace the original mass interpolation scheme, Equation (1.14), by

$$\mathbf{M}_e(x_e) = \begin{cases} x_e \bar{\mathbf{M}}_e, & x_e > 0.1 \\ 10^{q-1} x_e^q \bar{\mathbf{M}}_e, & x_e \leq 0.1 \end{cases} \quad (1.30)$$

with $q = 2p$. This ensures that the mass to stiffness ratio cannot exceed 10^{p-1} .

4.4. Flowchart and Numerical Examples

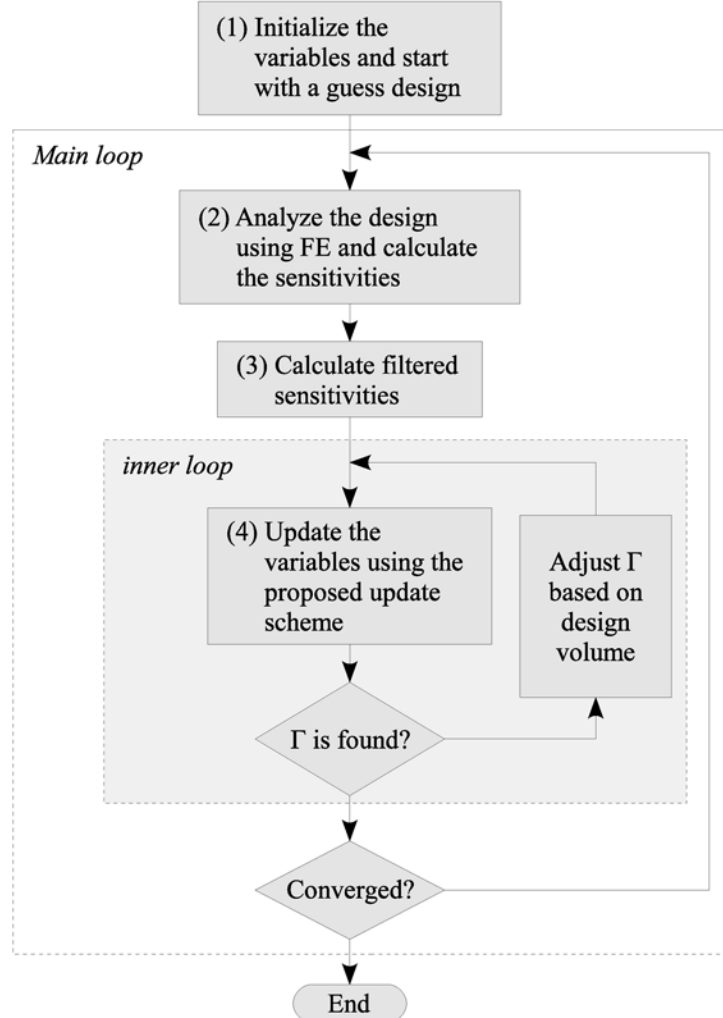
A flowchart of the proposed solution algorithm is depicted in Figure 2. The solution starts from an initial guess design. A uniform distribution of material defined as $x_e = \bar{v} / v_t$, $e = 1, \dots, N$ with v_t denoting the total volume of the design domain is usually used as an initial design. The main loop starts by analyzing the current design using finite element analysis. Based on FE results, the sensitivities are calculated using Equation (1.18). The sensitivities are then filtered using Equation (1.29). The updated variables are calculated in an inner loop. In the inner loop, starting with a positive value for the Lagrange multiplier Γ , the updated variables are calculated using Equation (1.28). The volume of this new design is checked and the new value of Γ is adjusted using the bisection approach. The inner loop continues until the value of Γ converges. The updated design is then replaces the old one and the procedure is repeated until a convergence criterion is satisfied.

The convergence criterion used here is defined as

$$\left| \frac{\sum_{i=k-l+1}^k \lambda_{(i)} - \sum_{i=k-l}^{k-1} \lambda_{(i)}}{\sum_{i=k-l+1}^k \lambda_{(i)} + \sum_{i=k-l}^{k-1} \lambda_{(i)}} \right| \leq \varepsilon \quad (1.31)$$

where $\lambda_{(i)}$ is the value of the objective function at the i -th iteration and k denotes the last iteration. This condition compares the value of the objective function in the last and second last l iterations and assumes convergence is achieved when the relative error is smaller than a predefined tolerance $0 < \varepsilon \ll 1$. In all examples reported here $l = 5$ and $\varepsilon = 0.001$ were used.

Figure 2. The flowchart of the proposed solution algorithm



Example 1: Reinforcement of a Planar Frame

As the first example we consider a frame in plane stress. The maximum volume of used material should be limited to half of the volume of the whole frame ($\bar{v} / v_t = 50\%$). The initial design is depicted in Figure 3 (leftmost). The outer frame is fixed to be solid and is non-designable. Note that if we do not consider the non-designable outer frame, the optimization program will obviously shorten the frame.

The $3 \times 12\text{m}$ domain is discretized using a 30×120 mesh of 4 node square bi-linear elements. A consistent mass matrix formulation has been used (see e.g. Zienkiewicz et al. 2005). The stiffness and density of the base material are assumed as $\bar{E} = 2 \times 10^5 \text{ MPa}$ and $\rho = 8000 \text{ kg/m}^3$ respectively. A penalty power of $p = 4$, a filtering radius of $R = 30\text{cm} = 3h$, and move limit of $\eta = 0.2$ have been used. The ratio between the stiffness of solid and void areas is selected as $\bar{E} : E = 10^9$.

The obtained topologies at different iterations are shown in Figure 3.

Figure 3. The initial design and topologies of the first example at different iteration numbers

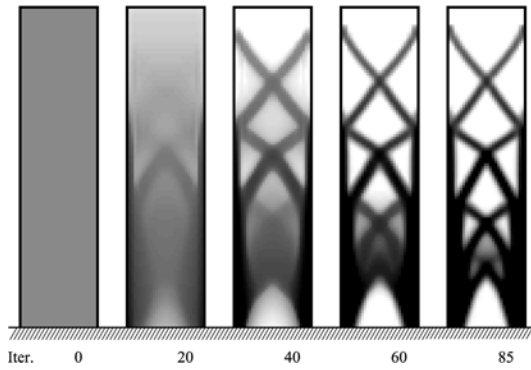


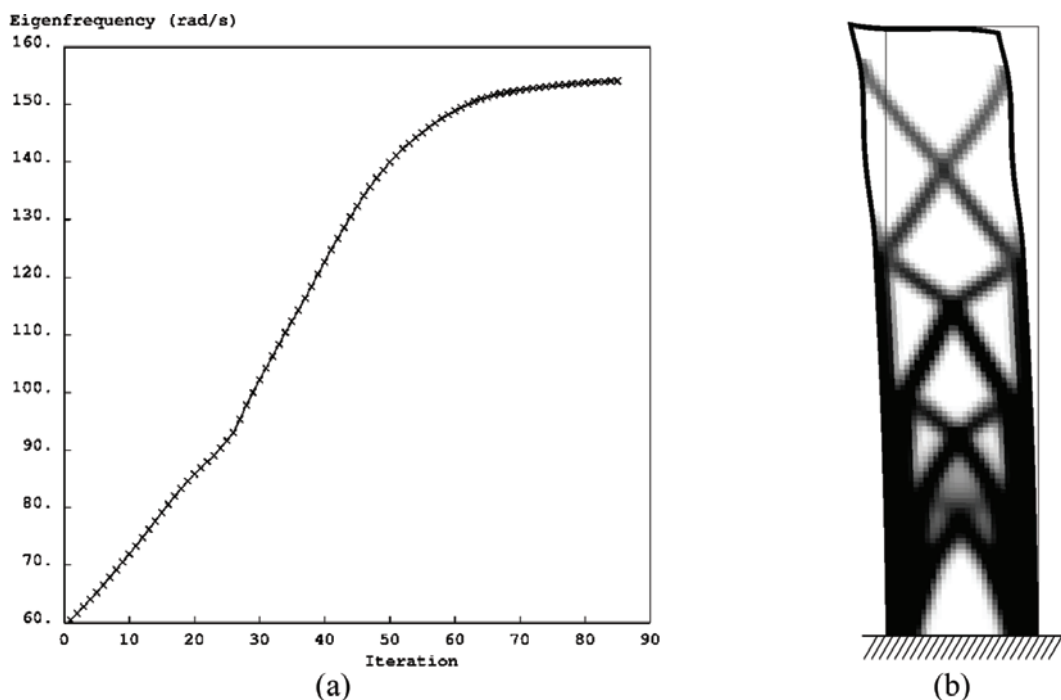
Figure 4 shows the values of the fundamental frequency and the first eigenmode. The fundamental frequency has increased from 60.4 rad/s in initial design to 154.1 rad/s after 85 iterations showing 155% increase. Note that the values of the fundamental frequency also depend on the penalty factor. If we analyze these designs with

$p = 1$, the initial and final eigenfrequencies will change to 105.2 rad/s and 174.0 rad/s respectively.

5. MULTIPLE EIGENFREQUENCIES

By steadily increasing (or decreasing) an eigenfrequency, it is possible that its value reaches adjacent eigenfrequencies resulting in multiple eigenfrequencies. The problem of multiple eigenvalues in structural optimization was first addressed by Olhoff and Rasmussen (1977). It is shown by Haug and Rousselet (1980) that the multiple eigenvalues are not differentiable in the Fréchet sense and can only be expected to be Gâteaux (directionally) differentiable. This finding rules out the validity of sensitivities calculated by Equation (1.18) in case of multiple eigenfrequencies. Ignoring this fact in topology optimization will result in oscillation of

Figure 4. Evolution history of the fundamental frequency (a) and the first eigenmode of the optimal design (b) in example 1



the objective function and suboptimal solutions as shown in the following example.

Example 2: Clamped-Clamped Beam

Consider the problem of maximization of the fundamental frequency of a clamped-clamped beam with volume fraction of 50% and material properties similar to example 1. All algorithmic parameters are similar to example 1. The structure has been discretized into 30×240 identical 4-node bi-linear square elements. The initial and the final solutions and the evolution of the first three eigenfrequencies are shown in Figure 5.

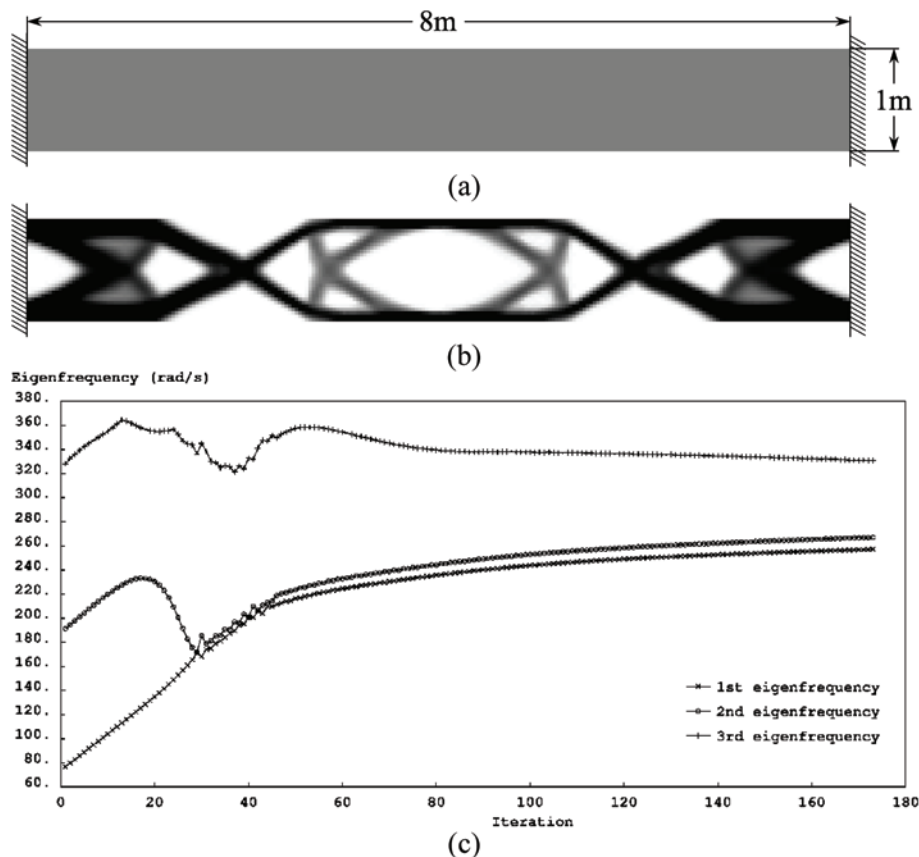
It can be seen that after 29 iterations, the first two eigenfrequencies coalesce. Using the single

modal sensitivities of Equation (1.18), decreases the objective function instead of increasing it. This produces oscillation after the point of coalesce and the algorithm converges at a suboptimal solution (Figure 5b).

5.1. Simple Approaches to Avoid Multiple Eigenfrequencies

A number of simple approaches can be used to avoid multiple eigenfrequencies. Kosaka and Swan (1999) proposed a symmetry reduction approach in which a symmetry condition is imposed on the design variables to ensure a symmetric solution. In their paper, Kosaka and Swan (1999) noted that in a symmetric structure, the multiple

Figure 5. Example 2 without treatment: initial design (a), final solution (b), and evolution of the eigenfrequencies (c)



eigenvalues are differentiable (in the Fréchet sense). Note that in this approach the symmetry reduction is not applied in the analysis and the analysis is based on the full structure. Using symmetry reduced structure for analysis cannot be validated in eigenfrequency optimization since the eigenmodes are not necessarily symmetric even for a symmetric structure.

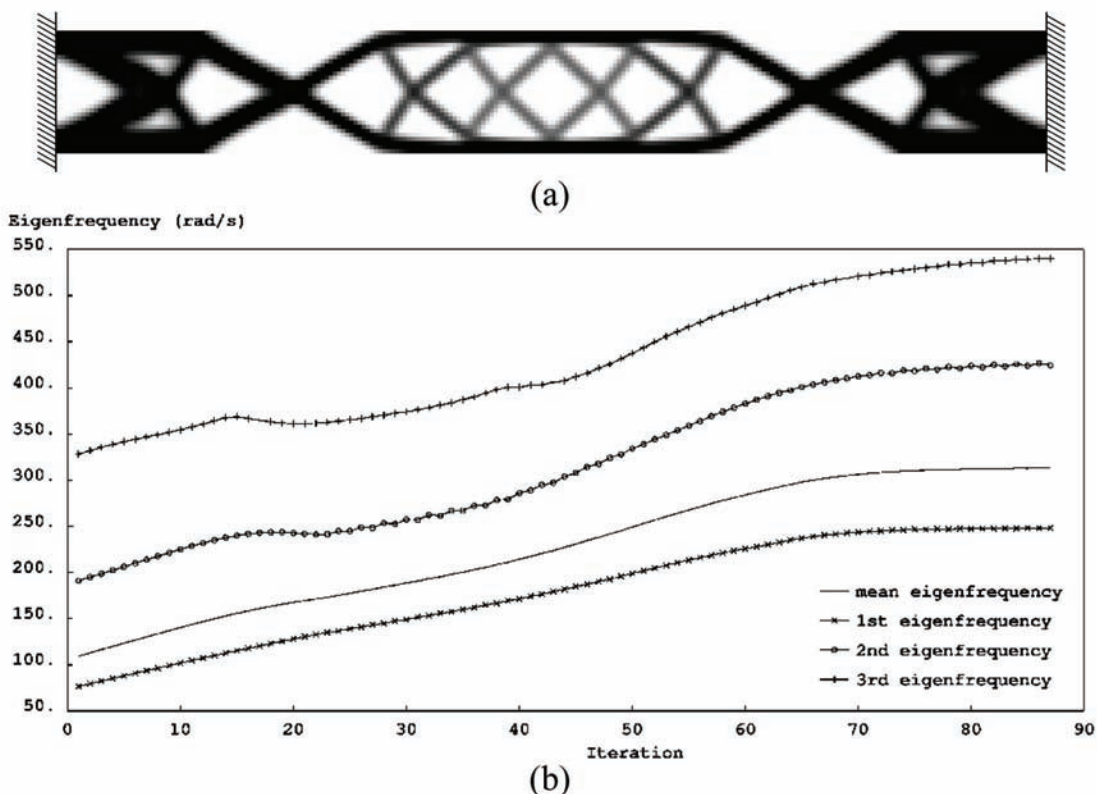
Another approach to avoid repeated eigenfrequencies is to add an extra condition to the optimization problem ensuring that the eigenfrequencies are distant from each other. For example one may reformulate problem (1.15) as follows (Bendsøe and Sigmund 2003).

$$\begin{aligned}
 & \max_{x_1, x_2, \dots, x_N} \beta \\
 \text{such that } & \alpha^j \lambda_j \geq \beta, \quad j = 1, 2, \dots, N_d \\
 & \mathbf{K}\Phi_j = \lambda_j \mathbf{M}\Phi_j, \quad j = 1, 2, \dots, N_d \\
 & \sum_{e=1}^N x_e v_e \leq \bar{v} \\
 & 0 \leq x_e \leq 1, \quad e = 1, 2, \dots, N
 \end{aligned} \tag{1.32}$$

with $\alpha < 1$, for example $\alpha = 0.95$. This formulation is known as *bound formulation*. Note that with $\alpha = 1$, Problem (1.32) is equivalent to Problem (1.15).

It is also possible to turn around the multiple eigenvalue problem by including adjacent eigenfrequencies in the objective function. For example Yang et al. (1999b) used the arithmetic mean of the eigenvalues as the objective function when

Figure 6. Solving example 2, using mean eigenfrequency as objective function: final solution (a) and evolution of the objective function and the first three eigenfrequencies (b)



they fell within a small distance from each other. A more generalized mean eigenvalue objective function has been considered by Ma et al. (1995). For example considering the harmonic mean of the first two eigenvalues, we can define the following objective function

$$\lambda^* = 2\left(\lambda_1^{-1} + \lambda_2^{-1}\right)^{-1} \quad (1.33)$$

Using this objective function in example 2 results in a smooth increase for the first two eigenvalues. Figure 6 shows the final solution and the evolution history of the first three eigenvalues considering the objective function defined in Equation (1.33) in example 2.

5.2. Sensitivity Analysis of Multiple Eigenvalues

It is also possible to solve the multimodal eigenfrequency optimization problems directly. Using a perturbation technique, Bratus and Seyranian (1983) calculated the sensitivities of multiple eigenvalues. Here we follow Seyranian et al. (1994) and Lund (1994) to present the sensitivity analysis of multiple eigenfrequencies.

Assume an m -fold multiple eigenvalue

$$\lambda_j = \tilde{\lambda}, \quad j = 1, \dots, m \quad (1.34)$$

Due to multiplicity, any linear combination of the corresponding eigenvectors will satisfy the main eigenvalue problem $\mathbf{K}\Phi_j = \lambda_j \mathbf{M}\Phi_j$. Now assume the following linear combination

$$\tilde{\Phi}_j = \sum_{k=1}^m \alpha_{jk} \Phi_k, \quad j = 1, \dots, m \quad (1.35)$$

where the coefficients α_{jk} are unknown. If we apply a perturbation ε to the i -th optimization variable the vector of design variables changes to $\mathbf{x} + \varepsilon \Delta \mathbf{x}_i$ where $\Delta \mathbf{x}_i$ denotes a vector of size N ,

all of its components being zero except for its i -th component which is 1.

Due to this perturbation, the stiffness and mass matrices will change to

$$\begin{aligned} \mathbf{K}(\mathbf{x} + \varepsilon \Delta \mathbf{x}_i) &= \mathbf{K} + \varepsilon \frac{\partial \mathbf{K}}{\partial x_i} + o(\varepsilon), \\ \mathbf{M}(\mathbf{x} + \varepsilon \Delta \mathbf{x}_i) &= \mathbf{M} + \varepsilon \frac{\partial \mathbf{M}}{\partial x_i} + o(\varepsilon) \end{aligned} \quad (1.36)$$

and the eigenvalues and the eigenvectors will change to

$$\lambda_j(\mathbf{x} + \varepsilon \Delta \mathbf{x}_i) = \tilde{\lambda} + \varepsilon \mu_j + o(\varepsilon), \quad j = 1, \dots, m \quad (1.37)$$

$$\Phi_j(\mathbf{x} + \varepsilon \Delta \mathbf{x}_i) = \tilde{\Phi}_j + \varepsilon \nu_j + o(\varepsilon), \quad j = 1, \dots, m \quad (1.38)$$

where μ_j and ν_j are the unknown sensitivities of the multiple eigenvalues and eigenvectors respectively. $o(\varepsilon)$ indicates higher order terms. Note that $\mu_j \equiv \mu_j(\mathbf{x}, \Delta \mathbf{x}_i)$ and $\nu_j \equiv \nu_j(\mathbf{x}, \Delta \mathbf{x}_i)$, i.e. the sensitivities depend on $\Delta \mathbf{x}_i$.

Using the perturbed values of Eqs. (1.36), (1.37), and (1.38) in the main eigenvalue problem, after ignoring the higher terms, one obtains

$$\left(\frac{\partial \mathbf{K}}{\partial x_i} - \tilde{\lambda} \frac{\partial \mathbf{M}}{\partial x_i} \right) \tilde{\Phi}_j + (\mathbf{K} - \tilde{\lambda} \mathbf{M}) \nu_j = \mu_j \mathbf{M} \tilde{\Phi}_j \quad (1.39)$$

Premultiplying Equation (1.39) by Φ_s^T , $s = 1, \dots, m$, the second term in the left-hand side will cancel out and one obtains the following m equations

$$\Phi_s^T \left(\frac{\partial \mathbf{K}}{\partial x_i} - \tilde{\lambda} \frac{\partial \mathbf{M}}{\partial x_i} \right) \tilde{\Phi}_j = \mu_j \Phi_s^T \mathbf{M} \tilde{\Phi}_j, \quad s = 1, \dots, m \quad (1.40)$$

We now substitute Equation (1.35) in Equation (1.40) and use Equation (1.6) to write

$$\sum_{k=1}^m \alpha_{jk} \left[\Phi_s^T \left(\frac{\partial \mathbf{K}}{\partial x_i} - \tilde{\lambda} \frac{\partial \mathbf{M}}{\partial x_i} \right) \Phi_k - \mu_j \delta_{sk} \right] = 0, \quad s = 1, \dots, m \quad (1.41)$$

This linear system can be solved to calculate the coefficients α_{jk} . A non-trivial solution only exists if

$$\det \left[\Phi_s^T \left(\frac{\partial \mathbf{K}}{\partial x_i} - \tilde{\lambda} \frac{\partial \mathbf{M}}{\partial x_i} \right) \Phi_k - \mu_j \delta_{sk} \right] = 0, \quad s, k = 1, \dots, m \quad (1.42)$$

This subeigenvalue problem can be solved to calculate the sensitivities $\mu_j, j = 1, \dots, m$ due to the increment of the i -th optimization variable.

If the vector of design variables undergo an increment of the form $\alpha \mathbf{e}$ with $\mathbf{e} = (\Delta x_1, \Delta x_2, \dots, \Delta x_N)^T$ and $\|\mathbf{e}\| = 1$, one can easily generalize Equation (1.42) to

$$\det \left[\mathbf{f}_{sk}^T \mathbf{e} - \mu \delta_{sk} \right] = 0, \quad s, k = 1, \dots, m \quad (1.43)$$

where

$$\mathbf{f}_{sk}^T = \left(\Phi_s^T \left(\frac{\partial \mathbf{K}}{\partial x_1} - \tilde{\lambda} \frac{\partial \mathbf{M}}{\partial x_1} \right) \Phi_k, \Phi_s^T \left(\frac{\partial \mathbf{K}}{\partial x_2} - \tilde{\lambda} \frac{\partial \mathbf{M}}{\partial x_2} \right) \Phi_k, \dots, \Phi_s^T \left(\frac{\partial \mathbf{K}}{\partial x_N} - \tilde{\lambda} \frac{\partial \mathbf{M}}{\partial x_N} \right) \Phi_k \right)^T, \\ s, k = 1, \dots, m \quad (1.44)$$

are known as the generalized gradient vectors (Seyranian et al. 1994). Note that \mathbf{f}_{sk} are vectors of length N , thus $\mathbf{f}_{sk}^T \mathbf{e}$ are scalars. Also note that due to symmetry of the stiffness and mass matrices $\mathbf{f}_{sk} = \mathbf{f}_{ks}$.

The solutions of subeigenvalue problem of Equation (1.43) are the sensitivities of the multiple eigenvalues. This equation was initially introduced by Bratus and Seyranian (1983).

5.3. Solution Algorithm

Assume that Φ is an $N_d \times m$ matrix whose columns are the eigenvectors Φ_1, \dots, Φ_m . Also consider the vector $\mathbf{d} = (d_1, d_2, \dots, d_N)^T$ defined as

$$d_e = \frac{\partial \mathbf{K}}{\partial x_e} - \tilde{\lambda} \frac{\partial \mathbf{M}}{\partial x_e}, \quad e = 1, \dots, N \quad (1.45)$$

Then the subeigenvalue problem of Equation (1.43) can be stated in the following matrix form

$$\mathbf{A} - \mu \mathbf{I} = 0 \quad (1.46)$$

where $\mathbf{A} = \Phi^T \Phi \mathbf{d}^T \mathbf{e}$ is a symmetric $m \times m$ matrix and $\mathbf{I}_{m \times m}$ is the unity matrix.

Following Cox and Overton (1992) and Overton (1992), the necessary optimality conditions to solve problem (1.15) is that there exists an $m \times m$ symmetric positive semidefinite matrix Λ with $\text{trace}(\Lambda) = 1$ such that

$$\begin{aligned} \tilde{D}_e &= \Lambda : (\Phi^T d_e \Phi) - \Gamma v_e = \gamma_e \\ \Gamma \left(\bar{v} - \sum_{e=1}^N x_e v_e \right) &= 0; \quad \bar{v} - \sum_{e=1}^N x_e v_e \geq 0; \quad \Gamma \geq 0 \\ x_e = 0 &\Rightarrow \gamma_e \leq 0 \\ 0 < x_e < 1 &\Rightarrow \gamma_e = 0 \\ x_e = 1 &\Rightarrow \gamma_e \geq 0 \\ e &= 1, \dots, N \end{aligned} \quad (1.47)$$

where the Frobenius matrix inner product is defined as $\mathbf{A} : \mathbf{B} = \text{trace}(\mathbf{A}^T \mathbf{B})$.

The proof of optimality conditions in (1.47) will not be presented here. Enthusiast reader is referred to Cox and Overton (1992), Overton (1992), and Seyranian et al. (1994).

Note that for the case of simple eigenvalues ($m = 1$), one should have $\Lambda = 1$ and optimality conditions in (1.47) reduce to (1.21). Comparing (1.47) with (1.21), one may note that the only difference is that the sensitivities $\partial \lambda / \partial x_e$ in (1.21) have been

replaced by $\Lambda : (\Phi^T d_e \Phi)$ in (1.47). The only issue here is to find a suitable matrix Λ .

Similar to Equation (1.24), we consider the following increment vector

$$\Delta x_e = \tilde{D}_e = \Lambda : (\Phi^T d_e \Phi) - \Gamma v_e, \quad e = 1, \dots, N \quad (1.48)$$

To illustrate the calculation of Λ , we consider the simplest multiple case of $m = 2$. We assume that the two eigenvalues are repeated if

$$\frac{\lambda_2 - \lambda_1}{\lambda_1} \leq \delta \quad (1.49)$$

with δ being a small positive tolerance. In this case we have

$$\Phi = (\Phi_1, \Phi_2) \quad (1.50)$$

We also introduce the following positive semidefinite symmetric matrix

$$\Lambda^* = \begin{pmatrix} \Lambda_{11}^* & \Lambda_{12}^* \\ \Lambda_{12}^* & \Lambda_{22}^* \end{pmatrix} \quad (1.51)$$

based on which we define

$$\Lambda = \frac{\Lambda^*}{\text{trace}(\Lambda^*)} \quad (1.52)$$

to ensure that $\text{trace}(\Lambda) = 1$.

Substituting Equation (1.51) in Equation (1.48) and using Eqs. (1.45) and (1.44), we may rewrite Equation (1.48) in the following form

$$\Delta x = \Lambda_{11}^* \mathbf{f}_{11} + 2\Lambda_{12}^* \mathbf{f}_{12} + \Lambda_{22}^* \mathbf{f}_{22} - \Gamma \mathbf{v} \quad (1.53)$$

The change in the multiple eigenvalues $\Delta\lambda_1$ and $\Delta\lambda_2$ due to Δx can be calculated by solving the

following quadratic equation which is emerged from Equation (1.43)

$$\det \begin{pmatrix} \mathbf{f}_{11}^T \Delta x - \Delta\lambda & \mathbf{f}_{12}^T \Delta x \\ \mathbf{f}_{12}^T \Delta x & \mathbf{f}_{22}^T \Delta x - \Delta\lambda \end{pmatrix} = 0 \quad (1.54)$$

We are interested in finding Λ_{ij}^* such that Equation (1.54) results in two positive eigenvalues $\Delta\lambda_1 > 0$ and $\Delta\lambda_2 > 0$. There are several ways to achieve this. Here we assume the following

$$\Delta\lambda_1 = \mathbf{f}_{11}^T \Delta x = 1 \quad (1.55)$$

$$\Delta\lambda_2 = \mathbf{f}_{22}^T \Delta x = 1 - \frac{\lambda_2 - \lambda_1}{\lambda_1} \quad (1.56)$$

$$\mathbf{f}_{12}^T \Delta x = 0 \quad (1.57)$$

Equation (1.57) implies that the matrix in Equation (1.54) is diagonal, hence the eigenvalues are equivalent to the diagonal terms as stated in Eqs. (1.55) and (1.56). In Equation (1.55) we considered an increase of 1 for the lowest eigenvalue. If the two eigenvalues are different, the increase assigned to the second eigenvalue in Equation (1.56) will be slightly lower than 1. This is to reduce the difference between the two repeated eigenvalues.

Substituting Equation (1.53) in Eqs. (1.55) to (1.57), we obtain a set of three equations which can be solved to yield the three unknown coefficients Λ_{11}^* , Λ_{22}^* , and Λ_{12}^* . These equations can be summarized as

$$\begin{bmatrix} \mathbf{f}_{11}^T \mathbf{f}_{11} & \mathbf{f}_{11}^T \mathbf{f}_{22} & \mathbf{f}_{11}^T \mathbf{f}_{12} \\ \mathbf{f}_{22}^T \mathbf{f}_{11} & \mathbf{f}_{22}^T \mathbf{f}_{22} & \mathbf{f}_{22}^T \mathbf{f}_{12} \\ \text{symm.} & \mathbf{f}_{12}^T \mathbf{f}_{12} & \end{bmatrix} \begin{Bmatrix} \Lambda_{11}^* \\ \Lambda_{22}^* \\ 2\Lambda_{12}^* \end{Bmatrix} = \begin{Bmatrix} 1 + \Gamma \mathbf{f}_{11}^T \mathbf{v} \\ 1 - \frac{\lambda_2 - \lambda_1}{\lambda_1} + \Gamma \mathbf{f}_{22}^T \mathbf{v} \\ \Gamma \mathbf{f}_{12}^T \mathbf{v} \end{Bmatrix} \quad (1.58)$$

By solving Equation (1.58) one finds Λ^* which is used in Equation (1.52) to find Λ and

subsequently Δx from Equation (1.53). Like the single modal case, to find the value of the Lagrange multiplier Γ an inner bisection loop can be used.

Figure 7 shows the final solution and the evolution history of the first three eigenfrequencies of the problem of example 2 using the above approach. It can be seen that the multiple eigenvalues evolve smoothly and a better solution is achieved.

Table 1 compares the final value of the first three eigenfrequencies of example 2 obtained using the three approaches considered here. As expected, using the multiple eigenvalue sensitivities yields the best result.

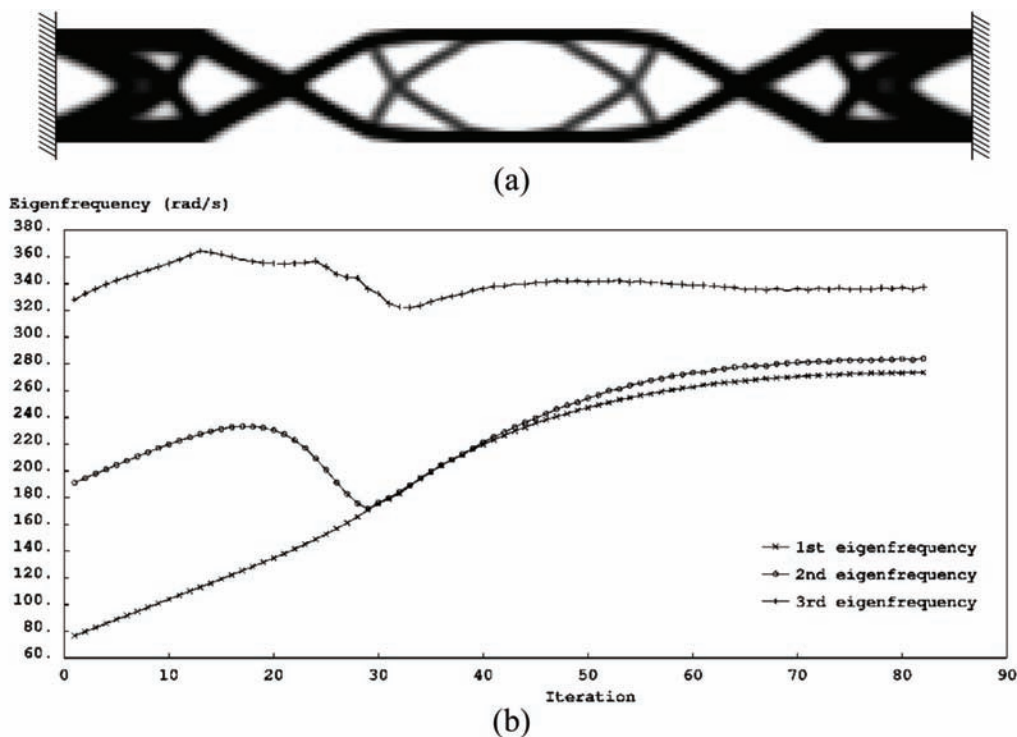
6. CONTROLLING THE NATURAL FREQUENCIES

In dynamic design of structures one usually requires to control the natural frequencies rather

than increasing them. For an objective function defined as a combination of natural frequencies, the optimization problem can usually be addressed by minimal modification of the eigenfrequency maximization problem. Typically one just needs to update the sensitivities. One example of such objective functions was defined in Equation (1.33) and dealt with in the preceding section. Other examples include maximizing the gap between two natural frequencies (see e.g. Du and Olhoff 2007 and Zhao et al. 1997) or designing structures with a specified set of frequencies or eigenmode shapes (see e.g. Xie and Steven 1996, Yang et al. 1999b, Maeda et al. 2006) among others.

A common practical case is where the excitation frequency is known and it is desired to move the natural frequencies as far away as possible from the excitation frequency. A suitable objective function can be defined as

Figure 7. Solving example 2, using multiple eigenvalue sensitivities: final solution (a) and evolution of the first three eigenfrequencies (b)



$$f = \sum_{j \in J} |\omega_j^2 - \Omega^2| \quad (1.59)$$

in which Ω is the excitation frequency and $J \subseteq \{1, \dots, N_d\}$ is a set of natural frequencies considered. If we only consider the closest natural frequencies to Ω , the problem reduces to maximizing the gap between the adjacent natural frequencies. Maximizing the fundamental frequency is a special case of this problem with $\Omega = 0$.

Maximizing the gap between two natural frequencies can lead to multiple eigenfrequencies (Du and Olhoff 2007). The following example illustrates this.

Example 3: Planar Frame with Non-Structural Mass

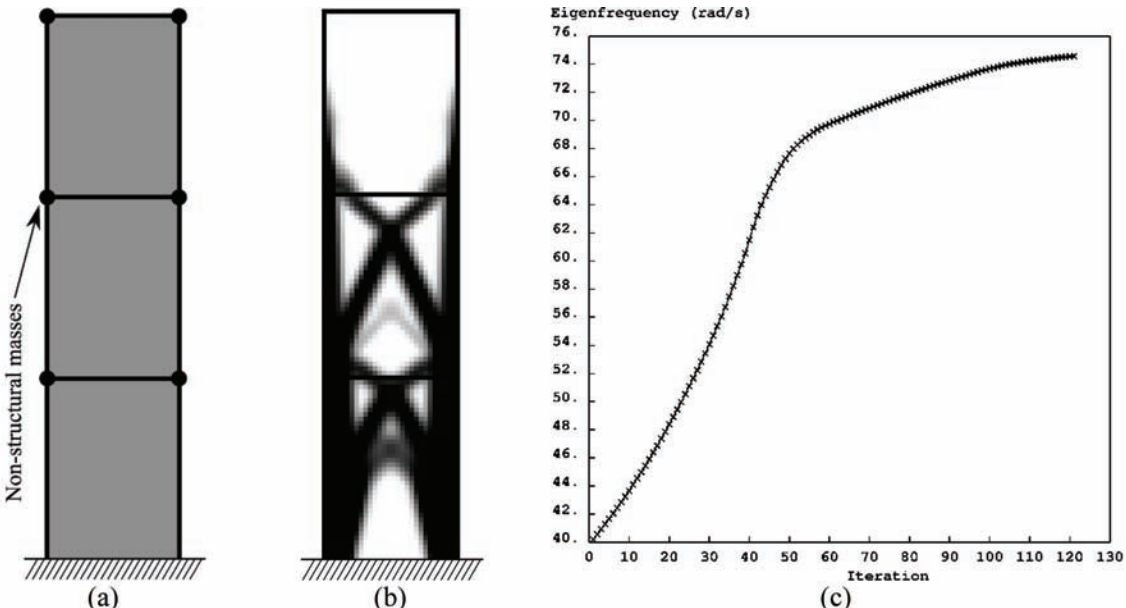
A three-level planar frame is considered with 6 non-structural masses of 20,000kg each attached to it as shown in Figure 8a. The ratio between the stiffness of solid and void areas is reduced to $\bar{E} : E = 100$. All other parameters are similar to example 1.

We first maximize the fundamental frequency of the frame. The evolution history of the fundamental frequency and the final solution are shown in Figures 8b and 8c respectively. The fundamental frequency has increased by 85% from 40.2 to 74.6rad/s.

Table 1. Comparison of the results of the three approaches used to solve example 2

Approach	ω_1 (rad/s)	ω_2 (rad/s)	ω_3 (rad/s)
Using single eigenvalue sensitivities (1.18)	257.1	267.1	330.9
Using the mean eigenvalue (1.33) as objective function	248.0	424.4	540.2
Using multiple eigenvalue sensitivities (1.43)	273.5	284.0	337.6

Figure 8. Example 3: initial design (a), final solution (b), and evolution of the fundamental frequency (c)



The first four natural frequencies of the initial structure are $\omega_1 = 40.2$, $\omega_2 = 163$, $\omega_3 = 215$, and $\omega_4 = 326$ (rad/s). We now assume an excitation frequency of 175 rad/s which falls between the second and the third natural frequencies, and try to move the natural frequencies of the structure away from this frequency. The problem can be simplified to maximizing the gap between the second and the third natural frequencies, i.e., maximizing the following objective function

$$f = \omega_3^2 - \omega_2^2 \quad (1.60)$$

The solution procedure explained in section 5.3 has been adopted. The optimal topology and the evolution history of the first four natural frequencies are depicted in Figure 9. The optimization algorithm, tries to increase the third natural frequency while decreasing the second natural frequency. After nearly 15 iterations, the third eigenfrequency coalesced with the fourth one but

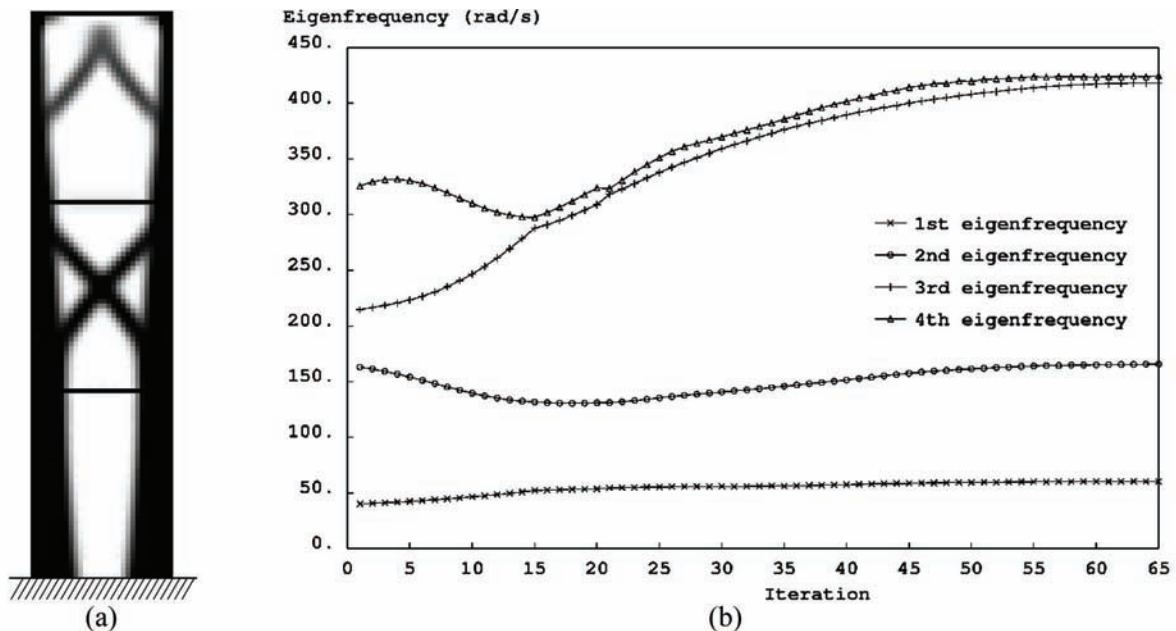
this multiple eigenfrequency has been handled well by the algorithm.

7. FORCED VIBRATION

In previous sections we have focused on free vibration and did not include external forces in our formulations. This section deals with topology optimization in forced vibration where the external dynamic forces are explicitly considered in the problem formulation. Similar to previous sections we ignore damping effects, uncertainties of the forces, geometry, and materials and consider linear elastic material behavior.

Applications of topology optimization in forced vibration have been initially studied by Ma et al. (1993) and Ma et al. (1995) using a homogenization approach. Ma et al. (1995) briefly discussed the forced vibration problem under periodic loads and defined the dynamic compliance

Figure 9. Maximizing the gap between the third and the second eigenfrequencies of the frame of example 3: final solution (a) and evolution of the first four eigenfrequencies (b). The first four eigenfrequencies of the optimal structure are $\omega_1 = 74.6$, $\omega_2 = 190$, $\omega_3 = 397$, and $\omega_4 = 408$ (rad/s).



as the objective function to be minimized. Min et al. (1999) minimized the dynamic compliance for structures under impulsive loads. The topology design of structures under periodic loads has been studied more extensively by Jog (2002) where he proposed a new positive-definite definition of dynamic compliance as the average input power over a cycle. Jog (2002) also studied the problem of minimizing the vibration amplitude at certain control points. Topology design of structures subjected to design-dependent dynamic loads (e.g. hydrodynamic pressure loading) has been addressed by Olhoff and Du (2005). In more recent publications in this area, alternative approaches in using topology optimization to control the structural responses in a frequency interval has been studied by Jensen (2007) and Yoon (2010b).

Consider a harmonic external force of form

$$\mathbf{p} = \mathbf{p}_c \cos \Omega t \quad (1.61)$$

where \mathbf{p}_c does not depend on time. The equation of motion for a discretized undamped system in forced vibration takes the form

$$\mathbf{M}\ddot{\mathbf{u}} + \mathbf{K}\mathbf{u} = \mathbf{p}_c \cos \Omega t \quad (1.62)$$

To solve this problem, we consider $\mathbf{u} = \mathbf{u}_c \cos \Omega t$ using which in Equation (1.62) gives

$$(\mathbf{K} - \Omega^2 \mathbf{M}) \mathbf{u}_c = \mathbf{p}_c \quad (1.63)$$

or

$$(\mathbf{K} - \Omega^2 \mathbf{M}) \mathbf{u} = \mathbf{p} \quad (1.64)$$

Comparing with equilibrium equation in static state, $\mathbf{K} - \Omega^2 \mathbf{M}$ can be termed as “dynamic stiffness”. Note that unlike the static stiffness, the dynamic stiffness matrix is not necessarily positive definite.

7.1. Objective Function and Problem Formulation

Under static loads, the compliance defined as

$$c = \mathbf{p}^T \mathbf{u} \quad (1.65)$$

is proportional to the strain energy of the structure and is a typical objective function used in topology optimization of structures. Minimizing the compliance maximizes the stiffness of the structure. Under dynamic loads, the value of c defined in Equation (1.65) varies with time. For structures subjected to periodic loads, we consider the average of c over a cycle, i.e.

$$\bar{c} = \frac{\Omega}{2\pi} \int_0^{2\pi/\Omega} \mathbf{p}^T \mathbf{u} dt \quad (1.66)$$

as the objective function to be minimized. Here $T = 2\pi/\Omega$ is the time period. Note that this measure is not always positive, and thus, in problem formulation, one should consider the absolute value (or square) of average compliance as the objective function. Otherwise, for $\bar{c} < 0$, the optimization algorithm will push the structure towards resonance.

In absence of damping, $\mathbf{u} = \mathbf{u}_c \cos \Omega t$. Using this and $\mathbf{p} = \mathbf{p}_c \cos \Omega t$ in Equation (1.66), we can write

$$\bar{c} = \frac{\Omega \mathbf{p}_c^T \mathbf{u}_c}{2\pi} \int_0^{2\pi/\Omega} \cos^2 \Omega t dt = \frac{1}{2} \mathbf{p}_c^T \mathbf{u}_c \quad (1.67)$$

The average compliance minimization problem can now be formulated as follows

$$\begin{aligned} \min_{x_1, x_2, \dots, x_N} \quad & c_m = 2 |\bar{c}| = |\mathbf{p}_c^T \mathbf{u}_c| \\ \text{such that} \quad & (\mathbf{K} - \Omega^2 \mathbf{M}) \mathbf{u}_c = \mathbf{p}_c \\ & \sum_{e=1}^N x_e v_e \leq \bar{v} \\ & 0 < x_{\min} \leq x_e \leq 1, e = 1, 2, \dots, N \end{aligned} \quad (1.68)$$

7.2. Sensitivity Analysis

In order to calculate the sensitivities, we rewrite the dynamic compliance by adding an (arbitrary) adjoint vector multiplied by a zero function

$$c_m = |\mathbf{p}_C^T \mathbf{u}_C| + \tilde{\mathbf{u}}^T [(\mathbf{K} - \Omega^2 \mathbf{M}) \mathbf{u}_C - \mathbf{p}_C] \quad (1.69)$$

Differentiating with respect to the design variables and rearranging the terms, we obtain

$$\frac{\partial c_m}{\partial x_e} = [\text{sign}(\bar{c}) \mathbf{p}_C^T + \tilde{\mathbf{u}}^T (\mathbf{K} - \Omega^2 \mathbf{M})] \frac{\partial \mathbf{u}_C}{\partial x} + \tilde{\mathbf{u}}^T \left(\frac{\partial \mathbf{K}}{\partial x} - \Omega^2 \frac{\partial \mathbf{M}}{\partial x} \right) \mathbf{u}_C \quad (1.70)$$

where $\text{sign}()$ is the sign function. Sensitivities of the dynamic compliance can now be written as

$$\frac{\partial c_m}{\partial x_e} = \tilde{\mathbf{u}}^T \left(\frac{\partial \mathbf{K}}{\partial x} - \Omega^2 \frac{\partial \mathbf{M}}{\partial x} \right) \mathbf{u}_C \quad (1.71)$$

in which the adjoint vector is selected such that

$$(\mathbf{K} - \Omega^2 \mathbf{M}) \tilde{\mathbf{u}} = -\text{sign}(\bar{c}) \mathbf{p}_C \quad (1.72)$$

Comparing Equation (1.72) with Equation (1.63), the adjoint vector is found to be $\tilde{\mathbf{u}} = -\text{sign}(\mathbf{p}_C^T \mathbf{u}_C) \mathbf{u}_C$ which can be substituted in Equation (1.71) to simplify the latter to

$$\frac{\partial c_m}{\partial x_e} = -\text{sign}(\bar{c}) \mathbf{u}_C^T \left(\frac{\partial \mathbf{K}}{\partial x} - \Omega^2 \frac{\partial \mathbf{M}}{\partial x} \right) \mathbf{u}_C \quad (1.73)$$

Having the sensitivities calculated, an appropriate solution method such as the method of moving asymptotes (MMA) can be employed to solve the minimization problem. One can also use the OC-based solution procedure proposed in section 4.2. The optimality criteria to solve Problem (1.68) can be expressed as

$$D_e = -\frac{\partial c_m}{\partial x_e} - \Gamma v_e = \gamma_e, \quad e = 1, \dots, N \quad (1.74)$$

with additional conditions similar to (1.21). The negative sign for $\partial c_m / \partial x$ in Equation (1.74) is added because it relates to a minimization problem.

7.3. Examples

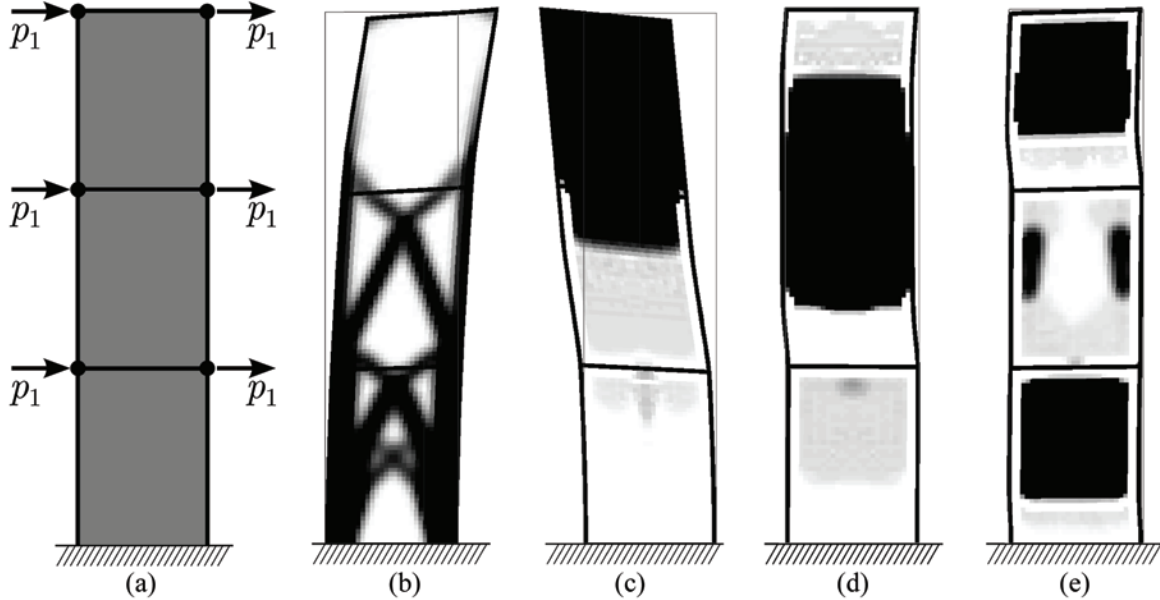
The frame in example 3 is considered under forced vibration. It is assumed that 6 identical horizontal periodic loads of magnitude $p_1 = 500$ kN and frequency of Ω are applied at locations of the concentrated masses as shown in Figure 10a. Note that for linear elastic materials, changing the force magnitude will only change the values of the objective function but the evolution pattern of the objective function values and the final topology will remain unchanged. This is not true for nonlinear problems.

Deformed shapes of optimum topologies obtained for different load frequencies are shown in Figure 10b-e. It can be seen that for high frequencies, the optimum material distribution tends to form damping masses.

When the input frequency is greater than the fundamental frequency of the initial structure, the optimization algorithm reduces the fundamental frequency. This increases the static compliance and can lead to disintegrated designs (clearly observable in Figure 10e). To prevent this disintegration, one can introduce an upper bound condition on static compliance in the problem formulation (Olhoff and Du 2005). One can also include the static compliance in the objective function as shown in Figure 10.

When the structure is subjected to a number of loads with different frequencies, one can define a multi-objective optimization problem to handle the case. This is of practical importance, for example when one approximates a periodic load using Fourier series. In the following example,

Figure 10. Minimizing the dynamic compliance of the frame of example 3 under periodic loading: external periodic loads (a), and deformed shape of final topologies for different input frequencies; $\Omega = 0$ (static loading) (b), $\Omega = 60 \text{ rad/s}$ (c), $\Omega = 175 \text{ rad/s}$ (d), and $\Omega = 330 \text{ rad/s}$ (e). The first four natural frequencies of the initial structure are $\omega_1 = 40.2$, $\omega_2 = 163$, $\omega_3 = 215$, and $\omega_4 = 326$ (rad/s).



we consider the structure to be subjected to a periodic load $\mathbf{p}_1 = \mathbf{p}_{C_1} \cos \Omega t$ and a static load \mathbf{p}_2 (with frequency of zero). The objective function is considered as

$$c_m = |\mathbf{p}_{C_1}^T \mathbf{u}_{C_1}| + \mathbf{p}_2^T \mathbf{u}_2 \quad (1.75)$$

where

$$(\mathbf{K} - \Omega^2 \mathbf{M}) \mathbf{u}_{C_1} = \mathbf{p}_{C_1} \quad \text{and} \quad \mathbf{K} \mathbf{u}_2 = \mathbf{p}_2 \quad (1.76)$$

Sensitivities of this objective function can be calculated as

$$\frac{\partial c_m}{\partial x} = -\text{sign}(\mathbf{p}_{C_1}^T \mathbf{u}_{C_1}) \mathbf{u}_{C_1}^T \left(\frac{\partial \mathbf{K}}{\partial x} - \Omega^2 \frac{\partial \mathbf{M}}{\partial x} \right) \mathbf{u}_{C_1} - \mathbf{u}_2^T \frac{\partial \mathbf{K}}{\partial x} \mathbf{u}_2 \quad (1.77)$$

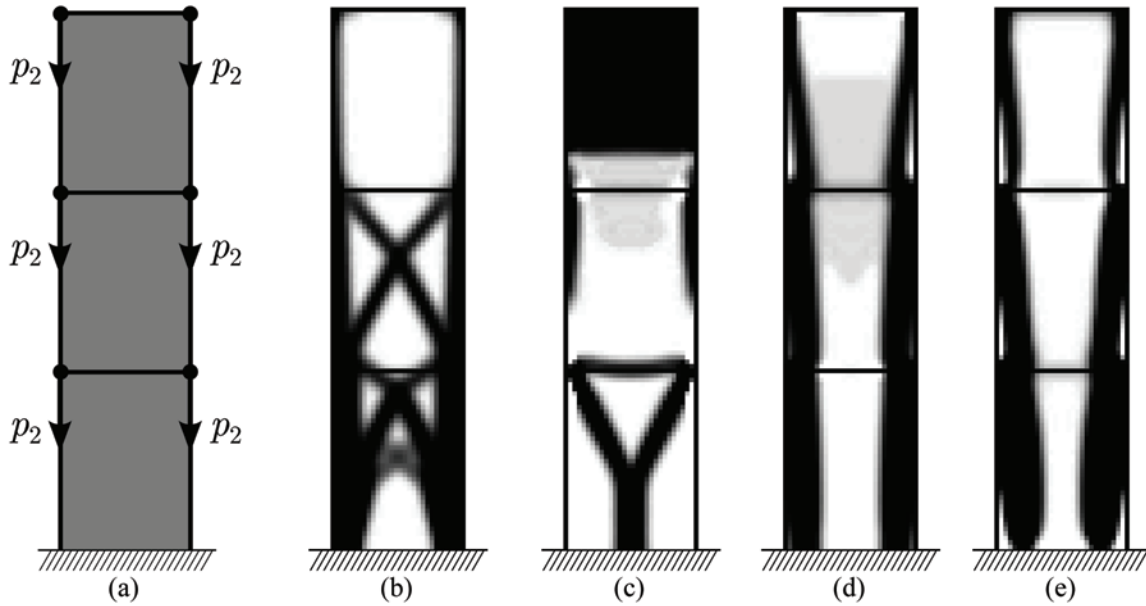
The previous example is considered under the dynamic loads (\mathbf{p}_1) in Figure 10a and the static loads (\mathbf{p}_2) shown in Figure 11a. The ratio between the magnitude of the loads is $p_2:p_1 = 5$. Various optimal topologies resulted from using various input frequencies of \mathbf{p}_1 are illustrated in Figure 11b-e.

In a similar manner one can optimize the topology of a structure under any combination of static and periodic loads with different frequencies.

8. OTHER CONSIDERATIONS

So far we have simplified the optimization problems by ignoring the damping effects and non-linear material behavior. We have also limited our study to small deformations. Considering large deformations will lead to geometrically non-linear problems.

Figure 11. Minimizing the dynamic compliance of the frame of example 3 under a combination of periodic loading of Figure 10a and static loading: external static loads (a), and final topologies for different input frequencies of the periodic load; $\Omega = 0$ (b), $\Omega = 60 \text{ rad/s}$ (c), $\Omega = 175 \text{ rad/s}$ (d), and $\Omega = 330 \text{ rad/s}$ (e)



Including either geometrical or material non-linearity in problems causes the stiffness matrix to be load-dependent. The equilibrium equations in such problems are commonly solved by the Newton-Raphson method. Finding eigenfrequencies will require a subsequent modal analysis.

Sensitivity analysis of a general displacement-based functional in a geometrically and materially non-linear system has been formulated by Jung and Gea (2004). This formulation can be used to calculate sensitivities of compliance-like objective functions. Similar procedure of deriving the sensitivities of an energy functional for a non-linear system is presented in Section 9.1.

In geometrically non-linear problems, the extremely soft “void” elements of the SIMP material model can be troublesome showing zero or even negative tangent stiffness and causing serious convergence problems (see e.g. Buhl et al. 2000). A new approach called Element Connectivity Parameterization has been proposed by Yoon and Kim (2005) to address this problem. This approach

proves to be useful in topology optimization of non-linear structures under dynamic loads (Yoon 2010a, 2011). Another approach to solve this issue is eliminating the void elements (see Section 9.1).

Considering damping effects will also change the sensitivities of the objective functions considered. In the following we update the previously derived sensitivities in presence of damping.

8.1. Forced Vibration with Damping

The equation of motion under a periodic load takes the form

$$\mathbf{M}\ddot{\mathbf{u}} + \mathbf{C}\dot{\mathbf{u}} + \mathbf{K}\mathbf{u} = \mathbf{p} = \mathbf{p}_c \cos \Omega t \quad (1.78)$$

Introducing the complex displacement $\mathbf{z} = (\mathbf{z}_c + i\mathbf{z}_s)e^{i\Omega t}$, and assuming \mathbf{u} to be the real part of \mathbf{z} , we rewrite this equation in the complex space as

$$\mathbf{M}\ddot{\mathbf{z}} + \mathbf{C}\dot{\mathbf{z}} + \mathbf{K}\mathbf{z} = \mathbf{p}_c e^{i\Omega t} \quad (1.79)$$

Separating the real and imaginary parts, we obtain

$$\begin{cases} \mathbf{B}\mathbf{z}_C - \Omega\mathbf{C}\mathbf{z}_S = \mathbf{p}_c \\ \mathbf{B}\mathbf{z}_S + \Omega\mathbf{C}\mathbf{z}_C = 0 \end{cases} \quad (1.80)$$

where $\mathbf{B} = \mathbf{K} - \Omega^2\mathbf{M}$. Calculating \mathbf{z}_S from the second equation in (1.80) yields

$$\mathbf{z}_S = -\Omega\mathbf{B}^{-1}\mathbf{C}\mathbf{z}_C \quad (1.81)$$

After substituting in the first equation in (1.80), we get

$$\hat{\mathbf{K}}\mathbf{z}_C = \mathbf{p}_c \quad (1.82)$$

where

$$\hat{\mathbf{K}} = \mathbf{B} + \Omega^2\mathbf{C}\mathbf{B}^{-1}\mathbf{C} \quad (1.83)$$

The displacement vector \mathbf{u} is the real part of \mathbf{z} , so

$$\mathbf{u} = \Re((\mathbf{z}_C + i\mathbf{z}_S)e^{i\Omega t}) = (\cos \Omega t)\mathbf{z}_C - (\sin \Omega t)\mathbf{z}_S \quad (1.84)$$

Using this and $\mathbf{p} = \mathbf{p}_c \cos \Omega t$ in Equation (1.66), we can write

$$\bar{c} = \frac{\Omega}{2\pi} \int_0^{2\pi/\Omega} (\mathbf{p}_c^T \mathbf{z}_C \cos^2 \Omega t - \mathbf{p}_c^T \mathbf{z}_S \cos \Omega t \sin \Omega t) dt = \frac{1}{2} \mathbf{p}_c^T \mathbf{z}_C \quad (1.85)$$

Differentiating with respect to design variable x_e , we obtain

$$\frac{\partial \bar{c}}{\partial x_e} = \frac{1}{2} \mathbf{p}_c^T \frac{\partial \mathbf{z}_C}{\partial x_e} \quad (1.86)$$

But from Equation (1.82),

$$\frac{\partial \hat{\mathbf{K}}}{\partial x_e} \mathbf{z}_C + \hat{\mathbf{K}} \frac{\partial \mathbf{z}_C}{\partial x_e} = 0 \Rightarrow \hat{\mathbf{K}} \frac{\partial \mathbf{z}_C}{\partial x_e} = -\frac{\partial \hat{\mathbf{K}}}{\partial x_e} \mathbf{z}_C \quad (1.87)$$

which can be used in Equation (1.86) to yield

$$\frac{\partial \bar{c}}{\partial x_e} = \frac{1}{2} \mathbf{p}_c^T \frac{\partial \mathbf{z}_C}{\partial x_e} = \frac{1}{2} \mathbf{z}_C^T \hat{\mathbf{K}} \frac{\partial \mathbf{z}_C}{\partial x_e} = -\frac{1}{2} \mathbf{z}_C^T \frac{\partial \hat{\mathbf{K}}}{\partial x_e} \mathbf{z}_C \quad (1.88)$$

We thus need to calculate $\partial \hat{\mathbf{K}} / \partial x_e$. Before proceeding we note that

$$\mathbf{B}^{-1}\mathbf{B} = \mathbf{I} \Rightarrow \frac{\partial \mathbf{B}^{-1}}{\partial x_e} \mathbf{B} + \mathbf{B}^{-1} \frac{\partial \mathbf{B}}{\partial x_e} = 0 \Rightarrow \frac{\partial \mathbf{B}^{-1}}{\partial x_e} = -\mathbf{B}^{-1} \frac{\partial \mathbf{B}}{\partial x_e} \mathbf{B}^{-1} \quad (1.89)$$

in which we used the fact that \mathbf{B} is symmetric, i.e. $\mathbf{B}^T = \mathbf{B}$. Differentiating Equation (1.83) and making use of Equation (1.89) and symmetry of \mathbf{B} and \mathbf{C} , we obtain

$$\frac{\partial \hat{\mathbf{K}}}{\partial x_e} = \frac{\partial \mathbf{B}}{\partial x_e} - \Omega^2 \mathbf{C} \mathbf{B}^{-1} \frac{\partial \mathbf{B}}{\partial x_e} \mathbf{B}^{-1} \mathbf{C} + 2\Omega^2 \frac{\partial \mathbf{C}}{\partial x_e} \mathbf{B}^{-1} \mathbf{C} \quad (1.90)$$

Pre- and post-multiplying by \mathbf{z}_C and using Equation (1.81), we achieve

$$\mathbf{z}_C^T \frac{\partial \hat{\mathbf{K}}}{\partial x_e} \mathbf{z}_C = \mathbf{z}_C^T \frac{\partial \mathbf{B}}{\partial x_e} \mathbf{z}_C - \mathbf{z}_S^T \frac{\partial \mathbf{B}}{\partial x_e} \mathbf{z}_S - 2\Omega \mathbf{z}_C^T \frac{\partial \mathbf{C}}{\partial x_e} \mathbf{z}_S \quad (1.91)$$

Substituting in Equation (1.88) and replacing \mathbf{B} by $\mathbf{K} - \Omega^2\mathbf{M}$, we obtain

$$\begin{aligned} \frac{\partial \bar{c}}{\partial x_e} &= \frac{1}{2} \left[\mathbf{z}_S^T \left(\frac{\partial \mathbf{K}}{\partial x_e} - \Omega^2 \frac{\partial \mathbf{M}}{\partial x_e} \right) \mathbf{z}_S - \mathbf{z}_C^T \left(\frac{\partial \mathbf{K}}{\partial x_e} - \Omega^2 \frac{\partial \mathbf{M}}{\partial x_e} \right) \mathbf{z}_C \right] \\ &\quad + \Omega \mathbf{z}_C^T \frac{\partial \mathbf{C}}{\partial x_e} \mathbf{z}_S \end{aligned} \quad (1.92)$$

If we now define the objective function as $c_m = 2|\bar{c}|$, for the sensitivities of this function we can write

$$\frac{\partial c_m}{\partial x_e} = \text{sign}(\bar{c}) \begin{cases} \mathbf{z}_s^T \left(\frac{\partial \mathbf{K}}{\partial x_e} - \Omega^2 \frac{\partial \mathbf{M}}{\partial x_e} \right) \mathbf{z}_s - \\ \mathbf{z}_c^T \left(\frac{\partial \mathbf{K}}{\partial x_e} - \Omega^2 \frac{\partial \mathbf{M}}{\partial x_e} \right) \mathbf{z}_c + 2\Omega \mathbf{z}_c^T \frac{\partial \mathbf{C}}{\partial x_e} \mathbf{z}_s \end{cases} \quad (1.93)$$

Ignoring damping effects, we have $\mathbf{C} = 0$, $\mathbf{z}_s = 0$, and $\mathbf{z}_c = \mathbf{u}_c$, and thus the above equation reduces to Equation (1.73).

The vectors \mathbf{z}_c and \mathbf{z}_s in Equation (1.93) can be obtained by solving Equation (1.80). Given the damping matrix \mathbf{C} , the term $\partial \mathbf{C} / \partial x_e$ is also calculable. For example, assuming the Reyliagh damping formulation of Equation (1.2), we have $\partial \mathbf{C} / \partial x_e = a_M \partial \mathbf{M} / \partial x_e + a_K \partial \mathbf{K} / \partial x_e$. Having the sensitivities, one can solve the optimization problem using a suitable solution algorithm.

8.2. Free Vibration with Damping

Using a similar approach followed in the previous section, in case of free vibration, Eqs. (1.79) and (1.80) need to be changed to

$$\mathbf{M}\ddot{\mathbf{z}} + \mathbf{C}\dot{\mathbf{z}} + \mathbf{K}\mathbf{z} = 0, \quad \mathbf{z} = (\mathbf{z}_c + i\mathbf{z}_s)e^{i\omega t}, \quad (1.94)$$

$$\begin{cases} \mathbf{B}\mathbf{z}_c - \omega \mathbf{C}\mathbf{z}_s = 0 \\ \mathbf{B}\mathbf{z}_s + \omega \mathbf{C}\mathbf{z}_c = 0 \end{cases} \quad (1.95)$$

respectively where ω is a natural frequency and

$$\mathbf{B} = \mathbf{K} - \omega^2 \mathbf{M} \quad (1.96)$$

From the second equation in (1.95), for \mathbf{z}_s we can write

$$\mathbf{z}_s = -\omega \mathbf{B}^{-1} \mathbf{C} \mathbf{z}_c \quad (1.97)$$

which after substituting in the first equation of (1.95), gives

$$\hat{\mathbf{K}} \mathbf{z}_c = 0, \quad \hat{\mathbf{K}} = \mathbf{B} + \omega^2 \mathbf{C} \mathbf{B}^{-1} \mathbf{C} \quad (1.98)$$

Using Equation (1.98), we can now write

$$\frac{\partial \hat{\mathbf{K}}}{\partial x_e} \mathbf{z}_c = -\hat{\mathbf{K}} \frac{\partial \mathbf{z}_c}{\partial x_e} \Rightarrow \mathbf{z}_c^T \frac{\partial \hat{\mathbf{K}}}{\partial x_e} \mathbf{z}_c = -\mathbf{z}_c^T \hat{\mathbf{K}} \frac{\partial \mathbf{z}_c}{\partial x_e} = 0 \quad (1.99)$$

Differentiating Equation (1.98), we get

$$\begin{aligned} \frac{\partial \hat{\mathbf{K}}}{\partial x_e} &= \frac{\partial \mathbf{B}}{\partial x_e} + 2\omega^2 \frac{\partial \mathbf{C}}{\partial x_e} \mathbf{B}^{-1} \mathbf{C} - \\ &\quad \omega^2 \mathbf{C} \mathbf{B}^{-1} \frac{\partial \mathbf{B}}{\partial x_e} \mathbf{B}^{-1} \mathbf{C} + 2\omega \frac{\partial \omega}{\partial x_e} \mathbf{C} \mathbf{B}^{-1} \mathbf{C} \end{aligned} \quad (1.100)$$

Pre- and post-multiplying this equation by \mathbf{z}_c and using Equation (1.97), we obtain

$$\begin{aligned} \mathbf{z}_c^T \frac{\partial \hat{\mathbf{K}}}{\partial x_e} \mathbf{z}_c &= \mathbf{z}_c^T \frac{\partial \mathbf{B}}{\partial x_e} \mathbf{z}_c - 2\omega \mathbf{z}_c^T \frac{\partial \mathbf{C}}{\partial x_e} \mathbf{z}_s - \\ &\quad \mathbf{z}_s^T \frac{\partial \mathbf{B}}{\partial x_e} \mathbf{z}_s - 2 \frac{\partial \omega}{\partial x_e} \mathbf{z}_c^T \mathbf{C} \mathbf{z}_s = 0 \end{aligned} \quad (1.101)$$

Differentiating Equation (1.96), we have

$$\frac{\partial \mathbf{B}}{\partial x_e} = \frac{\partial \mathbf{K}}{\partial x_e} - \omega^2 \frac{\partial \mathbf{M}}{\partial x_e} - 2\omega \frac{\partial \omega}{\partial x_e} \mathbf{M} \quad (1.102)$$

Substituting this equation in Equation (1.101) and rearranging yields

$$\frac{\partial \omega}{\partial x_e} = \frac{\mathbf{z}_c^T \left(\frac{\partial \mathbf{K}}{\partial x_e} - \omega^2 \frac{\partial \mathbf{M}}{\partial x_e} \right) \mathbf{z}_c - \mathbf{z}_s^T \left(\frac{\partial \mathbf{K}}{\partial x_e} - \omega^2 \frac{\partial \mathbf{M}}{\partial x_e} \right) \mathbf{z}_s - 2\omega \mathbf{z}_c \frac{\partial \mathbf{C}}{\partial x_e} \mathbf{z}_s}{2(\mathbf{z}_c^T \mathbf{C} \mathbf{z}_s + \omega \mathbf{z}_c^T \mathbf{M} \mathbf{z}_c + \omega \mathbf{z}_s^T \mathbf{M} \mathbf{z}_s)} \quad (1.103)$$

If we normalize the vectors \mathbf{z}_c and \mathbf{z}_s with respect to \mathbf{M} , for sensitivities of $\lambda = \omega^2$, we can write

$$\frac{\partial \lambda}{\partial x_e} = 2\omega \frac{\partial \omega}{\partial x_e} = \frac{\mathbf{z}_c^T \left(\frac{\partial \mathbf{K}}{\partial x_e} - \omega^2 \frac{\partial \mathbf{M}}{\partial x_e} \right) \mathbf{z}_c - \mathbf{z}_s^T \left(\frac{\partial \mathbf{K}}{\partial x_e} - \omega^2 \frac{\partial \mathbf{M}}{\partial x_e} \right) \mathbf{z}_s - 2\omega \mathbf{z}_c \frac{\partial \mathbf{C}}{\partial x_e} \mathbf{z}_s}{\frac{\mathbf{z}_c^T \mathbf{C} \mathbf{z}_s}{\omega} + 2} \quad (1.104)$$

It is easy to verify that in the without damping this equation reduces to Equation(1.18). Having the sensitivities, one can solve the optimization problem using a suitable solution algorithm.

9. MAXIMIZING ENERGY ABSORPTION

Apart from controlling natural frequencies and dynamic compliance, improving energy absorption characteristics is also of significant importance in seismic design of structures. In recent years, active and passive energy dissipating devices have been widely studied and utilized to increase energy absorption of structural systems (Soong and Spencer 2002). Topology optimization can be used to maximize energy absorption of these devices. In this section we consider the problem of maximizing the energy absorption of passive energy dissipaters which make use of yield deformation of metals to mitigate the excitation energy. These kinds of energy dissipating devices are popular due to low cost of fabrication and maintenance and easy installation (Ghabraie et al. 2010).

We consider an energy damping device which is made of a 100 mm-long cut of a standard structural wide-flange section with depth, flange width, web thickness, and flange thickness of 161.8, 152.2, 8, and 11.5 mm respectively. This device can be installed in braces connections (Chan and Albermani 2008) or beam-column connections

(Oh et al. 2009) as depicted in Figure 12a. In these installations the device will deform mainly in shear (Figure 12a). The design domain is the inner part of the web as shown in Figure 12b. The two 15 mm strips on the boundaries of the web are non-designable.

We use the BESO method here and introduce a simple technique to solve shape optimization problems using BESO. Restricting the topology of the design and performing shape optimization instead of topology optimization is useful when the fabrication cost is an important factor. We also address a simple approach to obtain periodic designs which are produced by repeating a fixed pattern.

Considering a volume constraint, the energy absorption maximization problem can be stated as

$$\begin{aligned} & \max_{x_1, x_2, \dots, x_N} \Pi_p \\ \text{such that } & \mathbf{r} = \mathbf{p} - \hat{\mathbf{p}} = 0 \\ & \sum_{e=1}^N x_e v_e = \bar{v} \\ & 0 \leq x_e \leq 1, \quad e = 1, 2, \dots, N \end{aligned} \quad (1.105)$$

where Π_p is the total plastic dissipation. Because the problem involves plastic behavior, one needs to solve a non-linear equilibrium system of the form

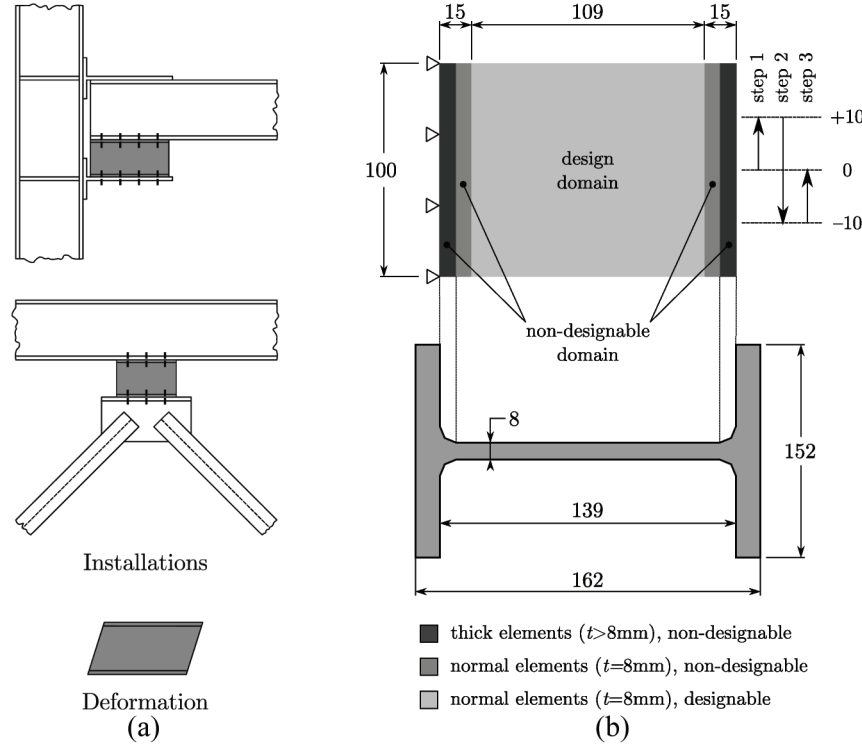
$$\mathbf{r} = \mathbf{p} - \hat{\mathbf{p}} = 0 \quad (1.106)$$

This requires an iterative solver to eliminate the residual force vector \mathbf{r} defined as the difference between the external and internal force vectors, \mathbf{p} and $\hat{\mathbf{p}}$ respectively.

The internal force vector is defined as

$$\hat{\mathbf{p}} = \sum_{e=1}^N \int_{v_e}^N \mathbf{G}_e^T \mathbf{B}_e^T \sigma_e \, dv = \sum_{e=1}^N \mathbf{G}_e^T \mathbf{q}_e \quad (1.107)$$

Figure 12. A passive energy dissipating device: (a) Installation and deformation; (b) designable and non-designable domains and loading. Dimensions are in mm



where \mathbf{G}_e is the matrix that transforms the local nodal values of element e to the global nodal values, \mathbf{B} is the strain-displacement matrix and $\boldsymbol{\sigma}$ represents the local element stress vector. The stress vector can be expressed as

$$\boldsymbol{\sigma}_e = \mathbf{D}_e \boldsymbol{\varepsilon}_e \quad (1.108)$$

with $\boldsymbol{\varepsilon}$ being the strain vector and \mathbf{D} the stress-strain matrix. Similar to Eqs. (1.10) and (1.12) we can define the relationship between \mathbf{D} and the design variables in the following form

$$\mathbf{D}_e(x_e) = x_e \bar{\mathbf{D}}_e \quad (1.109)$$

in which $\bar{\mathbf{D}}_e$ is the stress-strain matrix of element e in its solid state.

We consider the energy damping device to undergo a full loading cycle consisting of an upward displacement of 10 mm followed by a 20 mm downward displacement and finally a 10 mm upward displacement to its original position (Figure 12b). Due to this loading, the total plastic dissipation would be equal to the total strain energy

$$\Pi_p = \Pi = \oint \mathbf{p} \cdot d\mathbf{u} = \sum_{e=1}^N \oint \mathbf{p}_e \cdot d\mathbf{u}_e \quad (1.110)$$

Using the trapezoidal rule for integration, (1.110) can be written in the form

$$\Pi_p = \lim_{n \rightarrow \infty} \frac{1}{2} \sum_{i=1}^n \left(\mathbf{u}_{(i)}^T - \mathbf{u}_{(i-1)}^T \right) \left(\mathbf{p}_{(i)} + \mathbf{p}_{(i-1)} \right) \quad (1.111)$$

where the subscripts in parentheses indicate the integration divisions.

9.1. Bidirectional Evolutionary Structural Optimization (BESO)

The BESO method has been used in eigenfrequency optimization (see e.g. Yang et al. 1999b, Huang et al. 2010) as well as in maximizing energy absorption (see e.g. Huang et al. 2007, Ghabraie et al. 2010). This method solves the topology optimization problem in two steps. At first, the optimization algorithm finds the most and least efficient elements to be added and removed respectively. Then, it adjusts the number of adding and removing elements based on the volume constraint.

This method is capable of totally removing the elements, hence one does not require to represent voids with a very soft material. This approach, usually known as *hard kill* approach, results in faster solutions for only solid elements remain in the finite element model. Moreover, this approach works well in geometrically non-linear problems as it is not prone to the instabilities caused by soft elements in the SIMP material model (Buhl et al. 2000, Yoon and Kim 2005). Zhou and Rozvany (2001) showed that in certain cases the hard kill approach may result in non-optimal solutions and thus this approach need to be applied with care. In shape optimization, however, using the hard kill approach will not cause such problems.

Another advantage of the BESO method is that the solutions will not contain any intermediate design variables ($0 < x < 1$) or grey areas. In this method the boxing constraints $0 \leq x_e \leq 1$, $e = 1, \dots, N$ change to binary constraints of the form $x_e \in \{0, 1\}$, $e = 1, \dots, N$. This is particularly helpful if one wants to impose shape restrictions as the boundaries of solids and voids can be clearly defined in the black-white solutions of BESO.

In BESO, the so-called *sensitivity numbers* are used to evaluate the efficiency of the elements. Sensitivity numbers might be assigned intuitively

or calculated rigorously. Either way, they are defined such that a higher sensitivity number represents higher efficiency.

Considering the definition of the objective function in Equation (1.111), the sensitivities of this function can be calculated as

$$\frac{\partial \Pi_p}{\partial x_e} = \lim_{n \rightarrow \infty} \frac{1}{2} \sum_{i=1}^n \left[\left(\frac{\partial \mathbf{u}_{(i)}^T}{\partial x_e} - \frac{\partial \mathbf{u}_{(i-1)}^T}{\partial x_e} \right) (\mathbf{p}_{(i)} + \mathbf{p}_{(i-1)}) + (\mathbf{u}_{(i)}^T - \mathbf{u}_{(i-1)}^T) \left(\frac{\partial \mathbf{p}_{(i)}}{\partial x_e} + \frac{\partial \mathbf{p}_{(i-1)}}{\partial x_e} \right) \right] \quad (1.112)$$

The first term in the right hand side cancels out because on the boundaries with essential boundary conditions $\partial \mathbf{u} / \partial x = 0$ and elsewhere $\mathbf{p} = 0$. Hence the above equation reduces to

$$\frac{\partial \Pi_p}{\partial x_e} = \lim_{n \rightarrow \infty} \frac{1}{2} \sum_{i=1}^n (\mathbf{u}_{(i)}^T - \mathbf{u}_{(i-1)}^T) \left(\frac{\partial \mathbf{p}_{(i)}}{\partial x_e} + \frac{\partial \mathbf{p}_{(i-1)}}{\partial x_e} \right) \quad (1.113)$$

On the other hand, differentiating Equation (1.106) and using Eqs. (1.107) to (1.109), we obtain

$$\frac{\partial \mathbf{p}}{\partial x_e} = \frac{\partial \hat{\mathbf{p}}}{\partial x_e} = \mathbf{G}_e^T \mathbf{q}_e, \quad e = 1, \dots, N \quad (1.114)$$

Substituting Equation (1.114) in Equation (1.113), we can write

$$\frac{\partial \Pi_p}{\partial x_e} = \lim_{n \rightarrow \infty} \frac{1}{2} \sum_{i=1}^n (\mathbf{u}_{(i)}^T - \mathbf{u}_{(i-1)}^T) \mathbf{G}_e^T (\mathbf{q}_{e(i)} + \mathbf{q}_{e(i-1)}) \quad (1.115)$$

Using the trapezoidal numerical integration scheme and recalling the definition of the strain energy in Eqs. (1.110) and (1.111), the above equation reduces to

$$\frac{\partial \Pi_p}{\partial x_e} = \lim_{n \rightarrow \infty} \sum_{i=1}^n (\pi_{e(i)} - \pi_{e(i-1)}) = \pi_e \quad (1.116)$$

where π_e is the total strain energy of element e upon completion of the load cycle. Huang and Xie (2008) derived these sensitivities using the adjoint method and verified it using a simple example.

We may now define the sensitivity numbers for problem (1.105) as follows

$$\alpha_e = \frac{\partial \Pi_p}{\partial x_e} = \pi_e, \quad e = 1, 2, \dots, N \quad (1.117)$$

Based on this definition and using first order approximation, we can write

$$\Delta \Pi_p = \sum_{e=1}^N \alpha_e \Delta x_e \quad (1.118)$$

Note that in Equation (1.118) adding element e will be reflected by $\Delta x_e = 1 - 0 = 1$ and removing it results in $\Delta x_e = -1$. Thus during the solution procedure, if one introduces the a th element and removes the r th element, the change in the objective function can be estimated as

$$\Delta \Pi_p = \frac{\partial \Pi_p}{\partial x_a} - \frac{\partial \Pi_p}{\partial x_r} = \alpha_a - \alpha_r \quad (1.119)$$

As we are interested in maximizing Π_p , it is clear from Equation (1.119) that the elements with highest sensitivity numbers should be added to the design domain while the elements with lowest sensitivity numbers should be removed.

9.2. Adding and Removing the Elements

After ranking the efficiency of the elements, the algorithm should select the number of elements to be added and removed such that the volume constraint is satisfied. Generally in BESO, one starts the solution with an initial volume which is not necessarily equal to the volume limit \bar{v} . The design is then updated using the sensitivity

numbers and the algorithm tries to move the volume towards the volume limit gradually. Thus, if the current volume is bigger than \bar{v} the algorithm will increase the number of removing elements and vice versa. The procedure continues until no further significant improvement can be achieved.

The algorithms to update the solutions in the BESO method have been improved over time. One of the most recent algorithms is proposed by Huang and Xie (2007). In this algorithm, at each iteration k , the target volume of the next iteration is calculated using a small positive controlling parameter called the *evolutionary volume ratio* (R_v)

$$v^{(k+1)} = v^{(k)} \left(1 + \text{sign}(\bar{v} - v^{(k)}) R_v \right) \quad (1.120)$$

where superscripts enclosed in parentheses indicate the iteration number. Then the number of adding and removing elements are calculated such that the volume of the next design becomes equal to $v^{(k+1)}$ and the total number of added elements do not exceed $v^{add} = v_t \times R_a$ in which R_a is another controlling parameter known as the *maximum allowable admission ratio*.

If one starts BESO with an initial design volume equal to \bar{v} , the volume will be kept constant during the optimization procedure and the number of adding and removing elements at each iteration would be equal to each other. In this case R_v will have no effect on the optimization procedure and the maximum number of adding and removing elements is only controlled by R_a . Thus with a fixed volume, the effect of the R_a factor is similar to the move limit η in Equation (1.28).

9.3. Mirroring and Filtering Sensitivity Numbers

Due to the nonlinear nature of Problem (1.105), the loading sequence affects the mechanical responses. As a result, the optimal shape flips by mirroring the loading sequence. In real life, how-

ever, the direction of the load is uncertain. Thus one needs to consider two displacement cycles: a $\uparrow\downarrow\uparrow$ cycle as well as a $\downarrow\uparrow\downarrow$ cycle. But knowing that the results of these two displacement cycles are mirrored images of each other, it is not necessary to analyze the model under both of these loading conditions. Instead, one can add the sensitivities of the mirrored elements together to account for both displacement cycles. The sensitivity numbers are thus corrected as

$$\bar{\alpha}_e = \alpha_e + \alpha_{\tilde{e}} \quad (1.121)$$

where $\bar{\alpha}_e$ is the corrected sensitivity number of element e and \tilde{e} is the element which is located at the same location as e in the mirrored model.

Like the SIMP method, the BESO method is also prone to the formation of checkerboard patterns and mesh dependency. A filtering technique, similar to Equation (1.29) can be employed to overcome these problems in the BESO algorithm

$$\hat{\alpha}_e = \frac{\sum_{e=1}^N \bar{\alpha}_j w_{ij}}{\sum_{j=1}^N w_{ij}} \quad (1.122)$$

Another significance of filtering in the BESO method is extrapolating the sensitivity numbers to void elements. If one uses a hard kill approach, void elements are removed from the structure and their sensitivities cannot be evaluated directly. In other words, all void elements will have a sensitivity number of zero. The filtering scheme in Equation (1.122) extrapolates the sensitivities to the void elements in the neighborhood of the solid elements. This extrapolation leads the BESO algorithm to add the elements in the vicinity of the elements with high sensitivity numbers.

9.4. Restricting the Topology

Topology optimization techniques like BESO can naturally introduce new holes or fill the current holes in the design domain. However this behavior might produce complicated shapes which might be costly to fabricate. To prevent the BESO algorithm from introducing new holes, we restrict the designable domain to the elements at the boundaries of the shape at each iteration. The designable domain at each iteration is defined as

$$\mathcal{D} = \{e \mid \exists i, j \in \mathcal{B} : i, j \in e \wedge i \neq j\} \quad (1.123)$$

where \mathcal{B} is the set of boundary nodes defined as

$$\mathcal{B} = \{i \mid \exists e_m \in \mathcal{S}, e_v \in \mathcal{V} : i \in e_m \cap e_v\} \quad (1.124)$$

with \mathcal{S} and \mathcal{V} denoting the sets of solid and void elements respectively.

9.5. Numerical Examples

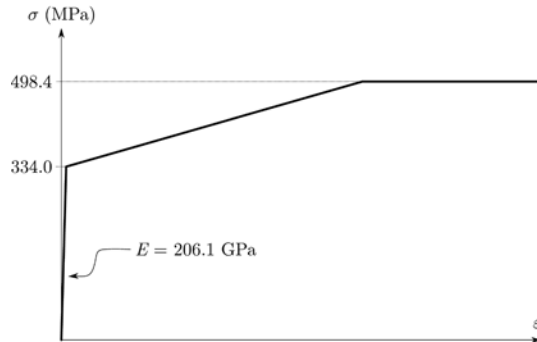
In the following numerical examples we fix the volume to simplify the approach. Another benefit of using fixed volume is that the results of different iterations are comparable to each other.

The modulus of elasticity of the material is considered as 206.1 GPa and the tensile yield stress is assumed to be 334 MPa. The material model considered is depicted in Figure 13.

Example 4: Simple Damper

We use the proposed BESO algorithm to optimize the shape of a simple damper. The target volume is 82% of the design domain. The initial and the final solutions are depicted in Figures 14a and 14b respectively. The evolution history of the objective function is plotted in Figure 14c. It can be verified that the energy absorption of the optimal solution

Figure 13. The idealized material model used for modeling the energy dissipating device



is considerably higher (37.4% improvement) than the initial design.

Example 5. Slit Damper

We now consider shape optimization of a slit damper. The initial design is depicted in Figure 14d. In order to preserve the periodicity of the design, one needs to impose an additional constraint to the optimization algorithm. To this end, we partition the design domain into four cells. To make the cells identical, the sensitivity numbers of elements are replaced by the mean value of sensitivity numbers of corresponding elements in all cells. Putting this mathematically, we write

$$\alpha_i = \frac{1}{N_{cell}} \sum_{j=1}^{N_{cell}} \alpha_{i,j} \quad (1.125)$$

where α_i is the average (corrected) sensitivity number of element i in all cells, N_{cell} is the number of cells, and $\alpha_{i,j}$ is the (original) sensitivity number of the element i in cell j .

The obtained solution is illustrated in Figure 14e. The evolution history of the objective function is plotted in Figure 14f. Again a significant improvement (64.3%) in energy absorption is observable.

Ghabraie et al. (2010) have used a smoothing postprocessor based on Bézier curves to

smooth the jagged boundaries of the solutions. The smoothed versions of the initial and optimal solution are analyzed and their stress distributions are compared in Figure 15. It can be seen that the optimal solution provides an even stress distribution and the stress concentration areas visible in the initial design have been dissipated. This even stress distribution improves the responses of this design against low cycle fatigue. This has been verified through experimental tests by Ghabraie et al. (2010).

Figure 16 compares the force-displacement curves of the initial and final solutions. The optimal solution shows a stiffer response than the initial design.

10. CONCLUSION

This chapter reviewed the application of topology optimization techniques in seismic design of structures. Two established topology optimization methods, namely SIMP and BESO, have been introduced and their application has been illustrated using numerical examples.

Eigenfrequency optimization of linear elastic structures in free vibration has been addressed using the SIMP method. Sensitivity analysis of eigenfrequencies has been explained and a simple solution procedure has been presented based on optimality criteria. Possible numerical instabilities have been mentioned and possible treatments have been discussed.

The problems involving multiple eigenfrequencies have been considered and simple approaches to bypass these problems have been discussed. The sensitivities of multiple eigenfrequencies have been calculated and the optimality criteria have been presented. A simple approach to solve these problems has been proposed and successfully applied to a simple problem. The problem of maximizing the gap between two eigenfrequencies has also been addressed. This problem is of practical significance when it is desired to push

Figure 14. Solutions of examples 4 and 5. The initial designs (a,d), the final designs (b,e), and the evolution history of the objective functions (c,f). Dark grey elements are non-designable

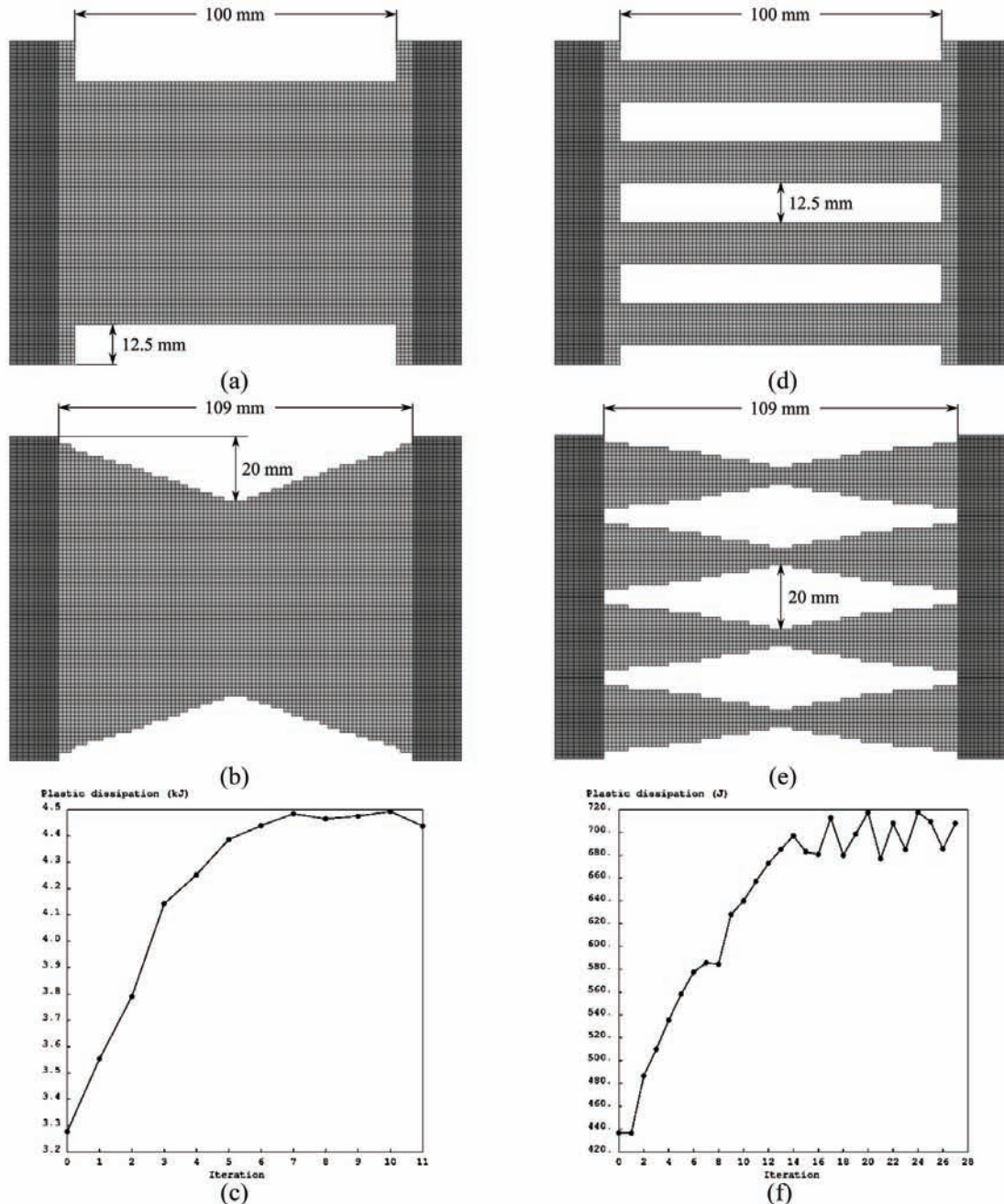


Figure 15. Comparing stress distribution in initial (a) and final (b) smoothed designs. Stresses are in MPa.

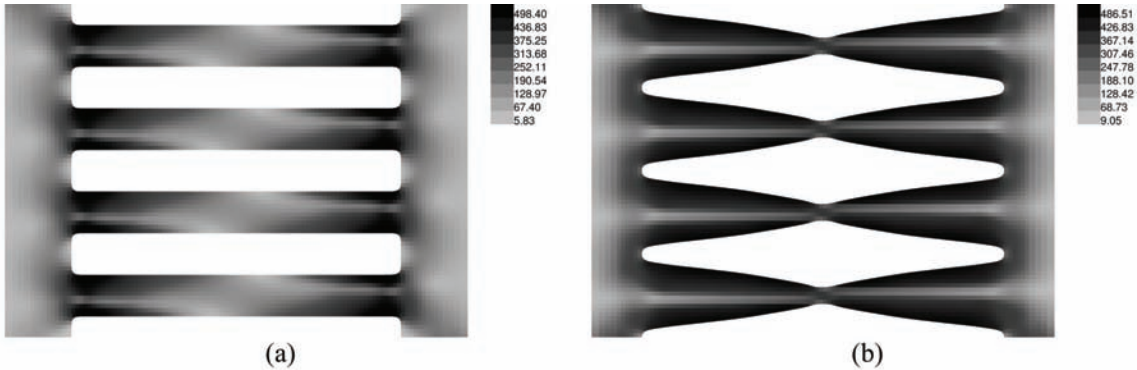
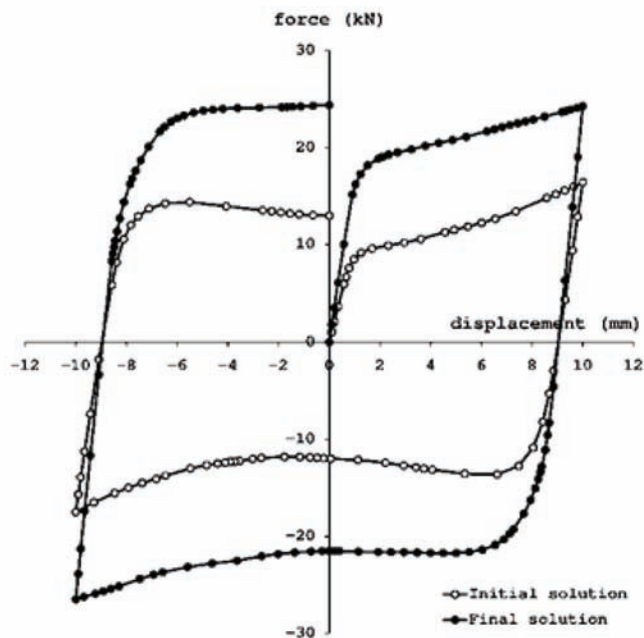


Figure 16. Comparing force-displacement graphs in initial and final smoothed designs



eigenfrequencies of a structure away from a given excitation frequency.

Topology optimization of structures under periodic loads has been discussed. An average dynamic compliance measure has been considered as the objective function to be minimized. Sensitivities of this objective function have been computed. Numerical examples have been solved to illustrate the applications of the optimization

method. Topology design of structures under a combination of periodic (and static) loads with different frequencies has been addressed. This is of practical importance, for example when a periodic load is expanded using Fourier series.

Issues and difficulties of considering the non-linear material and geometry behavior of the system have been briefly discussed. The sensitivities of eigenfrequencies and dynamic

compliance of structures in presence of damping have been derived.

The BESO technique has been modified and used to maximize the energy absorption of a passive metallic damper. Sensitivity analysis of the non-linear system has been presented. Simple approaches to achieve shape optimization and periodic solutions have been addressed. It has been illustrated that the optimized solution not only provides higher energy absorption capacities but also offers smoother stress distribution resulting in better fatigue resistance.

It has been shown that in seismic design of structures, topology optimization techniques can be useful in both conceptual design of structural systems (e.g. maximization of fundamental frequency of a frame) and detailed design of structural members (e.g. maximization of energy absorption of passive dampers). These techniques are capable of dealing with different objective functions and different material models.

REFERENCES

- Bendsøe, M. P. (1989). Optimal shape design as a material distribution problem. *Structural Optimization*, 1(4), 193–202. doi:10.1007/BF01650949
- Bendsøe, M. P., & Kikuchi, N. (1988). Generating optimal topologies in structural design using a homogenization method. *Computer Methods in Applied Mechanics and Engineering*, 71(2), 197–224. doi:10.1016/0045-7825(88)90086-2
- Bendsøe, M. P., & Sigmund, O. (1999). Material interpolation schemes in topology optimization. *Archive of Applied Mechanics*, 69(9–10), 635–654.
- Bendsøe, M. P., & Sigmund, O. (2003). *Topology optimization - Theory, methods, and applications*. Berlin, Germany: Springer.
- Beyer, H.-G., & Sendhoff, B. (2007). Robust optimization – A comprehensive survey. *Computer Methods in Applied Mechanics and Engineering*, 196(33–34), 3190–3218. doi:10.1016/j.cma.2007.03.003
- Bratus, A. S., & Seyranian, A. P. (1983). Bimodal solutions in eigenvalue optimization problems. *Journal of Applied Mathematics and Mechanics*, 47(4), 451–457. doi:10.1016/0021-8928(83)90081-3
- Buhl, T., Pedersen, C. B. W., & Sigmund, O. (2000). Stiffness design of geometrically nonlinear structures using topology optimization. *Structural and Multidisciplinary Optimization*, 19(2), 93–104. doi:10.1007/s001580050089
- Chan, R. W. K., & Albermani, F. (2008). Experimental study of steel slit damper for passive energy dissipation. *Engineering Structures*, 30(4), 1058–1066. doi:10.1016/j.engstruct.2007.07.005
- Chopra, A. K. (1995). *Dynamics of structures – Theory and applications to earthquake engineering*. Upper Saddle River, NJ: Prentice Hall International.
- Cox, S. J., & Overton, M. L. (1992). On the optimal design of columns against buckling. *SIAM Journal on Mathematical Analysis*, 23(2), 287–325. doi:10.1137/0523015
- Culmann, K. (1866). *Die graphische Statik*. Zürich, Switzerland: Mayer und Zeller.
- Díaz, A. R., & Kikuchi, N. (1992). Solutions to shape and topology eigenvalue optimization problems using a homogenization method. *International Journal for Numerical Methods in Engineering*, 35(7), 1487–1502. doi:10.1002/nme.1620350707
- Du, J., & Olhoff, N. (2007). Topological design of freely vibrating continuum structures for maximum values of simple and multiple eigenfrequencies and frequency gaps. *Structural and Multidisciplinary Optimization*, 34(2), 91–110. doi:10.1007/s00158-007-0101-y

- Elnashai, A. S., & Chryssanthopoulos, M. (1991). Effect of random material variability on seismic design parameters of steel frames. *Earthquake Engineering & Structural Dynamics*, 20(2), 101–114. doi:10.1002/eqe.4290200202
- Ghabraie, K., Chan, R., Huang, X., & Xie, Y. M. (2010). Shape optimization of metallic yielding devices for passive mitigation of seismic energy. *Engineering Structures*, 32(8), 2258–2267. doi:10.1016/j.engstruct.2010.03.028
- Haug, E. J., & Rousselet, B. (1980). Design sensitivity analysis in structural mechanics. II: Eigenvalue variations. *Journal of Structural Mechanics*, 8(2), 161–186. doi:10.1080/03601218008907358
- Huang, X., & Xie, Y. M. (2007). Convergent and mesh-independent solutions for the bi-directional evolutionary structural optimization method. *Finite Elements in Analysis and Design*, 43(14), 1039–1049. doi:10.1016/j.finel.2007.06.006
- Huang, X., & Xie, Y. M. (2008). Topology optimization of nonlinear structures under displacement loading. *Engineering Structures*, 30(7), 2057–2068. doi:10.1016/j.engstruct.2008.01.009
- Huang, X., Xie, Y. M., & Lu, G. (2007). Topology optimization of energy-absorbing structures. *International Journal of Crashworthiness*, 12(6), 663–675. doi:10.1080/13588260701497862
- Huang, X., Zuo, Z. H., & Xie, Y. M. (2010). Evolutionary topological optimization of vibrating continuum structures for natural frequencies. *Computers & Structures*, 88(5–6), 357–364. doi:10.1016/j.compstruc.2009.11.011
- Jensen, J. S. (2007). Topology optimization of dynamics problems with Padé approximants. *International Journal for Numerical Methods in Engineering*, 72(13), 1605–1630. doi:10.1002/nme.2065
- Jog, C. S. (2002). Topology design of structures subjected to periodic loading. *Journal of Sound and Vibration*, 253(3), 687–709. doi:10.1006/jsvi.2001.4075
- Jung, D., & Gea, H. C. (2004). Topology optimization of nonlinear structures. *Finite Elements in Analysis and Design*, 40(11), 1417–1427. doi:10.1016/j.finel.2003.08.011
- Karush, W. (1939). *Minima of functions of several variables with inequalities as side constraints*. Master's thesis, Department of Mathematics, University of Chicago, Chicago, Illinois.
- Kharmanda, G., Olhoff, N., Mohamed, A., & Lemaire, M. (2004). Reliability-based topology optimization. *Structural and Multidisciplinary Optimization*, 26(5), 295–307. doi:10.1007/s00158-003-0322-7
- Kosaka, I., & Swan, C. C. (1999). A symmetry reduction method for continuum structural topology optimization. *Computers & Structures*, 70(1), 47–61. doi:10.1016/S0045-7949(98)00158-8
- Kuhn, H. W., & Tucker, A. W. (1951). Nonlinear programming. In *Proceedings of 2nd Berkeley Symposium* (pp. 481–492). Berkeley, CA: University of California Press.
- Kuwamura, H., & Kato, B. (1989). Effects of randomness in structural members' yield strength on the structural systems' ductility. *Journal of Constructional Steel Research*, 13(2–3), 79–93. doi:10.1016/0143-974X(89)90007-2
- Lund, E. (1994). *Finite element based design sensitivity analysis and optimization*. Unpublished doctoral dissertation, Institute of Mechanical Engineering, Aalborg University, Denmark.
- Ma, Z. D., Cheng, H. C., & Kikuchi, N. (1995). Topological design for vibrating structures. *Computer Methods in Applied Mechanics and Engineering*, 121(1–4), 259–280. doi:10.1016/0045-7825(94)00714-X

- Ma, Z. D., Kikuchi, N., & Hagiwara, I. (1993). Structural topology and shape optimization for a frequency response problem. *Computational Mechanics*, 13(3), 157–174. doi:10.1007/BF00370133
- Maeda, Y., Nishiwaki, S., Izui, K., Yoshimura, M., Matsui, K., & Terada, K. (2006). Structural topology optimization of vibrating structures with specified eigenfrequencies and eigenmode shapes. *International Journal for Numerical Methods in Engineering*, 67(5), 597–628. doi:10.1002/nme.1626
- Michell, A. G. M. (1904). The limits of economy of material in frame structures. *Philosophical Magazine*, 6(8), 589–597.
- Min, S., Kikuchi, N., Park, Y. C., Kim, S., & Chang, S. (1999). Optimal topology design of structures under dynamic loads. *Structural Optimization*, 17(2–3), 208–218.
- Oh, S. H., Kimb, Y. J., & Ryu, H. S. (2009). Seismic performance of steel structures with slit dampers. *Engineering Structures*, 31(9), 1997–2008. doi:10.1016/j.engstruct.2009.03.003
- Olhoff, N., & Du, J. (2005). Topological design of structures subjected to forced vibration. In J. Herskovits (Ed.), *Proceedings of the 6th World Congress of Structural and Multidisciplinary Optimization*, Rio de Janeiro, Brazil, 30 May–03 June.
- Olhoff, N., & Rasmussen, S. H. (1977). On single and bimodal optimum buckling loads of clamped columns. *International Journal of Solids and Structures*, 13(7), 605–614. doi:10.1016/0020-7683(77)90043-9
- Overton, M. L. (1992). Large-scale optimization of eigenvalues. *SIAM Journal on Optimization*, 2(1), 88–120. doi:10.1137/0802007
- Papadrakakis, M., Lagaros, N. D., & Plevris, V. (2005). Design optimization of steel structures considering uncertainties. *Engineering Structures*, 27(9), 1408–1418. doi:10.1016/j.engstruct.2005.04.002
- Pedersen, N. L. (2000). Maximization of eigenvalues using topology optimization. *Structural and Multidisciplinary Optimization*, 20(1), 2–11. doi:10.1007/s001580050130
- Prager, W. (1969). *Optimality criteria derived from classical extremum principles*. Technical report, SM Studies Series. Ontario, Canada: Solid Mechanics Division, University of Waterloo.
- Prager, W. (1974). A note on discretized Michell structures. *Computer Methods in Applied Mechanics and Engineering*, 3(3), 349–355. doi:10.1016/0045-7825(74)90019-X
- Querin, O. M. (1997). *Evolutionary structural optimisation stress based formulation and implementation*. Unpublished Doctoral dissertation, Department of Aeronautical Engineering, University of Sydney, Sydney, Australia.
- Querin, O. M., Steven, G. P., & Xie, Y. M. (1998). Evolutionary structural optimisation (ESO) using a bidirectional algorithm. *Engineering Computations*, 15(8), 1031–1048. doi:10.1108/02644409810244129
- Rozvany, G. I. N. (1972a). Grillages of maximum strength and maximum stiffness. *International Journal of Mechanical Sciences*, 14(10), 651–666. doi:10.1016/0020-7403(72)90023-9
- Rozvany, G. I. N. (1972b). Optimal load transmission by flexure. *Computer Methods in Applied Mechanics and Engineering*, 1(3), 253–263. doi:10.1016/0045-7825(72)90007-2
- Rozvany, G. I. N., Zhou, M., & Birker, T. (1992). Generalized shape optimization without homogenization. *Structural Optimization*, 4(3–4), 250–252. doi:10.1007/BF01742754

- Seyranian, A. P., Lund, E., & Olhoff, N. (1994). Multiple eigenvalues in structural optimization problems. *Structural and Multidisciplinary Optimization*, 8(4), 207–227.
- Sigmund, O., & Petersson, J. (1998). Numerical instabilities in topology optimization: A survey on procedures dealing with checkerboards, mesh dependencies and local minima. *Structural and Multidisciplinary Optimization*, 16(1), 68–75.
- Soong, T. T., & Spencer, B. F. Jr. (2002). Supplemental energy dissipation: State-of-the-art and state-of-the-practice. *Engineering Structures*, 24(3), 243–259. doi:10.1016/S0141-0296(01)00092-X
- Svanberg, K. (1987). The method of moving asymptotes—A new method for structural optimization. *International Journal for Numerical Methods in Engineering*, 24(2), 359–373. doi:10.1002/nme.1620240207
- Xie, Y. M., & Steven, G. P. (1993). A simple evolutionary procedure for structural optimization. *Computers & Structures*, 49(5), 885–896. doi:10.1016/0045-7949(93)90035-C
- Xie, Y. M., & Steven, G. P. (1996). Evolutionary structural optimization for dynamic problems. *Computers & Structures*, 58(6), 1067–1073. doi:10.1016/0045-7949(95)00235-9
- Yang, X. Y., Xie, Y. M., Steven, G. P., & Querin, O. M. (1999a). Bidirectional evolutionary method for stiffness optimization. *American Institute of Aeronautics and Astronautics Journal*, 37(11), 1483–1488.
- Yang, X. Y., Xie, Y. M., Steven, G. P., & Querin, O. M. (1999b). Topology optimization for frequencies using an evolutionary method. *Journal of Structural Engineering*, 125(12), 1432–1438. doi:10.1061/(ASCE)0733-9445(1999)125:12(1432)
- Yoon, G. H. (2010a). Maximizing the fundamental eigenfrequency of geometrically nonlinear structures by topology optimization based on element connectivity parameterization. *Computers & Structures*, 88(1–2), 120–133. doi:10.1016/j.compstruc.2009.07.006
- Yoon, G. H. (2010b). Structural topology optimization for frequency response problem using model reduction schemes. *Computer Methods in Applied Mechanics and Engineering*, 199(25–28), 1744–1763. doi:10.1016/j.cma.2010.02.002
- Yoon, G. H. (2011). Topology optimization for nonlinear dynamic problem with multiple materials and material-dependent boundary condition. *Finite Elements in Analysis and Design*, 47(7), 753–763. doi:10.1016/j.finel.2011.02.006
- Yoon, G. H., & Kim, Y. Y. (2005). Element connectivity parameterization for topology optimization of geometrically nonlinear structures. *International Journal of Solids and Structures*, 42(7), 1983–2009. doi:10.1016/j.ijsolstr.2004.09.005
- Zhao, C. B., Steven, G. P., & Xie, Y. M. (1997). Evolutionary optimization of maximizing the difference between two natural frequencies of a vibrating structure. *Structural Optimization*, 13(2–3), 148–154. doi:10.1007/BF01199234
- Zhou, M., & Rozvany, G. I. N. (2001). On the validity of ESO type methods in topology optimization. *Structural and Multidisciplinary Optimization*, 21(1), 80–83. doi:10.1007/s001580050170
- Zienkiewicz, O. C., Taylor, R. L., & Zhu, J. Z. (2005). *The finite element method: Its basis and fundamentals*. Oxford, UK: Elsevier Butterworth-Heinemann.

KEY TERMS AND DEFINITIONS

Compliance Minimization: In structural optimization under static loads, minimizing the mean compliance is equivalent to maximizing the structural stiffness. Under dynamic loads, the average of mean compliance over a cycle can be considered as an objective function.

Eigenfrequency Control: Topology optimization techniques can be used to increase or decrease any of natural frequencies of a structural system.

Passive Dampers: These devices are used to enhance the energy dissipation capability of structural systems to mitigate seismic hazard.

Sensitivity Analysis: In solving an optimization problem, finding the derivatives of the objective function with respect to the design variables is sometimes referred to as sensitivity analysis.

Shape Optimization: Finding the best shape of the elements of a structural system in which the overall layout, topology and connectivity of the elements is previously determined is known as shape optimization.

Sizing Optimization: Finding the optimum dimensions of the elements in a structural system when the overall layout, connectivity and shape of the elements are fixed is termed as sizing optimization.

Topology Optimization: The problem of finding the best topology and layout of the elements of a structural system is known as topology optimization.

Chapter 11

Overall Conceptual Seismic Design and Local Seismic Capacity Design for Components of Bridges

Wan-Cheng Yuan

Tongji University, China

Yu-Guo Zheng

Tongji University and Hunan University of Science and Technology, China

Pak-Chiu Cheung

Tongji University, China

ABSTRACT

From the perspective of “overall conceptual seismic design,” four design strategies are presented to decrease and balance the seismic force and displacement demands for some bridges working in a linear and elastic state: the adjustment of the layout and detail of piers and expansion joints for a typical long span continuous girder bridge, the adoption of a new-type spatial bridge tower for a long span cable-stayed bridge, the study on the isolation mechanism of an elastic cable seismic isolation device for another cable-stayed bridge, and the study on the seismic potential and performance for long span SCC (steel-concrete composite) bridges. From the perspective of “local seismic capacity design,” three earthquake resistant strategies are presented to achieve economical, applicable, and valid seismic design of local components of bridges working in a nonlinear state: the adoption and the study on a new cable sliding friction aseismic bearing, the study on the seismic capacities of single-column bridge piers wholly and locally reinforced with steel fiber reinforced concrete (SFRC), the study on the seismic capacities, and the hysteretic performance and energy dissipation capabilities of bridge pile group foundations strengthened with the steel protective pipes (SPPs). Research results show that these seismic design strategies are effective to improve the seismic performance of bridges.

DOI: 10.4018/978-1-4666-1640-0.ch011

INTRODUCTION

To give clear and correct directions for seismic design optimization of bridges, the “overall conceptual seismic design” and the “local seismic capacity design” methods are proposed to obtain uniform and rational seismic demands and improved seismic capacities of structural components in seismic design of bridges.

There are many methods to realize seismic design optimization so as to improve the seismic performance of structures (Gong, 2003; Li, 1997; Liu, 2003; Vagelis, 2009; Zou, 2002). However, the structural seismic design optimization will be in wrong direction and invalid unless the initial structural seismic design itself is appropriate and rational. It is hoped that the strategies and methods proposed in the chapter are able to give clear and correct directions for seismic design optimization of bridges.

There are two paths to improve the seismic design of bridges so as to make the seismic demands more uniform and rational along structural components. One is to reduce the seismic demands as much as possible, and the other is to increase the seismic capacities. Correspondingly there are two design methods, the overall linear seismic conceptual design and the local nonlinear seismic capacity design. From overall to local design strategies, some new ideas and strategies of seismic design which can effectively improve seismic performance of bridges are proposed separately in this chapter.

Overall conceptual seismic design is a conceptual design method applicable for the whole structure based on the linear seismic analysis. When the components of bridges work in an elastic state during the earthquakes, the conceptual design will be an effective and efficient strategy. From the perspective of overall conceptual seismic design, four conceptual seismic design strategies are proposed focusing on the whole structure.

1. Taking a long span continuous girder bridge as an example, an optimal design for the layout and detail of the bridge components, including geometry of piers, arrangement of piers, location of expansion joint or braking pier, is carried out so as to reduce the seismic demands in the transverse direction as much as possible. The seismic performance of the bridges with different adjustments in different site conditions is calculated respectively. Based on the comparison of the results, the forms of some piers and the locations of expansion joints are required to be adjusted to improve the bending stiffness distribution for the bridge.
2. Taking a long span cable-stayed bridge as an instance, the original design proposal makes use of the inverted Y shape bridge tower, while the seismic design dominated by the first longitudinal vibration mode may lead to overlarge relative displacement between the girder and the tower. In order to solve the critical problem, a new-type spatial bridge tower is proposed by integrated analyses of the structural dynamic characteristics, design displacement and seismic responses. Compared with the original tower, the new spatial tower improves the seismic performance of the bridge significantly.
3. With respect to the elastic cable seismic isolation device installed between the girder and the lower horizontal beam of the tower to mitigate excessive seismic effects, the influences of the elastic cable stiffness on the dynamic characteristics and the seismic demands are investigated by parametric finite element analyses of a real cable-stayed bridge. The seismic isolation mechanism of the elastic cables is discussed.
4. Girders of the SCC bridge are composed of the structural steel and the concrete. Compared with a conventional concrete girder bridge with the same span, the superstructure height and weight are gener-

ally less. Therefore the substructure can be made of hollow or more flexible piers under earthquakes so that the total cost can be reduced greatly. Response spectrum analyses are carried out for two design proposals of a typical four-span continuous bridge, the “reinforced concrete bridge with solid column piers” and the “SCC bridge with hollow column piers”. Seismic responses of the two design proposals are compared with each other to discuss the seismic potential of the SCC bridge. The seismic performance of a long span SCC arch bridge is also studied by response spectrum analyses.

Because of the stochastic characteristics of earthquakes, keeping bridges work in an elastic state permanently is impossible and unreasonable. When the components of a bridge locally become plastic, the overall conceptual seismic design method is not applicable because of the limitations of overall linear analyses. Compared with the overall design, the local seismic capacity design is a method of great benefit for its economy, applicability and validity. It is a detail design strategy for local regions of components based on the nonlinear seismic analysis. From this perspective, three design strategies according to the local method are presented in the chapter.

1. Excessive displacements and forces often cause damage or collapse of bridges under earthquakes. Taking a currently used frictional isolation bearing as an example, the seismic forces can be reduced under severe earthquakes but the seismic displacements induced by lateral forces are generally unconstrained. Therefore, a new aseismic bearing system named as “cable sliding friction aseismic bearing” is developed for bridges. It combines the advantages of pot bearings with the excellent displacement restraining capabilities of cables. The performance criteria and several design parameters are

determined for the new bearing by theoretical analyses, experimental testing and numerical simulations. A constructed girder-arch composite bridge installed with the new bearing is studied and evaluated.

2. It is well known that the potential plastic hinge regions are vulnerable and crucial in bridge piers under earthquakes, while a structure made of steel fiber reinforced concrete (SFRC) has good ductility performance and energy dissipation capabilities. Therefore a new idea is put forward in that the SFRC is locally applied in the potential plastic hinge region of a bridge pier in an earthquake region both for saving cost and increasing the seismic capacities. Then a nonlinear material constitutive model is established for SFRC and applied to analyze the seismic capacities of single-column bridge piers reinforced with SFRC. Compared with the single-column bridge pier wholly reinforced with SFRC, the plastic hinge length and the reasonable range locally reinforced with SFRC are determined for the pier.
3. Steel protective pipe (SPP) is a widely adopted measure to make the construction of pile group foundations convenient. But the influences of the SPPs on the seismic performance of the foundations need further studies. The seismic capacities of a pile group foundation strengthened by the SPPs are analyzed and compared with the normal pile group foundation with RC piles by the pushover method. By using the modified Park-Ang damage index (Park & Ang, 1985; Park, Ang, & Wen, 1985) and the fiber beam-column finite element model, the hysteretic performance and energy dissipation capabilities are studied based on numerical simulations and low cycle loading experiments for the foundation.

BACKGROUND

For the bridge engineers, the conceptual seismic design is the first but most important stage in a bridge design that involves numerous complex and time-consuming tasks. Any optimization in the conceptual design phase will lead to greater cost savings than those at the detail design stage when decisions become more restricted. Though in strict terms, the structural seismic design optimization follows rigorous formulations and needs definite algorithms, the choices and adjustments of structural systems from the perspective of “overall conceptual seismic design” will innovatively give meaningful enlightenments and correct directions for seismic design optimization of structures. Instead of deferring seismic analyses to the detail design stage, it is emphasized that adequate seismic planning should be implemented early in the conceptual design.

For continuous girder bridges, past conceptual design used to focus on the longitudinal seismic behavior, perhaps because most previous damage reports referred to longitudinal support unseating or structural collapse (Yang, 1999). However, some transverse damages have been caused in Wenchuan Earthquake because of the lack of transverse earthquake resistances (Yuan & Sun, 2008). Pier's vertical torsion under earthquakes also increases the transverse deformation of the girders. Although a bidirectional ductility design will be effective to increase pier's torsional stiffness and transverse ductility capacity so as to improve the transverse seismic performance, but it may decrease the shear resistance significantly (Fan, 1997). Therefore it is necessary to study the transverse seismic performance of a continuous girder bridge to select the best structural form under different site situations. Accordingly the structure's dynamic characteristics should adapt to the site conditions and the demands should be uniform and rational along the structural components so as to decrease the overall seismic demands.

Generally the ductility approach and the seismic mitigation and isolation approach are two common strategies in the conceptual design of a bridge. The ductility method requires detailed reinforced concrete design for shear resistances and confinement design at the potential plastic hinges of piers in order to resist earthquake actions (Fan & Zhuo, 2001). The seismic mitigation and isolation approach protects the substructure through additional means of energy dissipation by shifting the structural fundamental frequency away from the dominant frequencies of the ground motions. However, the above two methods are not satisfactory for a long span floating cable-stayed bridge in view of the significant excessive displacement demands at the tower top and the girder ends under earthquakes. Hence a new conceptual design strategy is formulated to improve the seismic performance of a long span floating cable-stayed bridge through rational configuration of bridge tower forms. Accordingly a new-type spatial tower is proposed to replace the generally used inverted Y shape tower for an optimal balance between the seismic force and displacement demands of the bridge.

Cable-stayed bridges are classified into different categories by the connection types between the tower and the girder, such as the floating system (no restraint between the girder and towers), the semi-floating system (partial restraint between the girder and towers), the fixed system (full restraint between the girder and towers), and so on. They are widely constructed in seismic zones for their good seismic performance (Walther, Houriet, Isler, Moia, & Klein, 1999). However, the floating connection may cause excessive seismic displacement demands at the girder ends while the fixed connection may lead to excessive force demands at the tower bottom (Ye, Hu & Fan, 2004). So the seismic isolation connection types between the tower and the girder, especially the elastic cable connection, are adopted by more cable-stayed bridges. It is important to study the seismic isolation mechanism of the elastic cables, since the

seismic performance is directly correlated with the cable stiffness for the floating cable-stayed bridge installed with them.

The SCC bridge combines the mechanical advantages of steel and concrete, making the bridge more reasonable and durable. Since 1950s, much research has been carried out to promote the development of SCC bridges. Many countries such as USA and Japan developed the design guidelines and specifications (Brozzetti, 2000; Hayward, 1988). Recently, a growing concern is mainly about the seismic performance of this kind of bridges during earthquakes. So a typical SCC continuous girder bridge and an SCC arch bridge are mainly studied to discuss the seismic potential and performance of SCC bridges.

Since the seismic mitigation and isolation design has received growing attention and become a major research topic, various isolation devices including rubber bearings, frictional bearings and roller bearings have been developed for bridges (Kunde & Jangid, 2003). Pot bearings are widely used in long span railway and highway bridges for their higher vertical load bearing capacities and better deformation ability. It can be assigned to be fixed or frictional in horizontal directions depending on the design demands of the bridges. However, the pot bearing cannot restrain the excessive seismic displacements when sliding, and cannot reduce the seismic forces when fixed. Considering the restraint measures of the pot bearing, a new seismic isolation bearing, known as cable sliding friction aseismic bearing is introduced. This type of bearings can be regarded as the combination of pot bearings and restraining cables and has both advantages of them.

Considering the seismic vulnerability of potential plastic hinge regions of bridge piers, more and more bridge piers are reinforced with SFRC in earthquake regions for its better ductility performance and energy dissipation capacities (Gao, 2009). For the simplest single-column bridge pier, the seismic performance of the piers globally and locally reinforced with SFRC are

studied and compared. Also current seismic design guidelines of various countries give different proposals for estimating the plastic hinge length of a single-column pier reinforced with SFRC (Zhu, Fu, Wang, & Yuan, 2010). There is a need therefore to clarify these differences to facilitate the application of SFRC to bridge piers.

Pile group foundations are widely used in long span cable-stayed bridges and suspension bridges. Many post-earthquake damage investigations and theoretical studies show that the pile group foundations are usually vulnerable components under earthquakes (Zhou, 2008). Generally, they are considered to be strengthened with the steel protective pipes (SPPs) for the construction convenience. But the seismic performance is still not fully determined. Based on numerical simulations and scale-model experiments, seismic capacities, hysteretic behavior and energy dissipation capabilities are reviewed in this chapter.

OVERALL CONCEPTUAL SEISMIC DESIGN FOR BRIDGES

In order to decrease the seismic demands in the conceptual design phase, the main concern of the engineers is to make an optimal arrangement of structural components to let the structure's dynamic characteristics adapt to the site conditions and the seismic demands become more uniform and rational along structural components. Overall conceptual seismic design is applicable for the global structure design based on the linear seismic analysis. In the following sections, four design strategies are reviewed from the overall conceptual seismic design viewpoint: (i) optimal design for layout and detail of continuous girder bridge; (ii) design of towers for long span floating cable-stayed bridge; (iii) seismic isolation mechanism of elastic cables in cable-stayed bridge; (iv) seismic potential and performance for long span SCC bridges.

Optimal Design for Layout and Detail of Continuous Girder Bridge

The continuous girder bridge is one of the most commonly used bridge structural forms. The substructure has major effects on the bridge's dynamic properties and the seismic demands in different site conditions. Considering both the longitudinal and transverse responses of the bridge, many efforts of the optimal design are put on the substructures, especially on piers. In view of the design acceleration response spectrum for normal bridges in Chinese code shown in Figure 1 (Ministry of transport of the People's Republic of China, 1989), the acceleration response spectrum varies according to the structural fundamental period and the type of site. So in designing a continuous girder bridge as a complete structure, the stiffness distribution of some piers can be adjusted to decrease seismic forces and improve the seismic performance for different site conditions.

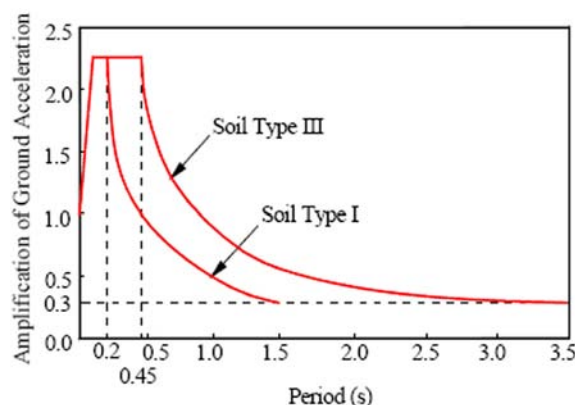
In the design acceleration response spectrum, the amplifications of ground acceleration are respectively $2.25 \times (0.2 / T)$ and $2.25 \times (0.45 / T)^{0.95}$ for soil type I and soil type III according to Chinese code (Ministry of transport of the People's Republic of China, 1989), which is only used as seismic inputs for the bridge. So the seismic im-

portance coefficient and the synthetic influence coefficient are both assumed to be 1.

For an example continuous girder bridge with 25 spans, each span being 29 m long, the finite element model is shown in Figure 2. The structure is separated into 5 parts by 4 expansion joints. There are three types of piers, the solid single-column pier (SSP), the hollow single-column pier (HSP) and the solid twin-column pier (STP), with heights ranging from 5.5 m to 48 m. The bridge is analyzed based on response spectrum method by a combination of transverse and vertical seismic action. The peak ground acceleration equals 0.41g.

For the original bridge, the response spectrum analysis results including the pier top displacements, the pier bottom shear forces and normal stresses are displayed in Table 1 for both soil Type I (rock and stiff soils) and soil Type III (soft to medium clays and sands). It can be seen that both the response magnitudes and variations along these piers are relatively large due to the uneven distribution of the piers' stiffness. New strategies are suggested in the following sections to adjust the piers' stiffness distribution adapt to the site conditions and to avoid the uneven seismic force demands caused by the transverse rotation of girders so as to make the demands more uniform and rational along the structural components.

Figure 1. Design response spectrum (Ministry of transport of the People's Republic of China, 1989)



Conceptual Seismic Design Strategies for Soil Type I

From the code design response spectrum (Figure 1), the specific period $T_g = 0.2$ s for soil Type I is relatively small, beyond which the acceleration amplification decreases rapidly. This means that any increase in the structural period can decrease the seismic force demands significantly, if the structural fundamental period exceed the specific period. Therefore, reducing the lateral flexural stiffness (i.e. shifting to larger fundamental period) can efficiently enhance the seismic performance in the transverse direction. Based on

Figure 2. Finite element model of the continuous girder bridge

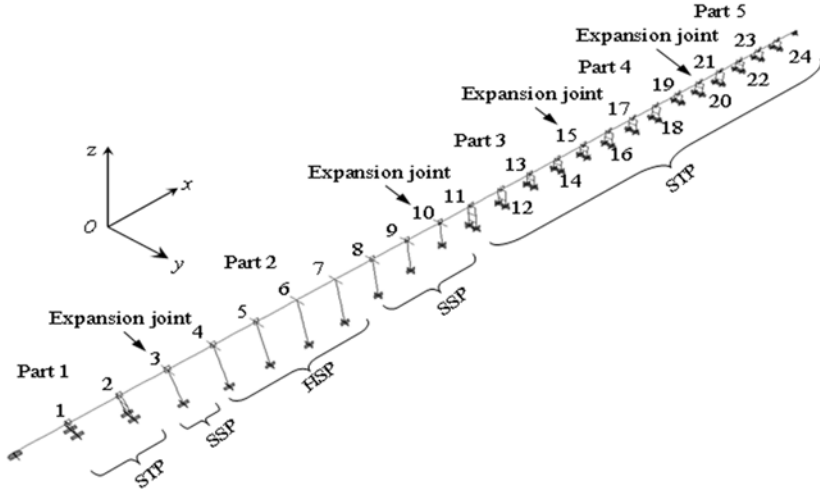


Table 1. Seismic demands of the original continuous girder bridge

Pier No.	Pier type	Bending stiffness($\times 10^3$ kN/m)	Soil type I condition			Soil type III condition		
			Disp. (m)	Shear stress (MPa)	Normal stress (MPa)	Disp. (m)	Shear stress (MPa)	Normal stress (MPa)
1	STP	521.0	0.024	4.630	4.340	0.047	9.290	8.710
2	STP	52.60	0.047	0.960	1.170	0.095	1.890	2.320
3	SSP	7.640	0.071	0.390	7.630	0.140	1.460	15.800
4	HSP	3.170	0.066	0.071	4.740	0.130	0.220	8.960
5	HSP	2.800	0.061	0.079	4.380	0.120	0.220	7.760
6	HSP	2.490	0.055	0.110	4.890	0.110	0.280	7.470
7	HSP	2.800	0.050	0.082	3.840	0.100	0.200	6.180
8	SSP	6.320	0.047	0.260	4.160	0.095	0.660	7.410
9	SSP	11.70	0.043	0.260	4.820	0.086	0.880	9.850
10	SSP	29.20	0.039	0.650	9.160	0.078	2.590	18.290

in this consideration, a new-type pier, named as close twin-column pier (CTP), is proposed to upgrade some piers of the bridge (Figure 3). The CTP is built by vertically dividing the SSP into two parts along the axial symmetrical plane but close to each other. The pier's transverse stiffness can be reduced by 45% to 50%, but the longitudinal flexural stiffness is still maintained. Hence the corresponding acceleration amplification is reduced greatly in the transverse direction. Accordingly the piers No. 3, 8, 9 and 10 are selected to

be replaced by the CTP and the response spectrum analysis results are shown in Table 2.

Comparing the results in Table 2 with Table 1, it can be seen that all the stress demands and some displacement demands are greatly mitigated after some of the bridge piers are changed to the CTPs. Although the pier top displacement demands at pier No. 5 to pier No. 10 increase in some degree, the values themselves are still small and do not exceed the requirements of the code (Ministry of transport of the People's Republic

Figure 3. Conceptual design strategy for bridge pier in soil type I condition

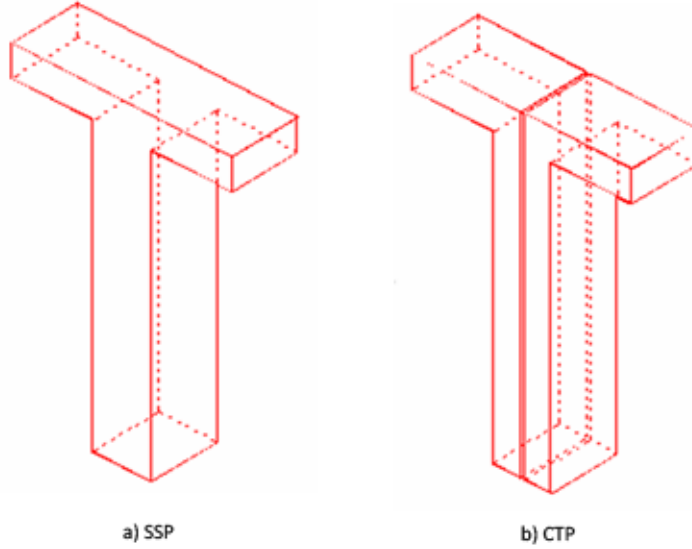


Table 2. Seismic demands of the upgraded bridge for soil type I condition

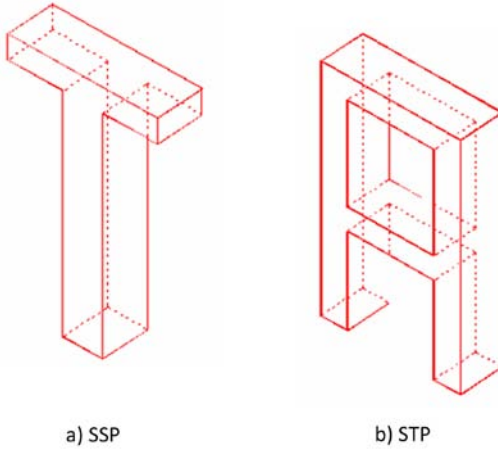
Pier No.	Pier type	Bending stiffness ($\times 10^3$ kN/m)	Disp. (m)	Shear stress (MPa)	Normal stress (MPa)
1	STP	521.0	0.022	4.340	4.070
2	STP	52.60	0.044	0.910	1.100
3	CTP	4.170	0.066	0.210	2.460
4	HSP	3.170	0.065	0.066	4.850
5	HSP	2.800	0.063	0.065	4.030
6	HSP	2.490	0.060	0.080	4.410
7	HSP	2.800	0.059	0.063	3.760
8	CTP	3.450	0.058	0.270	2.740
9	CTP	61.30	0.056	0.200	2.310
10	CTP	16.00	0.054	0.370	4.110

of China, 1989). Specially, the seismic demand variations along these piers decrease and this conceptual design strategy specifically makes the seismic demands more uniform and rational along the structural components and enhances the seismic performance in the transverse direction efficiently.

Conceptual Seismic Design Strategies for Soil Type III

Compared with the soil Type I, the specific period $T_g = 0.45$ s for soil Type III is relatively large. It is obvious that the large deformation becomes the critical problem for long span bridges in this soil type. So the above proposed upgrading measures for soil Type I would not be applicable.

Figure 4. Conceptual design strategy for bridge pier in soil type III condition



Therefore for soil Type III, the conceptual design strategies are proposed as follows: (i) relocate the expansion joint at pier No. 10 to No. 8 in order to adjust the stiffness distribution of the superstructure and to avoid the uneven seismic force demands caused by the transverse rotation of girders, (ii) separate the SSPs No. 8, 9 and 10 into STPs (Figure 4) to modify the transverse stiffness thus to restrict the seismic displacements for these piers. The seismic demands are listed in Table 3 for the upgraded bridge.

From the comparison between the results in Table 3 and those in Table 1, it can be seen that the displacements, the shear and normal stresses are all reduced, indicating that the proposed conceptual design strategies can improve the seismic performance of the bridge.

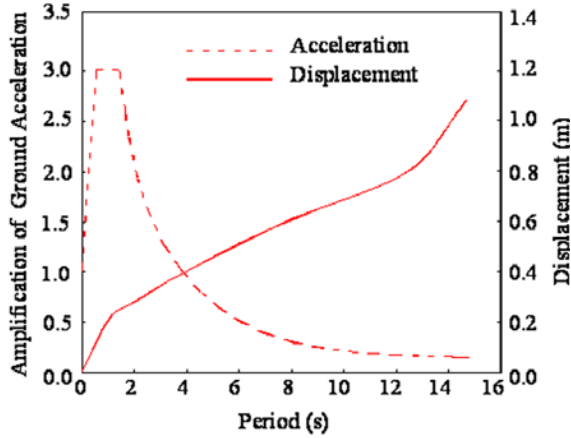
Design of Towers for Long Span Cable-Stayed Bridge

From the perspective of overall conceptual seismic design, both force and displacement demands should be taken into consideration. However the force and displacement responses are usually mutually contradictory. As can be seen from the design response spectra (Figure 5) for a special bridge, the Sutong Yangtze River Bridge in China (Yan & Yuan, 2004), in the long period range the acceleration amplification is relatively small and yet the displacement amplification may be too large to be tolerated. So for the flexible cable-stayed bridge, a structural period lengthening would be effective to reduce the force demands and yet ineffective to decrease the excessive displacement demands at the tower top and the deck ends. It is obvious that the flexural stiffness of the tower has a major influence on the fundamental period of the cable-stayed bridge. Therefore it is preferable

Table 3. Seismic demands of the upgraded bridge for soil type III condition

Pier No.	Pier type	Bending stiffness ($\times 10^3$ kN/m)	Disp. (m)	Shear stress (MPa)	Normal stress (MPa)
1	STP	521.0	0.030	5.840	5.480
2	STP	52.60	0.060	1.200	1.460
3	SSP	4.170	0.089	0.920	9.360
4	HSP	3.170	0.098	0.180	6.790
5	HSP	2.800	0.110	0.210	7.320
6	HSP	2.490	0.120	0.270	8.310
7	HSP	2.800	0.130	0.250	8.680
8	STP	24.60	0.140	2.780	1.770
9	STP	30.50	0.120	2.840	2.310
10	STP	43.20	0.094	3.150	1.900

Figure 5. Design response spectra for the Sutong Yangtze River Bridge (Yan & Yuan, 2004)



to adopt an optimal tower type for the bridge's fundamental period within a proper range so that acceptable force and displacement demands can be achieved in the seismic conceptual design phase.

The Sutong Yangtze River Bridge (Yan & Yuan, 2004), whose finite element model is shown in Figure 6, is a long span floating cable-stayed bridge originally with inverted Y shape bridge towers. The spans are 100 m, 100 m, 300 m, 1088 m, 300 m, 100 m, 100 m and the superstructure is designed as a floating system without connec-

tions to the towers. The design acceleration and displacement response spectra are shown in Figure 5 and the peak value of the design horizontal ground acceleration is $0.197g$, which is about twice of the vertical acceleration input.

Conceptual Seismic Design

Flexible structures always have relatively long fundamental periods. From dynamic analysis, the fundamental period of the above cable-stayed bridge is estimated as 13.40 s, a typical long period. Since the fundamental period is much affected by the flexural stiffness of the tower, a new-type spatial tower scheme is proposed as shown in Figure 7b after a series of response spectrum analyses and comparisons. The bending stiffness of the proposed alternative tower (65.5×10^3 kN/m) is 9.66 times of the original tower (6.78×10^3 kN/m), while the weight (1.17×10^6 kN) is just 1.83 times of the original (0.638×10^6 kN). In conclusion the proposed spatial tower can significantly increase the flexural stiffness yet with relatively small additional material cost. The fundamental period of the bridge with the proposed spatial towers is reduced from 13.40 s to 5.87 s.

Figure 6. Finite element model of the Sutong Yangtze River Bridge

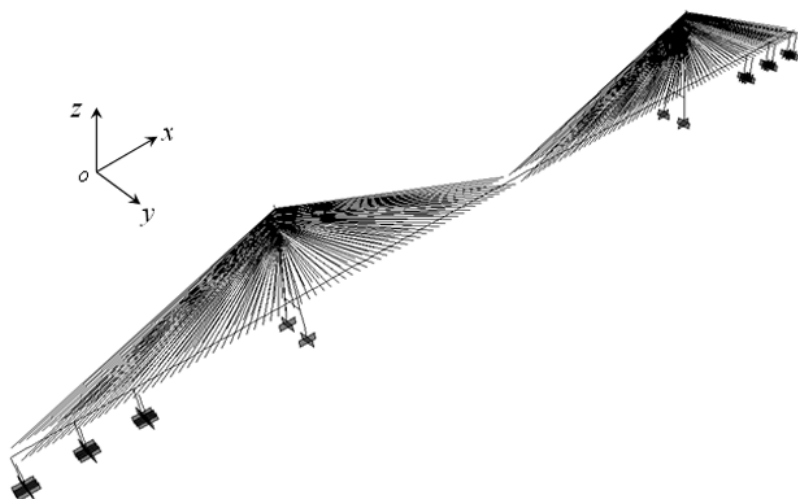
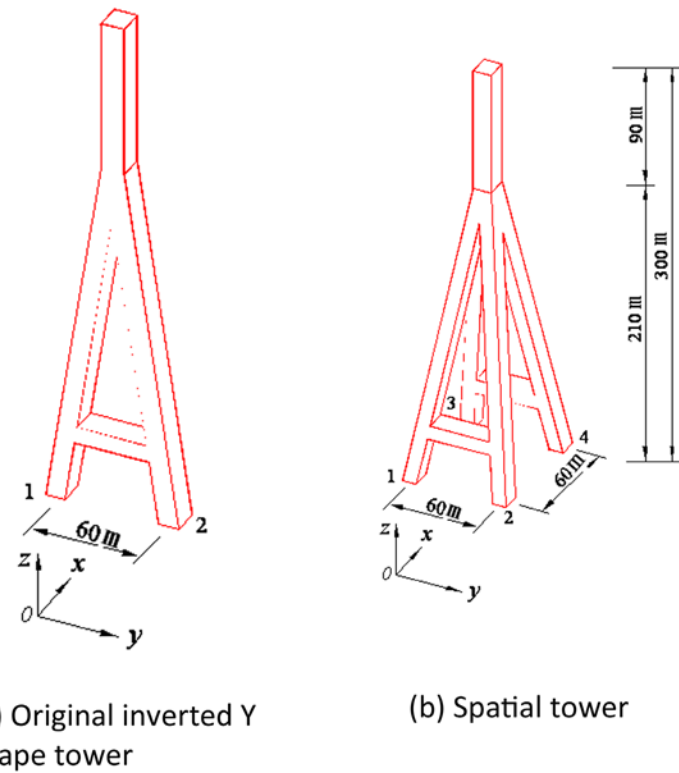


Figure 7. Original and alternative spatial bridge towers



(a) Original inverted Y shape tower

(b) Spatial tower

Comparison of Seismic Responses

By using the design response spectra (Figure 5) which are from the geological safety evaluation in the field and fit for the site situation for the bridge, the response spectrum analyses are conducted respectively in the longitudinal direction and in the transverse direction under corresponding horizontal and vertical ground motions. The displacement demand comparisons are shown in Table 4 for the original design tower model and the alternative spatial tower model. It can be seen that the maximum longitudinal seismic displacements at the deck end, the tower top and the midspan are reduced significantly for the spatial tower model. Since the spatial towers' constraint to the deck becomes stronger, the transverse displacement at the midspan of the alternative model is also reduced. Although the transverse displacement of

the tower top increases from 0.20 m to 0.41 m, this 0.41 m figure is considered small and practically acceptable for the long span cable-stayed bridge.

The force demand comparisons are shown in Table 5 between the original inverted Y shape and the proposed spatial tower models. The total force demands at the spatial tower bottoms are slightly larger than those at the inverted Y tower, while the demands in each column No. 1, 2, 3 and 4 (Figure 7) of the spatial tower model are less than or almost equal to those of the original one. It can be concluded that the conceptual design strategy for the cable-stayed bridge, which adopts the spatial tower to replace the original inverted Y shape tower, enables the seismic demands more uniform along the structural components and obtain a balance between the force and displacement demands.

Table 4. Seismic displacement comparisons

Model	Location	Longitudinal displacement (m)	Transverse displacement (m)
Original inverted Y shape tower model	Girder end	1.030	-
	Tower top	1.110	0.200
	Span center	1.040	0.950
Alternative spatial tower model	Girder end	0.440	-
	Tower top	0.390	0.410
	Span center	0.450	0.870

Seismic Isolation Mechanism of Elastic Cables in Cable-Stayed Bridge

The excessive seismic displacement of the girder end is one of the challenges to the cable-stayed bridge designers, since it may exceed the deformation capacities of expansion joints. There may also be excessive seismic bending moment at the tower bottom. Isolation devices are usually adopted to avoid excessive demands, including the system of elastic cables installed between the tower and the deck. For a floating cable-stayed bridge without elastic cables, the seismic force is transmitted from the deck to the tower mainly depending on the inclined cables. However, the elastic cables become one of the main force transmission paths

once the bridge installed with them, which may change the overall seismic force distribution of the bridge.

As a case study, consider a long span floating cable-stayed bridge with spans 55 m, 165 m, 165 m and 55 m and the finite element model is shown in Figure 8. There are sliding bearings at the subsidiary and side piers and no bearings between the tower and the deck girder from the original design scheme of the bridge.

Parametric Analyses

Based on dynamic analyses and parametric simulations, in which the elastic cables are simulated as elastic bearing connection elements, the variations of the bridge fundamental period corresponding to the elastic cable stiffness are shown in Figure 9 and the relationship between the vibration modes and the stiffness is shown in Table 6.

It can be seen that the fundamental period decreases rapidly when the elastic cable stiffness increases from 0 to 10×10^5 kN/m. At the stiffness values larger than 10×10^5 kN/m, the period variation is small. It is also shown in Table 6 that the vibration modes do not change when the cable stiffness increases from 0 to 5×10^5 kN/m. On the contrary, at stiffness of 30×10^5 kN/m, the first mode of vibration changes from a girder longitudinal drift to a tower lateral bending in the same direction. This may be due to the rational elastic cable stiffness leading to a change in the dy-

Table 5. Seismic force comparisons at the tower bottom

Model	Column number (Figure 7)	Longitudinal direction		Transverse direction	
		Shear force ($\times 10^3$ kN)	Bending moment ($\times 10^6$ kN.m)	Shear force ($\times 10^3$ kN)	Bending moment ($\times 10^6$ kN.m)
(i)Original inverted Y shape tower model	1 (or 2)	30.90	2.290	47.60	1.670
(ii)Spatial tower model	1 (or 2)	32.20	2.030	42.60	1.300
	3 (or 4)	32.20	2.030	32.00	1.220
((ii)-(i))/(i) (%)	1 (or 2)	4.2	-11.4	-10.5	-22.2
	3 (or 4)	4.2	-11.4	-32.8	-26.9

Figure 8. Finite element model of the cable-stayed bridge with elastic cables

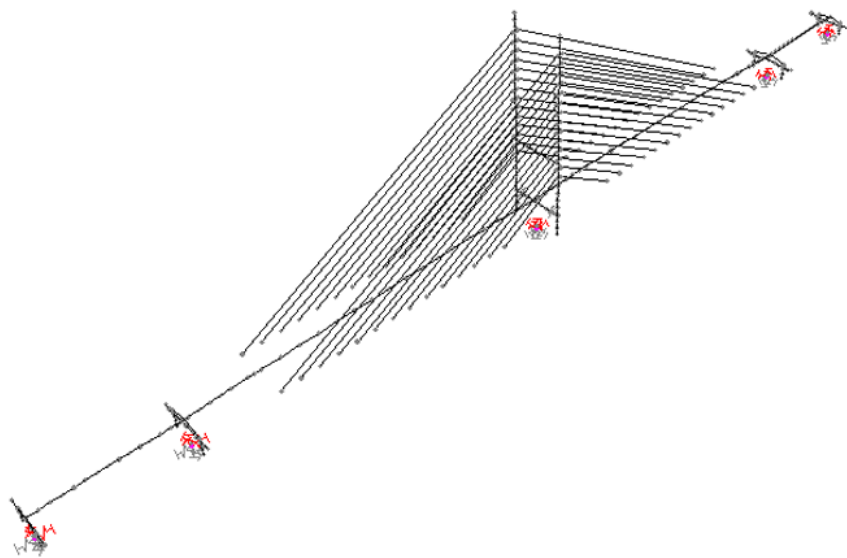


Figure 9. Fundamental period versus elastic cable stiffness

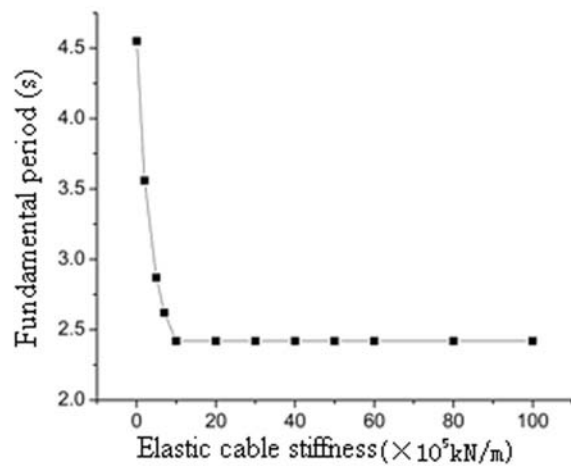
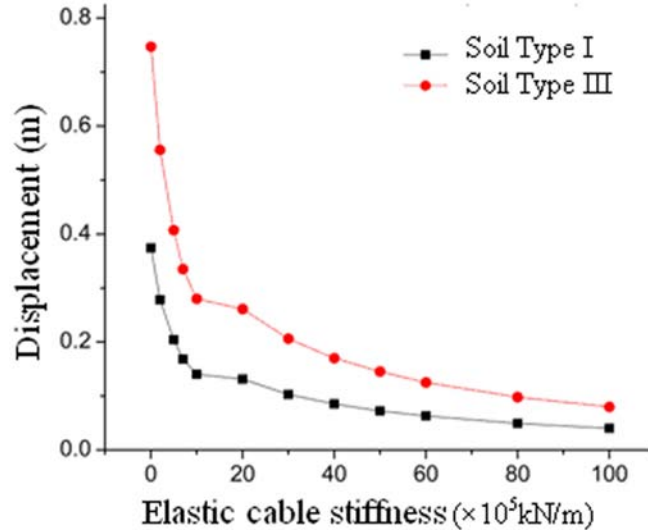


Table 6. Vibration mode versus elastic cable stiffness

Mode order	Elastic cable stiffness (kN/m)		
	0	5×10^5	30×10^5
1	Girder longitudinal drift	Girder longitudinal drift	Tower lateral bending in same direction
2	Tower lateral bending in same direction	Tower lateral bending in same direction	Reversely symmetric vertical bending
3	Reversely symmetric vertical bending	Reversely symmetric vertical bending	Tower lateral bending in different direction
4	Tower lateral bending in different direction	Tower lateral bending in different direction	Girder longitudinal drift

Figure 10. Girder end displacement versus elastic cable stiffness



namic characteristics, thus being able to reduce the seismic demands and improve the seismic performance of the bridge.

The variations of the girder end displacement demands are shown in Figure 10 for two different site situations (Ministry of Transport of the People's Republic of China, 2008), based on results from elastic response spectrum analyses. The relationships are shown in Figure 11 between the tower-girder relative displacement and the stiffness. It can be seen that the displacement demands decrease rapidly as the cable stiffness increases from 0 to 30×10^5 kN/m and their decreasing rate becomes insignificant after the stiffness exceeds 30×10^5 kN/m.

On the other hand, the variations of the tower bottom seismic force demands are shown in Figure 12 for the same two different site conditions. It can be seen that the bending moment demands fluctuate in relatively small amplitude when the cable stiffness increases, while the shear force demands monotonously increase.

Therefore it is concluded that the elastic cables change the seismic force transmission and distribution significantly. The stiffness range from 20×10^5 to 70×10^5 kN/m is practically acceptable

for the elastic cables, in which the displacement demands are reduced significantly while the moment and shear force demands have little changes. Thus the rational elastic cable stiffness adjusting strategy may achieve the seismic demand uniformity along the structural components and a balance between the force and displacement demands during the conceptual design.

Seismic Isolation Mechanism

From the parametric analyses, it can be seen that if the cable stiffness increases the fundamental period of the bridge will decrease rapidly, the vibration modes will change, the displacements will decrease rapidly, the bending moments will fluctuate in small amplitude and the shear force will monotonically increase.

The above analyses reveal the core of the seismic isolation mechanism of the elastic cables, the change of structure system and the transformation of the force transmission path in the bridge tower. Because of the limiting function of the elastic cables, a floating cable-stayed bridge gradually turns into a semi-floating system, and finally a tower-girder rigid connection system when the

Overall Conceptual Seismic Design and Local Seismic Capacity Design

Figure 11. Tower-girder relative displacement versus elastic cable stiffness

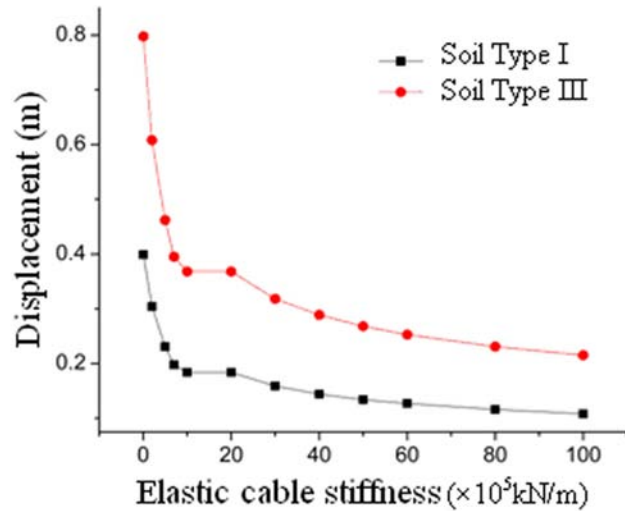


Figure 12. Seismic force demands versus elastic cable stiffness

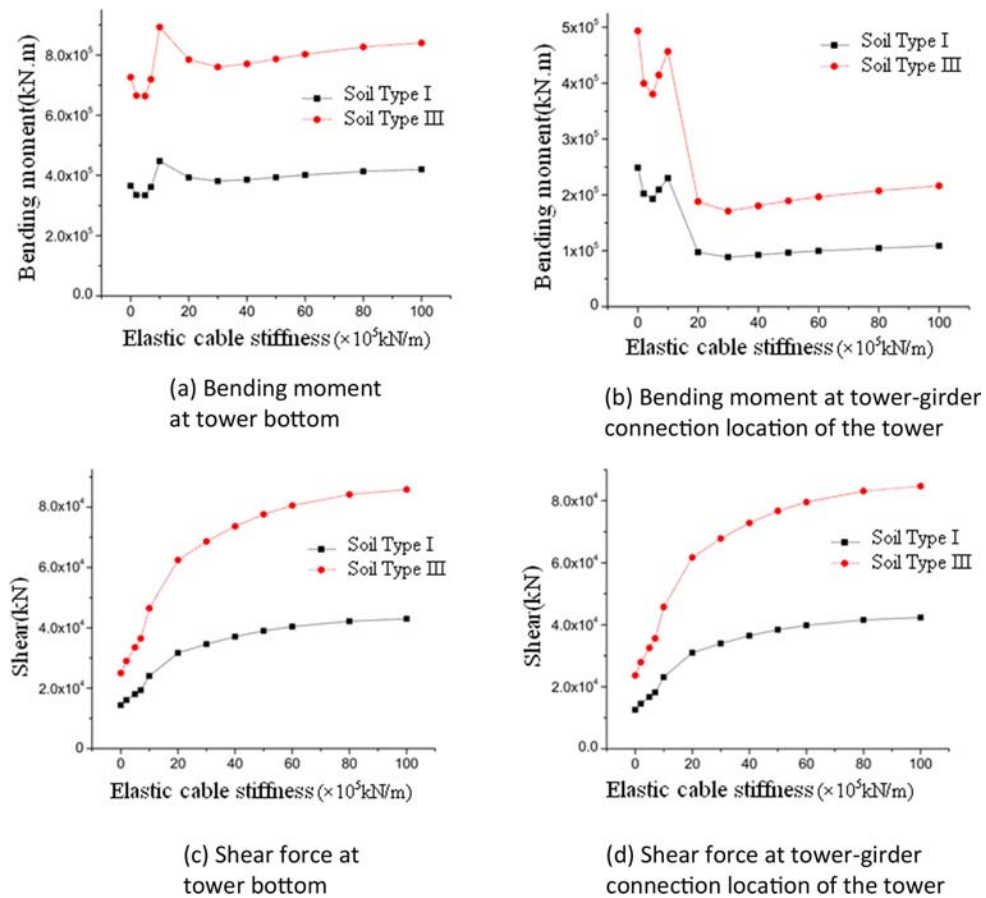


Table 7. Seismic response comparisons of RC and SCC continuous girder bridges

Design scheme	Superstructure mass ($\times 10^6$ kg)	Pier area (m 2)	Pier stiffness ($\times 10^6$ kN/m)	Period (s)	Shear ($\times 10^3$ kN)	Moment ($\times 10^3$ kN.m)	Disp. (m)
(i) RC	3.900	4.050	0.199	0.880	3.430	24.00	0.017
(ii) SCC	2.118	2.200	0.189	0.670	2.470	17.30	0.013
(ii)/(i) (%)	54.3	54.3	95.0	76.1	72.0	72.1	76.5

cable stiffness increases. It is obvious that the change of the system, namely the increase of the bridge stiffness will cause a decrease of the fundamental period and an increase of the horizontal brake force of the girder. The transformation of the force transmission path is the main reason why the seismic demands change along the curves shown in Figure 10 to 12. For a floating cable-stayed bridge without elastic cables under earthquakes, the large horizontal forces produced by the girder, whose acting point is usually at upper zones of the tower, are all transmitted to the tower by the stayed-cables. But the elastic cables can share most of the seismic forces and transmit them to lower zones of the tower for a cable-stayed bridge installed with them.

Seismic Potential and Performance for Long Span SCC Bridges

To illustrate the advantage of steel-concrete composite (SCC) system, a typical four span bridge with spans of 25 m, 30 m, 30 m and 25 m, deck 18 m wide, and piers 7 m high was ever studied (Turkington, Carr, Cooke, & Moss, 1989). In this section, there are two design schemes for the bridge: (i) a conventional reinforced concrete (RC) continuous girder bridge supported by solid form piers and (ii) an SCC continuous girder bridge supported by hollow form piers, all basic properties being shown in Table 7. The seismic responses of both design schemes from elastic response spectrum analyses (Ministry of Transport of the People's Republic of China, 2008) are also shown in Table 7. It can be seen that the SCC scheme

with the same span and deck width has a lighter superstructure, less pier stiffness and fundamental period. The seismic shear force and bending moment at the pier bottom are 72.0% and 72.1% of those from the initial reinforced concrete scheme. Moreover, the pier top displacement is only 76.5% of that in design scheme (i). The seismic potential of the SCC bridge system is significant.

A major highway bridge located in the city of Hangzhou, China, the Jiubao Bridge consists of an SCC continuous girder system for the northern approach (55 m, 85 m, 85 m, 90 m), an arch with SCC girder system for the main bridge (three 210 m spans) and another SCC continuous girder system for the southern approach (90 m, nine 85 m, 55 m). The SCC deck is a reinforced concrete slab on top of steel box girders. The superstructure is supported by sliding and pot bearings, both types being fixed in the transverse direction. In the longitudinal direction the bearings are designed to be fixed at pier PN4, PS1, PS5, PS6 and PS7 as shown in the finite element model in Figure 13.

It was suggested that the girders of the SCC bridge might be replaced by equivalent concrete girders with weight twice as heavy as the SCC ones. Response spectrum analyses were performed (Cao, 2009) and the results are shown in Table 8 for the bridge, and it is clear that the long span SCC bridge has lower seismic force and displacement demands than the RC one. Hence, the SCC system has higher seismic potential and better seismic performance.

Figure 13. Finite element model of the Jiubao Bridge

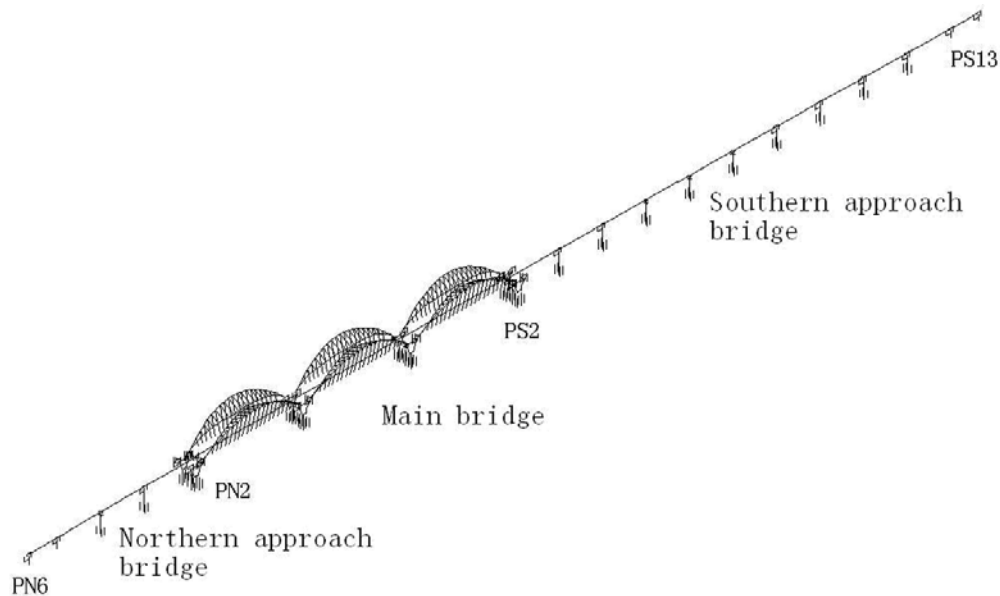


Table 8. Seismic response comparisons of the arch bridges with RC and SCC girders

Girder	Southern approach			Main bridge		
	Shear-PS6 ($\times 10^3$ kN)	Moment-PS6 ($\times 10^3$ kN.m)	Displacement of bearing-PS2 (m)	Shear-PS1 ($\times 10^3$ kN)	Moment-PS1 ($\times 10^3$ kN.m)	Displacement of bearing-PN1(m)
(i) RC	8.450	156.10	0.290	10.492	138.85	0.240
(ii) SCC	5.195	95.53	0.190	7.894	102.89	0.190
(ii)/(i) (%)	61.5	61.2	65.5	75.2	74.1	79.2

Solutions and Recommendations

From the perspective of overall linear conceptual seismic design, several new design strategies have been presented. For a typical long span continuous girder bridge, the forms of piers and the locations of expansion joints are adjusted respectively for different site conditions to improve the stiffness distribution. Based on code design response spectra, theoretical analyses and numerical simulations show that both the displacement and stress demands are greatly mitigated, and the demand variations along the piers are decreased as well after adopting the strategies.

For a long span floating cable-stayed bridge, a new-type spatial bridge tower is proposed to replace the originally designed inverted Y shape tower. Analysis results show that the longitudinal seismic displacements can be reduced significantly for a bridge with the spatial tower. The transverse displacement at the midspan of the spatial tower model is also reduced. Although the transverse displacement of the tower top increases to some extent, the magnitude of the displacement is relatively small and practically acceptable for the cable-stayed bridge. Moreover, the seismic force demands in each column of the spatial tower model are less than or almost equal to those of the original model.

With respect to the elastic cable seismic isolation device, the isolation mechanism, the influences of the elastic cable stiffness on the bridge structural dynamic characteristics, the force transmission paths and the displacement and force demands have been discussed for another floating cable-stayed bridge. Numerical analysis results show that the fundamental period of the bridge decreases rapidly when the cable stiffness increases. The vibration modes will change if the cable stiffness increases to some extent, and the displacement demands decrease rapidly when the stiffness increases. The bending moment demands fluctuate in small amplitude, while the seismic shear force demands monotonically increase.

For the new-type SCC bridge, the seismic potential is further confirmed based on response spectrum analyses of a four span continuous girder bridge and a long span SCC arch bridge. Analysis results show that the SCC continuous girder bridge with same span and deck width has lighter superstructure, less pier stiffness and fundamental period. Also the shear force and bending moment at the pier bottom and the displacement at pier top all decrease significantly. For the long span SCC arch bridge, it also has lower seismic force and displacement demands than a reinforced concrete bridge.

LOCAL SEISMIC CAPACITY DESIGN FOR COMPONENTS OF BRIDGES

Earthquakes have a habit of identifying structural weaknesses and concentrating damage at these locations (Priestley, Seible & Calvi, 1992). Lots of investigations on earthquake disaster show that bridge damage caused by earthquakes mainly focuses on local regions and weak points of bridge components, such as bearing failures, pier failures, pile foundation failures, expansion joint failures, and so on. Considering the stochastic characteristics of earthquakes, keeping bridges in elastic state permanently is impossible and unreasonable.

When the components of bridge locally become plastic, the overall conceptual seismic design is not applicable because of the limitation of overall linear analyses. The local nonlinear seismic capacity design is therefore beneficial for its economy, applicability and validity.

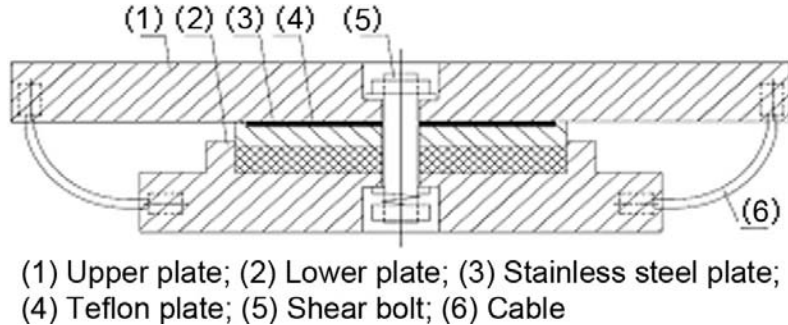
Innovation of Cable Sliding Friction Aseismic Bearing for Bridges

The girders of continuous bridges are generally supported by bearings which transmit loads to underlying piers and abutments. Bearing system generally comprises a fixed bearing on one pier and several frictional bearings on other piers. Under minor or moderate horizontal earthquake actions, almost all the superstructure's earthquake-induced forces are transmitted to the fixed pier which may thus be damaged because of the excessive shear force or bending moment. If the fixed bearing is designed to fail under severe earthquakes so as to protect the pier system, all the other frictional bearings will be mobilized to slide so that the bridge system will be difficult to maintain equilibrium.

A new cable sliding friction aseismic bearing (Figure 14) is invented and presented, which is composed of the pot bearing, some cables and a shear bolt. Through reasonable design, the bearing may perform as same as a fixed bearing system, namely keep in service under minor or moderate earthquakes. Moreover, the shear bolt of the new bearing will fail during severe earthquakes, and then a bearing originally used as a fixed bearing will be converted into a frictional one. Hence, the seismic force can be shared by all the piers not only by the fixed pier, while the excessive seismic displacement can be restricted by the cables attached to the base of the bearing.

As an improved type of frictional isolation devices, the new bearing is characterized by its insensitivity to the frequency content of earthquake excitations. It can be used in conventional girder-system bridges, cable-stayed bridges, suspension bridges and other similar structures. Compared

Figure 14. Schematic diagram of cable sliding friction aseismic bearing



to other isolation bearings, this bearing has the advantages of simplicity in principle, wide application, mature technique, stable performance and low cost (Yuan, Cao, Cheung, Wang & Rong, 2010).

Performance Criteria

Based on the above design strategies, three performance objectives are proposed for a cable sliding friction aseismic bearing as follows.

1. If the expected deformation of the bearing is less than the design free displacement, the cables should not be mobilized and the new bearing functions as a conventional pot bearing.
2. Under minor and moderate earthquakes, the shear bolt in a fixed-type bearing should not break so that the bearing keeps service and need not be replaced. With respect to a sliding-type bearing, the friction capacities between the stainless steel plate and the Teflon plate should bear the horizontal ground motions and dissipate the seismic energy.
3. Under severe earthquakes with the breaking of the shear bolt, the bearing should function as a frictional bearing to mitigate the seismic forces and dissipate the seismic energy, while excessive relative displacement between

the superstructure and the pier should be restrained by the cables.

Design Parameters

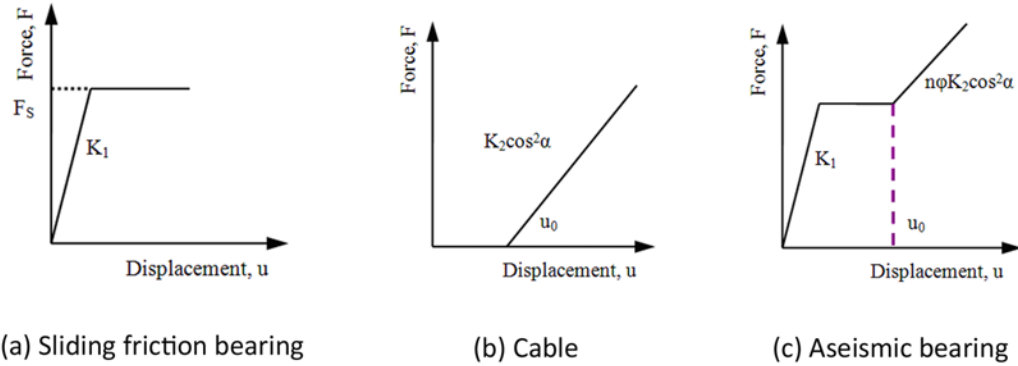
Depending on the above performance objects, some important design parameters, such as the characteristics of the cables, the shear strength of the bolt and the integral stiffness of the bearing should be studied carefully as follows, except for the available characteristics of the pot bearing from the manufacturers.

1. Characteristics of the cables

According to the geometry dimensions of the bearing, each cable's length L can be calculated as Eq. (1), where L_{xy} is the projective distance of the cable in horizontal plane, H is the bearing total height, A and B are length and width of the upper plate, C and D are length and width of the lower plate, δ_x and δ_y are the design displacement in the bearing's longitudinal and transverse direction.

$$\left\{ \begin{array}{l} L_{xy} = \sqrt{[\delta_x + (A - C)/2]^2 + [\delta_y + (B - D)/2]^2} \\ L = \sqrt{H^2 + L_{xy}^2} \end{array} \right. \quad (1)$$

Figure 15. Stiffness models



The axial stiffness of a cable member is defined as $K_2 = EA_1/L$, where E is the elastic modulus of the cables, A_1 is the cable section area and L is the cable length.

2. Shear strength of the bolt

Considering the requirements under service loads, the horizontal shear resisting capacity of the fixed-type pot bearing should not be less than 10% of the vertical load bearing capacity (Cao, 2009). Depending on the performance objects, the shear bolt should be out of service during severe earthquakes. So it is suggested that the shear strength of the bolt be within 10% to 15% of its vertical load capacity.

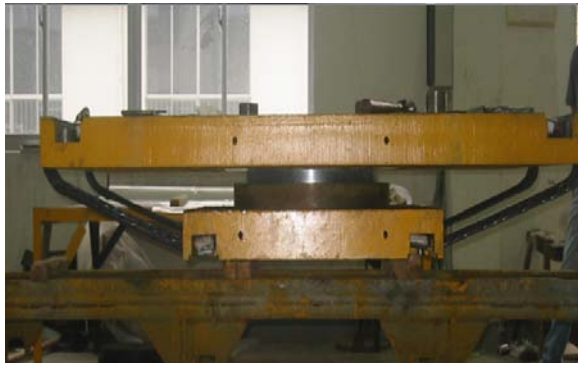
3. Integral stiffness of the bearing

The lateral stiffness of a frictional bearing can be simplified as an ideal bilinear model as shown in Figure 15a, where K_1 denotes the elastic stiffness of the bearing and F_s denotes the critical friction force which is calculated as $F_s = \mu N$ where μ is the friction coefficient and N is the vertical force on the bearing. The cables can be regarded as completely elastic material since they should not yield, whose load-displacement curve is shown in Figure 15b, where K_2 is the stiffness of the

cables, u_0 denotes the design free displacement when the bearing is in normal service load and α is the angle between the longitudinal direction of the cable when engages at a lateral displacement of u_0 and the direction of the horizontal relative displacement of the friction bearing. So combined with the characteristics of the frictional bearing and the cables, the integral stiffness model of the cable sliding friction aseismic bearing can be shown in Figure 15c, where n is the number of cables and φ is a coefficient that represents the equivalent linearization of cable stiffness under severe earthquakes.

Depending on pseudo-static cyclic loading experiments and finite element analyses for a prototype cable sliding friction aseismic bearing (Figure 16) where the maximum vertical load is 5000 kN, the actual values of the bearing's characteristics, such as the static and dynamic friction coefficients of the bearing's sliding surface, the cable stiffness, the experimental hysteretic curves of the bearing and the corresponding skeleton curves, can be obtained (Cao, 2009; Yuan, Cao, Cheung, Wang & Rong, 2010). The experimental results show that the static and dynamic friction coefficients decrease as the vertical load increases. Through the experiments and calculations, the coefficient φ is suggested to be 0.373 for its application in theoretical analysis models of the new

Figure 16. Prototype bearing



bearing. The results also show that the experimental hysteretic curves agree with the numerical ones well and the displacement restraining capacity of the cables is significant.

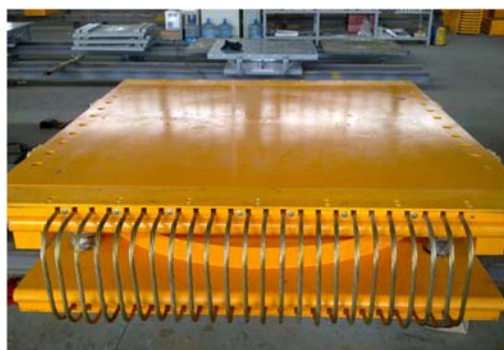
Application Study

From the above theoretical assumptions and analyses, the new cable sliding friction aseismic bearing seems sound and acceptable. After some conformation improvements in order to be fit for the requirements and convenience of manufacturers, the modified shop-manufactured bearing shown in Figure 17 is applied in a girder-arch composite bridge with spans of three 210m, whose finite element model is shown in Figure 18 and

the fixed pier is PS1. For the new cable sliding friction aseismic bearing used only on the fixed pier PS1 in the bridge, the vertical load bearing capacity is 35000 kN, the friction coefficient is 0.02 and the shear strength of the shear bolt is 3500 kN. The seismic responses are evaluated by using an artificial synthetic ground motion (Figure 19), whose excess probability is 3% in 100 years (Cao, 2009). The artificial synthetic ground motion is applied in the longitudinal direction at the base of the piles and abutments, while the vertical ground motion is two thirds of it.

Since the stiffness of the cables is very important for the new bearing, it is necessary to analyze the seismic demand variations of the bridge along with the stiffness of the cables. Parametric analyses are conducted and the results are shown in Figure 20, in which the left vertical coordinate indicates the seismic shear force at the bottom of pier PS1 and the right one indicates the maximum longitudinal seismic displacement of the deck end. It can be seen that the seismic displacements of the deck end decrease rapidly, while the seismic shear forces at the bottom of pier PS1 do not increase too much, as the cable stiffness increases. Yet the shear forces increases a little and the deck displacement changes slightly when the cable stiffness gradually increases from 1×10^5 to 3×10^5 kN/m.

Figure 17. Modified shop-manufactured bearing



(a) The bearing ready to be delivered to site



(b) Site installation of the bearing

Figure 18. Finite element model of the girder-arch composite bridge

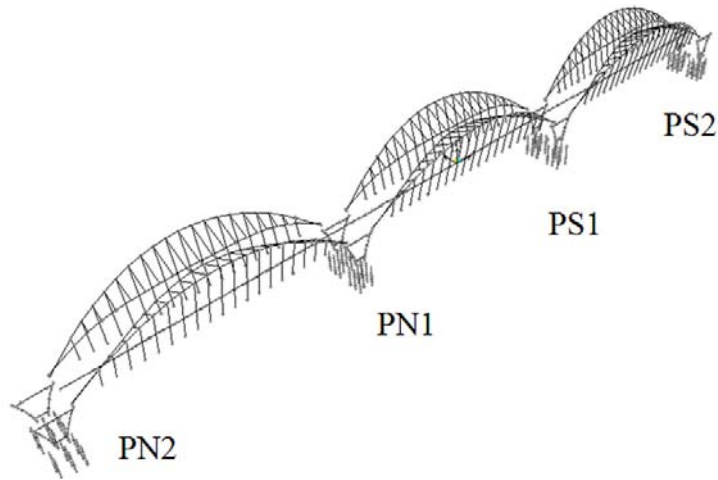


Figure 19. Synthetic seismic wave

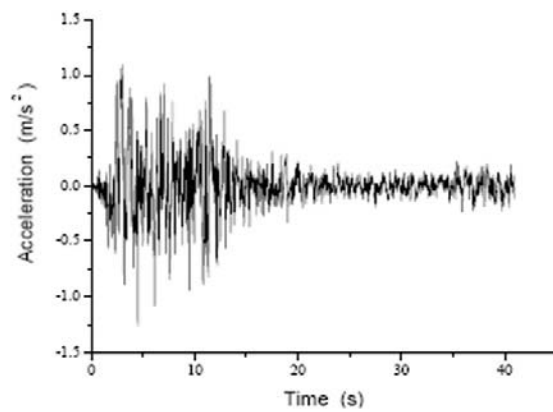


Figure 20. Seismic demands versus the cable stiffness

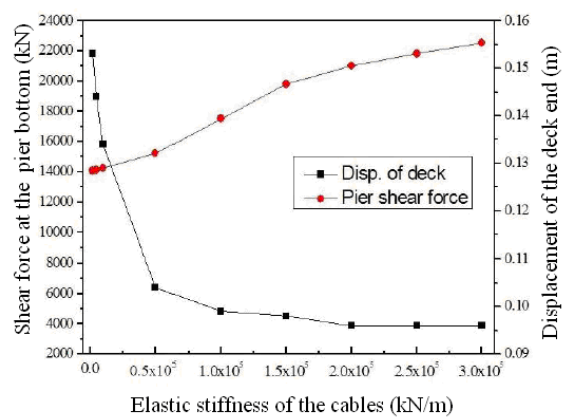


Table 9. Two different design schemes with different arrangements of bearings

Design scheme	Pier PN2	Pier PN1	Pier PS1	Pier PS2
Original design	Sliding bearings	Sliding bearings	Conventional fixed bearings	Sliding bearings
Alternative design	Sliding bearings	Sliding bearings	Proposed cable sliding friction aseismic bearings	Sliding bearings

For the nonlinear time history analysis of the bridge, two design schemes are considered, (i) the original design with the conventional fixed bearings on the fixed pier PS1; (ii) the alternative design with the cable sliding friction aseismic bearings on the same pier. Besides, all other bearings are the same sliding ones for the two design schemes and the arrangement of the bearings is listed in Table 9.

Considering the seismic demand variations of the bridge along with the stiffness of the cables and many cables used in the new bearing resulting in the larger supplied stiffness, so the cable stiffness in the horizontal direction is taken as about 3.0×10^5 kN/m in the application study. After the analyses, shear force demands at pier bottoms and deck-pier relative displacements are shown in Table 10. Note that the shear force is normalized with the deck weight. For the shear force comparisons, the bearings at PS1 are of conventional fixed type in the theoretical models of the bridge, because the bearings in fixed conditions have relative more disadvantageous seismic force demands. For the deck-pier relative displacement comparisons, the fixed bearings are assumed to have lost fixity and be free to move during a severe earthquake, focusing the performance of the original and the new bearings. It can be seen that the shear force demand at PS1 is much larger than those at the other three piers by using the original bearing on the fixed pier PS1. Yet the excessive

demands are significantly reduced by 59%, when the new bearing takes the place of the original one. And other shear forces are also reduced at the pier bottoms of other piers except for the almost equal shear forces at the pier bottoms of the pier PN2. Furthermore, the possible maximum displacements of the deck relative to the piers during a severe earthquake that causes the conventional fixed bearings at pier PS1 to lose fixity may range from 268 mm to 280 mm. Yet the deck displacements at all four piers are controlled to be less than 160 mm by using the new bearing.

Moreover, the seismic capacity checks are shown in Table 11 for the most unbeneficial pile of the bridge. It can be seen that the checks cannot pass when the original bearing is used on the fixed pier PS1. However, the checks can pass when the new bearing replaces the original one. So it can be concluded that the new bearing can decrease the seismic demands and be effective to protect the bridge piers and foundations.

Seismic Performance of Bridge Piers Reinforced with SFRC

There have been numerous studies on steel fiber reinforced concrete (SFRC), most of which aimed at the constitutive behavior (Zollo, 1997). These studies generally ignored an important fact that the SFRC is more likely conducted in confined conditions. Ramesh, Seshu and Prabhakar have made experimental analyses of 90 specimens and pointed out that the SFRC confined by lateral ties has improved material properties (Ramesh, Seshu & Prabhakar, 2003). Then a constitutive model of SFRC, which has been widely accepted, is offered as Figure 21. The constitutive equations are also shown as Eq. (2), (3) and (4), in which $C_i = (P_b - P_{bb})(f_v/f_c)\sqrt{b/s}$ and RI is the reinforced index.

$$P = f'_c (1 + 0.55C_i)(1.0228 + 0.1024(RI))A_g + f_y A_g \quad (2)$$

Overall Conceptual Seismic Design and Local Seismic Capacity Design

Table 10. Seismic demand comparisons of the bridge with different bearings

Design scheme	Pier location	Shear force demands of piers		Deck-pier relative displacement	
		Base Shear (W_d)	% of original	Displacement (mm)	% of original
Original design	PN2	0.0473	-	280	-
	PN1	0.0545	-	273	-
	PS1	0.0914	-	268	-
	PS2	0.0524	-	268	-
Alternative design	PN2	0.0491	104%	152	54%
	PN1	0.0474	87%	142	52%
	PS1b	0.0537	59%	128	48%
	PS2	0.0473	90%	113	42%

Table 11. Check comparisons of the unbeneficial pile for different bearings

Design scheme	Pier location	Seismic Demand		Moment capacity ($\times 10^3$ kN·m)	Check
		Axis force ($\times 10^3$ kN)	Moment ($\times 10^3$ kN·m)		
Original design	PN2	9.633	18.45	22.15	Yes
	PN1	10.872	15.39	22.59	Yes
	PS1	1.546	22.94	18.64	No
	PS2	9.591	18.48	22.13	Yes
Alternative design	PS1	4.081	15.23	19.90	Yes

Figure 21. Constitutive model of SFRC

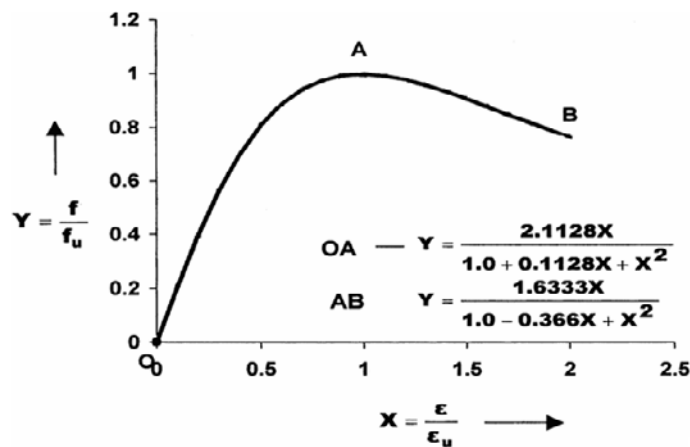
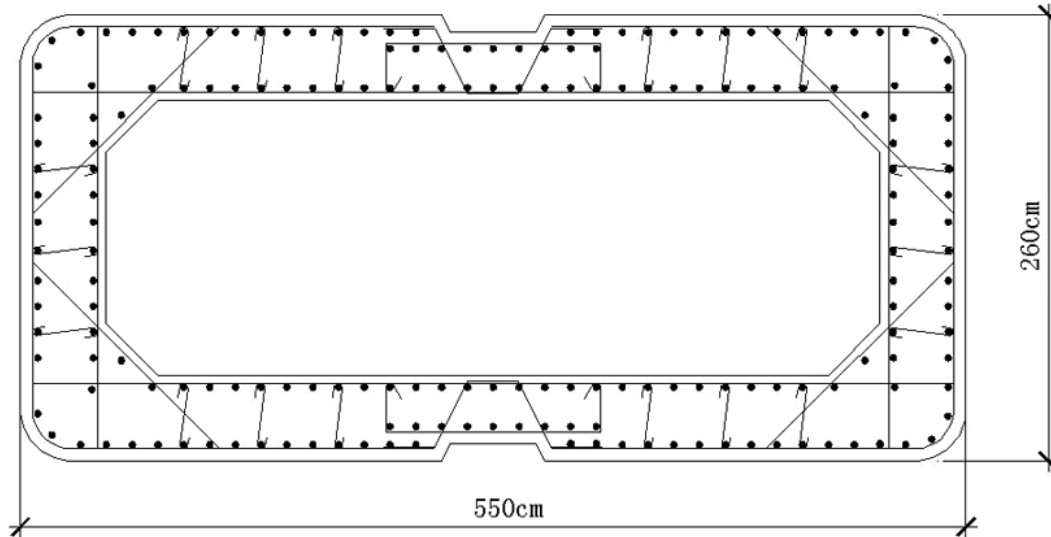


Figure 22. Section of single-column pier



$$\varepsilon_u = \varepsilon_c (1 + 5.2C_i) (0.9899 + 0.2204(RI)) \quad (3)$$

$$\varepsilon_{0.85u}/\varepsilon_u = 1.8847 + 0.121(RI) \quad (4)$$

Seismic Capacity of Section Reinforced with SFRC

To study the seismic capacity of a section reinforce with SFRC, a series of finite element models are established for some typical single-column piers reinforced with SFRC and for some alternative piers with plain confined concrete (CRC), whose section is shown in Figure 22 and design parameters are shown in Table 12 for the pier model M1, M2, M3 and M4. The longitudinal reinforcement ratio is 2.2% and the lateral reinforcement ratio is 0.8% for these piers. For the SFRC, the yielding stress and strain are 50 MPa and 6.188×10^{-3} and the ultimate stress and strain are 42.5 MPa and 13.88×10^{-3} . The yielding stress and strain are 38 MPa and 3.730×10^{-3} and the ultimate stress and strain are 32.3 MPa and 7.030×10^{-3} for the CRC.

Table 12. Typical single-column piers

Pier model	Concentrated load at the top of pier ($\times 10^3$ kN)	Height of pier (m)
M1	30	10
M2	30	15
M3	30	20
M4	30	25

For these typical single-column pier models, M1, M2, M3 and M4 reinforced with SFRC and CRC, pushover analyses are conducted for them respectively. Then the capacity curve comparisons are shown in Figure 23 and the curvature ductility comparisons are shown in Table 13. It can be seen that the bending strength is improved if the SFRC replaces the CRC for all the piers. It is also shown in Table 13 that the curvature ductility of sections adopting SFRC is better than those adopting CRC. The comparisons between the results in Table 13 and the ones in Figure 23 show that the improvement extent of the ductility is much higher than that of the bending strength after adopting the SFRC, which indicates that it's a

Figure 23. Capacity curve comparisons between piers reinforced with SFRC and CRC

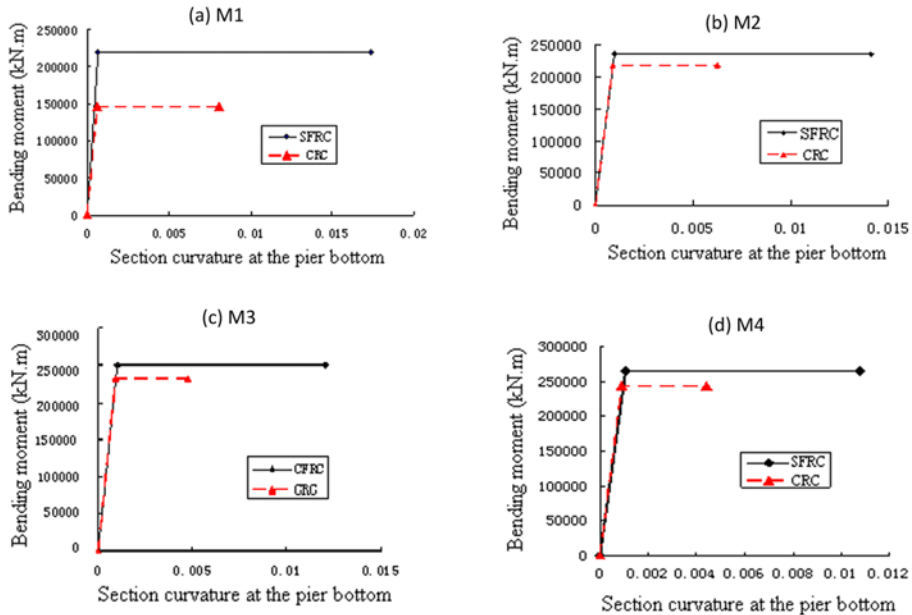


Table 13. Curvature ductility comparisons between piers reinforced with SFRC and CRC

Pier model	Yield curvature ($\times 10^{-3}$)	Ultimate curvature ($\times 10^{-3}$)	Curvature ductility factor	Ratio of curvature ductility factor (ii)/(i) (%)
(i) M1(CRC)	0.615	8.097	13.166	201.7
(ii) M1(SFRC)	0.654	17.381	26.576	
(i) M2(CRC)	0.915	6.277	6.860	206.4
(ii) M2(SFRC)	0.997	14.112	14.154	
(i) M3(CRC)	0.912	4.733	5.190	288.5
(ii) M3(SFRC)	0.999	12.085	12.097	
(i) M4(CRC)	0.899	4.401	4.895	263.8
(ii) M4(SFRC)	1.046	10.769	10.295	

more effective way to improve the ductility rather than to enhance the bending strength.

Bridge Piers Reinforced with SFRC

From the above analysis results, it is clear that the SFRC can efficiently improve the ductility capacity of bridge piers. However, only partial regions of a bridge pier may enter plasticity under

earthquakes from the capacity design principles (Priestley, Seible & Calvi, 1992). It means that the whole bridge pier reinforced with SFRC may be a tremendous waste. Therefore, it is necessary to study the seismic capacities of bridge piers wholly and locally reinforced with SFRC.

For a group of piers M3 and M4 (Table 12), the lengths of local region reinforced with SFRC (LR-SFRC) are assumed to be 4 m and 5 m respec-

Figure 24. Capacity curve comparisons between piers wholly and locally reinforced with SFRC

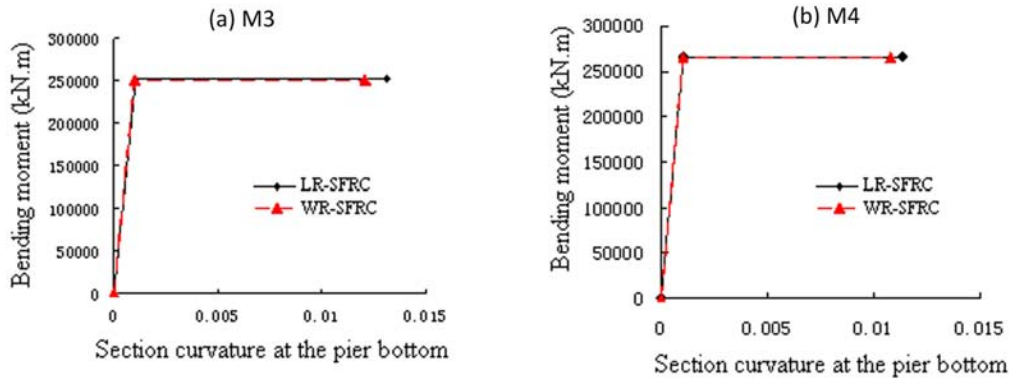


Table 14. Curvature ductility comparisons between piers wholly and locally reinforced with SFRC

Pier model	Yield curvature ($\times 10^{-3}$)	Ultimate curvature ($\times 10^{-3}$)	Curvature ductility factor	Ratio of curvature ductility factor (ii)/(i) (%)
(i) M3(WR-SFRC)	0.999	12.085	12.097	103.6
(ii) M3(LR-SFRC-4m)	1.047	13.111	12.522	
(i) M4(WR-SFRC)	1.046	10.769	10.295	106.2
(ii) M4(LR-SFRC-5m)	1.038	11.344	10.929	

tively at the pier bottoms. For another compared group of piers M3 and M4 (Table 12), it is assumed that the piers are wholly reinforced with SFRC (WR-SFRC). Based on pushover analyses, the capacity curve comparisons are shown in Figure 24 and the curvature ductility comparisons are shown in Table 14 between the piers wholly and locally reinforced with SFRC. It can be seen that applying the SFRC locally in a reasonable region at the bottom of the single-column pier almost has the same effect in improving the ductility and the bending strength as applying the SFRC in the whole pier. So considering the economy, it is more advantageous to applying SFRC in a local region of the bridge pier rather than applying SFRC in the whole pier.

Plastic Hinge Length and Reasonable Range Locally Reinforced with SFRC

For the third group of piers M3 and M4 (Table 12), the lengths of the local region reinforced with SFRC are assumed to be 2.0 m and 2.5 m respectively at the pier bottoms. Based on pushover analyses, the results show that a local CRC region above the CRC-SFRC interface has already yielded, while the pier bottom range reinforced with SFRC has not yet yielded. It is obvious that the local region reinforced with SFRC has not attained the predicted aim to increase the section capacities for the third group of pier models because of the unreasonable range reinforced with SFRC.

So, it is very important to determine the reasonable range of the local region reinforced with SFRC for bridge piers, namely the plastic hinge lengths. While referring to the present seismic guidelines

Table 15. Plastic hinge lengths according to different guidelines

Pier model	New Zealand	Euro Code 8	AASHTO
M3	3.750	1.840	1.890
M4	4.000	2.240	2.290

of several countries, it is shown in Table 15 that the plastic hinge lengths differ from each other greatly for the pier M3 and M4 reinforced with SFRC (Zhu, Fu, Wang & Yuan, 2010).

Then for a single-column bridge pier, the reasonable length l_c of local region reinforced with SFRC is given as Eq. (5), in which f_{cy} and f_{fy} are respectively the compressive yield stresses of the original reinforced concrete and the SFRC.

$$l_c = (1 - f_{cy} / f_{fy})l \quad (5)$$

Considering the extra-strength of the original reinforced concrete, the equation can be modified as the following Eq. (6), where ϕ is the extra-strength coefficient. And the coefficient ϕ is suggested to be 1.2 to 1.4.

$$l_c = (1 - f_{cy} / \phi f_{fy})l \quad (6)$$

Seismic Performance of Pile Group Foundations Strengthened with SPPs

The pile group foundations consisting of a group of piles and a cap supported by the pile group are widely used in large bridge projects. The pile group foundations are usually vulnerable components under earthquakes. Steel protective pipes (SPPs) are always used in construction as formworks for the underwater in situ concrete piles. After the bridge is completed, the SPPs can be of perma-

nently existence and be taken as a part of the piles and a strengthening measure for the pile. But the seismic performance is still not fully determined for the pile group foundations with SPPs.

Seismic Capacity

In order to investigate the effect of the SPPs on the seismic performance of the foundation, a real pile group foundation comprising of 9 reinforced concrete piles and a cap (Figure 25) is taken as an example. Four different scale-models are established to study the seismic capacity of the pile group foundation: (i) Model 1, all piles without SPPs, (ii) Model 2, only edge piles strengthened with SPPs in local regions from the pile top to the second plastic hinge under the ground surface, (iii) Model 3, only the edge piles strengthened with SPPs along the total pile height, and (iv) Model 4, all the piles strengthened with SPPs along the total pile height. For latter three models, the area of SPP accounts for 1.4% of the whole section area. Other parameters of the models are listed in Table 16.

Depending on the results of pushover analyses, the seismic capacity comparisons are shown in Figure 26 for Model 1 to 4. The seismic capacity variations for the edge pile in Model 3 are presented in Figure 27 along with the steel protective pipe ratio (SPPR) ranging from 0 to 2.5%. Moreover the section curvature variations in yielding state and in ultimate state are presented in Figure 28 for edge piles in Model 3. It can be seen that the seismic capacities, including the ductility and the lateral resistance of the pile group foundation strengthened with SPPs, is better than those of the foundation without SPP. The lateral resistance of the edge piles increases, while the maximum curvature decreases significantly along with the increasing of the SPPR. Therefore the potential is significant for the pile group foundation strengthened with SPPs.

Figure 25. Pile group foundation system

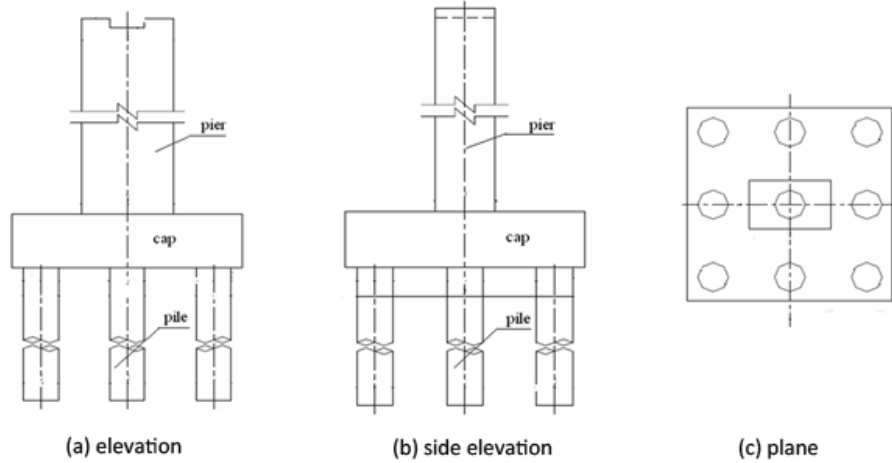


Table 16. Design parameters of the pile group foundation models

Model	Scale	Diameter (cm)	Height (cm)	Free Segment height(cm)	Pile space(cm)	Main reinforcement ratio	Hoop reinforcement ratio	Vertical Force at the pier top (kN)
1-8	1:20	9.0	72.0	49.0	44.5	0.871	0.379	75.0

Low Cycle Loading Experiments

From the above analyses results, it can be concluded that the pile group foundation strengthened with SPPs has better seismic capacities than the foundation without the SPP. So it is necessary to further study the energy dissipation and hysteretic performance under earthquakes in order to promote the application of the pile group foundation strengthened with SPPs. Then another four scale-models, Model 5 to 8, are established, whose design parameters are listed in Table 16 too. Model 5 and 6 are normal reinforced concrete (RC) pile group foundations and Model 7 and 8 are foundations strengthened with SPPs, whose pipe wall thickness is 0.1cm and length is 40cm beginning from the pile top. Moreover, the low cycle loading experiments (Figure 29) were conducted for these models in the electro-hydraulic servo loading system in Tongji University. The

amplitude of the cycles was variable from 2 mm to 80 mm and the frequency of the applied signal was equal to 0.02 Hz (Zhou, 2008).

Considering the modified Park-Ang damage index (Park & Ang, 1985; Park, Ang, & Wen, 1985), the fiber beam element finite element model (Figure 30) was established for these models and the low cycle loading experiments were simulated by the finite element method.

After the experiments and finite element analyses, the numerical and experimental hysteretic curves between the lateral force and the pier top displacement are shown in Figure 31. It can be shown that the strength of the models strengthened with SPPs is about 1.77 times and the ultimate displacement is about 1.66 times of the ones of the RC models. Additionally, the hysteretic energy dissipation capabilities of the models strengthened with SPPs are more than 2.15 times of the RC models, while the equivalent viscous

Figure 26. Seismic capacity comparisons

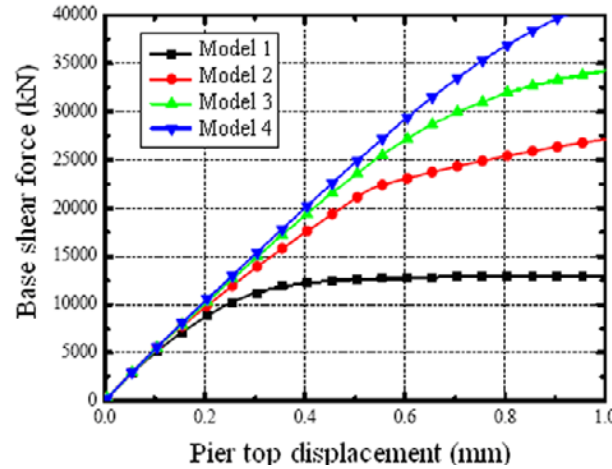


Figure 27. Seismic capacity variations of the edge pile in Model 3

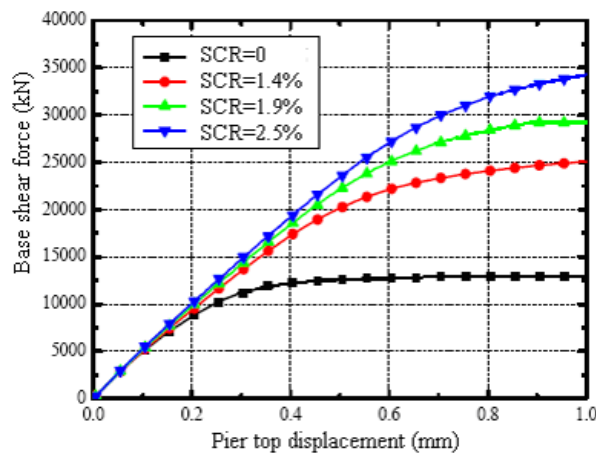


Figure 28. Section curvature variations of the edge pile in Model 3

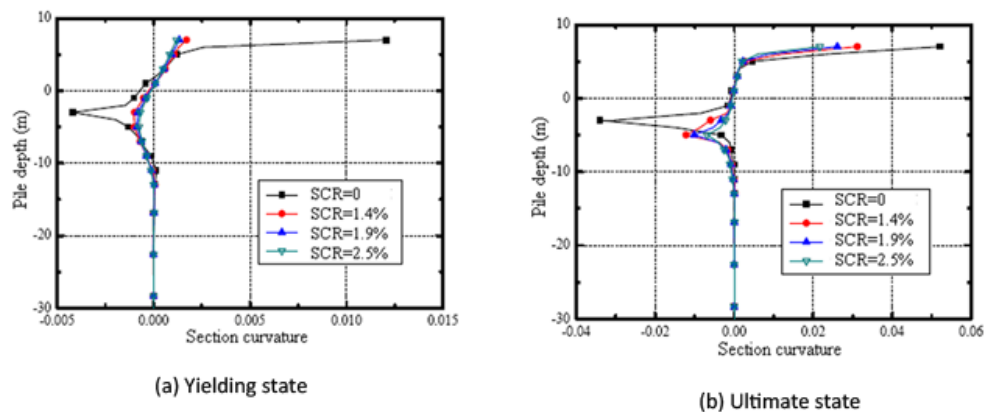


Figure 29. Low cycle loading experiments

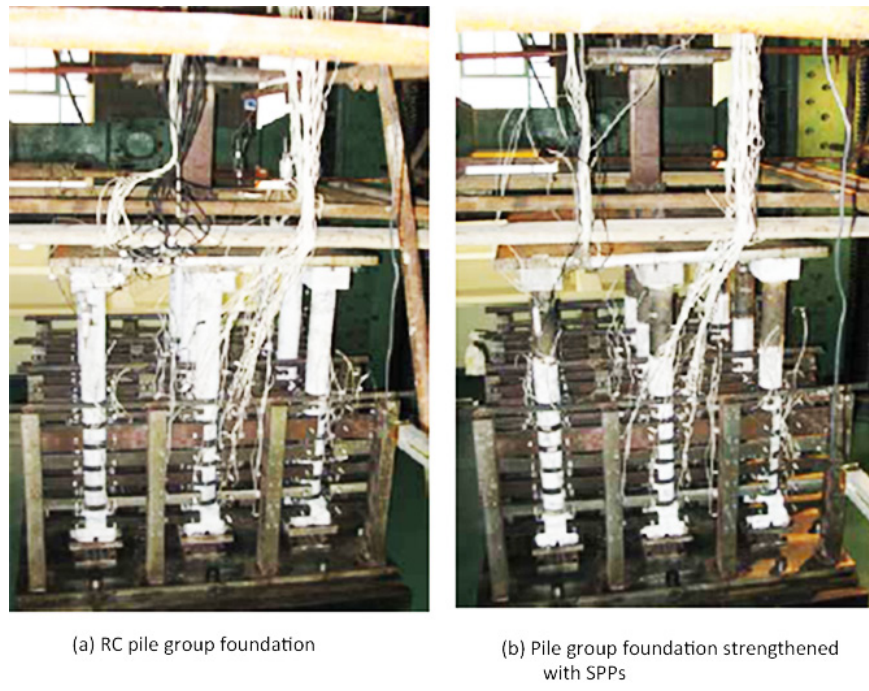


Figure 30. Finite element model and fiber element sections

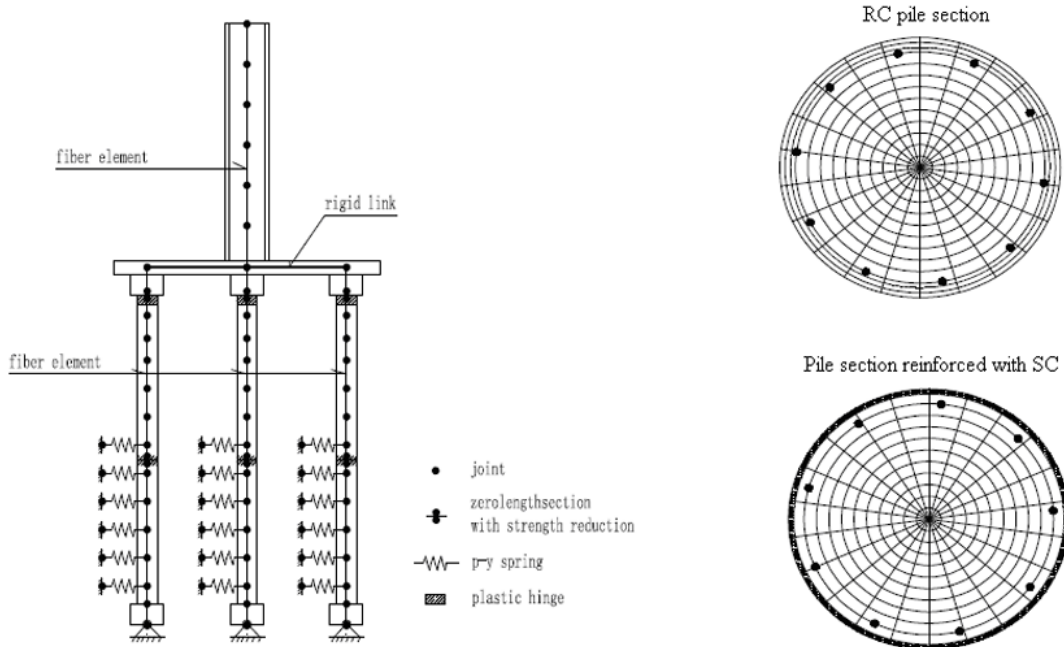
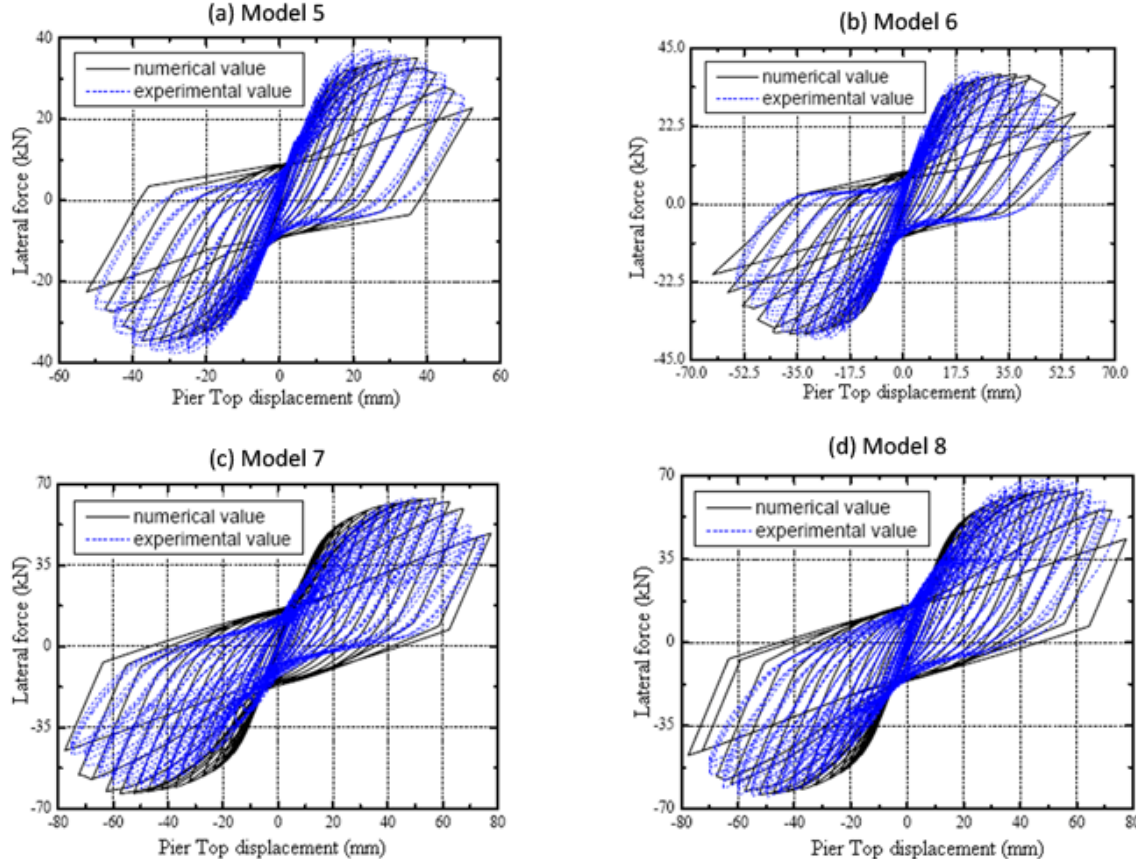


Figure 31. Hysteretic curves



damping ratio is reduced by 41.7%. The pinching effects of RC models are more obvious, while the hysteretic loops are plumper for models strengthened with SPPs. Comparisons between the experimental and numerical responses show that the numerical results agree with the experimental trends well.

Solutions and Recommendations

To realize more economical, applicable and valid seismic design of bridges, some local element seismic design strategies are presented to improve the seismic capacities for bridges. Considering the disadvantages of some typical isolation devices, a new cable sliding friction aseismic bearing is invented. Its performance criteria and some

important design parameters are determined by theoretical analyses and experiment testing. The application of the new bearing in a girder-arch composite bridge shows that the relative seismic displacements between the girder and piers are reduced significantly and the seismic forces at almost all the pier bottoms are also reduced when the new bearing replaces the original frictional one on the fixed pier.

Based on the proposed nonlinear material constitutive model of SFRC, the seismic capacities of single-column bridge piers wholly and locally reinforced with SFRC are studied by the pushover method. Analysis results show that the bending strength and the curvature ductility of the piers are improved if the SFRC replaces the CRC. The improvement extent of the ductility is

much higher than the bending strength. Seismic capacity comparisons between the piers wholly and locally strengthened with SFRC show that applying SFRC locally in a reasonable area of the single-column pier almost has the similar effect in improving the ductility and the bending strength as applying the SFRC in the whole pier. Then the plastic hinge length and the reasonable range locally strengthened with SFRC are clearly determined, considering that the present seismic guidelines of several countries have different definitions of the plastic hinge length for the single-column bridge pier reinforced with SFRC.

For pile group foundations reinforce with SPPs, the seismic capacities, the hysteretic performance and energy dissipation capabilities are studied by numerical simulations and low cycle loading experiments. The pushover analysis results show that the seismic capacity, including the ductility and the lateral resistance of the pile group foundation reinforced with SPPs, is better than the original one without SPPs. The lateral resistance of the edge piles increases, while the maximum curvature decreases significantly along with the increasing of the SPPR. The experiments and the finite element analysis comparisons show that the strength and the ultimate displacement of the foundation models strengthened with SPPs are better those of the RC ones. The hysteretic energy dissipation capabilities of the models strengthened with SPPs are much better than those of the RC models, while the equivalent viscous damping ratio is reduced by 41.7%. The pinching effects of RC models are more obvious, while the hysteretic loops are plumper for models strengthened with SPPs. Comparisons between the experimental and numerical responses show that the numerical results agree with the experimental trends well.

FUTURE RESEARCH DIRECTIONS

As an important lifeline project, seismic design of bridges should be paid more and more attention.

Undoubtedly, there are still many aspects need to be studied to obtain more optimal seismic performance for bridges, while this chapter mainly focuses on two methods: (i) the overall conceptual seismic design for whole bridges in a linear and elastic state; (ii) local seismic capacity design for components of bridges in a nonlinear and plastic state. The seismic design strategies proposed in the chapter consider the displacement requirements of bridges greatly, but they are still not enough to attain the complete displacement-based design. So the displacement-based design methods should be further promoted in the future, since the limitations of the force-based design methods are more and more obvious for bridges.

The overall conceptual seismic design mainly focuses on typical bridges in this chapter. With the increase of irregular bridges constructed in earthquake regions, more attention should be paid to their seismic performance, and how to conduct the overall conceptual seismic design and local seismic capacity design of them in the future. Moreover, the stochastic seismic performance of bridges with the cable sliding friction aseismic bearing should be emphasized in future research, since the determinate seismic performance has been carefully studied in the chapter. For the pile group foundation strengthened with SPPs, the erosion problem of steel pipes and its influences on the seismic design of foundations should be further promoted.

CONCLUSION

To give clear and correct directions for seismic design optimization of bridges, some new seismic design strategies are presented to obtain uniform and rational seismic demands and improved seismic capacities of structural components in seismic design of bridges, according to two design methods: the “overall conceptual seismic design” and the “local seismic capacity design”.

From the perspective of overall linear conceptual seismic design for several typical bridges, four design strategies are mainly introduced in the chapter to make the structure's dynamic characteristics adapt to the site conditions and let the seismic demands become more uniform and rational along structural components: optimal design for layout and detail of continuous girder bridge, design of towers for long span floating cable-stayed bridge, seismic isolation mechanism of elastic cables in cable-stayed bridge, and seismic potential and performance for long span SCC bridges. For a long span continuous girder bridge, the optimal adjustments of the piers form and locations of expansion joints are proposed to make the stiffness distribution better suit to the site conditions. For a long span cable-stayed bridge, a new-type spatial bridge tower is proposed to replace the original inverted Y shape tower based on elastic response spectrum analyses. The influences of the cable stiffness on the dynamic characteristics, seismic displacement and forces are investigated for another floating system cable-stayed bridge installed with the elastic cables seismic isolation device. For the new-type SCC bridge, the seismic potential is further confirmed based on response spectrum analyses of a four span continuous girder bridge and a long span SCC arch bridge. Amounts of numerical analyses and result comparisons show that the proposed overall conceptual seismic design strategies can decrease the seismic demands and achieve a balance between the seismic force and displacement, and thus improve the seismic performance for bridges.

From the perspective of local nonlinear seismic capacity design for components, three strategies, innovation of cable sliding friction aseismic bearing for bridges, bridge piers reinforced with SFRC and pile group foundations strengthened with SPPs are proposed to improve the seismic capacities for components of bridges. Based on the advantages of typical frictional isolation devices and displacement restraining capabilities of cables, a new cable sliding friction aseismic bearing is

invented and its seismic performance is studied by the theoretical analysis and experimental testing. The seismic capacities of bridge piers wholly and locally reinforced with SFRC are studied based on the presented nonlinear material constitutive model of SFRC and the plastic hinge length and the reasonable range locally reinforced with SFRC are determined for the single-column bridge pier. For pile group foundations reinforced with SPPs, its seismic capacities, hysteretic performance and energy dissipation capabilities are studied by numerical simulations and low cycle loading experiments. Theoretical analyses, experimental studies and some effective comparisons show that the presented local seismic design strategies of components of bridges are economical, applicable and valid.

ACKNOWLEDGMENT

This research is supported by the Ministry of Science and Technology of China (most recently under Grant No. SLDRC09-B-08), the National Natural Science Foundation of China (most recently under Grants No. 50978194 and No. 90915011), and Kwang-Hua Foundation for College of Civil Engineering at Tongji University. Such support is gratefully acknowledged by the authors.

REFERENCES

- Brozzetti, J. (2000). Design development of steel-concrete composite bridges in France. *Journal of Constructional Steel Research*, 55, 229–243. doi:10.1016/S0143-974X(99)00087-5
- Cao, X. (2009). *Design strategy on aseismic capacity of large bridge*. Doctoral dissertation, Tongji University, Shanghai, China.
- Fan, L. (Ed.). (1997). *Seismic resistance of bridge*. Shanghai, China: Tongji University Press.

Overall Conceptual Seismic Design and Local Seismic Capacity Design

- Fan, L., & Zhuo, W. (Eds.). (2001). *Seismic ductility design of bridge*. Beijing, China: People's Communication Press.
- Gao, Y. (2009). *Study on aseismic capacity of elevated pile cap foundations of large bridge*. Doctoral dissertation, Tongji University, Shanghai, China.
- Gong, Y. (2003). Performance-based design of steel building frameworks under seismic loading. Doctoral dissertation, University of Waterloo, Waterloo, Canada.
- Hayward, A. (1988). *Cheaper steel-concrete composite bridges*. In C. D. Buckner & I. Viest (Eds.), *Composite Construction in Steel and Concrete: Proceedings of an Engineering Foundation Conference*, New England College, Henniker, New Hampshire, June 7-12, 1987 (pp. 194-206). New York, NY: American Society of Civil Engineers.
- Kunde, M. C., & Jangid, R. S. (2003). Seismic behavior of isolated bridges: A-state-of-the-art review. *Electronic Journal of Structural Engineering*, 3, 140–170.
- Li, D. (1997). *Multi-objective optimum design of static and seismic-resistant structures with genetic algorithm, fuzzy logic and game theory*. Doctoral dissertation, University of Missouri-Rolla, Rolla, USA.
- Liu, M. (2003). *Development of multi-objective optimization procedures for seismic design of steel moment frame structures*. Doctoral dissertation, University of Illinois at Urbana Champaign, Urbana, USA.
- Ministry of Transport of the People's Republic of China. (1989). *Specifications for earthquake resistant design in highway Engineering (JTJ 004-89)*. Beijing, China: People's Communication Press.
- Ministry of Transport of the People's Republic of China. (2008). *Guidelines for seismic design of highway bridges (JTG/TB02-01-2008)*. Beijing, China: People's Communication Press.
- Park, Y. J., & Ang, A. H. S. (1985). Seismic damage model for reinforced concrete. *Journal of Structural Engineering*, 111(4), 722–739. doi:10.1061/(ASCE)0733-9445(1985)111:4(722)
- Park, Y. J., Ang, A. H. S., & Wen, Y. K. (1985). Seismic damage analysis of reinforced concrete buildings. *Journal of Structural Engineering*, 111(4), 740–757. doi:10.1061/(ASCE)0733-9445(1985)111:4(740)
- Plevris, Y. (2009). *Innovative computational techniques for the optimum structural design considering uncertainties*. Doctoral dissertation, National Technical University of Athens, Athens, Greece.
- Priestley, M. J. N., Seible, F., & Calvi, G. M. (1996). *Seismic design and retrofit of bridges*. New York, NY: John Wiley & Sons, Inc. doi:10.1002/9780470172858
- Ramesh, K., Seshu, D. R., & Prabhakar, M. (2003). Constitutive behaviour of confined fibre reinforced concrete under axial compression. *Cement and Concrete Composites*, 25, 343–350. doi:10.1016/S0958-9465(02)00051-3
- Turkington, D. H., Carr, A. J., Cooke, N., & Moss, P. J. (1989). Seismic design of bridges on lead-rubber bearings. *Journal of Structural Engineering*, 115(12), 3000–3016. doi:10.1061/(ASCE)0733-9445(1989)115:12(3000)
- Walther, R., Houriet, B., Isler, W., Moia, P., & Klein, J. (1988). *Cable stayed bridges*. London, UK: Thomas Telford, Ltd.
- Yan, D., & Yuan, W. (2004). Conceptual seismic design for long span cable-stayed bridges. *Journal of Tongji University*, 32(10), 1344–1348.

Yang, Y. (1999). *Seismic resistance of bridge and fractal characteristics*. Master's thesis, Tongji University, Shanghai, China.

Ye, A., Hu, S., & Fan, L. (2004). Seismic displacement control for super-long-span cable-stayed bridges. *China Civil Engineering Journal*, 37(12), 38–43.

Yuan, W., Cao, X., Cheung, P., Wang, B., & Rong, Z. (2010, August). *Development of cable-sliding friction aseismic bearing for bridges*. Paper presented at the 5th Civil Engineering Conference in the Asian Region and Australasian Structural Engineering Conference 2010, Sydney, Australia.

Yuan, Y., & Sun, B. (2008, October). General introduction of engineering damage of Wenchuan Ms 8.0 Earthquake. *Journal of Earthquake Engineering and Engineering Vibration*, 28, 59–73.

Zhou, M. (2008). *Experimental and theoretical studies on seismic performance of elevated pile caps*. Doctoral dissertation, Tongji University, Shanghai, China.

Zhu, Z., Fu, Y., Wang, B., & Yuan, W. (2010, August). *Seismic study on bridge piers reinforced with SFRC in local region*. Paper presented at the 5th Civil Engineering Conference in the Asian Region and Australasian Structural Engineering Conference 2010, Sydney, Australia.

Zollo, R. F. (1997). Fiber-reinforced concrete: An overview after 30 years of development. *Cement and Concrete Composites*, 19, 107–122. doi:10.1016/S0958-9465(96)00046-7

Zou, X. (2002). *Optimal seismic performance-based design of reinforced concrete buildings*. Doctoral dissertation, Hong Kong University of Science and Technology, Hong Kong, China.

ADDITIONAL READING

Cao, X., Xiong, Y., Fu, Y., Guo, P., Han, P., & Yuan, W. (2010, August). *Seismic design of Hangzhou Jiu-bao bridge*. Paper presented at the 5th Civil Engineering Conference in the Asian Region and Australasian Structural Engineering Conference 2010, Sydney, Australia.

Cao, X., Xiong, Y., Fu, Y., & Yuan, W. (2010). Analysis of structure-water interaction of bridge under earthquake excitation. *Structural Engineers*, 26(4), 69–73.

Cao, X., Yuan, W., Gao, Y., & Wei, K. (2010). Aseismic design of long-span continuous beam-arch combination bridges. *Earthquake Resistant Engineering and Retrofitting*, 32(3), 30–35.

Gao, Y., Yuan, W., & Jin, X. (in press). Soil-structure-water interaction of a cable-stayed bridge under seismic excitation. *Journal of Central South University of Technology*.

Wei, K., Guo, P., Han, P., Yuan, W., & Cao, X. (2010). Seismic responses of a long multi-span composite bridge under traveling wave excitation. *Structural Engineers*, 26(2), 119–125.

Wei, K., Yuan, W., & Cao, X. (2010). Study on aseismic potential and performance for composite bridge. *Engineering Mechanics*, 27(Sup. I), 275–279.

Wei, K., Yuan, W., & Cao, X. (2010, August). *Seismic analyses of long span steel-concrete composite bridge*. Paper presented at the 5th Civil Engineering Conference in the Asian Region and Australasian Structural Engineering Conference 2010, Sydney, Australia.

Yan, D., & Yuan, W. (2003). Conceptual design of earthquake resistance for multi-span continuous bridges in transverse direction. *Journal of Tongji University*, 31(11), 1275–1279.

Yang, Y., Yuan, W., & Fan, L. (2000). Earthquake ground motions and site effects on seismic performance of bridges in shanghai zone. *Journal of Tongji University*, 28(3), 348–352.

Yuan, W., Zhou, M., & Yan, D. (2008, October). *Study and trend on conceptual seismic design for bridges in China*. Paper presented at the 14th Conference on Earthquake Engineering, Beijing, China.

Zhou, M., Yuan, W., & Zhang, Y. (2008, October). *Analysis of pile equivalent anchorage length for elevated pile caps under lateral load*. Paper presented at the 14th Conference on Earthquake Engineering, Beijing, China.

Zhou, M., Zhang, Y., & Yuan, W. (2011). Fracture and damage mechanism of RC pile group foundation under low cycle loading. *Key Engineering Materials*, 452-453, 665–668. doi:10.4028/www.scientific.net/KEM.452-453.665

Zhu, Z., Fu, Y., Guo, P., & Yuan, W. (2010). Seismic study on bridge columns reinforced with SFRC in plastic-hinged range. *Structural Engineers*, 26(5), 73–78.

KEY TERMS AND DEFINITIONS

Bridge Pier Reinforced with SFRC: The pier whose material is steel fiber reinforced concrete in the whole pier or in local regions.

Cable-Sliding Friction Aseismic Bearing:

The new-type bearing which is composed of the pot bearing, some cables and a shear bolt.

Close Twin-Column Pier System: a pier system made up of two symmetrical adjoining parts (right and left part) which are half of the solid single-column pier divided along the vertical mid-plane.

Elastic Cable Seismic Mitigation and Isolation Device: The elastic cables equipped between the tower and the girder which can adjust the stiffness distribution of the cable-stayed bridges.

Local Seismic Capacity Design: A seismic design method which focuses on increasing the seismic capacities of components or local elements of a whole bridge in a nonlinear state.

Overall Conceptual Seismic Design: A conceptual seismic design method which focuses on the optimal design of whole structural system in a linear and elastic state to make the structure's dynamic characteristics adapt to the site conditions and achieve more uniform and rational seismic demands of structural components.

Pile Group Foundation Strengthened with SPPs: The pile group foundation whose piles are strengthened with the outer steel protective pipes in the whole pile or in local regions.

Spatial Tower: The tower model which is composed of four single columns in space to replace the inverted Y shape tower in plane.

Steel-Concrete Composite Bridge: The bridge whose girder is composed of structural steel and reinforced concrete.

Chapter 12

Optimum Design of Structures for Earthquake Loading by a Cellular Evolutionary Algorithm and Neural Networks

Saeed Gholizadeh
Urmia University, Iran

ABSTRACT

The present chapter deals with optimum design of structures for earthquake induced loads by taking into account nonlinear time history structural response. As the structural seismic optimization is a time consuming and computationally intensive task, in this chapter, a methodology is proposed to reduce the computational burden. The proposed methodology consists of an efficient optimization algorithm and a hybrid neural network system to effectively predict the nonlinear time history responses of structures. The employed optimization algorithm is a modified cellular genetic algorithm which reduces the required generation numbers compared with the standard genetic algorithm. Also, the hybrid neural network system is a combination of probabilistic and generalized regression neural networks. Numerical results demonstrate the computational merits of the proposed methodology for seismic design optimization of structures.

INTRODUCTION

Optimum design of structures is a process of selecting the design variables such that an objective function is minimized while all of the design constraints are satisfied. During the last decades, structural optimization problems have

been solved using gradient-based algorithms. As the mathematical programming based methods need gradient calculations, the considerable part of the optimization process is devoted to the sensitivity analysis and the computational work of these methods is usually high. Optimal design of real-world structures subject to seismic loading is

DOI: 10.4018/978-1-4666-1640-0.ch012

one of the major concerns in the field structural engineering. When structures are subjected to severe earthquakes a huge amount of inertia loads is imposed to the structures. In this case, considering linear elastic behavior and ignoring the nonlinear structural responses during the optimization process may lead to vulnerable structural systems. Therefore, seismic design codes suggest that, under severe earthquake events, the structures should be designed to deform inelastically. To achieve structural seismic design optimization it is necessary that the nonlinear structural time history analysis to be performed many times. In this case, the computational burden of the optimal seismic design process is so large that could prevent designer from comprehensively exploring the design space, and could ultimately result in unsuitable structures. Consequently, it is necessary to employ efficient computational strategies to achieve optimal seismic design of structures spending low computational costs.

In the last decades, soft computing procedures have been widely used to solve massive and complex engineering problems. Soft computing includes many components and the most attractive ones are meta-heuristic optimization algorithms and neural networks. As meta-heuristic or evolutionary optimization algorithms need not gradient calculations they are more robust than the mathematical programming based techniques and usually present better global behavior. Beside the mentioned computational advantages, the disadvantage of these methods is a slow rate of convergence towards the global optimum. A neural network is an interconnected network of simple processing elements. The processing elements interact along paths of variable connection strengths which when suitably adapted can collectively produce complex overall desired behavior. Neural networks operate as black box, model-free, and adaptive tools to capture and learn significant structures in data. Their computing abilities have been proven in the fields of prediction, pattern recognition, and optimization.

They are suitable particularly for problems too complex to be modelled and solved by classical mathematics and traditional procedures.

The main objective of this chapter is to propose a computationally efficient methodology to optimum design of structures subject to earthquake loading considering inelastic structural behaviour. To achieve this task, an efficient genetic algorithm (GA) based evolutionary optimization algorithm is employed to reduce the required analyses. Also, a hybrid neural network system is employed to effectively predict the nonlinear time history responses of structures during the optimization process.

BACKGROUND

During the last years, a number of researchers have employed evolutionary algorithms to optimal design of structures subject to dynamic loadings. Kocer and Arora (1999, 2002) employed GA for the optimal design of H-frame transition poles and latticed towers conducting nonlinear time-history analysis. They proposed the use of GA and Simulated Annealing (SA) for the solution of discrete variable problems, although the computational time required was excessive. Salajeghehand Heidari (2005) incorporated wavelet transforms and neural networks into the GA-based optimization processes to predict linear structural responses for a specific earthquake time history loading. Lagaros *et al.* (2006) examined the influence of various design procedures on the dynamic performance of real-scale steel buildings. Gholizadeh and Salajegheh (2009) employed meta-heuristic particle swarm optimization (PSO) algorithm, fuzzy inference systems (FIS) and radial basis function (RBF) neural network for optimizing linear structures subject to earthquake loading. Gholizadeh and Salajegheh (2010a) incorporated wavelet RBF neural network into a hybrid PSO-GA optimization algorithm for seismic optimization of a real-scale steel building considering

linear behavior. Computational performance of GA and PSO examined by Gholizadeh (2010) for dynamic design optimization of structures considering nonlinear responses while a surrogate model employed to predict the structural responses during the optimization process. Also, Gholizadeh and Samavati (2011) designed structures subject to earthquake for optimum weight considering linear responses by a combination of wavelet transforms, RBF neural networks and an improved GA. Lagaros and Papadrakakis (2011) employed back-propagation (BP) neural network to predict nonlinear seismic responses of 3D frame structures. They specified that the predicted responses may be used in the framework of performance based design of structures to reduce the computational effort. The proposed methodology in this chapter consists of two main computational strategies outlined as follows:

In the first strategy, an efficient evolutionary optimization algorithm is employed. The main drawback of the evolutionary algorithms, especially GA, is a slow rate of convergence. In the present chapter, a GA based structural optimization algorithm that can increase the probability of achieving the global optimum with accelerated convergence emphasizing on structural nonlinear time history analysis reduction is employed. For this purpose, the concepts of cellular automata (CA) (Von Neumann, 1966) and GA are hybridized and the resulted hybrid algorithm is called cellular genetic algorithm (CGA). In the CGA, a small dimensioned grid is selected and the artificial evolution is evolved by a novel crossover and traditional mutation operations. In each iteration, cellular crossover operation produces a new design at each site according to the fitness index of neighboring cells of each site. As the size of the population is small, the optimization process converges to a pre-mature solution. In each process, the best solution is saved. For creating a new population the saved best solution is transformed to the new population and the remaining ones are randomly selected. Thereafter, the optimization

process is repeated to achieve a new solution. The process of creating the new population with elite sites is continued until the method converges. However, employing the CGA the number of the required generations is considerably reduced during the optimization process, but due to this fact that the seismic optimization process requires a great number of nonlinear time history analyses the overall time of the optimization process is still very long.

In the second strategy, in order to reduce the computational burden of the nonlinear time history analysis, a hybrid neural network system (HNNS) based on generalized regression neural network (GRNN) (Wasserman, 1993) is employed. In this case, instead of performing nonlinear dynamic analysis by finite element method (FEM) a neural network model is used to predict the necessary nonlinear time history responses during the optimization process. By employing the natural frequencies as the inputs of neural networks, better performance generality can be obtained. As the natural frequencies are required during the optimization process, evaluating of these by analytic methods can impose additional computational burden to the process. In order to prevent from this difficulty, another GRNN is employed to effectively predict the frequencies. During the optimization process many designs are examined and due to considering nonlinear response analysis it is probable that some of them lose their stability during the ground motion and the nonlinear dynamic analysis fails to converge. It is evident that such designs should be rejected. As during the optimization process, GRNN is employed to evaluate the responses instead of the exact nonlinear time history analysis, it is necessary to detect such instable structures. For this purpose, a probabilistic neural network (PNN) (Wasserman, 1993) is used. Using the PNN, evaluating the time history responses of the instable structures is ignored during the optimization process and this makes the optimization process more efficient.

As a test example, a 72-bar space steel tower subjected to the El Centro earthquake is optimized considering nonlinear time history responses. The numerical results indicate that the hybrid methodology is a powerful and efficient tool for optimal design of structures subjected to earthquake loadings.

MAIN FOCUS OF THE CHAPTER

Main focus of the present chapter is to provide an efficient soft computing based methodology to achieve optimum design of structures subject to earthquake. The methodology is a serial integration of evolutionary algorithms for performing optimization and neural network for predicting nonlinear time history responses of structures. The various issues of the proposed methodology are described in the following subsections.

Optimal Design Problem Formulation

The dynamic equilibrium for a finite element system subjected to earthquake loading can be written in the following usual form:

$$\mathbf{M}\ddot{\mathbf{Z}}(t) + \mathbf{C}\dot{\mathbf{Z}}(t) + \mathbf{K}\mathbf{Z}(t) = \mathbf{MI}\ddot{\mathbf{u}}_g(t) \quad (1)$$

where \mathbf{M} , \mathbf{C} , \mathbf{K} , \mathbf{I} , $\ddot{\mathbf{Z}}(t)$, $\dot{\mathbf{Z}}(t)$, $\mathbf{Z}(t)$, $\ddot{\mathbf{u}}_g(t)$ and t are mass matrix, damping matrix, stiffness matrix, unit matrix, acceleration vector, velocity vector, displacement vector, ground acceleration and the time, respectively.

The problem of structural optimization for earthquake induced loads can be formulated as follows:

$$\text{Minimize } f(\mathbf{X}), \mathbf{X}; \mathbf{X}_i \in \mathbb{R}^d; i = 1, \dots, n \quad (2)$$

Subject to

$$g_j(X, Z(t), \dot{Z}(t), \ddot{Z}(t), t) \leq 0; j = 1, \dots, m \quad (3)$$

$$X_i^L \leq X_i \leq X_i^U; i = 1, \dots, n$$

where f , X , g , m and n are objective function, design variables vector, behavioral constraint, the number of constraints and the number of design variables, respectively. Also X_i^L and X_i^U are lower and upper bounds on the i th design variable. A given set of discrete values is presented by R^d .

In this chapter, for the time-dependent nonlinear optimization problems, only the displacement constraints are considered in Box 1. where d_j and $d_{j,all}$ are the displacement of the j th node, and its allowable value, respectively.

To perform dynamic time history analysis considering geometrical and material nonlinearities, ANSYS software (ANSYS, 2006) are employed. It uses a step-by-step implicit numerical integration procedure based on Newmark's method to solve the dynamic equilibrium. In order to consider the transient nature of earthquake loading a simple bilinear stress-strain relationship with kinematic hardening is adopted. As confirmed in (Lagaros *et al.*, 2006) this law provides accurate results for many practical applications.

Box 1.

$$g_j(X, Z(t), \dot{Z}(t), \ddot{Z}(t), t) = \frac{d_j(X, Z(t), \dot{Z}(t), \ddot{Z}(t), t)}{d_{j,all}} - 1 \leq 0; j = 1, \dots, m \quad (4)$$

As all the constraints are time-dependent the consideration of all the constraints requires an enormous amount of computational effort. Here, the conventional method (Arora, 1999) is employed to deal with time-dependent constraints. In this method the time interval is divided into n_{gp} subintervals and the time-dependent constraints are imposed at each time grid point. Let the j th time-dependent constraint be written as:

$$g_j(X, Z(t), \dot{Z}(t), \ddot{Z}(t), t) \leq 0, 0 \leq t \leq t_i \quad (5)$$

where t_i is time interval over which the constraints need to be imposed.

Because the total time interval is divided into n_{gp} subintervals, the constraint (5) is replaced by the constraints at the $n_{gp}+1$ time grid points as:

$$g_j(X, Z(t_\alpha), \dot{Z}(t_\alpha), \ddot{Z}(t_\alpha), t_\alpha) \leq 0; \alpha = 0, \dots, n_{gp} \quad (6)$$

The above constraint function can be evaluated at each time grid point after the structure has been analyzed. The objective function of constrained structural optimization problems is defined in Box 2 where $\tilde{\Delta}$ and r_p are the feasible search space, and an adjusting penalty factor respectively.

Cellular Genetic Algorithm

Cellular automata (CA) represents simple mathematical idealizations of physical systems in which

Box 2.

$$f(X) = \begin{cases} f(X) & \text{if } X \in \tilde{\Delta} \\ f(X) + \sum_{\alpha=0}^{n_{gp}} r_p \left[\sum_{j=1}^m \left(\max(g_j(X, Z(t_\alpha), \dot{Z}(t_\alpha), \ddot{Z}(t_\alpha), t_\alpha), 0) \right)^2 \right] & \text{otherwise} \end{cases} \quad (7)$$

space and time are discrete, and physical quantities are taken from a finite set of discrete values. In its basic form, a cellular automaton consists of a regular uniform grid of sites or cells with a discrete variable in each cell which can take on a finite number of states. The state of the cellular automaton is then completely specified by the values $s_i = s_i(t)$ of the variables at each cell i . During time, cellular automata evolve in discrete time steps according to a parallel state transition determined by a set of local rules: the variables $s_i^{k+1} = s_i(t_{k+1})$ at each site i at time t_{k+1} are updated synchronously based on the values of the variables $s_{n_c}^k$ in their n_c neighborhood at the preceding time instant t_k . The neighborhood n_c of a cell i is typically taken to be the cell itself and a set of adjacent cells within a given radius r . Thus, the dynamics of a cellular automaton can be formally represented as follows (Biondini *et. al.*, 2004):

$$s_i^{k+1} = \theta(s_i^k, s_{n_c}^k), i - r \leq n_c \leq i + r \quad (8)$$

where the function θ is the evolutionary rule of the automaton.

A proper choice of the neighborhood plays a crucial role in determining the effectiveness of such a rule. In this chapter, the widely used Moore neighborhood (Von Neumann, 1966) of interaction, by $r=1$, is adopted.

The CA technique can be combined with the evolutionary algorithms to solve optimization problems. One of the most popular evolutionary algorithms is GA. In the field of structural

optimization some of researchers (Canvurt & Hajela, 2005; Rajasekaran, 2001; Gholizadeh & Salajegheh, 2010b) have combined the concepts of CA and GA to create cellular genetic algorithms (CGA). The CGA presented in this chapter is a modified version of the CGA proposed by Gholizadeh and Salajegheh (2010b) and is denoted as modified cellular genetic algorithm (MCGA). In the MCGA, as well as the CGA, individuals of a selected population are set on discrete locations of a 2D grid. The state variables of each site are the design variables. In the MCGA, the evolution process is accomplished locally, with probabilistic interaction rules applied synchronously to each central site, and using information only from members of its Moore neighborhood. When the population has been updated, the evolutionary rules of the automaton are repeated until one of the stopping criteria is met. In both the CGA and MCGA, the objective function of the optimization problem is employed to define the fitness of each design vector. In the MCGA the evolutionary rule of the automaton includes the cellular crossover operation (CCO) and the mutation operation (MO) applied to the sites.

In the GA type evolutionary algorithms crossover operation creates one or more offspring from the selected parents. Many different methods have been proposed for crossing over in the GA such as point crossover method. In this simple method one or more points in the chromosome are randomly selected as the crossover points. Then the variables between these points are merely swapped between two parents. The problem with these point crossover methods is that no new information is introduced. But the blending methods mitigate this difficulty by finding ways to combine variables values from the two parents into new variable values in the offspring. For instance in (Haupt & Haupt, 2004) such method has been proposed so that a single offspring variable value X^o is produced from combination of the two corresponding parents' variable values as follows:

$$X^o = (1 - \beta)X^d + \beta X^m \quad (9)$$

where β is a random number on interval $[0, 1]$, X^d and X^m are variables in the father and mother chromosomes, respectively.

These types of crossovers can not provide sufficient information for a comprehensive search of the design space in the complex and large-scaled problems. Therefore the found solutions are usually local optima. In the MCGA a powerful crossover operation is employed that provides sufficient information for comprehensive and fast exploration of the design space.

In the MCGA model, a population of potential designs is structured in a 2D grid. In this case, each site contains a real-valued string describing of a design and therefore the state of the cellular automaton in each site is a vector of design variables.

$$s_i \rightarrow X_i = \{x_1, x_2, \dots, x_n\}^T, i = 1, 2, \dots, n_c \quad (10)$$

The CCO acts on the design variables and combines the information available at the central sites and their immediate neighbors. In this case, a virtual individual is produced by using the fitness indices of the individual in the immediate neighbors of each central site as follows (Gholizadeh & Salajegheh, 2010b):

$$\bar{X}_i = X^{best} + \left(\sum_{j=1}^{n_c} (X_i^{best} - X_{i,j}) f_j \right) / \sum_{j=1}^{n_c} f_j \quad (11)$$

where X^{best} is the best solution found up to current iteration. X_i^{best} is the best individual in immediate neighbors of i th central cell. $X_{i,j}$ is the j th individual in immediate neighbors of i th central cell and f_j is its fitness value.

In creation of \bar{X}_i the effect of individuals having better fitness values is higher and vice versa. In each discrete time step, the CCO combines the central cell with the virtual individual and pro-

duces a new design at each site according to the following equation:

$$s_i^{k+1} = \theta(s_i^k, s_{n_e}^k) \rightarrow X_i^{k+1} = (1 - \beta)X_i^k + \beta\bar{X}_i^k \quad (12)$$

The MO in the framework of the MCGA is similar to that used in the standard GA. In the real-valued model of mutation, the value of the mutated design variable is replaced by a randomly selected value from the R^d . It has been already demonstrated that the low values of mutation probability (0.001 to 0.004) is more effective, therefore, in this chapter also the value of 0.004 is considered.

The MCGA is elitism based multi-stage evolutionary algorithm. In the optimization process by MCGA, n individuals of a randomly selected small initial population are set on locations of a 2D grid and the search in the first process is commenced. As the size of the population is small, the optimization process rapidly converges and the best solution found in this stage, say ${}^1X^{best}$, is saved. In the next stage, a new elite population is created based on the philosophy of giving more chance to survive the elite individuals. In this case, ${}^1X^{best}$ is copied to the \sqrt{n} randomly selected cells and the remaining cells are selected as follows:

$${}^2X_j = N({}^1X^{best}, \sigma {}^1X^{best}), j = 1, 2, \dots, (n - \sqrt{n}) \quad (13)$$

where $N({}^1X^{best}, \sigma {}^1X^{best})$ represents a random number normally distributed with the mean of ${}^1X^{best}$ and the variance of $\sigma {}^1X^{best}$. Various values for σ are examined and the best results are obtained by $\sigma = 0.15$.

In this case a new optimization process is achieved. The process of selecting elite populations and achieving optimization processes are continued until the method converges. In fact in the CGA proposed by Gholizadeh and Salajegheh

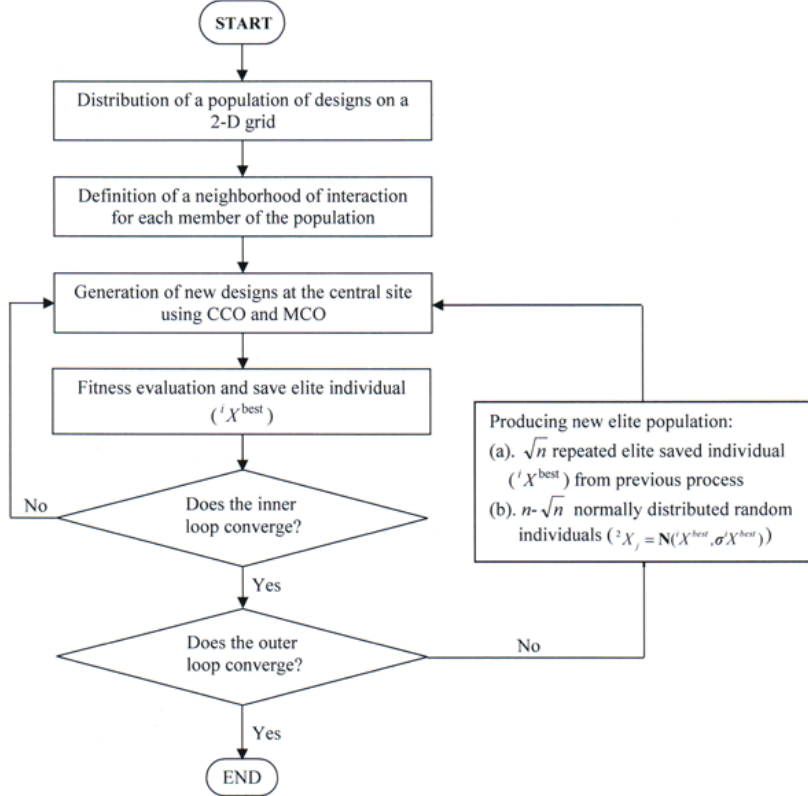
(2010b) the remaining cells are selected based on a pure random selection but in the MCGA these cells are selected by normal distribution about the elite individual of the previous stage. In this case, the MCGA compared with CGA can provide better performance for controlling the balance between exploration (global investigation of the search place) and exploitation (the fine search around a local optimum). Therefore, the MCGA increases the probability of finding better solutions spending lower computational cost. The flowchart of the proposed MCGA algorithm is shown in Figure 1.

Hybrid Neural Network System

A hybrid neural network system (HNNS) is employed to efficiently and accurately predict the nonlinear time history responses of the structures. In this neural system, GRNN and PNN, both from the radial basis function neural networks family, are serially integrated.

GRNN is a memory-based network that provides estimates of continuous and discrete variables and converges to the underlying regression surface. GRNN has a one pass learning algorithm with highly parallel structure. It does not require an iterative training procedure. The principal advantages of GRNN are fast learning and convergence to the optimal regression surface as the number of samples becomes large. GRNN approximates any arbitrary function between input and output vectors, drawing the function estimate directly from the training data (Specht, 1990). GRNN is often used for function approximation. It is a two layer feed forward network. The first layer of GR consists of RBF neurons with Gaussian activation functions while the output layer consists of linear neurons. In the first layer it has as many neurons as there are input-output vectors in training set. Specifically, the first layer weight matrix is set to the transpose of the matrix containing the input vectors. The second layer also has as many neurons as input-output vectors, but here the weight matrix is set to the matrix containing the output vectors.

Figure 1. Flowchart of MCGA



$$\mathbf{W}_1 = \mathbf{P}^T \quad (14)$$

$$\mathbf{W}_2 = \mathbf{T} \quad (15)$$

where \mathbf{W}_1 , \mathbf{W}_2 , \mathbf{P} and \mathbf{T} are the first layer weight, the second layer weight, input and desired outputs matrices, respectively.

The PNN is mainly used for classification problems. To train the PNN a supervised training is accomplished. Typically, a PNN consists of an input layer, a RBF layer, and a competitive (C) layer.

During the training stage, a training set of N_s data samples is used. The number of the neurons in the first layer is identical to N_s . Also, the weight matrix of this layer is set to the transpose of the input matrix (Wasserman, 1993). The number of the neurons in the competitive layer, which is

identical to the count of the classes, is denoted by N_c . Based on these assignments, the PNN is created with zero error on training samples (Wasserman, 1993). After training, a testing set of N_T new data samples are used to test the generalization of the PNN. When a new input vector is presented, the RBF layer computes the distances between it and the training samples. Then RBF activation function is used to produce a vector whose elements indicate how close the input vector is to the training sample. Thus, the RBF layer neurons with weight vectors quite far from the input vector produce output values near zero, while neurons with weight vectors quite close to it provide output values near one. Typically, several neurons may be active to varying degrees. The competitive layer sums these contributions for each class of inputs to produce a vector of probabilities. Finally, the second layer produces

a 1 corresponding to the largest element of the RBF layer neurons and 0's elsewhere. Thus, the network classifies the input vector into a specific k ($k = 1, 2, \dots, N_C$) class because that class has the maximum probability of being correct. The key advantage of PNN over the other networks is its rapid training. Since the number of layers in the PNN architecture is fixed and all the synaptic weights are directly assigned using training samples, this procedure can be finished in only one epoch and no error correction procedure is necessary. It has been proved that with enough training data a PNN is guaranteed to converge to a Bayesian classifier, which usually owns the optimal classification capability (Wasserman, 1993).

The first step in training of HNNS is to select a data set. In the sampling process, N_s structures based on their design variable vectors are selected. The natural frequencies (F_i) and nonlinear time history responses (R_i) of all the selected structures are computed by the conventional FEM. In (Gholizadeh *et. al.*, 2009) it has been demonstrated that the best candidates as the inputs of the neural networks for predicting the time history responses of structures are natural frequencies. In this chapter also the natural frequencies are employed as the inputs. During the optimization process evaluating of the frequencies by analytic methods increases the computational effort of the process. In order to prevent from this, a GRNN is trained to predict the natural frequencies. The inputs and outputs of this GRNN, denoted as frequency predictor, are design variables (X_i) and natural frequencies (F_i) of the selected structures, respectively. During the nonlinear time history analysis of a structure, it is probable that the structure loses its overall stability and the analysis procedure can not converge. Thus, before training a neural network to predict the nonlinear responses, it is important to detect stable and unstable structures. In this case, classifier neural networks can be employed. In the present chapter, a PNN is trained to achieve this

important task. All of the N_s selected structures are considered in the classification phase. Naturally, considering stable and unstable structures the number of classes, N_C , is equal to 2. In the training phase of the PNN, the inputs are F_i and the output is 1 for stability and 2 for instability of the corresponding structure. Employing N_{s1} stable and N_{s2} unstable structures, the PNN is trained to detect stable and unstable structures during the optimization process.

The last stage in training the HNNS is to train a network to predict the nonlinear time history responses of the N_{s1} stable structures. For this purpose, another GRNN is considered. This network is denoted as response predictor. The inputs and outputs of the GRNN are F_i and R_i of the N_{s1} stable structures.

In order to evaluate the accuracy of the approximate nonlinear time history responses against their corresponding actual ones (obtained by conventional FE analysis), two evaluation metrics are used.

$$RRMSE = \left(\left(\frac{1}{n_{gp} - 1} \sum_{i=1}^{n_{gp}} (z_i - \tilde{z}_i)^2 \right) / \left(\frac{1}{n_{gp}} \sum_{i=1}^{n_{gp}} (z_i)^2 \right) \right)^{\frac{1}{2}} \quad (16)$$

$$R^2 = 1 - \left(\sum_{i=1}^{n_{gp}} (z_i - \tilde{z}_i)^2 \right) / \left(\sum_{i=1}^{n_{gp}} (z_i - \bar{z})^2 \right) \quad (17)$$

where z_i and \tilde{z}_i are the i th component of the exact and approximate responses, respectively. The mean value of exact vectors component is expressed by \bar{z} .

In the normal mode when an unseen new sample (X_{new}) is presented to the trained HNNS during the optimization process, at first the frequency predictor GRNN predicts its natural frequencies (F_{new}). Then these frequencies are presented to the PNN to recognize the stability or instability of the structure. If the structure is unstable, it will be rejected else the response predictor GRNN

predicts the nonlinear time history responses of the structure (R_{new}).

The outline of the HNNS in training and normal modes is shown in Figure 2.

Fundamental Steps of the Methodology

As explained, in the proposed methodology MCGA is employed to achieve optimization task while HNNS is employed to predict the required structural responses. Fundamental steps of the methodology are as follows:

Step1: Data generation: A number of structures are randomly selected and their natural frequencies and nonlinear time history responses for earthquake loading are computed.

Step2: Structural identification: a PNN is trained to detect stable and instable structures based on their natural frequencies.

Step3: Frequency evaluation: a GRNN is trained to predict the natural frequencies of the structures during the optimization process.

Step4: Nonlinear responses evaluation: another GRNN is trained to predict the nonlinear time history responses of the structures during the optimization process.

Step5: Design optimization: optimal design process is achieved by MCGA incorporating HNNS.

Numerical Results

To show the computational advantages of the proposed methodology a 72-bar truss subjected to 15 seconds of the El Centro (S-E 1940) earthquake record is designed for optimal weight. The structure is shown in Figure 3. The earthquake record is applied in x direction. Young's modulus, yield stress and mass density are $2.1 \times 10^{10} \text{ kg/m}^2$, $2.4 \times 10^7 \text{ kg/m}^2$ and 7850 kg/m^3 , respectively. A simple bilinear stress-strain relationship with kinematic hardening by the modulus of $6.3 \times 10^8 \text{ kg/m}^2$ is

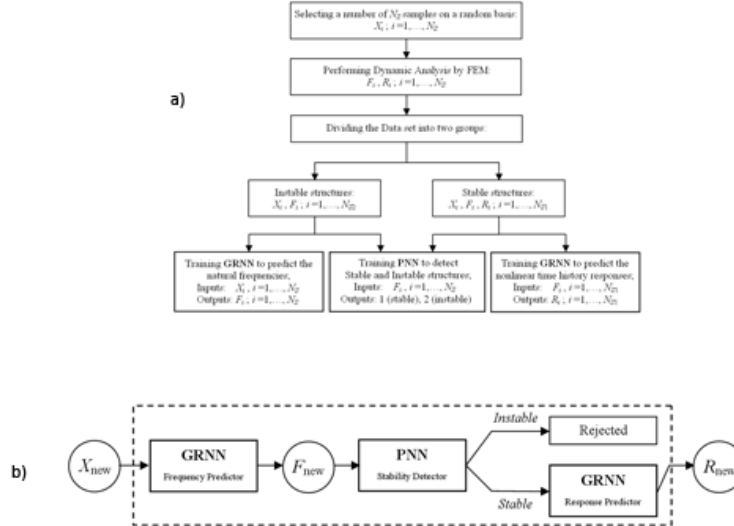
considered. The mass of 10000 kg is lumped at nodes of 1 to 4 of the structure. The 72 structural members are divided into 9 groups, as follows: (1) A1-A4, (2) A5-A12, (3) A13-A16, (4) A17-A24, (5) A25-A28, (6) A29-A36 (7) A37-A40, (8) A41-A48 and (9) A49-A72. The cross-sectional areas of the elements can be chosen from the standard Pipe profile list given as: (2.54, 11.2, 12.3, 13.9, 15.2, 17.2, 18.9, 21.4, 25.7, 26.4, 32.1 and 33.1) 10^{-4} m^2 . As the nonlinear structural behavior is considered only the displacement constraints are included. In this case, the displacement of top node of the structure is limited to 2 cm. The constraints are checked at 750 grid points with time step of 0.02 seconds. The computational time is measured in terms of CPU time required by a PC Pentium IV 3000 MHz.

To train and test the HNNS a training set of 161 samples are randomly selected and their natural frequencies and nonlinear time history responses are evaluated by the conventional FEM. During this process it is revealed that among all the selected structures, in case of 11 ones the nonlinear dynamic analysis does not converge. Therefore, in the data there are 150 stable structures ($N_{S1}=150$) and 11 instable ones ($N_{S2}=11$). The time spent to FE analysis of 165 structures is 320 min.

A GRNN is trained to predict the natural frequencies of the structures during the optimization process. The inputs and outputs of the GRNN are design variables ($X_i, i=1,2,\dots,161$) and frequencies ($F_i, i=1,2,\dots,161$) of the selected structures, respectively. Due to symmetry of the structure, its 1st, 3rd and 5th natural frequencies are considered. From the 161 selected structures, 107 and 54 ones are randomly selected to train and test the network, respectively. In this case, the size of the GRNN is 9-110-3. The results of testing the generalization of the GRNN are given in Table 1. The time spent to train and test the GRNN is 0.6 min.

In order to train the PNN, 107 samples including 100 stable and 7 instable structures are considered. Also to test the PNN, 54 samples includ-

Figure 2. Outlines of the HNNS in (a) training and (b) normal modes



ing 50 stable and 4 instable ones are considered, respectively. The testing results of PNN, shown in Figure 4(a), indicate that there is good conformance between exact results and predicted ones by PNN. However by adding more instable structures to the data set the accuracy of the PNN can be improved. The time spent to train and test the PNN is 1.0 min.

In order to predict the top node displacement of the structure another GRNN is trained. As the instable structures will be rejected during the optimization process, therefore the GRNN is only trained to predict the nonlinear responses of the stable structures. In this case, the training set includes the N_{s1} stable structures including their

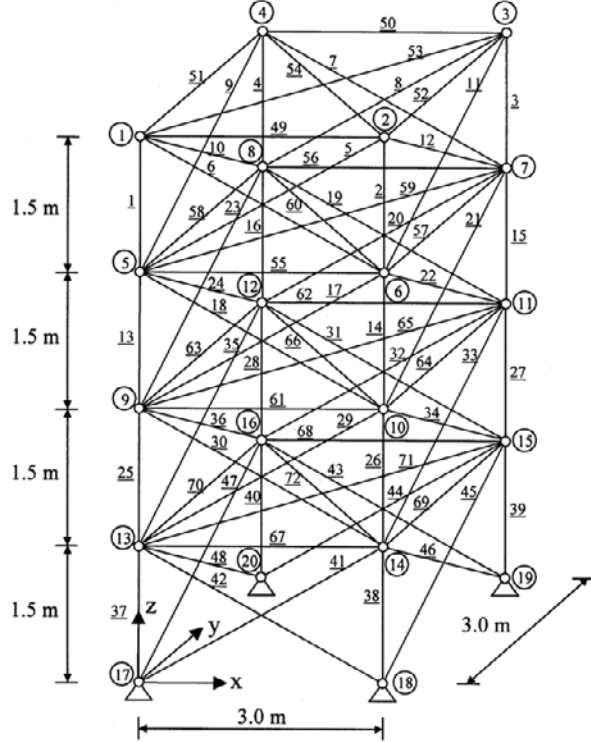
corresponding natural frequencies as the inputs and the nonlinear time history displacements of the top node as the outputs. To train and test the network 100 and 50 samples are considered, respectively. The size of the GRNN is 3-100-750. The results of testing the performance generality of the GRNN are shown in Figure 4(b). The time spent to train and test the network is 1.35 min. The results imply that the generalization of the GRNN is appropriate.

The optimization task is achieved by the CGA and MCGA with 30 individuals using the exact nonlinear dynamic Analysis(ENDA) and approximate analysis by HNNS (HNNS). The maximum number of generations is limited to 100. In each optimization case, ten independent optimal design processes are performed and the best solution found, the average number of generations and the average time of optimization are given as the final results. In the optimization process based on approximate analysis, to distinguish feasible and infeasible solutions, the criterion proposed by Vanderplaats (1999) is involved: if the sum of the violated constraints is less than 0.005, the corresponding solution is feasible, otherwise the

Table 1. Testing errors of the GRNN

<i>Natural frequencies</i>	<i>Mean error (%)</i>	<i>Maximum error (%)</i>
f_1	0.7320	2.1042
f_3	0.1420	1.1308
f_5	0.4792	1.6149
Average	0.4511	1.6166

Figure 3. 72-Bar space steel truss



solution is infeasible. It should be noted that, in the optimization by CGA and MCGA incorporating HNNS, the necessary responses during the optimization are predicted by the HNNS and to assess the feasibility of the final optimal solution its responses are evaluated by the conventional FE time history nonlinear analysis. The final results of optimization are given in Table 2.

It is demonstrated that the MCGA is superior to the CGA. It can be also observed that the best solution is obtained by MCGA using HNNS in terms of weight, time, and accuracy. The top node time history displacements of the solutions achieved by HNNS (CGA+HNNS and MCGA+HNNS) are compared with their corresponding actual ones in Figure 5. Also, the stress-strain hysteretic curves corresponding to the element 14 of the optimal structures are shown in Figure 6. These curves imply that the structural behavior is highly nonlinear.

DISCUSSION

Training of the HNNS includes three steps. In the first step, a GRNN is trained to predict the first, third and fifth natural frequencies of the structures. The training task is achieved in 0.6 min and the results show that the average error is 0.4511%. This means that the generalization of the trained GRNN is appropriate. In the second step, a PNN is trained to recognize stable structures from the unstable ones. The time spent is 1 min and the numerical results of testing indicate that accuracy of the PNN is good. As the final step, another GRNN is trained to predict the time history displacement the top node of the structure. In this case, the mean RRMSE and R^2 of the predicted responses are 0.0387 and 0.9971, respectively. The numerical results of testing reveal that the generality of the HNNS is proper to provide accurate and reliable results during the optimization phase.

Figure 4. (a) Testing results of PNN and (b) RRMSE and R^2 of the predicted responses by GRNN

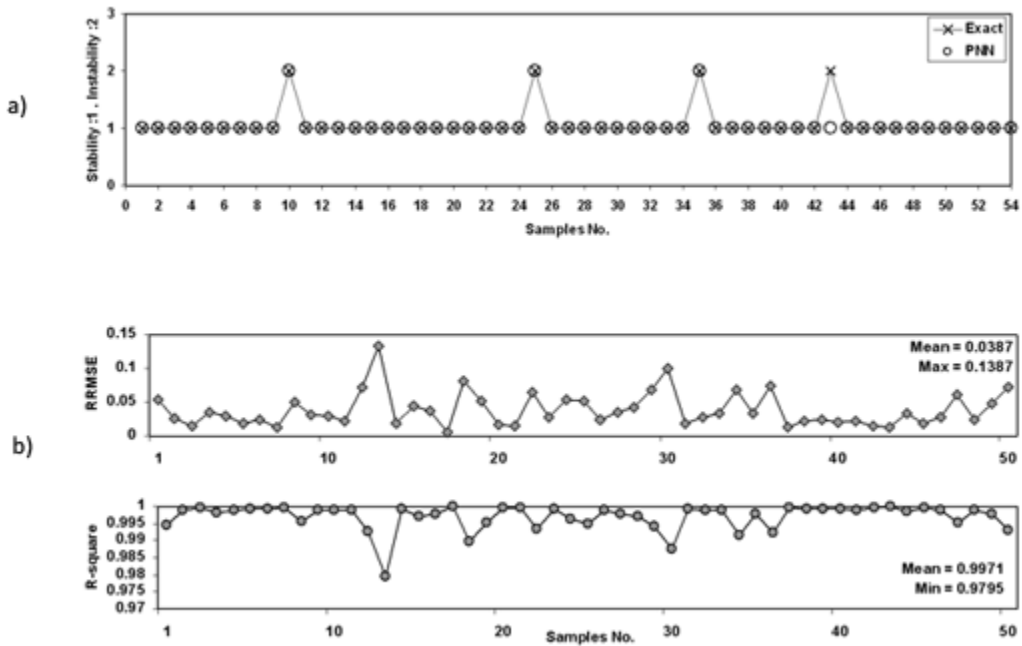
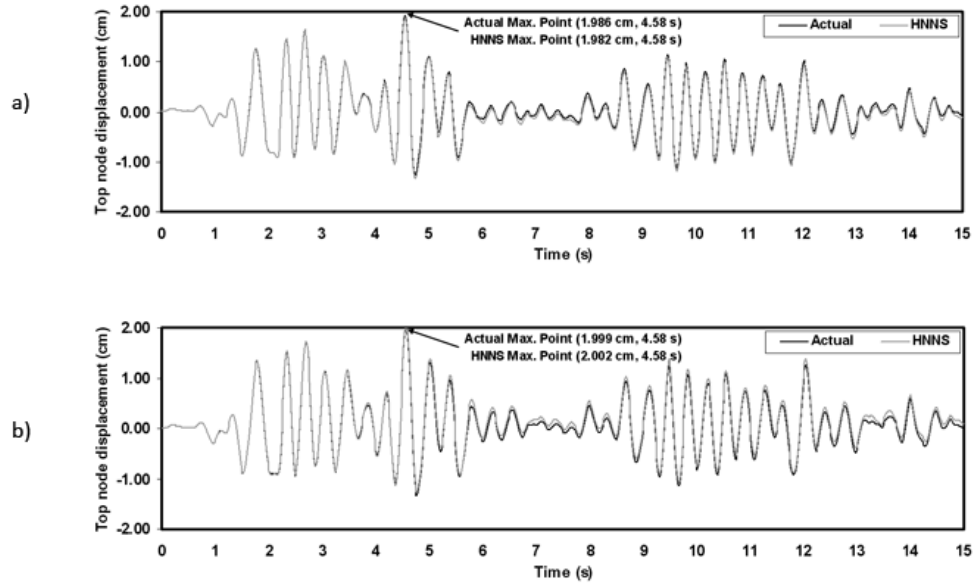


Table 2. Optimum designs

Element Groups No.	CGA		MCGA	
	ENDA	HNNS	ENDA	HNNS
1	1	1	1	1
2	1	1	1	1
3	1	1	1	1
4	2	2	2	2
5	2	3	3	2
6	2	2	2	2
7	6	4	3	3
8	2	2	2	2
9	1	1	1	1
Weight (kg)	1099.6	1089.1	1081.4	1076.2
The average number of generations	74	78	66	63
The sum of the violated constraints	0.0000	0.0000	0.0000	0.0020
The average Optimization time (min)	4110.0	1.22	3600.0	0.95
Data generating time (min)	-	320.0	-	320.0
Training time (min)	-	3.0	-	3.0
Overall time (min)	4110.0	324.2	3600.0	324.0
RRMSE, R^2	-	0.0732, 0.9951	-	0.0668, 0.9975

Figure 5. The top node displacements of the optimal design found by (a) CGA+HNNS and (b) MCGA+HNNS compared with the corresponding actual ones



The optimization task is achieved by CGA and MCGA incorporating ENDA and HNNS. The numerical results show that all of the solutions are feasible and the stress-strain hysteretic curves corresponding to the elements of the optimal structures imply that the structural behavior is highly nonlinear. The results obtained by MCGA are better than that of the CGA in terms of structural weight, required generations and prediction accuracy. The weight of the optimal structure found by CGA using ENDA and its required generations are 1099.6 and 74, respectively while these of the MCGA are 1081.4 and 66, respectively. Also the corresponding weight and required generation to the CGA+HNNS are 1089.1 and 78 while for MCGA+HNNS process are 1076.2 and 63, respectively. Therefore it can be observed that MCGA is superior to CGA and the best results are provided by the MCGA+HNNS process. According to the results the overall time of optimization using HNNS is significantly reduced by a factor of 0.09 compared with the optimization using ENDA.

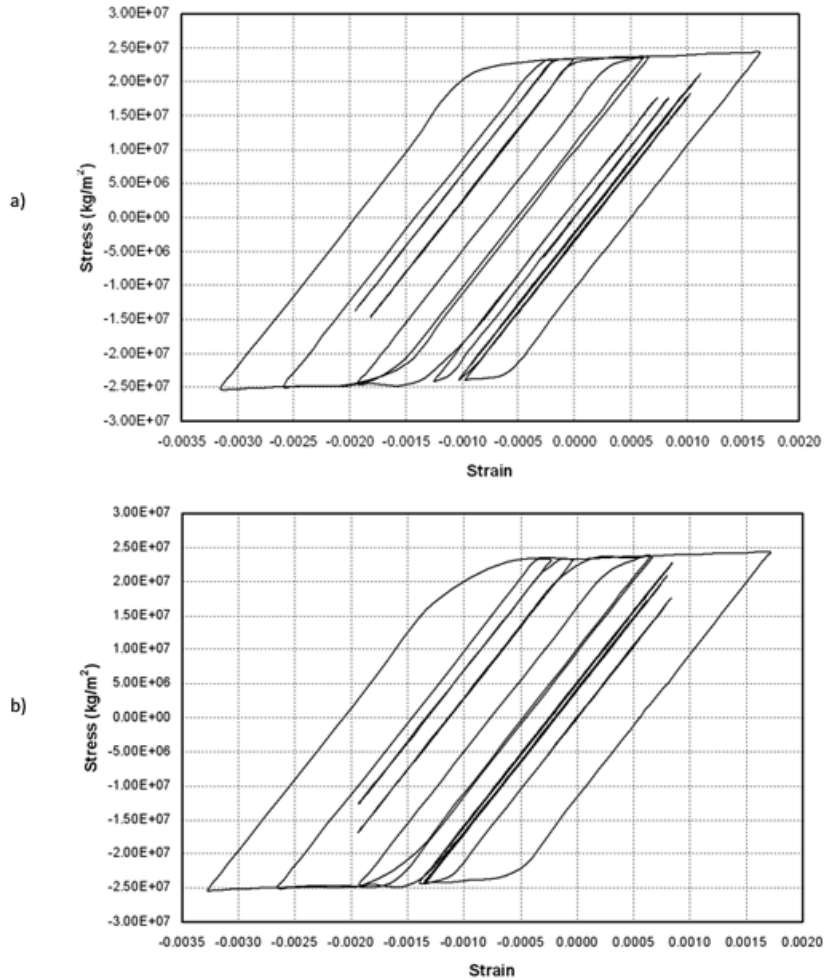
FUTURE RESEARCH DIRECTIONS

In this chapter, a single earthquake record is applied to the structure. For the future researches, a bank of natural or artificial records scaled according to a seismic design code and considering hazard levels may be used. Also, other optimization algorithms with higher performance may be investigated. To improve response prediction accuracy, other neural network models such as fuzzy network can be used. As the computational work of the methodology is low, it also can be used to solve the massive seismic reliability based optimization problems.

CONCLUSION

An efficient hybrid neural network based optimization algorithm is presented to achieve design optimization of structures subjected to earthquake time history loading with inelastic behavior. A modified cellular genetic algorithm denoted as

Figure 6. The stress-strain hysteretic curves of the element 14 of the optimal structures (a) CGA+HNNS and (b) MCGA+HNNS



MCGA is proposed for performing optimization task. The MCGA is a multi-stage optimization algorithm based on renewing the population in each stage using elitism. In order to mitigate the computational rigors of the nonlinear time history analysis, a hybrid neural network system termed as HNNS is employed. The PNN and GRNN are serially integrated in the framework of the HNNS. By using the HNNS the necessary nonlinear time history responses of the structures during the optimization process are accurately predicted. Optimization is achieved by CGA and MCGA

using exact and predicted structural nonlinear responses. The numerical results imply that the computational performance of the MCGA is better than that of the CGA. Also it is observed that by employing the HNNS the overall time of optimization is about 0.09 times of the time required by exact optimization while the errors due to all the approximations are small. Therefore, it can be finally concluded that the proposed methodology is a powerful tool to design optimization of structures subject to earthquake loading considering nonlinear behavior.

REFERENCES

- ANSYS Incorporated. (2006). *ANSYS release 10.0*, 2006.
- Arora, J. S. (1999). Optimization of structures subjected to dynamic loads. In Leondes, C. T. (Ed.), *Structural dynamic systems computational techniques and optimization* (pp. 1–73). Gordon and Breach Science Publishers.
- Biondini, F., Bontempi, F., Frangopol, D. M., & Malerba, P. G. (2004). Cellular automata approach to durability analysis of concrete structures in aggressive environments. *Journal of Structural Engineering*, 130(11), 1724–1737. doi:10.1061/(ASCE)0733-9445(2004)130:11(1724)
- Canjurt, O. E., & Hajela, P. (2005). A cellular framework for structural analysis and optimization. *Computer Methods in Applied Mechanics and Engineering*, 194(30-33), 3516–3534. doi:10.1016/j.cma.2005.01.014
- Gholizadeh, S. (2010). Structural optimization for earthquake loading with nonlinear responses by surrogate modeling based evolutionary algorithms. *Asian Journal of Civil Engineering*, 11(1), 25–42.
- Gholizadeh, S., & Salajegheh, E. (2009). Optimal design of structures for time history loading by swarm intelligence and an advanced metamodel. *Computer Methods in Applied Mechanics and Engineering*, 198(37-40), 2936–2949. doi:10.1016/j.cma.2009.04.010
- Gholizadeh, S., & Salajegheh, E. (2010a). Optimal seismic design of steel structures by an efficient soft computing based algorithm. *Journal of Constructional Steel Research*, 66(1), 85–95. doi:10.1016/j.jcsr.2009.07.006
- Gholizadeh, S., & Salajegheh, E. (2010b). A cellular genetic algorithm for structural optimisation. In B. H. V. Topping, J. M. Adam, F. J. Pallarés, R. Bru, & M. L. Romero, (Ed.), *Proceedings of the Tenth International Conference on Computational Structures Technology, DATE*, (pp. 1-14). Stirlingshire, UK: Civil-Comp Press.
- Gholizadeh, S., Salajegheh, J., & Salajegheh, E. (2009). An intelligent neural system for predicting structural response subject to earthquake. *Advances in Engineering Software*, 40(8), 630–639. doi:10.1016/j.advengsoft.2008.11.008
- Gholizadeh, S., & Samavati, O. A. (2011). Structural optimization by wavelet transforms and neural networks. *Applied Mathematical Modelling*, 35(2), 915–929. doi:10.1016/j.apm.2010.07.046
- Haupt, R. L., & Haupt, S. E. (2004). *Practical genetic algorithms*. New Jersey: Wiley-Interscience Publication.
- Kocer, F. Y., & Arora, J. S. (1999). Optimal design of H-frame transmission poles for earthquake loading. *Journal of Structural Engineering*, 125(11), 1299–1308. doi:10.1061/(ASCE)0733-9445(1999)125:11(1299)
- Kocer, F. Y., & Arora, J. S. (2002). Optimal design of latticed towers subjected to earthquake loading. *Journal of Structural Engineering*, 128(2), 197–204. doi:10.1061/(ASCE)0733-9445(2002)128:2(197)
- Lagaros, N. D., Fragiadakis, M., Papadrakakis, M., & Tsompanakis, Y. (2006). Structural optimization: A tool for evaluating dynamic design procedures. *Engineering Structures*, 28(12), 1623–1633. doi:10.1016/j.engstruct.2006.02.014
- Lagaros, N. D., & Papadrakakis, M. (2011). (in press). Neural network based prediction schemes of the non-linear seismic response of 3D buildings. *Advances in Engineering Software*.

- Rajasekaran, S. (2001). Optimization of large scale three dimensional reticulated structures using cellular genetics and neural networks. *International Journal of Space Structures*, 16(4), 315–324. doi:10.1260/026635101760832244
- Salajegheh, E., & Heidari, A. (2005). Optimum design of structures against earthquake by wavelet neural network and filter banks. *Earthquake Engineering & Structural Dynamics*, 34(1), 67–82. doi:10.1002/eqe.417
- Specht, D. F. (1990). Probabilistic neural networks. *Neural Networks*, 3(1), 109–118. doi:10.1016/0893-6080(90)90049-Q
- Vanderplaats, G. N. (1999). *Numerical optimization techniques for engineering design*. USA: VR and D, Inc.
- Von Neumann, J. (1966). *Theory of self-reproducing automata* (Burks, A. W., Ed.). University of Illinois Press.

Chapter 13

Fuzzy Identification of Seismically Excited Smart Systems

JinSeop Kim

Massachusetts Institute of Technology, USA

Yeesock Kim

Worcester Polytechnic Institute, USA

Tahar El-Korchi

Worcester Polytechnic Institute, USA

ABSTRACT

In this chapter, a nonlinear modeling framework to identify nonlinear behavior of smart structural systems under seismic excitations is proposed. To this end, multi-input-multi-output (MIMO) autoregressive exogenous (ARX) input models and Takagi-Sugeno (TS) fuzzy models are coalesced as the MIMO ARX-TS fuzzy model. The premised part of the proposed MIMO ARX-TS fuzzy model is optimized using the hierarchical clustering (HRC) algorithm, while its consequent parameters are optimized via the weighted linear least squares estimation. The performance of the proposed model is investigated using the dynamic response of a three-story shear planer frame structure equipped with a magnetorheological (MR) damper subject to earthquake disturbances. Furthermore, the impact of the HRC algorithm on the performance of the MIMO ARX-TS fuzzy model is compared with that of the subtractive and the fuzzy C-means clustering algorithms. The equivalence of the original and identified data is numerically shown to prove that the HRC MIMO ARX-TS fuzzy model introduced here is effective in estimating nonlinear behavior of a seismically excited building-MR damper system.

DOI: 10.4018/978-1-4666-1640-0.ch013

1. INTRODUCTION

The development of an accurate explicit mathematical model of dynamical systems is one of the most important tasks in structural health monitoring and control system design for hazard prediction and mitigation of dynamical systems because precise mathematical information related to the dynamic systems is used for damage prediction and/or calculation of control forces (Kerber et al. 2007; Yen & Langari 1998; Lin et al. 2001; Bani-Hani 1999; Kim et al. 2011). However, it is still challenging to derive a mathematical model of nonlinear dynamic systems (Moon & Aktan 2006). An example of such nonlinear dynamic systems can be sought when highly nonlinear hysteretic actuators/dampers are applied to structural systems for efficient energy dissipation: the structure integrated with the nonlinear control devices behaves nonlinearly although the structure itself is usually assumed to remain linear (Yi et al. 2001; Ramallo et al. 2004). Because the structure integrated with the nonlinear hysteretic control device is intrinsically nonlinear, it is challenging to develop an appropriate mathematical model for the integrated nonlinear system including the interaction effects between the structural system and the nonlinear control device while it plays a key role in both structural health monitoring and controlling system (Dyke et al. 1998).

Such a challenging nonlinear problem has made a number of researchers pay a great deal of attention to system identification (SI) approaches in recent years (Adeli & Jiang 2006). The nonlinear SI methodologies can be categorized into two parts: parametric and nonparametric SI approaches (Bani-Hani et al. 1999). A parametric SI method is to directly identify physical quantities such as the stiffness and damping of the structural systems (Lin et al. 2001; Lin & Betti 2004; Yang & Lin 2004); while a nonparametric SI method is to train the input-output map of the structural

systems (Hung et al. 2003). Among them, the nonparametric SI approach is effective for the complex nonlinear problems of large civil infrastructures, in particular, one of the nonparametric nonlinear SI methodologies that have been widely used in the field of large civil structures is neural network (NN) because it is more readily useful than the parametric SI approach to identify incomplete and incoherent measurements of large civil structures, in general (Smith & Chase 1993; Masri et al. 2000; Hung et al. 2003), although conventional NN models have drawbacks of the slow convergence rate and the potential to local minima due to the characteristics of the black-box model (Chassiakos & Masri 1996). On the other hand, another popular nonparametric SI method for modeling complex nonlinear dynamic systems is the fuzzy logic theory because it is effective to represent complex nonlinearities and uncertainties of dynamic systems in a more transparent way (Langari 1999). Since Zadeh's paper(1965), the fuzzy logic has been widely applied to various SI problems (Wang & Langari 1995). In particular, there have been a number of studies on the TS fuzzy model in recent years, which provides an effective representation of nonlinear systems with the aid of fuzzy sets, fuzzy rules, and a set of local linear models (Filev 1991; Du & Zhang 2008; Abonyi et al. 2000; Wang & Langari 1996; Johansen & Babuska 2003; Takagi & Sugeno 1985; Chen et al. 2007). On the other hand, the fuzzy logic theory in the field of large scale civil infrastructures has been mainly used for nonlinear fuzzy control system design (Tani et al. 1998; Wang & Lee 2002; Ahlawat & Ramaswamy 2004; Dounis et al. 2007; Loh et al. 2003; Shook et al. 2008; Casciati 1997; Yan & Zhou 2006; Choi & Schurter & Roschke 2001; Zhou et al. 2003; Faravelli & Rossi 2002; Al-Dawod et al. 2004; Battaini et al. 2004; Symans & Kelly 1999; Subramaniam et al. 1996; Kim et al. 2004; Pourzeynali et al. 2007; Kim et al. 2009; Nomura et al. 2007; Gu &

Oyadji 2008). However, few investigations are found in the field of the nonlinear fuzzy SI for civil building structures subjected to earthquake loadings (Adeli & Jiang 2006; Jiang & Adeli 2005). Adeli and Jiang developed a fuzzy wavelet neural network (FWNN) model for nonlinear SI of high-rise building structures. In their work, the multi-input-single-output (MISO) FWNN was trained by a hybrid Levenberg-Marquardt least-squares algorithm. However, their approach does not adopt a fuzzy model as an input-output mapping function, but uses a fuzzy C-mean clustering technique only as one of data mining methods for use in a neural network model. Furthermore, no investigation has been conducted on a nonlinear Takagi-Sugeno (TS) fuzzy SI for use with building structures equipped with a highly nonlinear hysteretic control device such as magnetorheological (MR) damper. Without the TS fuzzy model for the nonlinear building-MR damper systems, it is very difficult to design a parallel distributed compensation (PDC)-based TS fuzzy control system for damage mitigation of seismically excited civil structures equipped with MR damper systems (Kim et al. 2009) and it would not be easy to develop a damage detection algorithm for the seismically excited structure-MR damper system. The reason is that the PDC-based TS fuzzy control design framework requires that a TS fuzzy controller, i.e., a nonlinear fuzzy controller, has the same premise parameters as a TS fuzzy model, i.e., dynamic model of the building-MR damper system (Kim et al. 2009; Kim et al. 2010). Therefore, this chapter proposes a fuzzy modeling framework based on the TS fuzzy model for identifying nonlinear behavior of the building-MR damper systems subjected to earthquake disturbances: hierarchical clustering-based (HRC) multi-input, multi-output (MIMO) autoregressive exogenous (ARX) Takagi-Sugeno (TS) fuzzy model; HRC MIMO ARX-TS fuzzy model. The advantages of the proposed HRC

MIMO ARX-TS fuzzy model can be summarized as follows: 1) The proposed modeling framework can be directly applied to the structure-MR damper system without the decoupling process because it is a nonlinear SI method; 2) it is more appropriate to identify incomplete and incoherent measurements of large civil structures than typical parametric SI approaches; and 3) it provides a systematic design framework for the PDC-based nonlinear TS fuzzy controller.

In the rest of this chapter, first the HRC MIMO ARX-TS fuzzy identification framework is described, following by simulation results involving the time histories of the excitation input signals and the associated system output responses.

2. FUZZY LOGIC MODEL

In general, it is still challenging to develop a mathematical model for a dynamic model equipped with the MR damper system because the nonlinear dynamic system has multiple operating regions. In this section, a fuzzy modeling framework will be presented to model nonlinear behavior of structure-MR damper systems: first, the fundamentals on fuzzy logic models are summarized; and then HRCARXTS fuzzy model is introduced; and finally, simulation results are discussed.

2.1. Membership Functions and Fuzzy Sets

Membership functions (MFs) and fuzzy sets are the cornerstone of a fuzzy logic-based system that is appropriate for modeling complex nonlinear systems with uncertain parameters. There exist always a variety of uncertainties in engineering problems, e.g., “the structural damage is very large” and “the performance of an MR damper is sensitive to high temperature.” However, questions would arise: “How much damage would be

thought as very large quantity?" or "Which degree of temperature is high?" In reality, it is impossible to model the uncertain variables in a conventional way; while, MFs can be used for modeling such variables as an element of a fuzzy set. Fuzzy sets are constructed from MFs. For example, a fuzzy set of the structural damage can be constructed as three MFs, e.g., small, medium, and large. This fuzzy set is used for constructing the premise part of IF-THEN rules, i.e., IF STATEMENT.

2.2. Fuzzy Rules

A fuzzy rule base has a set of fuzzy IF-THEN rules; e.g., "if a building structure has large damage, a controller is operated such that an alarm is rung twice", "if the structural damage is medium, the controller is operated such that the alarm is rung once", and "if there is no damage in the building structure, the controller is not operated." The set of IF-THEN rules is blended into an integrated system through fuzzy reasoning methods.

2.3. Fuzzy Reasoning

Fuzzy reasoning is a mechanism to perform the fuzzy inference system that derives conclusions from a family of IF-THEN rules, i.e., fuzzy reasoning is a methodology to organize a set of the IF-THEN rules. Takagi and Sugeno (1985) developed a systematic methodology for a fuzzy reasoning using linear functions in the consequent part. Because the TS-fuzzy model uses linear functions in the consequent part, the defuzzification procedure is not required. A typical fuzzy rule for the TS fuzzy model has the form

$$\begin{aligned} R_j : & \text{ If } z_{FZ}^1 \text{ is } p_{1,j} \text{ and } z_{FZ}^2 \text{ is } p_{2,j} \text{ and... and } z_{FZ}^i \text{ is } p_{i,j} \\ & \text{ Then } y = f(z_{FZ}^1, \dots, z_{FZ}^i), \end{aligned} \quad (1)$$

where R_j is the j^{th} fuzzy rule; z_{FZ}^i are premise variables that can be either input or output values; $p_{i,j}$ are fuzzy sets centered at the j^{th} operating point; $y = f(z_{FZ}^1, \dots, z_{FZ}^i)$ can be any type of function in terms of the premise vector $\mathbf{z}_{FZ} = [z_{FZ}^1, \dots, z_{FZ}^i]$. The TS fuzzy model-based reasoning is to simply compute weighted mean values

$$y_{\text{final}} = \frac{\sum_{j=1}^{N_r} w_j y_j}{\sum_{j=1}^{N_r} w_j}, \quad (2)$$

where w_j is the fuzzy interpolation parameters; N_r is the number of the fuzzy rules. To appropriate model nonlinear behavior of dynamic systems, ARX input models are applied to the consequence part of the TS fuzzy model.

3. AUTOREGRESSIVE-EXOGENOUS INPUT TAKAGI-SUGENO FUZZY MODEL

A nonlinear dynamic system can be described by the following multivariable nonlinear model

$$\dot{\mathbf{z}} = \mathbf{f}(t, \mathbf{z}, \mathbf{u}), \quad (3)$$

where t is the time variable; \mathbf{z} is a state vector; \mathbf{u} is an input vector; and \mathbf{f} represents a multivariable nonlinear dynamic system. The nonlinear dynamic model can be described by the multiple multi-input multi output (MIMO) ARX input-based TS fuzzy model (MIMO ARX-TS) fuzzy model

Box 1.

$$\mathbf{z}_{\text{FZ}} \in \{y_1(k-1), \dots, y_1(k-n), \dots, y_p(k-n), u_1(k-1), \dots, u_1(k-m), \dots, u_p(k-m)\}.$$

R_j: If z_{FZ}^1 is $p_{1,j}$ and z_{FZ}^2 is $p_{2,j}$ and... and z_{FZ}^i is $p_{i,j}$
 Then $\mathbf{y}(k) = \sum_{i=1}^n \mathbf{a}_{i,j} \mathbf{y}(k-i) + \sum_{i=1}^m \mathbf{b}_{i,j} \mathbf{u}(k-i)$,
 (4)

where n is the number of delay steps in the output signals; m is the number of delay steps in the input signals; $\mathbf{y}(k)$ is the output; $\mathbf{u}(k)$ is the input; $\mathbf{a}_{i,j}$ and $\mathbf{b}_{i,j}$ are the consequent parameters (see Box 1).

Note that the number of the fuzzy rules corresponds to the number of local linear MIMO ARX models, i.e., the mth local linear MIMO ARX dynamic model represents the mth fuzzy rule that describes behavior of a nonlinear dynamic system in a local linear operating region. However, a question would arise on how to blend the multiple local linear MIMO ARX dynamic models into an integrated nonlinear dynamic system model, i.e., how to construct a bridge across the multiple MIMO ARX models. One solution is found in the fuzzy logic-based interpolation (Yen & Langari 1998). The multiple local linear MIMO ARX models at the specific operating point z_{FZ}^i can be blended

$$\hat{\mathbf{y}}(k) = \sum_{i=1}^n \sum_{j=1}^{N_r} w_j(z_{\text{FZ}}^i) \mathbf{a}_{i,j} \mathbf{y}(k-i) + \sum_{i=1}^m \sum_{j=1}^{N_r} w_j(z_{\text{FZ}}^i) \mathbf{b}_{i,j} \mathbf{u}(k-i), \quad (5)$$

where $0 \leq w_j(z_{\text{FZ}}^i) \leq 1$ is the normalized true value of the j^{th} rule,

$$w_j(z_{\text{FZ}}^i) = \frac{\prod_{i=1}^{n_i} \mu_{i,j}(z_{\text{FZ}}^i)}{\sum_{j=1}^{N_r} \prod_{i=1}^{n_i} \mu_{i,j}(z_{\text{FZ}}^i)}, \quad (6)$$

where $\mu_{i,j}(z_{\text{FZ}}^i)$ is the grades of membership of z_{FZ}^i ; N_r is the number of local linear dynamic models; and n_i is the number of premise variables. Once the MIMO ARX-TS fuzzy model is set up, the premise parameters $\mathbf{P}_{i,j}$ and the consequent parameters $\mathbf{a}_{i,j}$ and $\mathbf{b}_{i,j}$ are determined such that the MIMO ARX-TS fuzzy model describes behavior of a nonlinear dynamic system. In this study, the premise parameters are determined via clustering techniques, including the hierarchical, the fuzzy C-means, and the subtractive clustering algorithms, and the consequent part is optimized using the weighted linear least squares estimation algorithm.

4. OPTIMIZATION OF MIMO ARX-TS FUZZY MODEL

In the MIMOARX-TS fuzzy identification model, the parameters of the premise and consequent parts are optimized such that the MIMOARX-TS fuzzy model effectively represents nonlinear behavior of the physical system. In particular, it is desirable to group a large data set into subsets of data with similar patterns for efficient determination of the premise part, i.e., the small number of MFs but reasonable pattern recognition. Appropriate meth-

ods for the grouping are clustering techniques that extract the center information of the subset of data within a large data set. In this study, the hierarchical clustering algorithm is applied; and then, the solution is compared with the other benchmark clustering algorithms, such as the fuzzy C-means and the subtractive clustering algorithms.

4.1. Premise Part

The hierarchical clustering algorithm determines the membership of data to their clusters by constructing the hierarchical organization of a given set of data, revealing the membership of each datum differently at distinct hierarchy levels (Ward 1963; Clauset et al. 2008). Once the hierarchy is established, one of the levels can be chosen either to yield a desired number of clusters or to optimize an objective function, depending on the problem at hand. To describe the algorithm, the dissimilarity or distance between a pair of data u_p is first considered as

$$d_{IJ} = \|u_p(I) - u_p(J)\|, \quad (7)$$

where the definition of distance can take any well-behaved metric for distance. In addition, the distance between a pair of sets can be defined as a function of the distances of all the pairs of data which are extracted from respective sets, i.e.,

$$D_{uv} = F\{d_{IJ} : I \in U_p, J \in V_p\}, \quad (8)$$

where F can be the minimum, the maximum, the average, or any other functions of the elements, d_{IJ} . In this study, we choose the Euclidean distance for d_{IJ} and the minimum for F .

The algorithm starts with allocating each data point to its own set, so that each set contains only one data point. Then, the distances of all the pairs

of sets are evaluated to find the minimum distance pair, and the sets thus found are merged into a set. By repeating this, the number of sets decreases by 1 at each iteration, so the desired number N_q of the sets are obtained after $(N-N_q)$ iterations. The center of each cluster can be calculated from the locations of data points composing it. Note that while the procedure described above is called the agglomerative hierarchical clustering, a divisive strategy can also be applied to obtain the same result. Note also that our choice of distance metrics produces the equivalent result as splitting the set at the (N_q-1) locations where the distances between adjacent data points are farthest, since we are concerned in the clustering of one dimensional data in this study.

4.2. Consequent Part

Once the premise part is optimized, the consequent part parameters can be optimized with the weighted linear least squares algorithm. Based on Gauss's celebrated principle of least square (Gauss 1963), the linear least squares algorithm can be formulated as a quadratic optimization problem that minimizes the error between true values and estimated model outputs

$$\text{Min } J = \frac{1}{2} \mathbf{e}(k)^T \mathbf{e}(k), \quad (9)$$

where $\mathbf{e}(k) = \hat{\mathbf{y}}(k) - \tilde{\mathbf{y}}(k)$; i.e., the error $\mathbf{e}(k)$ is the difference between the estimation model $\hat{\mathbf{y}}(k)$ and the true values $\tilde{\mathbf{y}}(k)$. Note that the normal linear least squares formulation can be easily extended into the weighted linear least squares by introducing a factor of weight. Thus, in what follows, the normal linear least squares estimator is derived first and then the weight factor is added into the normal least squares. A linear estimation model for use with the linear least squares algorithm is

$$\hat{\mathbf{y}}(k) = \mathbf{H}(k),_j. \quad (10)$$

where $\mathbf{H}(k)$ is a set of independent specified basis and $,_j$ is the matrices of parameters to be estimated. On the other hand, the true model can be thought as a contaminated estimation model

$$\tilde{\mathbf{y}}(k) = \mathbf{H}(k),_j + \mathbf{e}(k). \quad (11)$$

From Eq. (11), the error dynamics is given by

$$\mathbf{e}(k) = \tilde{\mathbf{y}}(k) - \mathbf{H}(k),_j. \quad (12)$$

Using the fact that a scalar equals its transpose, substituting Eq. (12) into Eq. (9) leads to the following objective function

$$J = J(.,_j) = \frac{1}{2} [\tilde{\mathbf{y}}(k)^T \tilde{\mathbf{y}}(k) - 2\tilde{\mathbf{y}}(k)^T \mathbf{H}(k),_j + ,_j^T \mathbf{H}(k)^T \mathbf{H}(k),_j]. \quad (13)$$

In this problem, the goal is to find $,_j$ such that the objective function J is minimized. For minimization of the quadratic function of Eq. (13), the following necessary condition can be derived

$$\nabla_{,j} J = \mathbf{H}(k)^T \mathbf{H}(k),_j - \mathbf{H}(k)^T \tilde{\mathbf{y}}(k) = 0, \quad (14)$$

where $\nabla_{,j} J$ is a Jacobian matrix, the first partial derivative of J with respect to $,_j$. For solution of this equation, the following analytical least squares estimator is available

$$\theta_j = [\mathbf{H}(k)^T \mathbf{H}(k)]^{-1} \mathbf{H}(k)^T \tilde{\mathbf{y}}(k). \quad (15)$$

By simply adding an appropriate weighting parameter of w_j^e , the linear least squares estima-

tion can be easily extended into a weighted least squares estimator

$$\theta_j = [\mathbf{H}(k)^T w_j^e \mathbf{H}(k)]^{-1} \mathbf{H}(k)^T w_j^e \tilde{\mathbf{y}}(k), \quad (16)$$

where w_j^e is the appropriate weighting parameter and

$$\mathbf{H}(k) = [\mathbf{y}(k-1)^T, \dots, \mathbf{y}(k-n)^T, \mathbf{u}(k-1)^T, \dots, \mathbf{u}(k-m)^T] \quad (17)$$

and

$$\theta_j = [\mathbf{a}_{1,j}, \dots, \mathbf{a}_{n,j}, \mathbf{b}_{1,j}, \dots, \mathbf{b}_{m,j}]. \quad (18)$$

The nonlinear HRC MIMO ARX-TS fuzzy modeling approach proposed in this chapter can be summarized: 1) nonlinear behavior of a building-MR damper system are represented by a family of multiple MIMO ARX input models that are integrated into a nonlinear time-varying model through fuzzy rules; 2) the premise part of the multiple MIMO ARX-TS fuzzy model is determined by using the HRC algorithm; 3) the consequent part parameters are optimized by a family of weighted linear least squares. Finally, the effectiveness of the HRC MIMO ARX-TS fuzzy model is demonstrated from a benchmark building structure in the following section. Note that the proposed HRC MIMO ARX-TS fuzzy model was used for a semiactive nonlinear fuzzy control system design (Kim et al. 2009).

5. CASE STUDY

5.1. MR Damper

In recent years, smart control systems have been considered for large civil structures because it

combines the best features of both active and passive control systems. Smart control devices include variable-orifice dampers, variable-stiffness devices, variable-friction dampers, controllable-fluid dampers, shape memory alloy actuators, piezoelectrics, etc. (Hurlebaus & Gaul 2006). In particular, one of the controllable-fluid dampers, magnetorheological (MR) damper has attracted considerable attention in recent years due to its appealing characteristics. In general, an MR damper consists of a hydraulic cylinder, magnetic coils, and MR fluid comprising micron-sized magnetically polarizable particles floating within oil-type fluid. The MR damper is operated as a passive damper; however, when a magnetic field is applied to the MR fluid, it is changed into a semi-solid state in a few milliseconds. This is one of the most unique aspects of the MR dampers compared to active systems: the malfunction of the active control system might occur if some control feedback components, e.g., wires and sensors, are broken for some reasons during severe earthquake events, while a semiactive system operates as a passive damping system although the control feedback components are not functioning properly. Its characteristics are summarized in Kim et al. (2009).

To fully use the best features of the MR damper, a mathematical model that portrays the nonlinear behavior of the MR damper has to be developed first. However, this is challenging because the MR damper is a highly nonlinear hysteretic device. In this study, a modified Bouc-Wen model is used to predict the dynamic behavior of the MR damper force because it accurately predicts the dynamic behaviors at both low and high velocity regions as shown in figure 1 (Spencer et al. 1997), where the MR damper force $f_{\text{MR}}(t)$ predicted by the modified Bouc-Wen model is governed by the following differential equations

$$f_{\text{MR}} = c_{\text{BW}}^1 \dot{y}_{\text{BW}} + k_{\text{BW}}^1 (x_{\text{BW}} - x_{\text{BW}}^0), \quad (19)$$

$$\begin{aligned} \dot{z}_{\text{BW}} = & -\gamma |\dot{x}_{\text{BW}} - \dot{y}_{\text{BW}}| z_{\text{BW}} |z_{\text{BW}}|^{l-1} - \beta (\dot{x}_{\text{BW}} - \dot{y}_{\text{BW}}) |z_{\text{BW}}|^l \\ & + A_{\text{BW}} (\dot{x}_{\text{BW}} - \dot{y}_{\text{BW}}), \end{aligned} \quad (20)$$

$$\dot{y}_{\text{BW}} = \frac{1}{(c_{\text{BW}}^0 + c_{\text{BW}}^1)} \{ \alpha z_{\text{BW}} + c_{\text{BW}}^0 \dot{x}_{\text{BW}} + k_{\text{BW}}^0 (x_{\text{BW}} - y_{\text{BW}}) \}, \quad (21)$$

$$\alpha = \alpha_a + \alpha_b u_{\text{BW}}, \quad (22)$$

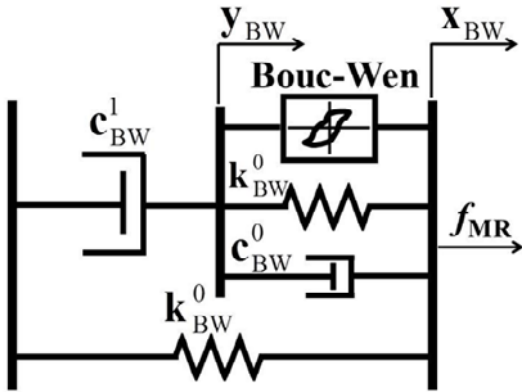
$$c_{\text{BW}}^1 = c_{\text{BW}}^{1a} + c_{\text{BW}}^{1b} u_{\text{BW}}, \quad (23)$$

$$c_{\text{BW}}^0 = c_{\text{BW}}^{0a} + c_{\text{BW}}^{0b} u_{\text{BW}}, \quad (24)$$

$$\dot{u}_{\text{BW}} = -\eta (u_{\text{BW}} - v_{\text{BW}}), \quad (25)$$

where z_{BW} and α , called the evolutionary variables, describe the hysteretic behavior of the MR damper; c_{BW}^0 is the viscous damping parameter at high velocities; c_{BW}^1 is the viscous damping parameter for the force roll-off at low velocities; α_a , α_b , c_{BW}^{0a} , c_{BW}^{0b} , c_{BW}^{1a} , and c_{BW}^{1b} are parameters that account for the dependence of the MR damper force on the voltage applied to the current driver; k_{BW}^0 controls the stiffness at large velocities; k_{BW}^1 represents the accumulator stiffness; x_{BW}^0 and x_{BW} are the initial and arbitrary displacements of the spring stiffness k_{BW}^1 , respectively; γ , β , l and A_{BW} are adjustable shape parameters of the hysteresis loops, i.e., the linearity in the unloading and the transition between pre-yielding and post-yielding regions; v_{BW} and u_{BW} are input and output voltages of a first-order filter, respectively; and η is the time constant of the first-order filter. Note that nonlinear phenomena occur when the highly nonlinear MR dampers are applied to structural systems for effective energy dissipation. Such an integrated structure-MR damper system behaves

Figure 1. Modified Bouc-Wen model for MR damper



nonlinearly although the structure itself is usually assumed to remain linear.

5.2. Building-MR Damper System

To demonstrate the effectiveness of the HRC MIMO ARX-TS fuzzy model proposed in this study, a 3-story shear planar frame structure employing an MR damper is investigated. An example of a building structure employing an MR damper is depicted in Figure 2. The associated equation of motion is given by

$$\mathbf{M}\ddot{\mathbf{x}} + \mathbf{C}\dot{\mathbf{x}} + \mathbf{K}\mathbf{x} = \mathbf{f}_{\text{MR}}(t, x_1, \dot{x}_1, v_1) - \mathbf{M}\ddot{\mathbf{w}}_g, \quad (26)$$

where the system matrices are;

$$\mathbf{M} = \begin{bmatrix} m_1 & 0 & 0 \\ 0 & m_2 & 0 \\ 0 & 0 & m_3 \end{bmatrix} \quad (27)$$

is the mass matrix,

$$\mathbf{C} = \begin{bmatrix} c_1 + c_2 & -c_2 & 0 \\ -c_2 & c_2 + c_3 & -c_3 \\ 0 & -c_3 & c_3 \end{bmatrix} \quad (28)$$

is the damping matrix,

$$\mathbf{K} = \begin{bmatrix} k_1 + k_2 & -k_2 & 0 \\ -k_2 & k_2 + k_3 & -k_3 \\ 0 & -k_3 & k_3 \end{bmatrix} \quad (29)$$

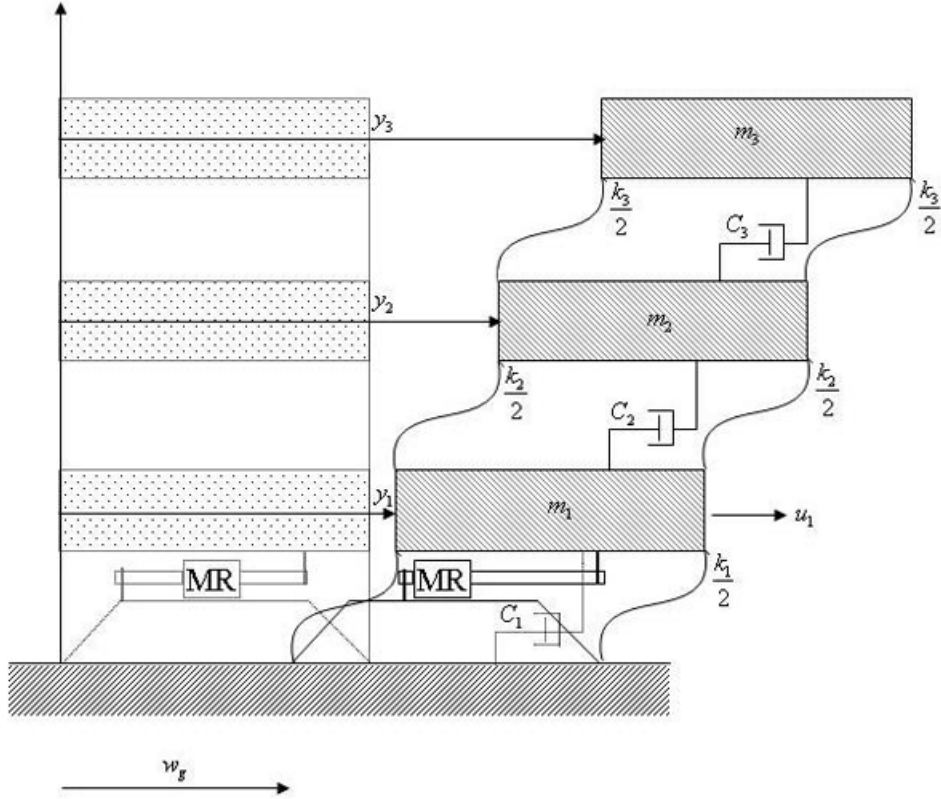
is the stiffness matrix,

$$\mathbf{f}_{\text{MR}}(t, x_1, \dot{x}_1, v_1) = \begin{bmatrix} f_{\text{MR}}(t, x_1, \dot{x}_1, v_1) \\ 0 \\ 0 \end{bmatrix} \quad (30)$$

is the MR damper force vector; $\ddot{\mathbf{w}}_g$ denotes the ground acceleration, m_i are the mass of the i th floor, k_i is the stiffness of the i th floor columns, c_i is the damping of the i th floor columns, the vector \mathbf{x} is the displacement relative to the ground, $\dot{\mathbf{x}}$ is the velocity, $\ddot{\mathbf{x}}$ is the acceleration, x_1 and \dot{x}_1 are the displacement and the velocity at the 1st floor level relative to the ground, respectively, v_1 is the voltage level to be applied, and “ and \triangleright are location matrices of control forces and disturbance signal, respectively. The second order differential equation can be converted into a set of first order differential equations in state space as

$$\begin{aligned} \dot{\mathbf{z}}_{6 \times 1} &= \mathbf{A}_{6 \times 1}^* \mathbf{z}_{6 \times 1} + \mathbf{B}_{6 \times 3}^* \mathbf{f}_{\text{MR}}(t, z_1, z_4, v_1)_{3 \times 1} - \mathbf{E}_{6 \times 3}^* \ddot{\mathbf{w}}_g_{3 \times 1} \\ \mathbf{y}_{9 \times 1} &= \mathbf{C}_{9 \times 6}^* \mathbf{z}_{6 \times 1} + \mathbf{D}_{9 \times 3}^* \mathbf{f}_{\text{MR}}(t, z_1, z_4, v_1)_{3 \times 1} + \mathbf{n}_{9 \times 1}, \end{aligned} \quad (31)$$

Figure 2. A 3-story shear planer frame structure employing an MR damper



where

$$\mathbf{A}^* = \begin{bmatrix} \mathbf{0} & \mathbf{I} \\ -\mathbf{M}^{-1}\mathbf{K} & -\mathbf{M}^{-1}\mathbf{C} \end{bmatrix} \quad (32)$$

is the state matrix,

$$\mathbf{B}^* = \begin{bmatrix} \mathbf{0} \\ \mathbf{M}^{-1}\mathbf{F} \end{bmatrix} \quad (33)$$

is the input matrix,

$$\mathbf{C}^* = \begin{bmatrix} \mathbf{I} & \mathbf{0} \\ \mathbf{0} & \mathbf{I} \\ -\mathbf{M}^{-1}\mathbf{K} & -\mathbf{M}^{-1}\mathbf{C} \end{bmatrix} \quad (34)$$

is the output matrix,

$$\mathbf{D}^* = \begin{bmatrix} \mathbf{0} \\ \mathbf{0} \\ \mathbf{M}^{-1}\mathbf{F} \end{bmatrix} \quad (35)$$

is the feed-through matrix,

$$\mathbf{E}^* = \begin{bmatrix} \mathbf{0} \\ \mathbf{F} \end{bmatrix} \quad (36)$$

is the disturbance location matrix,

$$\mathbf{F} = \begin{bmatrix} -1 & 1 & 0 \\ 0 & -1 & 1 \\ 0 & 0 & -1 \end{bmatrix} \quad (37)$$

is the location matrix that a Chevron brace is located within the building structure, \mathbf{n} is the noise vector, z_1 and z_4 are the displacement and the velocity at the 1st floor level of the three-story building structure, respectively, \mathbf{I} is the identity matrix, and $\mathbf{0}$ is the zero matrix. Note that in the earthquake engineering applications, the earthquake disturbance excites all the floor levels within the building structure as the inertia forces, i.e. is a 3×1 vector with the same component of the 1940 El-Centro earthquake. Properties of the three story building structure are adopted from a scaled model (Dyke et al. 1996) of a prototype building structure that was developed by Chung et al. (1989). The mass of each floor $m_1 = m_2 = m_3 = 98.3$ kg; the stiffness of each story $k_1 = 516,000$ N/m, $k_2 = 684,000$ N/m, and $k_3 = 684,000$ N/m; and the damping coefficients of each floor $c_1 = 125$ Ns/m, $c_2 = 50$ Ns/m, and $c_3 = 50$ Ns/m. In addition, a SD-1000 MR damper whose parameters are given in Table 1 is installed on the 1st floor level using a Chevron brace, which leads to a nonlinear dynamic model, i.e., a building-MR damper system. Based on the physical model, a set of input-output data is generated for training the proposed HRC MIMO ARX-TS fuzzy system identification procedures. Note that it is challenging to identify \mathbf{M} , \mathbf{C} , and \mathbf{K} matrices through a linear time-invariant (LTI) model framework because the building structures employing MR dampers are nonlinear time-varying systems. Therefore, it is recommended to develop a nonlinear time-varying model framework for modeling the building-MR damper system.

5.4. Simulation Results

To demonstrate the effectiveness of the proposed HRC MIMOARX-TS fuzzy models, a three-story building structure employing an MR damper is investigated. Two input signals, which are a disturbance signal and a control signal, are applied to the benchmark three-story building structure to generate output data. Figure 3 shows the first input signal, which is an artificial earthquake used as a disturbance input signal such that the spectrum of the random signal includes the frequency characteristics of the earthquake ground acceleration. The second input is the MR damper force signal as shown in Figure 4. On the other hand, the 3rd floor acceleration and the 1st floor displacement responses are selected as output signals.

The model order of the MIMOARX-TS fuzzy model is chosen to be $n = m = 2$. Note that the number and the type of the MFs are determined via trial-and-errors. Although the architecture of the MIMOARX-TS fuzzy model can be optimized via an optimization procedure (e.g., genetic algorithm), it is beyond the scope of the present chapter. However, the authors intend to optimize the architecture of the MIMO ARX-TS fuzzy model in near future. Note that the performance of the identified model can be improved by increasing either the order of the MIMO ARX-TS fuzzy model or the number of the MFs, resulting in the larger dimension of the fuzzy rule base. Figure 5 and Figure 6 compare the displacement and acceleration responses of the original simulation model with those of the identified HRC MIMO ARX-TS fuzzy model, respectively. As can be seen from the figures, overall good agreements between the original values and the identified HRC MIMO ARX-TS fuzzy models are found in the time histories of both displacement and acceleration responses.

Table 2 shows the error of the identified MIMO ARX-TS fuzzy model: represents the mean

Table 1. Parameters for SD-1000 MR damper model

Parameter	Value	Parameter	Value
c_{BW}^{0a}	21.0 Nscm ⁻¹	α_a	140 Ncm ⁻¹
c_{BW}^{0b}	3.50 Nscm ⁻¹ V ⁻¹	α_b	695 Ncm ⁻¹ V ⁻¹
k_{BW}^0	46.9 Ncm ⁻¹	γ	363 cm ⁻²
c_{BW}^{1a}	283 Nscm ⁻¹	β	363 cm ⁻²
c_{BW}^{1b}	2.95 Nscm ⁻¹ V ⁻¹	A_{BW}	301
k_{BW}^1	5.00 Ncm ⁻¹	l	2
x_{BW}^0	14.3 cm	η	190 s ⁻¹

Table 2. Error quantities of the MIMO ARX-TS fuzzy model

	Fuzzy C-means Clustering		Hierarchical Clustering		Subtractive Clustering	
	\hat{y}_1	\hat{y}_2	\hat{y}_1	\hat{y}_2	\hat{y}_1	\hat{y}_2
$E[(\tilde{y} - \hat{y})^2]$	3.194 × 10⁻⁴	0.468	3.685×10^{-4}	0.460	5.354×10^{-4}	0.666
$\left[1 - \frac{ \tilde{y} - \hat{y} }{ \tilde{y} - \bar{y} }\right] \times 100$	81.540	78.881	80.492	78.947	78.756	76.379

Figure 3. Artificial earthquake

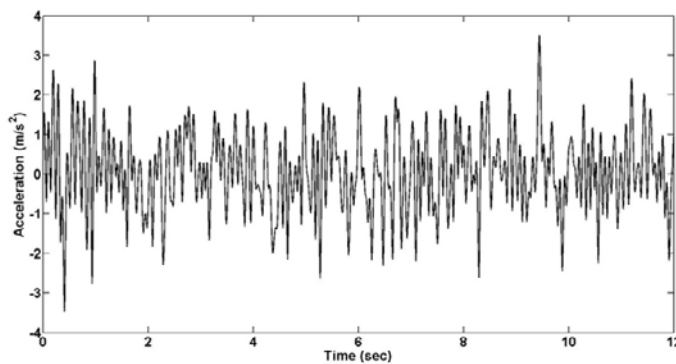


Figure 4. Magnetorheological (MR) damper force

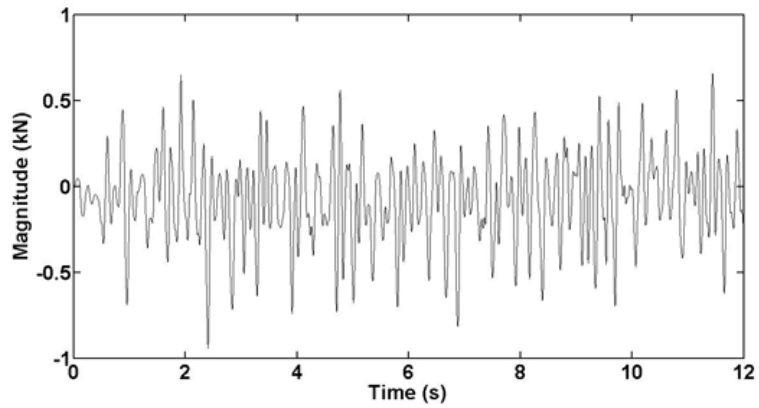


Figure 5. Comparison of original data and MIMO ARX-TS fuzzy model: Displacement

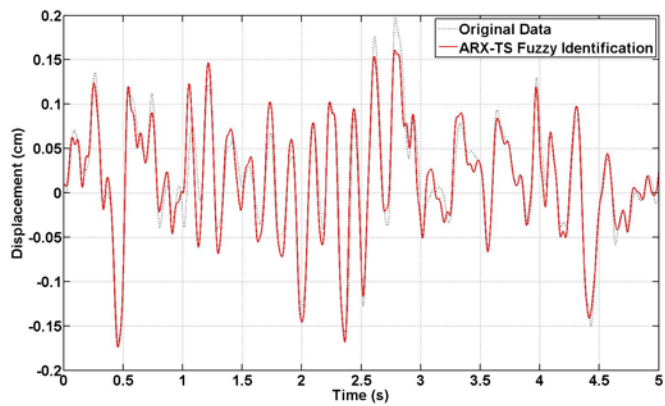
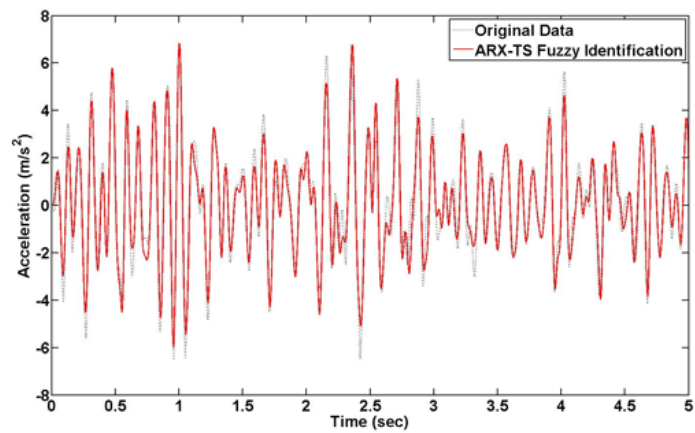


Figure 6. Comparison of original data and MIMO ARX-TS fuzzy model: Acceleration



squared errors (MSE); is the fitting rate (FR), e.g., if the proposed fuzzy models produce the same responses as the simulation model, FR is 100; is the output of the proposed MIMO ARX-TS fuzzy models; and are the output data from the simulation model and the associated mean value, respectively. The performance of the proposed HRC approach is compared with benchmark clustering algorithms, the fuzzy C-means and the subtractive clustering techniques. It is found from Table 2 that the proposed HRC MIMO ARX-TS fuzzy model outperforms over the other methods in terms of acceleration responses (i.e.,). The performance of identifying displacement (i.e.,) and acceleration responses using the proposed HRC MIMO ARX-TS fuzzy model is much better than the one of the subtractive clustering-based approach. It is, however, shown from the table that the identified displacement response of the fuzzy C-means clustering-based approach is better than that of the proposed HRC MIMO ARX-TS fuzzy model. In other words, the proposed HRC-approach effectively identifies the acceleration responses while the fuzzy C-means clustering approach better captures the behavior of displacement responses. Note that accelerometers are selected in the field of large-scale civil infrastructures in general in order to implement structural control systems and/or structural health monitoring systems because the acceleration responses are readily available, compared to other quantities such as displacements and velocities.

6. FUTURE RESEARCH DIRECTIONS

In near future, the authors intend to optimize the architecture of the proposed HRC MIMO ARX-TS fuzzy model. Also, it is recommended that the proposed models be validated using a variety of other disturbance signals.

7. CONCLUSION

In this chapter, a nonlinear fuzzy logic modeling framework has been proposed to model nonlinear behavior of structural systems employing smart control devices: the hierarchical clustering-based (HRC) multi-input, multi-output (MIMO) Autoregressive eXogenous (ARX) Takagi-Sugeno (TS) fuzzy model (HRC MIMO ARX-TS fuzzy model). The HRC MIMO ARX-TS fuzzy model is developed through the integration of the HRC technique, a family of local linear ARX input models, TS fuzzy model and weighted least squares estimator. The proposed modeling framework can be directly applied to the structure-MR damper system without the decoupling process because it is inherently a nonlinear system identification (SI) method; 2) it is more appropriate to identify incomplete and incoherent measurements of large civil structures than typical parametric SI approaches; and 3) it provides a systematic design framework for the parallel distributed compensation (PDC)-based nonlinear TS fuzzy controller. To demonstrate the effectiveness of the proposed HRC MIMO ARX-TS fuzzy model, a seismically excited building-MR damper system is investigated. It is demonstrated from the time history response analysis that the proposed fuzzy model is effective in identifying nonlinear behavior of the building-MR damper system subjected to earthquakes.

REFERENCES

- Abonyi, J., Babuska, R., Verbruggen, H. B., & Szeifert, F. (2000). Incorporating prior knowledge in fuzzy model identification. *International Journal of Systems Science*, 31, 657–667. doi:10.1080/002077200290966

- Adeli, H., & Jiang, X. (2006). Dynamic fuzzy wavelet neural network model for structural system identification. *Journal of Structural Engineering*, 132, 102–111. doi:10.1061/(ASCE)0733-9445(2006)132:1(102)
- Ahlawat, A. S., & Ramaswamy, A. (2004). Multiobjective optimal fuzzy logic control system for response control of wind-excited tall buildings. *Journal of Engineering Mechanics*, 130, 524–530. doi:10.1061/(ASCE)0733-9399(2004)130:4(524)
- Al-Dawod, M., Samali, B., Kwok, K. C. S., & Naghdy, F. (2004). Fuzzy controller for seismically excited nonlinear buildings. *Journal of Engineering Mechanics*, 130, 407–415. doi:10.1061/(ASCE)0733-9399(2004)130:4(407)
- Åström, K. J., & Eykhoff, P. (1971). System identification-A survey. *Automatica*, 7, 123–162. doi:10.1016/0005-1098(71)90059-8
- Bani-Hani, K., Ghaboussi, J., & Schneider, S. P. (1999). Experimental study of identification and control of structures using neural network Part 1: Identification. *Earthquake Engineering & Structural Dynamics*, 28, 995–1018. doi:10.1002/(SICI)1096-9845(199909)28:9<995::AID-EQE851>3.0.CO;2-8
- Battaini, M., Casciati, F., & Faravelli, L. (2004). Controlling wind response through a fuzzy controller. *Journal of Engineering Mechanics*, 130, 486–491. doi:10.1061/(ASCE)0733-9399(2004)130:4(486)
- Casciati, F. (1997). Checking the stability of a fuzzy controller for nonlinear structures. *Microcomputers in Civil Engineering*, 12, 205–215. doi:10.1111/0885-9507.00057
- Chassiakos, A. G., & Masri, S. F. (1996). Identification of structural systems by neural networks. *Mathematics and Computers in Simulation*, 40, 637–656. doi:10.1016/0378-4754(95)00012-7
- Chen, Y., Yang, B., Abraham, A., & Peng, L. (2007). Automatic design of hierarchical Takagi-Sugeno type fuzzy systems using evolutionary algorithms. *IEEE Transactions on Fuzzy Systems*, 15, 385–397. doi:10.1109/TFUZZ.2006.882472
- Choi, K. M., Cho, S. W., Jung, H. J., & Lee, I. W. (2004). Semi-active fuzzy control for seismic response reduction using magnetorheological dampers. *Earthquake Engineering & Structural Dynamics*, 33, 723–736. doi:10.1002/eqe.372
- Chung, L. L., Lin, R. C., Soong, T. T., & Reinhorn, A. M. (1989). Experiments on active control for MDOF seismic structures. *Journal of Engineering Mechanics*, 115, 1609–1627. doi:10.1061/(ASCE)0733-9399(1989)115:8(1609)
- Clauzel, A., Moore, C., & Newman, M. E. J. (2008). Hierarchical structure and the prediction of missing links in networks. *Nature*, 453, 98–101. doi:10.1038/nature06830
- Dounis, A. I., Tiropanis, P., Syrcos, G. P., & Tseles, D. (2007). Evolutionary fuzzy logic control of base-isolated structures in response to earthquake activity. *Structural Control and Health Monitoring*, 14, 62–82. doi:10.1002/stc.83
- Du, H., & Zhang, N. (2008). Application of evolving Takagi-Sugeno fuzzy model to nonlinear system identification. *Applied Soft Computing*, 8, 676–686. doi:10.1016/j.asoc.2007.05.006
- Dyke, S. J., Spencer, B. F. Jr, Sain, M. K., & Carlson, J. D. (1996). Modeling and control of magnetorheological dampers for seismic response reduction. *Smart Materials and Structures*, 5, 565–575. doi:10.1088/0964-1726/5/5/006
- Dyke, S. J., Spencer, B. F. Jr, Sain, M. K., & Carlson, J. D. (1998). An experimental study of MR dampers for seismic protection. *Smart Materials and Structures*, 7, 693–703. doi:10.1088/0964-1726/7/5/012

- Faravelli, L., & Rossi, R. (2002). Adaptive fuzzy control: Theory versus implementation. *Journal of Structural Control*, 9, 59–73. doi:10.1002/stc.5
- Filev, D. P. (1991). Fuzzy modeling of complex systems. *International Journal of Approximate Reasoning*, 5, 281–290. doi:10.1016/0888-613X(91)90013-C
- Gauss, K. F. (1963). *Theory of the motion of the heavenly bodies moving about the sun in conic sections: A Translation of Theoria Motus*. New York, NY: Dover Publications.
- Gu, Z. Q., & Oyadji, O. (2008). Application of MR damper in structural control using ANFIS method. *Computers & Structures*, 86, 427–436. doi:10.1016/j.compstruc.2007.02.024
- Hung, S. L., Huang, C. S., Wen, C. M., & Hsu, Y. C. (2003). Nonparametric identification of a building structure from experimental data using wavelet neural network. *Computer-Aided Civil and Infrastructure Engineering*, 18, 356–368. doi:10.1111/1467-8667.t01-1-00313
- Hurlebaus, S., & Gaul, L. (2006). Smart structure dynamics. *Mechanical Systems and Signal Processing*, 20, 255–281. doi:10.1016/j.ymssp.2005.08.025
- Jang, J. S. R., Sun, C. T., & Mizutani, E. (1997). *Neuro-fuzzy and soft computing: A computational approach to learning and machine intelligence*. Upper Saddle River, NJ: Prentice Hall.
- Jang, J. S. R., Sun, C. T., & Mizutani, E. (1997). *Neuro-fuzzy and soft computing*. Upper Saddle River, NJ: Prentice Hall.
- Jiang, X., & Adeli, H. (2005). Dynamic wavelet neural network for nonlinear identification of highrise buildings. *Computer-Aided Civil and Infrastructure Engineering*, 20, 316–330. doi:10.1111/j.1467-8667.2005.00399.x
- Johansen, T. A. (1994). Fuzzy model based control: Stability, robustness, and performance issues. *IEEE Transactions on Fuzzy Systems*, 2, 221–234. doi:10.1109/91.298450
- Johansen, T. A., & Babuška, R. (2003). Multi-objective identification of Takagi-Sugeno fuzzy models. *IEEE Transactions on Fuzzy Systems*, 11, 847–860. doi:10.1109/TFUZZ.2003.819824
- Kerber, F., Hurlebaus, S., Beadle, B. M., & Stöbener, U. (2007). Control concepts for an active vibration isolation system. *Mechanical Systems and Signal Processing*, 21, 3042–3059. doi:10.1016/j.ymssp.2007.04.003
- Kim, H. S., & Roschke, P. N. (2006). Design of fuzzy logic controller for smart base isolation system using genetic algorithm. *Engineering Structures*, 28, 84–96. doi:10.1016/j.engstruct.2005.07.006
- Kim, S. B., Yun, C. B., & Spencer, B. F. Jr. (2004). Vibration control of wind-excited tall buildings using sliding mode fuzzy control. *Journal of Engineering Mechanics*, 130, 505–510. doi:10.1061/(ASCE)0733-9399(2004)130:4(505)
- Kim, Y., Hurlebaus, S., & Langari, R. (2010). Control of a seismically excited benchmark building using linear matrix inequality-based semiactive nonlinear fuzzy control. *Journal of Structural Engineering*, 136, 1023–1026. doi:10.1061/(ASCE)ST.1943-541X.0000192
- Kim, Y., Langari, R., & Hurlebaus, S. (2009). Semiactive nonlinear control of a building using a magnetorheological damper system. *Mechanical Systems and Signal Processing*, 23, 300–315. doi:10.1016/j.ymssp.2008.06.006
- Kim, Y., Langari, R., & Hurlebaus, S. (2010). Model-based multi-input, multi-output supervisory semiactive nonlinear fuzzy controller. *Computer-Aided Civil and Infrastructure Engineering*, 25, 387–393. doi:10.1111/j.1467-8667.2009.00649.x

- Langari, R. (1999). Past, present and future of fuzzy control: A case for application of fuzzy logic in hierarchical control. *Proceedings, 18th International Conference of the North American Fuzzy Information Processing Society-NAFIPS*, New York City, New York, (pp.760-765).
- Lin, J. W., & Betti, R. (2004). On-line identification and damage detection in non-linear structural systems using a variable forgetting factor approach. *Earthquake Engineering & Structural Dynamics*, 33, 419–444. doi:10.1002/eqe.350
- Lin, J. W., Betti, R., Smyth, A. W., & Longman, R. W. (2001). On-line identification of non-linear hysteretic structural systems using a variable trace approach. *Earthquake Engineering & Structural Dynamics*, 30, 1279–1303. doi:10.1002/eqe.63
- Liu, W. Y., Xiao, C. J., Wang, B. W., Shi, Y., & Fang, S. F. (2003). Study on combining subtractive clustering with fuzzy c-means clustering. *Proceedings of Second International Conference on Machine Learning and Cybernetics*, Xi'an, China, (pp. 2659-2662).
- Loh, C. H., Wu, W. Y., & Lin, P. Y. (2003). Displacement control of isolated structures with semi-active control devices. *Journal of Structural Control*, 10, 77–100. doi:10.1002/stc.18
- Masri, S. F., Smyth, A. W., Chassiakos, A. G., Caughey, T. K., & Hunter, N. F. (2000). Application of neural networks for detection of changes in nonlinear systems. *Journal of Engineering Mechanics*, 126, 666–676. doi:10.1061/(ASCE)0733-9399(2000)126:7(666)
- Moon, F. L., & Aktan, A. E. (2006). Impacts of epistemic (bias) uncertainty on structural identification of constructed (civil) systems. *The Shock and Vibration Digest*, 38, 399–420. doi:10.1177/0583102406068068
- Nomura, Y., Furuta, H., & Hirokane, M. (2007). An integrated fuzzy control system for structural vibration. *Computer-Aided Civil and Infrastructure Engineering*, 22, 306–316. doi:10.1111/j.1467-8667.2007.00487.x
- Pedrycz, W. (1984). An identification algorithm in fuzzy relational systems. *Fuzzy Sets and Systems*, 13, 153–167. doi:10.1016/0165-0114(84)90015-0
- Pourzeynali, S., Lavasani, H. H., & Modarayi, A. H. (2007). Active control of high rise building structures using fuzzy logic and genetic algorithms. *Engineering Structures*, 29, 346–357. doi:10.1016/j.engstruct.2006.04.015
- Ramallo, J. C., Yoshioka, H., & Spencer, B. F. Jr. (2004). A two-step identification technique for semiactive control systems. *Structural Control and Health Monitoring*, 11, 273–289. doi:10.1002/stc.43
- Schurter, K. C., & Roschke, P. N. (2001). Neuro-fuzzy control of structures using magnetorheological dampers. *Proceedings of the American Control Conference*, Arlington, Virginia, (pp. 1097-1102).
- Sharifi, R., Kim, Y., & Langari, R. (2010). Sensor fault isolation and detection of smart structures. *Smart Materials and Structures*, 19, 1–15. doi:10.1088/0964-1726/19/10/105001
- Shook, D. A., Roschke, P. N., Lin, P. Y., & Loh, C. H. (2008). GA-optimized fuzzy logic control of a large-scale building for seismic loads. *Engineering Structures*, 30, 436–449. doi:10.1016/j.engstruct.2007.04.008
- Smith, A. H., & Chase, J. G. (1993). Identification of structural system parameters using the cascade-correlation neural network. *Journal of Dynamic Systems, Measurement, and Control*, 116, 790–792. doi:10.1115/1.2899280

- Spencer, B. F. Jr, Dyke, S. J., Sain, M. K., & Carlson, J. D. (1997). Phenomenological model for magnetorheological dampers. *Journal of Engineering Mechanics*, 123, 230–238. doi:10.1061/(ASCE)0733-9399(1997)123:3(230)
- Subramaniam, R. S., Reinhorn, A. M., Riley, M. A., & Nagarajaiah, S. (1996). Hybrid control of structures using fuzzy logic. *Microcomputers in Civil Engineering*, 11, 1–17. doi:10.1111/j.1467-8667.1996.tb00305.x
- Symans, M., & Kelly, S. W. (1999). Fuzzy logic control of bridge structures using intelligent semi-active seismic isolation systems. *Earthquake Engineering & Structural Dynamics*, 28, 37–60. doi:10.1002/(SICI)1096-9845(199901)28:1<37::AID-EQE803>3.0.CO;2-Z
- Takagi, T., & Sugeno, M. (1985). Fuzzy identification of systems and its applications to modeling and control. *IEEE Transactions on Systems, Man, and Cybernetics*, 15, 116–132.
- Tanaka, K., & Sugeno, M. (1992). Stability analysis and design of fuzzy control systems. *Fuzzy Sets and Systems*, 45, 135–156. doi:10.1016/0165-0114(92)90113-I
- Tani, A., Kawamura, H., & Ryu, S. (1998). Intelligent fuzzy optimal control of building structures. *Engineering Structures*, 20, 184–192. doi:10.1016/S0141-0296(97)00077-1
- Wang, A. P., & Lee, C. D. (2002). Fuzzy sliding mode control for a building structure based on genetic algorithms. *Earthquake Engineering & Structural Dynamics*, 31, 881–895. doi:10.1002/eqe.127
- Wang, L., & Langari, R. (1995). Decomposition approach for fuzzy systems identification. *Proceedings of the 34th IEEE Conference on Decision and Control*, New Orleans, LA, USA, (pp. 261-265).
- Wang, L., & Langari, R. (1996). Complex systems modeling via fuzzy logic. *IEEE Transactions on Systems, Man, and Cybernetics. Part B, Cybernetics*, 26, 100–106. doi:10.1109/3477.484441
- Ward, J. H. Jr. (1963). Hierarchical grouping to optimize an objective function. *Journal of the American Statistical Association*, 58, 236–244. doi:10.2307/2282967
- Yager, R. R., & Filev, D. P. (1993). Unified structure and parameter identification of fuzzy models. *IEEE Transactions on Systems, Man, and Cybernetics*, 23, 1198–1205. doi:10.1109/21.247902
- Yan, G., & Zhou, L. L. (2006). Integrated fuzzy logic and genetic algorithms for multi-objective control of structures using MR dampers. *Journal of Sound and Vibration*, 296, 368–382. doi:10.1016/j.jsv.2006.03.011
- Yang, G., Spencer, B. F. Jr, Carlson, J. D., & Sain, M. K. (2002). Large-scale MR fluid dampers: Modeling and dynamic performance considerations. *Engineering Structures*, 24, 309–323. doi:10.1016/S0141-0296(01)00097-9
- Yang, Y. N., & Lin, S. (2004). On-line identification of non-linear hysteretic structures using an adaptive tracking technique. *International Journal of Non-linear Mechanics*, 39, 1481–1491. doi:10.1016/j.ijnonlinmec.2004.02.010
- Yang, Y. N., & Lin, S. (2005). Identification of parametric variations of structures based on least squares estimation and adaptive tracking technique. *Journal of Engineering Mechanics*, 131, 290–298. doi:10.1061/(ASCE)0733-9399(2005)131:3(290)
- Yen, J., & Langari, R. (1998). *Fuzzy logic-intelligence, control, and information*. Upper Saddle River, NJ: Prentice Hall.

- Yi, F., Dyke, S. J., Caicedo, J. M., & Carlson, J. D. (2001). Experimental verification of multinput seismic control strategies for smart dampers. *Journal of Engineering Mechanics*, 127, 1152–1164. doi:10.1061/(ASCE)0733-9399(2001)127:11(1152)
- Zadeh, L. A. (1965). Fuzzy sets. *Information and Control*, 8, 338–353. doi:10.1016/S0019-9958(65)90241-X

Chapter 14

Health Assessment of Engineering Structures Using Graphical Models

Abbas Moustafa

Minia University, Egypt

Sankaran Mahadevan

Vanderbilt University, USA

ABSTRACT

A hybrid qualitative-quantitative health assessment of structures using the bond graph theory is presented in this chapter. Bond graph (BG) is an energy-based graphical-modeling tool for physical dynamic systems, actuators, and sensors. BG provides domain-independent framework for modeling dynamic systems with interacting components from multiple domains. Discrete structures are modeled using one-to-one bond graph elements, while continuous structures are modeled using finite-mode bond graphs. BG facilitates the construction of temporal causal graph (TCG) that links the system response to the damaged component or faulty sensor. TCG provides qualitative damage isolation, which is not possible using most existing system identification techniques. This leads to rapid isolation of damage and significant reduction in computations. Quantitative identification of damage size is performed by analyzing the substructure containing the damaged component, using the nonlinear least-squares optimization technique, thus reducing the computations. The health assessment algorithm developed in this chapter combines the Generic Modeling Environment (GME), the Fault Adaptive Control Technology (FACT) software, and Matlab Simulink®. Numerical illustrations on BG modeling of a hydraulic actuator and system identification of a fifteen-story shear building and a high-rise structure under earthquake loads are provided.

DOI: 10.4018/978-1-4666-1640-0.ch014

1. INTRODUCTION

This chapter proposes a graphical, domain-independent, energy-based framework that is capable of modeling multidisciplinary systems with interacting components from structural, mechanical, electrical, and hydraulic domains. This framework is based on the bond graph (BG) theory introduced by Paynter (1961) and developed by Karnopp, Rosenberg and Margolis (Rosenberg & Karnopp 1983, Karnopp & Margolis, 2006). For example, an electrical circuit and a mechanical system can be described with the same bond graph model. The use of bond graphs in electrical and mechanical engineering is well established. This method, however, has not received significant research attention in civil engineering. The BG model of a dynamic system represents the system equations of motion implicitly in a graphical form using bond graph elements. These elements model inertial, stiffness, damping and external forces. BG elements include serial and parallel junctions that govern the dynamic equilibrium of the structure subsystems.

Civil structures deteriorate over time and experience damage due to natural events such as earthquakes and wind. Structural health monitoring (SHM) is a process that aims at providing accurate and in-time information of the structural health condition of existing structures. A comprehensive review on recent advances in health assessment of structures can be found in Doebling et al (1998), Alvin et al (2003), Chang et al (2003), Koh et al (2003), Lui & Ge (2005), Gonzalez & Zapico (2008) and Moustafa et al (2010). System identification (SI) techniques can be grouped into parametric and non-parametric methods. The parametric methods identify changes in the structure global parameters (e.g. natural frequencies, mode shapes and modal damping) or in the local parameters (e.g. members stiffnesses and damping) to characterize the structural damage (Doebling et al 1998, Alvin et al. 2003, Chang et al, 2003, Koh et al, 2003, Lui & Ge,

2005). In general, the parametric methods can detect the damage location but require complete measurements and extensive computations for large structures. The non-parametric methods, on the other hand, require less measurement and have better adaptability to large structures but provide a global assessment on the health status of the structure (Gonzalez & Zapico, 2008).

Sensor performance also degrades with time under varying environmental conditions (Koh et al, 2003, De Oliveira et al, 2004, Elouedi et al, 2004, Blackshire et al, 2006, Glisic & Inaudi 2007). Different degradation mechanisms have been observed in different types of sensors (surface-bonded or fully-embedded) under various environmental effects such as temperature- and moisture-cycling (Elouedi et al, 2004, Blackshire et al, 2006, Glisic & Inaudi 2007). Sensor performance is particularly relevant in the field of road infrastructure where the loading conditions affecting the main structure (traffic loads, temperature cycling, etc.) also affect the sensor measurements. Details on recent sensor technologies can be found in (Ansari 2005, Manders et al, 2006). While sensor faults are difficult to be handled using existing SI techniques, bond graphs are capable of modeling both the system components and the sensors. This enables damage detection in both structural components and sensors. Bond graphs facilitate also the extraction of damage signatures off-line before sensor data collection thus providing rapid identification of the damage location through qualitative comparison of predicted and observed signatures. The quantification of the damage size is performed by analyzing the substructure containing the damaged component only, thus, reducing the computational costs. The idea of using BG in system identification of frame structures was introduced by these authors (Moustafa et al, 2010).

The bond graph technique is different from most existing SI methods since it provides: (1) graphical-modeling tool for dynamic systems under time-varying loads, (2) domain-independent modeling tool for dynamic analysis and health

assessment of physical systems across multiple domains, (3) rapid qualitative identification of damage locations, (4) the ability to identify sensor faults, (5) the ability to perform online diagnosis based on continuous monitoring, (6) reduction of data processing errors due to absence of transformation to frequency domain or approximations in feature selection, and (7) rapid quantification of damage size since only the substructure containing damage is analyzed. Finally, it may be noted that the research carried out in this chapter represents a novel application of bond graphs and structural optimization to the health assessment of frame structures under earthquake loads. The next section provides a brief overview on bond graph theory.

2. BOND GRAPH THEORY AND TERMINOLOGY

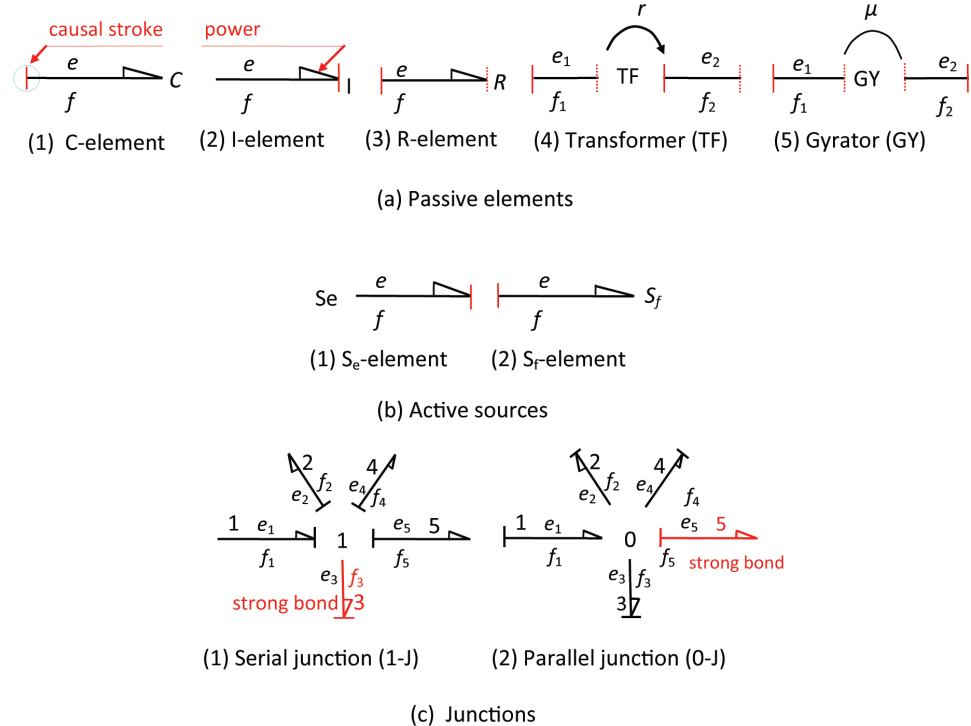
Bond graph is a graphical domain-independent framework capable of modeling dynamic systems across multiple domains (e.g. structural, electrical, mechanical, and hydraulic), thus providing a unified framework for dynamic analysis and SI of multidisciplinary systems. For instance, a hydraulic actuator composed of electrical, hydraulic and mechanical components can be modeled easily using bond graphs. Bond graph is a domain-independent framework. For instance, a SDOF mechanical system and an electrical circuit can be represented using the same bond graph model (an example is given later). The BG theory is based on the energy conservation and energy exchange among system components. Irrespective of the domain, power is the product of the two conjugate variables effort e and flow f . In structural and mechanical systems, e and f describe the force and velocity (for translation) or torque and angular velocity (for rotation) at a point in the system. In each domain there is such a combination of variables for which a physical interpretation exists. In electrical networks, e and f are voltage and current. In hydraulics, they are pres-

sure and volume flow, and for thermodynamic systems, they are temperature and entropy flow.

Bond graph elements consist of five primitives (passive elements), two ideal sources (active elements), and two junctions (see Figure 1). The five primitives are the Capacitance (C), the Inertance (I), the Resistor (R), the transformer (TF) and the Gyrator (GY). The source elements are the effort source S_e and the flow source S_f , which produce energy. The two junctions are the serial junction (1-J) and the parallel junction (0-J), which connect various elements together. Bonds are energy transfer pathways that connect elements and junctions and are represented as half arrows. This half arrow defines the positive direction of energy flow. Effort and flow signals are the information transferred through these pathways. Figure 2 shows the tetrahedron state demonstrating the relations related by C-, I-, and R-elements in structural engineering setting (Paynter 1961). The vertices represent the pair, effort and momentum and the pair, flow and displacement. The associated directed arrows imply that momentum and displacement are computed by integrating effort and flow, respectively. I- and C-elements represent the state variables of the system that accumulate net flow (I-element stores momentum and C-element stores displacement). Brief descriptions of bond graph elements are provided below with emphasis on translating concepts to structural engineering (see Table 1 and Figure 1).

1. **C-element (Figure a(1)):** C-element relates effort to time integral of flow (i.e., displacement) and is used to model linear or rotational springs, or stiffness of a structural member. The constitutive relation for a spring modeled as a C-element is $e = 1 / C \int_{-\infty}^t f dt$, where e is the force in the spring, f is the velocity and C is a constant ($k = 1 / C$ = stiffness). The C-element receives flow (cause) and produces effort

Figure 1. Bond graph elements: (a) passive elements (b) active sources (c) junctions



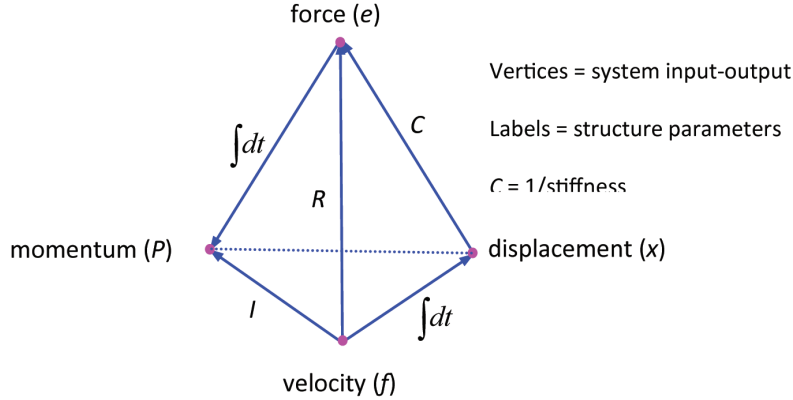
- (effect). The small vertical line in Figure a(1) is the causal stroke representing the integral causality relation (constitutive equation). The half arrow defines the direction of power flow (power = $e \times f$).
2. **I-element (Figure 1(a2)):** I-element models inertial effects in structural systems, and inductance effects in electrical or fluid systems. For a mass m subjected to a force p ,
$$f = (1/m) \int_{-\infty}^t e dt = (1/m) \int_{-\infty}^t p dt .$$

This relation represents the Newton's second law of motion. Herein, the effort history is integrated to generate flow thus I-element receives effort (cause) and generates flow (effect).

 3. **R-element (Figure 1(a3)):** R-element models energy dissipation components, such as, dampers, dashpots, electrical resistors and valves or losses in fluid lines. For a linear

- damper, e and f are related through a linear relation ($e = R f$). R-elements can have the causal stroke at either ends.
4. **TF-element (Figure 1(a4)):** TF-element can represent an ideal electrical transformer or a massless lever. It can also represent the mode shape at a point in the structure. TF-element does not store or absorb energy. It conserves power and transmits the factors of power with power scaling as defined by the transformer modulus r . The balance relation between the power variables for the transformer of Figure 1(a4) is $e_1 f_1 = e_2 f_2$, which leads to $f_2 = r f_1$ or $e_2 = (1/r) e_1$.
 5. **GY-element (Figure 1(a5)):** The gyrator establishes the relationship between flow to effort and effort to flow, gain keeping the power on the ports the same. The simplest gyrator is a mechanical gyroscope or an ideal DC motor. Gyrators are used when power

Figure 2. Tetrahedron of state showing the relations of state variables and the constitutive relations in structural engineering (Paynter 1961)



from one energy domain is transferred to another domain. The Gyrator modulus μ defines the relation between effort and flow. For the GY of Figure 1(a5), $e_2 = \mu f_1$ and $e_1 = \mu f_2$.

6. **Effort and flow sources (S_e , S_f) (Figures 1(b1) & 1(b2)):** These are active BG elements since they produce energy. In struc-

tural systems, S_e represents an external force, and S_f represents an input velocity to the system. The causal stroke implies that either the effort (force) or flow (velocity) is generated by the source and is imposed on the system. In either case, the half arrow is pointing away from the source indicating

Table 1. Conversion of Bond graph elements and terminology to structural engineering

Bond graph term	Corresponding term in structural engineering	Units
Capacitance (C)	Models member or spring stiffness $k = 1 / C$	N / m
Inductance (I)	Models inertia effects, mass $m = I$	N s ² / m
Resistance (R)	Models damping, friction or resistance forces $D = R$	N s / m
Transformer (TF)	Massless lever or participation factor in modal analysis	--
Gyrator (GY)	Mechanical gyrator or ideal DC motor	--
Effort (e)	Force or torque $F(t) = e(t)$	N
Flow (f)	Velocity or angular velocity $\dot{u}(t) = f(t)$	m / s
Displacement		m
Effort source S_e		--
Flow source S_f		--
Power		N m / s
Energy E	A source that exerts a force on the system (e.g. an actuator)	N m
Momentum P	A source that exerts a velocity on the system	N s
	Power = effort × flow = $e \times f$	
	$E = \int e f dt$	
	$P = \int e dt$	

that power flows from the source into the system.

7. **Serial and parallel junctions (Figures 1(c1) & 1(c2)):** A serial or 1-junction has equality of flows (velocities), and efforts (forces) sum up to zero. The equality of velocities or displacements represents the continuity condition between substructures that is known in FEM analysis. The summation represents the D'Alembert's principle that implies dynamic equilibrium of forces acting on the system or a substructure of it. This junction represents a common velocity point in a structural system. Thus, a 1-J can model the velocity at a floor level in a multi-story building.

In a 1-junction only one bond, referred to as strong bond, brings the information of flow (velocity) and other bonds receive it (i.e., only one bond is open ended and other bonds are stroked away from the junction). According to Figure 1(c1), bond 3 is the strong bond and thus the flow is governed by bond 3 and is imposed on other bonds. Conversely, the effort is determined by other bonds and is imposed on bond 3. Strong bonds are used in constructing TCG from BG as demonstrated in the next section.

The constitutive relation of power for the 1-junction of Figure 1(c1) is given by:

$$e_1 f_1 - e_2 f_2 - e_3 f_3 - e_4 f_4 - e_5 f_5 = 0 \quad (1)$$

Since the 1-junction has equality of flows, Eq. (1) leads to:

$$e_1 - e_2 - e_3 - e_4 - e_5 = 0 \quad (2)$$

Eq. (2) represents the D'Alembert's dynamic equilibrium principle. The 0-junction (0-J) is the counterpart of the 1-junction and represents common effort (force) points in the system (Figure 1(c2)). Thus a 0-J has equal efforts, and the flows

sum to zero. In a 0-J, the strong bond determines the effort at the junction and is stroked nearer to the junction. The constitutive relations for the 0-J are:

$$e_1 = e_2 = e_3 = e_4 = e_5; \quad f_1 - f_2 - f_3 - f_4 - f_5 = 0 \quad (3)$$

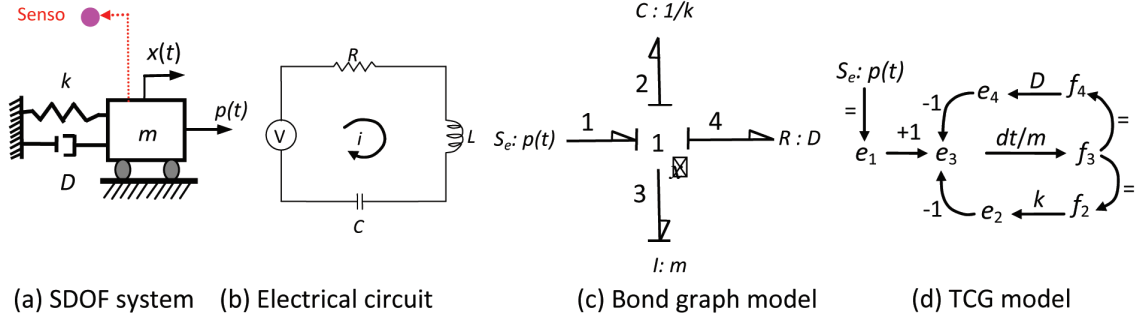
Equations (1, 2 and 3) and the constitutive equations for BG elements define the relations among the system parameters and responses, which represent the basis for the SI technique developed in this chapter.

This section provided a brief description of BG theory and terminology. The modeling of discrete systems, including SDOF and MDOF systems and an actuator composed of hydraulic and mechanical components, using bond graphs is developed in section 3. Continuous structures are tackled in Sections 3 and 4, respectively. The derivation of temporal causal graphs from bond graphs is explained in Section 5. Section 6 develops the modeling of sensors using the bond graph theory. The development of the health assessment methodology is presented in Sections 7 and 8. Numerical illustrations are provided in Section 9.

3. MODELING DISCRETE DYNAMIC STRUCTURES USING BOND GRAPHS

This section demonstrates the construction of bond graphs for discrete dynamic structures. First, we consider SDOF and MDOF structures. Subsequently, we demonstrate the modeling procedure for an actuator composed of hydraulic and mechanical components. Discrete structures are those structures having lumped properties (inertia, damping and stiffness). Verifications of bond graphs are provided by deriving the equations of motion of the structure from the bond graph model which are shown to be identical to those obtainable from structural dynamics theory.

Figure 3. Single-domain representation of mechanical and electrical systems using bond graphs



3.1 Single-Degree-of-Freedom (SDOF) System

Figure 3(a) shows a SDOF system driven by an external dynamic load $p(t)$. The system is characterized by a single flow f_3 (velocity \dot{x}) and is thus represented by a 1-junction with I-, C-, R- and Se-elements representing the inertial, spring, damping and external forces, respectively. Note that the 1-J has equal flows ($f_1 = f_2 = f_3 = f_4$) and efforts sum to zero ($e_1 - e_2 - e_3 - e_4 = 0$). The BG model of Figure 3(c) represents the equation of motion of the system in an implicit form. To derive this equation from the BG of Figure 3(c), consider the inertial force e_3 given by the constitutive relation of the I-element as:

$$m\ddot{x} = e_3 = e_1 - e_2 - e_4 \quad (4)$$

Substituting

$$\dot{x}_3 = \ddot{x}(t), \quad e_1 = p(t),$$

$$e_2 = (1/C) \int f_2 dt = kx(t), \text{ and}$$

$$e_4 = R f_4 = R f_3 = D \dot{x}(t),$$

where D is the damping coefficient, in the above equation, we get:

$$m \ddot{x}(t) + D \dot{x}(t) + k x(t) = p(t) \quad (5)$$

The free-body diagram of the forces acting on the SDOF system (dynamic equilibrium of the system using D'Alembert principle) leads to Eq. (5) obtained from the BG model of Figure 3(c). The electrical circuit of Figure 3(b) is also represented using the same bond graph model. This example demonstrates use of bond graphs as a unified tool for modeling dynamic systems from different energy domains. Note that Figure 3(d) represents the Temporal Causal Graph (TCG) which will be discussed later.

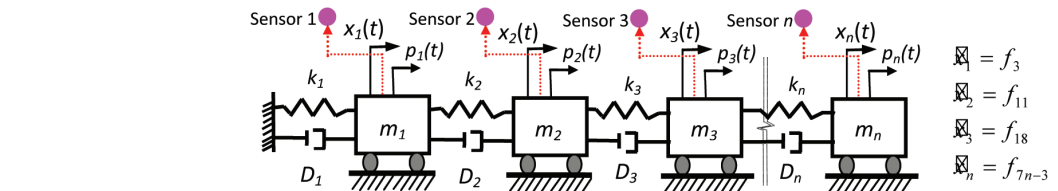
3.2 Multi-Degree-of-Freedom (MDOF) Systems

3.2.1 Construction of Bond Graph Model

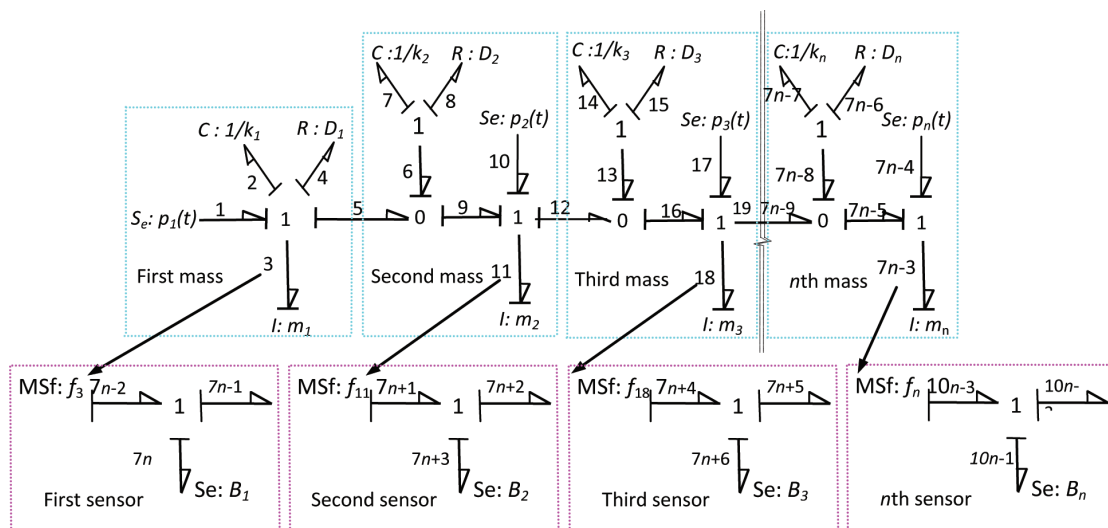
Figure 4(a) depicts an n-DOF system with each mass driven by a dynamic load $p_i(t)$ and characterized by a distinct flow or velocity $\dot{x}_i(t)$. Referring to section 3.1 and Figure 4(a), the steps of constructing bond graphs for MDOF systems can be summarized as follows:

1. Model each mass velocity as 1-J. Insert I- and Se-elements to model inertial and external forces.

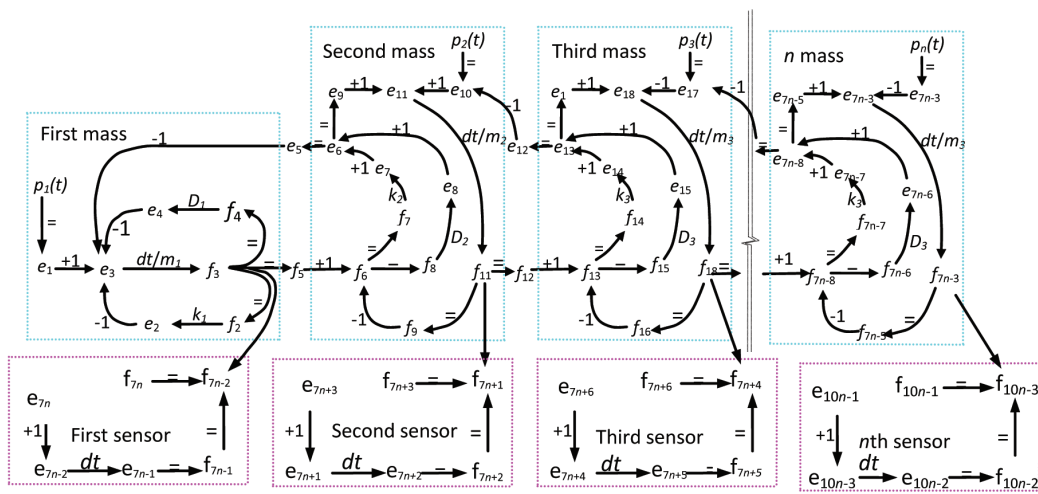
Figure 4. BG and TCG representation of MDOF discrete dynamic systems and sensors



(a) Mechanical system



(b) Bond graph model



(c) TCG model

2. Insert 0-J between 1-J to accommodate force-generating elements (stiffness and damping forces).
3. Simplify the resulting bond graph by removing the zero velocity at the support points.
4. Assign numbers, and directions to bonds using the half arrow (defines the direction of power).
5. Assign causality to bond graph elements and bonds (details provided in next subsection).

These procedures result in the lumped parameters of damping (D_1, D_2, \dots, D_n), stiffness (k_1, k_2, \dots, k_n) and inertia (m_1, m_2, \dots, m_n) being interconnected using energy conserving junctions producing the topological bond graph model shown in Figure 4(b). Each mass is represented as a separate block connected to neighboring blocks through bonds. Sensors are also modeled as separate blocks for measuring displacements and are discussed in Section 6. Note that Figure 4(c) represents the TCG which will be discussed later.

3.2.2 Causality Assignment and Bond Graph Verification

To assign causality to BGs we assign fixed causalities to sources. Integral causality is assigned to storage elements (I- and C-elements) and is propagated through junctions. I- and C-elements have integral causality since cause is integrated to provide effect. Causality is then assigned to R-elements and bonds connecting junctions. The procedure is continued until the entire BG is assigned causality.

The BG model of Figure 4(b) represents the equations of motion of the n -DOF system in an implicit form. The verification of the BG model is performed by deriving the system equations of motion from the BG and comparing them with those from structural dynamics theory. The derivation of the system equations from the bond graph is systematic and can be easily coded. The system state variables are associated with the

energy storage elements. For the I-element, the state variable is flow and for the C-element the state variable is effort. The n -DOF system has $2n$ state variables (e.g., $e_2, f_3, e_7, f_{11}, e_{14}, f_{18}, \dots$). Each flow variable represents the velocity of the associated mass and efforts represent the stiffness forces in the springs. The inertial force of the first mass is given as (bond 3) in Box 1.

Note the substitutions of equality of flows and balance of efforts at 1-junctions and equality of efforts and balance of flows at 0-junctions. Similarly, the inertial force in bond 11, (see Box 2).

Considering the inertial force of the $(n-1)^{th}$ mass, one gets: (see Box 3).

Finally, the equilibrium equation of the forces acting on the n^{th} mass can be shown to be shown in Box 4.

Combining Eqs. (6-9), the equations of motion of the n -DOF structure is given in a matrix form in Box 5.

Eq. (10) represents the well known equation of motion of the n -DOF structure derivable using structural dynamics principles (Clough & Penzien 2003, Chopra 2007). Note that, if the structure is subjected to ground acceleration $\ddot{y}(t)$, the forces at the floor levels are given as $p_i(t) = -m_i \ddot{y}(t); i = 1, 2, \dots, n$.

Thus the BG is simply a topological representation of the system equations of motion, using elements that exchange efforts and flows. The BG model is correct only if the correct equations of motion of the system can be derived from it. The above example derived the equations of motion for an n -DOF system by hand for sake of explanation. This derivation can be also automated (Manders et al, 2006).

3.3 Hydraulic Actuator System

This section illustrates the modeling of multidisciplinary dynamic systems using BG. Figure 5(a) shows a simplified model of a hydraulic actuator

Box 1.

$$\begin{aligned}
 m_1 \dot{f}_3 &= e_3 = e_1 - e_2 - e_4 - e_5 = p_1 - (1/C_1) \int f_2 dt - D_1 f_4 - e_6 = p_1 - k_1 x_1 - D_1 f_3 - e_7 - e_8 \\
 &= p_1 - k_1 x_1 - D_1 \dot{x}_1 - (1/C_2) \int f_7 dt - D_2 f_8 = p_1 - k_1 x_1 - D_1 \dot{x}_1 - k_2 \int f_6 dt - D_2 f_6 \\
 &= p_1 - k_1 x_1 - D_1 \dot{x}_1 - k_2 \int (f_5 - f_9) dt - D_2 (f_5 - f_9) \\
 &= p_1 - k_1 x_1 - D_1 \dot{x}_1 - k_2 (x_1 - x_2) - D_2 (\dot{x}_1 - \dot{x}_2) \\
 m_1 \ddot{x}_1 + (D_1 + D_2) \dot{x}_1 - D_2 \dot{x}_2 + (k_1 + k_2) x_1 - k_2 x_2 &= p_1(t)
 \end{aligned} \tag{6}$$

Box 2.

$$\begin{aligned}
 m_2 \dot{f}_{11} &= e_{11} = e_9 + e_{10} - e_{12} = e_6 + p_2 - e_{13} = e_7 + e_8 + p_2 - e_{14} - e_{15} \\
 &= (1/C_2) \int f_7 dt + D_2 f_8 + p_2 - (1/C_3) \int f_{14} dt - D_3 f_{15} \\
 &= k_2 (x_1 - x_2) + D_2 (\dot{x}_1 - \dot{x}_2) + p_2 - k_3 (x_2 - x_3) - D_3 (\dot{x}_2 - \dot{x}_3) \\
 m_2 \ddot{x}_2 - D_2 \dot{x}_1 + (D_2 + D_3) \dot{x}_2 - D_3 \dot{x}_3 - k_1 x_1 + (k_2 + k_3) x_2 - k_3 x_3 &= p_2(t)
 \end{aligned} \tag{7}$$

Box 3.

$$m_{n-1} \ddot{x}_{n-1} - D_{n-1} \dot{x}_{n-1} + (D_{n-1} + D_n) \dot{x}_{n-1} - D_n \dot{x}_n - k_{n-1} x_{n-1} + (k_{n-1} + k_n) x_{n-1} - k_n x_n = p_{n-1}(t) \tag{8}$$

Box 4.

$$m_n \ddot{x}_n - D_n \dot{x}_{n-1} + D_n \dot{x}_n - k_n x_{n-1} + k_n x_n = p_n(t) \tag{9}$$

Box 5.

$$\begin{aligned}
 &\left[\begin{array}{cccccc} m_1 & 0 & 0 & \dots & 0 & 0 \\ 0 & m_2 & 0 & \dots & 0 & 0 \\ \dots & \dots & \dots & \dots & \dots & \dots \\ 0 & 0 & 0 & \dots & m_{n-1} & 0 \\ 0 & 0 & 0 & \dots & 0 & m_n \end{array} \right] \begin{bmatrix} \ddot{x}_1(t) \\ \ddot{x}_2(t) \\ \dots \\ \ddot{x}_{n-1}(t) \\ \ddot{x}_n(t) \end{bmatrix} + \begin{bmatrix} D_1 + D_2 & -D_2 & 0 & \dots & 0 & 0 & 0 \\ -D_2 & D_2 + D_3 & -D_3 & \dots & 0 & 0 & 0 \\ \dots & \dots & \dots & \dots & \dots & \dots & \dots \\ 0 & 0 & 0 & \dots & -D_{n-1} & D_{n-1} + D_n & -D_n \\ 0 & 0 & 0 & \dots & 0 & -D_n & D_n \end{bmatrix} \begin{bmatrix} \dot{x}_1(t) \\ \dot{x}_2(t) \\ \dots \\ \dot{x}_{n-1}(t) \\ \dot{x}_n(t) \end{bmatrix} \\
 &\begin{bmatrix} k_1 + k_2 & -k_2 & 0 & \dots & 0 & 0 \\ -k_2 & k_2 + k_3 & -k_3 & \dots & 0 & 0 \\ \dots & \dots & \dots & \dots & \dots & \dots \\ 0 & 0 & 0 & \dots & -k_{n-1} & k_{n-1} + k_n \\ 0 & 0 & 0 & \dots & 0 & -k_n \end{bmatrix} \begin{bmatrix} x_1(t) \\ x_2(t) \\ \dots \\ x_{n-1}(t) \\ x_n(t) \end{bmatrix} = \begin{bmatrix} p_1(t) \\ p_2(t) \\ \dots \\ p_{n-1}(t) \\ p_n(t) \end{bmatrix}
 \end{aligned} \tag{10}$$

(used in aircrafts) with interacting components from mechanical and hydraulic domains. The actuator is composed of a single chamber and a piston of cross-sectional area A. The amount of fluid entering the chamber q_{in} through a hydraulic pump is controlled by the control valve. The pressure difference between right and left sides of the chamber ($p_r - p_l$) results in a force that controls the movement of the piston a distance $u(t)$. The piston is attached by a rigid rod to a mass M that is connected to a spring and a damper which model the aerodynamic effects. The displacement is controlled either manually or automatically based on a feedback system. The description of the actuator parameters are given in Table 2.

The bond graph model for the actuator of Figure 5(a) is shown in Figure 5(b). Note that Figure 5(c) represents the TCG which will be discussed later. The reservoir is represented by an effort source Se and the pump is represented by a transformer TF₁ with efficiency parameter PE. The valve is represented by a resistor $R_1 = R_v$. The difference in the chamber's pressure $p_r - p_l$ (i.e. e_3) is represented by a 0-Junction that ensures equal pressures ($e_3 = e_4 = e_5$). The fluid compressibility is represented by a C-element $C_1 = V_0\beta$. The pressure difference in bond 5 ($e_5 = p_r - p_l = e_3 = e_4$) is multiplied by the cross-sectional area of the piston A to provide the force acting on the mass M. This is represented by the transformer element TF₂, connecting bonds 5 and 6, with the transformer parameter A. The inertial effect of the mass M is modeled by an I-element. The spring is represented by a C-element and the damper is represented by an R-element $R_2 = B$. The displacement $u(t)$ is the time integral of the flow (velocity) in bond 7. There are three state

variables (two capacitors and one inductance) namely e_4 , e_8 and f_7 . Thus the equation of motion is of a third order. To verify the BG model, the effort e_4 can be calculated as the force in the first spring (bond 4) in Box 6.

Similarly, the equation governing the second capacitor is given as:

$$\dot{e}_8 = (1 / C_2)f_8 = kf_7 \quad (12)$$

The equation for the inductance element is given as:

$$M\ddot{f}_7 = \dot{e}_7 = \dot{e}_6 - \dot{e}_8 - \dot{e}_9 = A\dot{e}_4 - \dot{e}_8 - \dot{e}_9 \quad (13)$$

Substituting Eqs. (11) and (12) into Eq. (13) and making use of $\dot{e}_9 = B\dot{f}_7$, we get:

$$M\ddot{f}_7 = (1 / C)(Aq_{in} - A^2f_7) - kf_7 - B\dot{f}_7 \quad (14)$$

Substituting $f_7 = \dot{u}(t)$, $\dot{f}_7 = \ddot{u}(t)$, $\ddot{f}_7 = \ddot{u}(t)$ into Eq. (14) and simplifying leads to:

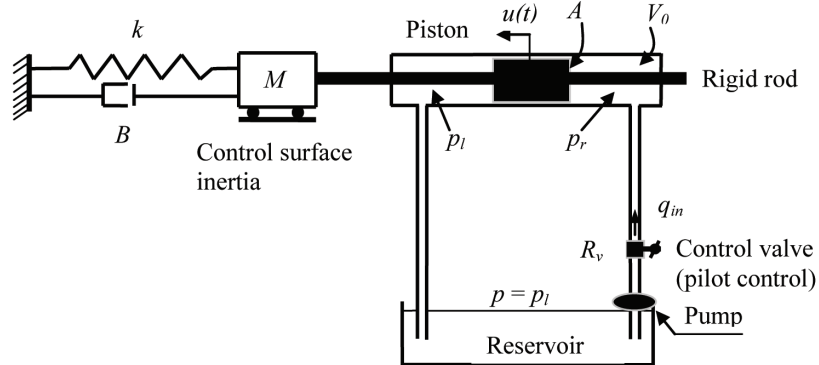
$$MC_1 \frac{\partial^3 u(t)}{\partial t^3} + BC_1 \frac{\partial^2 u(t)}{\partial t^2} + (kC_1 + A^2) \frac{\partial u(t)}{\partial t} = Aq_{in} \quad (15)$$

Equation (15) represents the equation of motion governing the dynamics of the hydraulic actuator that can be obtained using traditional mechanical system derivation. Therefore, the mathematical basis of bond graphs is the same as the classical dynamic theory. One should not, however, overlook the advantages of bond graphs (e.g., topological modeling tool, modeling sensors, qualitative

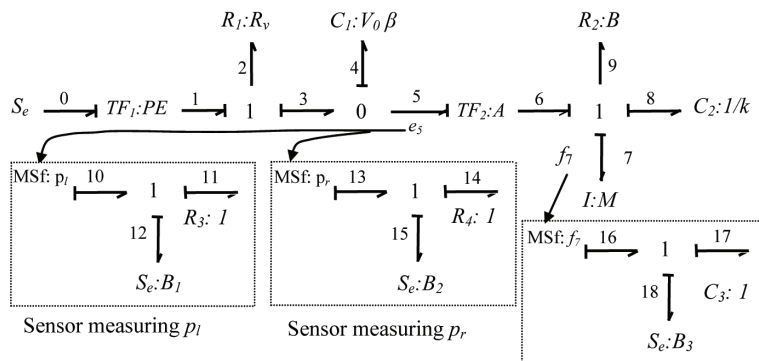
Box 6.

$$\dot{e}_4 = (1 / C_1)f_4 = (1 / C_1)(f_3 - f_5) = (1 / C_1)(S_f - Af_7) = (1 / C_1)(q_{in} - Af_7) \quad (11)$$

Figure 5. Single domain representation of a hydraulic actuator having interacting components from mechanical and hydraulic domains

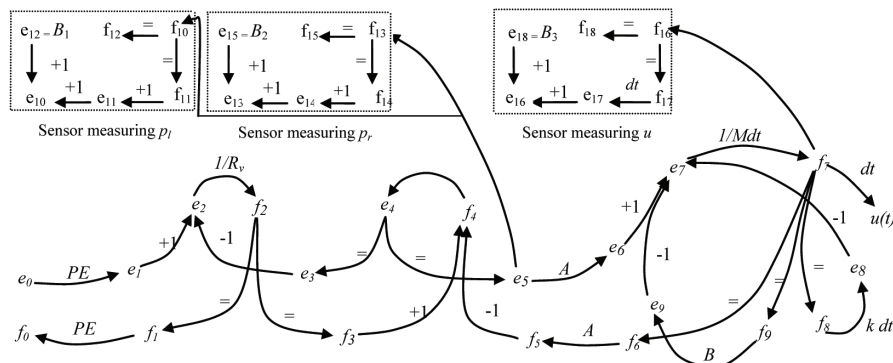


(a) Simple hydraulic actuator



*Note that: $e_5 = p_r - p_l$

(b) Bond graph model



(c) TCG model

Table 2. Description of the actuator parameters

Parameter	Description
A	Cross sectional area of the piston
V_0	Volume of the chamber
β	Bulk density of the fluid
R_v	Resistance of the valve
Se	Effort source
P_r	Chamber's pressure at right side
P_l	Chamber's pressure at left side
$P_r - P_l$	Pressure difference
M	Mass
k	Spring stiffness
B	Damping coefficient
$u(t)$	Displacement of the mass

damage identification, etc.) which are not provided by most existing system identifications methods. The next section demonstrates the modeling of continuous structures using bond graphs.

4. MODELING CONTINUOUS STRUCTURES USING FINITE-MODE BOND GRAPHS

This section demonstrates the modeling of continuous structures such as beams and frames using bond graphs. The modeling methodology is based on the normal mode approach (Clough & Penzien 2003, Chopra 2007) and is known as finite-mode bond graph (Karnopp et al, 2006). To do this, the external force (represented by an effort source S_e) is connected to a 0-junction that is connected to n 1-junctions using transformers (Figure 6(a)). The 0-J decomposes the external forces into their modal components. The 1-junctions represent the vibration modes retained and the transformers represent the mode shape evaluated at the point of application of the external force. The displacement of the i th 1-J represents the contribution to the structure response in the generalized coordinates. The I-, C- and R-elements (inertia, stiffness and damping forces) connected to the 1-junction represent the modal forces.

Figure 6(a) depicts the modeling of continuous dynamic systems using the finite-mode bond graphs. The transformers ensure that each mode is excited by the corresponding modal force. The number of modes to be retained in the dynamic analysis varies based on the boundary conditions and the dynamic characteristics of the structure (Clough & Penzien 2003, Chopra 2007). The associated TCG is shown in Figure 6(b) and will be discussed later.

The dynamic analysis of continuous structures using the finite-mode bond graph approach requires performing free vibration analysis to determine the natural frequencies and mode shapes of the structure, see, e.g., Clough & Penzien, 2003 and Chopra, 2007. The free vibration analysis is carried out based on the boundary conditions of the structure and can be performed analytically or numerically (e.g. using the finite element method). The natural frequencies and mode shapes are then used to quantify the parameters of the bond graph elements (I, C, R and TF) for each mode of vibration. In general, the first few modes usually provide fairly acceptable results.

5. CONSTRUCTING TEMPORAL CAUSAL GRAPH FROM BOND GRAPH

The step that follows the construction of the bond graph model is to use this model to develop a framework that facilitates damage detection and isolation. This is achieved by deriving the temporal causal graph (TCG) from the bond graph (Mosterman & Biswas, 1999). The TCG represents the constitutive relations of BG elements and junctions in graphical form. More precisely, the TCG represents causal relations among the system variables and parameters. The TCG is a directed graph in which the vertices represent the system variables and the directed edges express the relation between the vertices. The labels on the edges determine the type of causal relation

between the variables. These relations are similar to the forms of Eqs. (1, 2 and 3 but in a qualitative form ($=, +1, -1$). For instance, Eq. (3) reveals that the efforts e_1 and e_2 are equal, the flows f_1 and f_2 have $+1$ relation (i.e., increase in f_1 leads to increase in f_2 and vice-versa) and f_2 and f_3 have -1 relation (i.e., increase in f_1 leads to decrease in f_2 and vice-versa). The directions of the arrows in the TCG are defined based on the strong bond. Thus, a strong bond in a 1-junction governs the flow of the strong bond with arrows directed towards the flows of other bonds. The efforts of other bonds will have arrows directed towards the effort of the strong bond. A strong bond in a 0-J governs the effort at the junction with arrows directed towards efforts of other bonds.

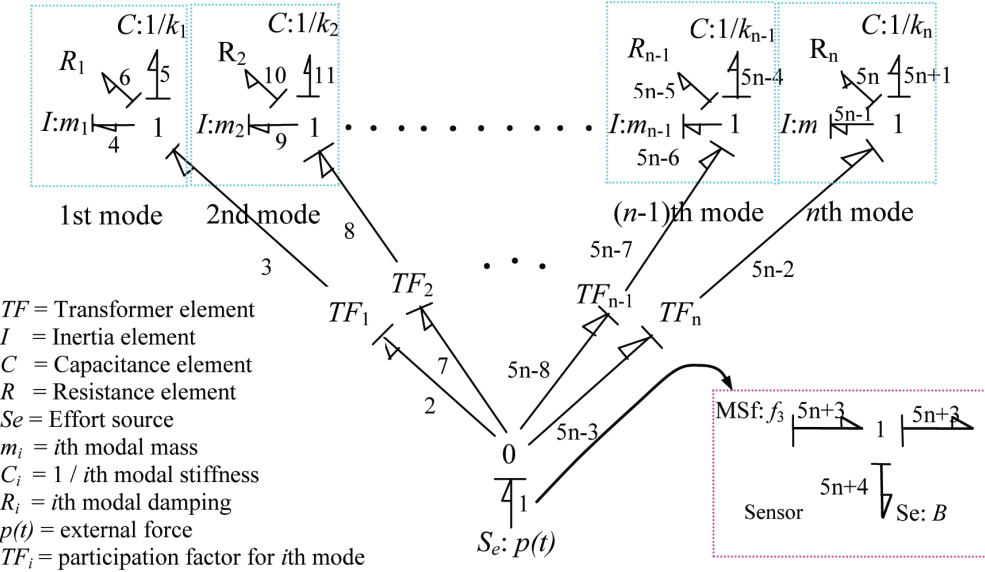
To construct the TCG for the SDOF system of Figure 3(a) from the BG model, it is first noted that the 1-J has equal flows and efforts sum to zero. We start with the external force $p(t)$, being imposed on the system, directed towards e_1 . Since bond 3 is the strong bond, thus f_3 determines the flow and e_1, e_2, e_4 determine the effort at the junction. Therefore, the flow arrows are drawn directed from f_3 to f_2, f_4 with equal signs (equal flow joint) and the efforts arrows are directed from e_1, e_2, e_4 to e_3 . The labels on the arrows connecting efforts are determined from the equation $e_3 = e_1 - e_2 - e_4$. Thus, the arrow connecting e_3 and e_2 carries the label -1 indicating the $-$ sign between e_3 and e_2 . To complete the TCG model we translate the constitutive relations for I-, C- and R-elements. For the I-element $e_3 = m\dot{f}_3$ or $f_3 = 1/m \int e_3 dt$ thus the label is dt/m (i.e. effort is integrated to provide flow). For the R-element, the equation is $e_4 = Df_4$ and thus the label is D (being multiplied by f_4 to give e_4). For the C-element, $e_2 = k \int f_2 dt$, thus the arrow carries the label k . This completes the TCG of the SDOF system.

To build the TCG for the MDOF system of Figure 4, we start by constructing the TCG for each

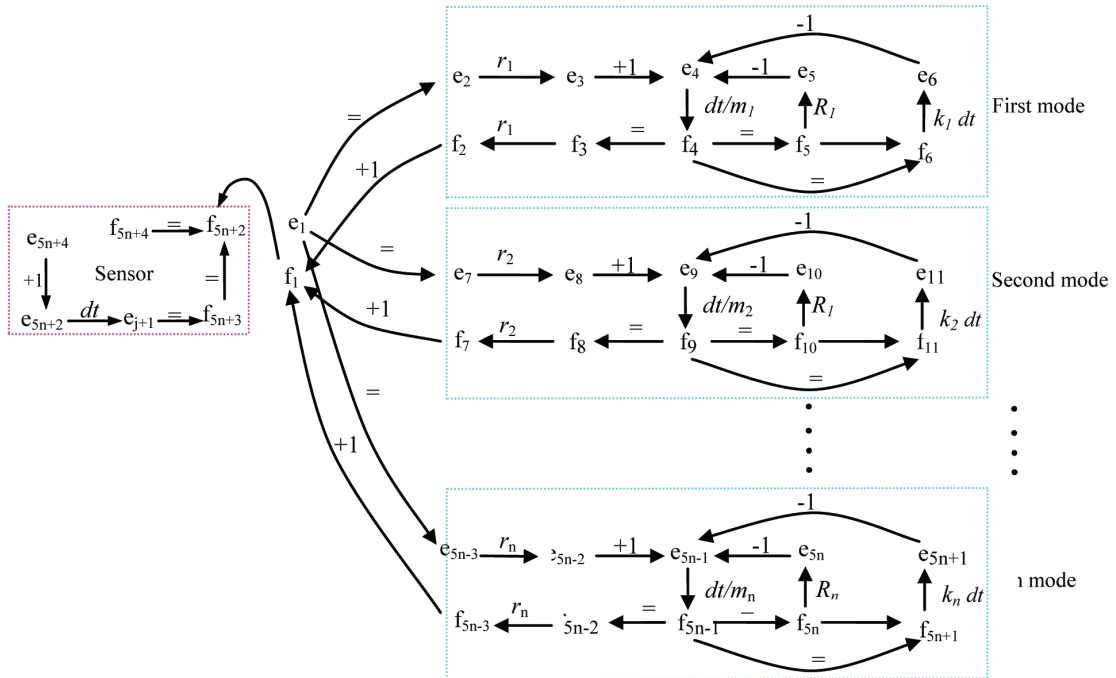
mass and then the connecting bonds (e.g. bonds 5 and 12). Note that the TCG for the second, third, ..., nth masses are identical and that each bond graph block is represented by an associated TCG block. The procedures are systematic and can be coded (Manders et al, 2006).

The temporal causal graph for the actuator of Figure 5(a) is shown in Figure 5(c). The energy source S_e defines the effort direction from e_0 to e_1 operated by the pump efficiency PE. The direction of the flow takes the opposite direction (i.e. from f_1 to f_0). Bond 2 is the strong bond (indicated by the causal stroke or the perpendicular line away from the junction) at the 1-junction (common flow junction $f_1 = f_2 = f_3$) and thus f_2 defines the flow at the junction. Accordingly f_2 is connected with f_1 and f_3 with arrows starting from f_2 and pointing towards f_1 and f_3 . Since $f_1 = f_2 = f_3$, therefore $=$ sign is shown in these arrows. Conversely, the effort is determined by e_1 and e_3 and thus the arrows are directed from e_1 and e_3 towards e_2 due to the relation $e_1 - e_2 - e_3 = 0$ (or $e_2 = e_1 - e_3$) at the 1-junction, $+1$ and -1 signs are shown above the arrows that connect e_2 with e_1 and e_3 , respectively. Bond 4 is the strong bond for the 0-junction (common effort junction $e_3 = e_4 = e_5$). Therefore, the effort is defined by bond 4. Accordingly, e_4 is connected with e_3 and e_5 by arrows pointing to e_3 and e_5 with equality sign. The flow is determined by f_3 and f_5 ($f_3 - f_4 - f_5 = 0$ or $f_4 = f_3 - f_5$) and thus the arrows connect f_3 and f_5 to f_4 with $+1$ and -1 signs, respectively. These signs are determined from the relation $f_4 = f_3 - f_5$. The efforts e_5 and e_6 are related by the area of the piston with an arrow pointing from e_5 to e_6 . The arrows for the flows f_5 and f_6 take the opposite direction. The strong bond of the last 1-junction ($f_6 = f_7 = f_8 = f_9$) is bond 7 and thus the flow at this junction is defined by f_7 . Accordingly f_7 is connected to f_6, f_8 and f_9 by arrows pointing from f_7 towards f_6, f_8 and f_9 with equality sign. The effort at the junction is defined by e_6, e_8 and e_9 and is shown by arrows connecting these efforts to e_7 . The effort relation at the 1-junction is $e_6 - e_7 - e_8 - e_9 = 0$ or $e_7 = e_6 - e_8 - e_9$.

Figure 6. Finite-mode BG and TCG representation of continuous dynamic systems and sensors



(a) Bond graph model



(b) TCG model

Accordingly, the arrows carry the signs 1, -1 and -1, respectively. The constitutive relation for the resistor R1 is $e_2 = R_v f_2$ or $f_2 = 1 / R_v e_2$ which is represented by an arrow connecting e2 to f2 and carries the constant 1/Rv. The constitutive relation for the C-element C1 is $e_4 = 1 / C_1 \int f_4 dt = (1 / V_0 \beta) \int f_4 dt$ and is represented by an arrow connecting f4 to e4 and carries the constant $(1 / V_0 \beta)$. The constitutive relation for the I-element is $e_7 = M \dot{f}_7$ or $\dot{f}_7 = 1 / M \int e_7 dt$ which is represented by an arrow connecting e7 and f7 pointing towards f7 and carries the term $1/M dt$. The constitutive relation for the second C-element is $e_8 = 1 / C_2 \int f_8 dt = k \int f_8 dt$ and is represented by an arrow connecting f8 to e8 and carries the term $k dt$. The flow f_7 is integrated to compute the displacement $u(t)$. This completes the TCG model for the actuator.

The TCG model of the continuous systems derived from the bond graph model of Figure 6(a) is shown in Figure 6(b). The derivation of the TCG follows the same procedures explained above. Again, each modal mass is represented by a separate TCG block. The modeling of a sensor that measures the structure tip displacement is also included and is explained in the next section.

6. MODELING SENSOR FAULTS USING BOND GRAPHS

A typical health monitoring system consists of a network of sensors that collect measurements data periodically or continuously during short or long terms. For civil structures, such as bridges, tunnels, dams, power plants, high-rise buildings and historical monuments, the most relevant measurement parameters are (Ansari, 2005, Manders et al, 2006): (a) Mechanical, such as, strain, deformation, displacement, crack opening, stress and forces, (b) Physical or environmental,

such as, temperature, humidity, and pore pressure, and (c) Chemical, such as, chloride penetration, sulfate penetration, pH, carbonatation penetration, rebar oxidation, steel oxidation, and timber decay.

Conventional sensors based on mechanical and electrical transducers are able to measure most of these parameters. Fiber-optic sensors offer superior performance compared with conventional sensors and have been used during the last few years in SHM of civil structures. More details on recent sensor technologies can be found in Ansari (2005) and Manders et al (2006).

In general, sensor performance and reliability degrade with time under varying environmental conditions and externally applied loadings (Ansari, 2005, Blackshire et al, 2006, Manders et al, 2006, Glisic & Inaudi 2007). Different degradation mechanisms have been observed in different types of sensors (e.g. surface-bonded or fully-embedded) under various environmental effects such as temperature- and moisture-cycling (Blackshire et al, 2006, Glisic & Inaudi 2007). Deviations in measurements could result from damage in structural components or due to faults in the sensors. Sensor performance is particularly relevant in the field of road infrastructure where the loading conditions affecting the main structure (traffic loads, temperature cycling, etc.) also affect the sensor measurements. In such situations, the use of traditional system identification methods may not provide accurate identification of actual damage cause since these methods do not account for sensor faults. On the other hand, bond graphs can easily model both the physical system and sensors (Daigle et al, 2006).

Faults in sensors could result in bias or drift in measured values. A biased measurement deviates from its true value by a constant B. Drift is the growth of deviations over time. For a sensor measuring the displacement response, a bias fault implies that the actual measured displacement d_m is the sum of the true displacement d_t and the bias B . The sensor is modeled as a modulated

source of flow (MSf) representing the relation $d_m(t) = d_t(t) + B$ (Figure 4(b)). Thus, for the displacement sensor measuring the displacement of the first mass $e_{7n-2} = dm$, $e_{7n-1} = dt$ and $e_{7n} = B1$. The C-element ($C = 1$) integrates the true velocity to give the true displacement. This leads to $e_{7n-2} = d_{7n-1} + B_1$ or $d_m(t) = d_t(t) + B_1$. In case of drift, the bias quantity $B1$ is replaced with a time drift function (i.e., $d_m(t) = d_t(t) + d_{drift}(t)$). Each sensor fault is represented by separate BG and TCG blocks.

7. EXTRACTION OF DAMAGE SIGNATURES FROM TEMPORAL CAUSAL GRAPH

This section describes the extraction of the damage signature matrix that lists the qualitative effects of changes in system components on system response measurements. This step is performed off-line using the TCG model before the collection of sensor data. The TCG is derived as described in Section 5. The TCG links damages to their causal effects on measurements, called damage signatures, which represent 0th through k th order derivative changes on a measurement residual at the instant of damage occurrence. They provide the discriminatory power in the damage isolation approach.

The damage signature derivation consists of two steps: backward propagation (BP) and forward propagation (FP). First, the TCG is used to perform a BP from possible deviant measurements to generate possible damage causes. This identifies a set of parameters that could be the reason for the damage (e.g. k and D in the SDOF example). It also determines whether the cause is above normal (+) or below normal (-). In the FP step we use each of these damage causes to derive its signatures on the system measurements (e.g. effect of decrease in k or D on x). The damage signature of the SDOF structure of Figure 4 is given in Table 3. Herein,

the BP of positive deviation in $x(t)$ leads identifying the damage causes as reduction in either k or D . The FP for reductions in k and D leads to the damage signature 00+ (see table 3).

Consider the MDOF structure of Figure 4. An example is shown in Figure 7(a) for a deviant displacement $x_1(t)$ being above normal. From the TCG of Figure 4(c), an increase in $x_1(t)$ initiates backward propagation along $f_3 \xrightarrow{dt} x_1$ and implies that the first derivative of f_3 is above normal (f_3+). The step along $f_3 \xrightarrow{+1} e_3$ implies e_3 above normal (e_3+), and $e_3 \xleftarrow{-1} e_2$ implies e_2 below normal and along $e_2 \xleftarrow{k_1} f_2$ implies k_1 below normal, and so on. Eventually, we arrive at $k_1, k_2, k_3, D_1, D_2, D_3$ below normal due to $x_1(t)$ being above normal.

The forward propagation starts from one of the damage causes identified in the previous step by propagating the change in this parameter and tracing its signature on the system measurements. An example of k_1- (k_1 below normal) is shown in Figure 7(b). The signature of k_1- on x_1 is derived by assuming that k_1 decreases and following the path shown in Figure 7(b), extracted from Figure 4(c). A decrease in k_1 implies a decrease in e_2 from the relation $e_2 = k_1 \int f_2 dt$ and is indicated with a downward arrow. This implies an increase in e_3 since $e_2 = e_1 - e_3 - e_4 - e_5$ (shown with an upward arrow). The increase in e_3 implies an increase in the first derivative of f_3 from the relation $f_3 = (1/m) \int_{-\infty}^t e_3 dt$ (shown with two upward arrows), and so on. Finally, this forward propagation implies an increase in the second derivative of x_1 which is indicated by three upward arrows and the signature is 00+. The signatures of $k_2, k_3, D_1, D_2, D_3, B_1, B_2, B_3, dr_1, dr_2$ and dr_3 on the system responses x_1, x_2 and x_3 are extracted following the same procedure and are shown in Table 4.

In Table 4, damage signatures are shown up to the first nonzero direction of change. Damage scenarios which produce discontinuities on the

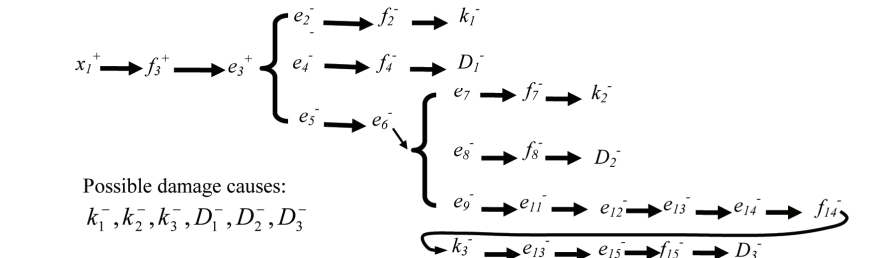
Table 3. Damage signatures for the SDOF building up to the first non zero direction of change

Damage type	Damage in structural components				Sensor faults			
	k^-	D^-	k^+	D^+	B^-	B^+	dr^-	dr^+
Damage signature (x)	00+	00+	00-	00-	-	+	0-	0+

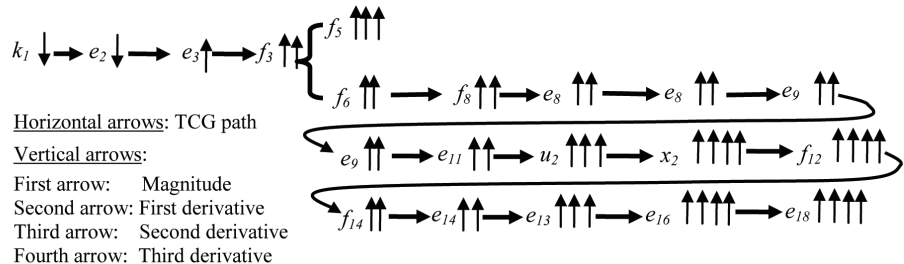
measurements (0th order changes) provide additional discriminatory power. Higher order effects eventually manifest as first order effects, and since we can only measure magnitude and slope reliably, only the first change (and whether it was discontinuous) is useful. If we measure displacement, the damage signatures represent a qualitative measure that reflects how a displacement observation could be affected by a change in one of the structure parameters. It is observed from Table 4 that the damage in the stiffness parameter of k_1 , k_2 and k_3 have different signatures on the measurements x_1 , x_2 and x_3 . On the other hand, the

signature of damage in k_1 is the same as the signature of damage in D_1 (same observation is valid for k_2 and D_2). Considering that the MDOF system models a multi-story building, this observation is consistent since the reduction in either the stiffness or the damping coefficient implies damage to the columns of the same floor. When multiple causes are identified in the qualitative step, then all those causes are included in the quantification step which helps to discriminate between them.

Figure 7. Damage signature extraction



(a) Backward propagation to find possible damage causes



(b) Forward propagation to establish a damage signature

Table 4. Damage signatures for the MDOF building up to the first non zero direction of change

Response quantity	Damage in structural components						Sensor faults					
	k_1^-	k_2^-	k_3^-	D_1^-	D_2^-	D_3^-	B_1^+	B_2^+	B_3^+	dr_1^+	dr_2^+	dr_3^+
x_1	00+	00+	000-	00+	00+	000-	+	0	0	0+	00	00
x_2	000+	00-	00-	000+	00-	00-	0	+	0	00	0+	00
x_3	0000+	000-	00-	0000+	000-	00-	0	0	+	00	00	0+

8. HYBRID QUALITATIVE-QUANTITATIVE SYSTEM IDENTIFICATION TECHNIQUE

The health assessment method developed here consists of damage detection, qualitative damage isolation, and quantitative damage identification (Figure 8). Here, p is the external load and r is the residual, the difference between the current structural response x , obtained from sensor measurements, and the undamaged structural response \hat{x} , determined using the BG model. Note that the BG and TCG models and the damage signatures are derived before the sensor data collection. This makes the damage detection, isolation and quantification efficient and inexpensive. The steps to be discussed in the next subsections are done after the collection of the sensor health monitoring data.

8.1 Damage Detection and Symbol Generation

The detection scheme is based on comparison of measurements from damaged and undamaged structures. This leads to estimating the residuals, which, when statistically significant, imply damage occurrence. Since measurements contain noise, a statistical test (Z-test) is used to examine if the structure is damaged or not (Biswas et al, 2003). The deviation of the residual $r(t)$ from zero is defined for the last N_2 samples and the variance of $r(t)$ is estimated for a larger data points N_1 , where $N_1 \gg N_2$ as follows:

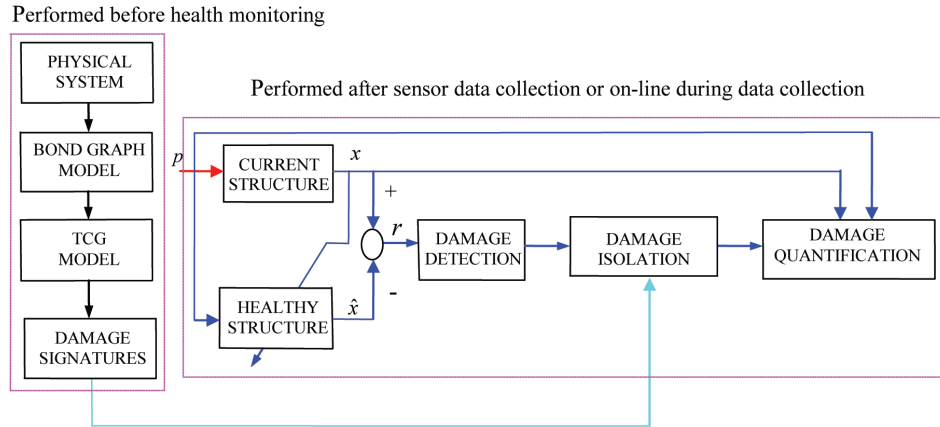
$$\hat{\mu}_{N_2}(t_j) = \frac{1}{N_2} \sum_{i=j-N_2}^j r(t_i); \quad \hat{\sigma}_{N_1}^2(t_j) = \frac{1}{N_1} \sum_{i=j-N_1}^j [r(t_i) - \hat{\mu}_{N_2}(t_j)]^2 \quad (16)$$

The symbol generation step follows the comparison of the measurements from healthy and damaged structures. If the measurement of the damaged structure at a given point of time is above normal, a (+) symbol is assigned, and if below normal, a (-) symbol is assigned.

8.2 Qualitative Damage Isolation

The damage isolation step begins once damage is detected. Having developed the damage signatures matrix in Section 6, this step is a monitoring of system response measurements over time and comparison with the damage signatures matrix to identify possible damage causes. For the MDOF structure of Figure 4, the system measurements are the displacements x_1, x_2, \dots, x_n . These measurements are compared with those for the undamaged structure. The damage that matches the damage signature is the cause of damage. If multiple causes are identified, the quantitative step in next section is used to discriminate between them. This qualitative approach is very fast, due to off-line development of the damage signature beforehand, and thus enables on-line health assessment.

Figure 8. Damage identification for dynamic systems



8.3 Quantitative Damage Identification

The qualitative damage isolation described above identifies the damaged component without quantifying the damage size. For discrete structures (i.e. the MDOF system that models a multi-story building), the qualitative isolation identifies which floor has damage. The damage size is quantified by applying nonlinear optimization using the least-

squares method to the substructure containing the damaged floor only. This offers substantial savings in the computational effort. For instance, if the damage is isolated in the columns of the first or the second floor we consider the substructure containing the first two floors. Thus, the equations of motion for the first two floors are given in Box 7.

These two equations can be recast in a matrix form in Box 8.

Box 7.

$$\begin{aligned} m_1 \ddot{x}_1(t) + [D_1 + D_2] \dot{x}_1(t) - D_2 \dot{x}_2(t) + [k_1 + k_2] x_1(t) - k_2 x_2(t) &= p_1(t) \\ m_2 \ddot{x}_2(t) - D_2 \dot{x}_1(t) + [D_2 + D_3] \dot{x}_2(t) - D_3 \dot{x}_3(t) - k_2 x_1(t) + [k_2 + k_3] x_2(t) - k_3 x_3(t) &= p_2(t) \end{aligned} \quad (17)$$

Box 8.

$$\begin{bmatrix} \dot{x}_1 & \dot{x}_1 - \dot{x}_2 & 0 & x_1 & x_1 - x_2 & 0 \\ 0 & \dot{x}_2 - \dot{x}_1 & \dot{x}_2 - \dot{x}_3 & 0 & x_2 - x_1 & x_2 - x_3 \end{bmatrix} \begin{bmatrix} D_1 \\ D_2 \\ D_3 \\ k_1 \\ k_2 \\ k_3 \end{bmatrix} = \begin{bmatrix} p_1(t) - m_1 \ddot{x}_1(t) \\ p_2(t) - m_2 \ddot{x}_2(t) \end{bmatrix} \quad (18)$$

Box 8.

$$\begin{bmatrix} \dot{x}_{n-1} - \dot{x}_{n-2} & \dot{x}_{n-1} - \dot{x}_n & x_{n-1} - x_{n-2} & x_{n-1} - x_n \\ 0 & \dot{x}_n - \dot{x}_{n-1} & 0 & x_n - x_{n-1} \end{bmatrix} \begin{bmatrix} D_{n-1} \\ D_n \\ k_{n-1} \\ k_n \end{bmatrix} = \begin{bmatrix} p_{n-1}(t) - m_{n-1}\ddot{x}_{n-1}(t) \\ p_n(t) - m_n\ddot{x}_n(t) \end{bmatrix} \quad (19)$$

Box 9.

$$\begin{bmatrix} \dot{x}_{i-2} - \dot{x}_{i-3} & \dot{x}_{i-2} - \dot{x}_{i-1} & 0 & x_{i-2} - x_{i-3} & x_{i-2} - x_{i-1} & 0 \\ 0 & \dot{x}_{i-1} - \dot{x}_{i-2} & \dot{x}_{i-1} - \dot{x}_i & 0 & x_{i-1} - x_{i-2} & x_{i-1} - x_i \end{bmatrix} \begin{bmatrix} D_{i-2} \\ D_{i-1} \\ D_i \\ k_{i-2} \\ k_{i-1} \\ k_i \end{bmatrix} = \begin{bmatrix} p_{i-2}(t) - m_{i-2}x_{i-2}(t) \\ p_{i-1}(t) - m_{i-1}x_{i-1}(t) \end{bmatrix} \quad (20)$$

The number of unknown system parameters here is $s = 6$. If damage is qualitatively isolated in one of the columns of the top two floors, the equations governing the motion of the substructure containing the top two floors are given in Box 8.

In this case, s reduces to 4. If the damaged columns are located between the third floor and the $(n-3)$ th floor, the equations of motion that describe the damaged substructure are given in Box 9.

Herein, $s = 6$ and $3 \leq i \leq n - 2$. Equations (18), (19) or (20) can be written in matrix form as:

$$[\mathbf{A}(t)]_{2 \times s} [\mathbf{R}]_{s \times 1} = [\mathbf{p}(t)]_{2 \times 1} \quad (21)$$

where, $\mathbf{A}(t)$ is a matrix of system responses, \mathbf{R} is a vector of the unknown system stiffness and damping parameters, $\mathbf{p}(t)$ is a vector of the external excitation and the inertia forces and $s = 4$ or 6. Considering that the structural response is measured for a time duration $T = l \Delta t$ where l

is the discrete number of time instants and Δt is the time step, Eq. (21) can be rewritten as:

$$[\mathbf{A}(t)]_{(l \times 2) \times s} [\mathbf{R}]_{s \times 1} = [\mathbf{p}(t)]_{(l \times 2) \times 1} \quad (22)$$

Alternatively, Eq. (22) can be expressed as:

$$\sum_{i=1}^s A_{ji} R_i = p_j; j = 1, 2, \dots, s \times l \quad (23)$$

Assuming \hat{R}_i is the predictor of the i th parameter R_i , the total error in this estimate is given by:

$$\varepsilon = \sum_{j=1}^{s \times l} [p_j - \sum_{i=1}^s A_{ji} \hat{R}_i]^2 \quad (24)$$

To minimize the total error, ε is differentiated with respect to R_j and is set to zero which leads to:

$$\sum_{j=1}^{s \times l} [\sum_{i=1}^s A_{ji} \hat{R}_i] A_{jq} = \sum_{j=1}^{s \times l} p_j A_{jq}; q = 1, 2, \dots, s \quad (25)$$

Eq. (25) gives s (4 or 6) simultaneous algebraic equations which when solved provide the system parameters including the stiffness and damping coefficient of the damaged columns.

Thus, the quantitative damage identification is performed for the substructure that contains the damaged component by minimizing the error in the identified structural parameters. This offers tremendous savings in the computations. Damage quantification of continuous systems follows the same procedures and is discussed in the next section.

9. NUMERICAL ILLUSTRATIONS

Two numerical examples are considered to demonstrate the use of bond graphs for dynamic analysis and health assessment of discrete and continuous systems. The first example considers a 15-story building under earthquake load. The second example demonstrates the health assessment of a high-rise building subjected to simulated Kanai-Tajimi acceleration using the finite-mode bond graphs.

The bond graph models of both structures are created using the Fault Adaptive Control Technology (FACT) software (Mosterman & Biswas, 1999) in the Generic Modeling Environment (GME-6, 2006) to generate a simulation model (Matlab Simulink model) (Mathworks, 1999) that is used to simulate the structural response. FACT contains a library of bond graph elements (i.e., I-, C-, R-, S_c -, S_f -, TF- and GY-elements and connecting bonds) that are used to assemble the bond graph model in GME. The displacement, velocity, and acceleration responses for the building are computed using the simulation model. The bond

graph damage detection, diagnosis and identification algorithm is executed using Matlab.

9.1 Health Assessment of a Fifteen-Story Shear Building under Earthquake Load

This example studies dynamic analysis and health assessment of a 15-story shear building under the first horizontal acceleration of the 1995 Kobe earthquake (Takatori station) scaled to 0.30 g PGA (PEER, 2005). We investigate the dynamic analysis of the structure first. The numerical values of floor masses, columns stiffnesses and damping used in the BG simulation analyses are given in Table 5. This structure was modeled using a fifteen degree-of-freedom mechanical system with linear behavior.

9.1.1 Health Assessment of the Structure

Damage in structural components is simulated as reduction of 20% in the stiffness parameters of the fourteenth floor (case 1) and the first floor (case 2). Damage in the sensors is modeled as bias or drift in the fourteenth floor or first floor sensors. The procedures described in Sections 3 and 5 are used to generate the BG and TCG models of the structure. The BG and TCG models are constructed from those shown in Figure 4 by duplicating the blocks of the third floor and third sensor. The damage signatures are derived as described in Section 7.

9.1.1.1 Damage in Structural Components

We first study damage in the structural components. For noise-free measurements, a reduction of 20% is introduced to the stiffness of the fourteenth floor. The damage criterion is taken as deviation in response measurements by more than 5% from corresponding values of healthy structure. The damage was successfully detected to be in

Table 5. Numerical values for mass, stiffness and damping coefficient for the 15-story building

Floor No.	1	2	3	4	5	6	7	8
Mass (kg)	103.2	97.2	97.2	95.3	100.2	108.1	76.6	80.0
Stiffness $\times 10^3$ (N/m)	64.5	63.4	72.7	72.1	68.7	52.3	48.5	51.5
Damping (N s/m)	645	634	727	721	687	523	600	650
Floor No.	9	10	11	12	13	14	15	
Mass (kg)	90.0	90.0	108.1	76.6	80.0	90.0	70.0	
Stiffness $\times 10^3$ (N/m)	48.1	68.7	52.3	48.5	51.5	48.1	16.8	
Damping (N s/m)	700	687	523	600	650	700	168	

the columns of the fourteenth floor due to deviation of displacement measurements x_{14} . Similar analyses with 2%, 4% and 6% noise level are also carried out and the identification algorithm detects and isolates the damage to be in the fourteenth floor. Herein, the Z-test is used to detect the damage. The parameters N_1, N_2, α were taken as 50, 5 and 1.0, respectively. The quantitative identification scheme described in Section 7 leads to identifying the stiffness and damping parameters of the last two floors, see Table 6. For noise-free measurements, the identified stiffness and damping parameter of the last two floors contain very small errors. For 2% noise measurements, the reduction in the stiffness was identified close 19%. The accuracy of the identified parameters was seen to decrease for higher values of noise (see Table 6). Denoising of sensor measurements will definitely improve the accuracy of the identified parameters.

It was found that the time step of the ground acceleration of 0.01 s provides inaccurate results. Therefore, interpolation of the ground acceleration at smaller time period of 0.005 s was performed. Similar analyses with damage simulated as reduction in the stiffness of the first floor columns were also conducted and the health assessment algorithm was found to detect and isolate the damage successfully. Some of these results are provided in Table 6. Note that $s = 6$ in this case.

9.1.1.2 Faults in Sensors

Damage in sensors is performed by simulating sensor measurements of the fourteenth floor displacement as bias (0.02 m) or drift ($0.002 t$) functions from the true measurements at $t = 5.0$ s (Figure 9). The diagnosis algorithm correctly detects the fault to be in the sensor at the fourteenth floor, since no other damage cause provides similar damage signatures. To quantify the bias value, the two measurements at the fourteenth floor are subtracted. Notwithstanding that the bias function contains noise, the average value, however, was found to be about 0.019 m which is close to the correct value. Alternatively, the true and measured data can be denoised before computing the bias value. For the noise-free case, the difference leads to correctly quantifying the bias value to be 0.02 m.

Further numerical analyses with faults simulated in the sensor measuring the displacement response of the first floor were also conducted. The health assessment algorithm successfully detects, isolates, and quantifies the correct damage to be in the first floor sensor.

9.2 Health Assessment of a High-Rise Building under Simulated Kanai-Tajimi Acceleration

In the previous example discrete structures were modeled using one-to-one bond graph elements.

Table 6. Actual and identified parameters for the 15-story shear building due to structural damage

Parameter	Actual values	Identified values			
		Noise-free	2% noise	4% noise	6% noise
k_{14}^*	38480	38469 (0.03%)	38415 (0.17%)	38291 (0.49%)	38118 (0.94%)
D_{14}	700	695.36(0.66%)	690.72 (1.33%)	676.87 (3.30%)	698.75 (4.57%)
k_{15}	16800	16797 (0.02%)	16761 (0.23%)	16694 (0.63%)	16610 (1.13%)
D_{15}	168	166.34(0.99%)	164.68 (1.98%)	159.71 (4.94%)	155.89 (7.21%)
k_1^{**}	51600	51596 (0.01%)	51223 (0.73%)	50652 (1.84%)	50272 (2.57%)
D_1	645	643 (0.31%)	660.80 (2.46%)	678.68 (5.22%)	687.95 (6.66%)
k_2	63400	63392 (0.02%)	62935 (0.73%)	62230 (1.85%)	61760 (2.59%)
D_2	634	632 (0.32%)	656.15 (3.49%)	682.05 (7.58%)	696.09 (9.79%)
k_3	72700	72688 (0.02%)	72157 (0.75%)	71335 (1.88%)	70786 (2.63%)
D_3	727	724 (0.41%)	754.73 (3.81%)	787.71 (8.35%)	805.91 (10.85%)

Note: The numbers in parentheses indicates % error in identified parameter.

* Case 1: Damage in columns of fourteenth floor.

** Case 2: Damage in columns of first floor.

The modeling of continuous dynamic systems using bond graphs is carried out using finite-mode bond graphs as described before. This example demonstrates the health assessment of a reinforced concrete high-rise building using the finite-mode bond graphs. It may be recalled here that the modal analysis technique is used to model the continuous system with an equivalent discretized multi-degree-of-freedom system. The bond graph and temporal causal graph models of the building are shown in Figure 6. The bond graph and TCG graph model the structural components and the sensor as well. The structure is taken to be subjected to a simulated Kanai-Tajimi random ground acceleration at the support points and the response measurement is taken as the displacement at the tip point of the structure. The input acceleration and simulated displacement measurements with 5% noise are shown in Figure 10.

The structure properties used in simulating the sensor measurements are taken as $h = 75.00$ m, $E = 2.0 \times 10^{10}$ N/m 2 and mass density of 2500 kg/m 3 . The structure is taken to have a uniform cross sectional area of 8.00 m outer diameter and 7.20 m inner diameter. A modal viscous damping of 5% damping ratio is assumed for all modes. The first 5 modes are considered in the health

assessment analysis. The free vibration analysis was carried out analytically (Blevins, 1979).

Damage in the structural components is modeled as a reduction of 20% in the stiffness of the structure. The sensor fault is modeled as either bias of 0.02 m or drift function of 0.002 t , at $t = 5.0$ s. Figure 10 shows the input load and simulated noisy measurements (5% noise level). Possible damage scenarios are taken as changes in modal stiffness and damping in all modes. It should be noted here that the transformer index (TF = the participation factor) is a positive quantity for odd modes and is negative for even modes. For the case of structural damage, the identification algorithm detects damage and isolates it to be in the modal stiffness or modal damping. Similarly, the identification algorithm successfully isolates the sensor fault (bias or drift) to be the sensor.

In this example, damage detection and qualitative damage isolation are carried out. It is possible to perform damage quantification using the least-squares method to quantify the modal parameters. To do this, additional sensors should be placed for collecting required measurements for the quantification process. Given that changes in the modal parameters of the structure provide a measure of the structural damage at the global

Figure 9. Example 1: Sensor measurements with 5% noise (a) Fourteenth floor displacement with damage in structural components (b) Fourteenth floor displacement with sensor bias

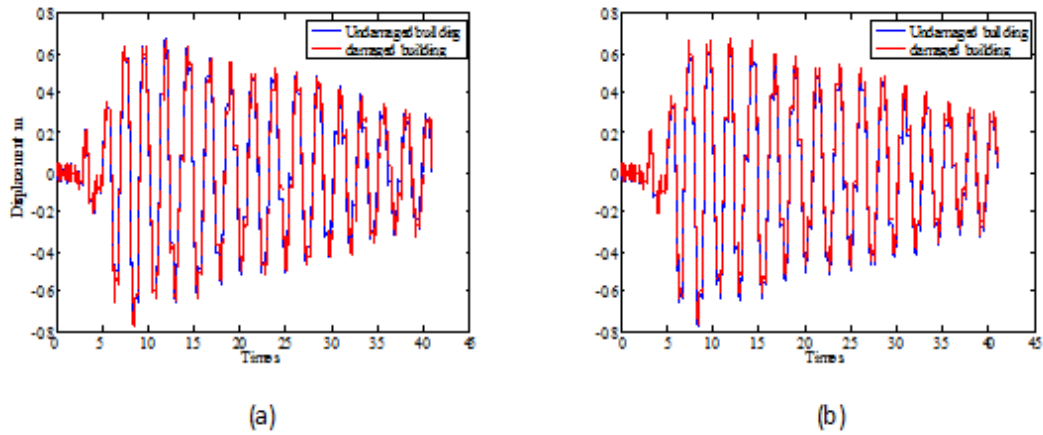
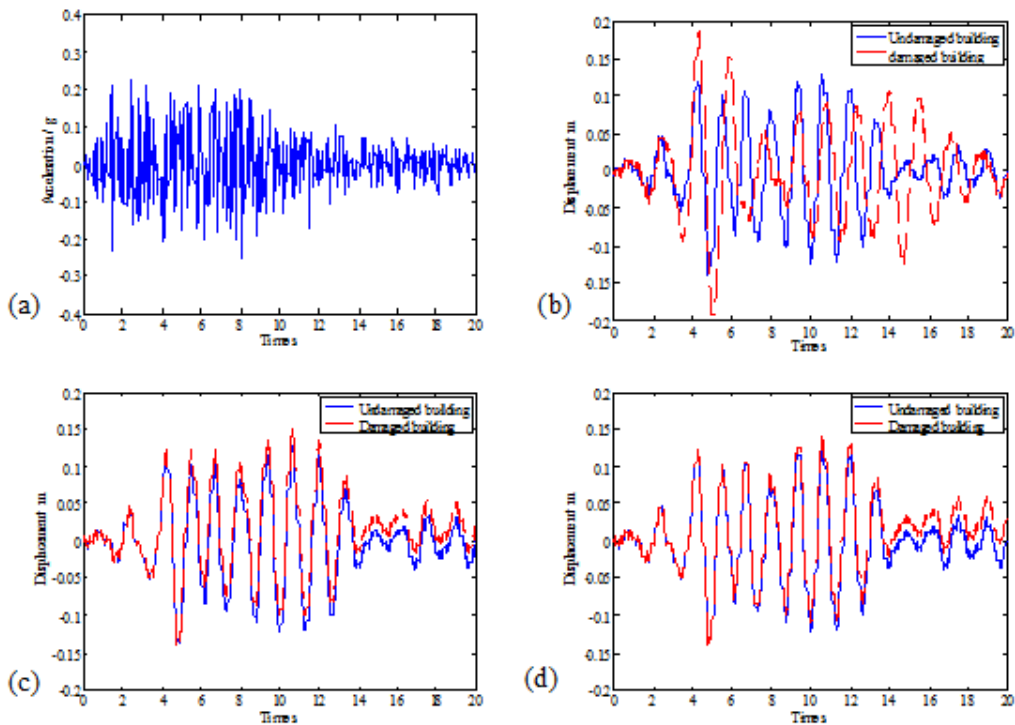


Figure 10. Example 2: Input-output measurements with 5% noise (a) Simulated Kanai-Tajimi acceleration (b) Tip displacement with damage in structural components (15% reduction in ω_1) (c) Tip displacement with sensor bias 0.02 m (d) Tip displacement with sensor drift 0.002 t



level and not at the local level, this step was not considered in this chapter.

10. CONCLUDING REMARKS AND FUTURE CHALLENGES

A new graphical energy-based framework for dynamic analysis and health assessment of dynamic systems is developed in this chapter. This framework is based on the bond graph theory, the associated temporal causal graphs, the derived damage signatures and the least-squares optimization method. The framework is different from other frameworks in the sense that it enables performing qualitative system identification first, thus reducing the computations significantly. Subsequently, damage quantification is carried out if necessary. BG is shown to represent the system equations of motion in an implicit graphical form. The TCG links the system response to changes in the system components and sensor measurements which facilitates deriving qualitative effects of changes in system response on system components. The advantages of the BG framework are: (1) Simple graphical-modeling tool for dynamic systems, (2) Unified (domain-independent) framework for dynamic analysis and health assessment of dynamic systems across multiple domains (e.g., structural, mechanical, electrical, hydraulic, etc.), (3) Rapid qualitative identification of the damage location, thus reducing the computations, (4) The ability to identify sensor faults, (5) The ability to perform online diagnosis, based on continuous monitoring, (6) Reduction of data processing, online computations and associated errors due to absence of transformation to other domain or approximations in feature selection, and (7) Rapid quantification of damage size since only the substructure containing damage is analyzed.

In this chapter, linear structural behavior and relatively simple structures are considered. More complex systems, continuum elements and non-

linear material behavior need to be studied. The study also considered a single damage to occur at a time. The inclusion of multiple damages will be considered in a future work. Notwithstanding these shortcomings, it is believed that bond graphs will open the door for new useful applications in system identification and structural control of engineering structures. The issue of sensor performance is particularly relevant in the field of road infrastructure where the loading conditions affecting the main structure (traffic load, temperature cycling, etc.) affect also the sensor performance. It is difficult, however, to consider all these concerns in this chapter.

ACKNOWLEDGMENT

This study was partly supported by funds from the U. S. Air Force Research Laboratory (Grant No. USAF- 0060-43-0001). This support is greatly acknowledged.

REFERENCES

- Alvin, K. F., Robertson, A. N., Reich, G. W., & Park, K. C. (2003). Structural system identification: from reality to models. *Computers & Structures*, 81(12), 1149–1176. doi:10.1016/S0045-7949(03)00034-8
- Ansari, F. (2005). *Sensing issues in civil structural health monitoring*. Springer. doi:10.1007/1-4020-3661-2
- Biswas, G., Simon, G., Mahadevan, N., Narasimhan, S., Ramirez, J., & Karsai, G. (2003). A robust method for hybrid diagnosis of complex systems. *Proceedings of 5th Symposium on Fault Detection, Supervision and Safety for Technical Processes* (pp. 1125-1131). Washington, DC.

- Blackshire, J. L., Martin, S., & Cooney, A. (2006). Characterization and modeling of bonded piezoelectric sensor performance and durability in simulated aircraft environments. *Proceedings of 3rd European Workshop on Structural Health Monitoring*, Granada, Spain.
- Blevins, R. D. (1979). *Formulas for natural frequency and mode shape*. New York, NY: Litton Education Publishing Inc.
- Chang, P. C., Flatau, A., & Liu, S. C. (2003). Review paper: Health monitoring of civil infrastructure. *Structural Health Monitoring*, 2(3), 257–267. doi:10.1177/1475921703036169
- Chopra, A. K. (2007). *Dynamics of structures* (3rd ed.). Englewood Cliffs, NJ: Prentice-Hall.
- Clough, R. W., & Penzien, J. (2003). *Dynamics of structures* (3rd ed.). Computers & Structures Inc.
- Daigle, M., Koutsoukos, X., & Biswas, G. (2006). Distributed diagnosis of coupled mobile robots. *IEEE International Conference on Robotics and Automation*, (pp. 3787-3794).
- De Oliveira, R., Frazao, O., Santos, J. L., & Marques, A. T. (2004). Optic fibre sensor for real-time damage detection in smart composite. *Computers & Structures*, 82(17-19), 1315–1321. doi:10.1016/j.compstruc.2004.03.028
- Doebling, S. W., Farrar, C. R., & Prime, M. B. (1998). A summary review of vibration-based damage identification methods. *The Shock and Vibration Digest*, 30(2), 91–105. doi:10.1177/058310249803000201
- Elouedi, Z., Mellouli, K., & Smets, P. (2004). Assessing sensor reliability for multisensor data fusion within the transferable belief model. *IEEE Transactions on Systems, Man, and Cybernetics. Part B, Cybernetics*, 34(1), 782–787. doi:10.1109/TSMCB.2003.817056
- Glisic, B., & Inaudi, D. (2007). *Fibre optic methods for structural health monitoring*. Chichester, UK: John Wiley & Sons. doi:10.1002/9780470517819
- GME-6. (2006). *A generic modeling environment, GME 6 user's manual*. Vanderbilt University. Retrieved from <http://www.isis.vanderbilt.edu>
- Gonzalez, M. P., & Zapico, J. L. (2008). Seismic damage detection in buildings using neural networks and modal data. *Computers & Structures*, 86(3-5), 416–426. doi:10.1016/j.compstruc.2007.02.021
- Karnopp, D. C., Margolis, D. L., & Rosenberg, R. C. (2006). *System dynamics, modeling and simulation of mechatronic systems*. John Wiley & Sons.
- Koh, C. G., Chen, Y. F., & Liaw, C.-Y. (2003). A hybrid computational strategy for identification of structural parameters. *Computers & Structures*, 81(2), 107–117. doi:10.1016/S0045-7949(02)00344-9
- Lui, E. M., & Ge, M. (2005). Structural damage identification using system dynamic properties. *Computers & Structures*, 83(27), 2185–2196. doi:10.1016/j.compstruc.2005.05.002
- Manders, E. J., Biswas, G., Mahadevan, N., & Karsai, G. (2006). Component-oriented modeling of hybrid dynamic systems using the generic modeling environment. *Proceedings of 4th Workshop on Model-Based Development of Computer Based Systems*.
- Mathworks. (1999). *Simulink: Dynamic system simulation for Matlab*. Mathworks Inc.
- Mosterman, P. J., & Biswas, G. (1999). Diagnosis of continuous valued systems in transient operating regions. *IEEE Transactions, Man, and Cybernetics-Part A*, 29(6), 554–565. doi:10.1109/3468.798059

- Moustafa, A., Mahadevan, S., Daigle, M., & Biswas, D. (2010). Structural and sensor system damage identification using the bond graph approach. *Structural Control and Health Monitoring*, 17, 178–197. doi:10.1002/stc.285
- Pacific Earthquake Engineering Research (PEER) Center.* (2005). Retrieved from <http://peer.berkeley.edu>
- Paynter, H. M. (1961). *Analysis and design of engineering systems*. MIT Press.
- Rosenberg, R. C., & Karnopp, D. C. (1983). *Introduction to physical system dynamics*. McGraw-Hill.
- Sankararaman, S., & Mahadevan, S. (2011). (in press). Uncertainty quantification in structural damage diagnosis. *Structural Control and Health Monitoring*. doi:10.1002/stc.400

Chapter 15

Optimal Design of Nonlinear Viscous Dampers for Protection of Isolated Bridges

Alexandros A. Taflanidis
University of Notre Dame, USA

Ioannis G. Gidaris
University of Notre Dame, USA

ABSTRACT

A probabilistic framework based on stochastic simulation is presented in this chapter for optimal design of supplemental dampers for multi - span bridge systems supported on abutments and intermediate piers through isolation bearings. The bridge model explicitly addresses nonlinear characteristics of the isolators and the dampers, the dynamic behavior of the abutments, and the effect of pounding between the neighboring spans to each other as well as to the abutments. A probabilistic framework is used to address the various sources of structural and excitation uncertainties and characterize the seismic risk for the bridge. Stochastic simulation is utilized for evaluating this seismic risk and performing the associated optimization when selecting the most favorable damper characteristics. An illustrative example is presented that considers the design of nonlinear viscous dampers for protection of a two-span bridge.

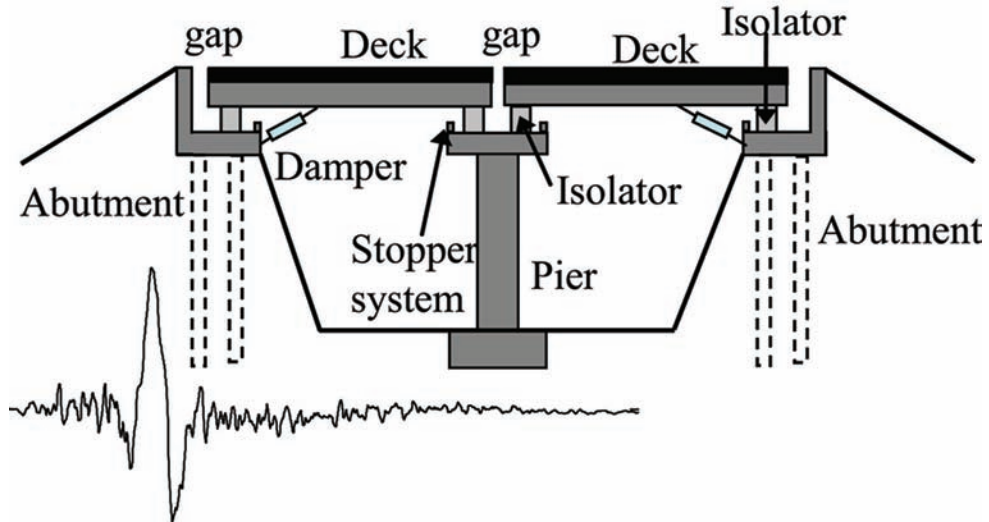
INTRODUCTION

Applications of seismic isolation techniques to bridges (Figure 1) have gained significant attention over the last decade (Jangid, 2008; Jónsson, Bessason, & Haflidason, 2010; Makris & Zhang, 2004; Perros & Papadimitriou, 2009; Tsopelas, Constantinou, Okamoto, Fujii, & Ozaki, 1996;

Wang, Fang, & Zou, 2010). Lead-rubber bearings or friction pendulum systems are selected for this purpose in order to isolate the bridge deck from its support, at the abutments and potentially at the locations of intermediate piers. This configuration provides enhanced capabilities for energy dissipation during earthquake events while also accommodating thermal movements during the life-cycle of operation of the bridge. It is associated though with large displacement for the bridge

DOI: 10.4018/978-1-4666-1640-0.ch015

Figure 1. Two-span base-isolated bridge

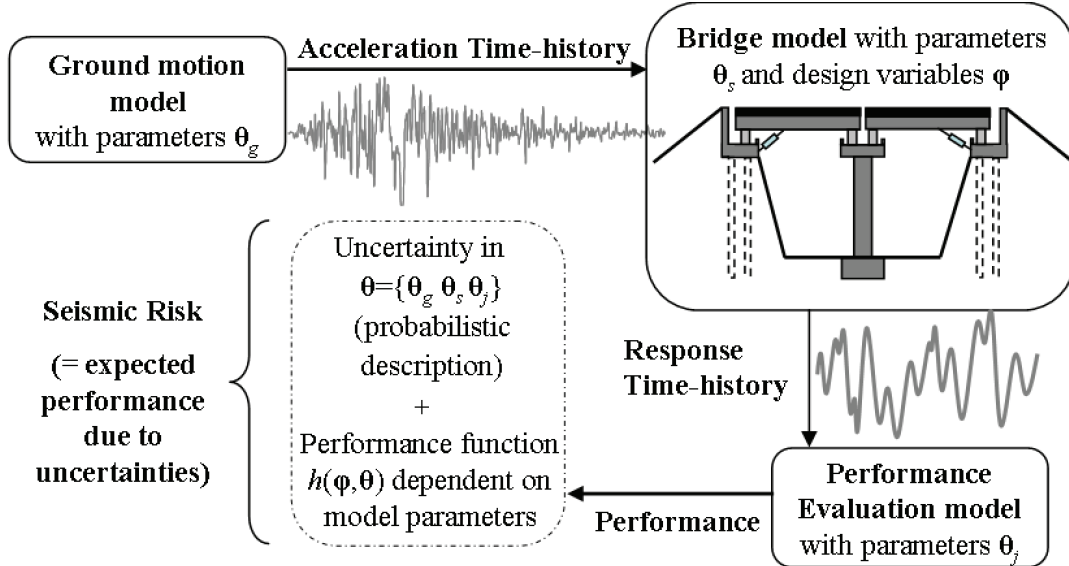


deck relative to its supports, especially under near fault earthquake ground motions (Dicleli, 2006; Dimitrakopoulos, Makris, & Kappos, 2010; Shen, Tsai, Chang, & Lee, 2004). These motions include frequently a strong, longer period component (pulse) that has important implications for flexible, isolated structures (Bray & Rodriguez-Marek, 2004; Mavroeidis & Papageorgiou, 2003). For base-isolated bridge systems, such large displacements under strong ground motions may lead to (i) large inelastic deformations and formation of plastic hinges at the piers and abutments and (ii) pounding of the deck between adjacent spans or to intermediate seismic stoppers or to the abutments supporting the ends of the bridge (Dimitrakopoulos, Makris, & Kappos, 2009; Dimitrakopoulos et al., 2010; Ruanggrassamee & Kawashima, 2003). Such pounding will then lead to high impact stresses and increased shear forces for both the bridge deck and its supports (abutments and piers).

This overall behavior associated with excessive vibrations will ultimately lead to significant damages that affect not only the serviceability but also the structural integrity of the bridge system. For controlling such vibrations, application of seismic dampers has been proposed and applied to iso-

lated bridges (Hwang & Tseng, 2005; Makris & Zhang, 2004; Ruanggrassamee & Kawashima, 2003). The explicit consideration of the hysteretic behavior of the isolators and the highly nonlinear behavior of the dampers in the design process, as well as the proper modeling of soil-structure interaction at the foundations of the bridge are some of the main challenges encountered in the design of such dampers. Linearization techniques are frequently adopted for modeling the bridge system (Hwang & Tseng, 2005); this simplifies the analysis, but there is great doubt if it can accurately predict the combined effect of the non-linear viscous damping, provided by the dampers, along with the non-linear hysteretic damping, provided by the isolators, while appropriately addressing the soil-structure interaction characteristics and the nonlinearities introduced by pounding effects. Another challenge is the explicit consideration of the variability of future excitations and of the properties of the structural system since a significant degree of sensitivity has been reported between these characteristics and the overall system performance (Dimitrakopoulos et al., 2009; Perros & Papadimitriou, 2009).

Figure 2. Schematic of augmented system and seismic risk description



This chapter presents a methodology that addresses all aforementioned challenges for the design of supplemental dampers for seismically isolated, short-spanned bridges. A probabilistic framework is proposed for addressing the various sources of uncertainty and quantifying the overall performance. This is established by characterizing the relative plausibility of different properties of the system and its environment (representing future excitations) by appropriate probability models. Seismic risk is then defined as the expected value of the system performance over these models. Stochastic simulation is implemented for evaluation of the multidimensional probabilistic integral representing seismic risk and an efficient algorithm (Kleinmann, Spall, & Naiman, 1999; Spall, 1998) is adopted for performing the associated optimization and selecting the optimal damper parameters. This establishes a versatile, simulation-based framework for detailed characterization of seismic risk that puts no restrictions in the complexity of the modeling approach adopted. Thus, the bridge response is evaluated through nonlinear dynamic analysis allowing for direct incorporation of all important sources of nonlin-

earities into the model used at the design stage. A realistic model is also discussed for description of near-fault ground motions. This model establishes a direct link, in a probabilistic sense, between our knowledge about the characteristics of the seismic hazard in the structural site and future ground motions. An efficient probabilistic sensitivity analysis is also discussed for investigating the influence of each of the uncertain model parameters to the overall seismic risk.

PROBABILISTIC DESIGN FRAMEWORK

Evaluation of seismic risk for isolated bridges requires adoption of appropriate models for (i) the bridge system itself, (ii) the excitation (ground motion), and (iii) the system performance (Figure 2). The combination of the first two models provides the structural response. The performance evaluation model assesses, then, the favorability of this response based on the selected performance criteria.

The characteristics of the models for the seismically isolated bridge and for future earthquake excitations, described in the next two sections are not known with absolute certainty. Uncertainties may pertain to (i) the properties of the bridge system, for example, related to stiffness or damping characteristics and traffic loads; to (ii) the variability of future seismic events, i.e., the moment magnitude or the epicentral distance; to (iii) the predictive relationships about the characteristics of the excitation given a specific seismic event, for example duration of strong ground motion or peak acceleration; or to (iv) parameters related to the performance of the system, for example, thresholds defining fragility of system components. A probability logic approach provides a rational and consistent framework for quantifying all these uncertainties and explicitly incorporating them into the system description. In this approach, probability can be interpreted as a means of describing the incomplete or missing information (Jaynes, 2003) about the system under consideration and its environment, representing the seismic hazard, through the entire life-cycle (Taflanidis & Beck, 2009a).

To formalize these ideas denote the vector of controllable system parameters, referred to herein as design variables, be $\boldsymbol{\varphi} \in \Phi \subset \mathbb{R}^{n_\varphi}$, where Φ denotes the admissible design space with volume V_φ . These variables are related to the adjustable characteristics of the damper application, for example viscosity properties or damper size. Let $\boldsymbol{\theta} \in \Theta \subset \mathbb{R}^{n_\theta}$, denote the augmented vector of model parameters where Θ represents the space of possible model parameter values. Vector $\boldsymbol{\theta}$ is composed of all the model parameters for the individual structural system, excitation, and performance evaluation models indicated in Figure 2. The seismic performance of the bridge, for specific design $\boldsymbol{\varphi}$ and model description $\boldsymbol{\theta}$, is characterized by the performance measure $h(\boldsymbol{\varphi}, \boldsymbol{\theta}) : \mathbb{R}^{n_\varphi \times n_\theta} \rightarrow \mathbb{R}^+$, which ultimately quantifies seismic utility or risk according to the de-

signer criteria (an example is discussed in the illustrative application considered later). The conventions that lower values for $h(\boldsymbol{\varphi}, \boldsymbol{\theta})$ correspond to better performance, i.e. it is associated with risk and ultimately corresponds to a risk measure, is used herein.

For addressing the uncertainty in $\boldsymbol{\theta}$ a probability density function (PDF) $p(\boldsymbol{\theta})$, is assigned to it, quantifying the relative likelihood of different model parameter values. This PDF incorporates our available knowledge about the structural system and its environment into the respective knowledge, and should be selected based on this knowledge (Jaynes, 2003). In this setting, the overall performance, i.e. seismic risk, is described by the following probabilistic integral that corresponds to the expected value of $h(\boldsymbol{\varphi}, \boldsymbol{\theta})$

$$C(\boldsymbol{\varphi}) = \int_{\Theta} h(\boldsymbol{\varphi}, \boldsymbol{\theta}) p(\boldsymbol{\theta}) d\boldsymbol{\theta} \quad (1)$$

Different selections for $h(\boldsymbol{\varphi})$ lead to different characterization for seismic risk; for example, if $h(\boldsymbol{\varphi}, \boldsymbol{\theta}) = C_{in}(\boldsymbol{\varphi}, \boldsymbol{\theta}) + C_{lj}(\boldsymbol{\varphi}, \boldsymbol{\theta})$, where $C_{in}(\boldsymbol{\varphi}, \boldsymbol{\theta})$ corresponds to the initial cost and $C_{lj}(\boldsymbol{\varphi}, \boldsymbol{\theta})$ to the additional cost over the lifetime due to repairs or downtime, then risk corresponds to life cycle cost (Taflanidis & Beck, 2009a), if $h(\boldsymbol{\varphi}, \boldsymbol{\theta}) = I_F(\boldsymbol{\varphi}, \boldsymbol{\theta})$, where $I_F(\boldsymbol{\varphi}, \boldsymbol{\theta})$ is the indicator function for some event F (one if F has occurred and zero if not), then risk corresponds to the probability of unacceptable performance (Taflanidis & Beck, 2009b).

The probabilistically-robust stochastic design (Taflanidis & Beck, 2008) is then established by selecting the design variables that minimizes seismic risk $C(\boldsymbol{\varphi})$

$$\boldsymbol{\varphi}^* = \arg \min_{\boldsymbol{\varphi} \in \Phi} \left\{ C(\boldsymbol{\varphi}) \mid f_c(\boldsymbol{\varphi}) \geq 0 \right\} \quad (2)$$

Where \arg stands for “argument that minimizes” and $f_c(\boldsymbol{\varphi})$ is a vector of deterministic constraints, related, for example, to location or space constraints for the dampers. Note that in this

formulation, all performance requirements against future natural hazards are directly incorporated in the objective function. Finally, the constraints in Equation 2 may be incorporated into the definition of admissible design space Φ , which leads to the simplified expression:

$$\boldsymbol{\varphi}^* = \arg \min_{\boldsymbol{\varphi} \in \Phi} C(\boldsymbol{\varphi}) \quad (3)$$

For evaluation of Equation 1 and the optimization in Equation 3 an approach based on stochastic simulation will be discussed in detail later. Along with the comprehensive risk quantification and the bridge and excitation models described next that establishes a versatile, end-to-end simulation based framework for detailed characterization and optimization of seismic risk. This framework puts no restrictions in the complexity of the models used allowing for incorporation of all important sources of nonlinearities and adoption of advanced models for characterization of the ground motion. Thus, it allows an efficient, accurate estimation of the seismic risk by appropriate selection of the characteristics of the stochastic analysis. Next we will discuss in detail the bridge and excitation models used in this study, and then proceed to the computational framework for performing the optimization in Equation 3.

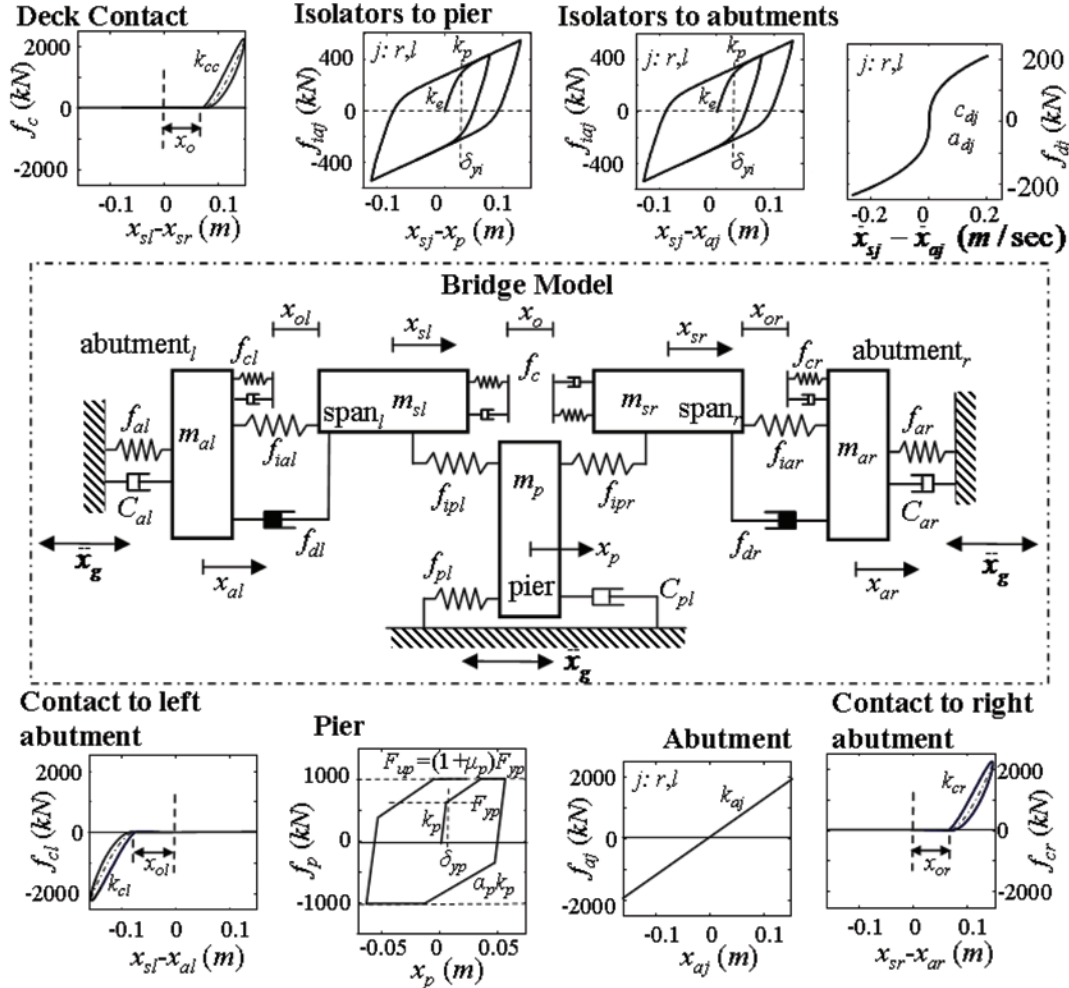
BRIDGE MODEL

For simplicity of the analysis, we will assume a two-span (as in Figure 1), straight bridge, whose fundamental behavior in the longitudinal direction can be adequately characterized with a planar (two-dimensional) model. It is noted that the bridge is assumed to be parallel to the direction of the seismic wave propagation and also that it does not fall in the category of long-span bridges. The ideas discussed in the following sections, related to probabilistic modeling and design, can be directly extended, though, to more complex

cases, for example, skewed bridges, for which a complete three dimensional model is required to accurately capture their response under seismic excitation. Each span of the bridge is modeled here as a rigid body. For appropriately addressing at the design stage the pounding between adjacent spans, soil-structure interaction characteristics and the nonlinear behavior of isolators and dampers, nonlinear dynamic analysis is used (Makris & Zhang, 2004; Saadeghvaziri & Yazdani-Motlagh, 2008; Zhang, Makris, & Delis, 2004). The pounding with the abutment and the dynamic characteristics of the latter are incorporated in the analysis by modeling the abutment as a mass (Saadeghvaziri & Yazdani-Motlagh, 2008) connected to the ground by a spring and a dashpot, with stiffness and damping properties that are related to the local soil conditions (Zhang et al., 2004). The vibration behavior of the isolators, the dampers and the pier is incorporated by appropriate nonlinear models (Ruangrassamee & Kawashima, 2003; Taflanidis, 2009; Taflanidis & Beck, 2009a; Zhang et al., 2004). The pounding between adjacent spans, or to the abutments, is approximated here as a Hertz contact force with an additional non-linear damper to account for energy losses (Muthukumar & DesRoches, 2006).

A schematic of the bridge model with two spans, supported by seismic isolators to the abutments and to the intermediate pier is illustrated in Figure 3. The two spans and abutments are distinguished by using the convention right and left for each of them. The gap between the two spans is denoted by x_o and the gap between the left or right span and the corresponding abutment by x_{ol} or x_{or} , respectively. Let also x_p , x_{sl} , x_{sr} , x_{al} , x_{ar} denote, respectively, the displacement relative to the ground of the pier, the left and right span of the bridge and the left and right abutment. The total mass for the pier, the left and right span of the bridge and the left and right abutment are denoted, respectively, by m_p , m_{sl} , m_{sr} , m_{al} , m_{ar} . This total mass includes both the weight of each component as well as the live loads due to ve-

Figure 3. Schematic model for two-span bridge system with seismic isolators and supplemental dampers



hicle traffic. Additionally let \$C_p\$, \$C_{al}\$, \$C_{ar}\$ denote, respectively, the damping coefficient for the pier and the left and right abutment. The equation for the seismically isolated system is then derived by equilibrium conditions as:

$$\begin{aligned}
 m_{sl}\ddot{x}_{sl} + (f_{ial} + f_{cl} + f_{dl}) + f_{ipl} + f_c &= 0 \\
 m_{sr}\ddot{x}_{sr} + (f_{iar} + f_{cr} + f_{dr}) + f_{ipr} - f_c &= 0 \\
 m_p\ddot{x}_p + C_p\dot{x}_p + f_p - f_{ipl} - f_{ipr} &= -m_p\ddot{x}_g \\
 m_{al}\ddot{x}_{al} + C_{al}\dot{x}_{al} + f_{al} - (f_{ial} + f_{cl} + f_{dl}) &= -m_{al}\ddot{x}_g \\
 m_{ar}\ddot{x}_{ar} + C_{ar}\dot{x}_{ar} + f_{ar} - (f_{iar} + f_{cr} + f_{dr}) &= -m_{ar}\ddot{x}_g
 \end{aligned} \tag{4}$$

where \$\ddot{x}_g\$ is the ground acceleration; \$f_c\$, \$f_{cl}\$ and \$f_{cr}\$ are the impact forces due to pounding between the two spans or between the spans and the left or right, respectively, abutments; \$f_{dl}\$ and \$f_{dr}\$ are the left and right damper forces; and \$f_{ial}\$, \$f_{ipl}\$ or \$f_{iar}\$, \$f_{ipr}\$ are the forces of the isolators that support the left or right span of the bridge to the abutment and the pier, respectively; \$f_p\$ corresponds to the restoring force for the pier which is modeled as hysteretic bilinear force with ultimate strength as depicted in Figure 3. Strength and stiffness deterioration may be additionally incorporated

into this model (Taflanidis & Beck, 2009a). All these forces are discussed in more detail next.

The hysteretic behavior of each isolator is modeled by a Bouc-Wen model which is described by the following basic differential equation (Taflanidis, 2009):

$$\delta_{yi}\dot{z} = \alpha_{is}\dot{x}_b - z^2(\gamma_{is} \operatorname{sgn}(\dot{x}_b z) + \beta_{is})\dot{x}_b \quad (5)$$

where x_b is the displacement of the isolator, which corresponds to the relative displacement of the span relative to its support; z is a dimensionless hysteretic state-variable that is constrained by values ± 1 ; δ_{yi} is the yield displacement; and α_{is} , β_{is} , and γ_{is} are dimensionless quantities that characterize the properties of the hysteretic behavior. Typical values for these parameters are used here, taken as $\alpha_{is}=1$, $\beta_{is}=0.1$, and $\gamma_{is}=0.9$ (Taflanidis, 2009). The isolator forces f_i may be then described based on the state-variable z and the relative isolator displacement x_b . For friction-pendulum isolators and lead-rubber bearings, these forces are given respectively, by (Taflanidis, 2009):

$$f_i = k_p x_b + \mu N_t z \quad (6)$$

$$f_i = k_p x_b + (k_e - k_p)\delta_{yi}z \quad (7)$$

where k_p is the post yield stiffness, N_t the average normal force at the bearing, μ is the coefficient of friction, k_e the pre yield stiffness. For the left span x_b is given by $x_b=x_{sl}-x_{al}$ and $x_b=x_{sl}-x_p$ for the isolators supporting it to the abutment and the pier, respectively. For the right span the corresponding quantities are $x_b=x_{sr}-x_{ar}$ and $x_b=x_{sr}-x_p$, respectively.

The force due to pounding between the adjacent spans is modelled as a single-sided Hertz contact force with an additional damper that incorporates in the analysis the energy dissipated during the contact (Muthukumar & DesRoches, 2006)

$$f_c = \begin{cases} 0 & ; \text{if } x_{sl} - x_{sr} < x_o \\ k_{cc}(x_{sl} - x_{sr} - x_o)^{\beta_c} + c_{cc}(\dot{x}_{sl} - \dot{x}_{sr}) & ; \text{if } x_{sl} - x_{sr} \geq x_o \end{cases} \quad (8)$$

where k_{cc} is the contact stiffness, c_{cc} the non-linear damper coefficient and β_c the contact exponent, taken here with the nominal value for Hertz type of impact, i.e. $\beta_c=1.5$ (Muthukumar & DesRoches, 2006). The damper coefficient may be expressed in terms of the ratio of relative velocities of the pounding bodies before and after the contact, called coefficient of restitution e_{cc} , as (Muthukumar & DesRoches, 2006):

$$c_{cc} = 0.75k_{cc} \frac{|x_{sl} - x_{sr} - x_o|^{\beta_c}}{|v_{con}|} (1 - e_{cc}^2) \quad (9)$$

where v_{con} is the relative velocity at the initiation of contact. The contact stiffness is a function of the elastic properties and the geometry of the colliding bodies. For elastic contact between two isotropic spheres with radius R_1 and R_2 , the following relationship holds (Werner, 1960)

$$k_c = \frac{4}{3\pi(\delta_1 + \delta_2)} \sqrt{\frac{R_1 R_2}{R_1 + R_2}} \quad (10)$$

where δ_i , $i=1,2$ is a material parameter for the i th body given by

$$\delta_i = \frac{1 - v_i^2}{\pi E_i} \quad (11)$$

with v_i and E_i representing its Poisson's ratio and modulus of elasticity, respectively. To calculate(10) each of the spans can be roughly approximated as a sphere with radius (Muthukumar & DesRoches, 2006)

$$R_i = \sqrt[3]{\frac{3m_i}{4\pi\rho}} \quad (12)$$

Box 1.

$$f_{cl} = \begin{cases} 0 & ; \text{if } x_{sl} - x_{al} > -x_{ol} \\ -k_{cl} |x_{sl} - x_{al} + x_{ol}|^{\beta_c} + c_{cl} (\dot{x}_{sl} - \dot{x}_{al}) & ; \text{if } x_{sl} - x_{al} \leq -x_{ol} \end{cases} \quad (13)$$

Box 2.

$$f_{cr} = \begin{cases} 0 & ; \text{if } x_{sr} - x_{ar} < x_{or} \\ k_{cr} (x_{sr} - x_{ar} - x_{or})^{\beta_c} + c_{cr} (\dot{x}_{sr} - \dot{x}_{ar}) & ; \text{if } x_{sr} - x_{ar} \geq x_{or} \end{cases} \quad (14)$$

where ρ is the material density and m_i corresponds to the mass of the span. R_i and δ_i are calculated based on the total mass and material properties of each span and then the contact stiffness k_{cc} is equal to k_c given by Equation 10.

The force due to pounding of the left span to the left abutment is modeled as left-sided contact force in Box 1 and similar modeling holds for the pounding of the right span to the right abutment (see Box 2).

The contact parameters k_{cl} , k_{cr} and c_{cl} , c_{cr} are defined similarly to the case of contact between the spans, using the properties (mass, velocity) of the colliding bodies of interest. The restitution coefficients for collision of the left or right span to their neighboring abutments are denoted by e_{cl} and e_{cr} respectively.

The damper forces depend on the type of application. For simplicity only the case of passive viscous dampers is discussed here, but the framework presented in the next sections is directly extendable to the design of other type of dampers as well. For fluid viscous dampers the damper forces are a function of the relative velocity across the end points of the damper. For the damper connecting the left span to the corresponding abutment (Makris & Zhang, 2004) they may be described in Box 3.

$$f_{dl} = c_d \operatorname{sgn}(\dot{x}_{sl} - \dot{x}_{al}) |\dot{x}_{sl} - \dot{x}_{al}|^{a_d} \quad (15)$$

where c_d is the damping coefficient and a_d an exponent parameter. These adjustable characteristics are the controllable damper parameters to be selected at the design stage. Note that for $a_d=1$ relationship 15 corresponds to a linear viscous damper. Maximum forcing capabilities for the damper, related to cost constraints, may be incorporated into the model as a saturation of the damper force to f_{\max} leading to (see Box 4).

For the damper connecting the right span to the abutment the damper force is similarly expressed in Box 4.

EXCITATION MODEL

The analysis and design of any seismic structural system needs to be performed considering potential damaging future ground motions. For base-isolated bridges this translates to consideration of near-fault ground motions.

The last two decades numerous models have been proposed for ground motion modeling (Atkinson & Silva, 2000; Shinozuka, Deodatis, Zhang, & Papageorgiou, 1999) that incorporate important characteristics of the seismic source as well as of the earth medium. Other studies

Box 3.

$$f_{dl} = \begin{cases} f_{\max} \operatorname{sgn}(\dot{x}_{sl} - \dot{x}_{al}) & ; \text{ if } c_d |\dot{x}_{sl} - \dot{x}_{al}|^{a_d} > f_{\max} \\ c_d \operatorname{sgn}(\dot{x}_{sl} - \dot{x}_{al}) |\dot{x}_{sl} - \dot{x}_{al}|^{a_d} & ; \text{ if } c_d |\dot{x}_{sl} - \dot{x}_{al}|^{a_d} \leq f_{\max} \end{cases} \quad (16)$$

Box 4.

$$f_{dr} = \begin{cases} f_{\max} \operatorname{sgn}(\dot{x}_{sr} - \dot{x}_{ar}) & ; \text{ if } c_d |\dot{x}_{sr} - \dot{x}_{ar}|^{a_d} > f_{\max} \\ c_d \operatorname{sgn}(\dot{x}_{sr} - \dot{x}_{ar}) |\dot{x}_{sr} - \dot{x}_{ar}|^{a_d} & ; \text{ if } c_d |\dot{x}_{sr} - \dot{x}_{ar}|^{a_d} \leq f_{\max} \end{cases} \quad (17)$$

have focused on the estimation of the spatial variability of the seismic ground motions which is a result of the transmission of the waves from the source through the different earth strata to the ground surface (Zerva, 2008). The latter effect is considered to be very crucial in the design of elongated structures such as long – span bridges. An important factor of the spatial variability is the site response effect (i.e. the difference at the local soil conditions at two stations), especially for structures situated in regions with rapidly changing local soil conditions and for bridges with short or medium length spans (Der Kiureghian, 1996). Moreover, other researchers have developed models that address the nonstationarity of the ground motions by accounting the time variation of both intensity and frequency content (Conte & Peng, 1997; Rezaeian & Der Kiureghian, 2008). An alternative tool for modeling uncertainty of future earthquake loads is the critical excitation method in which the ground motion is represented as a product of a Fourier series and an envelope function and in general involves estimating the excitation producing the maximum response from a class of allowable inputs (Abbas, 2011; Takewaki, 2002).

For the proposed probabilistic framework, a complete stochastic model for characterizing the acceleration time-history of near-fault excitations is required, that addresses all important sources of

uncertainty. Such a model was proposed recently in (Taflanidis, Scruggs, & Beck, 2008) and is briefly discussed next. According to it the high-frequency and long-period components of the motion are independently modeled and then combined to form the acceleration time history. It is pointed out that the spatial variation of the seismic input is not been taken into account, because the bridge systems we focus on are relatively short-spanned.

High – Frequency Component

The fairly general, point source stochastic method (Boore, 2003) is selected for modeling the higher-frequency (>0.1–0.2 Hz) component of ground motions. This approach corresponds to ‘source – based’ stochastic ground motion models, developed by considering the physics of the fault rupture at the source as well as the propagation of seismic waves through the entire ground medium till the structural site. It is based on a parametric description of the ground motion’s radiation spectrum $A(f, M, r)$, which is expressed as a function of the frequency, f , for specific values of the earthquake magnitude, M , and epicentral distance, r . This spectrum consists of many factors which account for the spectral effects from the source (source spectrum) as well as propagation through the earth’s crust up to the structural site. The duration of the ground motion is addressed

through an envelope function $e(t;M,r)$, which again depends on M and r . These frequency and time domain functions, $A(f;M,r)$ and $e(t;M,r)$, completely describe the model and their characteristics are provided by predictive relationships that relate them directly to the seismic hazard, i.e., to M and r . More details on them are provided in (Boore, 2003; Taflanidis et al., 2008). Particularly, the two-corner point-source model by Atkinson & Silva (2000) can be selected for the source spectrum because of its equivalence to finite fault models. This equivalence is important because of the desire to realistically describe near-fault motions and adaptation of a point-source model might not efficiently address the proximity of the site to the source (Mavroeidis & Papageorgiou, 2003). The spectrum developed by Atkinson & Silva (2000) has been reported in their studies to efficiently address this characteristic.

The time-history (output) for a specific event magnitude, M , and source distance, r , is obtained according to this model by modulating a white-noise sequence $\mathbf{Z}_w = [\mathbf{Z}_w(i\Delta t); i=1,2,\dots, N_T]$ by $e(t;M,r)$ and subsequently by $A(f;M,r)$ through the following steps: the sequence \mathbf{Z}_w is multiplied by the envelope function $e(t;M,r)$ and then transformed to the frequency domain; it is normalized by the square root of the mean square of the amplitude spectrum and then multiplied by the radiation spectrum $A(f;M,r)$; finally it is transformed back to the time domain to yield the desired acceleration time history. The model parameters consist of the seismological parameters, M and r , describing the seismic hazard, the white-noise sequence \mathbf{Z}_w and the predictive relationships for $A(f;M,r)$ and $e(t;M,r)$. Figure 4 shows functions $A(f;M,r)$ and $e(t;M,r)$ for different values of M and r . It can be seen that as the moment magnitude increases the duration of the envelope function also increases and the spectral amplitude becomes larger at all frequencies with a shift of dominant frequency content towards the lower-frequency regime. Reduction of r primarily contributes to an overall increase of the spectral amplitude. Alternatively, a

“record-based” stochastic ground motion could be used for modelling the high frequency component of the ground motion. An example of such a model is the one developed recently by Rezaeian & Der Kiureghian (2008), which has the advantage that additionally addresses spectral nonstationarities.

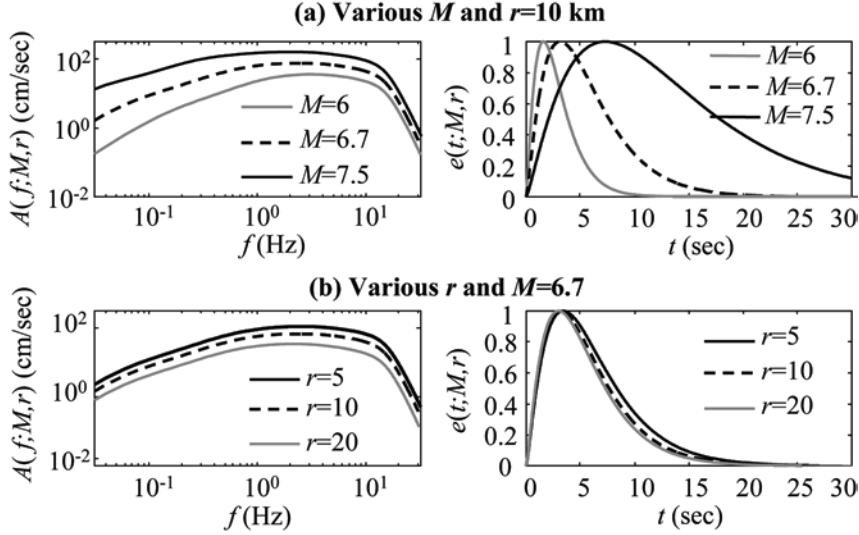
Long Period Pulse

For describing the pulse characteristic of near-fault ground motions, the simple analytical model developed by Mavroeidis & Papageorgiou (2003) is selected. This model is based on an empirical description of near-fault ground motions and has been calibrated using actual near-field ground motion records from all over the world. According to it, the pulse component of near-fault motions is described through the following expression for the ground motion velocity pulse:

$$V(t) = \begin{cases} \frac{A_p}{2} \left[1 + \cos\left(\frac{2\pi f_p}{\gamma_p} (t - t_o)\right) \right] \cos[2\pi f_p(t - t_o) + \nu_p] & \text{if } t \in \left[t_o - \frac{\gamma_p}{2f_p}, t_o + \frac{\gamma_p}{2f_p}\right] \\ = 0 & \text{otherwise} \end{cases} \quad (18)$$

where $A_p, f_p, \nu_p, \gamma_p$, and t_o describe the signal amplitude, prevailing frequency, phase angle, oscillatory character (i.e., number of half cycles), and time shift to specify the envelope's peak, respectively. Note that all parameters have an unambiguous physical meaning. A number of studies (Alavi & Krawinkler, 2000; Bray & Rodriguez-Marek, 2004; Mavroeidis & Papageorgiou, 2003) have been directed towards developing predictive relationships that connect these pulse characteristics to the seismic hazard of a site. These studies link the amplitude and frequency of near-fault pulse to the moment magnitude and epicentral distance of seismic events, but they also acknowledge that significant uncertainty exists in such relationships. This indicates that a probabilistic characterization is more appropriate. For example, according to the study by Bray and Rodriguez-Marek (2004) the following relationships hold for the pulse frequency f_p and the peak ground velocity A_v

Figure 4. Radiation spectrum and envelope function, for various M , r



$$\ln f_p = \ln \hat{f}_p + e_f \quad (19)$$

$$\ln A_v = \ln \hat{A}_v + e_v \quad (20)$$

where \hat{f}_p and \hat{A}_v are median values (provided through a regression analysis), and e_f and e_v are prediction errors following a Gaussian distribution with zero mean and large standard deviation. For rock sites the predictive relationships for the median values are (Bray & Rodriguez-Marek, 2004)

$$\ln \hat{f}_p = 8.60 - 1.32M \quad (21)$$

$$\ln \hat{A}_v = 4.46 + 0.34M - 0.58\ln(r^2 + 7^2) \quad (22)$$

whereas the standard deviation for the prediction errors e_f and e_v is estimated as 0.4 and 0.39, respectively. Note that according to Equation 22 the pulse amplitude, which is directly related to the peak ground velocity (Mavroeidis & Papageorgiou, 2003), varies almost inversely proportional to the epicentral distance. This indicates a strong

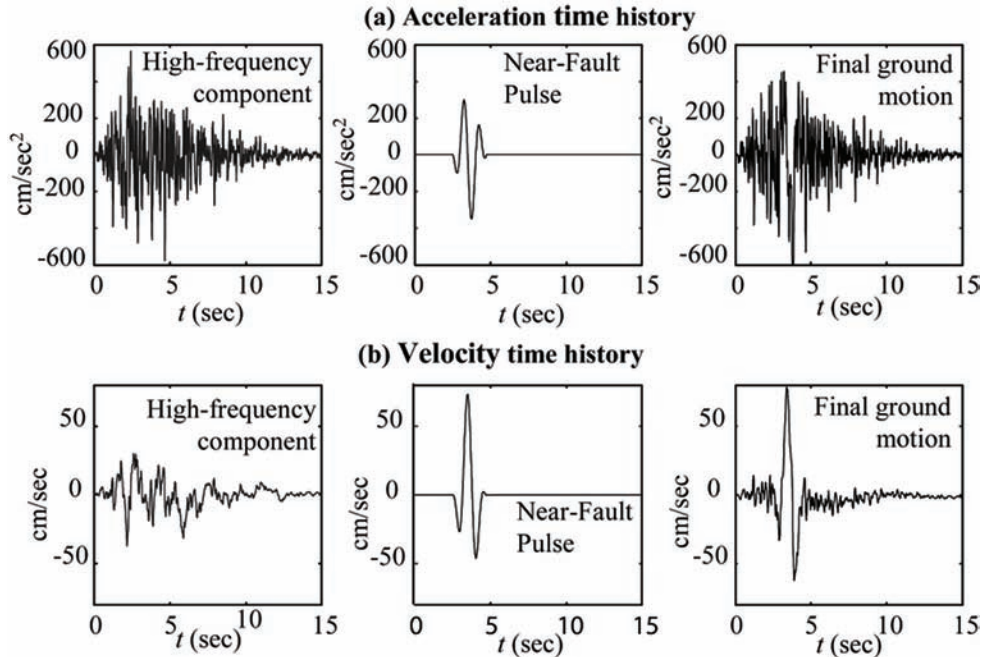
correlation between the existence of the pulse and the proximity of the structural site to the seismic source/fault. For epicentral distances larger than 15-20 km the pulse component according to this equation is negligible (Bray & Rodriguez-Marek, 2004).

For the rest of the pulse parameters, the phase and the number of half cycles, no clear link to the seismic hazard of the structural site has been yet identified. They need to be considered as independent model parameters. The study (Mavroeidis & Papageorgiou, 2003) provides relevant values for these parameters by fitting Equation 18 to a suite of recorded near-fault ground motions.

Near-Fault Excitation Model

The *stochastic model* for near-fault motions is finally established by combining the above two components through the methodology initially developed in (Mavroeidis & Papageorgiou, 2003). The model parameters consist of the seismological parameters M and r , the additional parameters for the velocity pulse, v_p , γ_p , the white noise sequence \mathbf{Z}_w , and the predictive relationships for f_p , A_v , and

Figure 5. Sample near-fault ground motion; acceleration and velocity time histories



for the characteristics of $A(f; M, r)$ and $e(t; M, r)$. The following procedure describes the final model:

1. Generate the high-frequency component of the acceleration time history by the stochastic method.
2. Generate a velocity time history for the near-field pulse using Equation 18. The pulse is shifted in time to coincide with the peak of the envelope $e(t; M, r)$. This defines the value of the time shift parameter t_0 . Differentiate the velocity time series to obtain an acceleration time series.
3. Calculate the Fourier transform of the acceleration time histories generated in steps 1 and 2.
4. Subtract the Fourier amplitude of the time series generated in step 2 from the spectrum of the series generated in 1.
5. Construct a synthetic acceleration time history so that its Fourier amplitude is the one calculated in step 4 and its Fourier phase

coincides with the phase of the time history generated in step 2.

6. Finally superimpose the time histories generated in steps 2 and step 5.

Figure 5 illustrate a near-fault ground motion sample for an earthquake $M=6.7$, $r=5\text{km}$ and parameters for the near-fault pulse $\gamma_p=1.7$, $v_p=\pi/6$. Both the acceleration and velocity time histories of the synthetic ground-motion are presented. The existence of the near-fault pulse is evident when looking at the velocity time history.

STOCHASTIC ANALYSIS, OPTIMIZATION, AND SENSITIVITY

Stochastic Analysis

Since the nonlinear models considered for the bridge and the excitation are complex and include a large number of uncertain model parameters the

multi-dimensional integral in Equation 1 defining seismic risk and involved in optimization in Equation 3 cannot be calculated, or even accurately approximated, analytically. An efficient alternative approach is to estimate the integral by *stochastic simulation* (Taflanidis & Beck, 2008). Using a finite number, N , of samples of $\boldsymbol{\Theta}$ drawn from some importance sampling density $p_{is}(\boldsymbol{\Theta})$, an estimate for (1) is given by the *stochastic analysis*:

$$\hat{C}(\boldsymbol{\Phi}) = \hat{C}(\boldsymbol{\Phi}, \Omega) = \frac{1}{N} \sum_{i=1}^N h(\boldsymbol{\Phi}, \boldsymbol{\Theta}^i) \frac{p(\boldsymbol{\Theta}^i)}{p_{is}(\boldsymbol{\Theta}^i)} \quad (23)$$

where vector $\boldsymbol{\Theta}^i$ denotes the sample of the uncertain parameters used in the i^{th} simulation and Ω denotes the entire samples set $\{\boldsymbol{\Theta}^i\}$ used in the evaluation. As $N \rightarrow \infty$, then $\hat{C} \rightarrow C$ but even for finite, large enough N , Equation 23 gives a good approximation for the integral in Equation 1. The importance sampling density $p_{is}(\boldsymbol{\Theta})$ may be used to improve the efficiency of this estimation. This is established by focusing on regions of the $\boldsymbol{\Theta}$ space that contribute more to the integrand of the probabilistic integral in Equation 1 (Taflanidis & Beck, 2008), i.e. by selecting a proposal density that resembles that integrand. If $p_{is}(\boldsymbol{\Theta})=p(\boldsymbol{\Theta})$ then the evaluation in Equation 23 corresponds to direct Monte Carlo integration. For problems with large number of model parameters, as the application discussed here, choosing efficient importance sampling densities for all components of $\boldsymbol{\Theta}$ is challenging and can lead to convergence problems for the estimator of Equation 23; thus it is preferable to formulate importance sampling densities only for the important components of $\boldsymbol{\Theta}$, i.e. the ones that have biggest influence on the seismic risk, and use $q(\cdot)=p(\cdot)$ for the rest (Taflanidis & Beck, 2008). For seismic risk applications the characteristics of the hazard, especially the moment magnitude or epicentral distance are generally expected to have the strongest impact on the calculated risk (Taflanidis & Beck, 2009a), so

selection of importance sampling densities may preliminary focus on them.

Optimization for the Design Variables under Uncertainty

The optimal design choice is finally given by the optimization under uncertainty problem (Spall, 2003):

$$\boldsymbol{\Phi}^* = \arg \min_{\boldsymbol{\Phi} \in \Phi} \hat{C}(\boldsymbol{\Phi}) \quad (24)$$

The estimate of the objective function for this optimization involves an unavoidable estimation error and significant computational cost since N evaluations of the model response are needed for each stochastic analysis. These features that make this optimization problem challenging. Many numerical techniques and optimization algorithms have been developed to address such challenges in design optimization under uncertainty (Royset & Polak, 2004; Ruszcynski & Shapiro, 2003; Spall, 2003). Such approaches may involve one or more of the following strategies: (i) use of common random numbers to reduce the relative importance of the estimation error when comparing two design choices that are “close” in the design space, (ii) application of exterior sampling techniques which adopt the same stream of random numbers throughout all iterations in the optimization process, thus transforming the stochastic problem into a deterministic one, (iii) simultaneous perturbation stochastic search techniques, which approximate at each iteration the gradient vector by performing only two evaluations of the objective function in a random search direction, and (iv) gradient-free algorithms (such as evolutionary algorithms) which do not require derivative information. References (Spall, 2003; Taflanidis & Beck, 2008) provide reviews of appropriate techniques and algorithms for such optimization problems. The very efficient Simultaneous Perturbation Stochastic Approximation (SPSA)

with Common Random Numbers (CRN) will be employed in this study and is briefly reviewed next.

Simultaneous Perturbation Stochastic Approximation

Simultaneous-perturbation stochastic approximation (SPSA) (Kleinmann et al., 1999; Spall, 2003) is an efficient stochastic search method. It is based on the observation that one properly chosen simultaneous random perturbation in all components of ϕ provides as much information for optimization purposes in the long run as a full set of one at a time changes of each component. Thus, it uses only two evaluations of the objective function, in a direction randomly chosen at each iteration, to form an approximation to the gradient vector. It also uses the notion of stochastic approximation (Kushner & Yin, 2003) which can significantly improve the computational efficiency of stochastic search applications (Spall, 2003). The latter approximation is performed by establishing (through proper recursive formulas) an equivalent averaging across the iterations of the optimization algorithm, instead of getting higher accuracy estimates for the objective function at each iteration, that is averaging over one single iteration.

The implementation of SPSA takes the iterative form:

$$\Phi_{k+1} = \Phi_k - \alpha_k \mathbf{g}_k(\Phi_k, \Omega_k) \quad (25)$$

where $\Phi_1 \in \Phi$ is the chosen point to initiate the algorithm and the j^{th} component for the Common Random Number (CRN) simultaneous perturbation approximation to the gradient vector in the k^{th} iteration, $\mathbf{g}_k(\Phi_k, \Omega_k)$, is given by:

$$g_{k,j} = \frac{\hat{C}(\Phi_k + c_k \Delta_k, \Omega_k) - \hat{C}(\Phi_k - c_k \Delta_k, \Omega_k)}{2c_k \Delta_{k,j}} \quad (26)$$

where Ω_k is the sample set used at iteration k and $\Delta_k \in \mathbb{R}^{n_\varphi}$ is a vector of mutually independent random variables that defines the random direction of simultaneous perturbation for Φ_k and that satisfies the statistical properties given in (Spall, 2003). A symmetric Bernoulli ± 1 distribution is typically chosen for the components of Δ_k . The selection for the sequences $\{c_k\}$ and $\{\alpha_k\}$ is discussed in detail in (Kleinmann et al., 1999). A choice that guarantees asymptotic convergence to Φ^* is $\alpha_k = \alpha/(k + w)^\beta$ and $c_k = c_1/k^\zeta$, where $4\zeta - \beta > 0$, $2\beta - 2\zeta > 1$, with $w, \zeta > 0$ and $0 < \beta \leq 1$. This selection leads to a rate of convergence that asymptotically approaches $k^{-\beta/2}$ when CRN is used (Kleinmann et al., 1999). The asymptotically optimal choice for β is, thus, 1. In applications where efficiency using a small number of iterations is sought after, use of smaller values for β are suggested in (Spall, 2003). For complex design optimizations, where the computational cost for each iteration of the algorithm is high, the latter suggestion should be adopted. Note that the same set of random numbers is selected for the two estimates of the objective function at each iteration used to calculate the gradient in Equation 26. This reduces the variance of the difference of these estimates thus creating a consistent estimation error (Glasserman & Yao, 1992; Taflanidis & Beck, 2008) and improving the efficiency of the estimate in Equation 26 (reduces relative importance of estimation error). Across the iterations of the optimization algorithm, though, this sample set is not the same; thus there is no dependence of the optimal solution on it (i.e. the approach here does not correspond to an exterior sampling technique).

Regarding the rest of the parameters for the sequences $\{c_k\}$ and $\{\alpha_k\}$: w is typically set to 10% of the number of iterations selected for the algorithm and the initial step c_1 is chosen “close” to the standard deviation of the prediction error for the stochastic estimate in Equation 23. The value of α can be determined based on the estimate of

Box 5.

$$\pi(\theta_i | \Phi) = \int \pi(\Theta | \Phi) d\mathbf{x}_i = \frac{1}{\int_{\Theta} h(\Phi, \Theta) p(\Theta) d\Theta} \int h(\Phi, \Theta) p(\Theta) d\mathbf{x}_i \propto p(\theta_i) \int h(\Phi, \Theta) p(\mathbf{x}_i | \theta_i) d\mathbf{x}_i \quad (28)$$

\mathbf{g}_i and the desired step size for the first iteration. Some initial trials are generally needed in order to make a good selection for α , especially when little prior insight is available for the sensitivity of the objective function to each of the design variables. Convergence of the iterative process is judged based on the value $\|\Phi_{k+1} - \Phi_k\|$ in the last few steps, for an appropriate selected vector norm. Blocking rules can also be applied in order to avoid potential divergence of the algorithm, especially in the first iterations (Spall, 2003).

Probabilistic Sensitivity Analysis for Model Parameters

An extension of the optimization framework may be established to additionally quantify the importance of each of the model parameters in affecting the overall risk. Foundation of this methodology is the definition of an auxiliary probability density function that is proportional to the integrand of the seismic risk integral for each design configuration

$$\pi(\Theta | \Phi) = \frac{h(\Phi, \Theta) p(\Theta)}{\int_{\Theta} h(\Phi, \Theta) p(\Theta) d\Theta} \propto h(\Phi, \Theta) p(\Theta) \quad (27)$$

where \propto denotes proportionality and the denominator in $\pi(\Theta | \Phi)$ is simply a normalization constant that will not be explicitly needed. The sensitivity analysis is established by comparing this auxiliary distribution $\pi(\Theta | \Phi)$ and the prior probability model $p(\Theta)$; based on the definition of $\pi(\Theta | \Phi)$ in Equation 27 such a comparison provide information for $h(\Phi, \Theta)$. Thus, bigger discrepancies between distributions $\pi(\Theta | \Phi)$ and $p(\Theta)$ indicate greater importance of Θ in affecting the system performance, since they ultimately correspond to higher values for $h(\Phi, \Theta)$. More importantly, though, this idea can be implemented to each specific model parameter θ_i (or even to group of them), by looking at the marginal distribution $\pi(\theta_i | \Phi)$. This distribution is given by (see Box 5), where \mathbf{x}_i corresponds to the rest of the components of Θ , excluding θ_i . Comparison between this marginal distribution $\pi(\theta_i)$ and the prior distribution $p(\theta_i)$ expresses the *probabilistic* sensitivity of the seismic risk with respect to θ_i . Uncertainty in all other model parameters and stochastic excitation is explicitly considered by appropriate integration of the joint probability distribution $\pi(\Theta | \Phi)$ to calculate the marginal probability distribution $\pi(\theta_i | \Phi)$.

A quantitative metric to characterize this sensitivity is the relative information entropy, which is a measure of the difference between probability distributions $\pi(\theta_i | \Phi)$ and $p(\theta_i)$ (Jaynes, 2003) over the entire space of possible model parameter values

$$D(\pi(\theta_i | \Phi) || p(\theta_i)) = \int \pi(\theta_i | \Phi) \log \left(\frac{\pi(\theta_i | \Phi)}{p(\theta_i)} \right) d\theta_i \quad (29)$$

The importance of each parameter (or sets of them) is then directly investigated by comparison of the relative information entropy value *for each of them*; larger values for the relative entropy indicate bigger importance.

An analytical expression, though, is not readily available for the marginal distribution $\pi(\theta_i | \Phi)$ since evaluation of Equation 28 is challenging. An alternative stochastic-sampling approach is

Box 6.

$$\tilde{\pi}(\theta_i | \boldsymbol{\varphi}) = \frac{1}{n\sigma_{li}\sqrt{2\pi}} \sum_{k=1}^n e^{-\frac{(\theta_i - \theta_i^k)^2}{2\sigma_{li}^2}}; \quad \sigma_{li} = 1.06 \cdot n^{-1/5} \sigma_{si} \quad (30)$$

discussed next. This approach is based on exploiting the information in samples of $\boldsymbol{\theta}$ from the joint distribution $\pi(\boldsymbol{\theta}|\boldsymbol{\varphi})$. Such samples may be obtained by any appropriate stochastic sampling algorithm, for example by the accept-reject method (Robert & Casella, 2004). Furthermore this task may be integrated within the stochastic analysis: each of the samples $\boldsymbol{\theta}^i$ used for the estimation in Equation 23 can be selected as a candidate sample $\boldsymbol{\theta}^c$ in the context of the Accept-Reject algorithm. The required samples from $\pi(\boldsymbol{\theta}|\boldsymbol{\varphi})$ are obtained at a small additional computational effort over the risk assessment task, since they require no new simulations for the bridge model response. Projection, now, of the samples from $\pi(\boldsymbol{\theta}|\boldsymbol{\varphi})$ to the space of *each* of the model parameters provides samples for the marginal distributions $\pi(\theta_i|\boldsymbol{\varphi})$ for each of them separately. Thus using the same sample set this approach provides simultaneously information for all model parameters. For scalar quantities, as in the case of interest here, the relative entropy may be efficiently calculated (Beirlant, Dudewicz, Gyorfi, & Van der Meulen, 1997; Mokkadem, 1989) by establishing an analytically approximation for $\pi(\theta_i|\boldsymbol{\varphi})$, based on the available samples, through Kernel density estimation. This estimate will not necessarily have high accuracy, but it can still provide an adequate approximation for computing the information entropy integral. A Gaussian Kernel density estimator may be used for this purpose (Martinez & Martinez, 2002). Using the n available samples for θ_i , with θ_i^k denoting the k -th sample and σ_{si} the standard deviation for these samples, the approximation for $\pi(\theta_i|\boldsymbol{\varphi})$ would be (see Box 6).

For establishing better consistency in the relative information entropy calculation $p(\theta_i)$ may also be approximated by Equation 30 based on samples, even when an analytical expression is available for it. This way, any type of error introduced by the Kernel density estimation is similar for both of the densities compared. The approximation for the relative information entropy is then (Beirlant et al., 1997)

$$D\left(\pi(\theta_i | \boldsymbol{\varphi}) || p(\theta_i)\right) \approx \int_{b_{i,l}}^{b_{i,u}} \tilde{\pi}(\theta_i | \boldsymbol{\varphi}) \log \left(\frac{\tilde{\pi}(\theta_i | \boldsymbol{\varphi})}{\tilde{p}(\theta_i)} \right) d\theta_i \quad (31)$$

where the last scalar integral can be numerically evaluated, for example using the trapezoidal rule, and $[b_{i,l}, b_{i,u}]$ is the region for which samples for $\pi(\theta_i | \boldsymbol{\varphi})$ and $q(\theta_i)$ are available. This approach ultimately leads to an efficient sampling-based methodology for calculating the relative information entropy for different parameters, which can be performed concurrently with the risk assessment, exploiting the readily available system model evaluations for minimizing the computational burden. Comparing the values for this entropy between the various model parameters leads then to a direct identification of the importance of each of them in affecting risk. Parameters with higher value for the relative entropy will have greater importance. Furthermore direct comparison of samples from the distributions $\pi(\theta_i | \boldsymbol{\varphi})$ and $p(\theta_i)$ could provide additional insight about what specific values for each parameter contribute more to the risk (Taflanidis & Beck, 2009c).

ILLUSTRATIVE EXAMPLE

Models and Uncertainty Description

The design of nonlinear viscous dampers for a two-span seismically isolated concrete bridge is considered as illustrative example. The model described previously is adopted for the bridge and probability distributions are established, based on our available knowledge, for all parameters that are considered as uncertain. All probability models are described here in terms of the mean (or median) value, characterizing most probable model, and the coefficient of variation, characterizing the potential spread for each parameter. For variables whose values are expected to be correlated, such dependency is expressed through their correlation coefficient.

The length of the span of the bridges is equal to 30 and 34 m, respectively. The mass of the pier is taken as $m_p = 100$ ton. For the pier restoring force f_p as illustrated in Figure 3, the initial stiffness k_p , post-yield stiffness coefficient α_p , over-strength factor μ_p and yield displacement δ_{yp} , have mean values 70 kN/mm, 10%, 30% and 0.04 m, respectively. All these parameters are treated as independent Gaussian variables with coefficient of variation 10%. For the nominal, i.e. most probable, model this assumption corresponds to period of 0.237 sec based on the initial stiffness. The damping coefficient C_p is selected based on modal damping assumption, using the initial period of the pier. The damping ratio ζ_p is treated as uncertain variable following a log-normal distribution with median 3% and coefficient of variation 25%.

The mass of the left and right abutments are taken, respectively, as $m_{al} = 400$ ton, $m_{ar} = 500$ ton. For the right and left abutment restoring forces f_{ar} , f_{al} the stiffness's k_{ar} and k_{al} , respectively, are modelled as correlated Gaussian variables with mean value 2500 kN/mm (Saadeghvaziri & Yazdani-Motlagh, 2008), coefficient of variation 15%, and correlation coefficient 50%. For the nominal, i.e. most probable, model this assumption corresponds

to period of 0.079 sec for the left and 0.089 sec for the right abutment. Both damping coefficients C_{al} and C_{ar} are selected based on modal damping assumption. The damping ratios for each abutment ζ_{al} , ζ_{ar} are treated as correlated uncertain variables following a log-normal distribution with median 8%, coefficient of variation 20% and correlation coefficient 50%. The high correlation in the abutment model parameter characteristics is attributed to the common soil properties.

For the left and right span of the bridge the self-weight of the deck is taken as 1000 and 1200 ton respectively. Vehicle traffic is modeled as additional loads m_l and m_r for the left and right span, respectively, that follow independent exponential distributions with mean value 20 ton. The isolators connecting each span to its supports are lead-rubber bearings modeled by Equation 7. All isolators have same properties; post-yield stiffness $k_e = 3.0$ kN/mm, pre-yield stiffness $k_p = 30.0$ kN/mm, and yield displacement $\delta_y = 2.5$ cm. These choices correspond to a natural period of 2.57 sec and 2.81 sec for the right and left span, respectively, based on the post-yield stiffness and no vehicle traffic. The respective gap dimensions x_o , x_{ol} , x_{or} , whose potential variability is influenced by common weather conditions, are modeled as correlated log-normal variables with median 10 cm, coefficient of variation 20%, and large correlation coefficient, 70%.

The contact stiffnesses k_{cc} , k_{cl} , k_{cr} for the Hertz impact forces between the spans or between each span and the neighboring abutment are taken as independent log-normal variables with median value given by 10 and large coefficient of variation 40%, again reflecting our limited knowledge. For calculating the median value of k_c , Poisson's ratio is taken as 0.15, the modulus of elasticity as 30 GPa and the density 2.4 ton/m³. The equivalent sphere radius 12 for each span is calculated by considering their total mass, including vehicle traffic. The coefficients for restitution for the energy dissipated during contact for each span are modeled as independent, truncated in [0 1] Gaussian

variables with mean value 0.6 and coefficient of variation 20%.

The time-history for future near-fault ground motions is described by the excitation model presented earlier. The details for the functions $A(f, M, r)$ and $e(t, M, r)$ are the same as in (Taflanidis et al., 2008). The uncertainty in moment magnitude for seismic events, M , is modeled by the Gutenberg-Richter relationship truncated to the interval $[M_{\min}, M_{\max}] = [6, 8]$. Smaller than M_{\min} earthquakes are not expected to have significant impact on the base isolated structure [and also do not frequently contain a near-fault pulse component (Bray & Rodriguez-Marek, 2004)] whereas it is assumed that the regional faults cannot produce seismic events with larger than 8 magnitude. This choice leads to a truncated exponential PDF (Kramer, 2003):

$$p(M) = \frac{b_M \exp(-b_M M)}{\exp(-b_M M_{\min}) - \exp(-b_M M_{\max})} \quad (32)$$

The selection for the regional seismicity factor is $b_M = 0.9 \log_e(10)$, corresponding to fairly significant seismic activity. For the uncertainty in the event location, the epicentral distance, r , for the earthquake events is assumed to be a log-normal variable with median $r_m = 10$ km and large coefficient of variation 50%. For the near-field pulse, the pulse frequency f_p and the peak ground velocity A_v are selected according to the probabilistic models for the characteristics of near-field pulses in rock sites given earlier by Equations 19 and 20. This is equivalent to f_p and A_v being log-normal variables with median value the ones in Equations 21 and 22 and coefficient of variation 0.4 and 0.39, respectively. Note that either f_p and A_v , or e_f and e_v can be used as the uncertain parameters addressing the uncertainty in the pulse frequency and ground velocity amplitude; the first set corresponds to a representation with an unambiguous physical meaning but is correlated to the

moment magnitude and the epicentral distance, also uncertain parameters, through the conditional median values given by Equations 21 and 22. The second set corresponds to a more abstract representation but is independent of any other model parameters. Throughout the discussion in this paper both representations will be utilized, according to convenience, but the risk integral was actually formulated with respect to e_f and e_v . The probability models for the rest of the pulse model parameters, the number of half cycles and phase, are chosen, respectively, as truncated in $[1, \infty)$ Gaussian with mean value 2 and coefficient of variation 15%, and uniform in the range $[-\pi/2, \pi/2]$. These probability models are based on the values reported in (Mavroeidis & Papageorgiou, 2003) when tuning the analytical relationship in Equation 18 to a wide range of recorded near-fault ground motions.

The uncertain model parameter vector in this design problem consists of the bridge model parameters $\Theta_s = [k_p \alpha_p \mu_p \delta_{yp} \zeta_p k_{al} k_{ar} \zeta_{al} \zeta_{ar} m_{tl} m_{tr} x_o, x_{ol} x_{or} e_{cc} e_{cl} e_{cr} k_{cc} k_{cl} k_{cr}]$ the seismological parameter $\Theta_g = [M \, r]$, the additional parameters for the near-fault pulse $\Theta_p = [e_v \, e_f \, \gamma_p \, v_p]$ (with the former two related to A_v and f_p) and the white-noise sequence, \mathbf{Z}_w , so $\Theta = [\Theta_s \, \Theta_g \, \Theta_p \, \mathbf{Z}_w]^T$. Table 1 reviews these parameters along with their probability models.

Damper Configuration and Performance Characteristics

Nonlinear viscous dampers are applied to the connection of each of the two spans to its corresponding abutment, as illustrated in Figures 1 and 3. They are modeled by Equation 16 with maximum force capability for each damper, representing cost constraints (Taflanidis & Beck, 2009a), selected as 4000 kN. Coefficients a_d and c_d correspond to the design variables for the problem and for cost reduction (bulk ordering) are chosen the same for all dampers. The initial design space for each of them is defined as $a_d \in [0.3, 2]$ and $c_d \in [0.1, 30]$ MN (sec/m)^{ad}.

Table 1. Probability models for uncertain model parameters. In this table c.o.v=coefficient of variation, ρ =correlation coefficient, μ =mean value

k_p	Gaussian $\mu=70$ kN/mm c.o.v = 10%	ζ_{al} ζ_{ar}	Correlated log-normal median = 8%, c.o.v = 20%, ρ = 50%	r	Log-normal Median = 10km c.o.v = 50%
ζ_p	Log-normal median = 3% c.o.v = 25%	k_{al} K_{ar}	Correlated Gaussian $\mu=2500$ kN/mm c.o.v = 15%, ρ = 50%	M	Truncated exponential in [6 8] with parameter $0.9\log_e(10)$
				v_p	Uniform in $[0, \pi]$
μ_p	Gaussian $\mu=0.3$ c.o.v = 10%	x_o x_{ol} x_{or}	Correlated log-normal median = 10 cm c.o.v = 15%, ρ = 70%	α_p	Gaussian $\mu=0.1$ c.o.v = 20%
	Gaussian $\mu=0.03$ m c.o.v=10%			γ_p	Gaussian $\mu=2.0$ c.o.v=15%
m_{il} m_{ir}	Independent Exponential $M=20$ ton	k_{cc} k_{cl} k_{cr}	Independent log-normal median given by 10 c.o.v = 40%,	f_p	Lognormal Median Equation 21 c.o.v = 40%
k_{al} k_{ar}	Correlated Gaussian $\mu=2500$ kN/mm c.o.v = 15%, ρ 50%	e_{cc} e_{cl} e_{cr}	Independent Gaussian truncated in $[0 1]$ $\mu=0.6$ c.o.v = 15%	A_v	Log-normal Median Equation 22 c.o.v = 39%

The optimization problem is defined by Equation 24, in which the objective function is the seismic risk given by Equation 23. The admissible design space is defined in Box 7.where f_{dl} and f_{dr} correspond to the damper force for the left and right abutment, respectively.

Asimplified design problem is also considered where a_d is set to 1, corresponding to a linear viscous damper. This will allow for investigation of the performance improvement gained by considering nonlinear, rather than linear, damper implementation.

The bridge performance measure assumed in this study addresses potential seismic damages for all components of the bridge: the pier, the abutments, and the deck. The failure criteria used are: (i) the maximum pier shear V_p , associated with yielding and inelastic deformations for the pier, (ii) the maximum displacement for the left and right abutment z_p and z_l , respectively, associated with permanent deformations for the ground, and (iii) the maximum velocity for impact between the two spans v_o or between each of the spans and the left or right abutment v_l and v_r , respectively, associated with the damages that occur during pounding (Davis, 1992). The fragility related to

each of these quantities, i.e. the probability that the response will exceed some acceptable performance μ , is used for describing the system performance. These fragilities are assumed to have a lognormal distribution with median μ and coefficient of variation β . The probabilistic description for the fragility incorporates into the stochastic analysis model prediction errors (Goulet et al., 2007; Taflanidis & Beck, 2010). The seismic-risk occurrence measure is the average of these fragilities, see Box 8.where Φ_g is the standard Gaussian cumulative distribution function. The characteristics for the median of the fragility curves are $\mu_p=2200$ kN for the pier shear, $\mu_z=6$ mm for the abutment displacement and $\mu_v=10$ cm/sec for the impact velocity, whereas the coefficient of variation is set for all of them equal to $\beta_p=\beta_z=\beta_v=0.4$. Seismic risk is finally given by the integral in Equation 1 which in this case corresponds to probability of unacceptable performance for the base-isolated bridge. The maximum value for $C(\phi)$ is one while the minimum value for $C(\phi)$, corresponding to best possible performance, is zero.

Box 7.

$$\Phi : \left\{ c_{di} \in [0.1, 30] \text{MN} (\text{sec / m})^{a_d}; a_{di} \in [0.3, 2]; f_{dl}, f_{dr} \leq 4000 \text{ KN} \right\} \quad (33)$$

Box 8.

$$h(\Phi, \Theta) = \frac{1}{6} [\Phi_g \left(\frac{\ln(V_p) - \ln(\mu_p)}{\beta_p} \right) + \Phi_g \left(\frac{\ln(z_l) - \ln(\mu_z)}{\beta_z} \right) + \Phi_g \left(\frac{\ln(z_r) - \ln(\mu_z)}{\beta_z} \right) \\ + \Phi_g \left(\frac{\ln(v_o) - \ln(\mu_v)}{\beta_v} \right) + \Phi_g \left(\frac{\ln(v_l) - \ln(\mu_v)}{\beta_v} \right) + \Phi_g \left(\frac{\ln(v_r) - \ln(\mu_v)}{\beta_v} \right)] \quad (34)$$

Optimal Design

The bridge model, described by system of Equations 4, is created and analyzed in SIMULINK (Klee, 2007). The computations are performed for this study on the “Persephone” cluster at the HIgh Performance system Analysis and Design (HIPAD) laboratory at the University of Notre Dame (www.nd.edu/~hipad). The cluster is composed of 42 nodes, each having eight 2.56GHz Nehalem cores. All stochastic simulations are performed in parallel mode, taking advantage of the multi-core capacities of the high-performance computing cluster.

SPSA is used for the design optimization with selection of $N=2000$ for the estimate of Equation 23 and importance sampling densities established only for the moment magnitude, M , which is anticipated to be the most influential parameter within the ones included in vector Θ , based on results from previous studies on the risk assessment of flexible structures under near-fault excitations (Taflanidis & Jia, 2011). A truncated in [6 8] Gaussian with mean 6.8 and standard deviation 0.6 is selected for M .

Cumulative results from the optimization are presented in Table 2 which includes the optimal

design configuration for both nonlinear and linear damper implementation, the overall objective function $C(\Phi)$ as well as the expected fragility for each of the components. The results illustrate that the addition of the viscous dampers leads to significant improvement of fragility of the bridge; there is a big difference between the optimal $C(\Phi^*)$ and the uncontrolled performance $C(\Theta)$. All six components contributing to the overall fragility are characterized by a considerable reduction, with the maximum pounding velocities having by far the largest one. This illustrates that the viscous dampers can significantly reduce the undesirable collisions between the different spans, which can have devastating effects for the serviceability of the bridge, while simultaneously efficiently controlling other modes of failure for the bridge, as the pier shear or the abutment displacements. It should be also pointed out that the optimal linear damper configuration provides still a significant improvement over the uncontrolled bridge performance. Implementation, though, of nonlinear dampers provides a further reduction in the seismic risk for the bridge, especially with respect to the pier and abutment failure criteria. The exponent coefficient for the dampers under optimal design is 0.66, which corresponds to a

Table 2. Optimization results; units for c_d are MN (sec/m)^{ad}

Case	ϕ^*		$C(\phi^*)$	Probabilities of failure for individual components					
				V_p	z_l	z_r	v_o	v_l	v_r
Nonlinear Damper	c_d	9.7	0.029	0.047	0.034	0.055	0.006	0.0205	0.0093
	a_d	0.66							
Linear Damper	c_d	19.5	0.034	0.059	0.037	0.071	0.006	0.0208	0.0102
	a_d	1.00							
No Damper	c_d	0	0.256	0.284	0.179	0.247	0.253	0.332	0.244
	a_d	-							

Table 3. Sensitivity analysis results (normalised entropy) for total risk

No dampers (maximum relative entropy $D_m=0.565$)													
M	r	e_v	e_f	γ	v	A_v	f_p	m_{il}	m_{ir}	x_{ol}	x_{or}	x_o	k_{cl}
0.410	0.270	0.243	0.055	0.010	0.001	1.000	0.653	0.007	0.028	0.013	0.016	0.011	0.011
k_{cr}	k_c	e_{cl}	e_{cr}	e_{cc}	k_{al}	k_{ar}	ζ_{al}	ζ_{ar}	ζ_p	k_p	A_p	μ_p	δ_{yp}
0.007	0.006	0.005	0.004	0.002	0.003	0.002	0.003	0.003	0.001	0.003	0.005	0.004	0.005

Optimal nonlinear dampers (maximum relative entropy $D_m=1.08$)													
M	r	e_v	e_f	γ	v	A_v	f_p	m_{il}	m_{ir}	x_{ol}	x_{or}	x_o	k_{cl}
0.089	0.402	0.491	0.086	0.012	0.009	1.000	0.016	0.009	0.026	0.003	0.004	0.002	0.005
k_{cr}	k_c	e_{cl}	e_{cr}	e_{cc}	k_{al}	k_{ar}	ζ_{al}	ζ_{ar}	ζ_p	k_p	A_p	μ_p	δ_{yp}
0.006	0.007	0.003	0.001	0.001	0.031	0.026	0.003	0.002	0.005	0.004	0.003	0.004	0.002

significant degree of nonlinearity. This illustrates the importance of a design methodology that can efficiently address damper nonlinearities, so that a truly optimal design is identified.

Stochastic Sensitivity Analysis

Results for the sensitivity analysis are finally discussed. Table 3 includes the maximum relative entropy D_m and the normalised entropy for each parameter for the uncontrolled or optimal damper configuration. The normalised entropy, D_n , is defined by scaling the entropy for each parameter by the maximum, over all parameters, entropy. This is an explicit measure of the relative importance of each parameter to the seismic risk, with values closer to unity indicating higher importance.

The results in Table 3 illustrate that the pulse amplitude A_v is the most influential parameter in affecting the overall seismic risk. The uncertainty in the pulse amplitude, e_v , the moment magnitude, M , and the epicentral distance, r , have also a significant impact. As pointed out earlier A_v is actually influenced by all three previous ones, so the higher importance for it is anticipated. Similar remark holds for f_p , which is shown, though, to have considerable influence in the seismic risk only for the bridge without the dampers. Since both A_v and f_p are directly related to the impact of the near-fault pulse on the structure (amplitude of pulse and unison conditions, respectively), these results, especially the high importance of A_v and e_v , indicate that seismic risk does indeed have a big correlation to the near-fault character-

istics of the excitation for base-isolated bridge. All other excitation and structural parameters have negligible importance in affecting seismic risk. Only the gap sizes, contact stiffnesses, and live loads from the trucks seem to have some, small, significance.

The sensitivity pattern does change between the no-damper and optimal-damper-configuration cases. This is another important outcome of this study; it shows that addition of the dampers not only alters the seismic risk but also influences the risk factors that contribute more to this risk. Since addition of the dampers provides an overall reduction of seismic pounding occurrences (identified from the results of Table 2) the characteristics that have a stronger connection to this pounding are impacted more. It is interesting that the second most important model parameter for the no-damper case, the pulse frequency, has small

only importance for the system with optimized viscous dampers. This is an interesting outcome and can be attributed to resonance characteristics; the rigid type of connection to the abutments introduced through the dampers influences the vibration properties of the isolated-bridge and thus alters the frequencies of the near fault-pulse that have higher impact on it.

Sensitivity analysis results for individual components of the total performance are presented in Table 4. In particular the maximum pier shear V_p , the maximum displacement for right abutment z_r , and the maximum velocity for impact between the left span and abutment v_l are reported. Only the interesting model parameters are included in this table. For obtaining these results the risk occurrence measure in Equation 34 is substituted by the fragility of the corresponding component. Since this fragility has been already computed when

Table 4. Sensitivity analysis results for different response quantities

		No Dampers			Optimal Nonlinear Dampers		
		V	z_r	v_l	V_p	z_r	v_l
D_m		0.227	0.701	0.494	1.179	0.672	2.740
D_n	M	0.48	0.404	0.551	0.144	0.071	0.125
	r	0.30	0.251	0.214	0.372	0.540	0.245
	e_v	0.19	0.246	0.176	0.407	0.453	0.525
	e_f	0.15	0.042	0.080	0.034	0.155	0.053
	γ	0.01	0.007	0.005	0.012	0.010	0.006
	v	0.03	0.001	0.007	0.004	0.008	0.021
	A_v	1.00	1.000	1.000	1.000	1.000	1.000
	f_p	0.81	0.646	0.919	0.039	0.022	0.070
	m_{nl}	0.031	0.007	0.010	0.004	0.009	0.003
	m_r	0.073	0.023	0.016	0.012	0.011	0.005
	k_p	0.02	0.002	0.003	0.006	0.004	0.001
	x_{ol}	0.011	0.011	0.024	0.004	0.005	0.008
	x_{or}	0.012	0.016	0.028	0.002	0.006	0.018
	x_o	0.04	0.011	0.021	0.001	0.002	0.010
	k_{cl}	0.027	0.009	0.007	0.011	0.007	0.001
	k_{cr}	0.040	0.005	0.008	0.005	0.006	0.002
	k_c	0.09	0.004	0.006	0.005	0.010	0.003

calculating the initial risk occurrence measure, no new simulations are needed, and the results in Table 4 are obtained at a small additional computational cost (requiring only approximation of the densities through Kernel estimation and calculation of the relative entropy integral). These results demonstrate some significant variability, indicating that there is a big dependence of the sensitivity analysis and the importance of the various risk factors, on the exact performance quantification chosen. Especially interesting is the fact that for the bridge with the dampers, the epicentral distance and the pulse amplitude are the only important risk factors for all different quantifications.

FUTURE RESEARCH DIRECTIONS

The design of structural systems for seismic risk mitigation requires explicit consideration of the uncertainties for the characteristics of future excitations as well as for the system properties. The constant advances in computer and computational science, especially the widespread implementation of distributed computing, have created a new era for computer simulation and it is currently acknowledged that Simulation-Based Engineering Science constitutes a critical new paradigm for uncertainty quantification and propagation and is providing great new potentials for detailed modeling and solution of problems that were until recently considered computationally intractable. Future research efforts need to exploit these characteristics and focus on modeling approaches for quantification of seismic risk and computational frameworks for estimation of this risk that will explicitly address all important characteristics of the built systems and its environment, with no need to establish any type of approximations for computational simplicity. This will only be established through development of high fidelity numerical models for the dynamic behavior of structural systems and adoption of complex probabilistic

descriptions for the seismic hazard, exploiting an end-to-end simulation-based approach.

CONCLUSION

The design of supplemental dampers for seismic risk reduction of isolated multi-span bridges was the focus of this Chapter. The basis of the suggested approach is a probabilistic framework that explicitly addresses all sources of uncertainty, related either to future excitations or to the structural configuration, by appropriate probability models. In this setting, seismic risk is expressed by a multidimensional integral, corresponding to the expected value of the risk occurrence measure over the space of the uncertain model parameters. Through appropriate definition of the risk occurrence measure this approach facilitates diverse risk quantifications. Stochastic simulation was suggested for evaluation of the multidimensional integral describing risk and an efficient algorithm was discussed for performing the associated design optimization and selecting the optimal parameters for the damper implementation. An efficient sampling-based probabilistic importance analysis was also presented, based on information entropy principles, for investigating the influence of each of the model parameters on the overall seismic risk.

Due to the fact that the framework is based on stochastic simulation, consideration of complex nonlinear models for the bridge system and the excitation was feasible. The adopted bridge model explicitly addressed nonlinear characteristics of the isolators and the dampers, the dynamic behavior of the abutments and the effect of pounding between the neighboring spans to each other as well to the abutments. A realistic probabilistic model for future near-fault excitations was also considered. An illustrative example was presented that considered the design of nonlinear viscous dampers for protection of a two-span bridge. The fragility of the bridge system related to seismic pounding

but also to failure modes associated with the pier shear and the abutment deformations were adopted as the risk occurrence measure, with seismic risk ultimately corresponding to the probability of unacceptable performance. The addition of the dampers was shown to provide considerable risk reduction, especially with respect to the vulnerabilities associated with seismic pounding. Results from the sensitivity analysis demonstrated that the excitation properties, especially the amplitude of the pulse component of the ground motion, have the highest importance in affecting seismic risk and that the inclusion of the dampers did alter these sensitivity characteristics to a significant degree.

In closing, it is noted that the proposed methodology offers also significant practical advantages in real seismic design, since the optimal parameters of the viscous dampers can be efficiently estimated through a probabilistic framework which incorporates the various sources of uncertainty, as well as, the various nonlinearities related with the different bridge components. It is stressed that by considering the nonlinear damper implementation, significant performance improvement is achieved which in general results to more economic design.

REFERENCES

- Abbas, M. (2011). Damage-based design earthquake loads for single-degree-of-freedom inelastic structures. *Journal of Structural Engineering*, 137(3), 456–467. doi:10.1061/(ASCE)ST.1943-541X.0000074
- Alavi, B., & Krawinkler, H. (2000, January 30–February 4). *Consideration of near-fault ground motion effects in seismic design*. Paper presented at the 12th World Conference on Earthquake Engineering, Auckland, New Zealand.
- Atkinson, G. M., & Silva, W. (2000). Stochastic modeling of California ground motions. *Bulletin of the Seismological Society of America*, 90(2), 255–274. doi:10.1785/0119990064
- Beirlant, J., Dudewicz, E. J., Gyorfi, L., & Van der Meulen, E. C. (1997). Nonparametric entropy estimation: An overview. *International journal of Mathematical and Statistical Sciences*, 6(1), 17–40.
- Boore, D. M. (2003). Simulation of ground motion using the stochastic method. *Pure and Applied Geophysics*, 160, 635–676. doi:10.1007/PL00012553
- Bray, J. D., & Rodriguez-Marek, A. (2004). Characterization of forward-directivity ground motions in the near-fault region. *Soil Dynamics and Earthquake Engineering*, 24, 815–828. doi:10.1016/j.soildyn.2004.05.001
- Conte, J. P., & Peng, B. F. (1997). Fully nonstationary analytical earthquake ground-motion model. *Journal of Engineering Mechanics*, 123, 15–34. doi:10.1061/(ASCE)0733-9399(1997)123:1(15)
- Davis, R. O. (1992). Pounding of buildings modeled by an impact oscillator. *Earthquake Engineering & Structural Dynamics*, 21, 253–274. doi:10.1002/eqe.4290210305
- Der Kiureghian, A. (1996). A coherency model for spatially varying ground motions. *Earthquake Engineering & Structural Dynamics*, 25(1), 99–111. doi:10.1002/(SICI)1096-9845(199601)25:1<99::AID-EQE540>3.0.CO;2-C
- Dicleli, M. (2006). Performance of seismic-isolated bridges in relation to near-fault ground-motion and isolator characteristics. *Earthquake Spectra*, 22(4), 887–907. doi:10.1193/1.2359715
- Dimitrakopoulos, E., Makris, N., & Kappos, A. J. (2009). Dimensional analysis of the earthquake-induced pounding between adjacent structures. *Earthquake Engineering & Structural Dynamics*, 38(7), 867–886. doi:10.1002/eqe.872

- Dimitrakopoulos, E., Makris, N., & Kappos, A. J. (2010). Dimensional analysis of the earthquake response of a pounding oscillator. *Journal of Engineering Mechanics*, 136(3), 299–310. doi:10.1061/(ASCE)0733-9399(2010)136:3(299)
- Glasserman, P., & Yao, D. D. (1992). Some guidelines and guarantees for common random numbers. *Management Science*, 38(6), 884–908. doi:10.1287/mnsc.38.6.884
- Goulet, C. A., Haselton, C. B., Mitrani-Reiser, J., Beck, J. L., Deierlein, G., & Porter, K. A. (2007). Evaluation of the seismic performance of code-conforming reinforced-concrete frame building-From seismic hazard to collapse safety and economic losses. *Earthquake Engineering & Structural Dynamics*, 36(13), 1973–1997. doi:10.1002/eqe.694
- Hwang, J.-S., & Tseng, Y.-S. (2005). Design formulations for supplemental viscous dampers to highway bridges. *Earthquake Engineering & Structural Dynamics*, 34(13), 1627–1642. doi:10.1002/eqe.508
- Jangid, R. S. (2008). Stochastic response of bridges seismically isolated by friction pendulum system. *Journal of Bridge Engineering*, 13(4), 319–330. doi:10.1061/(ASCE)1084-0702(2008)13:4(319)
- Jaynes, E. T. (2003). *Probability theory: The logic of science*. Cambridge, UK: Cambridge University Press. doi:10.1017/CBO9780511790423
- Jónsson, M. H., Bessason, B., & Haflidason, E. (2010). Earthquake response of a base-isolated bridge subjected to strong near-fault ground motion. *Soil Dynamics and Earthquake Engineering*, 30(6), 447–455. doi:10.1016/j.soildyn.2010.01.001
- Klee, H. (2007). *Simulation of dynamic systems with MATLAB and SIMULINK*. Boca Raton, FL: CRC Press.
- Kleinmann, N. L., Spall, J. C., & Naiman, D. C. (1999). Simulation-based optimization with stochastic approximation using common random numbers. *Management Science*, 45(11), 1570–1578. doi:10.1287/mnsc.45.11.1570
- Kramer, S. L. (2003). *Geotechnical earthquake engineering*. Prentice Hall.
- Kushner, H. J., & Yin, G. G. (2003). *Stochastic approximation and recursive algorithms and applications*. New York, NY: Springer Verlag.
- Makris, N., & Zhang, J. (2004). Seismic response analysis of a highway overcrossing equipped with elastomeric bearings and fluid dampers. *Journal of Structural Engineering*, 130(6), 830–845. doi:10.1061/(ASCE)0733-9445(2004)130:6(830)
- Martinez, W. L., & Martinez, A. R. (2002). *Computational Statistics Handbook with MATLAB*. Boca Raton, FL: Chapman & Hall/CRC.
- Mavroeidis, G. P., & Papageorgiou, A. P. (2003). A mathematical representation of near-fault ground motions. *Bulletin of the Seismological Society of America*, 93(3), 1099–1131. doi:10.1785/0120020100
- Mokkadem, A. (1989). Estimation of the entropy and information for absolutely continuous random variables. *IEEE Transactions on Information Theory*, 35, 193–196. doi:10.1109/18.42194
- Muthukumar, S., & DesRoches, R. (2006). A Hertz contact model with non-linear damping for pounding simulation. *Earthquake Engineering & Structural Dynamics*, 35, 811–828. doi:10.1002/eqe.557
- Perros, K., & Papadimitriou, C. (2009). *Reliability analysis of bridge models with elastomeric bearings and seismic stoppers under stochastic earthquake excitations*. Paper presented at the 2009 ECCOMAS Thematic Conference on Computational Methods in Structural Dynamics and Earthquake Engineering.

- Rezaeian, S., & Der Kiureghian, A. (2008). A stochastic ground motion model with separable temporal and spectral nonstationarities. *Earthquake Engineering & Structural Dynamics*, 37, 1565–1584. doi:10.1002/eqe.831
- Robert, C. P., & Casella, G. (2004). *Monte Carlo statistical methods* (2nd ed.). New York, NY: Springer.
- Royset, J. O., & Polak, E. (2004). Reliability-based optimal design using sample average approximations. *Probabilistic Engineering Mechanics*, 19, 331–343. doi:10.1016/j.proben-gmech.2004.03.001
- Ruangrassamee, A., & Kawashima, K. (2003). Control of nonlinear bridge response with pounding effect by variable dampers. *Engineering Structures*, 25(5), 593–606. doi:10.1016/S0141-0296(02)00169-4
- Ruszczynski, A., & Shapiro, A. (2003). *Stochastic programming*. New York, NY: Elsevier.
- Saadeghvaziri, M. A., & Yazdani-Motlagh, A. R. (2008). Seismic behavior and capacity/demand analyses of three multi-span simply supported bridges. *Engineering Structures*, 30(1), 54–66. doi:10.1016/j.engstruct.2007.02.017
- Shen, J., Tsai, M.-H., Chang, K.-C., & Lee, G. C. (2004). Performance of a seismically isolated bridge under near-fault earthquake ground motions. *Journal of Structural Engineering*, 130(6), 861–868. doi:10.1061/(ASCE)0733-9445(2004)130:6(861)
- Shinozuka, M., Deodatis, G., Zhang, R. C., & Papageorgiou, A. S. (1999). Modeling, synthetics and engineering applications of strong earthquake wave motion. *Soil Dynamics and Earthquake Engineering*, 18(3), 209–228. doi:10.1016/S0267-7261(98)00045-1
- Spall, J. C. (1998). Implementation of the simultaneous perturbation algorithm for stochastic optimization. *IEEE Transactions on Aerospace and Electronic Systems*, 34, 817–823. doi:10.1109/7.705889
- Spall, J. C. (2003). *Introduction to stochastic search and optimization*. New York, NY: Wiley-Interscience. doi:10.1002/0471722138
- Taflanidis, A. A. (2009, 22–24 June). *Robust stochastic design of viscous dampers for base isolation applications*. Paper presented at the Computational Methods in Structural Dynamics and Earthquake Engineering, Rhodes, Greece.
- Taflanidis, A. A., & Beck, J. L. (2008). An efficient framework for optimal robust stochastic system design using stochastic simulation. *Computer Methods in Applied Mechanics and Engineering*, 198(1), 88–101. doi:10.1016/j.cma.2008.03.029
- Taflanidis, A. A., & Beck, J. L. (2009a). Life-cycle cost optimal design of passive dissipative devices. *Structural Safety*, 31(6), 508–522. doi:10.1016/j.strusafe.2009.06.010
- Taflanidis, A. A., & Beck, J. L. (2009b). Stochastic subset optimization for reliability optimization and sensitivity analysis in system design. *Computers & Structures*, 87, 318–331. doi:10.1016/j.compstruc.2008.12.015
- Taflanidis, A. A., & Beck, J. L. (2009c). Stochastic subset optimization for reliability optimization and sensitivity analysis in system design. *Computers & Structures*, 87(5-6), 318–331. doi:10.1016/j.compstruc.2008.12.015
- Taflanidis, A. A., & Beck, J. L. (2010). Reliability-based design using two-stage stochastic optimization with a treatment of model prediction errors. *Journal of Engineering Mechanics*, 136(12), 1460–1473. doi:10.1061/(ASCE)EM.1943-7889.0000189

Taflanidis, A. A., & Jia, G. (2011). A simulation-based framework for risk assessment and probabilistic sensitivity analysis of base-isolated structures. *Earthquake Engineering & Structural Dynamics*, 40(14). doi:10.1002/eqe.1113

Taflanidis, A. A., Scruggs, J. T., & Beck, J. L. (2008). Probabilistically robust nonlinear design of control systems for base-isolated structures. *Journal of Structural Control and Health Monitoring*, 15(3), 697–719. doi:10.1002/stc.275

Takewaki, I. (2002). Seismic critical excitation method for robust design: A review. *Journal of Structural Engineering*, 128(5), 665–672. doi:10.1061/(ASCE)0733-9445(2002)128:5(665)

Tsopelas, P., Constantinou, M. C., Okamoto, S., Fujii, S., & Ozaki, D. (1996). Experimental study of bridge seismic sliding isolation systems. *Engineering Structures*, 18(4), 301–310. doi:10.1016/0141-0296(95)00147-6

Wang, Q., Fang, H., & Zou, X.-K. (2010). Application of Micro-GA for optimal cost base isolation design of bridges subject to transient earthquake loads. *Structural and Multidisciplinary Optimization*, 41, 765–777. doi:10.1007/s00158-009-0470-5

Werner, G. (1960). *Impact: The theory and physical behaviour of colliding solids*. London, UK: Edward Arnold.

Zerva, A. (2008). *Spatial variation of seismic ground motions modeling and engineering applications*. Boca Raton, FL: CRC Press.

Zhang, J., Makris, N., & Delis, T. (2004). Structural characterization of modern highway overcrossings-Case study. *Journal of Structural Engineering*, 130(6), 846–860. doi:10.1061/(ASCE)0733-9445(2004)130:6(846)

ADDITIONAL READING

Bahi, J. M., Contassot-Vinier, S., & Couturier, R. (2008). *Parallel iterative algorithms. From sequential to grid computing*. Boca Raton, FL: Chapman & Hall/ CRC.

Christopoulos, C., & Filiatrault, A. (2006). *Principles of passive supplemental damping and seismic isolation*. Pavia, Italy: IUSS Press.

Clough, R. W., & Penzien, J. (1993). *Dynamics of structures*. New York, NY: Mc Graw-Hill Inc.

Cornell, C. A. (1968). Engineering seismic risk analysis. *Bulletin of the Seismological Society of America*, 58(5), 1583–1606.

Cox, R. T. (1961). *Algebra or probable inference*. Baltimore, MD: The Johns Hopkins University Press.

Elnashai, A., & Di Sarnio, L. (2008). *Fundamentals of earthquake engineering*. West Sussex, UK: John Wiley & Sons. doi:10.1002/9780470024867

Fujimoto, R. M. (2001). *Parallel simulation: Parallel and distributed simulation systems*. Paper presented at the 33rd Winter Simulation Conference, Arlington, Virginia.

Gavin, H. P., & Zaicenco, A. (2007). Performance and reliability of semi-active equipment isolation. *Journal of Sound and Vibration*, 306(1-2), 74–90. doi:10.1016/j.jsv.2007.05.039

Gosavi, A. (2003). *Simulation-based optimization: Parametric optimization techniques and reinforcement learning*. Norwell, MA: Kluwer Academic Publishers.

Haukaas, T., & Der Kiureghian, A. (2007). Methods and object-oriented software for FE reliability and sensitivity analysis with application to a bridge structure. *Journal of Computing in Civil Engineering*, 21(3), 151–163. doi:10.1061/(ASCE)0887-3801(2007)21:3(151)

- Jangid, R. S. (2007). Optimum lead-rubber isolation bearings for near-fault motions. *Engineering Structures*, 29, 2503–2513. doi:10.1016/j.engstruct.2006.12.010
- Katsanos, E. I., Sextos, A. G., & Manolis, G. D. (2010). Selection of earthquake ground motion records: A state-of-the-art review from a structural engineering perspective. *Soil Dynamics and Earthquake Engineering*, 30(4), 157–169. doi:10.1016/j.soildyn.2009.10.005
- Komodromos, P., Polycarpoy, P. C., Papaloizou, L., & Phocas, M. C. (2007). Response of seismically isolated buildings considering pounding. *Earthquake Engineering & Structural Dynamics*, 36, 1605–1622. doi:10.1002/eqe.692
- Lutes, L. D., & Sarkani, S. (1997). *Stochastic analysis of structural and mechanical vibrations*. Upper Saddle River, NJ: Prentice Hall.
- Marti, K. (2005). *Stochastic optimization methods*. Berlin, Germany: Springer.
- Naeim, F., & Kelly, J. M. (1999). *Design of seismic isolated structures: From theory to practise*. New York, NY: Wiley. doi:10.1002/9780470172742
- Nagarajaiah, S., & Narasimhan, S. (2006). Smart base isolated benchmark building. Part II - phase I sample controllers for linear isolation system. *Journal of Structural Control and Health Monitoring*, 13(2-3), 589–604. doi:10.1002/stc.100
- Narasimhan, S., Nagarajaiah, S., Gavin, H. P., & Johnson, E. A. (2006). Smart base isolated benchmark building part I: Problem definition. *Journal of Structural Control and Health Monitoring*, 13(2-3), 573–588. doi:10.1002/stc.99
- Narasimhan, S., Nagarajaiah, S., & Johnson, E. A. (2008). Smart base isolated benchmark building Part IV: Phase II sample controllers for nonlinear isolation systems. *Journal of Structural Control and Health Monitoring*, 13(2-3).
- Nickolls, J., Buck, I., Garland, M., & Skadron, K. (2008). Scalable parallel programming with CUDA. *Queue*, 6(2), 40–53. doi:10.1145/1365490.1365500
- Papadimitriou, C., Beck, J., & Katafygiotis, L. (1997). Asymptotic expansions for reliabilities and moments of uncertain dynamic systems. *Journal of Engineering Mechanics*, 123, 1219–1229. doi:10.1061/(ASCE)0733-9399(1997)123:12(1219)
- Papadimitriou, K. (1990). *Stochastic characterization of strong ground motion and application to structural response*. Pasadena, CA: Report No. EERL 90-03, California Institute of Technology.
- Politopoulos, I., & Pham, H., K. (2009). Sensitivity of seismically isolated structures. *Earthquake Engineering & Structural Dynamics*, 38(8), 989–1007. doi:10.1002/eqe.879
- Priestley, M. J. N., Seible, F., & Calvi, G. M. (1996). *Seismic design and retrofit of bridges*. New York, NY: John Wiley & Sons, INC. doi:10.1002/9780470172858
- Rubinstein, R. Y., & Kroese, D. P. (2008). *Simulation and the Monte Carlo method* (2nd ed.). Hoboken, NJ: Wiley.
- Suchard, M. A., Wang, Q., Chan, C., Frelinger, J., Cron, A., & West, M. (2009). Understanding GPU programming for statistical computation: studies in massively parallel massive mixtures. *Journal of Computational and Graphical Statistics*, 19(2), 419–438. doi:10.1198/jcgs.2010.10016

Taflanidis, A. A. (2010). Reliability-based optimal design of linear dynamical systems under stochastic stationary excitation and model uncertainty. *Engineering Structures*, 32(5), 1446–1458. doi:10.1016/j.engstruct.2010.01.023

Zhang, Y. F., & Iwan, W. D. (2002). Protecting base isolated structures from near-field ground motion by tuned interaction damper. *Journal of Engineering Mechanics*, 128(3), 287–295. doi:10.1061/(ASCE)0733-9399(2002)128:3(287)

KEY TERMS AND DEFINITIONS

Near-Fault Ground Motion: Seismic ground motions at small distances from epicenter of an earthquake that include a strong pulse component, evident in the velocity time history of the excitation.

Optimization Under Uncertainty: Optimization algorithms appropriate for problems for which the objective function or the constraints are computed through stochastic simulation.

Probabilistic Design (Robust Design): Design of systems that explicitly addresses the uncertainties in their model description.

Risk Quantification and Assessment: Methodologies for mathematical description of risk and for its evaluation.

Seismic Dampers: Devices used for energy dissipation (through mechanical or electrical means) in the vibration of structural systems due to seismic excitation

Seismic Isolation: Decoupling of structures (building, bridges) from the ground through use of flexible isolators, commonly lead-rubber or friction pendulum bearings.

Stochastic Simulation: Methodologies and algorithms that entail random sampling characteristics.

Compilation of References

- Abbas, A. M. (2006). Critical seismic load inputs for simple inelastic structures. *Journal of Sound and Vibration*, 296, 949–967. doi:10.1016/j.jsv.2006.03.021
- Abbas, A. M., & Manohar, C. S. (2002). Investigations into critical earthquake load models within deterministic and probabilistic frameworks. *Earthquake Engineering & Structural Dynamics*, 31, 813–832. doi:10.1002/eqe.124
- Abbas, A. M., & Manohar, C. S. (2005). Reliability-based critical earthquake load models. Part 2: Nonlinear structures. *Journal of Sound and Vibration*, 287, 883–900. doi:10.1016/j.jsv.2004.12.003
- Abbas, A. M., & Manohar, C. S. (2007). Reliability-based vector nonstationary random critical earthquake excitations for parametrically excited systems. *Structural Safety*, 29, 32–48. doi:10.1016/j.strusafe.2005.11.003
- Abbas, M. (2011). Damage-based design earthquake loads for single-degree-of-freedom inelastic structures. *Journal of Structural Engineering*, 137(3), 456–467. doi:10.1061/(ASCE)ST.1943-541X.0000074
- Abonyi, J., Babuska, R., Verbruggen, H. B., & Szeifert, F. (2000). Incorporating prior knowledge in fuzzy model identification. *International Journal of Systems Science*, 31, 657–667. doi:10.1080/002077200290966
- Abrahamson, N. A. (1993). *Non-stationary spectral matching program RSPMatch: user's manual*.
- Adamu, A., Karihaloo, B. L., & Rozvany, G. I. N. (1994). Minimum cost design of reinforced concrete beams using continuum-type optimality criteria. *Structural and Multidisciplinary Optimization*, 7(1), 91–102.
- Adeli, H., & Jiang, X. (2006). Dynamic fuzzy wavelet neural network model for structural system identification. *Journal of Structural Engineering*, 132, 102–111. doi:10.1061/(ASCE)0733-9445(2006)132:1(102)
- Ahlawat, A. S., & Ramaswamy, A. (2004). Multiobjective optimal fuzzy logic control system for response control of wind-excited tall buildings. *Journal of Engineering Mechanics*, 130, 524–530. doi:10.1061/(ASCE)0733-9399(2004)130:4(524)
- Akiyama, H. (1985). *Earthquake-resistant limit-state design for buildings*. Tokyo, Japan: University of Tokyo Press.
- Alavi, B., & Krawinkler, H. (2000, January 30–February 4). *Consideration of near-fault ground motion effects in seismic design*. Paper presented at the 12th World Conference on Earthquake Engineering, Auckland, New Zealand.
- Al-Dawod, M., Samali, B., Kwok, K. C. S., & Naghdy, F. (2004). Fuzzy controller for seismically excited nonlinear buildings. *Journal of Engineering Mechanics*, 130, 407–415. doi:10.1061/(ASCE)0733-9399(2004)130:4(407)
- Alexandrov, N., Dennis, J. Jr, Lewis, R., & Torczon, V. (1998). A trust-region framework for managing the use of approximation models in optimization. *Structural Optimization*, 15(1), 16–23. doi:10.1007/BF01197433
- Altay, N., & Greene, W. G. (2006). OR/MS research in disaster operations management. *European Journal of Operational Research*, 175, 475–493. doi:10.1016/j.ejor.2005.05.016

- Alvin, K. F., Robertson, A. N., Reich, G. W., & Park, K. C. (2003). Structural system identification: from reality to models. *Computers & Structures*, 81(12), 1149–1176. doi:10.1016/S0045-7949(03)00034-8
- Al-Widyan, K., & Angeles, J. (2005). Model-based formulation of robust design. *Journal of Applied Mechanics Transaction*, 127(3), 388–396. doi:10.1115/1.1829728
- American Concrete Institute. (2008). *ACI-318: Building code requirements for structural concrete and commentary*. ACI.
- Amin, M., & Ang, A. H.-S. (1968). Non-stationary stochastic models of earthquake motions. *Proceedings ASCE, Journal of Engineering Mechanics Division*, 94.
- Anderson, J., & Hough, S. (1984). A model for the shape of the Fourier amplitude spectrum of acceleration at high frequencies. *Bulletin of the Seismological Society of America*, 74(5), 1969–1993.
- Andrade, C., Alonso, C., Garcia, D., & Rodriguez, J. (1991). Remaining life time of reinforced concrete structures: effect of corrosion in mechanical properties of the steel, life prediction of corrodible structures. *Proceedings of the International Symposium of the National Association of Corrosion Engineers*, 12/1-12/11, Cambridge, U. K.
- Andrade, C., Alonso, C., & Molina, F. J. (1993). Cover cracking as a function of rebar corrosion: Part I: Experimental test. *Materials and Structures*, 26(3), 345–353.
- Ang, A. H.-S., Lee, J.-C., & Pires, J. A. (1997). Cost-effectiveness evaluation of design criteria. *Proceedings of the International Workshop on Optimal Performance of Civil Infrastructure Systems* (pp.1-16). New York, NY: ASCE.
- Ansari, F. (2005). *Sensing issues in civil structural health monitoring*. Springer. doi:10.1007/1-4020-3661-2
- ANSYS Incorporated. (2006). *ANSYS release 10.0*, 2006.
- Applied Technology Council. (1985). *ATC-13: Earthquake damage evaluation data for California*. Redwood City, CA: ATC.
- Arias, A. (1970). *A measure of earthquake intensity: Seismic design of nuclear power plants* (pp. 438–468). Cambridge, MA: MIT Press.
- Arora, J. S. (1999). Optimization of structures subjected to dynamic loads. In Leondes, C. T. (Ed.), *Structural dynamic systems computational techniques and optimization* (pp. 1–73). Gordon and Breach Science Publishers.
- Arora, J. S. (2004). *Introduction to optimum design*. San Diego, CA: Elsevier Academic Press.
- Arora, J. S., & Haug, E. J. (1979). Methods of design sensitivity analysis in structural optimization. *AIAA Journal*, 17(9), 970–974. doi:10.2514/3.61260
- Asadi, P. (2006) *Optimization of distribution of reinforcement in the seismic design of R/C frames*. MSc. Thesis Civil Eng. Dept., Sharif University of Technology.
- ASCE. (2007). *Seismic rehabilitation of existing buildings* (pp. 41–06). Reston, VA: ASCE Publications.
- Aschheim, M. (1999). Yield point spectra: A simple alternative to the capacity spectrum method. *SEAOC 1999 Convention*, (pp. 373-379).
- Aslani, H., & Miranda, E. (2005). Probability-based seismic response analysis. *Engineering Structures*, 27(8), 1151–1163. doi:10.1016/j.engstruct.2005.02.015
- Åström, K. J., & Eykhoff, P. (1971). System identification—A survey. *Automatica*, 7, 123–162. doi:10.1016/0005-1098(71)90059-8
- Atkinson, G. M., & Silva, W. (2000). Stochastic modeling of California ground motions. *Bulletin of the Seismological Society of America*, 90(2), 255–274. doi:10.1785/0119990064
- Atkinson, G., & Silva, W. (2000). Stochastic modeling of California ground motions. *Bulletin of the Seismological Society of America*, 90(2), 255–274. doi:10.1785/0119990064
- Au, S., & Beck, J. (2001). Estimation of small failure probabilities in high dimensions by subset simulation. *Probabilistic Engineering Mechanics*, 16(4), 263–277. doi:10.1016/S0266-8920(01)00019-4
- Baber, T., & Noori, M. N. (1985). Random vibration of degrading, pinching systems. *Journal of Engineering Mechanics*, 111(8), 1010–1026. doi:10.1061/(ASCE)0733-9399(1985)111:8(1010)

Compilation of References

- Baber, T., & Wen, Y. (1981). Random vibration hysteretic, degrading systems. *Journal of the Engineering Mechanics Division*, 107(6), 1069–1087.
- Baker, J. W., Lin, T., Shahi, S. K., & Jayaram, N. (2011). *New ground motion selection procedures and selected motions for the PEER transportation research program*. PEER Technical Report 2011/03. 106p.
- Baker, J. W. (2011). Conditional mean spectrum: Tool for ground motion selection. *Journal of Structural Engineering*, 137(3), 322–331. doi:10.1061/(ASCE) ST.1943-541X.0000215
- Baker, J. W., & Cornell, C. A. (2006). Spectral shape, epsilon and record selection. *Earthquake Engineering & Structural Dynamics*, 35, 1077–1095. doi:10.1002/eqe.571
- Balling, R. J., Pister, K. S., & Ciampi, V. (1983). Optimal seismic-resistant design of a planar steel frame. *Earthquake Engineering & Structural Dynamics*, 11, 541–556. doi:10.1002/eqe.4290110407
- Bamforth, P. B., & Price, W. F. (1996). *An international review of chloride ingress into structural concrete*. Rep. No. 1303/96/9092. Middlesex, UK: Taywood Engineering Ltd., Technology Division.
- Bani-Hani, K., Ghaboussi, J., & Schneider, S. P. (1999). Experimental study of identification and control of structures using neural network Part 1: Identification. *Earthquake Engineering & Structural Dynamics*, 28, 995–1018. doi:10.1002/(SICI)1096-9845(199909)28:9<995::AID-EQE851>3.0.CO;2-8
- Basoz, N., & Kiremidjian, A. (1999). Development of empirical fragility curves for bridges. *Proceedings of 5th US Conference on Lifeline Earthquake Engineering*, ASCE, New York, USA.
- Battaini, M., Casciati, F., & Faravelli, L. (2004). Controlling wind response through a fuzzy controller. *Journal of Engineering Mechanics*, 130, 486–491. doi:10.1061/(ASCE)0733-9399(2004)130:4(486)
- Baykasoglu, A., Owen, S., & Gindy, N. (1999a). Solution of goal programming models using a basic taboo search algorithm. *The Journal of the Operational Research Society*, 50(9), 960–973.
- Baykasoglu, A., Owen, S., & Gindy, N. (1999b). A taboo search based approach to find the Pareto optimal set in multiple objective optimization. *Engineering Optimization*, 31(6), 731–748. doi:10.1080/03052159908941394
- Bazant, Z. P., & Najjar, L. J. (1972). Nonlinear water diffusion in unsaturated concrete. [Paris, France.]. *Materials and Structures*, 5(25), 3–20.
- Beck, J. L., Papadimitriou, C., Chan, E., & Irfanoglu, A. (1998). *A performance-based optimal structural design methodology*. Report No. EERL 97-03, CA, USA.
- Beirlant, J., Dudewicz, E. J., Gyorfi, L., & Van der Meulen, E. C. (1997). Nonparametric entropy estimation: An overview. *International journal of Mathematical and Statistical Sciences*, 6(1), 17-40.
- Bendsøe, M. P. (1989). Optimal shape design as a material distribution problem. *Structural Optimization*, 1(4), 193–202. doi:10.1007/BF01650949
- Bendsøe, M. P., & Kikuchi, N. (1988). Generating optimal topologies in structural design using a homogenization method. *Computer Methods in Applied Mechanics and Engineering*, 71(2), 197–224. doi:10.1016/0045-7825(88)90086-2
- Bendsøe, M. P., & Sigmund, O. (1999). Material interpolation schemes in topology optimization. *Archive of Applied Mechanics*, 69(9–10), 635–654.
- Bendsøe, M. P., & Sigmund, O. (2003). *Topology optimization - Theory, methods, and applications*. Berlin, Germany: Springer.
- Ben-Tal, A., & Nemirovski, A. (2002). Robust optimization-methodology and applications. *Mathematical Programming*, 92(3), 453–480. doi:10.1007/s101070100286
- Bertero, V. V., & Zagajeski, S. W. (1979). *Optimal inelastic design of seismic-resistant reinforced concrete framed structures*. Paper presented at the Nonlinear Design of Concrete Structures, CSCE-ASCE-ACI-CEB International Symposium, Ontario, Canada.
- Bertolini, L. (2008). Steel corrosion and service life of reinforced concrete structures. *Structure and Infrastructure Engineering*, 4(2), 123–137. doi:10.1080/15732470601155490

- Bertsimas, D., & Sim, M. (2006). Tractable approximations to robust conic optimization problems. *Mathematical Programming*, 107(1-2), 5–36. doi:10.1007/s10107-005-0677-1
- Basset, S., & Jezequel, L. (2007). Optimization of structural dynamic behaviour based on effective modal parameters. *International Journal for Numerical Methods in Engineering*, 70(5), 523–542. doi:10.1002/nme.1890
- Beyer, H.-G., & Sendhoff, B. (2007). Robust optimization –A comprehensive survey. *Computer Methods in Applied Mechanics and Engineering*, 196(33–34), 3190–3218. doi:10.1016/j.cma.2007.03.003
- Bhattacharjya, S., & Chakraborty, S. (2009). Robust optimization of linear dynamic system with random parameters under stochastic earthquake excitation. *International Journal of Reliability Quality and Safety Engineering*, 16(3), 261–279. doi:10.1142/S0218539309003393
- Bhatti, M. A., & Pister, K. S. (1981). A dual criteria approach for optimal design of earthquake-resistant structural systems. *Earthquake Engineering & Structural Dynamics*, 9, 557–572.
- Biondini, F., Bontempi, F., Frangopol, D. M., & Malerba, P. G. (2004). Cellular automata approach to durability analysis of concrete structures in aggressive environments. *Journal of Structural Engineering*, 130(11), 1724–1737. doi:10.1061/(ASCE)0733-9445(2004)130:11(1724)
- Bjerager, P., & Krenk, S. (1989). Parametric sensitivity in first order reliability theory. *Journal of Engineering Mechanics*, 115(7), 1577–1582. doi:10.1061/(ASCE)0733-9399(1989)115:7(1577)
- Blackshire, J. L., Martin, S., & Cooney, A. (2006). Characterization and modeling of bonded piezoelectric sensor performance and durability in simulated aircraft environments. *Proceedings of 3rd European Workshop on Structural Health Monitoring*, Granada, Spain.
- Bland, J. (1998). Structural design optimization with reliability constraints using tabu search. *Engineering Optimization*, 30(1), 55–74. doi:10.1080/03052159808941238
- Blevins, R. D. (1979). *Formulas for natural frequency and mode shape*. New York, NY: Litton Education Publishing Inc.
- Bommer, J. J., & Acevedo, A. B. (2004). The use of real earthquake accelerograms as input to dynamic analysis. *Journal of Earthquake Engineering*, 1, 43–91. doi:10.1080/13632460409350521
- Boore, D. (2003). Simulation of ground motion using the stochastic method. *Pure and Applied Geophysics*, 160(3), 635–676. doi:10.1007/PL00012553
- Boore, D. M. (1983). Stochastic simulation of high-frequency ground motions based on seismological models of the radiated spectra. *Bulletin of the Seismological Society of America*, 73, 1865–1894.
- Boore, D. M. (2003). Simulation of ground motion using the stochastic method. *Pure and Applied Geophysics*, 160, 635–676. doi:10.1007/PL00012553
- Boore, D., Joyner, W., & Fumal, T. (1997). Equations for estimating horizontal response spectra and peak acceleration from western North American earthquakes: A summary of recent work. *Seismological Research Letters*, 68(1), 128–153. doi:10.1785/gssrl.68.1.128
- Bouazizi, M.-L., Ghanmi, S., & Bouhaddi, N. (2009). Multi-objective optimization in dynamics of the structures with nonlinear behavior: Contributions of the metamodels. *Finite Elements in Analysis and Design*, 45(10), 612–623. doi:10.1016/j.finel.2009.03.007
- Bouc, R. (1967). Forced vibration of mechanical systems with hysteresis. *Proceedings of the 4th Conference on Non-linear Oscillations*, Prague, Czechoslovakia, Sept. 5-9.
- Bozorgnia, Y., & Bertero, V. V. (2003). Damage spectra: Characteristics and applications to seismic risk reduction. *Journal of Structural Engineering*, 129(4), 1330–1340. doi:10.1061/(ASCE)0733-9445(2003)129:10(1330)
- Bozorgnia, Y., & Bertero, V. V. (Eds.). (2004). *Earthquake engineering*. New York, NY: CRC Press. doi:10.1201/9780203486245

Compilation of References

- Bratus, A. S., & Seyranian, A. P. (1983). Bimodal solutions in eigenvalue optimization problems. *Journal of Applied Mathematics and Mechanics*, 47(4), 451–457. doi:10.1016/0021-8928(83)90081-3
- Bray, J. D., & Rodriguez-Marek, A. (2004). Characterization of forward-directivity ground motions in the near-fault region. *Soil Dynamics and Earthquake Engineering*, 24, 815–828. doi:10.1016/j.soildyn.2004.05.001
- Brozzetti, J. (2000). Design development of steel-concrete composite bridges in France. *Journal of Constructional Steel Research*, 55, 229–243. doi:10.1016/S0143-974X(99)00087-5
- Brune, J. N. (1970). Tectonic stress and the spectra of seismic shear waves from earthquakes. *Journal of Geophysical Research*, 75, 4997–5009. doi:10.1029/JB075i026p04997
- Bucher, C., & Bourgund, U. (1990). A fast and efficient response surface approach for structural reliability problems. *Structural Safety*, 7(1), 57–66. doi:10.1016/0167-4730(90)90012-E
- Bucher, C., & Macke, M. (2005). Response surfaces for reliability assessment. In Nikolaidis, E., Ghiocei, D. M., & Singhal, S. (Eds.), *Engineering design reliability handbook*. Boca Raton, FL: CRC Press.
- Buhl, T., Pedersen, C. B. W., & Sigmund, O. (2000). Stiffness design of geometrically nonlinear structures using topology optimization. *Structural and Multidisciplinary Optimization*, 19(2), 93–104. doi:10.1007/s001580050089
- Buratti, N., Stafford, P. J., & Bommer, J. J. (2011). Earthquake accelerogram selection and scaling procedures for estimating the distribution of drift response. *Journal of Structural Engineering*, 137(3), 345–357. doi:10.1061/(ASCE)ST.1943-541X.0000217
- Caleman, T., Branch, M. A., & Grace, A. (1999). *Optimization toolbox for the use with Matlab. User's guide*. USA: The MATH WORKS Inc.
- California Department of Transportation. (2006). *Caltrans seismic design criteria*. Sacramento, CA: Author.
- California Department of Transportation. (2008). *Caltrans contract cost data*. Sacramento, CA: Author.
- Canuryt, O. E., & Hajela, P. (2005). A cellular framework for structural analysis and optimization. *Computer Methods in Applied Mechanics and Engineering*, 194(30-33), 3516–3534. doi:10.1016/j.cma.2005.01.014
- Cao, X. (2009). *Design strategy on aseismic capacity of large bridge*. Doctoral dissertation, Tongji University, Shanghai, China.
- Casciati, F. (1997). Checking the stability of a fuzzy controller for nonlinear structures. *Microcomputers in Civil Engineering*, 12, 205–215. doi:10.1111/0885-9507.00057
- Chai, Y. H., Romstad, K. M., & Bird, S. M. (1995). Energy-based linear damage model for high-intensity seismic loading. *Journal of Structural Engineering*, 121(5), 857–864. doi:10.1061/(ASCE)0733-9445(1995)121:5(857)
- Chan, C. M. (1997). How to optimize tall steel building frameworks. *Guide to structural optimization* (pp. 165–195). ASCE Manuals and Reports on Engineering Practice No.90.
- Chan, C. M., & Zou, X. K. (2004). Elastic and inelastic drift performance optimization for reinforced concrete building under earthquake loads. *Earthquake Engineering & Structural Dynamics*, 33(8), 929–950. doi:10.1002/eqe.385
- Chang, P. C., Flatau, A., & Liu, S. C. (2003). Review paper: Health monitoring of civil infrastructure. *Structural Health Monitoring*, 2(3), 257–267. doi:10.1177/1475921703036169
- Chang, S., & Shinozuka, M. (1996). Life cycle cost analysis with natural hazard risk. *Journal of Infrastructure Systems*, 2(3), 118–126. doi:10.1061/(ASCE)1076-0342(1996)2:3(118)
- Chan, R. W. K., & Albermani, F. (2008). Experimental study of steel slit damper for passive energy dissipation. *Engineering Structures*, 30(4), 1058–1066. doi:10.1016/j.engstruct.2007.07.005

- Charney, F. A. (2000). Needs in the development of a comprehensive performance based design optimization process. In M. Elgaaly (Ed.), *Advanced Technology in Structural Engineering - Structural Congress 2000*, ASCE, May 8-10, (CD-ROM).
- Chassiakos, A. G., & Masri, S. F. (1996). Identification of structural systems by neural networks. *Mathematics and Computers in Simulation*, 40, 637–656. doi:10.1016/0378-4754(95)00012-7
- Chaudhuri, A., & Chakraborty, S. (2004). Sensitivity evaluation in seismic reliability analysis of structures. *Computer Methods in Applied Mechanics and Engineering*, 193(1-2), 59–68. doi:10.1016/j.cma.2003.09.007
- Chaudhuri, A., & Chakraborty, S. (2006). Reliability of linear structures with parameter uncertainty under non-stationary earthquake. *Structural Safety*, 28(3), 231–246. doi:10.1016/j.strusafe.2005.07.001
- Cheng, F. Y., & Chang, C. C. (1988). *Safety-based optimum design of nondeterministic structures subjected to various types of seismic loads*. NSF Report, U.S. Department of Commerce, VA, NTIS No. PB90-133489/AS.
- Cheng, F. Y., & Botkin, M. E. (1976). Nonlinear optimum design of dynamic damped frames. *Journal of the Structural Division*, 102, 609–628.
- Cheng, F. Y., & Li, D. (1997). Multiobjective optimization design with Pareto genetic algorithm. *Journal of Structural Engineering*, 123(9), 1252–1261. doi:10.1061/(ASCE)0733-9445(1997)123:9(1252)
- Cheng, F. Y., & Truman, K. Z. (1982). Optimization algorithm of 3-D building systems for static and seismic loading. In Ames, W. F. (Ed.), *Modeling and simulation in engineering* (pp. 315–326). North-Holland Pub. Co.
- Chen, J., Che, J., Sun, H., Ma, H., & Cui, M. (2002). Structural dynamic optimization with probability constraints of frequency and mode. *Structural Engineering & Mechanics*, 13(5), 479–490.
- Chen, S. H., Song, M., & Chen, Y. D. (2007). Robustness analysis of vibration control structures with uncertain parameters using interval algorithm. *Structural Safety*, 29(2), 94–111. doi:10.1016/j.strusafe.2006.03.001
- Chen, Y., Yang, B., Abraham, A., & Peng, L. (2007). Automatic design of hierarchical Takagi-Sugeno type fuzzy systems using evolutionary algorithms. *IEEE Transactions on Fuzzy Systems*, 15, 385–397. doi:10.1109/TFUZZ.2006.882472
- Choi, E., DesRoches, R., & Nielson, B. (2004). Seismic fragility of typical bridges in moderate seismic zones. *Journal of Engineering Structures*, 26(2), 187–199. doi:10.1016/j.engstruct.2003.09.006
- Choi, H., & Kim, J. (2006). Energy-based design of buckling-restrained braced frames using hysteretic energy spectrum. *Engineering Structures*, 28, 304–311. doi:10.1016/j.engstruct.2005.08.008
- Choi, K. M., Cho, S. W., Jung, H. J., & Lee, I. W. (2004). Semi-active fuzzy control for seismic response reduction using magnetorheological dampers. *Earthquake Engineering & Structural Dynamics*, 33, 723–736. doi:10.1002/eqe.372
- Chopra, A. K. (1995). *Dynamics of structures – Theory and applications to earthquake engineering*. Upper Saddle River, NJ: Prentice Hall International.
- Chopra, A. K. (2007). *Dynamics of structures* (3rd ed.). Englewood Cliffs, NJ: Prentice-Hall.
- Chung, L. L., Lin, R. C., Soong, T. T., & Reinhorn, A. M. (1989). Experiments on active control for MDOF seismic structures. *Journal of Engineering Mechanics*, 115, 1609–1627. doi:10.1061/(ASCE)0733-9399(1989)115:8(1609)
- Clauset, A., Moore, C., & Newman, M. E. J. (2008). Hierarchical structure and the prediction of missing links in networks. *Nature*, 453, 98–101. doi:10.1038/nature06830
- Clough, R. W., & Penzien, J. (1975). *Dynamics of structures*. McGraw-Hill.
- Clough, R. W., & Penzien, J. (2003). *Dynamics of structures* (3rd ed.). Computers & Structures Inc.
- Coello, C. A. (2000). An updated survey of GA-based multi-objective optimization techniques. *ACM Computing Surveys*, 32(2), 109–143. doi:10.1145/358923.358929

Compilation of References

- Collins, K. R., Wen, Y. K., & Foutch, D. A. (1996). Dual-level seismic design: A reliability-based methodology. *Earthquake Engineering & Structural Dynamics*, 25(12), 1433–1467. doi:10.1002/(SICI)1096-9845(199612)25:12<1433::AID-EQE629>3.0.CO;2-M
- Colomi, A., Dorigo, M., & Maniezzo, V. (1992). An investigation of some properties of an ant algorithm. In R. Manner, & B. Manderick (Eds.), *Proceedings of the Parallel Problem Solving from Nature Conference (PPSN 92)*, (pp. 509-520). Brussels, Belgium: Elsevier Publishing.
- Colomi, A., Dorigo, M., & Maniezzo, V. (1992). Distributed optimization by ant colonies. In F. Varela & P. Bourgine (Eds.), *Proceedings of the First European Conference on Artificial Life*, (pp. 134-142). Paris, France: Elsevier Publishing.
- Comartin, C., Brvez, S., Naeim, F., Greene, M., Blondet, M., & Cherry, S. (2004). A challenge to the earthquake engineering professionals. *Earthquake Spectra*, 20(4), 1049–1056. doi:10.1193/1.1809130
- Computer and Structures, Inc. (CSI). (2000). *SAP2000/NL-PUSH software*, Version 7.40. Berkeley, CA: Computer and Structures, Inc.
- Conte, J. P., & Peng, B. F. (1997). Fully nonstationary analytical earthquake ground motion model. *Journal of Engineering Mechanics*, 123, 15–24. doi:10.1061/(ASCE)0733-9399(1997)123:1(15)
- Cornell, A. C. (2008). Uncertainty propagation in probabilistic seismic loss estimation. *Structural Safety*, 30(3), 236–252. doi:10.1016/j.strusafe.2006.11.003
- Cornell, C. A., Jalayer, F., Hamburger, R. O., & Foutch, D. A. (2002). Probabilistic basis for 2000 SAC federal emergency management agency steel moment frame guidelines. *Journal of Structural Engineering*, 128(4), 526–533. doi:10.1061/(ASCE)0733-9445(2002)128:4(526)
- Cosenza, C., Manfredi, G., & Ramasco, R. (1993). The use of damage functionals in earthquake engineering: A comparison between different methods. *Earthquake Engineering & Structural Dynamics*, 22, 855–868. doi:10.1002/eqe.4290221003
- COSMOS. (2005). *Consortium organizations for strong-motion observation systems*. Retrieved from <http://db.cosmos-eq.org/scripts/default.plx>
- Cox, S. J., & Overton, M. L. (1992). On the optimal design of columns against buckling. *SIAM Journal on Mathematical Analysis*, 23(2), 287–325. doi:10.1137/0523015
- Crisfield, M. A. (2000). *Non-linear finite element analysis of solids and structures, Vol. 1: Essentials; Vol. 2: Advanced topics*. New York, NY: John Wiley & Sons.
- Culmann, K. (1866). *Die graphische Statik*. Zürich, Switzerland: Mayer und Zeller.
- Daigle, M., Koutsoukos, X., & Biswas, G. (2006). Distributed diagnosis of coupled mobile robots. *IEEE International Conference on Robotics and Automation*, (pp. 3787-3794).
- Datta, T. K. (2010). *Seismic analysis of structures*. Singapore: John Wiley & Sons. doi:10.1002/9780470824634
- Davis, R. O. (1992). Pounding of buildings modeled by an impact oscillator. *Earthquake Engineering & Structural Dynamics*, 21, 253–274. doi:10.1002/eqe.4290210305
- De Donato, O. (1977). Fundamentals of elastic-plastic analysis. In Cohn, M. Z., & Maier, G. (Eds.), *Engineering plasticity by mathematical programming* (pp. 325–349). New York, NY: Pergamon Press.
- De la Llera, J., Esguerra, C., & Almazán, J. (2004). Earthquake behavior of structures with copper energy dissipators. *Earthquake Engineering & Structural Dynamics*, 33(3), 329–358. doi:10.1002/eqe.354
- De Oliveira, R., Frazao, O., Santos, J. L., & Marques, A. T. (2004). Optic fibre sensor for real-time damage detection in smart composite. *Computers & Structures*, 82(17-19), 1315–1321. doi:10.1016/j.compstruc.2004.03.028
- Deb, K. (2001). *Multi-objective optimization using evolutionary algorithms*. New York, NY: John Wiley & sons.
- Decanini, L. D., & Mollaoli, F. (2001). An energy-based methodology for the assessment of seismic demand. *Soil Dynamics and Earthquake Engineering*, 21, 113–137. doi:10.1016/S0267-7261(00)00102-0

- Der Kiureghian, A. (1996). A coherency model for spatially varying ground motions. *Earthquake Engineering & Structural Dynamics*, 25(1), 99–111. doi:10.1002/(SICI)1096-9845(199601)25:1<99::AID-EQE540>3.0.CO;2-C
- Diaaz, A. R., & Kikuchi, N. (1992). Solutions to shape and topology eigenvalue optimization problems using a homogenization method. *International Journal for Numerical Methods in Engineering*, 35(7), 1487–1502. doi:10.1002/nme.1620350707
- Dicleli, M. (2006). Performance of seismic-isolated bridges in relation to near-fault ground-motion and isolator characteristics. *Earthquake Spectra*, 22(4), 887–907. doi:10.1193/1.2359715
- Dimitrakopoulos, E., Makris, N., & Kappos, A. J. (2010). Dimensional analysis of the earthquake response of a pounding oscillator. *Journal of Engineering Mechanics*, 136(3), 299–310. doi:10.1061/(ASCE)0733-9399(2010)136:3(299)
- Doebling, S. W., Farrar, C. R., & Prime, M. B. (1998). A summary review of vibration-based damage identification methods. *The Shock and Vibration Digest*, 30(2), 91–105. doi:10.1177/058310249803000201
- Dolsek, M. (2009). Incremental dynamic analysis with consideration of modelling uncertainties. *Earthquake Engineering & Structural Dynamics*, 38(6), 805–825. doi:10.1002/eqe.869
- Dong, W. M., Chiang, W. L., & Shah, H. C. (1987). Fuzzy information processing in seismic hazard analysis and decision making. *Soil Dynamics and Earthquake Engineering*, 6(4), 202–226. doi:10.1016/0267-7261(87)90003-0
- Dorigo, M. (1992). *Optimization, learning and natural algorithms*. Milano, Italy: Politecnico di Milano.
- Dorigo, M., & Stützle, T. (2004). *Ant colony optimization*. The MIT Press.
- Dounis, A. I., Tiropanis, P., Syrcos, G. P., & Tseles, D. (2007). Evolutionary fuzzy logic control of base-isolated structures in response to earthquake activity. *Structural Control and Health Monitoring*, 14, 62–82. doi:10.1002/stc.83
- Drenick, R. F. (1977). The critical excitation of nonlinear systems. *Journal of Applied Mechanics*, 18, 333–336. doi:10.1115/1.3424047
- Du, H., & Zhang, N. (2008). Application of evolving Takagi-Sugeno fuzzy model to nonlinear system identification. *Applied Soft Computing*, 8, 676–686. doi:10.1016/j.asoc.2007.05.006
- Du, J., & Olhoff, N. (2007). Topological design of freely vibrating continuum structures for maximum values of simple and multiple eigenfrequencies and frequency gaps. *Structural and Multidisciplinary Optimization*, 34(2), 91–110. doi:10.1007/s00158-007-0101-y
- Du, X., & Chen, W. (2000). Towards a better understanding of modelling feasibility robustness in engineering design. *ASME Journal of Mechanical Design*, 122(4), 385–394. doi:10.1115/1.1290247
- Du, X., Sudijianto, A., & Chen, W. (2004). An interval framework for optimization under uncertainty using inverse reliability strategy. *ASME Journal of Mechanical Design*, 126(4), 562–570. doi:10.1115/1.1759358
- Du, Y. G., Clark, L. A., & Chan, A. H. C. (2005a). Residual capacity of corroded reinforcing bars. *Magazine of Concrete Research*, 57(3), 135–147. doi:10.1680/macr.2005.57.3.135
- Du, Y. G., Clark, L. A., & Chan, A. H. C. (2005b). Effect of corrosion on ductility of reinforcing bars. *Magazine of Concrete Research*, 57(7), 407–419. doi:10.1680/macr.2005.57.7.407
- Dyke, S. J., Spencer, B. F. Jr, Sain, M. K., & Carlson, J. D. (1996). Modeling and control of magnetorheological dampers for seismic response reduction. *Smart Materials and Structures*, 5, 565–575. doi:10.1088/0964-1726/5/5/006
- Dyke, S. J., Spencer, B. F. Jr, Sain, M. K., & Carlson, J. D. (1998). An experimental study of MR dampers for seismic protection. *Smart Materials and Structures*, 7, 693–703. doi:10.1088/0964-1726/7/5/012

Compilation of References

- EC2. (2004). *Eurocode 2. Design of concrete structures—Part 1: General rules and rules for buildings. (The European Standard EN 1992-1-1)*. Brussels, Belgium: European Committee for Standardisation.
- EC8. (2004). *Eurocode 8: Design of structures for earthquake resistance. (The European Standard EN 1998-1)*. Brussels, Belgium: European Committee for Standardisation.
- El Maaddawy, T., & Soudki, K. (2007). A model for prediction of time from corrosion initiation to corrosion cracking. *Journal of Cement and Concrete Composites*, 29(3), 168–175. doi:10.1016/j.cemconcomp.2006.11.004
- Elishakoff, I., & Ohsaki, M. (2010). *Optimization and anti-optimization of structures under uncertainty*. Singapore: Imperial College Press. doi:10.1142/9781848164789
- Elnashai, A. S., & Chryssanthopoulos, M. (1991). Effect of random material variability on seismic design parameters of steel frames. *Earthquake Engineering & Structural Dynamics*, 20(2), 101–114. doi:10.1002/eqe.4290200202
- Elouedi, Z., Mellouli, K., & Smets, P. (2004). Assessing sensor reliability for multisensor data fusion within the transferable belief model. *IEEE Transactions on Systems, Man, and Cybernetics. Part B, Cybernetics*, 34(1), 782–787. doi:10.1109/TSMCB.2003.817056
- Enevoldsen, I., & Sørensen, J. (1994). Reliability-based optimization in structural engineering. *Structural Safety*, 15(3), 169–196. doi:10.1016/0167-4730(94)90039-6
- Esteva, L., López, O. D., & Hernández, E. I. (2010). Seismic vulnerability functions of multi-story buildings: estimation and applications. *Structure and Infrastructure Engineering Special Issue: Vulnerability Assessment of Structures and Infrastructures*, 6(1-2), 3–16.
- Fajfar, P. (1992). Equivalent ductility factors, taking into account low-cyclic fatigue. *Earthquake Engineering & Structural Dynamics*, 21, 837–848. doi:10.1002/eqe.4290211001
- Fajfar, P. (2000). A nonlinear analysis method for performance-based seismic design. *Earthquake Spectra*, 16(3), 573–599. doi:10.1193/1.1586128
- Fajfar, P., & Krawinklere, H. (1997). *Seismic design methodologies for the next generation of codes*. Rotterdam, The Netherlands: Balkema.
- Fan, L. (Ed.). (1997). *Seismic resistance of bridge*. Shanghai, China: Tongji University Press.
- Fan, L., & Zhuo, W. (Eds.). (2001). *Seismic ductility design of bridge*. Beijing, China: People's Communication Press.
- Faravelli, L., & Rossi, R. (2002). Adaptive fuzzy control: Theory versus implementation. *Journal of Structural Control*, 9, 59–73. doi:10.1002/stc.5
- Fardis, M. N. (Ed.). (2010). *Advances in performance-based earthquake engineering*. New York, NY: Springer.
- Federal Emergency Management Agency. (2000). Prestandard and commentary for the seismic rehabilitation of buildings. *FEMA-356*. Washington, DC.
- Federal Emergency Management Agency. (2005). Improvement of nonlinear static seismic analysis procedure. *FEMA-440*. Washington, DC.
- Federal Emergency Management Agency. (2006). Next-generation performance-based seismic design guidelines. *FEMA-445*. Washington, DC.
- FEMA. (1997). *NEHRP guidelines for the seismic rehabilitation of buildings, FEMA 273*. Washington, DC: Federal Emergency Management Agency.
- FEMA. (2003). *NEHRP recommended provisions for seismic regulations for new buildings and other structures, FEMA 450, Part 1: Provisions*. Washington, DC: Federal Emergency Management Agency.
- FEMA. 356. (2000). *Prestandard and Commentary for the seismic rehabilitation of buildings*. Reston, VA: ASCE Publications.
- Feng, T. T., Arora, J. S., & Huang, E. J. (1977). Optimal structural design under dynamic loads. *International Journal for Numerical Methods in Engineering*, 11(1), 39–52. doi:10.1002/nme.1620110106
- Filev, D. P. (1991). Fuzzy modeling of complex systems. *International Journal of Approximate Reasoning*, 5, 281–290. doi:10.1016/0888-613X(91)90013-C

- Fleury, C. (1983). Dual methods for optimizing finite element flexural systems. *Computer Methods in Applied Mechanics and Engineering*, 37(3), 249–275. doi:10.1016/0045-7825(83)90078-6
- Fleury, C. (1989). CONLIN: An efficient dual optimizer based on convex approximation concepts. *Structural Optimization*, 1(2), 81–89. doi:10.1007/BF01637664
- Fleury, C., & Braibant, V. (1986). Structural optimization: A new dual method using mixed variables. *International Journal for Numerical Methods in Engineering*, 23(3), 409–428. doi:10.1002/nme.1620230307
- Foley, C. M. (2002). Optimized performance-based design for buildings. In Burns, S. A. (Ed.), *Recent advances in optimal structural design* (pp. 169–240). American Society of Civil Engineers.
- Foley, C. M., & Schinler, D. (2003). Automated design of steel frames using advanced analysis and object-oriented evolutionary computation. *Journal of Structural Engineering*, 129(5), 648–660. doi:10.1061/(ASCE)0733-9445(2003)129:5(648)
- Foschi, R. O. (2000). Modeling the Hysteretic response of mechanical connectors for wood structures. *Proceedings, World Timber Engineering Conference*, Whistler, B.C.
- Fragiadakis, M., & Lagaros, N. D. (2011). An overview to structural seismic design optimisation frameworks. *Computers & Structures*, 89(11-12), 1155–1165. doi:10.1016/j.compstruc.2010.10.021
- Fragiadakis, M., Lagaros, N. D., & Papadrakakis, M. (2006a). Performance-based earthquake engineering using structural optimisation tools. *International Journal of Reliability and Safety*, 1(1/2), 59–76. doi:10.1504/IJRS.2006.010690
- Fragiadakis, M., Lagaros, N. D., & Papadrakakis, M. (2006b). Performance-based multiobjective optimum design of steel structures considering life-cycle cost. *Structural and Multidisciplinary Optimization*, 32(1), 1–11. doi:10.1007/s00158-006-0009-y
- Fragiadakis, M., & Papadrakakis, M. (2008). Performance-based optimum seismic design of reinforced concrete structures. *Earthquake Engineering & Structural Dynamics*, 37(6), 825–844. doi:10.1002/eqe.786
- Frangopol, D. M. (2011). Life-cycle performance, management, and optimisation of structural systems under uncertainty: Accomplishments and challenges. *Structure and Infrastructure Engineering*, 7(6), 389–413. doi:10.1080/15732471003594427
- Fujita, K., Moustafa, A., & Takewaki, I. (2010). Optimal placement of viscoelastic dampers and supporting members under variable critical excitations. *Earthquakes and Structures*, 1(1), 43–67.
- Ganzerli, S., Pantelides, C. P., & Reaveley, L. D. (2000). Performance-based design using structural optimization. *Earthquake Engineering & Structural Dynamics*, 29(11), 1677–1690. doi:10.1002/1096-9845(200011)29:11<1677::AID-EQE986>3.0.CO;2-N
- Gao, Y. (2009). *Study on aseismic capacity of elevated pile cap foundations of large bridge*. Doctoral dissertation, Tongji University, Shanghai, China.
- Gao, X. W., & Bao, A. B. (1985). Probabilistic model and its statistical parameters for seismic load. *Earthquake Engineering and Engineering Vibration*, 5(1), 13–22.
- Gauss, K. F. (1963). *Theory of the motion of the heavenly bodies moving about the sun in conic sections: A Translation of Theoria Motus*. New York, NY: Dover Publications.
- Ghabraie, K., Chan, R., Huang, X., & Xie, Y. M. (2010). Shape optimization of metallic yielding devices for passive mitigation of seismic energy. *Engineering Structures*, 32(8), 2258–2267. doi:10.1016/j.engstruct.2010.03.028
- Ghanem, R., & Spanos, P. D. (1990). *Stochastic finite element analysis: A spectral approach*. Berlin, Germany: Springer.
- Ghobara, A., Abou-Elfath, H., & Biddah, A. (1999). Response-based damage assessment of structures. *Earthquake Engineering & Structural Dynamics*, 28, 79–104. doi:10.1002/(SICI)1096-9845(199901)28:1<79::AID-EQE805>3.0.CO;2-J
- Ghobarah, A. (2001). Performance-based design in earthquake engineering: State of development. *Journal of Engineering Structures*, 23(8), 878–884. doi:10.1016/S0141-0296(01)00036-0

Compilation of References

- Ghobarah, A., Abou-Elfath, H., & Biddah, A. (1999). Response-based damage assessment of structures. *Earthquake Engineering & Structural Dynamics*, 28(1), 79–104. doi:10.1002/(SICI)1096-9845(199901)28:1<79::AID-EQE805>3.0.CO;2-J
- Gholizadeh, S., & Salajegheh, E. (2010b). A cellular genetic algorithm for structural optimisation. In B. H. V. Topping, J. M. Adam, F. J. Pallarés, R. Bru, & M. L. Romero, (Ed.), *Proceedings of the Tenth International Conference on Computational Structures Technology, DATE*, (pp. 1-14). Stirlingshire, UK: Civil-Comp Press.
- Gholizadeh, S. (2010). Structural optimization for earthquake loading with nonlinear responses by surrogate modeling based evolutionary algorithms. *Asian Journal of Civil Engineering*, 11(1), 25–42.
- Gholizadeh, S., & Salajegheh, E. (2009). Optimal design of structures for time history loading by swarm intelligence and an advanced metamodel. *Computer Methods in Applied Mechanics and Engineering*, 198(37-40), 2936–2949. doi:10.1016/j.cma.2009.04.010
- Gholizadeh, S., & Salajegheh, E. (2010a). Optimal seismic design of steel structures by an efficient soft computing based algorithm. *Journal of Constructional Steel Research*, 66(1), 85–95. doi:10.1016/j.jcsr.2009.07.006
- Gholizadeh, S., Salajegheh, J., & Salajegheh, E. (2009). An intelligent neural system for predicting structural response subject to earthquake. *Advances in Engineering Software*, 40(8), 630–639. doi:10.1016/j.advengsoft.2008.11.008
- Gholizadeh, S., & Samavati, O. A. (2011). Structural optimization by wavelet transforms and neural networks. *Applied Mathematical Modelling*, 35(2), 915–929. doi:10.1016/j.apm.2010.07.046
- Glasserman, P., & Yao, D. D. (1992). Some guidelines and guarantees for common random numbers. *Management Science*, 38(6), 884–908. doi:10.1287/mnsc.38.6.884
- Glass, G. K., & Buenfeld, N. R. (2000). The influence of chloride binding on the chloride induced corrosion risk in reinforced concrete. *Corrosion Science*, 42(2), 329–344. doi:10.1016/S0010-938X(99)00083-9
- Glisic, B., & Inaudi, D. (2007). *Fibre optic methods for structural health monitoring*. Chichester, UK: John Wiley & Sons. doi:10.1002/9780470517819
- Glover, F. (1989). Tabu search - Part I. *ORSA Journal on Computing*, 1(3), 190-206.
- Glover, F. (1990). Tabu search - Part II. *ORSA Journal on computing*, 2(1), 4-32.
- GME-6. (2006). *A generic modeling environment, GME 6 user's manual*. Vanderbilt University. Retrieved from <http://www.isis.vanderbilt.edu>
- Goel, R. K. (1997). Seismic response of asymmetric systems: Energy-based approach. *Journal of Structural Engineering*, 123(11), 1444–1453. doi:10.1061/(ASCE)0733-9445(1997)123:11(1444)
- Goldberg, D. (1989). *Genetic algorithms in search, optimization, and machine learning*. Reading, MA: Addison Wesley.
- Gong, Y. (2003). Performance-based design of steel building frameworks under seismic loading. Doctoral dissertation, University of Waterloo, Waterloo, Canada.
- Gonzalez, M. P., & Zapico, J. L. (2008). Seismic damage detection in buildings using neural networks and modal data. *Computers & Structures*, 86(3-5), 416–426. doi:10.1016/j.compstruc.2007.02.021
- Groenwold, A., Etman, L., Snyman, J., & Rooda, J. (2007). Incomplete series expansion for function approximation. *Structural and Multidisciplinary Optimization*, 34(1), 21–40. doi:10.1007/s00158-006-0070-6
- Groenwold, A., & Wood, D. W. (2009). Globally convergent optimization algorithm using conservative convex separable diagonal quadratic approximations. *AIAA Journal*, 47(11), 2649–2657. doi:10.2514/1.41975
- Guedri, M., Ghanmi, S., Majed, R., & Bouhaddi, N. (2009). Robust tools for prediction of variability and optimization in structural dynamics. *Mechanical Systems and Signal Processing*, 23(4), 1123–1133. doi:10.1016/j.ymssp.2008.08.013

- Gunawan, S., & Azarm, S. (2005). Multi-objective robust optimization using a sensitivity region concept. *Structural and Multidisciplinary Optimization*, 29(1), 50–60. doi:10.1007/s00158-004-0450-8
- Gunawan, S., & Papalambros, P. Y. (2007). Reliability optimization with mixed continuous-discrete random variables and parameters. *Journal of Mechanical Design*, 129(2), 158–165. doi:10.1115/1.2406085
- Guo, X., Bai, W., Zhang, W., & Gao, X. (2009). Confidence structural robust design and optimization under stiffness and load uncertainties. *Computer Methods in Applied Mechanics and Engineering*, 198(41-44), 3378–3399. doi:10.1016/j.cma.2009.06.018
- Gu, Z. Q., & Oyadiji, O. (2008). Application of MR damper in structural control using ANFIS method. *Computers & Structures*, 86, 427–436. doi:10.1016/j.compstruc.2007.02.024
- Habibi, A. (2008). *Optimal seismic performance-based design of 2D reinforced concrete frames*. Doctoral dissertation, Tarbiat Modarres University, Tehran, Iran.
- Habibi, A., & Moharrami, H. (2010). Nonlinear sensitivity analysis of reinforced concrete frames. *Finite Elements in Analysis and Design*, 46(7), 571–584. doi:10.1016/j.finel.2010.02.005
- Haftka, R. T., & Gurdal, Z. (1992). *Elements of structural optimization*. Norwell, MA: Kluwer Academic Publishers.
- Haldar, A. (Ed.). (2006). *Recent developments in reliability-based civil engineering*. Singapore: World Scientific Publishing Co. Pte. Ltd. doi:10.1142/9789812707222
- Haldar, A., & Mahadevan, S. (2000). *Reliability assessment using stochastic finite element analysis*. USA: John Wiley and Sons.
- Hanks, T. G., & McGuire, R. K. (1981). The character of high frequency ground motions based on seismic shear waves. *Bulletin of the Seismological Society of America*, 71, 2071–2095.
- Hart, G. C., & Wong, K. (2000). *Structural dynamics for structural engineers*. New York, NY: John Wiley & Sons.
- Hasan, R., Xu, L., & Grierson, D. E. (2002). Push-over analysis for performance-based seismic design. *Computers & Structures*, 80(31), 2483–2493. doi:10.1016/S0045-7949(02)00212-2
- Haselton, C., Baker, J. W., Liel, A. B., & Deierlein, G. G. (2011). Accounting for ground motion spectral shape characteristics in structural collapse assessment through an adjustment for epsilon. *Journal of Structural Engineering*, 137(3), 332–344. doi:10.1061/(ASCE)ST.1943-541X.0000103
- Hassan, R., & Crossley, W. (2008). Reliability-based optimization under uncertainty including discrete variables. *Journal of Spacecraft and Rockets*, 45(2), 394–405. doi:10.2514/1.28827
- Haug, E. J., & Rousselet, B. (1980). Design sensitivity analysis in structural mechanics. II: Eigenvalue variations. *Journal of Structural Mechanics*, 8(2), 161–186. doi:10.1080/03601218008907358
- Haupt, R. L., & Haupt, S. E. (2004). *Practical genetic algorithms*. New Jersey: Wiley-Interscience Publication.
- Hayward, A. (1988). *Cheaper steel-concrete composite bridges*. In C. D. Buckner & I. Viest (Eds.), *Composite Construction in Steel and Concrete: Proceedings of an Engineering Foundation Conference*, New England College, Henniker, New Hampshire, June 7-12, 1987 (pp. 194-206). New York, NY: American Society of Civil Engineers.
- HAZUS-MH/MR3. (2007). FEMA's software program for estimating potential losses from disasters.
- He, W. L., & Agrawal, A. K. (2008). Analytical model of ground motion pulses for the design and assessment of seismic protective systems. *Journal of Structural Engineering*, 134(7), 1177–1188. doi:10.1061/(ASCE)0733-9445(2008)134:7(1177)
- Housner, G. W., & Hudson, D. E. (1958). The Port Hueneme earthquake of March 18, 1957. *Bulletin of the Seismological Society of America*, 48, 163–168.
- Huang, B., & Du, X. (2007). Analytical robustness assessment for robust design. *Structural and Multidisciplinary Optimization*, 34(2), 123–127. doi:10.1007/s00158-006-0068-0

Compilation of References

- Huang, X., & Xie, Y. M. (2007). Convergent and mesh-independent solutions for the bi-directional evolutionary structural optimization method. *Finite Elements in Analysis and Design*, 43(14), 1039–1049. doi:10.1016/j.finel.2007.06.006
- Huang, X., & Xie, Y. M. (2008). Topology optimization of nonlinear structures under displacement loading. *Engineering Structures*, 30(7), 2057–2068. doi:10.1016/j.engstruct.2008.01.009
- Huang, X., Xie, Y. M., & Lu, G. (2007). Topology optimization of energy-absorbing structures. *International Journal of Crashworthiness*, 12(6), 663–675. doi:10.1080/13588260701497862
- Huang, X., Zuo, Z. H., & Xie, Y. M. (2010). Evolutionary topological optimization of vibrating continuum structures for natural frequencies. *Computers & Structures*, 88(5–6), 357–364. doi:10.1016/j.compstruc.2009.11.011
- Hung, S. L., Huang, C. S., Wen, C. M., & Hsu, Y. C. (2003). Nonparametric identification of a building structure from experimental data using wavelet neural network. *Computer-Aided Civil and Infrastructure Engineering*, 18, 356–368. doi:10.1111/1467-8667.t01-1-00313
- Hurlebaus, S., & Gaul, L. (2006). Smart structure dynamics. *Mechanical Systems and Signal Processing*, 20, 255–281. doi:10.1016/j.ymssp.2005.08.025
- Hurtado, J. (2004). *Structural reliability – Statistical learning perspectives. Lecture Notes in Applied and Computational Mechanics*, 17. Springer Verlag.
- Hwang, H., Liu, J. B., & Chiu, Y.-H. (2001). *Seismic fragility analysis of highway bridges*. Tennessee, USA: Center of Earthquake Research and Information, The University of Memphis.
- Hwang, J.-S., & Tseng, Y.-S. (2005). Design formulations for supplemental viscous dampers to highway bridges. *Earthquake Engineering & Structural Dynamics*, 34(13), 1627–1642. doi:10.1002/eqe.508
- Hwang, K.-H., Lee, K.-W., & Park, G.-J. (2001). Robust optimization of an automobile rearview mirror for vibration reduction. *Structural and Multidisciplinary Optimization*, 21(4), 300–308. doi:10.1007/s001580100107
- INPRES. (1995). *Microzonificación Sísmica del Gran Mendoza*. Instituto Nacional de Prevención Sísmica, Publicación Técnica Nº 19.
- INPRES-CIRSOC 103. (1995). *Reglamento Argentino para construcciones sismorresistentes, Parte II: Construcciones de Hormigón Armado*, INTI.
- International Building Code*. (2006).
- International Conference of Building Officials. (1997). *Uniform building code*(UBC). Whittier, California, USA.
- Iyengar, R. N. (1972). Worst inputs and a bound on the highest peak statistics of a class of non-linear systems. *Journal of Sound and Vibration*, 25, 29–37. doi:10.1016/0022-460X(72)90593-7
- Jalayer, F., & Cornell, C. A. (2009). Alternative non-linear demand estimation methods for probability-based seismic assessments. *Earthquake Engineering & Structural Dynamics*, 38(8), 951–972. doi:10.1002/eqe.876
- Jangid, R. S. (2008). Stochastic response of bridges seismically isolated by friction pendulum system. *Journal of Bridge Engineering*, 13(4), 319–330. doi:10.1061/(ASCE)1084-0702(2008)13:4(319)
- Jang, J. S. R., Sun, C. T., & Mizutani, E. (1997). *Neuro-fuzzy and soft computing*. Upper Saddle River, NJ: Prentice Hall.
- Jaynes, E. T. (2003). *Probability theory: The logic of science*. Cambridge, UK: Cambridge University Press. doi:10.1017/CBO9780511790423
- Jensen, H. (2005). Structural optimization of linear dynamical systems under stochastic excitation: A moving reliability database approach. *Computer Methods in Applied Mechanics and Engineering*, 194(12-16), 1757–1778.
- Jensen, H. (2002). Reliability-based optimization of uncertain systems in structural dynamic. *AIAA Journal*, 40(4), 731–738. doi:10.2514/2.1705
- Jensen, H. (2006). Structural optimization of non-linear systems under stochastic excitation. *Probabilistic Engineering Mechanics*, 21(4), 397–409. doi:10.1016/j.probengmech.2006.02.002

- Jensen, H., & Beer, M. (2010). Discrete-continuous variable structural optimization of systems under stochastic loading. *Structural Safety*, 32(5), 293–304. doi:10.1016/j.strusafe.2010.03.007
- Jensen, H., Valdebenito, M., Schüller, G., & Kusanovic, D. (2009). Reliability-based optimization of stochastic systems using line search. *Computer Methods in Applied Mechanics and Engineering*, 198(49–52), 3915–3924. doi:10.1016/j.cma.2009.08.016
- Jensen, J. S. (2007). Topology optimization of dynamics problems with Padé approximants. *International Journal for Numerical Methods in Engineering*, 72(13), 1605–1630. doi:10.1002/nme.2065
- Jiang, X., & Adeli, H. (2005). Dynamic wavelet neural network for nonlinear identification of highrise buildings. *Computer-Aided Civil and Infrastructure Engineering*, 20, 316–330. doi:10.1111/j.1467-8667.2005.00399.x
- Jin, R., Chen, W., & Simpson, T. (2001). Comparative studies of metamodeling techniques under multiple modeling criteria. *Structural and Multidisciplinary Optimization*, 23(1), 1–13. doi:10.1007/s00158-001-0160-4
- Jog, C. S. (2002). Topology design of structures subjected to periodic loading. *Journal of Sound and Vibration*, 253(3), 687–709. doi:10.1006/jsvi.2001.4075
- Johansen, T.A. (1994). Fuzzy model based control: Stability, robustness, and performance issues. *IEEE Transactions on Fuzzy Systems*, 2, 221–234. doi:10.1109/91.298450
- Johansen, T. A., & Babuška, R. (2003). Multiobjective identification of Takagi-Sugeno fuzzy models. *IEEE Transactions on Fuzzy Systems*, 11, 847–860. doi:10.1109/TFUZZ.2003.819824
- Jónsson, M. H., Bessason, B., & Haflidason, E. (2010). Earthquake response of a base-isolated bridge subjected to strong near-fault ground motion. *Soil Dynamics and Earthquake Engineering*, 30(6), 447–455. doi:10.1016/j.soildyn.2010.01.001
- Jung, D., & Gea, H. C. (2004). Topology optimization of nonlinear structures. *Finite Elements in Analysis and Design*, 40(11), 1417–1427. doi:10.1016/j.finel.2003.08.011
- Jurecka, F., Ganser, M., & Bletzinger, K. U. (2007). Update scheme for sequential spatial correlation approximations in robust design optimization. *Computers & Structures*, 85(10), 606–614. doi:10.1016/j.compstruc.2006.08.075
- Kaisa, M. (1999). *Nonlinear multiobjective optimization*. USA: Kluwer Academic Publishers.
- Kalkan, E., & Kannath, S. K. (2008). Relevance of absolute and relative energy content in seismic evaluation of structures. *Advances in Structural Engineering*, 11(1), 1–18. doi:10.1260/136943308784069469
- Kalkan, E., & Luco, N. (Eds.). (2011). Earthquake ground motion selection and modification for nonlinear dynamic analysis of structures. *Journal of Structural Engineering*, 137(3), 277–467. doi:10.1061/(ASCE)ST.1943-541X.0000355
- Kang, B., Park, G. J., & Arora, J. S. (2006). A review of optimization of structures subjected to transient loads. *Structural and Multidisciplinary Optimization*, 31(2), 81–95. doi:10.1007/s00158-005-0575-4
- Kang, S.-C., Koh, H.-M., & Choo, J. F. (2010). An efficient response surface method using moving least squares approximation for structural reliability analysis. *Probabilistic Engineering Mechanics*, 25(4), 365–371. doi:10.1016/j.probengmech.2010.04.002
- Karlaftis, M. G., Kepaptsoglou, K. L., & Lampropoulos, S. (2007). Fund allocation for transportation network recovery following natural disasters. *Journal of Urban Planning and Development*, 133(1), 82–89. doi:10.1061/(ASCE)0733-9488(2007)133:1(82)
- Karnopp, D. C., Margolis, D. L., & Rosenberg, R. C. (2006). *System dynamics, modeling and simulation of mechatronic systems*. John Wiley & Sons.
- Karush, W. (1939). *Minima of functions of several variables with inequalities as side constraints*. Master's thesis, Department of Mathematics, University of Chicago, Chicago, Illinois.
- Kennedy, J., & Eberhart, R. (1995). Particle swarm optimization. *IEEE International Conference on Neural Networks*, Piscataway, NJ, (pp. 1942–1948).

Compilation of References

- Kerber, F., Hurlebaus, S., Beadle, B. M., & Stöbener, U. (2007). Control concepts for an active vibration isolation system. *Mechanical Systems and Signal Processing*, 21, 3042–3059. doi:10.1016/j.ymssp.2007.04.003
- Kharmanda, G., Olhoff, N., Mohamed, A., & Lemaire, M. (2004). Reliability-based topology optimization. *Structural and Multidisciplinary Optimization*, 26(5), 295–307. doi:10.1007/s00158-003-0322-7
- Khashaee, P. (2004). Damage-based seismic design of structures. *Earthquake Spectra*, 21(2), 371–387. doi:10.1193/1.1896366
- Kim, C., Wang, S., & Choi, K. K. (2005). Efficient response surface modelling by using moving least-squares method and sensitivity. *AIAA Journal*, 43(1), 2404–2411. doi:10.2514/1.12366
- Kim, H. S., & Roschke, P. N. (2006). Design of fuzzy logic controller for smart base isolation system using genetic algorithm. *Engineering Structures*, 28, 84–96. doi:10.1016/j.engstruct.2005.07.006
- Kim, S. B., Yun, C. B., & Spencer, B. F. Jr. (2004). Vibration control of wind-excited tall buildings using sliding mode fuzzy control. *Journal of Engineering Mechanics*, 130, 505–510. doi:10.1061/(ASCE)0733-9399(2004)130:4(505)
- Kim, Y., Hurlebaus, S., & Langari, R. (2010). Control of a seismically excited benchmark building using linear matrix inequality-based semiactive nonlinear fuzzy control. *Journal of Structural Engineering*, 136, 1023–1026. doi:10.1061/(ASCE)ST.1943-541X.0000192
- Kim, Y.-I., & Park, G. J. (2010). Nonlinear dynamic response structural optimization using equivalent static loads. *Computer Methods in Applied Mechanics and Engineering*, 199(9-12), 660–676. doi:10.1016/j.cma.2009.10.014
- Kim, Y., Langari, R., & Hurlebaus, S. (2009). Semiactive nonlinear control of a building using a magnetorheological damper system. *Mechanical Systems and Signal Processing*, 23, 300–315. doi:10.1016/j.ymssp.2008.06.006
- Kim, Y., Langari, R., & Hurlebaus, S. (2010). Model-based multi-input, multi-output supervisory semiactive nonlinear fuzzy controller. *Computer-Aided Civil and Infrastructure Engineering*, 25, 387–393. doi:10.1111/j.1467-8667.2009.00649.x
- Kiureghian, A. D., & Crempien, J. (1989). An evolutionary model for earthquake ground motion. *Structural Safety*, 6, 235–246. doi:10.1016/0167-4730(89)90024-6
- Klee, H. (2007). *Simulation of dynamic systems with MATLAB and SIMULINK*. Boca Raton, FL: CRC Press.
- Kleiber, M., & Hien, T. D. (1992). *The stochastic finite element method*. Chichester, UK: John Wiley and Sons.
- Kleinmann, N. L., Spall, J. C., & Naiman, D. C. (1999). Simulation-based optimization with stochastic approximation using common random numbers. *Management Science*, 45(11), 1570–1578. doi:10.1287/mnsc.45.11.1570
- Kocer, F. Y., & Arora, J. S. (1999). Optimal design of H-frame transmission poles for earthquake loading. *Journal of Structural Engineering*, 125(11), 1299–1308. doi:10.1061/(ASCE)0733-9445(1999)125:11(1299)
- Kocer, F. Y., & Arora, J. S. (2002). Optimal design of latticed towers subjected to earthquake loading. *Journal of Structural Engineering*, 128(2), 197–204. doi:10.1061/(ASCE)0733-9445(2002)128:2(197)
- Koh, C. G., Chen, Y. F., & Liaw, C.-Y. (2003). A hybrid computational strategy for identification of structural parameters. *Computers & Structures*, 81(2), 107–117. doi:10.1016/S0045-7949(02)00344-9
- Kong, J. S., Ababneh, A. N., Frangopol, D. M., & Xi, Y. (2002). Reliability analysis of chloride penetration in saturated concrete. *Journal of Probabilistic Engineering Mechanics*, 17(3), 302–315. doi:10.1016/S0266-8920(02)00014-0
- Kosaka, I., & Swan, C. C. (1999). A symmetry reduction method for continuum structural topology optimization. *Computers & Structures*, 70(1), 47–61. doi:10.1016/S0045-7949(98)00158-8
- Kovács, L. (1980). Combinatorial methods of discrete programming. *Mathematical Methods of Operation Research*, 2.

- Kramer, S. L. (2003). *Geotechnical earthquake engineering*. Prentice Hall.
- Krawinkler, H. (1994). Static pushover analysis. *Proceedings SEAONC 1994 Fall Seminar on the Developing Art of Seismic Engineering*. San Francisco, CA.
- Kuhn, H. W., & Tucker, A. W. (1951). Nonlinear programming. In *Proceedings of 2nd Berkeley Symposium* (pp. 481–492). Berkeley, CA: University of California Press.
- Kunde, M. C., & Jangid, R. S. (2003). Seismic behavior of isolated bridges: A-state-of-the-art review. *Electronic Journal of Structural Engineering*, 3, 140–170.
- Kurdi, M. H., Haftka, R. T., Schmitz, T. L., & Mann, B. P. (2008). A robust semi-analytical method for calculating the response sensitivity of a time delay system. *Journal of Vibration and Acoustics*, 130(6), 1–6. doi:10.1115/1.2981093
- Kushner, H. J., & Yin, G. G. (2003). *Stochastic approximation and recursive algorithms and applications*. New York, NY: Springer Verlag.
- Kuwamura, H., & Kato, B. (1989). Effects of randomness in structural members' yield strength on the structural systems' ductility. *Journal of Constructional Steel Research*, 13(2–3), 79–93. doi:10.1016/0143-974X(89)90007-2
- Lagaros, N. D., Fragiadakis, M., & Papadrakakis, M. (2004). Optimum design of shell structures with stiffening beams. *AIAA Journal*, 42(1), 175–184. doi:10.2514/1.9041
- Lagaros, N. D., Fragiadakis, M., Papadrakakis, M., & Tsompanakis, Y. (2006). Structural optimization: A tool for evaluating dynamic design procedures. *Engineering Structures*, 28(12), 1623–1633. doi:10.1016/j.engstruct.2006.02.014
- Lagaros, N. D., Garavelas, A. T., & Papadrakakis, M. (2008). Innovative seismic design optimization with reliability constraints. *Computer Methods in Applied Mechanics and Engineering*, 198(1), 28–41. doi:10.1016/j.cma.2007.12.025
- Lagaros, N. D., & Karlaftis, M. G. (2011). A critical assessment of metaheuristics for scheduling emergency infrastructure inspections. *Swarm and Evolutionary Computation*, 1(3), 147–163. doi:10.1016/j.swevo.2011.06.002
- Lagaros, N. D., Naziris, I. A., & Papadrakakis, M. (2010). The influence of masonry infill walla in the Framework of the performance-based design. *Journal of Earthquake Engineering*, 14, 57–79. doi:10.1080/13632460902988976
- Lagaros, N. D., & Papadrakakis, M. (2007). Robust seismic design optimization of steel structures. *Structural and Multidisciplinary Optimization*, 33(6), 457–469. doi:10.1007/s00158-006-0047-5
- Lagaros, N. D., & Papadrakakis, M. (2007). Seismic design of RC structures: A critical assessment in the framework of multi-objective optimization. *Earthquake Engineering & Structural Dynamics*, 36(12), 1623–1639. doi:10.1002/eqe.707
- Lagaros, N. D., & Papadrakakis, M. (2011). (in press). Neural network based prediction schemes of the nonlinear seismic response of 3D buildings. *Advances in Engineering Software*.
- Lagaros, N., Garavela, A. T., & Papadrakakis, M. (2008). Innovative seismic design optimization with reliability constraints. *Computer Methods in Applied Mechanics and Engineering*, 198, 28–41. doi:10.1016/j.cma.2007.12.025
- Langari, R. (1999). Past, present and future of fuzzy control: A case for application of fuzzy logic in hierarchical control. *Proceedings, 18th International Conference of the North American Fuzzy Information Processing Society-NAFIPS*, New York City, New York, (pp. 760–765).
- Lawler, E. L., Lenstra, J. K., Rinnooy Kan, A. H. G., & Shmoys, D. B. (1985). *The traveling salesman problem: A guided tour of combinatorial optimization*. New York, NY: Wiley.
- Lee, H. S., Tomosawa, F., & Noguchi, T. (1996). Effect of rebar corrosion on the structural performance of single reinforced beams. In Lacasse, M. A., & Vanier, D. J. (Eds.), *Durability of building material and components* (pp. 571–580). London, UK: E & FN Spon.
- Lee, K., & Park, G. (2001). Robust optimization considering tolerances of design variable. *Computers & Structures*, 79(1), 77–86. doi:10.1016/S0045-7949(00)00117-6
- Lewis, A. S. (2002). *Robust regularization*. Technical Report. Columbia: Simon Fraser University.

Compilation of References

- Li, D. (1997). *Multi-objective optimum design of static and seismic-resistant structures with genetic algorithm, fuzzy logic and game theory*. Doctoral dissertation, University of Missouri-Rolla, Rolla, USA.
- Li, G. (1998). *Reliability and performance based optimal design for seismic high-rising structures*. Ph.D. Dissertation, Dalian University of Technology, China.
- Liang, Q. Q. (2005). *Performance-based optimization of structures*. New York, NY: Spon Press. doi:10.4324/9780203334713
- Li, G., Zhou, R.-G., Duan, L., & Chen, W.-F. (1999). Multiobjective and multilevel optimization for steel frames. *Engineering Structures*, 21(6), 519–529. doi:10.1016/S0141-0296(97)00226-5
- Lin, J. W., & Betti, R. (2004). On-line identification and damage detection in non-linear structural systems using a variable forgetting factor approach. *Earthquake Engineering & Structural Dynamics*, 33, 419–444. doi:10.1002/eqe.350
- Lin, J. W., Betti, R., Smyth, A. W., & Longman, R. W. (2001). On-line identification of non-linear hysteretic structural systems using a variable trace approach. *Earthquake Engineering & Structural Dynamics*, 30, 1279–1303. doi:10.1002/eqe.63
- Liu, M. (2003). *Development of multi-objective optimization procedures for seismic design of steel moment frame structures*. Doctoral dissertation, University of Illinois at Urbana Champaign, Urbana, USA.
- Liu, W. Y., Xiao, C. J., Wang, B. W., Shi, Y., & Fang, S. F. (2003). Study on combining subtractive clustering with fuzzy c-means clustering. *Proceedings of Second International Conference on Machine Learning and Cybernetics*, Xi'an, China, (pp. 2659-2662).
- Liu, M. (2005). Seismic design of steel moment-resisting frame structures using multiobjective optimization. *Earthquake Spectra*, 21(2), 389–414. doi:10.1193/1.1902952
- Liu, M., Burns, S. A., & Wen, Y. K. (2003). Optimal seismic design of steel frame buildings based on life cycle cost considerations. *Earthquake Engineering & Structural Dynamics*, 32(9), 1313–1332. doi:10.1002/eqe.273
- Liu, M., Burns, S. A., & Wen, Y. K. (2005). Multiobjective optimization for performance-based seismic design of steel moment frame structures. *Earthquake Engineering & Structural Dynamics*, 34(3), 289–306. doi:10.1002/eqe.426
- Liu, M., Burns, S. A., & Wen, Y. K. (2006). Genetic algorithm based construction-conscious minimum weight design of seismic steel moment-resisting frames. *Journal of Structural Engineering*, 132(1), 50–58. doi:10.1061/(ASCE)0733-9445(2006)132:1(50)
- Liu, M., Wen, Y. K., & Burns, S. A. (2004). Life cycle cost oriented seismic design optimization of steel moment frame structures with risk-taking preference. *Engineering Structures*, 26(10), 1407–1421. doi:10.1016/j.engstruct.2004.05.015
- Loh, C. H., Wu, W. Y., & Lin, P. Y. (2003). Displacement control of isolated structures with semi-active control devices. *Journal of Structural Control*, 10, 77–100. doi:10.1002/stc.18
- Lui, E. M., & Ge, M. (2005). Structural damage identification using system dynamic properties. *Computers & Structures*, 83(27), 2185–2196. doi:10.1016/j.compstruc.2005.05.002
- Lund, E. (1994). *Finite element based design sensitivity analysis and optimization*. Unpublished doctoral dissertation, Institute of Mechanical Engineering, Aalborg University, Denmark.
- Lutes, L. D., & Sarkani, S. (1997). *Stochastic analysis of structural and mechanical vibrations*. Upper Saddle River, NJ: Prentice Hall.
- Maeda, Y., Nishiwaki, S., Izui, K., Yoshimura, M., Matsui, K., & Terada, K. (2006). Structural topology optimization of vibrating structures with specified eigenfrequencies and eigenmode shapes. *International Journal for Numerical Methods in Engineering*, 67(5), 597–628. doi:10.1002/nme.1626
- Mahin, S. A., & Bertero, V. V. (1981). An evaluation of inelastic seismic design spectra. *Journal of the Structural Division*, 107(ST9), 1777–1795.

- Makris, N., & Zhang, J. (2004). Seismic response analysis of a highway overcrossing equipped with elastomeric bearings and fluid dampers. *Journal of Structural Engineering*, 130(6), 830–845. doi:10.1061/(ASCE)0733-9445(2004)130:6(830)
- Mander, J. B., & Basoz, N. (1999). Seismic fragility curve theory for highway bridges. *Proceedings of the 5th US Conference on Earthquake Engineering TCLEE No. 16*, (pp. 31-40).
- Mander, J. B., Priestly, M. J. N., & Park, R. (1988). Theoretical stress-strain model for confined concrete. *Journal of the Structural Division*, 114(8), 1804–1826. doi:10.1061/(ASCE)0733-9445(1988)114:8(1804)
- Manders, E. J., Biswas, G., Mahadevan, N., & Karsai, G. (2006). Component-oriented modeling of hybrid dynamic systems using the generic modeling environment. *Proceedings of 4th Workshop on Model-Based Development of Computer Based Systems*.
- Manoharan, S., & Shanmuganathan, S. (1999). A comparison of search mechanisms for structural optimization. *Computers & Structures*, 73(1-5), 363-372.
- Marano, G. C., Greco, R., & Sgobba, S. (2010). A comparison between different robust optimal design approaches: Application to tuned mass dampers. *Probabilistic Engineering Mechanics*, 25(1), 108–118. doi:10.1016/j.probengmech.2009.08.004
- Marano, G. C., Sgobba, S., Greco, R., & Mezzina, M. (2008). Robust optimum design of tuned mass dampers devices in random vibrations mitigation. *Journal of Sound and Vibration*, 313(3-5), 472–492. doi:10.1016/j.jsv.2007.12.020
- Marano, G. C., Trentadue, F., & Greco, R. (2006). Optimal design criteria for elastic structures subject to random dynamic loads. *Engineering Optimization*, 38(7), 853–871. doi:10.1080/03052150600913028
- Marler, R. T., & Arora, J. S. (2004). Survey of multi-objective optimization methods for engineering. *Structural and Multidisciplinary Optimization*, 26(6), 369–395. doi:10.1007/s00158-003-0368-6
- Martinez, W. L., & Martinez, A. R. (2002). *Computational Statistics Handbook with MATLAB*. Boca Raton, FL: Chapman & Hall/CRC.
- Martin-Perez, B., Pantzopoulou, S. J., & Thomas, M. D. A. (2001). Numerical solution of mass transport equations in concrete structures. *Journal of Computers and Structures*, 79(13), 1251–1264. doi:10.1016/S0045-7949(01)00018-9
- Masri, S. F., Smyth, A. W., Chassiakos, A. G., Caughey, T. K., & Hunter, N. F. (2000). Application of neural networks for detection of changes in nonlinear systems. *Journal of Engineering Mechanics*, 126, 666–676. doi:10.1061/(ASCE)0733-9399(2000)126:7(666)
- Masson, G., Cogan, S., Bouhaddi, N., Lombard, J. P., & Bonini, J. (2002). Parameterized reduced models for efficient optimization of structural dynamic behavior. *Collection of Technical Papers - AIAA/ASME/ASCE/AHS/ASC Structures, Structural Dynamics and Materials Conference*, (pp. 1434-1440).
- Mathworks. (1999). *Simulink: Dynamic system simulation for Matlab*. Mathworks Inc.
- Mavroeidis, G. P., & Papageorgiou, A. P. (2003). A mathematical representation of near-fault ground motions. *Bulletin of the Seismological Society of America*, 93(3), 1099–1131. doi:10.1785/0120020100
- Mavroeidis, G., & Papageorgiou, A. (2003). A mathematical representation of near-fault ground motions. *Bulletin of the Seismological Society of America*, 93(3), 1099–1131. doi:10.1785/0120020100
- Ma, Z. D., Cheng, H. C., & Kikuchi, N. (1995). Topological design for vibrating structures. *Computer Methods in Applied Mechanics and Engineering*, 121(1-4), 259–280. doi:10.1016/0045-7825(94)00714-X
- Ma, Z. D., Kikuchi, N., & Hagiwara, I. (1993). Structural topology and shape optimization for a frequency response problem. *Computational Mechanics*, 13(3), 157–174. doi:10.1007/BF00370133
- McGee, R. (1999). Modeling of durability performance of Tasmanian bridges. *Proceedings of the ICASP8 Conference*, (pp. 297-306). Sydney, Australia.

Compilation of References

- McGuire, R. K. (1995). Probabilistic seismic hazard analysis and design earthquake: Closing the loop. *Bulletin of the Seismological Society of America*, 85, 1275–1284.
- Mehanny, S. S., & Deierlein, G. G. (2000). *Modeling of assessment of seismic performance of composite frames with reinforced concrete columns and steel beams*. Report No. 135, The John Blume Earthquake Research Center, Stanford University.
- Memari, A. M., & Madhkhani, M. (1999). Optimal design of steel frames subject to gravity and seismic codes' prescribed lateral forces. *Structural and Multidisciplinary Optimization*, 18(1), 56–66.
- Mendonca, D., Beroggi, G. E. G., van Gent, D., & Wallace, W. A. (2006). Designing gaming simulations for the assessment of Group decision support Systems in emergency response. *Safety Science*, 44, 523–535. doi:10.1016/j.ssci.2005.12.006
- Mendonca, D., Beroggi, G. E. G., & Wallace, W. A. (2001). Decision support for improvisation during emergency response operations. *International Journal of Emergency Management*, 1(1), 30–38. doi:10.1504/IJEM.2001.000507
- Michell, A. G. M. (1904). The limits of economy of material in frame structures. *Philosophical Magazine*, 6(8), 589–597.
- Mills-Curran, W. C., & Schmit, L. A. (1985). Structural optimization with dynamic behaviour constraints. *AIAA Journal*, 23(1), 132–138. doi:10.2514/3.8881
- Ministry of Transport of the People's Republic of China. (1989). *Specifications for earthquake resistant design in highway Engineering (JTJ 004-89)*. Beijing, China: People's Communication Press.
- Ministry of Transport of the People's Republic of China. (2008). *Guidelines for seismic design of highway bridges (JTG/T B02-01-2008)*. Beijing, China: People's Communication Press.
- Min, S., Kikuchi, N., Park, Y. C., Kim, S., & Chang, S. (1999). Optimal topology design of structures under dynamic loads. *Structural Optimization*, 17(2–3), 208–218.
- Mitropoulou, C., Lagaros, N. D., & Papadrakakis, M. (2010). Building design based on energy dissipation: A critical assessment. *Bulletin of Earthquake Engineering*, 8(6), 1375–1396. doi:10.1007/s10518-010-9182-x
- Moehle, J. P., & Mahin, S. A. (1991). Observations on the behavior of reinforced concrete buildings during earthquakes. American Concrete Institute SP-127. In Ghosh, S. K. (Ed.), *Earthquake-resistant concrete structures – Inelastic response and design*.
- Moharrami, H. (1993). *Design optimization of reinforced concrete frameworks*. Ph.D. Thesis, The University of Waterloo, Waterloo, Ontario, Canada
- Moharrami, H. (2006). *Optimality criteria: A robust nonlinear optimization algorithm*. The 7th International Congress on Civil Engineering, Tarbiat Modares University, Tehran, Iran.
- Moharrami, H., & Alavinashab, A. (2006). An optimization procedure for automated design of seismic resistant steel frames. *International Journal of Civil Engineering*, 4(2), 86–105.
- Moharrami, H., & Grierson, D. E. (1993). Computer-automated design of reinforced concrete frameworks. *Journal of Structural Engineering*, 119(7), 2036–2058. doi:10.1061/(ASCE)0733-9445(1993)119:7(2036)
- Mokkadem, A. (1989). Estimation of the entropy and information for absolutely continuous random variables. *IEEE Transactions on Information Theory*, 35, 193–196. doi:10.1109/18.42194
- Möller, O. (2001). *Metodología para evaluación de la probabilidad de falla de estructuras sismorresistentes y calibración de códigos*. Tesis de Doctorado en Ingeniería, Universidad Nacional de Rosario.
- Möller, O., & Foschi, R. (2003). Reliability evaluation in seismic design: A response surface methodology. *Earthquake Spectra*, 19(3), 579–603. doi:10.1193/1.1598200
- Möller, O., Foschi, R., Quiroz, L., & Rubinstein, M. (2008). Optimización de pórticos con acciones sísmicas: diferentes estrategias numéricas utilizando redes neuronales. [AMCA]. *Mecánica Computacional*, 28, 2583–2603.

- Möller, O., Foschi, R., Quiroz, L., & Rubinstein, M. (2009a). Performance-based seismic optimization implementing neural networks. In Frangopol, D. M. (Ed.), *Computational structural dynamics and earthquake engineering, structures and infrastructures series (Vol. II, pp. 547–564)*. Taylor & Francis Group.
- Möller, O., Foschi, R., Quiroz, L., & Rubinstein, M. (2009c). Structural optimization for performance-based design in earthquake engineering: Applications of neural networks. *Structural Safety*, 31(6), 490–499. doi:10.1016/j.strusafe.2009.06.007
- Möller, O., Foschi, R., Rubinstein, M., & Quiroz, L. (2006). Momento-curvatura de secciones de hormigón armado sismorresistentes utilizando redes neuronales. [AMCA.]. *Mecánica Computacional*, 25, 2145–2162.
- Möller, O., Foschi, R., Rubinstein, M., & Quiroz, L. (2007). Optimización de pórticos sismorresistentes utilizando redes neuronales y algoritmo sin cálculo de gradientes. [AMCA.]. *Mecánica Computacional*, 26, 1824–1839.
- Möller, O., Foschi, R., Rubinstein, M., & Quiroz, L. (2009b). Seismic structural reliability using different nonlinear dynamic response surface approximations. *Structural Safety*, 31(5), 432–442. doi:10.1016/j.strusafe.2008.12.001
- Moon, F. L., & Aktan, A. E. (2006). Impacts of epistemic (bias) uncertainty on structural identification of constructed (civil) systems. *The Shock and Vibration Digest*, 38, 399–420. doi:10.1177/0583102406068068
- Moore, R. E. (1979). *Methods and applications of interval analysis*. Philadelphia, PA: SIAM Bookmart, PA.
- Morinaga, S. (1996). *Remaining life of reinforced concrete structures after corrosion cracking. Durability of Building Material and Components* (pp. 127–136). London, UK: E & FN Spon.
- Mosterman, P. J., & Biswas, G. (1999). Diagnosis of continuous valued systems in transient operating regions. *IEEE Transactions, Man, and Cybernetics-Part A*, 29(6), 554–565. doi:10.1109/3468.798059
- Moustafa, A. (2002). *Deterministic/reliability-based critical earthquake load models for linear/nonlinear engineering structures*. Doctoral dissertation, Department of Civil Engineering, Indian Institute of Science, Bangalore, India.
- Moustafa, A., Takewaki, I., & Wijeyewickrema, A. K. (2010). Selection of earthquake records for time-history analysis of structures. Joint 7th International Conference on Urban Earthquake Engineering and 5th International Conference on Earthquake Engineering, 3-5 March, Tokyo, Japan.
- Moustafa, A. (2009). Critical earthquake load inputs for multi-degree-of-freedom inelastic structures. *Journal of Sound and Vibration*, 325, 532–544. doi:10.1016/j.jsv.2009.03.022
- Moustafa, A. (2009). Discussion of a new approach of selecting real input ground motions for seismic design: The most unfavourable real seismic design ground motions. *Earthquake Engineering & Structural Dynamics*, 38, 1143–1149. doi:10.1002/eqe.885
- Moustafa, A. (2010). Closure to discussion of critical earthquake load inputs for multi-degree-of-freedom inelastic structures. *Journal of Sound and Vibration*, 330, 356–360. doi:10.1016/j.jsv.2010.09.002
- Moustafa, A. (2010). Discussion of analytical model of ground motion pulses for the design and assessment of seismic protective systems. *Journal of Structural Engineering*, 137(1), 229–230. doi:10.1061/(ASCE) ST.1943-541X.134
- Moustafa, A. (2010). Identification of resonant earthquake ground motion. *Indian Academy of Sciences*, 35(3), 355–371.
- Moustafa, A. (2011). Damage-based design earthquake loads for SDOF inelastic structures. *Journal of Structural Engineering*, 137(3), 456–467. doi:10.1061/(ASCE) ST.1943-541X.0000074
- Moustafa, A., & Mahadevan, S. (2010). Probabilistic critical earthquake excitations using earthquake response spectra. [Building and Housing]. *Asian Journal of Civil Engineering*, 11(3), 295–319.

Compilation of References

- Moustafa, A., Mahadevan, S., Daigle, M., & Biswas, D. (2010). Structural and sensor system damage identification using the bond graph approach. *Structural Control and Health Monitoring*, 17, 178–197. doi:10.1002/stc.285
- Moustafa, A., & Takewaki, I. (2010). Characterization and modeling of near-fault pulse-like strong ground motion via damage-based critical excitation method. *Structural Engineering & Mechanics*, 34(6), 755–778.
- Moustafa, A., & Takewaki, I. (2010). Deterministic and probabilistic representation of near-field pulse-like ground motion. *Soil Dynamics and Earthquake Engineering*, 30, 412–422. doi:10.1016/j.soildyn.2009.12.013
- Moustafa, A., & Takewaki, I. (2010). Modeling critical strong ground motion sequences on inelastic structures. *Advances in Structural Engineering*, 13(4), 665–679. doi:10.1260/1369-4332.13.4.665
- Moustafa, A., & Takewaki, I. (2011). Response of nonlinear SDOF structures to random acceleration sequences. *Engineering Structures*, 33(4), 1251–1258. doi:10.1016/j.engstruct.2011.01.002
- Moustafa, A., Ueno, K., & Takewaki, I. (2010). Critical earthquake loads for SDOF inelastic structures considering evolution of seismic waves. *Earthquakes and Structures*, 1(2), 147–162.
- Muthukumar, S., & DesRoches, R. (2006). A Hertz contact model with non-linear damping for pounding simulation. *Earthquake Engineering & Structural Dynamics*, 35, 811–828. doi:10.1002/eqe.557
- Myers, R. H., & Montogmery, D. C. (1995). *Response surface methodology: Process and product optimization using designed experiments*. USA: John Wiley and Sons.
- Nakashima, M., Saburi, K., & Tsuji, B. (1996). Energy input and dissipation behavior of structures with hysteretic dampers. *Earthquake Engineering & Structural Dynamics*, 25, 483–496. doi:10.1002/(SICI)1096-9845(199605)25:5<483::AID-EQE564>3.0.CO;2-K
- National Standard of the People's Republic of China. (2001). *Chinese code for seismic design buildings (GB50011-2001)*. Beijing, China: New World Press.
- Newmark, N. M., & Hall, W. J. (1982). *Earthquake spectra and design. Monograph, Earthquake Engineering Research Institute*. EERI.
- Nigam, N. C. (1972). Structural optimization in random vibration environment. *AIAA Journal*, 10(4), 551–553. doi:10.2514/3.50151
- Oh, S. H., Kimb, Y. J., & Ryu, H. S. (2009). Seismic performance of steel structures with slit dampers. *Engineering Structures*, 31(9), 1997–2008. doi:10.1016/j.engstruct.2009.03.003
- Ohsaki, M., Kinoshita, T., & Pan, P. (2007). Multiobjective heuristic approaches to seismic design of steel frames with standard sections. *Earthquake Engineering & Structural Dynamics*, 36(11), 1481–1495. doi:10.1002/eqe.690
- Olhoff, N., & Du, J. (2005). Topological design of structures subjected to forced vibration. In J. Herskovits (Ed.), *Proceedings of the 6th World Congress of Structural and Multidisciplinary Optimization*, Rio de Janeiro, Brazil, 30 May–03 June.
- Olhoff, N., & Rasmussen, S. H. (1977). On single and bimodal optimum buckling loads of clamped columns. *International Journal of Solids and Structures*, 13(7), 605–614. doi:10.1016/0020-7683(77)90043-9
- OpenSees Development Team. (2009). *OpenSees: Open system for earthquake engineering simulation*. Berkeley, CA, USA.
- Otani, S. (1981). Hysteretic models of reinforced concrete for earthquake response analysis. *Journal of the Faculty of Engineering, University of Tokyo*, 36(2), 407–441.
- Overton, M. L. (1992). Large-scale optimization of eigenvalues. *SIAM Journal on Optimization*, 2(1), 88–120. doi:10.1137/0802007
- Owen, D. R. J., & Hinton, E. (1980). *Finite elements in plasticity- Theory and practice*. Swansea, UK: Pineridge Press.
- Pacific Earthquake Research (PEER) Center. (2011). Retrieved from http://peer.berkeley.edu/peer_ground_motion_database
- Papadrakakis, M., Charmpis, D. C., Lagaros, N. D., & Tsompanakis, Y. (Eds.). (2009). *Computational structural dynamics and earthquake engineering*. London, UK: Taylor & Francis.

- Papadrakakis, M., & Lagaros, N. (2002). Reliability-based structural optimization using neural networks and Monte Carlo simulation. *Computer Methods in Applied Mechanics and Engineering*, 191, 3491–3507. doi:10.1016/S0045-7825(02)00287-6
- Papadrakakis, M., Lagaros, N. D., & Plevris, V. (2005). Design optimization of steel structures considering uncertainties. *Engineering Structures*, 27(9), 1408–1418. doi:10.1016/j.engstruct.2005.04.002
- Park, Y. J., Reinhorn, A. M., & Kunnath, S. K. (1987). *IDARC: Inelastic damage analysis of frame shear-wall structures*. Technical Report NCEER-87-0008, National Center for Earthquake Engineering Research, State University of New York at Buffalo.
- Park, G. J., & Kang, B. S. (2003). Validation of a structural optimization algorithm transforming dynamic loads into equivalent static loads. *Journal of Optimization Theory and Applications*, 118(1), 191–200. doi:10.1023/A:1024799727258
- Park, G. J., Lee, T. H., Lee, K., & Hwang, K. H. (2006). Robust design: An overview. *AIAA Journal*, 44(1), 181–191. doi:10.2514/1.13639
- Park, K. J., Lee, J. N., & Park, G. J. (2005). Structural shape optimization using equivalent static loads transformed from dynamic loads. *International Journal for Numerical Methods in Engineering*, 63(4), 589–602. doi:10.1002/nme.1295
- Park, Y. J., & Ang, A. H. S. (1985). Mechanistic seismic damage model for reinforced concrete. *Journal of Structural Engineering*, 111(4), 722–739. doi:10.1061/(ASCE)0733-9445(1985)111:4(722)
- Park, Y. J., Ang, A. H. S., & Wen, Y. K. (1985). Seismic damage analysis of reinforced concrete buildings. *Journal of Structural Engineering*, 111(4), 740–757. doi:10.1061/(ASCE)0733-9445(1985)111:4(740)
- Park, Y. J., & Ang, A. H.-S. (1985). Mechanistic seismic damage model for reinforced concrete. *Journal of Structural Engineering*, 111(4), 722–739. doi:10.1061/(ASCE)0733-9445(1985)111:4(722)
- Park, Y. J., Ang, A. H.-S., & Wen, Y. K. (1985). Seismic damage analysis of reinforced concrete buildings. *Journal of Structural Engineering*, 111(4), 740–757. doi:10.1061/(ASCE)0733-9445(1985)111:4(740)
- Park, Y. J., Ang, A. H.-S., & Wen, Y. K. (1987). Damage-limiting aseismic design of buildings. *Earthquake Spectra*, 3(1), 1–26. doi:10.1193/1.1585416
- Paulay, T., & Priestley, M. J. N. (1992). *Seismic design of reinforced concrete and masonry buildings*. John Wiley & Sons, Inc. doi:10.1002/9780470172841
- Paynter, H. M. (1961). *Analysis and design of engineering systems*. MIT Press.
- Pecker, A. (Ed.). (2007). *Advanced earthquake engineering analysis*. Udine, Italy: Springer. doi:10.1007/978-3-211-74214-3
- Pedersen, N. L. (2000). Maximization of eigenvalues using topology optimization. *Structural and Multidisciplinary Optimization*, 20(1), 2–11. doi:10.1007/s001580050130
- Pedrycz, W. (1984). An identification algorithm in fuzzy relational systems. *Fuzzy Sets and Systems*, 13, 153–167. doi:10.1016/0165-0114(84)90015-0
- PEER. (2005). *Pacific Earthquake Engineering Research (PEER) center: NGA database*. Retrieved January 1, 2009, from <http://peer.berkeley.edu/nga/>
- Peizhuangm, W., Xihui, L., & Sanchez, E. (1986). Set-valued statistics and its application to earthquake engineering. *Fuzzy Sets and Systems*, 18(3), 347–356. doi:10.1016/0165-0114(86)90011-4
- Penelis, G. G., & Kappos, A. J. (1997). *Earthquake-resistant concrete structures*. London, UK: E & FN SPON.
- Pérez López, J. R. (2005). *Contribución a los métodos de optimización basados en procesos naturales y su aplicación a la medida de antenas en campo próximo*. Retrieved from <http://www.tesisenred.net/TDR-0305107-180847>
- Perez, R. E., & Behdinan, K. (2007). Particle swarm approach for structural design optimization. *Computers & Structures*, 85, 1579–1588. doi:10.1016/j.compstruc.2006.10.013

Compilation of References

- Perros, K., & Papadimitriou, C. (2009). *Reliability analysis of bridge models with elastomeric bearings and seismic stoppers under stochastic earthquake excitations*. Paper presented at the 2009 ECCOMAS Thematic Conference on Computational Methods in Structural Dynamics and Earthquake Engineering.
- Pezeshk, S. (1998). Design of framed structures: An integrated non-linear analysis and optimal minimum weight design. *International Journal for Numerical Methods in Engineering*, 41(3), 459–471. doi:10.1002/(SICI)1097-0207(19980215)41:3<459::AID-NME293>3.0.CO;2-D
- Philippacopoulos, A. J., & Wang, P. C. (1984). Seismic inputs for nonlinear structures. *Journal of Engineering Mechanics*, 110, 828–836. doi:10.1061/(ASCE)0733-9399(1984)110:5(828)
- Pinho, R. (2007). Non linear dynamic analysis of structures subjected to seismic action. In Pecker, A. (Ed.), *Advanced earthquake engineering analysis*. New York, NY: Springer Wien. doi:10.1007/978-3-211-74214-3_5
- Plevris, V. (2009). *Innovative computational techniques for the optimum structural design considering uncertainties*. Ph. D. dissertation, Institute of Structural Analysis and Seismic Research, National Technical University of Athens, June 2009.
- Plevris, V., Karlaftis, M. G., & Lagaros, N. D. (2010). A swarm intelligence approach for emergency infrastructure inspection scheduling. In Gopalakrishnan, K., & Peeta, S. (Eds.), *Sustainable and resilient critical infrastructure systems: Simulation, modeling, and intelligent engineering*. Springer. doi:10.1007/978-3-642-11405-2_8
- Pourzeynali, S., Lavasani, H. H., & Modarayi, A. H. (2007). Active control of high rise building structures using fuzzy logic and genetic algorithms. *Engineering Structures*, 29, 346–357. doi:10.1016/j.engstruct.2006.04.015
- Pradlwarter, H. J., & Schuëller, G. I. (1993). Equivalent linearization - A suitable tool for analyzing MDOF-systems. *Probabilistic Engineering Mechanics*, 8(2), 115–126. doi:10.1016/0266-8920(93)90005-G
- Prager, W. (1969). *Optimality criteria derived from classical extremum principles. Technical report, SM Studies Series*. Ontario, Canada: Solid Mechanics Division, University of Waterloo.
- Prager, W. (1974). A note on discretized Michell structures. *Computer Methods in Applied Mechanics and Engineering*, 3(3), 349–355. doi:10.1016/0045-7825(74)90019-X
- Prasad, B. (1983). Approximation, adaptation and automation concepts for large scale structural optimization. *Engineering Optimization*, 6(3), 129–140. doi:10.1080/03052158308902462
- Priestely, M. J. N., Calvi, G. M., & Kowalsky, M. J. (2007). *Displacement-based seismic design of structures*. Pavia, Italy: IUSS Press.
- Priestley, M. J. N., Seible, F., & Calvi, G. M. (1996). *Seismic design and retrofit of bridges*. New York, NY: John Wiley & Sons, Inc. doi:10.1002/9780470172858
- Priestley, M. J. N., Seible, F., & Calvi, G. M. (1996). *Seismic design and retrofit of bridges*. USA: John Wiley and Sons Inc. doi:10.1002/9780470172858
- Quek, S. T., Teo, Y. P., & Balendra, T. (1990). Non-stationary structural response with evolutionary spectra using seismological input model. *Earthquake Engineering & Structural Dynamics*, 19, 275–288. doi:10.1002/eqe.4290190210
- Querin, O. M. (1997). *Evolutionary structural optimisation stress based formulation and implementation*. Unpublished Doctoral dissertation, Department of Aeronautical Engineering, University of Sydney, Sydney, Australia.
- Querin, O. M., Steven, G. P., & Xie, Y. M. (1998). Evolutionary structural optimisation (ESO) using a bidirectional algorithm. *Engineering Computations*, 15(8), 1031–1048. doi:10.1108/02644409810244129
- Rajasekaran, S. (2001). Optimization of large scale three dimensional reticulated structures using cellular genetics and neural networks. *International Journal of Space Structures*, 16(4), 315–324. doi:10.1260/026635101760832244

- Ramallo, J. C., Yoshioka, H., & Spencer, B. F. Jr. (2004). A two-step identification technique for semiactive control systems. *Structural Control and Health Monitoring*, 11, 273–289. doi:10.1002/stc.43
- Ramesh, K., Seshu, D. R., & Prabhakar, M. (2003). Constitutive behaviour of confined fibre reinforced concrete under axial compression. *Cement and Concrete Composites*, 25, 343–350. doi:10.1016/S0958-9465(02)00051-3
- Reiter, L. (1990). *Earthquake hazard analysis*. New York, NY: Columbia University Press.
- Rezaeian, S., & Der Kiureghian, A. (2008). A stochastic ground motion model with separable temporal and spectral nonstationarities. *Earthquake Engineering & Structural Dynamics*, 37, 1565–1584. doi:10.1002/eqe.831
- Riddell, F. (1995). Inelastic design spectra accounting for soil conditions. *Earthquake Engineering & Structural Dynamics*, 24, 1491–1510. doi:10.1002/eqe.4290241106
- Robert, C. P., & Casella, G. (2004). *Monte Carlo statistical methods* (2nd ed.). New York, NY: Springer.
- Rodriguez, J., & Ortega, L. M. (1994). *Assessment of structural elements with corroded reinforcement*. *Corrosion and Corrosion Protection in Concrete*. Sheffield, UK: Sheffield Academic press.
- Rosenberg, R. C., & Karnopp, D. C. (1983). *Introduction to physical system dynamics*. McGraw-Hill.
- Rosset, J. O., & Polak, E. (2004). Reliability-based optimal design using sample average approximations. *Probabilistic Engineering Mechanics*, 19, 331–343. doi:10.1016/j.probengmech.2004.03.001
- Rozvany, G. I. N. (1972a). Grillages of maximum strength and maximum stiffness. *International Journal of Mechanical Sciences*, 14(10), 651–666. doi:10.1016/0020-7403(72)90023-9
- Rozvany, G. I. N. (1972b). Optimal load transmission by structure. *Computer Methods in Applied Mechanics and Engineering*, 1(3), 253–263. doi:10.1016/0045-7825(72)90007-2
- Rozvany, G. I. N., Zhou, M., & Birker, T. (1992). Generalized shape optimization without homogenization. *Structural Optimization*, 4(3–4), 250–252. doi:10.1007/BF01742754
- Ruangrassamee, A., & Kawashima, K. (2003). Control of nonlinear bridge response with pounding effect by variable dampers. *Engineering Structures*, 25(5), 593–606. doi:10.1016/S0141-0296(02)00169-4
- Rubinstein, M., Giuliano, A., & Möller, O. (2006). Diseño preliminar de estructuras sismorresistentes: un tratamiento unificado de los efectos traslacionales y rotacionales. *Memorias XIX Jornadas Argentinas de Ingeniería Estructural*, 49.
- Ruszczynski, A., & Shapiro, A. (2003). *Stochastic programming*. New York, NY: Elsevier.
- Saadeghvaziri, M. A., & Yazdani-Motlagh, A. R. (2008). Seismic behavior and capacity/demand analyses of three multi-span simply supported bridges. *Engineering Structures*, 30(1), 54–66. doi:10.1016/j.engstruct.2007.02.017
- Saetta, A. V., Schrefler, B. A., & Vitaliani, R. V. (1993). The carbonation of the concrete and the mechanism of moisture, heat and carbon dioxide flow through porous material. *Journal of Cement and Concrete Research*, 23(4), 761–772. doi:10.1016/0008-8846(93)90030-D
- Sahab, M. G., Ashour, A. F., & Toropov, V. V. (2005). Cost optimisation of reinforced concrete flat slab buildings. *Engineering Structures*, 27(3), 313–322. doi:10.1016/j.engstruct.2004.10.002
- Saikat, S., & Manohar, C. S. (2005). Inverse reliability based structural design for system dependent critical earthquake loads. *Probabilistic Engineering Mechanics*, 20, 19–31. doi:10.1016/j.probengmech.2004.03.006
- Saka, M. P. (1997). The theorems of structural variation for grillage systems. In Topping, B. H. V., & Leeming, M. B. (Eds.), *Innovation in computer methods for civil and structural engineering* (pp. 101–111). Edinburgh, UK: Civil Comp Press. doi:10.4203/ccp.50.8.2
- Salajegheh, E., & Heidari, A. (2005). Optimum design of structures against earthquake by wavelet neural network and filter banks. *Earthquake Engineering & Structural Dynamics*, 34(1), 67–82. doi:10.1002/eqe.417

Compilation of References

- Sankararaman, S., & Mahadevan, S. (2011). (in press). Uncertainty quantification in structural damage diagnosis. *Structural Control and Health Monitoring*. doi:10.1002/stc.400
- Saragoni, G., & Hart, G. (1974). Simulation of artificial earthquakes. *Earthquake Engineering & Structural Dynamics*, 2(3), 249–267. doi:10.1002/eqe.4290020305
- Sarkar, A. (2003). Linear stochastic dynamical system under uncertain load: Inverse reliability analysis. *Journal of Engineering Mechanics*, 129(6), 665–671. doi:10.1061/(ASCE)0733-9399(2003)129:6(665)
- Scharage, L. (1989). *Optimization modeling with LINGO*. Technical report, LINDO Systems inc., Chicago.
- Schuëller, G., & Jensen, H. (2008). Computational methods in optimization considering uncertainties- An overview. *Computer Methods in Applied Mechanics and Engineering*, 198(1), 2–13. doi:10.1016/j.cma.2008.05.004
- Schurter, K. C., & Roschke, P. N. (2001). Neuro-fuzzy control of structures using magnetorheological dampers. *Proceedings of the American Control Conference*, Arlington, Virginia, (pp. 1097-1102).
- SEAOC. (1995). *Vision 2000, performance based seismic engineering of buildings (Vol. I and II)*. Sacramento, CA: Structural Engineers Association of California.
- SEAOC. Vision Committee. (2002). *Performance based seismic design engineering*. Sacramento, CA: Structural Engineers Association of California (SEAOC) Report.
- Seyranian, A. P., Lund, E., & Olhoff, N. (1994). Multiple eigenvalues in structural optimization problems. *Structural and Multidisciplinary Optimization*, 8(4), 207–227.
- Sharifi, R., Kim, Y., & Langari, R. (2010). Sensor fault isolation and detection of smart structures. *Smart Materials and Structures*, 19, 1–15. doi:10.1088/0964-1726/19/10/105001
- Shen, J., Tsai, M.-H., Chang, K.-C., & Lee, G. C. (2004). Performance of a seismically isolated bridge under near-fault earthquake ground motions. *Journal of Structural Engineering*, 130(6), 861–868. doi:10.1061/(ASCE)0733-9445(2004)130:6(861)
- Shi, Y., & Eberhart, R. (1998). A modified particle swarm optimizer. *IEEE World Congress on Computational Intelligence*, Anchorage, AK, USA, (pp. 69-73).
- Shinozuka, M. (1970). Maximum structural response to seismic excitations. *Journal of Engineering Mechanics*, 96, 729–738.
- Shinozuka, M., Deodatis, G., Zhang, R. C., & Papageorgiou, A. S. (1999). Modeling, synthetics and engineering applications of strong earthquake wave motion. *Soil Dynamics and Earthquake Engineering*, 18(3), 209–228. doi:10.1016/S0267-7261(98)00045-1
- Shinozuka, M., Feng, M. Q., Kim, H.-K., & Kim, S.-H. (2000b). Nonlinear static procedure for fragility curve development. *Journal of Engineering Mechanics*, 126(12), 1287–1296. doi:10.1061/(ASCE)0733-9399(2000)126:12(1287)
- Shinozuka, M., Feng, M. Q., Lee, J., & Naanuma, T. (2000a). Statistical analysis of fragility curves. *Journal of Engineering Mechanics*, 126(12), 1224–1231. doi:10.1061/(ASCE)0733-9399(2000)126:12(1224)
- Shinozuka, M., & Henry, L. (1965). Random vibration of a beam column. *Journal of Engineering Mechanics*, 91, 123–143.
- Shinozuka, M., & Sato, Y. (1967). Simulation of non-stationary random processes. *Journal of Engineering Mechanics*, 93(1), 11–40.
- Shook, D. A., Roschke, P. N., Lin, P. Y., & Loh, C. H. (2008). GA-optimized fuzzy logic control of a large-scale building for seismic loads. *Engineering Structures*, 30, 436–449. doi:10.1016/j.engstruct.2007.04.008
- Sigmund, O., & Petersson, J. (1998). Numerical instabilities in topology optimization: A survey on procedures dealing with checkerboards, mesh dependencies and local minima. *Structural and Multidisciplinary Optimization*, 16(1), 68–75.
- Smith, A. H., & Chase, J. G. (1993). Identification of structural system parameters using the cascade-correlation neural network. *Journal of Dynamic Systems, Measurement, and Control*, 116, 790–792. doi:10.1115/1.2899280

- Somerville, P., Smith, N., Punyamurthula, S., & Sun, J. (1997). *Development of ground motion time histories for Phase 2 of the FEMA/SAC steel project*. SAC joint venture, California, USA. U.S. Geological Survey. (USGS). Retrieved from www.usgs.gov
- Son, Y. K., & Savage, G. J. (2007). Optimal probabilistic design of the dynamic performance of a vibration absorber. *Journal of Sound and Vibration*, 307(1-2), 20–37. doi:10.1016/j.jsv.2007.06.032
- Soong, T. T., & Spencer, B. F. Jr. (2002). Supplemental energy dissipation: State-of-the-art and state-of-the-practice. *Engineering Structures*, 24(3), 243–259. doi:10.1016/S0141-0296(01)00092-X
- Spall, J. C. (1998). Implementation of the simultaneous perturbation algorithm for stochastic optimization. *IEEE Transactions on Aerospace and Electronic Systems*, 34, 817–823. doi:10.1109/7.705889
- Spall, J. C. (2003). *Introduction to stochastic search and optimization*. New York, NY: Wiley-Interscience. doi:10.1002/0471722138
- Specht, D. F. (1990). Probabilistic neural networks. *Neural Networks*, 3(1), 109–118. doi:10.1016/0893-6080(90)90049-Q
- Spencer, B. F. Jr, Dyke, S. J., Sain, M. K., & Carlson, J. D. (1997). Phenomenological model for magnetorheological dampers. *Journal of Engineering Mechanics*, 123, 230–238. doi:10.1061/(ASCE)0733-9399(1997)123:3(230)
- Strasser, F. O., & Bommer, J. J. (2009). Review: Strong ground motions – Have we seen the worst? *Bulletin of the Seismological Society of America*, 99(5), 2613–2637. doi:10.1785/0120080300
- Subramaniam, R. S., Reinhorn, A. M., Riley, M. A., & Nagarajaiah, S. (1996). Hybrid control of structures using fuzzy logic. *Microcomputers in Civil Engineering*, 11, 1–17. doi:10.1111/j.1467-8667.1996.tb00305.x
- Svanberg, K. (1987). The method of moving asymptotes—A new method for structural optimization. *International Journal for Numerical Methods in Engineering*, 24(2), 359–373. doi:10.1002/nme.1620240207
- Svanberg, K. (2002). A class of globally convergent optimization methods based on conservative convex separable approximations. *SIAM Journal on Optimization*, 12(2), 555–573. doi:10.1137/S1052623499362822
- Swisher, J. R., Hyden, P. D., Jacobson, S. H., & Schruben, L. W. (2000). A survey of simulation optimization techniques and procedures. In J. A. Joines, R. R. Barton, K. Kang, & P. A. Fishwick (Eds.), *2000 Winter Simulation Conference*.
- Symans, M., & Kelly, S. W. (1999). Fuzzy logic control of bridge structures using intelligent semi-active seismic isolation systems. *Earthquake Engineering & Structural Dynamics*, 28, 37–60. doi:10.1002/(SICI)1096-9845(199901)28:1<37::AID-EQE803>3.0.CO;2-Z
- Taflanidis, A. A. (2009, 22–24 June). *Robust stochastic design of viscous dampers for base isolation applications*. Paper presented at the Computational Methods in Structural Dynamics and Earthquake Engineering, Rhodes, Greece.
- Taflanidis, A. A. (2010). Reliability-based optimal design of linear dynamical systems under stochastic stationary excitation and model. *Engineering Structures*, 32(5), 1446–1458. doi:10.1016/j.engstruct.2010.01.023
- Taflanidis, A. A., & Beck, B. L. (2008). An efficient framework for optimal robust stochastic system design using stochastic simulation. *Computer Methods in Applied Mechanics and Engineering*, 198(1), 88–101. doi:10.1016/j.cma.2008.03.029
- Taflanidis, A. A., & Beck, J. L. (2009a). Life-cycle cost optimal design of passive dissipative devices. *Structural Safety*, 31(6), 508–522. doi:10.1016/j.strsafe.2009.06.010
- Taflanidis, A. A., & Beck, J. L. (2009b). Stochastic subset optimization for reliability optimization and sensitivity analysis in system design. *Computers & Structures*, 87, 318–331. doi:10.1016/j.compstruc.2008.12.015
- Taflanidis, A. A., & Beck, J. L. (2009c). Stochastic subset optimization for reliability optimization and sensitivity analysis in system design. *Computers & Structures*, 87(5-6), 318–331. doi:10.1016/j.compstruc.2008.12.015

Compilation of References

- Taflanidis, A. A., & Beck, J. L. (2010). Reliability-based design using two-stage stochastic optimization with a treatment of model prediction errors. *Journal of Engineering Mechanics*, 136(12), 1460–1473. doi:10.1061/(ASCE)EM.1943-7889.0000189
- Taflanidis, A. A., & Jia, G. (2011). A simulation-based framework for risk assessment and probabilistic sensitivity analysis of base-isolated structures. *Earthquake Engineering & Structural Dynamics*, 40(14). doi:10.1002/eqe.1113
- Taflanidis, A. A., Scruggs, J. T., & Beck, J. L. (2008). Probabilistically robust nonlinear design of control systems for base-isolated structures. *Journal of Structural Control and Health Monitoring*, 15(3), 697–719. doi:10.1002/stc.275
- Tajimi, H. (1960). A statistical method of determining the maximum response of a building during earthquake. In G. W. Housner (Ed.), *Proceedings of the Second World Conference on Earthquake Engineering*, 11–18 July 1960 Tokyo and Kyoto, Japan, (pp. 781–797). Tehran, Iran: University press.
- Takagi, T., & Sugeno, M. (1985). Fuzzy identification of systems and its applications to modeling and control. *IEEE Transactions on Systems, Man, and Cybernetics*, 15, 116–132.
- Takeda, T., Sozen, M. A., & Nielsen, N. (1970). Reinforced concrete response to simulated earthquakes. *Journal of the Structural Division*, 96(ST12), 2557–2573.
- Takewaki, I. (2001). Probabilistic critical excitation for MDOF elastic-plastic structures on compliant ground. *Earthquake Engineering & Structural Dynamics*, 30, 1345–1360. doi:10.1002/eqe.66
- Takewaki, I. (2002). Seismic critical excitation method for robust design: A review. *Journal of Structural Engineering*, 128(5), 665–672. doi:10.1061/(ASCE)0733-9445(2002)128:5(665)
- Takewaki, I. (2002a). Seismic critical excitation method for robust design: A review. *Journal of Structural Engineering*, 128, 665–672. doi:10.1061/(ASCE)0733-9445(2002)128:5(665)
- Takewaki, I. (2002b). Robust building stiffness design for variable critical excitations. *Journal of Structural Engineering*, 128(12), 1565–1574. doi:10.1061/(ASCE)0733-9445(2002)128:12(1565)
- Takewaki, I. (2004). Bound of earthquake input energy. *Journal of Structural Engineering*, 130, 1289–1297. doi:10.1061/(ASCE)0733-9445(2004)130:9(1289)
- Takewaki, I. (2007). *Critical excitation methods in earthquake engineering*. Elsevier Science.
- Takewaki, I. (2009). *Building control with passive dampers*. Singapore: John Wiley & Sons. doi:10.1002/9780470824931
- Takewaki, I., Murakami, S., Fujita, K., Yoshitomi, S., & Tsuji, M. (2011). The 2011 off the Pacific coast of Tohoku earthquake and response of high-rise buildings under long-period ground motions. *Soil Dynamics and Earthquake Engineering*, 31(11), 1511–1528. doi:10.1016/j.soildyn.2011.06.001
- Tamura, H., Yamamoto, K., Tomiyama, S., & Hatono, I. (2000). Modelling and analysis of decision making problem for mitigating natural disaster risks. *European Journal of Operational Research*, 122(2), 461–468. doi:10.1016/S0377-2217(99)00247-7
- Tanaka, K., & Sugeno, M. (1992). Stability analysis and design of fuzzy control systems. *Fuzzy Sets and Systems*, 45, 135–156. doi:10.1016/0165-0114(92)90113-I
- Tangaramvong, S., & Tin Loi, F. (2011). Mathematical programming approaches for the safety assessment of semirigid elastoplastic frames. *International Journal of Solids and Structures*, 48(6), 1011–1023. doi:10.1016/j.ijsolstr.2010.12.003
- Tani, A., Kawamura, H., & Ryu, S. (1998). Intelligent fuzzy optimal control of building structures. *Engineering Structures*, 20, 184–192. doi:10.1016/S0141-0296(97)00077-1
- Tolson, B. A., Maier, H. R., Simpson, A. R., & Lence, B. J. (2004). Genetic algorithms for reliability-based optimization of water distribution systems. *Journal of Water Resources Planning and Management*, 130(1), 63–72. doi:10.1061/(ASCE)0733-9496(2004)130:1(63)

- Tomlin, J. (1970). Integer and non-linear programming. In *Branch and bound methods for integer and non-convex programming* (pp. 437–450). Amsterdam, The Netherlands: North Holland.
- Tsompanakis, Y., Lagaros, N. D., & Papadrakakis, M. (Eds.). (2008). *Structural design optimization considering uncertainties*. London, UK: Taylor & Francis.
- Tsopelas, P., Constantinou, M. C., Okamoto, S., Fujii, S., & Ozaki, D. (1996). Experimental study of bridge seismic sliding isolation systems. *Engineering Structures*, 18(4), 301–310. doi:10.1016/0141-0296(95)00147-6
- Turkington, D. H., Carr, A. J., Cooke, N., & Moss, P. J. (1989). Seismic design of bridges on lead-rubber bearings. *Journal of Structural Engineering*, 115(12), 3000–3016. doi:10.1061/(ASCE)0733-9445(1989)115:12(3000)
- Uang, C.-M., & Bertero, V.V. (1990). Evaluation of seismic energy in structures. *Earthquake Engineering & Structural Dynamics*, 19, 77–90. doi:10.1002/eqe.4290190108
- Uniform Building Code* (1997).
- USGS. (2008). *Documentation for the 2008 update of the United States national seismic hazard maps* (No. Open-File Report 2008-1128). Reston, VA: United States Geological Survey.
- USGS/EERI Advance Reconnaissance Team. (2010). *The Mw 7.0 Haiti earthquake of January 12, 2010*.
- Val, D. V. (2004). *Aspects of corrosion in reinforced concrete structures and its influence on structural safety*. Report No. 2002950, National Building Research Institute.
- Val, D., & Stewart, M. G. (2003). Life-cycle cost analysis of reinforced concrete structures in marine environments. *Journal of Structural Safety*, 25(4), 343–362. doi:10.1016/S0167-4730(03)00014-6
- Valdebenito, M., & Schuëller, G. (2011). Efficient strategies for reliability-based optimization involving non linear, dynamical structures. *Computers & Structures*, 89(19-29), 1797–1811.
- Vanderplaats, G. M. (1997). *DOT user's manual*. Colorado Springs, CO: VMA.
- Vanderplaats, G. N. (1999). *Numerical optimization techniques for engineering design*. USA: VR and D, Inc.
- Vanmarcke, E. H., Shinotsuka, M., Nakagiri, S., Schuëller, G. I., & Grigoriu, M. (1986). Random fields and stochastic finite elements. *Structural Safety*, 3(3), 143–166. doi:10.1016/0167-4730(86)90002-0
- Vidal, T., Catel, A., & Francois, R. (2004). Analyzing crack width to predict corrosion in reinforced concrete. *Cement and Concrete Research*, 34(1), 165–174. doi:10.1016/S0008-8846(03)00246-1
- Vision, S. E. A. O. C. (2000). *Committee. (1995). Performance based seismic engineering of buildings, part 2: Conceptual framework*. Sacramento, CA: Structural Engineers Association of California.
- Von Neumann, J. (1966). *Theory of self-reproducing automata* (Burks, A. W., Ed.). University of Illinois Press.
- Walther, R., Houriet, B., Isler, W., Moia, P., & Klein, J. (1988). *Cable stayed bridges*. London, UK: Thomas Telford, Ltd.
- Wang, L., & Langari, R. (1995). Decomposition approach for fuzzy systems identification. *Proceedings of the 34th IEEE Conference on Decision and Control*, New Orleans, LA, USA, (pp. 261–265).
- Wang, A. P., & Lee, C. D. (2002). Fuzzy sliding mode control for a building structure based on genetic algorithms. *Earthquake Engineering & Structural Dynamics*, 31, 881–895. doi:10.1002/eqe.127
- Wang, L., & Langari, R. (1996). Complex systems modeling via fuzzy logic. *IEEE Transactions on Systems, Man, and Cybernetics. Part B, Cybernetics*, 26, 100–106. doi:10.1109/3477.484441
- Wang, Q., Fang, H., & Zou, X. K. (2010). Application of micro-GA for optimal cost base isolation design of bridges subject to transient earthquake loads. *Structural and Multidisciplinary Optimization*, 36(5), 493–507.
- Wang, W. M., Peng, Y. H., Hu, J., & Cao, Z. M. (2009). Collaborative robust optimization under uncertainty based on generalized dynamic constraints network. *Structural and Multidisciplinary Optimization*, 38(2), 159–170. doi:10.1007/s00158-008-0271-2

Compilation of References

- Ward, J. H. Jr. (1963). Hierarchical grouping to optimize an objective function. *Journal of the American Statistical Association*, 58, 236–244. doi:10.2307/2282967
- Wen, Y. K., & Kang, Y. J. (1997). Optimal seismic design based on life-cycle cost. *Proceedings of the International Workshop on Optimal Performance of Civil Infrastructure Systems 1997*, (pp. 194-210). New York, NY: ASCE.
- Wen, Y. K., Ellingwood, B. R., & Bracci, J. M. (2004). *Vulnerability function framework for consequence-based engineering* (No. Project DS-4 Report). Urbana, IL: Mid-America Earthquake (MAE) Center.
- Wen, Y. K., & Kang, Y. J. (2001). Minimum building life-cycle cost design criteria. I: Methodology. *Journal of Structural Engineering*, 127(3), 330–337. doi:10.1061/(ASCE)0733-9445(2001)127:3(330)
- Wen, Y. K., & Kang, Y. J. (2001a). Minimum building life-cycle cost design criteria, I: Methodology. *Journal of Structural Engineering*, 127(3), 330–337. doi:10.1061/(ASCE)0733-9445(2001)127:3(330)
- Wen, Y. K., & Kang, Y. J. (2001b). Minimum building life-cycle cost design criteria, II: Applications. *Journal of Structural Engineering*, 127(3), 338–346. doi:10.1061/(ASCE)0733-9445(2001)127:3(338)
- Werner, G. (1960). *Impact: The theory and physical behaviour of colliding solids*. London, UK: Edward Arnold.
- Westermo, B. D. (1985). The critical excitation and response of simple dynamic systems. *Journal of Sound and Vibration*, 100, 233–242. doi:10.1016/0022-460X(85)90417-1
- Wong, K. K. F., & Yong, R. (2002). Earthquake response and energy evaluation of inelastic structures. *Journal of Engineering Mechanics*, 128(3), 308–317. doi:10.1061/(ASCE)0733-9399(2002)128:3(308)
- Xie, Y. M., & Steven, G. P. (1993). A simple evolutionary procedure for structural optimization. *Computers & Structures*, 49(5), 885–896. doi:10.1016/0045-7949(93)90035-C
- Xie, Y. M., & Steven, G. P. (1996). Evolutionary structural optimization for dynamic problems. *Computers & Structures*, 58(6), 1067–1073. doi:10.1016/0045-7949(95)00235-9
- Xi, Y., & Bazant, Z. P. (1999). Modeling chloride penetration in saturated concrete. *Journal of Materials in Civil Engineering*, 11(1), 58–65. doi:10.1061/(ASCE)0899-1561(1999)11:1(58)
- Xu, L., Gong, Y., & Grierson, D. E. (2006). Seismic design optimization of steel building frameworks. *Journal of Structural Engineering*, 132(2), 277–286. doi:10.1061/(ASCE)0733-9445(2006)132:2(277)
- Yager, R. R., & Filev, D. P. (1993). Unified structure and parameter identification of fuzzy models. *IEEE Transactions on Systems, Man, and Cybernetics*, 23, 1198–1205. doi:10.1109/21.247902
- Yamaguchi, H., & El-Abd, A. (2003). Effect of energy input characteristics on hysteretic damper efficiency. *Earthquake Engineering & Structural Dynamics*, 32, 827–843. doi:10.1002/eqe.250
- Yan, D., & Yuan, W. (2004). Conceptual seismic design for long span cable-stayed bridges. *Journal of Tongji University*, 32(10), 1344–1348.
- Yang, C. S., DesRoches, R., & Padgett, J. E. (2009). Fragility curves for a typical California box girder bridge. *Proceedings of the 2009 ASCE Technical Council on Lifeline Earthquake Engineering Conference*, San Francisco, California, USA.
- Yang, Y. (1999). *Seismic resistance of bridge and fractal characteristics*. Master's thesis, Tongji University, Shanghai, China.
- Yan, G., & Zhou, L. L. (2006). Integrated fuzzy logic and genetic algorithms for multi-objective control of structures using MR dampers. *Journal of Sound and Vibration*, 296, 368–382. doi:10.1016/j.jsv.2006.03.011
- Yang, G., Spencer, B. F. Jr, Carlson, J. D., & Sain, M. K. (2002). Large-scale MR fluid dampers: Modeling and dynamic performance considerations. *Engineering Structures*, 24, 309–323. doi:10.1016/S0141-0296(01)00097-9
- Yang, X. Y., Xie, Y. M., Steven, G. P., & Querin, O. M. (1999a). Bidirectional evolutionary method for stiffness optimization. *American Institute of Aeronautics and Astronautics Journal*, 37(11), 1483–1488.

- Yang, X. Y., Xie, Y. M., Steven, G. P., & Querin, O. M. (1999b). Topology optimization for frequencies using an evolutionary method. *Journal of Structural Engineering*, 125(12), 1432–1438. doi:10.1061/(ASCE)0733-9445(1999)125:12(1432)
- Yang, Y. N., & Lin, S. (2004). On-line identification of non-linear hysteretic structures using an adaptive tracking technique. *International Journal of Non-linear Mechanics*, 39, 1481–1491. doi:10.1016/j.ijnonlinmec.2004.02.010
- Yang, Y. N., & Lin, S. (2005). Identification of parametric variations of structures based on least squares estimation and adaptive tracking technique. *Journal of Engineering Mechanics*, 131, 290–298. doi:10.1061/(ASCE)0733-9399(2005)131:3(290)
- Yan, L., & Byrne, P. M. (1992). Lateral pile response to monotonic loads. *Canadian Geotechnical Journal*, 29, 955–970. doi:10.1139/t92-106
- Ye, A., Hu, S., & Fan, L. (2004). Seismic displacement control for super-long-span cable-stayed bridges. *China Civil Engineering Journal*, 37(12), 38–43.
- Yen, J., & Langari, R. (1998). *Fuzzy logic-intelligence, control, and information*. Upper Saddle River, NJ: Prentice Hall.
- Yi, F., Dyke, S. J., Caicedo, J. M., & Carlson, J. D. (2001). Experimental verification of multinput seismic control strategies for smart dampers. *Journal of Engineering Mechanics*, 127, 1152–1164. doi:10.1061/(ASCE)0733-9399(2001)127:11(1152)
- Yoon, G. H. (2010a). Maximizing the fundamental eigenfrequency of geometrically nonlinear structures by topology optimization based on element connectivity parameterization. *Computers & Structures*, 88(1–2), 120–133. doi:10.1016/j.compstruc.2009.07.006
- Yoon, G. H. (2010b). Structural topology optimization for frequency response problem using model reduction schemes. *Computer Methods in Applied Mechanics and Engineering*, 199(25–28), 1744–1763. doi:10.1016/j.cma.2010.02.002
- Yoon, G. H. (2011). Topology optimization for nonlinear dynamic problem with multiple materials and material-dependent boundary condition. *Finite Elements in Analysis and Design*, 47(7), 753–763. doi:10.1016/j.fin.2011.02.006
- Yoon, G. H., & Kim, Y. Y. (2005). Element connectivity parameterization for topology optimization of geometrically nonlinear structures. *International Journal of Solids and Structures*, 42(7), 1983–2009. doi:10.1016/j.ijsolstr.2004.09.005
- Yuan, W., Cao, X., Cheung, P., Wang, B., & Rong, Z. (2010, August). *Development of cable-sliding friction aseismic bearing for bridges*. Paper presented at the 5th Civil Engineering Conference in the Asian Region and Australasian Structural Engineering Conference 2010, Sydney, Australia.
- Yuan, Y., & Sun, B. (2008, October). General introduction of engineering damage of Wenchuan Ms 8.0 Earthquake. *Journal of Earthquake Engineering and Engineering Vibration*, 28, 59–73.
- Zadeh, L. A. (1965). Fuzzy sets. *Information and Control*, 8, 338–353. doi:10.1016/S0019-9958(65)90241-X
- Zahrah, T. F., & Hall, W. J. (1984). Earthquake energy absorption in sdof structures. *Journal of Structural Engineering*, 110, 1757–1772. doi:10.1061/(ASCE)0733-9445(1984)110:8(1757)
- Zerva, A. (2008). *Spatial variation of seismic ground motions modeling and engineering applications*. Boca Raton, FL: CRC Press.
- Zhang, J. (2003). *Performance-based seismic design using designed experiments and neural networks*. PhD Thesis, Department of Civil Engineering, University of British Columbia, Canada.
- Zhang, J., Makris, N., & Delis, T. (2004). Structural characterization of modern highway overcrossings-Case study. *Journal of Structural Engineering*, 130(6), 846–860. doi:10.1061/(ASCE)0733-9445(2004)130:6(846)
- Zhao, C. B., Steven, G. P., & Xie, Y. M. (1997). Evolutionary optimization of maximizing the difference between two natural frequencies of a vibrating structure. *Structural Optimization*, 13(2–3), 148–154. doi:10.1007/BF01199234

Compilation of References

- Zhou, M. (2008). *Experimental and theoretical studies on seismic performance of elevated pile caps*. Doctoral dissertation, Tongji University, Shanghai, China.
- Zhou, M., & Rozvany, G. I. N. (2001). On the validity of ESO type methods in topology optimization. *Structural and Multidisciplinary Optimization*, 21(1), 80–83. doi:10.1007/s001580050170
- Zhu, Z., Fu, Y., Wang, B., & Yuan, W. (2010, August). *Seismic study on bridge piers reinforced with SFRC in local region*. Paper presented at the 5th Civil Engineering Conference in the Asian Region and Australasian Structural Engineering Conference 2010, Sydney, Australia.
- Zienkiewicz, O. C., Taylor, R. L., & Zhu, J. Z. (2005). *The finite element method: Its basis and fundamentals*. Oxford, UK: Elsevier Butterworth-Heinemann.
- Zollo, R. F. (1997). Fiber-reinforced concrete: An overview after 30 years of development. *Cement and Concrete Composites*, 19, 107–122. doi:10.1016/S0958-9465(96)00046-7
- Zou, X. (2002). *Optimal seismic performance-based design of reinforced concrete buildings*. Doctoral dissertation, Hong Kong University of Science and Technology, Hong Kong, China.
- Zou, X. K., & Chan, C. M. (2001). Optimal drift performance design for nonlinear pushover response of concrete structures. *WCSMO-4: Proceedings of the Fourth World Congress of Structural and Multidisciplinary Optimization*, June 4-8, Dalian, China.
- Zou, X. K. (2008). Integrated seismic design optimization of nonlinear base-isolated RC buildings. *Structural and Multidisciplinary Optimization*, 36(5), 493–507. doi:10.1007/s00158-007-0184-5
- Zou, X. K., & Chan, C. M. (2005). An optimal resizing technique for seismic drift design of concrete buildings subjected to response spectrum and time history loadings. *Computers & Structures*, 83(19-20), 1689–1704. doi:10.1016/j.compstruc.2004.10.002
- Zou, X. K., & Chan, C. M. (2005a). An optimal resizing technique for seismic drift design of concrete buildings subjected to response spectrum and time history loadings. *Computers & Structures*, 83, 1689–1704. doi:10.1016/j.compstruc.2004.10.002
- Zou, X. K., & Chan, C. M. (2005b). Optimal seismic performance-based design of reinforced concrete buildings using nonlinear pushover analysis. *Engineering Structures*, 27, 1289–1302. doi:10.1016/j.engstruct.2005.04.001
- Zou, X. K., Chan, C. M., Li, G., & Wang, Q. (2007b). Multiobjective optimization for performance-based design of concrete structures. *Journal of Structural Engineering*, 133(10), 1462–1474. doi:10.1061/(ASCE)0733-9445(2007)133:10(1462)
- Zou, X. K., Teng, J. G., Xia, S. H., & Wong, Y. L. (2007a). Optimal performance-based seismic retrofit design of FRP-confined concrete buildings. *Composite Part B: Engineering International Journal*, 38, 584–597. doi:10.1016/j.compositesb.2006.07.016
- Zou, X. K., Wang, Q., Li, G., & Chan, C. M. (2010). Integrated reliability-based seismic drift design optimization of base-isolated concrete buildings. *Journal of Structural Engineering*, 136(10), 1282–1295. doi:10.1061/(ASCE) ST.1943-541X.0000216

About the Contributors

Vagelis Plevris is an Assistant Professor at the Department of Civil and Structural Engineering Educators, School of Pedagogical & Technological Education (ASPETE) in Athens, Greece and a Research Associate at the School of Civil Engineering, National Technical University of Athens (NTUA). He holds a Bachelor in Civil Engineering, an MSc in Earthquake Engineering, a PhD in Computational Mechanics from NTUA and also a Master in Business Administration from the Athens University of Economics and Business. His research work focuses mainly on computational earthquake engineering, design optimization, reliability analysis of structures and neural networks applications in structural engineering. His published research work includes more than 10 peer-reviewed journal papers, 4 contributed books as editor, 4 chapters in international scientific books, and 22 papers in international conferences.

Chara Ch. Mitropoulou is a post-doctoral researcher at the Institute of Structural Analysis and Seismic Research of the School of Civil Engineering, National Technical University of Athens. She holds BSc, MSc, and Ph.D. degrees in Civil Engineering from the National Technical University of Athens. She has participated in a number of research projects and consultancies in the areas of structural analysis and structural dynamics, shape, sizing and topology optimum design of structures, mathematical programming, performance based design of RC and steel structures as well as life cycle cost and fragility assessment of structures. Her publications include 4 book chapters, 2 papers in non-referred international scientific journals, 7 publications in referred international scientific journals, and 13 papers in conference proceedings.

Nikos D. Lagaros is a Lecturer at the Institute of Structural Analysis and Seismic Research of the School of Civil Engineering, National Technical University of Athens and at the School of Corps of Engineers of the Hellenic Army since 2007. He is serving as Treasurer of the Greek Association for Computational Mechanics, while he acts as NSF panellist at the Directorate for Engineering Civil, Mechanical and Manufacturing Innovation, since 2010. Dr. Lagaros provides consulting, peer-review, and expert-witness services to private companies and federal government agencies in Greece. A focus of his consulting work is the assessment of buildings after earthquake events and the development of technical software. The results of his research activity encompass a wide range of topics with an interdisciplinary character in the field of computational mechanics. His published research work contains: 70 peer-reviewed journal papers, 1 book, 6 contributed books, 2 international conference proceedings, 15 chapters in international books, and 135 papers in international conferences.

About the Contributors

Azadeh Alipour, PhD, is an Assistant Professor at the Department of Civil and Environmental Engineering of University of Massachusetts, Amherst. She received her Doctoral degree from the University of California, Irvine in 2010. Prior to joining to the University of Massachusetts, she was a postdoctoral scholar at University of California, Irvine. Dr. Alipour has served as a committee member in ASCE and ACI. Furthermore, she is a reviewer of *ASCE Journal of Bridge Engineering*, *ASCE Journal of Engineering Mechanics*, and *Journal of Structure and Infrastructure Engineering*. Her research interests include probabilistic performance evaluation of civil infrastructure components under multi-hazards, risk mitigation strategies for infrastructure systems under extreme conditions, and life-cycle engineering and management of civil infrastructures.

Luis Becerra is a Master's student of Civil Engineering at Santa Maria University, Valparaiso, Chile. The topic of his Master's thesis is the optimal design of structural systems subject to stochastic loading using an interior-point method for optimization.

Soumya Bhattacharjya, born on 12th March, 1979, is an Assistant Professor in the Department of Civil Engineering, Bengal Engineering and Science University, Shibpur, India. He completed his Bachelor of Engineering in Civil Engineering in 2002 from Bengal Engineering College, Shibpur, India and Master of Engineering with specialization in Structural Engineering in 2004 from Bengal Engineering and Science University, Shibpur, India. Subsequently, he obtained his PhD in Civil Engineering from the same university in the field of Robust Optimization of Structures in 2011. In general, Dr. Bhattacharjya's research interest lies in the field of reliability, optimization under uncertainty, steel structures, and composite mechanics.

Subrata Chakraborty is currently a Professor at the Bengal Engineering and Science University, Shibpur. He is a fellow of the Indian National Academy Engineering and the Institution of Engineers (India). Prof. Chakraborty did his Bachelor of Engineering in Civil Engineering from Bengal Engineering College, Shibpur, M. Tech. and Ph.D. from Indian Institute of technology, Kharagpur. He was a postdoctoral researcher at University of Cambridge, UK and University of Arizona, USA and Technical University of Aachen, Germany. In general, Prof. Chakraborty's research interest lies in the field of computational mechanics under uncertainty, structural health monitoring, vibration control, composite mechanics, et cetera. He has published extensively in peer reviewed journals, authored textbook and book chapters, and reviewed research articles for various national and international journals. As an independent researcher, Prof. Chakraborty has completed a number of research projects funded by various agencies and he is also active in important industrial consultancy.

Pak-Chiu Cheung is a Kwang-Hua Foundation visiting Professor of Civil Engineering at Tongji University, Shanghai, China. Also an adjunct Associate Professor at the Hong Kong Polytechnic University, he retired as a Structural Engineer from the Architectural Services Department of Hong Kong SAR Government in 2010 and was President of American Society of Civil Engineers Hong Kong Section for the session 2008-2009. He received his B.S. from the National Cheng-Kung University, Taiwan, in 1974, M.S. from Cornell University, New York, in 1976, and Ph.D. from the University of Canterbury, New Zealand, in 1991. Dr. Cheung's research interest focuses on seismic structural design.

Tahar El-Korchi is a Professor and Chair of the Civil and Environmental Engineering Department at Worcester Polytechnic Institute in Worcester, Mass. He has been at WPI since 1987. His teaching and research interests are in the smart materials and structures, structural composites and control, construction materials and processes, pavement engineering, and testing. He has authored and coauthored over 80 publications in this area, including a textbook on Pavement Engineering. He received funding through federal and state agencies including the NSF – PYI program. He is active in numerous organizations including TRB, FHWA, ACI, and ASCE. He is very active in the global perspective program at WPI where he directs the Panama and Morocco student project centers.

Amr Elnashai, is the Head of the Civil and Environmental Engineering Department, and Bill and Elaine Hall Endowed Professor at the University of Illinois at Urbana-Champaign, USA. He was Director of the NSF multi-institution interdisciplinary Mid-America Earthquake Center and NSF Network for Earthquake Engineering Simulation (NEES) Laboratory at Illinois. Amr obtained his MSc and PhD from Imperial College, University of London, UK and is a Fellow of the UK Royal Academy of Engineering. Before joining the University of Illinois in June 2001, Amr was Professor of Earthquake Engineering and Head of Section at Imperial College (1985-2001). He is founder and co-editor of the *Journal of Earthquake Engineering* and editorial board member of several other journals. Amr's technical interests are multi-resolution distributed analytical simulations, network analysis, large-scale hybrid testing and field investigations of the response of complex networks and structures to earthquakes. He has produced more than 250 research publications, including over 120 refereed journal papers, many conference, keynote and prestige lectures (including the Nathan Newmark Distinguished Lecture), research reports, 2 books and several book chapters, magazine articles and earthquake field investigation reports. Amr has successfully supervised 40 Doctoral and over 100 Master of Science theses.

Ricardo O. Foschi is Emeritus Professor, Civil Engineering, University of British Columbia, Vancouver, Canada. Dr. Foschi received his Ph.D in Engineering Mechanics from Stanford University in 1966, and has contributed many publications in different topics of applied mechanics, including behaviour of wood structures, reliability, and application of general probabilistic methods to different problems in engineering. His publications have appeared in national and international journals, as well as contributed book chapters. His continuing areas of research include reliability applications in earthquake engineering, performance-based design, and optimization applications.

Bora Gencturk is an Assistant Professor at the Civil and Environmental Engineering Department at the University of Houston. Bora obtained his MSc and PhD from University of Illinois at Urbana-Champaign. He is a member of several professional organizations including the American Society of Civil Engineers, American Concrete Institute and Earthquake Engineering Research Institute. Bora's technical interest are use of advanced materials for hazard mitigation and sustainable construction, life-cycle analysis of new and existing buildings subjected multiple hazards, development of small-scale structural testing methods, and vulnerability assessment of structures. Bora has produced more than 20 research publications, including two book chapters and five research reports.

About the Contributors

Kazem Ghabraie completed a Bachelor's and a Master's degree in Civil Engineering in University of Tehran, Iran. He obtained his PhD in Civil Engineering from RMIT University in Melbourne, Australia in 2009. Since 2010, he has been working as a Lecturer in University of Southern Queensland, Toowoomba, Australia. His research interests include non-linear finite element method and numerical structural optimization. Since 2002 he is working on topology optimization of structures as his main research area.

Saeed Gholizadeh was born in Urmia, Iran, in 1978. He received his B.Sc. degree in Civil Engineering from Urmia University in 2001, and his M.Sc. and Ph.D. degrees in Structural Engineering from University of Kerman as the first rank in 2003 and 2009, respectively. Dr. Gholizadeh has been with the Department of Civil Engineering, Urmia University, Iran, since 2009. His research interests include structural optimization, earthquake engineering, space structures, and soft computing. He has published over 50 journal papers, conference articles and book chapters in the above areas. Dr. Gholizadeh is a member of the Centre of Excellence for Fundamental Studies in Structural Engineering of Iran University of Science and Technology, member of the Iranian Institute of Spatial Structures and member of the editorial board of the *International Journal of Optimization in Civil Engineering*.

Ioannis Gidaris received his Diploma in Civil Engineering with major in Structural Engineering from the Civil Engineering Department of the Aristotle University of Thessaloniki in 2008. He completed the Master's program "Earthquake Resistant Design of Structures" in 2009 in the same department. He is currently a PhD student at the University of Notre Dame and his research interests are performance based seismic design of structures, assessment of the nonlinear response of structures subjected to earthquake excitations, life-cycle cost assessment, and Bayesian updating of deteriorating bridge infrastructure systems through monitoring data.

Héctor Jensen is Professor of Civil Engineering at Santa María University, Valparaíso, Chile. He received his degree of Mathematician Civil Engineer from University of Chile, Santiago, and his Ph.D. in Applied Mechanics from California Institute of Technology (Caltech), Pasadena, USA. Jensen's research expertise is in structural reliability based optimization, stochastic structural dynamics, and structural reliability.

Jin Seop Kim is a postdoctoral researcher at the Department of Brain and Cognitive Sciences at Massachusetts Institute of Technology (MIT), U. S. A. He studied for his Doctorate at the Department of Physics and Astronomy at Seoul National University, Republic of Korea. His research interests include critical phenomena and universality in statistical physics, structure and dynamics of complex systems, biophysics, and computational models of neural systems. At MIT he is studying the topology of neuronal systems at electron microscope resolution for macroscopic systems.

Yeesock Kim currently holds the position as the Assistant Professor of Structural Engineering at the Department of Civil and Environment Engineering at Worcester Polytechnic Institute (WPI), Massachusetts, USA. He was a postdoctoral researcher of Control Engineering at the Department of Mechanical Engineering at Texas A&M University, College Station, USA, in 2007-2010. He is the author of 6 book/book chapters, including 42 technical papers in various fields of smart structures, vibration control, system

identification, and control theory. At WPI, he teaches Smart Structures, Smart Infrastructure Analysis and Design, Structural Dynamics, and Structural Analysis and Design. He is also currently serving on the *IEEE Control Systems Society* Editorial Board.

Sankaran Mahadevan is a Professor at the Department of Civil & Environmental Engineering, Vanderbilt University, USA. He is also the Director of the NSF-IGERT Multidisciplinary Graduate Program in Reliability and Risk Engineering and Management. Dr. Mahadevan is a member of the American Society of Civil Engineers (ASCE) and has acted as an Associate Editor for the *Journal of Structural Engineering* (ASCE). Professor Mahadevan co-authored two books on reliability and statistical methods in engineering design and on reliability assessment using stochastic finite element analysis. He has more than 100 research papers published in reputable international journals and several book chapters. His research interest includes probabilistic computational mechanics, reliability and risk assessment, structural durability, fatigue and fracture, model verification and validation under uncertainty and reliability-based design optimization.

Hamid Moharrami is a Senior Professor in Tarbiat Modares University, Tehran, Iran, since October 1993. He received his B.Sc. from Amirkabir Universities of Technology, and M.Sc., from Sharif Universities of Technology, both in Tehran Iran. He continued his education at the University of Waterloo, Canada where, he got his Ph.D. in 1993 in Civil Engineering with a speciality in structural optimization. Dr. Moharrami's research interests include design optimization, nonlinear analysis, numerical analysis and experimental methods. He has been doing research in three branches of design optimization. One is developing new optimization algorithms or improving the existing algorithms. The second is the use of the optimization algorithm in various fields of Civil Engineering design problems. The third is the application of optimization algorithms, especially LP and QP in developing nonlinear structural analysis algorithms. His research endeavour has led to many fascinating solution schemes for design optimization of different types of structures including buildings, bridges, space structures, differential surge tanks, et cetera.

Oscar Moller is Professor, School of Civil Engineering, University of Rosario, Argentina, and the Institute of Applied Mechanics and Structures (IMAE), University of Rosario, Argentina. He is also Researcher with the Research Council of the University of Rosario, Argentina. Dr. Moller received his Doctoral degree in Engineering in 2001 from the School of Civil Engineering, University of Rosario, Argentina. Dr. Moller's interests are structural mechanics and dynamics, nonlinear response of structures, earthquake engineering, and issues of reliability in the context of seismic design. He has previously published in international journals and has had collaborations in book chapters in the area of earthquake engineering, focussing on reliability, performance-based design, and structural optimization algorithms.

Abbas Moustafa is an Associate Professor at the Department of Civil Engineering, Minia University, Egypt. He is also the chairman of the Department of Civil Engineering, High Institute of Engineering, Tamoh, Giza, Egypt. He is the editor of two books on earthquake resistant structures and geotechnical earthquake engineering. Dr. Moustafa got his Doctoral degree in 2002 from the Indian Institute of Science in earthquake engineering and structural reliability. He joined Vanderbilt University as a senior research associate. He worked for a funded research project by the US-Air Force on structural health

About the Contributors

monitoring using bond graphs. He joined also Nagasaki and Kyoto Universities as a JSPS research fellow. Dr. Moustafa has more than 25 research papers published in international journals, and he acts as a reviewer for a number of regional and international journals. His research interest includes earthquake engineering, seismic design, inelastic structures, optimum design, structural health monitoring, structural safety, base-isolation, structural control, and uncertainty modeling.

Marcelo Rubinstein is Professor, School of Civil Engineering, University of Rosario, Argentina, and the Institute of Applied Mechanics and Structures (IMAE), University of Rosario, Argentina, of which Professor Rubinstein is the Director of the Structures Laboratory. Professor Rubinstein received his Civil Engineering degree from the University of Rosario in 1962. His interests are structural mechanics and dynamics, structural design, bridge analysis and design, earthquake engineering, and behavior of structures with energy dissipation devices.

Fabián Savino is a Student and Research Assistant, School of Engineering and IMAE, University of Rosario, Argentina. Future interests focus on structural analysis and design, including computer applications and optimization of structures.

Juan Sepúlveda received his Diploma and Master's Degree in Civil Engineering from Santa María University, Valparaíso, Chile, in 2010. The topic of his Master's thesis is the optimal design of structural systems subject to stochastic loading considering discrete design variables.

Behrouz Shafei, PhD, is an Assistant Professor at the Department of Civil and Environmental Engineering of University of Massachusetts, Amherst. He received his Doctoral degree from the University of California, Irvine in 2011. Prior to joining to the University of Massachusetts, he was a postdoctoral scholar at University of California, Irvine. Dr. Shafei has been selected as ASCE 2012 New Face of Civil Engineering. Furthermore, he is the recipient of the Public Impact Distinguished Fellowship and James D. Cooper best paper award. Dr. Shafei's research addresses the deterioration of civil infrastructure components subjected to multiple environmental stressors. His investigation also includes the effects of spatial and temporal uncertainties on the estimation of the durability and state of deterioration.

Masanobu Shinotuka, PhD, PE, NAE, is a Distinguished Professor at the Department of Civil and Environmental Engineering of University of California, Irvine. He received his Doctoral degree from Columbia University in 1960. He is an Elected Member of the National Academy of Engineering, Distinguished Member of ASCE, and Fellow ASME. He has been the recipient of prestigious awards and medals, including the ASCE Theodore von Karman medal (1994), ASCE Nathan M. Newmark medal (1985), and ASCE Alfred M. Freudenthal medal (1978). Dr. Shinotuka is a world-renowned expert in applied mechanics and structural engineering. He has published several technical papers on random vibration, reliability of structural systems, structural control, and risk assessment of civil infrastructure components.

Alexandros Taflanidis is the Rooney Family Assistant Professor in the Department of Civil Engineering and Geological Sciences at the University of Notre Dame. Dr. Taflanidis received his diploma in Civil Engineering (2002) and Master's in "Earthquake Resistant Design of Structures" (2003) from

the Aristotle University of Thessaloniki. He received his PhD in 2008 in Civil Engineering with a minor in Control and Dynamical Systems from the California Institute of Technology. His research focuses on the implementation of advanced computational and simulation methodologies for assessment and mitigation of risk due to natural hazards (such as earthquakes, waves and hurricanes). He is also the Director of the High Performance System Analysis and Design (HIPAD) Lab at Notre Dame, pursuing fundamental research in the analysis and design of high-performance engineering systems in the presence of probabilistically characterized modeling uncertainties. The applications his group examines extend to seismic resistant design of structural systems, assessment of risk due to hurricanes in support of emergency responses, optimal monitoring and maintenance of bridge infrastructure systems, and optimization of offshore energy (wind/wave) conversion devices.

Marcos Valdebenito is Assistant Professor of Civil Engineering at Santa Maria University, Valparaiso, Chile. He received his Diploma and Master's Degree in Civil Engineering from Santa Maria University, Valparaiso, Chile, in January 2006 and his Doctoral Degree in Civil Engineering from the University of Innsbruck, Innsbruck, Austria, in February 2010. His fields of interest are simulation methods, reliability-based optimization, and reliability sensitivity.

Wan-Cheng Yuan is a Professor of Civil Engineering in the State Key Laboratory of Disaster Reduction in Civil Engineering, Tongji University in Shanghai, China. He was Head of the University's Department of Bridge Engineering from 1992 to 1996. He was a visiting Professor at the Hong Kong University of Science and Technology in 1997 and at Darmstadt University of Technology in Germany from 1993 to 1994. He received his B.S., M.S. and Ph.D. degrees from Tongji University in 1984, 1987, and 1990 respectively. Dr. Yuan's research interests cover various areas of bridge engineering, including seismic structural design, performance and safety assessment, bridge vibration, ductility of high-strength concrete, and bridge health monitoring. He received the First Class Prize of the National Competition for Progress in Science and Technology of China in 2009, the First Level Technology Advances Award from Shanghai City in 2008, and the Second Award in Science and Technology Advances Program from the Ministry of Education of China in 1995. He has authored and co-authored more than a hundred technical papers.

Yu-Guo Zheng is a Ph.D. Candidate in Bridge and Tunnel Engineering at Tongji University and presently a Lecturer in Civil Engineering at the Hunan University of Science and Technology, Xiangtan, China.

Xiao-Kang Zou obtained her Bachelor Degree and Master Degree of Civil Engineering in 1987 and 1990, respectively, in Northern Jiaotong University (currently called Beijing Jiaotong University) in Beijing, P.R. China. She obtained her PhD degree in 2002 from the Department of Civil Engineering, the Hong Kong University of Science and Technology. Her PhD topic is "Optimal Seismic Performance-Based Design of Reinforced Concrete Buildings." Currently, she works in AECOM Asia Company Ltd. in Hong Kong as a principal Engineer. She is mainly responsible for developing and applying elastic and inelastic optimization technique to design projects under wind load and seismic load.

Index

A

acceleration-displacement response spectrum (ADRS) 182
 aleatory uncertainties 129
 Ant Colony Optimization (ACO) 154, 165
 Autoregressive eXogenous (ARX) 323, 325, 336
 axial-moment hinge 216-217

B

back-propagation (BP) 308
 basic safety objective (BSO) 177
 Bi-directional ESO (BESO) 234
 bond graph (BG) 342-343
 bridge modelling
 abutments 84, 286, 289, 370-371, 374-375,
 377, 386, 388, 391-392
 pier columns 84
 superstructure model 84
 Bridge Piers Reinforced with SFRC 271, 291, 294,
 302, 304
 BWBM model 44

C

Cable-Sliding Friction Aseismic Bearing 304-305
 cable-stayed bridges 272
 fixed system 272
 floating system 272
 semi-floating system 272
 Capacitance (C) 344
 cellular automata (CA) 308, 310
 cellular crossover operation (CCO) 311
 cellular genetic algorithm (CGA) 308
 chloride binding capacity 78
 chloride content profile 80
 chloride-induced corrosion 77, 100

chloride transport mechanism 77
 capillary suction 77
 ionic diffusion 77
 permeation 77
 close twin-column pier (CTP) 275
 Close Twin-Column Pier System 305
 coefficient of variation (CoV) 156
 collapse performance level 4, 9-10, 13, 23, 25, 34-
 35, 37, 39, 129, 134, 141, 143, 148, 176-177,
 212, 217, 224, 271-272, 394
 interstory drift 3-4, 6-7, 10-12, 16-18, 35, 65-
 66, 70, 214, 225
 maximum global damage index 33, 35
 maximum local damage index 33, 35
 Collapse Prevention (CP) 10, 177, 224
 Combined Methods 184
 Common Random Numbers (CRN) 383
 complete quadratic combination (CQC) 212
 compliance minimization 250
 concentration cycle 77-78
 continuation method 239
 continuous girder bridges 272
 cumulative distribution function 92

D

damage detection 343
 damage indices 128, 145
 damage signature derivation 358
 backward propagation (BP) 358
 forward propagation (FP) 358
 deck drift ratio (DDR) 85
 depassivated 81
 Design (decision) Variables 4
 Design Parameters (DPs) 107
 deterministic and probabilistic seismic hazard analysis (DSHA and PSHA) 8
 deterministic design optimization (DDO) 107
 diffusion cycle 78

discrete formulation 51
ductility 132

E

earthquake loads 129, 131-132, 344
earthquake-resistant design of structures 129
Eigenfrequency Control 232, 268
Elastic Cable Seismic Mitigation and Isolation Device 305
elastic dynamic 3
evaporable water content 78
Evolutionary Algorithms (EA) 155
Evolutionary Structural Optimization (ESO) 234
exact nonlinear dynamic Analysis (ENDA) 316
excitation models 52

F

Fault Adaptive Control Technology (FACT) 342, 363
Finite Difference (FD) 188
fmincon algorithm 137
For single-objective seismic design optimization 2
fragility analysis 86
frictional bearings 273
fully stressed design (FSD) 186
fuzzy-decision theory 220
fuzzy inference systems (FIS) 307

G

generalized regression neural network (GRNN) 308
Generic Modeling Environment (GME) 342
genetic algorithms (GA) 6
gradient-based algorithms 5
ground motion uncertainties 24
Gyrator (GY) 344

H

hard kill approach 258
Hazard Levels 4, 7-10, 13, 17, 87, 153, 319
heuristic-based algorithms 5, 22
hierarchical clustering-based (HRC) 325, 336
High Performance system Analysis and Design (HIPAD) 389
hollow single-column pier (HSP) 274
homogenization method 233
hybrid design space (HDS) 106

I

Immediate Occupancy (IO) 10, 177, 224
Incremental Scheme 184, 190
Inertance (I) 344
initial cost 31
Initial Stiffness method 184
inspection and maintenance intervals 93
inspection scheduling 152, 159, 168, 173
inter-story drift responses 217
isolation design 273

L

life-cycle cost (LCC) 1, 20, 87, 99
Life Safety (LS) 10, 177, 224
life safety performance level 4, 9-10, 13, 23, 25, 34-35, 129, 153, 177, 217, 224
interstory drift 3-4, 6-7, 10-12, 16-18, 35, 65-66, 70, 214, 225
maximim local damage 33, 35
maximum global damage index 33, 35
Linear dynamic analysis 150, 178-179
Linear Programming (LP) 187
Linear static analysis 175, 178-179
linear time-invariant (LTI) 333
load and resistance factored design (LRFD) 175
local capacity design 271
local minima 238
local response quantities 217
longitudinal support unseating 272
lower bound Fourier amplitude spectra (LBFAS) 134

M

magnetorheological (MR) 323, 325, 330, 335
Markov Chain Monte Carlo procedure 53
Material Properties 3, 8, 11-12, 20, 83-84, 101, 153, 155, 168, 176, 234, 242, 291, 377
Matlab optimiztion toolbox 137
maximum allowable admission ratio 259
Membership functions (MFs) 325
metaheuristic optimization 168
meta-heuristic optimization algorithms 307
method of moving asymptotes (MMA) 237, 251
modified cellular genetic algorithm (MCGA) 311
moment hinge 215, 217
monotonic convergence 53, 72
Monte Carlo Simulation (MCS) 11, 115

moving least-squares method (MLSM) 108
multi degree of freedom (MDOF) 111
multi-input, multi-output (MIMO) 325, 336
multiple-objective seismic design optimization 2
Multi-Stripe Dynamic Analysis (MSDA) 158
mutation operation (MO) 311

N

National Oceanic and Atmospheric Administration (NOAA) 78
near-fault ground motions 372, 379
neural networks 24
neural network system (HNNS) 308, 312
Newton-Raphson method 184, 194, 253
Nonlinear dynamic analysis 26, 31, 33-34, 45-46, 129, 145, 148, 175, 178, 180-181, 196, 204, 308, 315-316, 372, 374
nonlinear static analysis 3, 153, 178-179, 212
nonlinear system identification 336
nonlinear time-history analysis method 129
non-stationary stochastic process 51, 55

O

Objective (merit) Function 4
OpenSees 83-84, 103
Operational (OP) 177
operational performance level 9, 20, 23, 25, 34, 171, 173, 177, 211
elastic displacement limit 34
interstory drift 3-4, 6-7, 10-12, 16-18, 35, 65-66, 70, 214, 225
Optimality Criteria (OC) 187, 210, 237
optimization under uncertainty 382
optimum path 165
optimum performance-based seismic design (OPBSD) 176
overall conceptual seismic design 270

P

parameter uncertainty 106
Pareto-Optimality 4-5
Pareto optimal set 221
Particle Swarm Optimization (PSO) 154, 307
passive dampers 151, 232, 264, 268
performance based design optimization (PBDO) 106
Performance-Based Design (PBD) 153, 175
performance-based seismic design (PBS) 6
Performance Levels 4, 9-13, 23-25, 34, 37-39, 177, 195, 200-202, 217, 219

pheromone 165
pheromone trail 165
pile-cap mass 25
pile group foundation strengthened with SPPs 296
plastic hinges 196, 214
plastification 189
pot bearings 273
probabilistic design 372
probabilistic neural network (PNN) 308
probability density function (PDF) 31, 110, 156, 373
pushover analysis 209

Q

Quadratic Programming (QP) 185, 187

R

radial basis function (RBF) 307
reinforced concrete (RC) 1-2, 77, 153, 208, 284, 297
reliability based design optimization (RBDO) 106
reliability-based optimization (RBO) 52
repair costs 31
Resistor (R) 344
response parameters 33
 DIES 31-33, 35
 DILO 33, 35
 DIST 33, 35-36
 UMAX 33, 35
response spectrum analysis 208
response surface method (RSM) 105, 108
risk quantification 374
roller bearings 273
root mean square (RMS) 112
rubber bearings 273

S

Saturated Design (SD) 118
SCC bridge 273
seismic dampers 371
seismic mitigation 273
Sensitivity Analysis 51-52, 114, 174, 176, 187-191, 193-196, 199, 201, 204-205, 236, 244, 251, 253, 261, 264-265, 268, 306, 372, 384, 390-393, 395-396
sensitivity based approach 107
sensitivity numbers 258
sensor faults 343
Sequential Linear Programming (SLP) 187
sequential quadratic programming (SQP) 121, 187
service failure 92-94, 100

shape optimization 233
 Simulated Annealing (SA) 6, 307
 simultaneous failure mode (SFM) 186
 Simultaneous Perturbation Stochastic Approximation (SPSA) 382
 single-degree-of-freedom (SDOF) 6, 348
 sizing optimization 232
 smart control 329
 Solid Isotropic Microstructures with Penalization (SIMP) 234
 solid twin-column pier (STP) 274
 Solution (objective function) Space 4
 Sorting Evolution Strategies II (NSES-II) 155
 Space of Design (decision) Variables or Search Space 4
 spatial tower 272, 278
 Steel-Concrete Composite Bridge 304-305
 steel fiber reinforced concrete (SFRC) 269, 271, 291
 steel protective pipes (SPPs) 269, 273, 296
 stoachastic model 380
 stochastic earthquake load 108, 115, 124
 stochastic structural optimization (SSO) 106, 111
 structural collapse 148, 176, 272
 Structural health monitoring (SHM) 343
 Structural optimization 1-6, 15, 21-23, 44, 50-53, 73-75, 105-106, 111, 126-127, 164, 174-176, 204-206, 209, 229, 232-235, 241, 258, 264-268, 306, 308-310, 321, 344
 shape optimization 1, 258
 sizing optimization 1
 topology optimization 1, 239, 256
 Structural variation theory studies 185

subset simulation 66
 system identification (SI) 324, 336, 343

T

taboo search (TS) 6, 14
 Takagi-Sugeno (TS) 323, 325, 336
 temporal causal graph (TCG) 342, 348, 354
 the peak ground acceleration (PGA) 8
 time-history 55, 379, 387
 topology optimization 233
 total cost 7, 23-25, 29-30, 38-41, 43, 45, 48, 77, 87-88, 271
 transformer (TF) 344
 Travelling Salesman Problem (TSP) 161
 tuned mass damper (TMD) 107

U

uncertain but bounded (UBB) 107
 uniform hazard spectra (UHS) 8
 upper bound Fourier amplitude spectra (UBFAS) 134
 U-shaped flexural plates (UFP) 69

V

virtual work 5, 210, 214, 228

W

weighted sum method (WSM) 109